PENN STATE

NASW-4435

MARS SAMPLE RETURN MISSION TWO ALTERNATE SCENARIOS

FINAL REPORT

By the 1990-91 Senior Spacecraft Design Students
Penn State Aerospace Engineering Department

Sponsored by the USRA Advanced Design Program

ABSTRACT

Two scenarios for accomplishing a Mars Sample Return mission are presented herein. Mission A is a low-cost, low-mass scenario, while Mission B is a high-technology, high-science alternative.

Mission A begins with the launch of one Titan IV rocket with a Centaur G' upper stage. The Centaur performs the trans-Mars injection burn and is then released. The payload consists of two lander packages and the Orbital Transfer Vehicle, which is responsible for supporting the landers during launch and interplanetary cruise. Near Mars, the landers separate -- one bound for a polar site and the other for an equatorial site. After descending to the surface, the landers deploy small, local rovers to collect samples. The rovers return these samples to the landers for loading on the Direct Return Rockets, which return the samples directly to the Earth's surface.

Mission B starts with four Titan IV launches, used to place the components of the Planetary Transfer Vehicle (PTV) into orbit. The fourth launch payload is able to move to assemble the entire vehicle by simple docking routines. Once complete, the PTV begins a low-thrust trajectory out from low Earth orbit, through interplanetary space, and into low Martian orbit. It deploys a communications satellite into a one-half sol orbit and then releases the lander package at 500 km altitude. The lander package contains the lander, the Mars Ascent Vehicle (MAV), two lighter-than-air rovers (called Aereons), and one conventional land rover. The entire package is contained within a biconic aeroshell. After release from the PTV, the lander package descends to the surface, where all three rovers are released to collect samples and map the terrain. The Aereons attempt to circumnavigate Mars and collect samples from a wide variety of sites, while the land rover examines a local area more thoroughly. The Aereons are equipped with small Sample Return Rockets which can return their samples to the lander in the event that an Aereon is incapable of returning to the lander itself. Once all samples have been collected, they are loaded onto the MAV and launched into orbit. The PTV then collects the samples and returns them to Earth orbit for recovery.

TABLE OF CONTENTS

INTRODUCTION

Penn State's design project for the 1990-91 academic year was the Mars Sample Return mission, currently under study by the Human and Robotic Spacecraft Office (HRSO) at Johnson Space Center.

From the Mars Rover Sample Return Mission Science Objectives Document [Ref. 1]: "The objectives of the MRSR mission are two-fold:

(1) "To reconstruct the geological, climatological, and biological history of Mars and determine the nature of its near-surface materials."

(2) "To obtain key environmental information and test key technologies necessary to maximize the safety and effectiveness of eventual human exploration."

A Mars Sample Return mission will "address the above goals by doing in situ analyses and returning a suite of intelligently selected samples representative of the planet's diversity."

The students participating in this year's design class were given a list of desired sample types and amounts, with the task being to acquire some or all of the sample set and return it to Earth by the year 2010. For the Fall '90 semester, the class was challenged to examine several alternate methods of achieving their mission and to evaluate the alternatives based on their own established criteria. For the Spring semester, the class was divided into two mission design teams, and each was given a mission scenario compiled from interesting features of the previous semester's designs. The two teams were composed of several groups, with each being responsible for a specific mission element of its team's scenario. Figures 1 and 2 depict the two mission scenarios. The suggested sample set is presented in Table 1.

This class comprises the required senior-level design sequence at Penn State and consists of two credits of conceptual and preliminary design in the Fall, followed by two credits of detailed design in the Spring.

Table 1: Suggested Sample Set

Regolith	50 g
Rock Fragments/Chips	1000 g
Pebbles	2085 g
Boulder Specimens	70 g
Core Sample	1256 g
Atmosphere	160 cm^3

Mission A Summary:

Mission A is a low-cost, low-mass mission scenario satisfying the following mission requirements:

1) All mission elements had to fit on one launch vehicle without assembly or construction in Earth orbit;

2) The trans-Mars injection had to be performed by the upper stage on the launch vehicle;

3) No Mars orbit operations, such as a satellite or a rendezvous, were permitted;

4) The mission had to use two landers, each with a small, land-based rover and a direct launch-to-Earth return vehicle.

These requirements were developed after a review of the previous semester's preliminary design work.

The scenario designed to meet these requirements can be seen in Figure 1. A single Titan IV/Centaur G' launch is used to boost the payload on a trajectory to Mars. The payload consists of two lander vehicles supported by an Orbital Transfer Vehicle (OTV). The OTV supports the landers during launch and interplanetary cruise and uses shared systems to reduce mass and avoid unnecessary duplication. This means that the OTV has access to the landers' communications, power, and computer systems. It does, however, have its own attitude and control system to make course corrections as necessary. As the OTV approaches Mars, it is jettisoned, and the two landers continue on independently -- one bound for a polar landing site and one for an equatorial site.

The landers aerocapture into separate orbits, and then proceed to land. They have blunt aeroshells similar in shape to those used on the Viking missions, but made to withstand both an aerocapture and an atmospheric entry. Once the entry process is complete, the aeroshells are jettisoned, and the parachutes deployed. The chutes slow the landers to a velocity of approximately 60 m/s at an altitude of 1.5 km. At this time, the chutes are discarded, and the retrorockets begin to fire. There are four retrorockets per lander, and they use a hydrazine/NTO propellant combination to slow the lander for a soft landing.

Once on the surface, the landers collect a contingency sample of regolith and atmosphere to insure at least a partial mission success should a rover fail. The landers are also responsible for collecting the core sample, which they do after obtaining the contingency samples. The Mars Sample Acquisition Vehicles (MSAVs) are then deployed.

The MSAVs are small, local rovers which range no more than one kilometer from the lander. Each MSAV is an articulated, three-body, six-wheeled vehicle powered by a modular radioisotope thermoelectric generator (MOD-RTG). It is semi-autonomous, and therefore dependent on instructions from Earth to execute complicated procedures. The MSAV has two arms: one for high-strength work and one for high-precision work. Both arms have access to a number of tools for acquiring samples and a variety of analysis

equipment to determine the fitness of a candidate sample. Samples worth keeping are placed in small teflon bags which are then placed in a basket on the rover. When the MSAV is done collecting samples, it returns to the lander. The lander uses its robotic arm to remove the basket from the rover and place it aboard the Direct Return Rocket.

The Direct Return Rocket (DRR) is a three-stage vehicle which is capable of returning a sample return capsule directly from the Martian surface to an Earth splashdown. The first two stages are simple, solid-propellant rocket stages using an advanced, high specific impulse propellant. Together, these stages move the payload into a low Mars orbit, and then perform the trans-Earth injection. The third stage of the DRR is the Earth Transfer Vehicle (ETV). It is based on the Kinetic Kill Vehicle (KKV) developed for the Strategic Defense Initiative and provides guidance, navigation, and control for the sample return capsule as it returns to Earth. Once the capsule has been placed on its reentry trajectory, the ETV detaches and the capsule continues on an unpowered entry. The small size of the capsule keeps it from generating much heat, so an ablative heat shield and passive thermal control devices are sufficient to protect the samples from damage.

This mission was costed using the Advanced Space Systems Costing Model developed by Kelly Cyr at Johnson Space Center [Ref 2]. Each mission element was costed separately, and the results are shown in Table 2.

Table 2: Mission A Costs (in millions of U.S. dollars)

Launch Costs (Titan IV/Centaur G')	265
Orbit Transfer Vehicle	552
Landers (2)	1746
Mars Sample Acquisition Vehicles (2)	708
Direct Return Rockets (2)	230
TOTAL MISSION COST	3236

Mission B Summary:

Mission B is a high-science return, high-technology scenario, and was designed under the following requirements:

1) Multiple launches were permitted, but Earth-orbit assembly was limited to simple docking routines (i.e. no on-orbit construction);

2) An orbital transfer vehicle, using radioisotope engines for propulsion, was to be used to transfer all mission elements from low Earth orbit to low Mars orbit and then back again upon completion of the mission. The transfer vehicle was to remain in Mars orbit while surface operations were conducted;

3) A communications and tracking satellite was to be included and deployed in an appropriate Mars orbit;

4) A lander was required, and was to be responsible for delivering three rovers to the planet's surface. Additionally, the lander was to include an ascent vehicle which would deliver the collected samples to the waiting transfer vehicle;

5) Two of the rovers were to be small, lighter-than-air (LTA) vehicles based on the Aereon principle. These rovers were required to attempt to circumnavigate Mars, collecting small amounts of samples from a large variety of sites. In case an LTA rover failed to return sufficiently close the lander, a mini-rocket could be included to attempt to launch the collected samples to the vicinity of the lander;

6) The third rover was to be a large, land-based rover responsible for investigating the area near the lander in detail. This rover was also to collect the majority of the samples, including those the LTA rovers were unable to collect due to weight limitations;

7) All rovers were to deliver their samples back to the lander for delivery to orbit via the ascent vehicle.

These requirements were developed after a review of the preliminary scenarios developed during the Fall '90 semester.

The mission designed to fulfill these requirements can be seen in Figure 2. Four Titan IV's launch their payloads into low Earth orbit. The first two payloads consist of one tank of ammonia each. The third payload consists of the communications satellite and the

lander package, which contains all the vehicles operating on the Martian surface. The final launch contains the Central Planetary Transfer Vehicle (CPTV) which consists of the third and final ammonia tank, the sample retrieval bay, and the transfer vehicle's subsystems. The CPTV then maneuvers on-orbit to rendezvous with and connect to the other sections.

Once the Planetary Transfer Vehicle is fully assembled, it begins a low-thrust spiral out of Earth orbit. The PTV's radioisotope engines produce thrust by heating a working fluid and expanding it out a diverging nozzle in a similar manner to a nuclear thermal engine. A decaying radioactive isotope provides the heat. Ammonia was chosen to be the working fluid due to its relatively high density and high specific impulse. This configuration results in a total thrust of approximately ten Newtons, with a specific impulse between 800 and 1200 seconds.

Upon reaching the vicinity of Mars, the PTV spirals into a low orbit. Along the way, it releases the communications satellite into a roughly circular 9300 km orbit which has an orbital period of approximately one-half a Martian day. This will allow the satellite to be in contact with each vehicle on the surface, including the Aereons, for a considerable amount of time each day.

After the PTV settles into a 500 km orbit, it releases the lander package, which subsequently begins an atmospheric entry. The lander package is contained in a biconic aeroshell which slows the lander to Mach 2 at an altitude of 6 km. At this time, the aeroshell is jettisoned, and the parachutes are deployed to slow the lander further. The conical ribbon chutes are made of Kevlar and are designed to bring the lander's speed to 60 m/s at an altitude of 1.5 km before being discarded as the retrorockets begin to fire. The retrorockets use a hydrazine/H_2O_2 combination and slow the lander sufficiently to provide a soft landing.

Once on the ground, the lander collects the contingency samples and loads them onto the Mars Ascent Vehicle (MAV) prior to releasing the rovers. The rovers are then deployed to collect their samples. The landing site is at Candor Mensa, a proposed landing

site for a manned mission, and has a number of geologically interesting features within range of the land rover.

The Aereons' primary mission is to collect information about the Martian surface as they attempt to circumnavigate the planet. The principal means of doing this is by using the instruments onboard to conduct in-situ analysis. Additionally, the Aereons will collect a few regolith and atmospheric samples along the way. The Aereons function using the Aereon principle developed by Dr. Solomon Andrews in 1862; it holds that certain orientations of an ellipsoid balloon generate thrust as the vehicle ascends or descends. Using this thrust, the Aereon can pilot its way to a specific location with some accuracy. The Aereon is filled with hydrogen gas which is stored in tanks on the lander until the Aereons are deployed. Additionally, there are ballast balloons which can be filled with Martian air as needed to cause the Aereon to ascend or descend. Once an Aereon has collected its samples (totalling no more than 7 kg per vehicle), it will attempt to return to the lander. Since the accuracy of the Aereons' navigation may be insufficient to bring them within range of the land rover, each is equipped with a small sample return rocket which has a range of approximately 200 km and is capable of carrying all of the Aereon's collected samples. These rockets are equipped with radio beacons, so that they can be located by the land rover.

The land rover is a large, three-bodied, six-wheeled vehicle with a range of at least 200 km. It is equipped with the Sample Acquisition Robotic System (SARS) -- a set of tools and scientific instruments which permit the rover to be very selective when examining a candidate sample. The SARS is also equipped with two robotic arms for acquiring the samples. A six degree-of-freedom (DOF) acquisition arm will perform jobs requiring high strength, while a seven DOF manipulator arm will perform those jobs that require more precision. The rover will use the SARS to collect almost 60 kg of samples, including regolith, core samples, boulder chips, pebbles, and rock fragments. As the samples are collected, the rover makes periodic stops at the lander to have its samples loaded onto the

MAV. This procedure will prevent all the samples from being lost in the case of a mission-ending accident for the rover. The rover also supports the Aereons by moving to retrieve samples from them or their sample return rockets, in the event that they are unable to return precisely to the lander.

This mission was also costed using the Advanced Space Systems Costing Model [Ref 2]. Each mission element was costed separately, and the resulting mission costs are shown in Table 3.

Table 3: Mission B Costs (in millions of U.S. dollars)

Launch Vehicles (4 Titan IV's)	1000
Planetary Transfer Vehicle	1200
Communications Satellite	367
Lander and MAV	2936
Land Rover	905
Aereons (2)	1266
TOTAL MISSION COST	7674

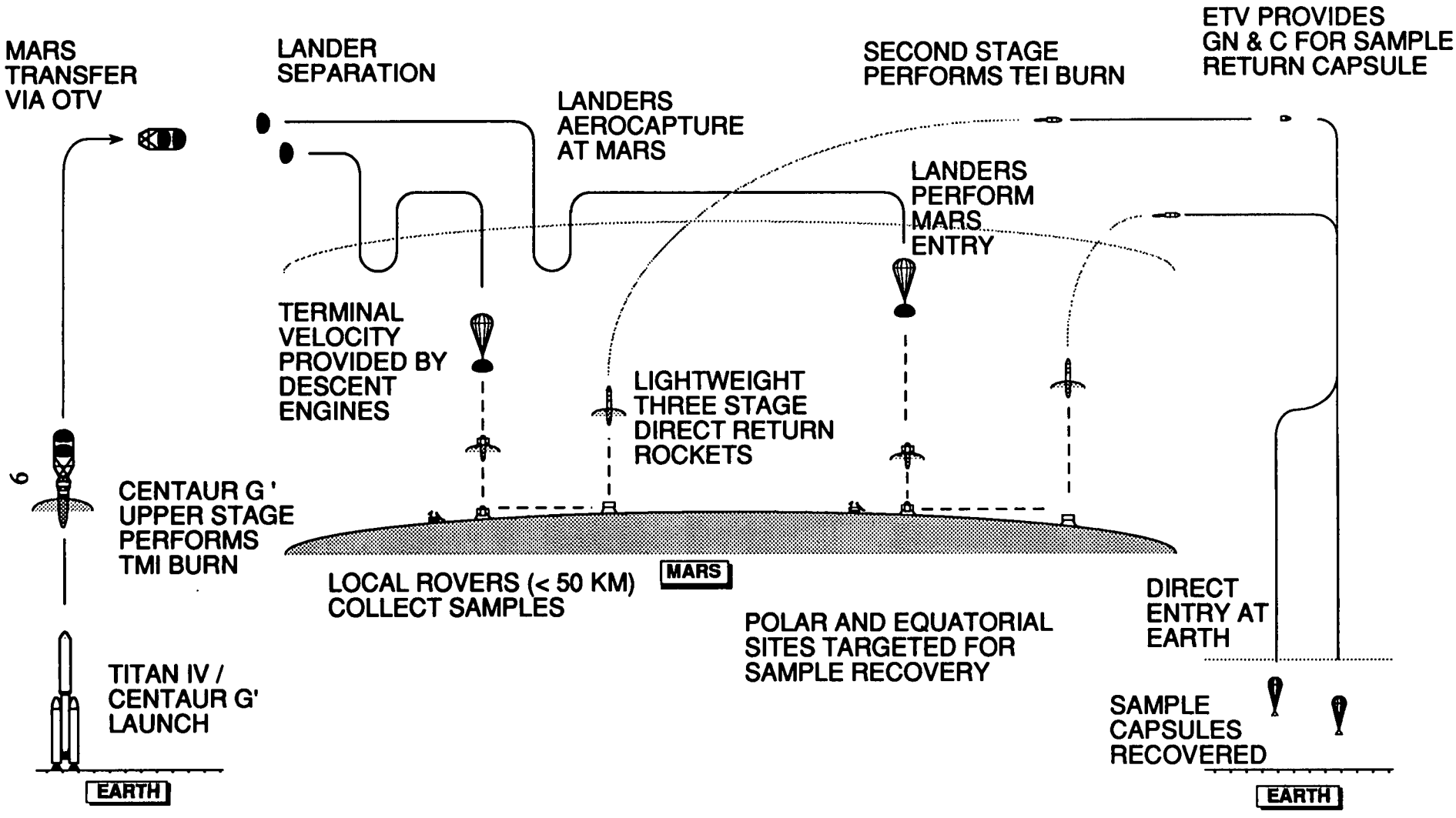

Figure 1: Mission A Scenario

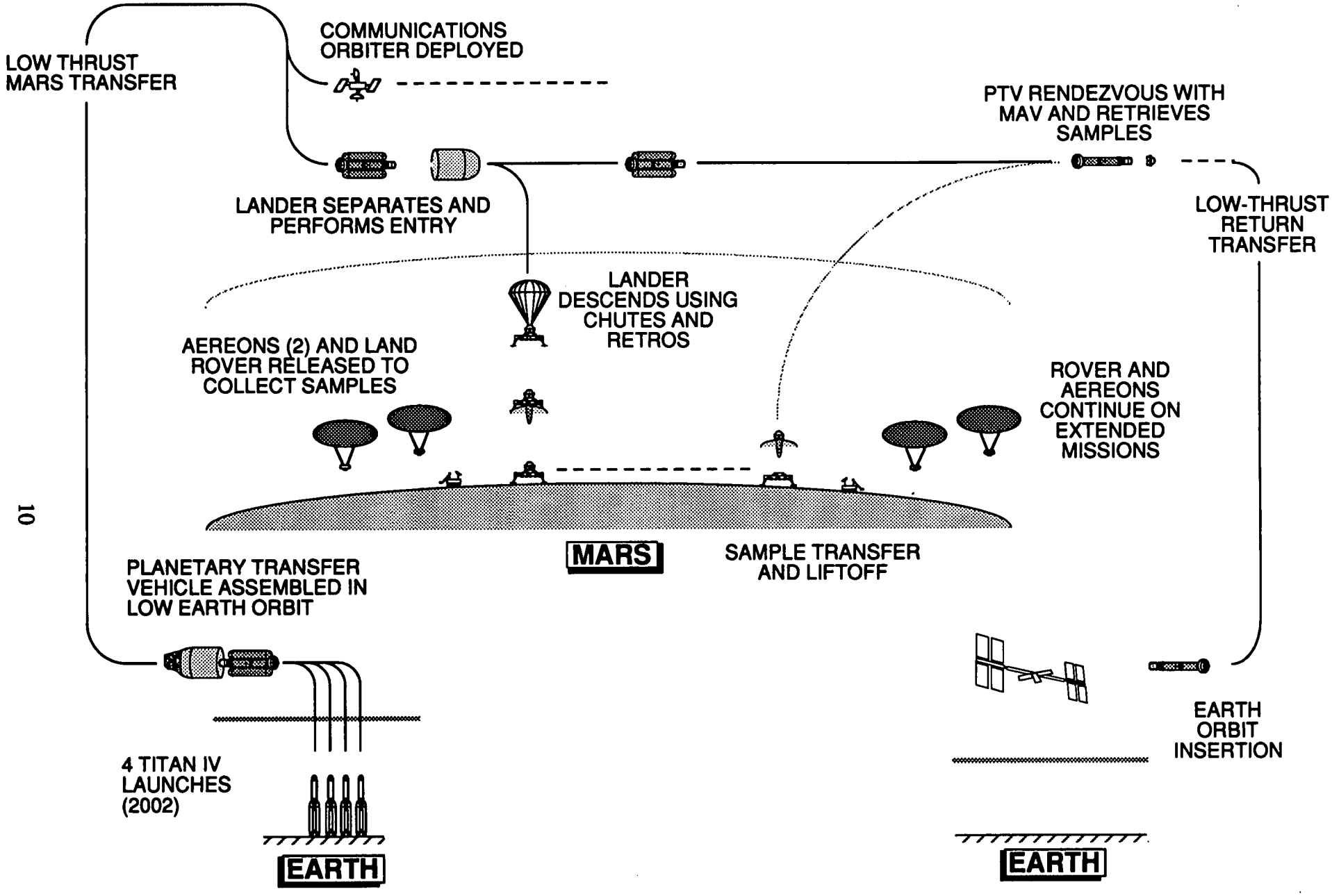

Figure 2: Mission B Scenario

REFERENCES

1. Carr, M. et al. Mars Rover Sample Return: Science Objectives Document. JPL Document No. D-6247. February 1, 1989.

2. Cyr, Kelly. "Cost Estimating Methods for Advanced Space Systems." SAWE Paper No. 1856, Index Category No. 29. July 29, 1988

MARS SAMPLE RETURN MISSION

TWO ALTERNATE SCENARIOS

PART I

A LOW COST, LOW MASS ALTERNATIVE

Chapter 1:

Launch, Transfer, and Return Phases

of a

Low Mass,
Multiple Lander,
Mars Sample Return Mission

(Mission Proposal A)

A final design report for Aerospace 401B

Group Members

Christopher Gazze
Andrew Greenjack
Scott Hirsch
Koch Ky
Tom Martin
Doug Schwer

The Pennsylvania State University

Abstract

This report contains the design of the launch, transfer, and return phases of a low mass, multiple-lander Mars sample return mission. The mission plan involves launching a package of two identical lander vehicles on a single Titan IV, landing them at different locations on the surface of Mars (one polar), collecting 5-6 kg of rock, soil, core, ice, and atmospheric samples with a roving vehicle, and returning the specimens safely and intact to Earth.

Analysis has determined that a Titan IV launch vehicle, with a Centaur G Prime upper stage, will be capable of boosting the 3500 kg lander package and Orbital Transfer Vehicle (OTV) and sending them on their way to Mars without difficulty. In this phase, a unique design will reduce mass by using shared lander and OTV subsystems. During the transfer, the OTV will provide the lander package with communication, guidance, and three-axis stabilization, using lander power, computers, and retrorockets in addition to its own systems. Upon arrival at Mars, it will split in two, enabling the landers to aerocapture into separate orbits.

Sample return will be accomplished by the Direct Return Rocket (DRR). The DRR is a 200 kg, four-stage system capable of returning 6 kg of sample material directly from the surface of Mars to an ocean splashdown on Earth. The rocket uses two solid, BeH_2-fueled booster stages to lift a 15 kg Earth Transfer Vehicle (ETV) and 17 kg (loaded) payload capsule into orbit and initiate transfer to Earth. During the trip, the ETV, which uses propulsion and computer tracking systems developed for the SDI "brilliant pebbles" program, provides guidance for the payload capsule, leaving it on the perfect trajectory for a direct reentry. During this last phase, the payload/reentry capsule takes advantage of its small size and mass to reenter safely at a speed of over 12,000 km/s, parachuting the samples to an ocean splashdown for easy recovery. Throughout the mission design, low mass and simplicity serve as the guiding philosophies.

Table of Contents

Acknowledgements

The members of Group Gazze would like to thank the following for their invaluable help in bringing this design effort to a completion. First, and most importantly, we would like to thank our 401B instructors, Dr. Robert Melton, Dr. Roger Thompson, Jay Burton, and Eric Bell, for the many hours of help and assistance given both inside and outside of the classroom. Secondly, we would like to thank design groups DiPippa and Matulevich for their assistance and cooperation. Additionally, we thank the many other faculty of the Aerospace Engineering Department at Penn State who have given their time to lend advice and expertise to this project, including Dr. Cengiz Camci and Dr. Mark Maughmer. We would also like to extend special thanks to Amy Meyers for all the last minute copying and slide production when the group was running late. Also, appreciation is extended to Mr. Terri Galati and Lt. Coffee at the Air Force Astronautics Laboratory for their helpful suggestions on the DRR booster design. Finally, we would like to thank USRA and NASA for the chance to participate in this program.

List of Figures

Page

List of Tables

Nomenclature

Symbol	Description
ACS	Attitude Control System for OTV
AP	Ammonium Perchlorate
ASAS	Advanced Solid Axial Stage
BC	Ballistic Coefficient
DRR	Direct Return Rocket
ETV	Earth Transfer Vehicle
HTPB	Hydroxally Terminated Polybutadiene
Isp	Specific Impulse
MMH-NTO	Monomethyl hydrazine - Nitrogen tetroxide
MPO	Mars Parking Orbit
OTV	Orbital Transfer Vehicle
Pk	Temperature Sensitivity of Propellant
RTG	Radioisotope Thermoelectric Generator
SDI	Strategic Defense Initiative
T-1000	Carbon-Carbon Composite Fiber
Wp	Weight of Parachute

1.0 Introduction

A low mass, multiple-lander, sample return mission is one alternative being developed for returning planetary samples from Mars. The mission plan involves launching a package of two identical lander vehicles on a single Titan IV; landing them at different locations on the surface of Mars (one polar); collecting 5-6 kg of rock, soil, core, ice, and atmospheric samples with a roving vehicle; and returning the specimens safely and intact to Earth.

This report details the launch, transfer, and return portions of this mission. It begins with a discussion of the Titan IV launch and the orbital trajectory selected for the trip to Mars. Following this is a description of the Orbital Transfer Vehicle, or OTV, designed to provide guidance and control, as well as support for the landers, during the launch and transfer phases of the mission. In the final section, design of the sample return system, the Direct Return Rocket (DRR), is given considerable treatment.

It is believed that these systems, when coupled with a suitable lander and effective rover currently being designed, will accomplish the mission at hand with simplicity, efficiency, reliability, and at low cost.

2.0 Launch and Orbital Transfer

The baseline launch vehicle for the mission is a Titan IV/Centaur G Prime with upgraded Hercules solid rocket boosters, as this vehicle is capable of supporting the mission requirement for a single Earth launch (Refer to Tables 2-1 through 2-3 for launch vehicle specifications). The payload is supported by an adapter from the Centaur's 22-point interface ring. The Orbital Transfer Vehicle's (OTV) octagonal support structure is attached to this interface by an octagonal support ring connected at eight points.

Table 2-1. Launch Vehicle Parameters

Launch Vehicle:	Titan IV/Centaur G Prime Upper Stage
Modification:	Hercules Solid Rocket Boosters
Vehicle Contractor:	Martin Marietta

Table 2-2. Engine Specifications

Stage Number	Engines	Propellants	Thrust
0	UA 1207	Solid	319,400,000 lb-sec
1	2 Aerojet LR-87 AJ11	N2O4/N2H4-UDMH	546,000 lb
2	1 Aerojet LR19-AJ11	N2O4/N2H4-UDMH	104,000 lb
Centaur G'	2 P&W RL 10A-3-A3	LOX/LH2	33,000 lb

Table 2-3. Payload Specifications

Maximum Payload Diameter	16.7 ft
Payload Fairing Length	29.3 ft
Total Centaur Cargo Element Mass	24,690 kg
Centaur Adapter Mass	120.5 kg

2.1 Earth Launch

A launch vehicle study developed preliminary estimates for a single launch scenario using a Titan IV with modified Centaur G Prime upper stage. This study included the launch window analysis that appears in Table 2-4, and allows for a 10-day window with a payload capability (for hyperbolic transfer to Mars) of 5465 kg. Including a mass margin of 10% (equivalent to a launch window of 80 days), the payload capability is 4756 kg.

At launch, the nominal ascent trajectory has a nearly due-east orientation to a 125 km circular parking orbit at 29.5° inclination. This corresponds to a daily one-hour launch window. The Centaur will perform an initial burn to insert itself into a parking orbit, and, after a short coast for orbit and attitude corrections, do a second burn to achieve the desired heliocentric transfer velocity. After the Centaur orients it for cruise flight and does a settling burn, the OTV and its lander package will separate from the Centaur adapter and continue towards Mars. Separation should occur approximately 10 minutes after completion of the second Centaur main engine burn. (Ref 2, pp 2-2,2-3)

Table 2-4. Launch Window Analysis Summary

Mission Class:	Conjunction (minimum energy transfer)
Median Earth Launch Date:	March 20, 2001
Earth Departure Orbit:	125 km circular
Earth Departure Delta-V:	3574 m/s
Earth/Mars Flight Time:	200 days
Mars Arrival Velocity:	3270 m/s
Mars Encounter Method:	Aerocapture into MPO 250 km x 33,500 km
Mars Stay Time:	551 days
Mars Departure Delta-V:	2733 m/s
Mars/Earth Flight Time:	200 days
Round Trip Time:	951 days

The Earth-Mars trajectory will be a Hohmann-like, conjunction class, heliocentric transfer. Cruise duration is nominally 200 days +/- 15 days depending upon the launch date (increasing for an earlier launch and decreasing for a later launch). During this phase of the mission, the OTV will orient itself using its sun and star reference sensors, maintaining three-axis stability with momentum wheels and attitude and control system (ACS) thrusters. The delta-v allocated for such attitude and control maneuvers is 50 m/sec.

Several trajectory correction maneuvers will be necessary to fix injection errors and accumulated drifts due to solar pressure, attitude correction pulses, and execution errors in the above maneuvers. These corrections will be executed on three separate occasions, the first immediately following Centaur separation, the second at the midpoint of the cruise flight, and the third just prior to lander separation. A total Δv of 50 m/sec has been assumed for these corrections. These maneuvers will be executed by the aft lander's MMH/NTO retrorockets in conjunction with the OTV-ACS.

Upon arrival at the edge of Mars' gravitational field, the landers will be separated from the OTV superstructure. This will begin by initially releasing the foreword lander at its attachment points. After the first lander clears the OTV, the second will be separated from the remaining superstructure in a similar manner. After assuming independent attitude control, each will fire their main engine and insert into the desired trajectory for aerocapture.

Each lander will capture into a 250 km x 33,500 km parking orbit, with one lander in a nominal 80 degree, near polar orbit and the other at a 35 degree inclination. The landers will be captured out of their hyperbolic trajectories and remain in the park orbit for a period of no less than 20 days. After this, a deorbit burn from the lander engines will initiate the final descent to the planet surface.

2.2 The Orbital Transfer Vehicle

The design of the Orbital Transfer Vehicle, or OTV, was characterized by requirements for low mass and high reliability. Its mission will be to support the two Martian lander craft throughout launch and transfer, while remaining within the payload capacity of a Titan IV/Centaur G Prime launch vehicle. Its responsibilities included structural support during launch, thermal control , power regulation, communications, guidance, navigation, and attitude control. The OTV, which will not have any purely scientific instrumentation, will be jettisoned following lander separation. The OTV with landers attached is depicted in Figure 2-1.

2.2.1 OTV Structure

OTV structure was primarily designed to support the landers during launch. Three separate truss structures were created to accomplish this task: one to support the upper lander, one to connect the OTV and landers, and an adaptor to connect the Centaur and OTV. Because accurate data could not be obtained on Titan IV launch loads, design analyses were performed using data for an Ariane rocket instead. As the Ariane is a much smaller and quicker booster, these load models should represent, in the very least, a worst case approximation; however, an additional safety factor of 1.5 was still included. The Ariane experiences a maximum axial loading during launch 7.9 g (compressive), and a maximum transverse loading of 1 g.

Because of the large (4.572 m) major axis of the landers' elliptical aeroshells, they will have to be stacked vertically in order to fit within the Titan IV's payload faring. Since the lower lander can sit directly on top of the Centaur's adapter ring, only a truss supporting the top lander was required for launch. An octagonal shape was chosen for this structure, allowing the aeroshell and lander design lengths to increase along the minor-axis (in case future design modifications require more space), without adding additional mass to the OTV.

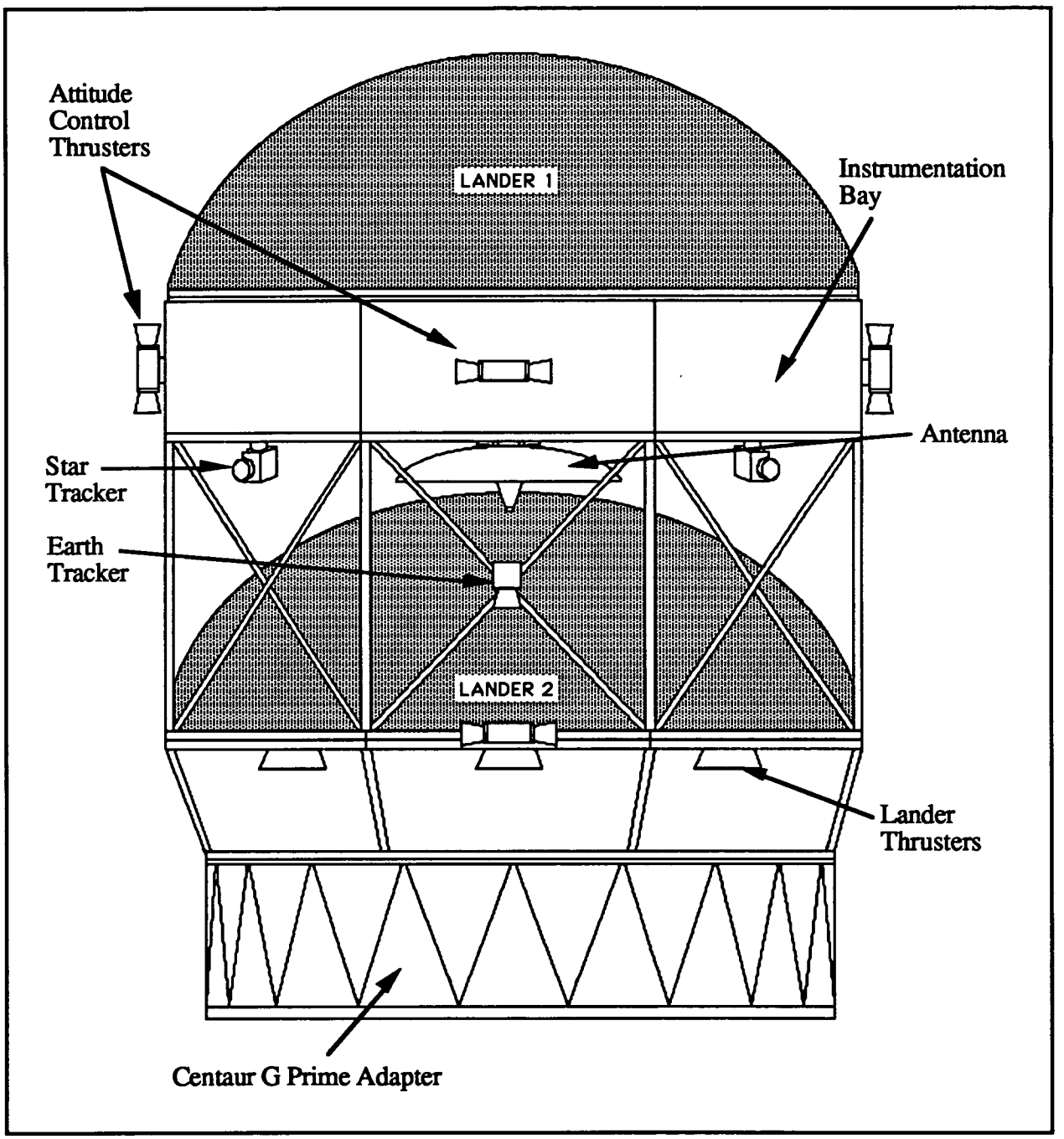

Figure 2-1. Orbital Transfer Vehicle with Landers

Cross beams were placed on the structure in order to carry any non-axial loading during launch. As these beams will experience highly compressive loads, co-circular cross sections were chosen for their high transverse moments of inertia and consequently high values of critical buckling stress. The landers and OTV will be secured together with an interface ring aligned and connected to the aeroshell with explosive bolts. There will also be four connections between the landers and support beams running beneath them. These beams are required to support the transverse loading of the landers, and to distribute the lander weight to other truss elements. I-beams were chosen for this application due to their ability to carry flexural loads well. Mass estimates for these beams were generated by a simplified analysis, and are presented in Table 2-5.

Table 2-5. Truss Structure Masses (SI Units)

Beam Length	Element Type[1]	Maximum Moment	Stress	Mass of Beam	Number of Beams
1.358	2	2937.5	1.89e+08	2.7165	2
2.316	1	8543.8	4.02e+08	5.7196	4
1.92	2	5871.9	3.79e+08	3.8407	13

[1]Type 1: Cross sectional area 882 mm^2, Moment of Inertia I_{xx} 744,420.3 mm^4
Type 2: Cross sectional area 714.42 mm^2, Moment of Inertia I_{xx} 488,414.1 mm^4

Finally, since the Centaur's own, 22 point adapter ring was smaller than the octagonal truss structure of the OTV, a second adaptor was designed so the two could be joined. A truss similar to the ones described above was designed; however, no advanced analysis was done.

2.2.2 Guidance, Navigation, and Attitude Control

The sensors used in the OTV guidance, navigation, and control subsystem are as follows: one digital sun-sensor, one analog sun-sensor, one Mars sensor, and two star trackers, as shown in Figure 2-1. One sun sensor is located toward the aft end of the OTV

and the other is at forward end to provide backup. The star trackers are situated to reference Polaris during the entire transfer. The Mars sensor is also situated at the forward end to provide Mars encounter navigation, while the Earth sensors are located towards the aft end of the second lander and for backup sensing. A breakdown of power requirements, mass, and accuracy of the different sensors is shown in Table 2-6.

Table 2-6. Attitude Sensing Instrument Statistics

Attitude Sensor	Accuracy	Mass	Power
2 Sun Sensors	0.005° to 3°	2 kg each	2 W each
2 Star Trackers	0.0028° to 0.0166°	5 kg each	10 W each
2 Horizon Sensors	0.1° to 1.0°	4 kg each	10 W each
TOTAL	N/A	22 kg	44 W

Estimates from Wertz and Wiley.
Averages are used for power and mass estimates.

The attitude control system (ACS) consists of twelve, 11 N, MMH-NTO thrusters and three momentum wheels. The thrusters provide coarse adjustments and momentum wheel desaturation. The three momentum wheels provide fine adjustment so exact attitude can be maintained. These momentum wheels are aligned along the three principal axes of the OTV. Table 2-7 shows some key features of the ACS.

2.2.3 Power and Communications Subsystems

Both the power and communications subsystems for the OTV are integrated with the lander subsystem. The communication subsystem for the OTV will provide the means of transmitting and receiving data. The lander will provide encoding and modulation for the data transmitted and the decoding and demodulation for received data. The frequency used for communication is in the S-band, as allocated by the General World Administrative Radio Conference. These units will be linked with an antenna on the OTV by coaxial

cables. The link will be interrupted by a waveguide cutter. The waveguide cutter's purpose is to disconnect the communication link between the antenna and the OTV at the time of lander separation. The waveguide cutter will also disconnect any power cables that the antenna will need.

The antenna used for the OTV is a 1.5 m diameter parabolic dish. Table 2-8 shows the antenna gain for frequencies in the S-band. The frequencies shown are the frequencies allocated for deep-space communications. The 2.115 GHz frequency is allocated for Earth-to-space communications and the 2.295 GHz frequency is allocated for space-to-Earth communications. An efficiency factor of 55% was used to calculate the results.

Table 2-7. ACS Specifications

Coarse Adjustment	
Type of Propellant	MMH-NTO Bipropellant
Isp	300 s
Vel. Change Required	100 m/s
Propellant Amount	140 kg
Dry Mass	30 kg
Power Requirements	10 W
Fine Adjustment	
Type	Momentum Wheel
Isp	N/A
Vel. Change Required	Negligible
Amount of Fuel	0 kg
Dry Mass	30 kg
Power Requirements	100 W
TOTAL MASS:	200 kg

Mass estimates obtained from Wertz and Wiley.

Table 2-8. Antenna Gain for the OTV

Frequency	Antenna Gain
2.115 GHz	26.248 dB
2.195 GHz	26.571 dB

The antenna is mounted on a retractable beam between the instrumentation bay and Lander 2. The beam will have motors powered by the lander's RTG that will enable the antenna to be extended out from the OTV. The retractable beam will also rotate, allowing the antenna to point towards Earth. This rotation is driven by a motor located in the OTV. The antenna is mounted on the end of the beam with a hinge. This enables the antenna to move within a plane. The movement is controlled by a motor located at the mount. The retractable beam is made of aluminum and is hollow, allowing the cables connecting the motor and the antenna to the lander to run through the beam, thus keeping the wires from becoming entangled during antenna positioning.

The OTV subsystems will draw power from the RTG's within the lander. Since the power available from the RTG's is approximately 500 W, additional power sources are not needed. Power systems provided by the OTV will then fall into two categories: the power cutter will provide a clean cut of the power between the RTG's and the OTV, and a power regulator will provide power distribution among the instrumentation. The power control subsystem will also provide controls in case power failure occurs.

The central feature of the power control subsystem is a dual bus design, each bus obtaining power from one lander RTG. For each bus a power regulator is provided to control the power output to different instruments. Each bus will be unregulated, requiring individual regulation devices at each instrument. This decision is based on the simplicity of the electrical system for the OTV. A power break down is provided in Table 2-9.

Table 2-9. Power Breakdown on OTV

Communications	100 W
Thermal Control	40 W
Attitude Sensing	44 W
Attitude Control	100 W
TOTAL POWER REQUIREMENTS	284 W

The power requirements in Table 2-9 represent the worst possible power usage at any particular time. For approximately half of the trip, the thermal control system will not require any power at all since the equilibrium temperature will be within instrument operational temperature range. The other subsystems, however, will require almost constant power usage.

2.2.4 Thermal Control Subsystem

Before a formal analysis of the thermal control subsystem was accomplished, several simplifying assumptions were made. First, it was assumed that the majority of heat would be radiation from the sun. Other major sources of heat, such as the power supply subsystem, will be located on the landers and controlled by the lander's own subsystems. Another simplifying assumption is that the instrumentation subsystem will be significantly isolated from the landers so that only the instrumentation area will be considered for thermal control. Allowable temperature ranges are presented in Table 2-10. Since heating is much simpler than refrigeration, the equilibrium temperature was designed to be underneath the highest operational temperature for the majority of instruments.

With these operational limits in mind, the equilibrium temperature was calculated with a mixed aluminized kapton and black paint surface over the panelling. Near Earth, this equilibrium temperature is 31.62° C. At the end of the trip, this equilibrium temperature sinks to -39.3° C. The mixture was chosen as opposed to other surface coatings because of the equilibrium heat in near Earth space. Other coatings studied had equilibrium temperatures above the operational temperatures of several instruments, requiring active cooling systems for the instruments.

Table 2-10. Instrument Temperature Range

Equipment Type	Non-operating (°C)	Operating Range (°C)
Communications		
Receiver	-30/55	10/45
Antenna	-170/90	-170/90
Electric Power		
Solar Array Wing	-160/80	-160/80
Shunt Assembly	-45/65	-45/65
Attitude Assembly		
Earth/Sun/Star Sensor	-30/55	-30/50
Angular Rate Assembly	-30/55	1/55
Propulsion		
Propellant Tank	10/50	10/50
Structure		
Pyrotechnic Mechanism	-170/55	-115/55
Separation Clamp	-40/40	-15/40

Adapted from Table 5.1, pg 266. Agrawal. *Design of Geosynchronous Spacecraft.* Prentice-Hall, Englewood Cliffs, NJ: 1986.

Since the equilibrium temperatures are below operational levels for many of the instruments, heating elements will be required for proper thermal control. Resistive heating elements are used to heat the instruments to within operational levels. The heaters are a relatively simple on/off closed-loop control type. Single layer thermal insulation will be provided on the MMH-NTO tanks in order to keep the tanks warm for longer periods of time between heating. Similar insulation will be provided for the other instrumentation; in particular, the Earth/Sun and Star Sensors.

3.0 The Direct Return Rocket

The primary function of any return vehicle designed for this mission is to transport the 5-6 kg of Martian soil, ice, core, and atmospheric samples safely back to Earth. When one considers the possibilities, there are a multitude of different ways of accomplishing this task; however, most of these options only serve to complicate system design and operation, or add unneeded mass.

For these reasons, the Direct Return Rocket (DRR) was designed to achieve this basic mission of sample return in the simplest manner possible. Thus, options such as orbital rendezvous, propulsive capture into Earth orbit, and shuttle retrieval were abandoned in favor of the simplicity of direct transfer and entry. Also, subsystems which involved simple or passive designs with few working parts were chosen over more complicated options whenever possible. The simplicity in design and operation which resulted translates directly into lower development and production costs, as well as greatly increased chances of mission success. In essence, the DRR is the "no frills" approach for returning samples to Earth.

In the sections which follow, the design and operation of the Direct Return Rocket will be described in considerable detail. In every instance, an attempt will be made to relate design choices to the basic guidelines of simplicity and low mass outlined above.

3.1 General Specifications

The DRR is a four stage system, capable of transporting up to 6 kg of sample material directly from the surface of Mars to an ocean splashdown on Earth. Weighing just under 200 kg, it is 2.3 m in length, 0.4 m in diameter, and consists of two solid booster stages, a transfer vehicle, and a payload/reentry capsule. These dimensions, unfortunately, make the DRR quite oblong, and present unique problems for integration with the lander vehicle. Complete specifications for the DRR are given in Figure 3-1 and Table 3-1.

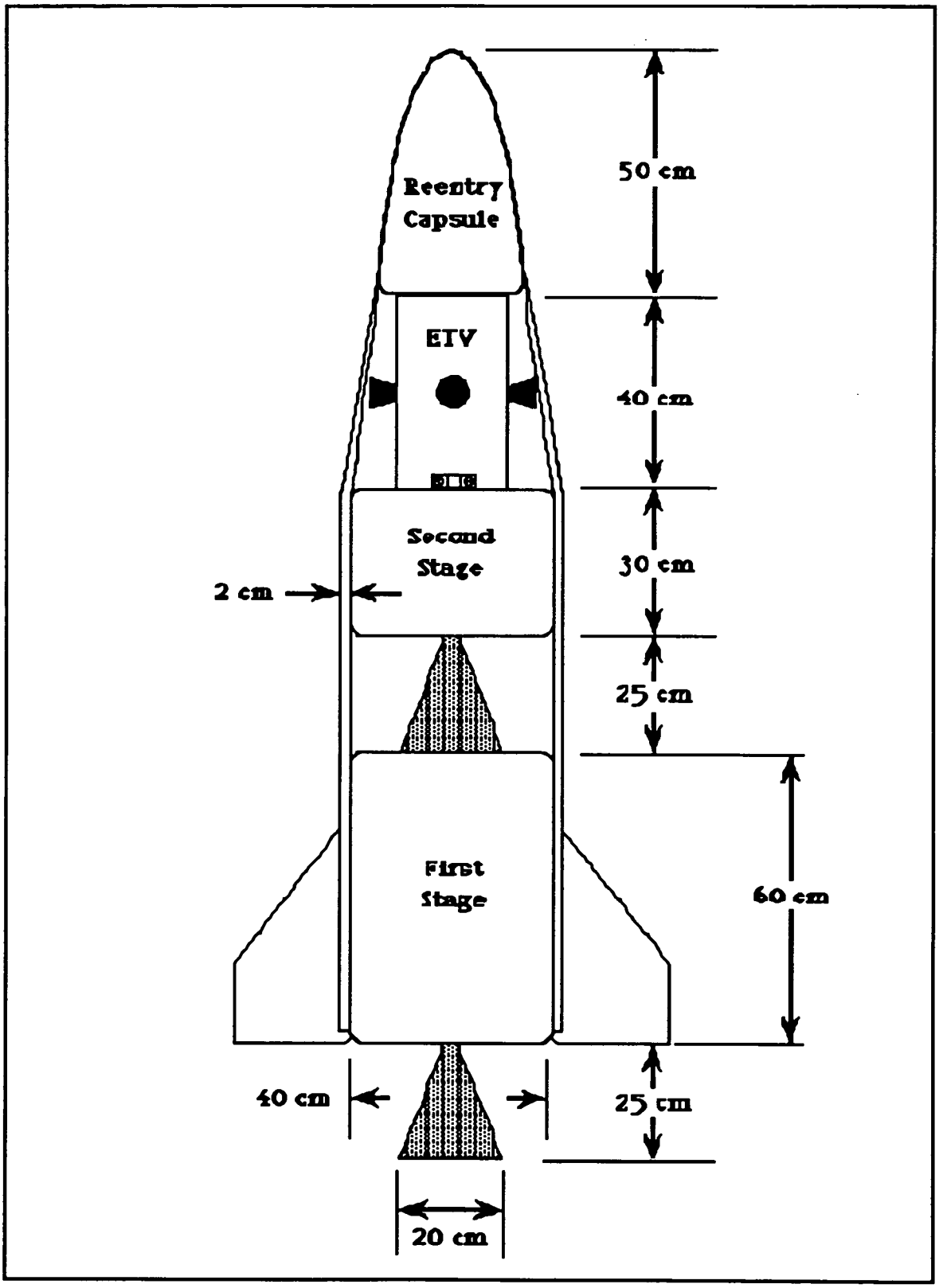

Figure 3-1. Direct Return Rocket Specifications

Table 3-1. DRR Stage Masses

Payload/Reentry Capsule	
Dry Mass	11.0 kg
Samples	6.0 kg
Earth Transfer Vehicle (ETV)	
Dry Mass	5.0 kg
MMH and NTO Fuel	10.0 kg
Booster Stages	
Second Stage	56.5 kg
First Stage	111.5 kg
Total	200.0 kg

The two solid booster stages, which represent the majority of the DRR mass, lift the 15 kg transfer unit and the 17 kg payload capsule into orbit, and send them on their way to Earth. Both stages use a similar design consisting of a metalized HTPB/AP propellant in a filament-wound, carbon-carbon case. The use of beryllium hydride (BeH_2) as a fuel provides an initially rapid-burning boost (i.e., high thrust), as well as a high I_{sp} for optimum performance at altitude. The first stage is responsible for lifting the rocket to a 150 km apoapsis, and the second provides the necessary delta-v to initiate the orbital transfer.

Following second stage burnout, the Earth Transfer Vehicle (ETV) provides active guidance and control throughout the trip back to Earth, separating only after aligning the payload/reentry capsule on the its final approach trajectory. Using mini-thruster and computer guidance technologies developed for the SDI "Brilliant Pebbles" program, the ETV accomplishes this mission with a dry mass of only 5 kg. Fully loaded with 10 kg of MMH/NTO fuel, it is capable of performing over 1.2 km/s of propulsive attitude, control, and trajectory correction maneuvers during the return trip. This large potential, coupled

with its state of the art computer tracking and guidance technology, enables the ETV to place the payload capsule onto its final reentry trajectory with pinpoint accuracy.

The payload/reentry capsule, which is the final stage of the DRR, protects the samples during the entire transfer and reentry procedures before parachuting them to an ocean splashdown for easy recovery. Fully loaded, the capsule weighs only 17 kg, yet subsystems include heat shield, insulation, parachute, flotation balloon, instrumentation, and homing beacon. Additionally, a liquid nitrogen bath provides refrigeration for the samples throughout the transfer, keeping them at a temperature below 100 K, even during reentry.

3.2 Booster Stages

In any booster system, the ratio of structural mass to payload mass is important. In the case of the Direct Return Rocket, payload mass is so small that stage dry mass becomes a critical influence on the rocket's overall delivery efficiency. Such a situation favors the choice of solid rockets over liquid systems, because solids possess considerably lower empty weights. Since solid systems also tend to be simpler to design, produce, and operate, they were the obvious choice for use in the DRR.

3.2.1 Propellant Development

The propellant designed for the DRR is a fairly standard HTPB/AP formulation with one exception--the use of BeH_2 as a fuel. The decision to use BeH_2 was based on a desire to compensate for the loss in performance normally associated with the selection of a solid propulsion system over a liquid one. It is estimated that a BeH_2 system will *deliver* I_{sp}'s around 375 seconds.[1] While this still cannot match the specific impulse generated by

[1]Oberth (1987, p 1-19) quotes a propellant Isp of 326 seconds for a typical BeH_2 system. Accordingly, vacuum Isp should be on the order of 400 seconds. Assuming an efficiency of about 94%, (typical for metalized systems), we should expect a delivered Isp of 375 seconds. Engineers at th Air Force Astronautics Laboratory working on the ASAS program, which uses solid Be as a fuel, have confirmed the reliability of this estimate.

a cryogenic, liquid hydrogen-liquid oxygen system, it definitely out-performs the storable liquids, especially at larger expansion ratios.

In proposing the use of BeH_2 as a fuel, it is recognized that the toxicity of the combustion products[2] may pose unique problems to its use in the DRR first stage; however, since Mars is widely believed to be devoid of life, and because the amounts of toxic gas would be small for this application, it is hoped that environmental impact studies will permit its use. In the event that this is not the case, the first stage propellant could be replaced with a modified version of an existing aluminized formulation. With an increase in chamber pressure and by shifting more of the propulsive responsibility to the second stage, such a change could be effected with a minimal increase in total rocket mass.

The remainder of the formulation, an HTPB/AP system, was chosen to provide the greatest flexibility and ease of development. Energetic systems were bypassed in favor of the more proven and reliable HTPB binders, while nitramines were similarly avoided as detonation-sensitive propellants would have complicated the mission unnecessarily. Additionally, the use of ammonium perchlorate (AP) as an oxidizer allows the maximum burn rate to be tailored and propellant mechanical properties to be improved through multi-modal distribution and particle size variation.

The largest technical challenge in developing a suitable BeH_2 propellant will probably arise in meeting processing and mechanical property requirements. Surface conditions on Mars will require a propellant with exceptional low temperature mechanical properties to avoid cracking of the grain during the landing and ignition processes. Of existing solid propellant systems, only tactical missiles, which are typically rated from 70° C down to - 60° C, provide examples of design for low temperature. As temperatures on

---

[2] In general, the use of beryllium is restricted to exo-atmospheric applications because of the toxicity of its oxide, BeO, which is generated during the combustion process. This fact is debatable, however, and recent studies have indicated that hot fired BeO (at temperatures over 1500 K) may not be toxic.

the Martian surface could well dip below 100 °C, the DRR propellant will obviously represent a considerable extension of present propellant capabilities.

Although this problem is far from insurmountable, it will necessitate a variety of formulation modifications which will all occur at the expense of performance. The most noticeable drawback will be a reduced solids loading, possibly as low as 85%. On the positive side, since propellant burning rate requirements are not particularly stringent (basically, rocket operation will be altered to fit the resulting burn rate rather than operational parameters necessitating the reverse, as usually occurs), extensive freedom will exist to vary AP particle sizes to achieve suitable processing and optimal mechanical properties. The remainder of the need for good mechanical properties will be met by heavy binder plasticization, with such inert ingredients as DOA, and the use of a good bonding agent, like TEPANOL.

3.2.2 Case and Nozzle Design

Since the DRR booster stages turned out to be highly similar, in scale as well as design, to the Advanced Solid Axial Stage[1] (ASAS), many of the design parameters from that program were adopted for these motors. Specifically, the case will be fabricated by filament winding T-1000, a carbon-carbon composite produced by Hercules, onto a sand mandrel. In order to reduce complexity, the case will be wound as one piece. Including the nozzle, the system should have a structural coefficient (dry mass to total mass ratio) of only $\varepsilon = 0.06$, but be capable of withstanding bursting pressures in excess of one million psia (6,900 MPa).

The nozzle will also be fabricated of carbon-carbon, densified to provide additional strength, and screwed into the aft portion of the case. According to ASAS research, rapid flow turning results in considerable nozzle impingement of particulate BeO from the

[1]The ASAS motor is currently being developed (under contract) by the Air Force Astronautics Laboratory (AFAL), Edwards AFB, CA.

exhaust plume. Thus, optimal nozzle configuration tends to be virtually conical, thereby increasing half-angle losses for a given nozzle length. Actual nozzle length was determined by striking a compromise between sufficient expansion ratio, the need to keep half-angle losses under 4% (which corresponds to a maximum nozzle half-angle of 23°), and the desire to keep DRR length as short as possible.

3.2.3 Motor Performance

Table 3-2 shows expected propellant, grain, and operational characteristics of the DRR booster stages. The data in this table represent assumed and predicted values for these quantities at the present time. Ultimately, however, these motor performance parameters will depend upon the final characteristics of propellant and grain design. The calculation of these expected quantities is detailed in Appendix A.

Propellant properties were arrived at by beginning with standard values for a metalized formulation and then estimating the effects of replacing the aluminum with beryllium hydride. The considerable weight and density differences between the two fuels is expected to lower exhaust molecular weight from 30 to around 23, and lower density from about 1.8 to 1.5 gm/cm^3. Also, the more energetic BeH_2 should give rise to higher chamber temperatures and a faster burning rate. It should be noted that the burning rate given in Table 3-2 is for ambient conditions. Depending on the temperature sensitivity of the propellant, π_k, the burn rate on the Martian surface should be considerably lower. A value of around 0.5 in/sec (1.27 cm/sec) was assumed for the calculations in this table.

Table 3-2. Expected Motor Characteristics

Property	Stage 1	Stage 2
Propellant		
Burn Rate, r_b (at 1000 psia and 300 K)	0.7 in/sec	0.7 in/sec
Molecular Weight, M	23	23
Chamber Temperature, T_c	4000 K	4000 K
Propellant Density, ρ_p	1.5 gm/cm^3	1.5 gm/cm^3
Temperature Sensitivity, π_k	.002 in/sec K	.002 in/sec K
Gamma, γ	1.2	1.2
Nozzle		
Throat Area, A^*	9 cm^2	4 cm^2
Expansion Ratio, A_e/A^*	35	78
Half Angle, θ	23°	23°
Mass Flow, m	3.3 - 6.1 kg/s	2.2 kg/s
Operation		
Chamber Pressure	1000-2000 psi	1500 psi
Thrust, T	11.6-23.25 kN	8.02 kN
Thrust to Weight Ratio, T/W	17	-
Specific Impulse, Isp	360 sec	372 sec
Burn Time, t_b	21 sec	24 sec

As stated previously, nozzle design was largely a compromise between conflicting desires to increase area ratio while keeping nozzle length as low as possible. Because length and half-angle limitations combined to essentially fix nozzle exit area, the ability to increase expansion ratio became entirely dependent on the ability to decrease throat area. Furthermore, since throat area is related to other propellant and motor characteristics by

$$\rho_p r_b A_b = C_d p_c A^* \qquad (3\text{-}1)$$

and since propellant design will essentially fix the burn rate, propellant density, and discharge coefficient in this equation, it is burning area and chamber pressure which will ultimately determine the achievable expansion ratio. Thus, it can be seen that motor performance will be largely dependent on the chosen grain design.

In addition to low burning area, this grain design will have to meet several other requirements as well. Most importantly, the grain will have to burn outwards in order to insulate the case from the high combustion temperatures. This means that a conical, a star-shaped, or perhaps a slotted grain design will have to be used. Also, grain configuration should reduce mechanical loadings as much as possible, and provide a neutral or slightly progressive burn.

In Table 3-2, a star shaped grain was used to produce a progressive first stage and neutral second stage design. The resulting nozzles were identical except for the lower throat area on the smaller second stage. The corresponding area ratios were 35 for the first stage and 78 for the second. Since the optimal expansion ratio at the surface is 423 (see Appendix A), grain designs which further decrease throat area in the first stage would obviously be desirable. A similar argument can be made for the second stage, where optimal expansion ratio is essentially infinite.

3.2.4 Trajectory and Stage Optimization

In order to evaluate first stage performance, a computer program was created to "fly" it, taking into account the effects of gravity and drag forces. Again, as with the motor performance predictions on which the program was based, the results are only rough estimates. Even so, depending on launch angle and burn profile, the DRR first stage was found capable of reaching either high apoapses with little orbital velocity, or rather low apoapses with much higher orbital velocities.

Naturally, the latter is the more desirable of the two cases, as it represents the smaller "gravity loss." Figure 3-2, which is based on a patched conic estimate of the total velocity needed for Earth transfer, illustrates this point by showing the rather weak dependence of escape velocity on apoapsis altitude. Thus, an optimum trajectory would carry the DRR to the smallest apoapsis necessary, while converting the remainder of the rocket's energy into velocity. The minimum altitude chosen for this apoapsis was approximately 150 km, in order to ensure that the craft was well out of the Martian atmosphere before firing the second stage.

Figure 3-3 combines the orbital requirements of Figure 3-2 with the results of the first stage performance program to describe acceptable combinations of stage mass ratios yielding escape conditions. The plot indicates that as much of the propulsive responsibility as possible should be shifted to the second stage, while still maintaining the first stage's ability to reach orbit. Mass ratios of 2.1 and 2.5 for the first and second stages respectively were chosen for this design.

To reduce complexity as well as the chances of system failure, the DRR will have no active guidance during its ascent. Instead, it will be launched from an angle and perform a gravity turn. As the DRR trajectory will be ballistic (e.g., including the planet), the second stage will have to be fired as soon as apoapsis is attained. Launch time on the planet will therefore be determined by the need to position the DRR apoapsis in proper alignment for transfer. Finally, although analysis indicates that launch angle is optimized near the horizontal, a minimum launch angle of 30° was established to ensure adequate obstacle clearance following launch.

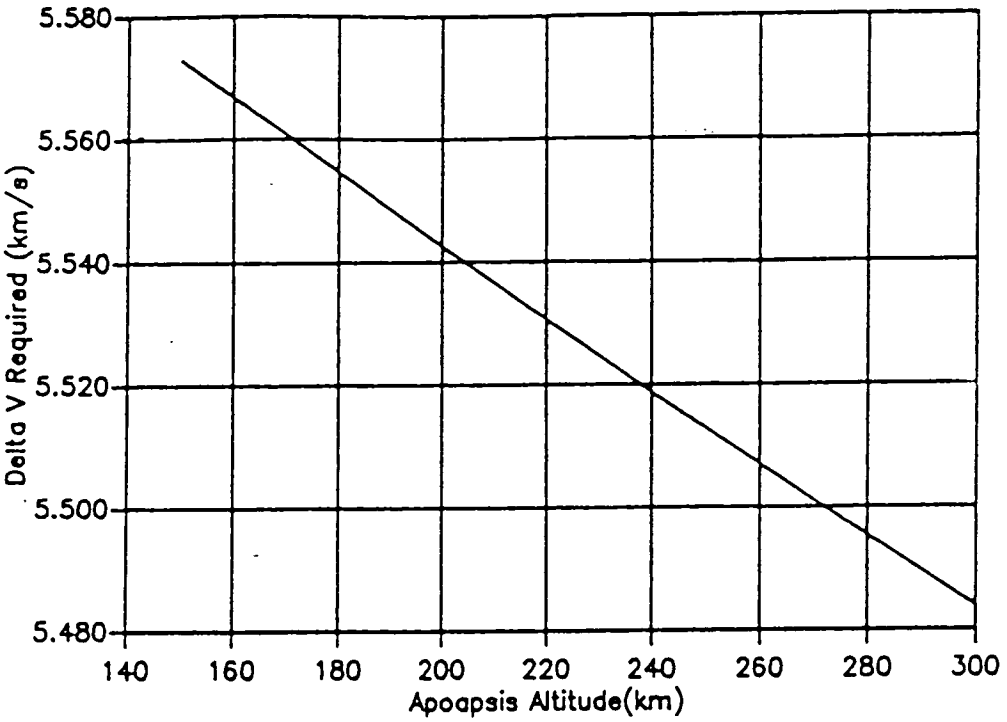

Figure 3-2. Total Δv Requirement for Earth Return as a Function of Apoapsis Altitude

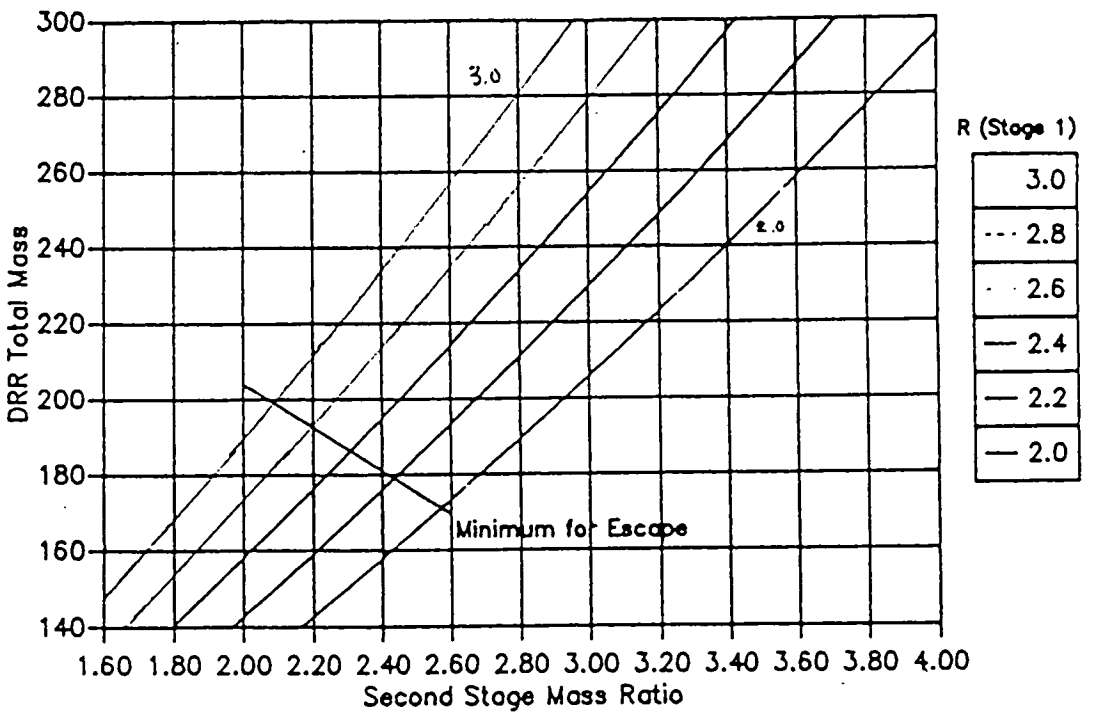

Figure 3-3. DRR Stage Mass Ratios

3.3 Earth Transfer Vehicle

The ETV represents the only really "intelligent" part of the DRR, since the other three stages are essentially "programmed in the factory." Thus, it will be up to the ETV to correct the trajectory errors introduced during the boost and transfer phases, maintain stability, control, and guidance during the transfer back, and provide an accurate reentry trajectory for the capsule section.

To accomplish these tasks, the ETV will have a total of 10 engines capable of generating over 1200 m/s of Δv. Four divert engines, spaced at 90° intervals around the ETV midsection, will provide for lateral movement, while four smaller attitude control engines located on the rear edge of the craft will control vehicle pitch. (See Figure 3-4.) The final two engines, mounted axially, will work together to provide trajectory corrections. The thruster system will be a pressure fed, MMH/NTO design, capable of firing rapid, millisecond bursts to achieve precision attitude and trajectory control.

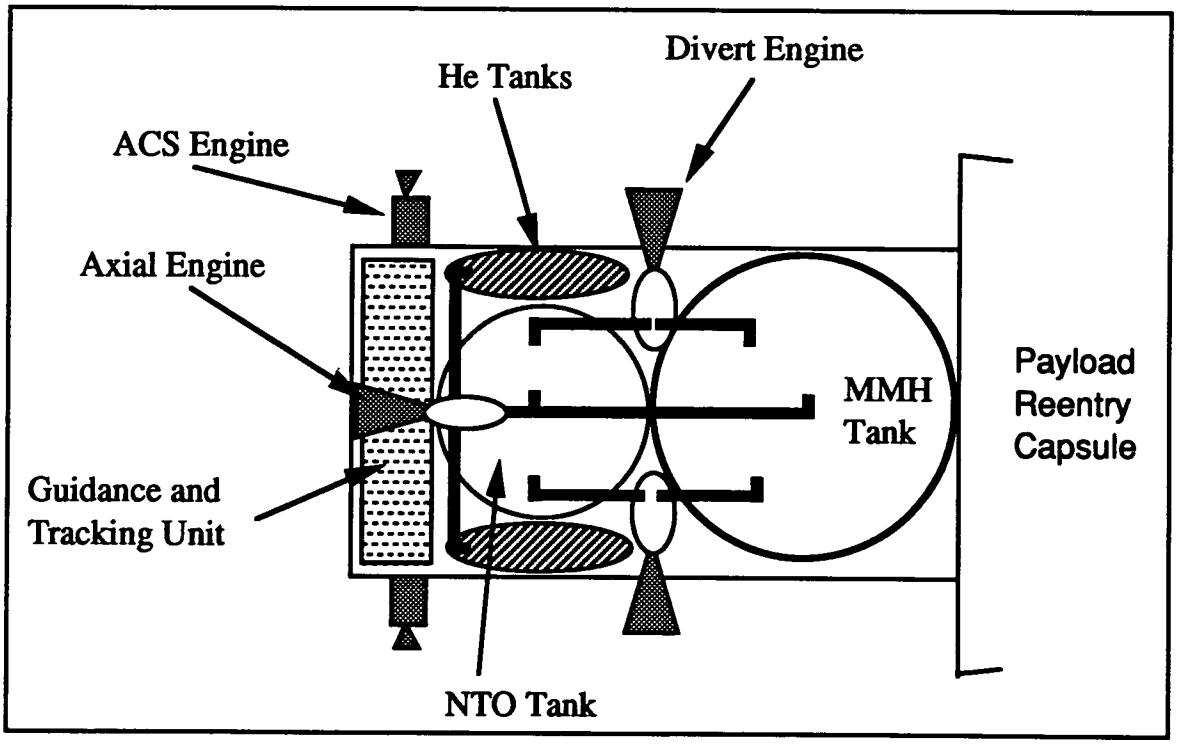

Figure 3-4. ETV Schematic

While the technologies for the ETV exist and have even been demonstrated to a large degree, they will have to be significantly adapted for this mission. Most importantly, the computer guidance systems will have to be largely reprogrammed for tracking planets and stars at great distances, while maintaining constant awareness of position and trajectory. The ETV, due to its position as part of the DRR payload, will be a mass critical system, because increases in its mass requirement will quickly multiply requirements down through the booster stages. In summary, the technical challenges of ETV design will obviously be quite demanding.

3.4 Payload/Reentry Capsule

The Payload/Reentry capsule is the portion of the DRR responsible for keeping the samples safe and intact during the long trip back from Mars. Like the ETV, the capsule is part of the DRR payload section, making its overall mass a critical design parameter. In fact, in order to keep the DRR 's mass under 200 kg, capsule empty mass was limited to only 11 kg. Despite this limitation, the capsule is still required to perform a variety of functions, including protecting, cushioning, and insulating the samples as well as keeping them refrigerated during the entire transfer and reentry procedures. Additionally, the capsule must be a reentry craft, providing a heat shield, parachute, flotation balloon, and homing beacon for safe descent and recovery. All of these systems, as well as 6 kg of soil, rock, and atmospheric samples are contained in a small, almost conical capsule, 28 cm in diameter and 50 cm long. A schematic of the capsule is shown in Figure 3-5, and it is amazing to realize that this figure is actually 40% of the full-scale capsule size. A mass breakdown is shown in Table 3-3.

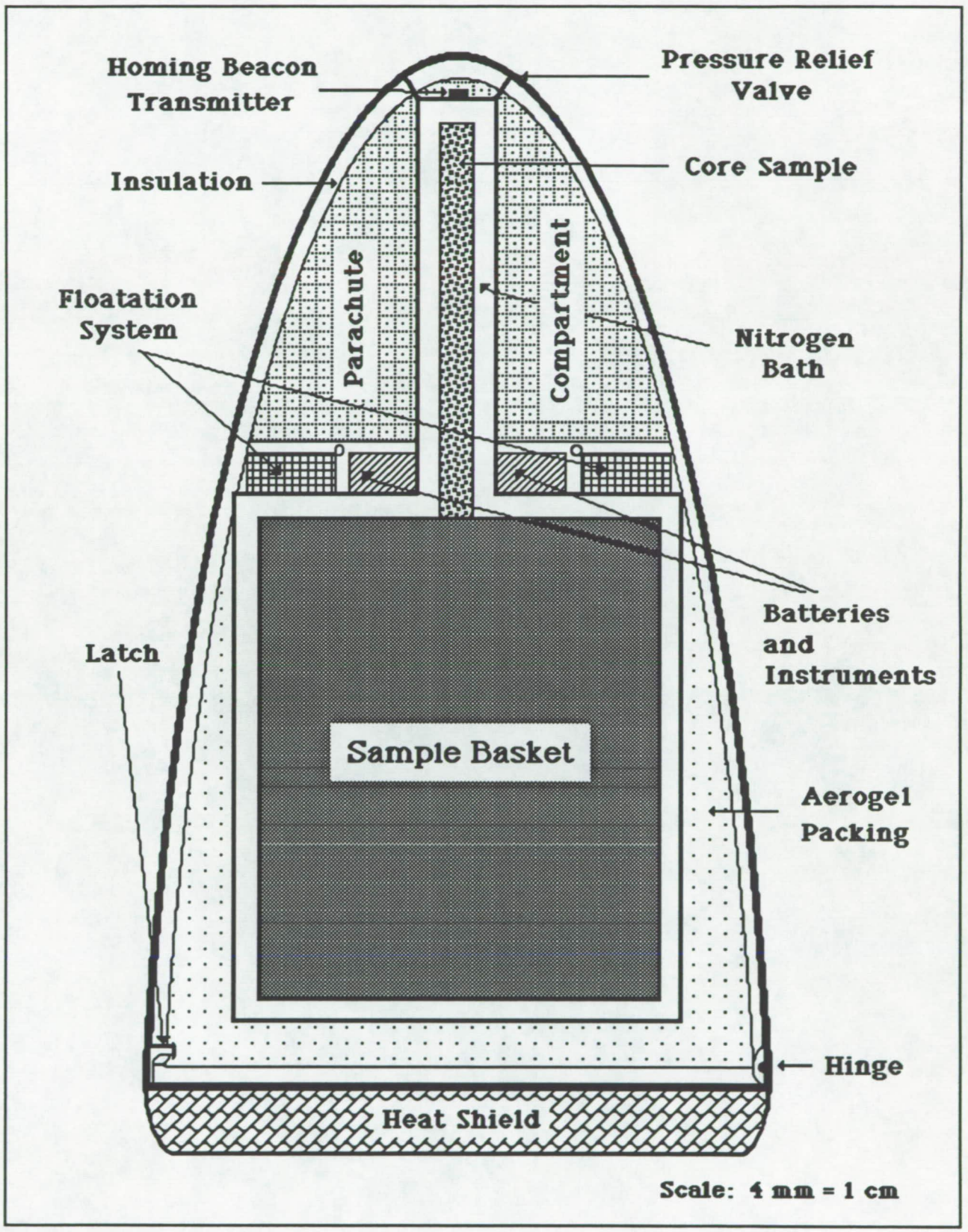

Figure 3-5. The Payload/Reentry Capsule

Table 3-3. Mass Breakdown of Reentry Capsule

Structural Mass	
Outer Carbon-Carbon Shell	1.50 kg
Insulation / Packing	
Inner Liner (Ceramic Silica Insulation)	0.40 kg
Aerogel Packing	0.10 kg
Reentry Protection	
Ablative Heat Shield	1.70 kg
Refrigeration System for Samples	
Nitrogen Bath Canister (Fiberglass)	0.17 kg
Liquid Nitrogen	2.00 kg
Descent / Retrieval System	
Parachute System	2.00 kg
Flotation System	0.20 kg
Beacon Transmitter	0.20 kg
Batteries / Accelerometers	1.50 kg
Miscellaneous (Explosive Bolts, etc)	1.23 kg
Collected Samples	
Martian Samples / Containment	6.00 kg
Total Mass of Reentry Capsule	**17.00 kg**

3.4.1 Capsule Structure

The outer shell of the capsule will be fabricated from a carbon-carbon composite. Carbon-carbon was chosen not only for its low density and high strength, but also for its ability to withstand high temperatures without significant degradation of these properties. Composites structures of this material, when coated to prevent oxidation, have been successfully used in space shuttle insulation tiles and found capable of withstanding temperatures over 2200° C (Sheehan, 1988, pp 920-921). With a density of 1.28

gm/cm^3 (Eliezer, 1989), a 3 mm thick carbon-carbon wall will have a mass of approximately 1.5 kg.

Directly beneath the outer shell will be a 1 cm thick layer of insulating material similar to the tiles used on the space shuttle. This lightweight ceramic insulation is basically a low density (32.0 kg/m^3) composite formed from graphite or carbon fibers mixed into a slurry of silica, alumina and boron fibers. Because it is liquid, it can be formed and kiln-dried to the exact shape of the capsule inner wall (Johnson Space Center, 1986, p 65). This ceramic insulation is capable of withstanding temperatures up to 2400°C (Space Shuttle Accident Report), and will form a crucial barrier between the capsule interior and the external environment, especially during reentry.

The majority of interior volume in the capsule is reserved for sample storage. Collected specimens (except for the core sample) will be packaged in small plastic bags and dropped into a doughnut-shaped, carbon-carbon cylinder on the rover. The core sample will also be packaged in a carbon-carbon case, inserted through the middle of this cylindrical container, and lowered into the Payload/Reentry capsule, which will swing down on hinges to facilitate the process. A fiberglass shell will enclose the entire sample storage area.

The remaining interior space not occupied by other capsule subsystems will be filled with a chemical packing substance called Aerogel. Aerogel is a mixture of 99.8% air and 0.2% silicon dioxide which has a density of 5 kg/m^3, or only four times greater than air at sea level. A tenuous web structure makes it extremely strong and capable of supporting over 100 times its mass without significant deflection (Pool, 1990). Additionally, it has a high melting point (above 1530 K) and possesses excellent thermal insulating properties. Its intricate framework prevents heat from either entering or escaping by convection, while its silica chains are too slender and circuitous to conduct much heat (Pool, 1990). The aerogel insulation for the payload/reentry capsule will be pre-formed and installed prior to departure from Earth.

3.4.2 Sample Refrigeration

Returning samples intact required they be kept at or below the temperature at which they were gathered. This is especially true for polar samples, which might contain volatiles. Such a requirement was not easily met for a capsule which had no mass available for heavy pumping or power generation equipment. Essentially, the system was required to be totally passive and non-circulating.

The resulting design involved simply placing the samples in a liquid nitrogen bath. Space for the bath was created by leaving a gap between the sample basket and fiberglass wall of the capsule storage area. The liquid N_2 is pumped into this 1 cm thick space from storage tanks on the lander just prior to DRR launch. As the capsule absorbs heat during the transfer and reentry procedures, the liquid N_2 is boiled away, escaping through numerous capillary tubes to one way pressure relief valves at the top of the capsule. The temperature of the bath is set by the pressure at which the valves release the gas, which corresponds to a certain critical vapor pressure of nitrogen. The pressure selected for this design was 3 atm, corresponding to a liquid temperature of 88 K (CRC, p D-219).

Each mole of nitrogen carries away 5.59 KJ of heat as it vaporizes (Mahan and Myers, p 106), giving the entire 2 kg reservoir the potential of carrying away almost 400 KJ of heat. This is an enormous potential when the capsule is not even expected to absorb half this amount during the entire reentry procedure. Thus, the samples and capsule should be kept very cold during the entire mission.

3.4.3 Capsule Reentry and Recovery

At the periapsis of its approach trajectory,the payload/reentry capsule will be moving at a speeds in excess of 12 km/s. Typically, it would be almost impossible to directly enter a spacecraft at such speeds due the incredible heat and temperature extremes which would result; however, the incredibly small size and mass of the payload capsule make such a procedure possible, and even quite easy. At an entry speed of 12 km/s, the

capsule should produce approximately 1.23 x 10^6 KJ of heat as it dissipates its kinetic energy. Of this, 99.9% will carried away in the boundary layer. Most of the remaining 1200 KJ will be dissipated by using an ablative heat shield on the bottom surface of the capsule.

The heat shield chosen, an AVCO 5026-39 ablator, will be capable of protecting the capsule's carbon-carbon skin from the expected 2500 K reentry temperature as well as carrying away heat in excess of 1100 KJ/kg (Regan, 1984). The material was proven on the Apollo missions and is to date considered one of the lightest materials known which can withstand such high reentry temperatures (Lockheed, 1990). A conservative formula for predicting needed heat shield mass (24.4 kg/m2) indicates that a about 1.5 kg of ablative material should be used on the payload/reentry capsule (Lockheed, 1990).

Figure 3-6 shows reentry profiles and dynamic loading for several different entry flight path angles[1]. Values were calculated for a reentry speed of 12 km/s and assumed a capsule ballistic coefficient given by

$$BC = M / (C_D * S) \qquad (3\text{-}2)$$

where M is the reentry vehicle mass, C_D is the drag coefficient, and S is the maximum cross sectional area (Regan, p. 100). A drag coefficient of 1.1 was used to model the capsule in this equation, based on a triangular shape with the flat face foreword (McCormick, p 173). With a mass of 17 kg and diameter of 28 cm, the capsule's ballistic coefficient was 236.22 kg/m^2. Figure 3-6 indicates that a more shallow entry angle tends to decrease dynamic loading considerably. For this reason, the reentry angle will be set

[1]These curves were generated with a computer program which uses the Allen and Eggars approximation and was written by Capt. David Vallado at the U.S. Air Force Academy. A program listing is provided in Appendix F.

just beyond -1 to ensure the capsule doesn't skip out. Thus, the capsule should experience dynamic loading of 10 to 30 g's during descent and reach terminal velocity around 20 km

When the reentry process is complete and the capsule has achieved its terminal velocity (at approximately 10 - 20 km), the entire top portion of the capsule will be jettisoned with the help of explosive bolts to deploy the capsule's parachute. The parachute will be a nylon canopy with a mean porosity of 25 and an average drag coefficient of 1.05. Required parachute weight was determined from the following equations (Brown, 1951:

$$D = (1 / Z) (8W / \pi \rho C_D) \quad (3\text{-}3)$$

$$W_p = (0.09673065) (D^2) \quad (3\text{-}4)$$

where Z is the desired terminal velocity, W the weight of the capsule, ρ the average density of the atmosphere, C_D the drag coefficient, D the diameter of the inflated parachute, and W_p is the required weight in SI units (Brown, 1951, pp 45, 156, 160-161). Performing these calculations for a terminal velocity of about 4.5 m/s (10 mph), one gets parachute mass and diameter estimates of 0.2 kg and 4.31 m respectively (See Appendix C). Note that while these calculations do not take into account the mass of the Kevlar rigging lines or capsule attachments, the total mass of the parachute system should still be far under the allocated amount.

When parachute deployment is completed, the heat shield will be jettisoned to prevent any excess heat from being conducted inward. The capsule will then continue to splashdown. While it will probably displace enough water to float on its own, a small, helium flotation balloon will be deployed anyway to increase its buoyancy (More information on the flotation balloon is available in Appendix D.). Finally, a small homing beacon will guide recovery personnel to the capsule.

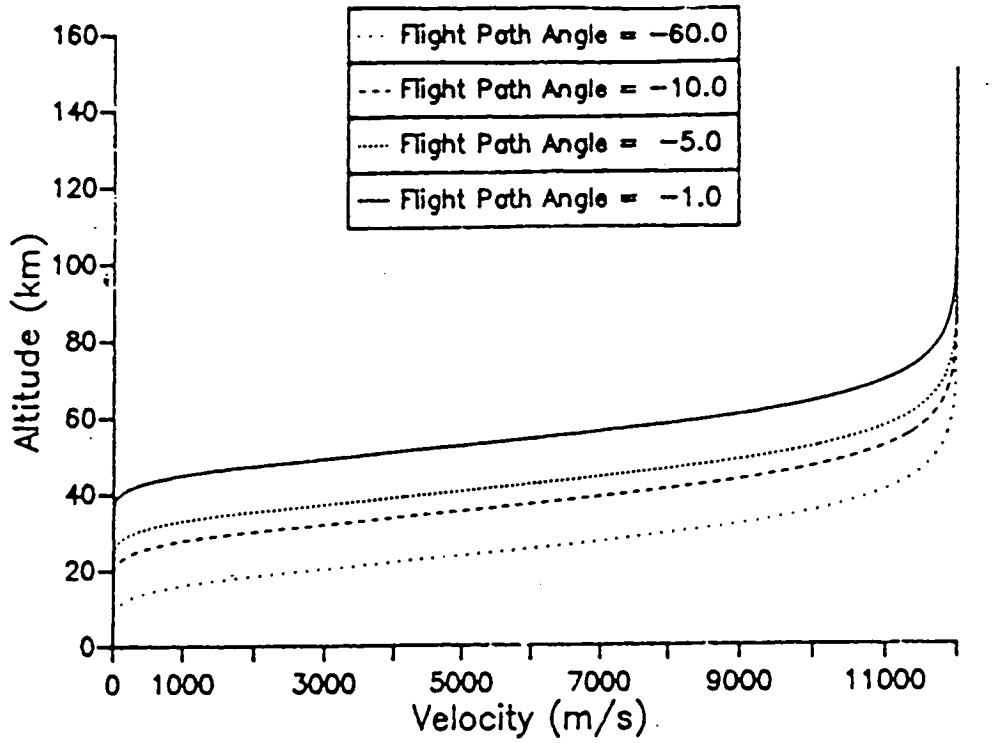

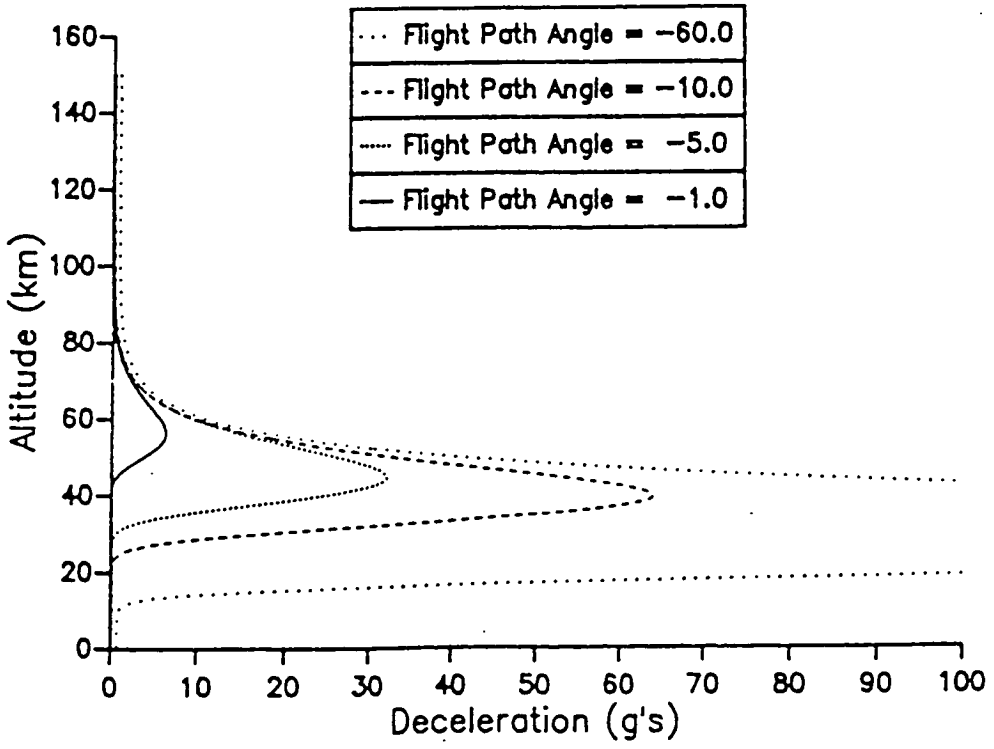

Figure 3-6. Reentry Deceleration and Dynamic Loading

4.0 Conclusions

The above designs were created with the themes of simplicity and low mass foremost in the designers' minds. As stated from the beginning, one of the largest payoffs of this type of design should be a below average cost, and this is indeed the case. Table 4-1 lists the costs associated with the launch, transfer, and return portions of the mission. These values are calculated in Appendix E.

Table 4-1. Launch, Transfer, and Mission Costs

Mission System	Cost (in millions)
Direct Return Rockets	$ 230
Orbital Transfer Vehicle	$ 552
Titan Launch	$ 265
TOTAL COST	$ 1000

At this point in the design process detailed analyses using advanced techniques and preliminary experimental development are needed. The OTV should be subjected to rigorous finite element analysis and optimized to reduce its considerable mass. Systems integration should proceed to develop the communication, computer, and power system interface between the lander and OTV. Also, detailed design should proceed on the OTV's attitude and control systems.

DRR propellant and grain designs are ready for both more detailed theoretical and experimental development. For the propellant, a reasonable baseline formulation should be

chosen and small scale mixing and hazard testing should be initiated. Also, a theoretical Isp program should be used to provide more accurate estimates of propellant properties. For the grain, a detailed burn back analysis needs to be performed and estimates of required mechanical properties developed. Adaptation of the ETV technology should start and capsule prototypes should be fabricated in the lab.

The designs developed in this effort should prove exceptionally capable of performing the mission of sample return, and this combination of low mass and simplicity in a Martian return mission is the best method of accomplishing the task at hand.

References

Agrawal, Brij N., **Design of Geosynchronous Spacecraft**, International Telecommunications Satellite Organization, Prentice-Hall, Inc. Englewood Cliffs,NJ, 1986.

Allen, David H., and Walter E. Haisler, **Introduction to Aerospace Structural Analysis**, John Wiley and Sons, New York, NY, 1985.

Bates, Roger R., D. Mueller and J. White, **Fundamentals of Astrodynamics**, 1971.

Brown, W.D., **Parachutes**, Sir Isaac Pittman and Sons, LTD, London, England, 1951.

Corliss, William R., **Scientific Satellites**, NASA SP-133, National Aeronautics and Space Administration, Washington D.C. , 1967.

Cruz, Manuel I., " Aerocapture and Aeroassisted Orbital Transfer," **Journal of the British Interplanetary Society**, Vol. 36, Jet Propulsions Laboratory, Pasadena, CA, 1983, pp. 395-404.

Cyr, Kelly, "Cost Estimating Methods for Advanced Space Systems," SAWE Paper No. 1856, 1988.

Eagle Engineering Inc., ELV DATA BASE, July 11, 1989.

Eliezer, S. and I. Gilath, " Spallation and Dynamic Fracture as an Effect of Laser Induced Shock Waves in Carbon Based Composite Materials ", United States Army, Johnson Space Center, **Nasa Tech Briefs**, " Lightweight Ceramic Insulation ", Volume 10, Number 3, Houston, Texas, May/June 1986.

French, James R., and Manuel I. Cruz, " Aerobraking for Circularizing Orbits and Aerocapture could more than Double Science Payload on some Planetary Spacecraft and make Possible many New Missions, such as a Titan Orbiter ", Jet Propulsions Laboratory, Pasadena, CA, 1982.

Handbook of Chemistry and Physics, 65 th Edition, CRC Press Inc., Boca Raton, FL, 1984.

Hankey, Wilburn L. , "Re-entry Aerodynamics", AIAA Education Series, American Institute of Aeronautics and Astronautics Inc., Washington D.C., 1988.

Hill and Peterson, **Mechanics and Thermodynamics of Propulsion**, Addison-Wesley Publishing Company, Reading, MA, 1970.

Incropera, F. and D. DeWitt, **Fundamentals of Heat and Mass Transfer** , 3 rd edition, John Wiley and Sons, New York, NY, 1990

Lockheed Missiles and Space Company, Inc., Thermal Protection Systems: Technology, Status and Challenges, Presented to NASA / L.B Johnson Space Center, Sunnyvale, CA, May 1990.

Mahon and Myers, **University Chemistry,** Benjamin/Cummings Publishing Company, Reading, MA, 1987.

Oberth, Adolf E., **Principles of Solid Propellant Development,** John Hopkins University Applied Physics Laboratory, Laurel, MD, September 1987.

Posner, E and R. Stevens, **IEEE Communications**, " Deep Space Communication-Past,Present, and Future ", Volume 22, Number 5, May 1984.

Regan, F.J., **Re-entry Vehicle Dynamics**, AIAA Education Series, American Institute of Aeronautics and Astronautics Inc., New York, NY, 1984.

Schindler, Robert C., "SDI Thinks Small," **Aerospace America,** Vol. 28, No. 4, April 1990, pages 22-25.

Vallado, Capt. D., **Methods of Astrodynamics, A Computer Approach,** Headquarters US Air Force Academy, Department of Astronautics, Version 2.0, Colorado Springs, CO, April 1990.

Wertz, J. and J. Larson, **Space Mission Analysis and Design,** Kluwer Academic Publishers, Norwell, MA, 1991.

Wood, Lowell,"From "smart rocks" Come "Brilliant Pebbles"," **Aerospace America,** Vol. 28, No. 4, April 1990, pages 18 - 20.

Yuen, J., **Deep Space Telecommunications Systems Engineering,** Plenum Publishing Corporation, New York, NY, 1983.

Appendix A

Calculation of Expected DRR Booster Performance

A. Calculation of Optimum Expansion Ratio for Stage 1 at the Surface

Since the atmospheric pressure on Mars is approximately 1/100 that of the Earth at sea level, $p_e = p_a = 0.147$ psi for optimal expansion. Then, for a chamber pressure of p_o = 1500 psia,

$$Me = \sqrt{\left\{\left(\frac{Po}{Pe}\right)^{\frac{\gamma-1}{\gamma}} - 1\right\}\left(\frac{2}{\gamma-1}\right)} = 6.05 \tag{1}$$

The corresponding area ratio for this condition is given by

$$\frac{Ae}{A^*} = \frac{1}{Me}\left[\frac{2}{\gamma+1}\left(1+\frac{\gamma-1}{2}Me^2\right)\right]^{\frac{\gamma+1}{2(\gamma-1)}} \tag{2}$$

B. Calculation of Expected Motor Performance

Given the propellant properties of Table 3-2 and a maximum exit area of 314 cm^2:

$$\mathbf{m} = \rho_p r_b A_b = C_D p_o A^* \tag{3}$$

The discharge coefficient is fixed by the propellant properties as

$$C_D = \sqrt{\gamma \frac{\overline{m}}{\overline{R}To}\left\{\left(\frac{2}{\gamma+1}\right)^{\frac{\gamma+1}{\gamma-1}}\right\}} = 5.322 \times 10^{-4}\ m/s \tag{4}$$

Assuming a chamber pressure of 1500 psia for the second stage and 1000 - 2000 psia for the first, and assuming minimum throat areas of 4 cm^2 and 9 cm^2 for the second and first stages respectively,

$$\mathbf{m} = 2.2\ kg/s\ (stage\ 2) \tag{5}$$

$$\dot{m} = 3.3 - 6.1 \text{ kg/s (stage 2)}$$

and since the propellant masses for stages 2 and 1 are 53 kg and 105 kg, the burning times are given as

$$\begin{aligned} t_b &= 24 \text{ sec (stage 2)} \\ t_b &= 21 \text{ sec (stage 1)} \end{aligned} \tag{6}$$

From the area ratios defined by the throat and exit areas

$$\begin{aligned} A_e / A^* &= 35 \text{ (stage 1)} \\ A_e / A^* &= 78 \text{ (stage 2)} \end{aligned} \tag{7}$$

$$\frac{Ae}{A^*} = \frac{1}{Me}\left[\frac{2}{\gamma+1}\left(1+\frac{\gamma-1}{2}Me^2\right)\right]^{\frac{\gamma+1}{2(\gamma-1)}} \tag{8}$$

Which yields

$$\begin{aligned} M_e &= 4.15 \text{ (stage 1)} \\ M_e &= 4.72 \text{ (stage 2)} \end{aligned} \tag{9}$$

Now the pressure ratios (p_o / p_e) can be found from the relation

$$\frac{Po}{Pe} = Pr = \left(1+\frac{\gamma-1}{2}Me^2\right)^{\frac{\gamma}{\gamma-1}} \tag{10}$$

$$\begin{aligned} &= 407 \quad \text{(Stage 1)} \\ &= 1131 \quad \text{(Stage 2)} \end{aligned}$$

Then the thrust coefficient is

$$C_T = \sqrt{\left\{\left(\frac{2}{\gamma+1}\right)^{\frac{\gamma+1}{\gamma-1}}\left(\frac{2\gamma^2}{\gamma-1}\right)\right\}}\sqrt{\left\{1-\left(\frac{1}{Pr}\right)^{\frac{\gamma-1}{\gamma}}\right\}} + \frac{Pe-Pa}{Po}\frac{Ae}{A^*} \tag{11}$$

$$\begin{aligned} C_T &= 1.8722 \quad \text{(stage 1)} \\ C_T &= 1.938 \quad \text{(stage 2)} \end{aligned}$$

And finally, thrust is given by

$$T = C_T p_o A^* = 11626 - 23252 \text{ N} \quad \text{(stage 1)} \qquad (12)$$
$$T = C_T p_o A^* = 8016 \text{ N} \quad \text{(stage 2)}$$

I_{sp} can also be found from its definition

$$I_{sp} = \mathbf{m}\, g_{sl} = 360 \quad \text{(stage 1)} \qquad (13)$$
$$I_{sp} = \mathbf{m}\, g_{sl} = 372 \quad \text{(stage 2)}$$

Appendix B

Determination of Masses for DRR Capsule Components

NOTE: Refer to Figure 3-5 for illustration of shapes and dimensions of particular components.

All mass estimates were determined by simply calculating the appropriate surface area of the DRR component, then multiplying by the appropriate thickness and density. This method works as long as the thicknesses are very small compared to the surface areas. Mass estimates were rounded up in order to allow for slight variations and margin of error.

A. Carbon-Carbon Outer Shell and Ceramic Silica Tile Insulator

The surface area of the outer shell was determined using, as a model, the parabolic ellipsoid given by the following equation.

$$S = \int_0^{2\pi} \int_0^{0.14} \sqrt{\frac{4r^2}{a^4} + 1}\,(r dr d\theta) = 0.3018779 m^2 \qquad (1)$$

Where a = 0.19799

Also, the volume of the endcap was modeled as a disc of radius 14 cm, and thickness 2 mm. The volume was then generated using the equation:

$$Vol = \pi r^2 h \qquad (2)$$

The density of carbon-carbon was taken to be $\rho = 1280\ kg/m^3$ (Eliezer, 1989).

Since the ceramic silica insulation layer is the same shape as the carbon-carbon outer shell, we assumed the same surface area as for the carbon-carbon shell. While the actual surface area will be slightly less, this will give a worse case approximation of the mass.

The thickness of the ceramic tile will be 1 cm thick, thus a volume can be determined using equation 2. The density of the ceramic silica was found to be $\rho = 96\ kg/m^3$ (Johnson Space Flight Center, 1986).

B. Mass Estimate of the Ablative Heat Shield

The area of the bottom of the DRR was determined by the following equation:

$$\text{Area} = \pi r^2 \qquad (3)$$

Where the radius is r = 14 cm.

An over-estimated mass per unit area of 24.412 kg/m^2 needed for an Earth reentry from Mars was used.

The mass was then simply determined my multiplying this estimate by the determined area.

C. Mass Estimate for the Aerogel Packing

The aerogel volume was divided into two separate sections. One section was the small disc located at near the bottom of the sample storage container. The second section was the volume between the outer shell and the sample collection basket.

In order to determine the volume of the disc, equation 2 was used with r = 14 cm and h = 6 cm.

The density of the aerogel was given as $\rho = 4.970$ kg/m^3 (Pool, 1990). By multiplying the volume obtained above by this density the mass of this particular section could be determined.

For the second section, the volume was obtained by an approximation of determining the area of the triangular section remaining, then revolving the edge, at a radius of 14 cm through an angle of 360 degrees. The area of the triangle was determined by:

$$\text{Area} = 1/2\ b\ h \qquad (4)$$

Where b = 2 cm, and h = 22 cm.

To determine the approximated volume of the section, the following equation was used:

$$\text{Vol} = (2\pi r)\ (\text{Area}) \qquad (5)$$

The mass of this particular section was then determined by multiplying this volume by the density indicated above for aerogel. To estimate the total mass of the aerogel packing, the masses of the two sections were simply added.

D. Mass estimate of the Sample Collection Container

It was intended to use 1 cm thick fiberglass to construct the sample collection basket which will store both the sample collection basket and the liquid nitrogen bath. To determine the mass of this structure, surface area was determined by using a radius of the cylinders which would be directly in the center of the fiberglass casing.

This component was also broken down into several sections in order to simplify computation.

The first section was the large cylinder in which the sample basket is placed. The surface area of this cylinder was determined using the equation:

$$S = 2 \pi r h \qquad (6)$$

where r = 10.3 cm, and h = 24.6 cm.

The next section in which the surface area was determined, was the casing around the upper portion of the core sample. This surface area was determined using equation 5, with r = 2.05 cm and h = 18.3 cm.

Two endcaps were then needed to seal the container. Each endcap had an area determined by equation 3 at r = 10.3 cm. Since two were needed, the area was then multiplyed by 2. Notice that we did not determine an area for the endcap at the top of the core sample because one of the endcaps in which the area was just determined would have to have a hole cut out to the exact dimension of the core endcap. So for simplification, we simply just left the that particular endcap solid instead of doughnut shaped.

At this time the total surface area of the entire canister was determined by simply adding the surface areas of all the sections mentioned.

From this surface area, the volume of the canister wall was calculated by simply multiplying by the thickness of the fiberglass casing.

Mass of the canister was then generated by multiplying the volume by the density of fiberglass, which is r = 32.0 kg/m^3 (Incropera, 1990)

Appendix C

Determination of Parachute Mass and Diameter

To determine the diameter, D, the equation used is

$$D = (1/z)[(8W)/(\pi \rho C_D)]^{(1/2)} \quad (1)$$

where

z = terminal velocity

W = total weight including parachute

ρ = average density of the atmosphere parachute deployment and sea level

C_D = coefficient of drag of the parachute = 1.05

We want the capsule to land in the water at approximately 10 mph, or $z = 4.4704$ m/s.

The capsule total mass is 17 kg. Therefore

$$W = (17 \text{ kg})(9.81 \text{ m}/\text{s}^2) = 166.77 \text{ N} \quad (2)$$

The parachute will open at approximately 4 km. The density for this altitude is

$$\rho = 1.0265 \text{ kg}/\text{m}^3$$

Using the equation for the diameter of the parachute

$$D = 1.654 \text{ m} = 5.427 \text{ ft}$$

Using this diameter for the parachute the mass and weight of the parachute can be estimated

$$W = (0.09673065 \text{ kg}/\text{m s}^2) D^2 \quad (3)$$

$$W = .264628 \text{ N}$$

From this we can calculate the mass of the parachute

$$M = W/(9.81 \text{ m}/\text{s}^2) = (.264628 \text{ N})/(9.81 \text{ m}/\text{s}^2) = 0.027 \text{ kg}$$

This, we feel, is an underestimate of the parachute material mass, also the diameter of the parachute was overestimated. Therefore, with the mass of the parachute material and the added mass due to the rings and the attachments, we feel 1 kg is a safe approximation of the mass for the entire parachute system.

Appendix D

Determination of the Flotation Balloon Parameters

The capsule's mass without the heat shield (i.e. at splashdown) is 14.497 kg. To keep the capsule afloat, we must displace at least 14.497 kg of salt water. For these calculations, we will take the mass of the capsule to be 15 kg and use the density of fresh water.

$$\rho = 1000 \text{ kg} / \text{m}^3$$

The mass of the capsule times gravity must equal the amount of water displaced by the capsule times the density of water times gravity.

$$F = \rho g V \tag{1}$$

The force of the capsule, F,

$$F = m g = (15 \text{ kg}) (9.81 \text{ m} / \text{s}^2) = 147.15 \text{ N} \tag{2}$$

This implies the volume of water that must be displaced is

$$V = F / \rho g = (147.15 \text{ N}) / (1000 \text{ kg} / \text{m}^3) (9.81 \text{ m} / \text{s}^2) \tag{3}$$

$$= 0.015 \text{ m}^3$$

The volume that the capsule displaces is 0.014 m^3. This means the balloon must displace 0.001 m^3. For a safety factor, we set the balloon displacement to be 0.005 m^3.

The shape of the balloon is a hollow disk with a height of 10.16 cm. The inner radius, r, is 20 cm. The outer radius, R, is unknown and must be solved for. The volume of the balloon is

$$V = 2 \pi r (R - r) h \tag{4}$$

Solving for R, we get

$$R = V / (2 \pi r h) + r \tag{5}$$

$$R = (0.005 \text{ m}^3) / [2 \pi (0.2 \text{ m}) (0.1016 \text{ m})] + 0.2 \text{ m}$$

$$= 0.2392 \text{ m}$$

Thus the width of the balloon is

$$w = R - r = 0.2392 \text{ m} - 0.2 \text{ m} = 0.0392 \text{ m} = 3.92 \text{ cm} \tag{6}$$

Appendix E

Evaluation of Mission Cost

The following NASA cost model [Cyr, 1988] was used to obtain preliminary estimates of mission expense:

$$\text{Cost} = .0000172(Q^{.5773})(W^{.6569})(58.95^{C})(1.0291^{Y})(G^{-.3485}) \qquad \text{(F-1)}$$

where Q is the number needed plus two, W is the system weight, C is a technology factor, Y is the mission year minus 1900, and G is the design generation (1 for this case). The mission departure year is 2003. The DRR was costed with a technology factor of 10 and the OTV with a factor of 7 corresponding to Q values of 2.4 and 2.25 respectively.

The cost of a Titan launch was estimated at $ 265 million. Results of the cost analysis can be found in Table 4-1.

Appendix F

Reentry Computer Program

```
*-----------------------------------------------------------------------
*                                                                      *
*                          REENTRY PROGRAM                             *
*                                                                      *
*                                                                      *
*     This Program calculates velocity and deceleration parameters     *
*   during reentry, using Allen and Eggars Approximations for any      *
*   altitude.                                                          *
*                                                                      *
*                                                                      *
*   AUTHOR: Capt Dave Vallado  USAFA/DFAS  719-472-4109  19 Dec 1989   *
*                                                                      *
*                                                                      *
*   Transposed for The Pennsylvania State University, Department of    *
*   Aerospace Engineering, Spacecraft Design Class (ie Group           *
*   Gazze) by Scott L. Hirsch.                                         *
*                                                                      *
*                                                                      *
*   Inputs:                                                            *
*                                                                      *
*                                                                      *
*                                                                      *
*      Vre             - Reentry Velocity                  m/s         *
*      Phire           - Reentry Flight Path Angle         deg         *
*      BC              - Ballistic Coefficient             kg/m2       *
*      delh            - decreasing altitude increment     km          *
*      alt             - altitude at which the                         *
*                        calculations begin                km          *
*                                                                      *
*                                                                      *
*   Outputs:                                                           *
*                                                                      *
*      V               - Velocity                          m/s         *
*      Decl            - Deceleration                      g's         *
*                                                                      *
*   Local Variables:                                                   *
*                                                                      *
*      grav            - Temporary variable to hold Weight             *
*                        Component                                     *
*      rho             - Atmospheric density               kg/m3       *
*      h               - Altitude                          km          *
*                                                                      *
*   Constants:                                                         *
*                                                                      *
*      Scaleht         - Scale height used to exponentially            *
*                        model the atmosphere (1.0/7.313)              *
*                                                                      *
*                                                                      *
*-----------------------------------------------------------------------*

1          implicit real*8(a-z)

*
```

```
*    Open a data file to dump all calculated data into
*
2         open(unit = 11, file = 'redat.dat', status = 'unknown')

3         scaleht = 1.0 / 7.315
*
*   Input all the needed parameters listed above
*
4         Print*,'Input the vehicle reentry velocity.'
5          read*,vre
6         Print*,'Now enter the reentry flight path angle in degrees'
7          read*,phire1
8         Print*,'Enter the Ballistic Coefficient of the reentry vehicle.'
9          read*,BC
10        Print*,'Input the altitude you wish to start calculations.'
11         read*,alt
12        Print*,'Lastly, enter the decrement factor through the atmos.'
13         read*,delh
*
*   Convert flight path angle to radians
*
14        pi = acos(-1.0)
15        phire = phire1*pi/180.0


16        do 10 h = alt,0.0,-delh

* DENSITY MODEL OF ATMOSPHERE
17            rho = 1.225 * exp( -scaleht * h )
* DETERMINATION OF VELOCITY AT A PARTICULAR ALTITUDE
18            v = vre * exp( (1000.0*rho)/(2.0*bc*scaleht*sin(phire)))
* DETERMINATION OF DECELERATION AT A PARTICULAR ALTITUDE
19            grav = 9.81 * sin(phire)
20            decl = ((-0.5*rho*v**2) / bc ) + grav
21            decl = decl / 9.81


22            write(11,15)h,v,decl
23 10        continue

24         close(11)

25 15     format(5x,f9.3,5x,f12.5,5x,f12.5,5x)
          stop
          end
```

CHAPTER 2:

LOW MASS, LOW COST LANDER DESIGN FOR A MARS SAMPLE RETURN MISSION

AEROSPACE 401B

DETAILED SPACECRAFT DESIGN

SUBMITTED BY:

GROUP MATULEVICH

GROUP MEMBERS:

KIRK BENTLEY
MARK DEL VECCHIO
ROBERT GARCIA
JONATHAN MATULEVICH
RAYMOND MORRISON
ALICE MUNNELLY
KIRK WHITMER

ABSTRACT

A low mass, low cost lander design for an unmanned Mars Sample Return Mission is investigated. The criteria used in this scenario were the following: the implementation of current technology; the design of two landers, one equatorial and one polar; the sharing of communications, computer and power subsystems; a soft landing capability on the Martian surface; and the ability to directly communicate from the Martian surface to Earth. The landers will begin in a low Martian orbit, descend to the surface, and perform surface operations so that the samples can be obtained. The samples will then be placed in a direct return rocket for transfer to Earth. Investigation into each of the lander subsystems necessary to fulfill the objectives of the lander scenario along with their integration is given and a total system cost is presented.

TABLE OF CONTENTS

LIST OF FIGURES

LIST OF TABLES

LIST OF APPENDICES

NOMENCLATURE

DIPS	Dynamic Isotope Power Source
DOF	Degrees of Freedom
DRR	Direct Return Rocket
FAA	Federal Aviation Administration
GPHS	General Purpose Heat Source
LFS	Lander Flight System
LRA	Lander Robotic Arm
MMH	Monomethyl Hydrazine
MSRM	Mars Sample Return Mission
NERVA	Nuclear Engine Rocket Vehicle Application
NTO	Nitrogen Tetroxide
RSDS	Rover Storage & Deployment System
RTG	Radio Isotope Thermal Electric Generator
SPDS	Stabilized Payload Deployment System

INTRODUCTION

An integral part of the Mars Sample Return Mission (MSRM), the Lander Flight System (LFS) conducts extensive surface operations on Mars. The lander portion of the mission begins in a stable Martian parking orbit and ends with the launch of the Direct Return Rocket (DRR) from the Martian surface. The subsystems utilized by the LFS include an aeroshell, propulsion, communication, power, core and contingency sample collection systems, rover deployment system, robotics, and a DRR launch system. A simplified schematic of the lander and its subsystems is shown in Figure 1.

In constructing the LFS, five criteria were taken into account; the first of which incorporates low cost/low mass design based on current technology. By using current technology, the overall cost of the mission may be reduced, because research and development will not have to be performed on a large scale. Subsystems utilizing current technology will have a higher level of reliability when related to overall mission performance. Low mass has been achieved through the use of a simple support structure containing all of the subsystems. Care was taken in designing the rail launch and rover deployment system to minimize mass through the use of lightweight and composite materials.

Secondly, two landers needed to be used to explore both the polar and equatorial regions; however, due to the similarity of the landers, only one will be discussed in this report. These regions were chosen for sample collection in the two extreme locations of the planet. Next, it was necessary to share systems between the Orbital Transfer Vehicle (OTV) and the landers during the transfer from Earth to Mars. The communications, computer, and power systems were used by the OTV in order to further reduce overall mission mass and cost. The sharing was achieved through the use of a module which allowed transfer of information and power to the OTV. The fourth criterion focused on the need to achieve a soft landing on the surface of the planet. Soft landing was carried out after descent through the Martian atmosphere and was necessary in order to avoid the damage of the lander in any way. Lastly, it was deemed necessary to have a direct communication link with Earth. This eliminates the need for an orbital satellite which

would again reduce the overall mission mass and cost.

Initial trade studies were done for each subsystem. Mass, volume, and power characteristics were taken into account in order to better locate and/or design each subsystem. An overall mass constraint of 1500 kg was placed on the LFS. Justification for each of the chosen subsystems will be presented in the following sections.

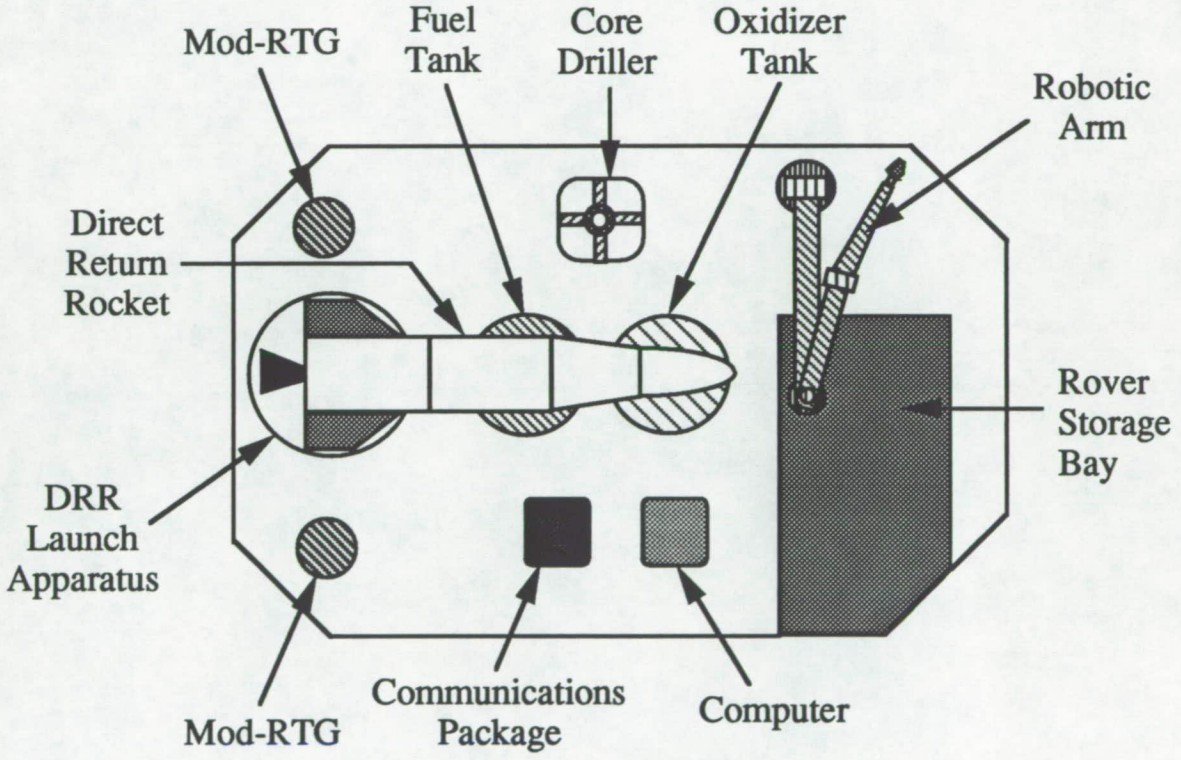

Figure 1: Lander Schematic (Top View)

SUBSYSTEMS

Power Generation

Many power generation systems were considered for this mission. The following criteria were used to evaluate the power generation systems: mass, specific power, volume, and thermoelectric conversion efficiency. The primary objective of the selection process was to find a system that was capable of generating 500 W with minimal mass and volume. Upon complete evaluation of all the available systems subject to the above criteria, the MOD - RTG was selected to power the subsystems of the lander. Based upon the selected criteria, a brief summary of the comparison and selection process follows.

The SP - 100 and NERVA derivative are representative of existing high mass and high power output systems. Current SP-100 and NERVA systems are rather large and are very heavy when compared to the MOD - RTG. These and related systems, in the multi-kilowatt, multi-megawatt range, cannot be effectively and efficiently scaled down to meet the needs of this mission (again based upon the criteria presented above). Scaling down of such systems to meet our needs at minimal mass would not be possible due to the complexity and number of components within the system design. Also, even if scaling down of the large mass systems was possible, they would generally not be a likely candidate for this mission based on the lack of reliability in the flight design. Table 1 gives a brief comparison of the current SP - 100, and NERVA derivative to the MOD - RTG [1]. As can be seen from Table 1, the first two systems in their original form would essentially be useless to this mission.

TABLE 1: HIGH WATTAGE SYSTEM COMPARISON

	SP - 100	NERVA	MOD - RTG
Power (kW)	100	1000	0.50
System Mass (kg)	2700	15200	60
Power/ Mass (kW/kg)	37.0	65.8	0.0084

Aside from the larger systems, a solar panel design was also considered in comparison to the MOD - RTG. Solar panels are widely used in space related applications and have proven their reliability over the years. Solar panels generally need a large amount of surface area and contain considerable support mass when used in gravity influenced environments.

In order to adequately compare the solar cells to the MOD-RTG, the panels on the Intelstat V were used as a reference [2]. The dimensions of these panels were 1.6 m x 2.0 m; it was calculated that such a system would provide approximately 467 W per panel on the panel surface. However, these estimates were formulated for the satellite in synchronous orbit above the Earth. Adjusting the power generation, assuming 100% absorption, the power would decline to around 201 W per panel on the Martian surface. It should be noted that all of these calculations were based on a thermoelectric conversion efficiency factor of 15% due to degradation and solar scattering. Also, the solar radiation incident upon the panels was assumed to be perpendicular over the entire operating time. This would allow the most flux to be incident upon the cells. All calculations related to the solar cell comparison can be found in Appendix A. A brief comparison of the solar panel system and the MOD - RTG can be seen in Table 2. It should be noted that the solar cells are considerably heavier when operating on the surface of the planet due to the support structure. This structure causes an increase in generator weight of about 100%.

TABLE 2: SOLAR CELL COMPARISON

	Solar Cells	MOD - RTG
Power (W)	401.98	494.80
Generator Mass (kg)	82.5	58.788
Power/ mass (W/kg)	6.43	8.40
Energy Storage (kg)	14.88	14.88
Power Conditioning and Structure (kg)	43.33	43.33
Volume (m^3)	0.064	0.066
Incident Surface Area (m^2)	6.4	0.2574
Generator Efficiency (%)	15.0	7.6
Total system mass (kg)	140.71	117.00

In the above comparison, the power conditioning and energy storage were assumed to be equal to simplify the comparison of the generators. Since the generator mass for the solar cells was larger than that of the MOD - RTG and produced a total power output less than the MOD - RTG, the solar cells were not as favorable as the RTG. Also, since the RTG was much more compact in terms of area and volume, the placement and/ or deployment of such a large panel of cells would not have to be considered. Once again, the MOD-RTG proved favorable to the opposing system.

Lastly, the MOD - RTG was compared to radioisotope generators of comparable size, mass, and power output. The GPHS - RTG, and the Stirling and Brayton DIPS engines were evaluated in comparison to the MOD - RTG. From these systems, the MOD - RTG proved to be the best system for the power source of this mission. This comparison can be seen in Table 3 [3].

TABLE 3: RADIOISOTOPE COMPARISON

	GPHS	MOD - RTG	Brayton	Stirling
System Mass (kg)	155.0	117.00	138.0	88.00
Generator Efficiency (%)	6.0	7.6	22.0	22.0
Power Output (W)	500.0	494.80	500.00	500.00
Radiator Area (m^2)	2.0	0.92	4.4	1.5
Power/ mass (W/kg)	5.3	8.4	5.8	10.2

The Brayton engine was eliminated due to its larger system mass and low specific power. The high thermoelectric converter efficiency does not account for the complexity in design and the lack of reliability. The GPHS was not utilized since the MOD - RTG was designed directly from GPHS technology. Also, the GPHS is heavier, and has a lower specific power and generator efficiency. The Stirling engine looks rather appealing at first due to its light mass, high efficiency, and high specific power; however, the engine has moving parts, like the Brayton engine, which increases its level of complexity. Unlike the MOD - RTG, friction exists within the engine caused by the moving parts. Since this mission is of considerable length, the friction in the engine might cause significant problems. Also, since the Stirling was originally a multi-kilowatt system which was scaled

down, the reliability of such a system is uncertain. Due to these factors, the Stirling engine will not be used.

The MOD - RTG represents the next generation of RTG technology. This thermoelectric generator was selected on the basis of its ability to adequately fulfill all requirements for the mission. A schematic of the RTG can be seen in Figure 2.

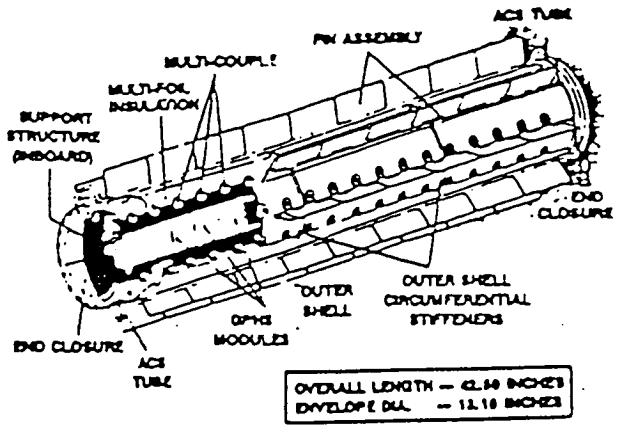

Figure 2: RTG CUTAWAY
(Ref: Hartman, 1988)

RTGs have been safely and reliably employed in space applications since the early 1960's. The MOD - RTG has been designed with the same level of reliability and safety in mind. The distinguishing feature of the MOD - RTG is its modular construction. The electrical output power can be varied, in increments, to meet the necessary power requirements of the lander. The modularity of the RTG can provide the spacecraft with power from as low as 20 W to as high as 494.8 W at a total mass of 60 kg for the RTG modules [4]. The modular variation produces essentially a linear power output from thirteen modules down to six. For operations with less than six modules, the behavior is unknown, but has a minimum of 20 W.

This mission will utilize two MOD - RTGs at a mass of about 30 kg each. The calculations done in order to scale a prototype MOD - RTG down to mission dimensions have been provided in Appendix B. From these calculations, all pertinent values for a single RTG can be found in Table 4.

TABLE 4: MOD-RTG FLIGHT DESIGN

Voltage	30.8 Volts
Power Output	247.35 Watts
Specific Power	8.4 Watts/ kg
Number of GPHS modules	13
Number of multicouples	104
Length	0.78 m
Diameter	0.33 m
Weight	30 kg
Operating Life	5 years
Storage Life	3 years

Radiative heating is a factor that must be considered when using an RTG for power generation. The RTG does contain a shielded generator housing; the shielding prevents any significant ionizing radiation from escaping the RTG, but the device certainly radiates heat. The radiation from the sun also contributes to the heating of the spacecraft, but not as significantly as the power units (calculations regarding the heating effects imposed on the lander by the RTGs and the sun can be found in Appendix C).

In order to analyze such heating effects, the mission time is allowed to approach infinity for simplicity in calculation of a steady-state temperature. This temperature was calculated to be approximately 305 K. This is not an unreasonably high number, but only a very simple heat transfer analysis was conducted on the lander taking into account only radiative heating. Conduction of heat through the lander structure was not considered due to the high level of complexity associated with the calculations. The estimate is rough because conduction of the radiation through the aeroshell was not calculated again due to the complexity level. Therefore, it can be concluded that the steady-state temperature may be higher than the calculated value.

Due to the complexity of the heat transfer process occurring in space, the use of heat pipes within the lander to heat the subsystems cannot be justified. Since the steady state temperature was approximated to be 32°C, the use of shielding has been incorporated. Formed Aluminum was placed on the three sides vertical to the RTGs, exposing one side to the rear of the lander for proper radiation removal. This substance was chosen based upon its high reflectivity and low transmissivity.

Communications

The communications system for the MSRM will have a mass of approximately 10 kg with a volume of 0.01 m^3. These figures result from modeling the system after a small personal computer. The system will also require about 80 W of power. Direct transmission to Earth will use an S-band high-gain antenna with a 75 cm diameter parabolic dish [5]. These approximations are based on the Viking Lander communication system. One limitation of the communication subsystem will occur when the lander enters the Martian atmosphere. At this time, the lander will experience a communications black-out which will hinder the transmission and reception of information.

Modeling the communication system after the one used on the Pioneer / Venus I mission will allow the transmitter to communicate directly with Earth for about 70 minutes per day at a data rate of 1200 bits per second [6]. This transmission rate can be increased but according to the power constraints which result from the low-mass criteria, a low transmission rate will be necessary. About 2 million bits can be delivered each day over this direct Mars-to-Earth link [5].

The lander will also contain two cameras with each located on opposite sides of the robotic arm. This will allow for adequate visualization of the arm's activities. The camera's scanning rate will be 500 bits per second for direct transmission to Earth [5]. This is similar to the direct transmission cameras used in the Viking mission. The direct transmission will permit real-time imaging of the Martian surface and the robotic arm's maneuvers.

There are several requirements dealing with communications that should be addressed before the mission design is completed. First, because the lander must perform entry maneuvers and maintain command control, the receiving antenna system should provide a specified gain in all directions from the lander. During Martian descent, the lander should be able to maintain communications with Earth regardless of its attitude. Also, the command link between Mars and Earth should be highly reliable. Finally, the whole system should allow for low power consumption, and should be lightweight. These specifications come from the telecommunications of the Surveyor spacecraft which was

designed for direct communication between the Moon and Earth [7]. The Mars lander meets similar needs; therefore, these requirements can be incorporated into the communications system for the Mars lander.

Several subsystems are important to investigate when choosing the communication system. The Mars lander will be exposed to large thermal gradients from the sun's radiation along with thermal radiation from Mars. Also, equipment in the lander will generate excess heat that must be removed. Radiation mirrors can be used to remove heat from the communications payload [8]. This is a process currently used for communications satellites. Further research is needed to determine the most efficient method to alleviate the lander of the excess heat. To maintain near constant temperature conditions, heaters may be switched on to make up for the heat reduction that occurs when the transponders are switched off. The transponders will consist of both receiver and transmitter signal-relay equipment. The parabolic antenna on the lander receives and transmits the downlink signals between Mars and Earth. The gain of the antenna is determined by:

$$G = \eta\left[\frac{\pi D}{\lambda}\right]^2 \qquad (1)$$

where h is the aperture efficiency, λ is the wavelength of the signal, and D is the reflector diameter [8]. The aperture is the area of a receiving or transmitting antenna through which all of the radiation is assumed to pass. Assuming the aperture efficiency is 0.91 the approximate gain for the Mars lander will be 5.05. If necessary, the gain of the antenna can be increased by increasing the reflector diameter [8].

More research and information is needed to adequately design the communication system for the lander. Some areas that need modification include the system's mass, volume, and power estimates, the size estimate of the reflector dish of the antenna, and the information transmission time. Also, ways to reduce the heat build-up among the instruments and ways to increase or decrease the gain of the antenna should be investigated.

Computer

The computer subsystem will be a variation of that used by a deep probe such as Magellan or Galileo with modifications made for this mission. Due to time constraints, a complete computer system design was not investigated, but several estimates were made. To conform to the low mass mission requirements, the sub-system will have a mass of approximately 15 kg. The computer will also use 25 W of power.

The computer will act as the control center of the lander. The primary function of the computer will be to instruct all of the remaining subsystems of the proper operating procedures. Some of these procedures include: regulating the power sent to all systems, commanding the communications subsystem of when and what to up and down link, providing entry corrections for the thrusters, instructing the core sampler when and how to take samples, and guiding the robotic arm in transferring the samples from the rover to the DRR.

Rover Storage And Deployment

A Rover Storage and Deployment System (RSDS) has been designed based on criteria related to the Stabilized Payload Deployment System (SPDS) used for handling a payload in the cargo bay of a Space Shuttle [9]. The RSDS must safely store the rover during launch, Earth to Mars transfer, and Mars descent. Thus, the system must allow for some vibration and/or movement of the rover. Once the lander is on the surface of Mars, the RSDS must be able to deploy the rover reliability.

The RSDS will be located at the edge of the lander. A shield will be present enclosing the RSDS. This shell is present in order to protect the lander subsystems from the conditions experienced once the aeroshell is removed. The lander will be descending at a very high velocity even after the parachutes are deployed. Also, debris from the surface blown by the thrusters may be detrimental. The part of the shield enclosing the RSDS will have to be removed before the rover can be deployed. Through the use of explosive bolts, the shielding about the RSDS will be blown off. Once this is accomplished, there will be no enclosure between the rover and the edge and bottom of the lander. A conceptual diagram of the basic RSDS concept is shown in Figure 3. The description and function of each component will be presented. Two arms, located on each side of the rover, are connected at the ends by a straight beam. Along this beam are three latch devices which will be connected to the hub of each wheel on the rover. When the rover is deployed, the arms will swing down from the weight of the rover until it reaches the ground. Once the rover is on the ground, the latches will release and the arms will retract upwards. Due to this system, the rover will have the option to move initially in two directions instead of one. Even if the lander was sitting with its bottom on the ground, the rover would be able to be deployed.

Figure 4 shows detailed views of the RSDS. Part (a) is a hollow rotation disk. The system is connected to the lander structure at this point. The rotation disk contains spring and damping devices. This allows the rover to slowly descend towards the ground and for the arms to retreat upwards once they are released from the rover, thus removing any obstruction. Figure 5 is a detailed view of part (a).

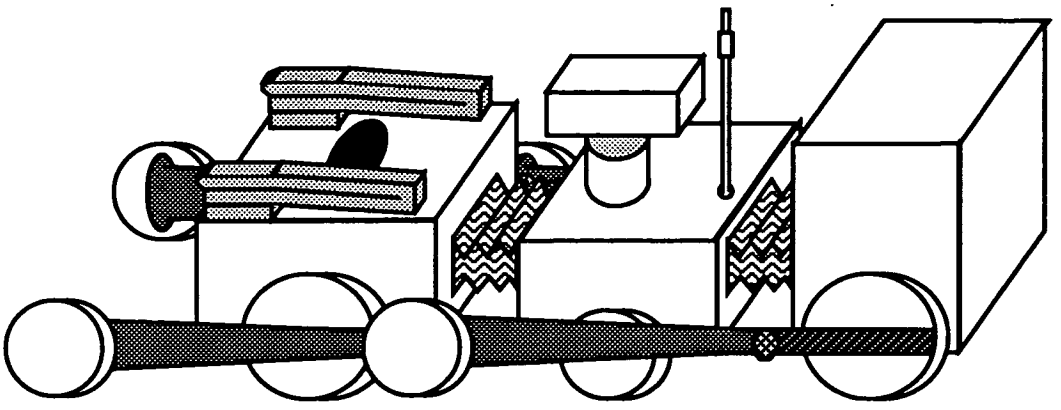

Inside Lander - Prior to Deployment

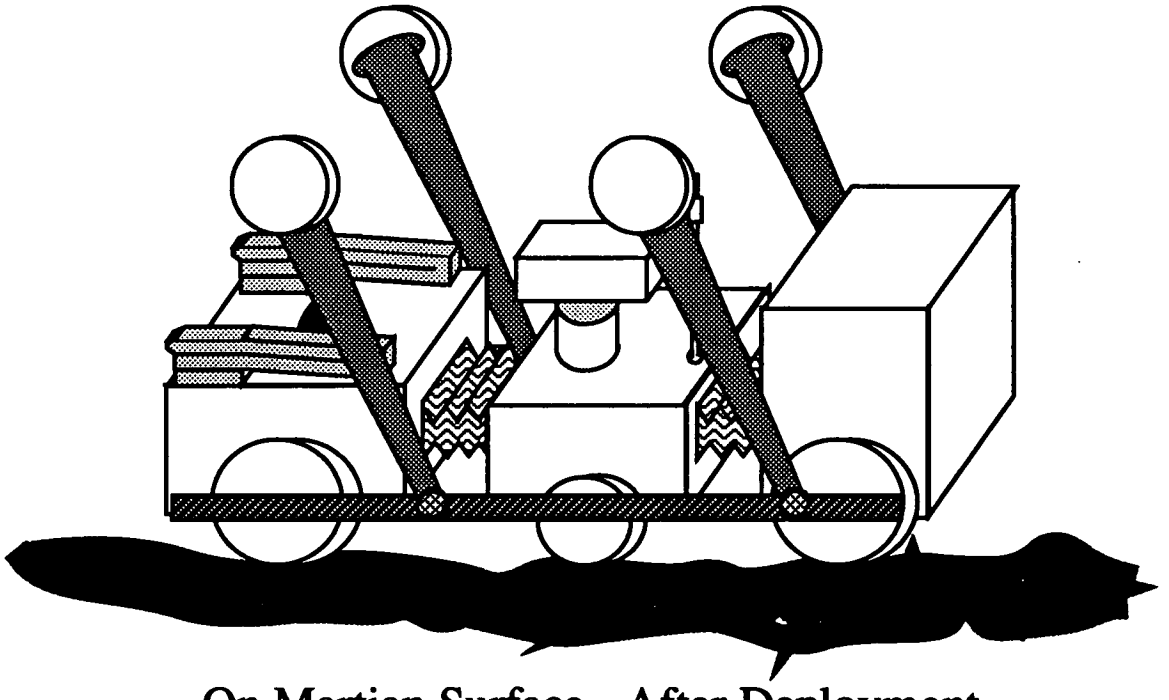

On Martian Surface - After Deployment

Figure 3: Rover Deployment System

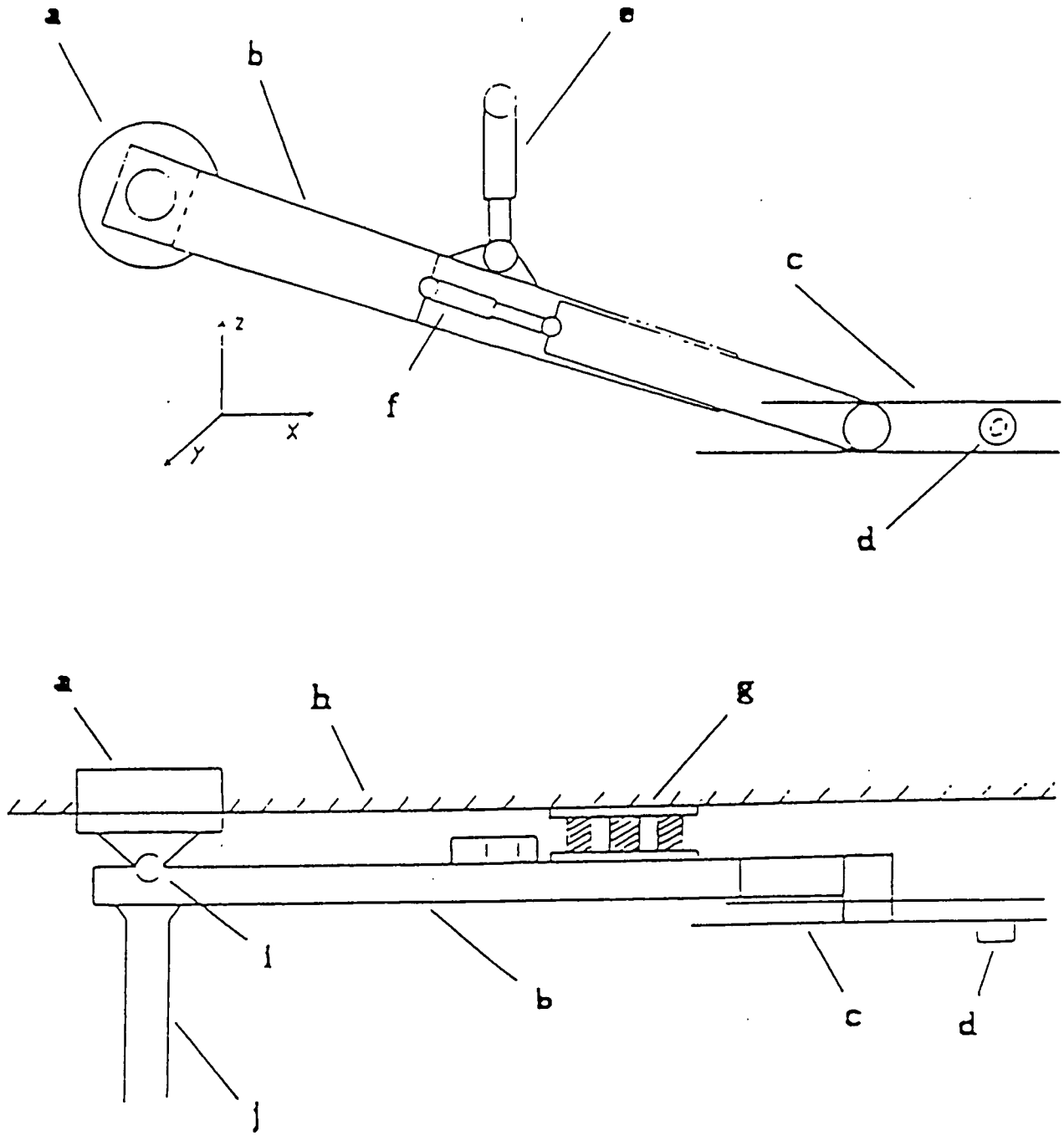

Figure 4: Basic Components of the RSDS

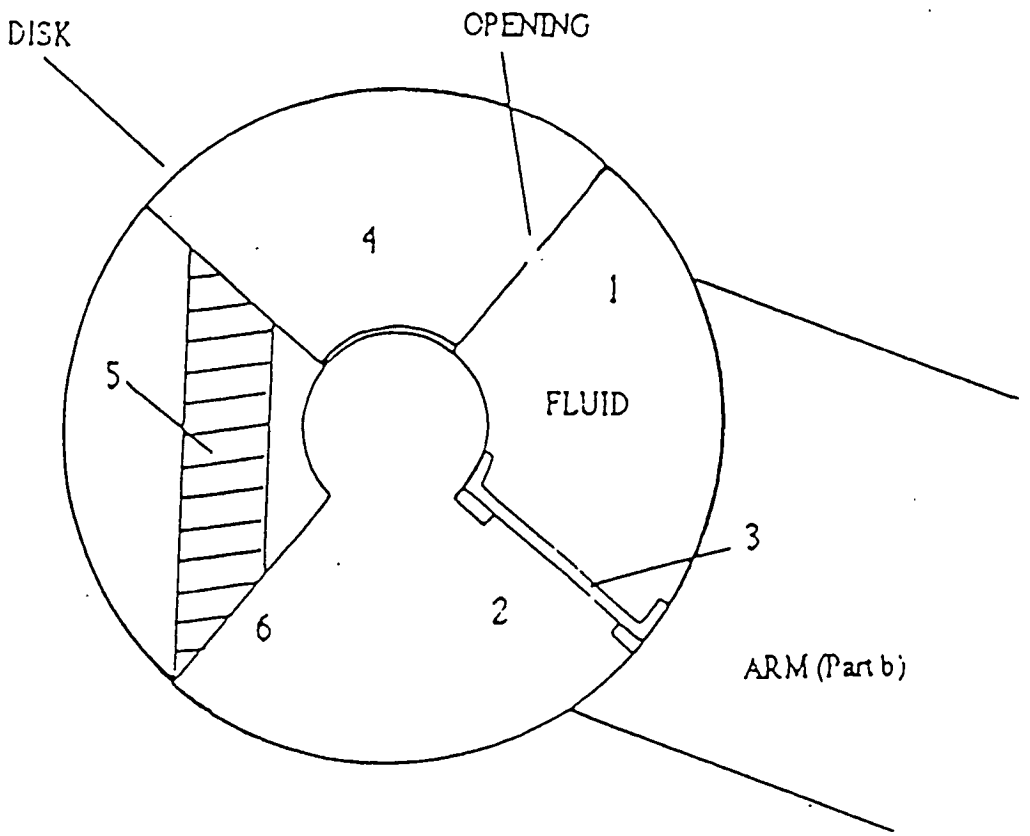

Figure 5: Conceptual View of Rotation Disk

The corresponding components of part (a) will be represented by numbers. The damping device will consist of a hydraulic fluid in a sealed compartment with only a small opening, as represented by #1. The opening will be covered with foil during Earth to Mars transfer to prevent the fluid from leaking out while in zero gravity.

Part of the wall structure of the lander will be placed against the inside surface of the disk, as represented by 2. Once the RSDS is activated, the disk will tend to rotate. Part 2 will push against part 3 which is free to slide around the inside of the disk. Part 3 will push against the fluid and the foil will break once enough pressure is created. The fluid will slowly evacuate the containment area, part 1, into another containment area, part 4, thus allowing the rover to slowly descend towards the surface. As the disk rotates, it will stretch the spring, part 5, attached to the structure of the lander wall, part 6, and the inside of the disk. Once the rover has been unlatched from the system, the spring will retract and pull the system up away from the rover. Due to lower temperatures on Mars, excess heat from the RTGs or the liquid nitrogen refrigeration unit will be channeled to the rotation disk.

Part (b) is the connection arm; it is one of the basic structural components of the system. It connects all of the constituents of the system together. It will be approximately 1 m long, 0.03 m wide, and 0.1m high. Part (c) is the latch beam. Three latches (d) are connected to this beam. It will be approximately 1.37 m long, 0.011 m wide, and 0.06 m high. Each latch will be connected to the hub of one of the rover's wheels, which will allow the rover to be held firmly in place. Part (c) also synchronizes the arms (b) and this eliminates any stresses on the rover. Part (e) is basically a shock absorber similar to those used on automobiles. It latches the RSDS in place during Earth surface to Mars surface transfer. It dampens vibration and motion in the z-direction. Part (e) unlatches to allow the system to swing towards the ground. Part (f) is also a shock absorption device very similar to (e). Part (b) is actually two beams, one inside the other, connected by (f). This controls vibration and motion in the x-direction. As can be observed, part (b) does not rest against the lander structure (h). Part (g) is another shock absorption system that lies between (b) and (h). It is basically a system of springs and rubber like pads connected to a flat plate. Part (g) dampens vibration in the y-direction. The RSDS thus allows the rover

to be held firmly in place and absorbs all the vibrations that could otherwise damage the rover. Part (i) is a joint between (a) and (b) which allows motion in the x-direction. Part (j) is a tie rod between the first two connection arms (b). It synchronizes the arms (b) and thus also helps eliminate any stresses from twisting on the rover. The total dimension of the RSDS will be approximately 1.83 m long, 1.22 m high, and 1.22 m wide. The approximate mass of the RSDS is 27.5 kg. The corresponding calculations are shown in Appendix D. It should be noted that the mechanics of the latch system has not been considered and is left to future work.

Rail Launch System

FLUID POWER

There are two basic guidance and control criteria which must be met before the DRR can be launched from the lander. First the DRR must be inclined from its initial horizontal position to the proper launch angle. Second, it must be pointed in the proper direction. Thus, in order to achieve the proper trajectory, the launch system utilized on the lander must be capable of rotation and lift.

The simplest mechanical process for guidance control involved the use of fluid power actuators. A linear actuator (cylinder) will be used for inclination of the launch system and a rotational actuator (a hydraulic motor) will be used to rotate the launch system. A fluid power system can position the platform with tolerances as precise as 2.5 micrometers. It can multiply forces simply and efficiently and is capable of providing constant force or torque regardless of speed changes. In general, a fluid power system uses fewer moving parts than comparable mechanical or electrical systems. Thus, it maximizes compactness and reliability [10].

Certain modifications need to be considered for the fluid power system to be used on the lander. Fluid power systems for general purposes do not consider their own mass as a factor. The components of the system for a low-mass criterion need to be constructed of very light-weight materials. The system will only be used for a short duration of time. It does not require extensive repeatability of its functions. By definition, fluid power systems use a working fluid to transmit power. Most systems are designed to operate with the working fluid at normal room temperatures. The average temperatures are much less on Mars than on Earth. This will not be a problem since excess heat generated by the RTGs will be dissipated to the working fluid and other components of the system. This will allow the fluid and other components of the system to operate at normal temperature conditions. The system will also be insulated by wrapping it in insulation. The suggested working fluid may be any common hydraulic fluid since the working temperature will be similar to normal working conditions. It is left to future work to determine the exact hydraulic fluid to use.

RAIL LAUNCHER:

A rail launch system was determined to be the best launch system for complying with the low mass criterion. Coordination with the design group responsible for the DRR indicated that two rails will be sufficient. Once the basic design and mass distribution within the DRR was known, design and mass estimates were determined. The length of the rails is 1.7 m. A scaled cross sectional view of the rails is shown in Figure 6. The diameter of the turret is 0.5 m. In order to reduce mass, the center of the turret is hollow. The inner diameter is 0.3 m. The cylinder will be connected 0.4 m from the base of the rails. Hinges will be located at the base of the rails and at the point of contact with the cylinder. The distance between the two rails is 0.346 m. The base of the cylinder will be supported by two braces connected to the turret. A conceptual design of the DRR rail launch system is shown in Figure 7.

The following describes the criteria used to determine the mass estimate. The length of the rail launch system will be approximately 1.7 m. The force applied from the fluid power cylinder will be located 0.4 m from the base of the launch system. This position was determined with the constraint that the turret would be 0.5 m in diameter. This diameter was chosen to be approximately the same as the DRR diameter. Another constraint considered was the maximum inclination of 30^{o} necessary for the launch system. The computational and geometrical calculations for the approximate cylinder position are shown in Appendix E. The rails were treated as cantilevered beams with their base located at the point where they connect to the turret. Using the following constraints, the approximate mass for the rails was determined. The rail configurations were basically I-beams with trapezoidal grooves constructed at the top to hold the DRR in place. The maximum deflection at the rail tip was 1.5 cm, and the material used was a strong aluminum alloy (2014-T6). The estimated mass was 3.6 kg per beam. The calculations pertaining to this estimate are shown in Appendix F. The sum of the hinges at the base of rail launch system and at the cylinder connection was calculated to be approximately 0.14 kg. The mass of each hinge was assumed to be approximately three times the mass of the pins.

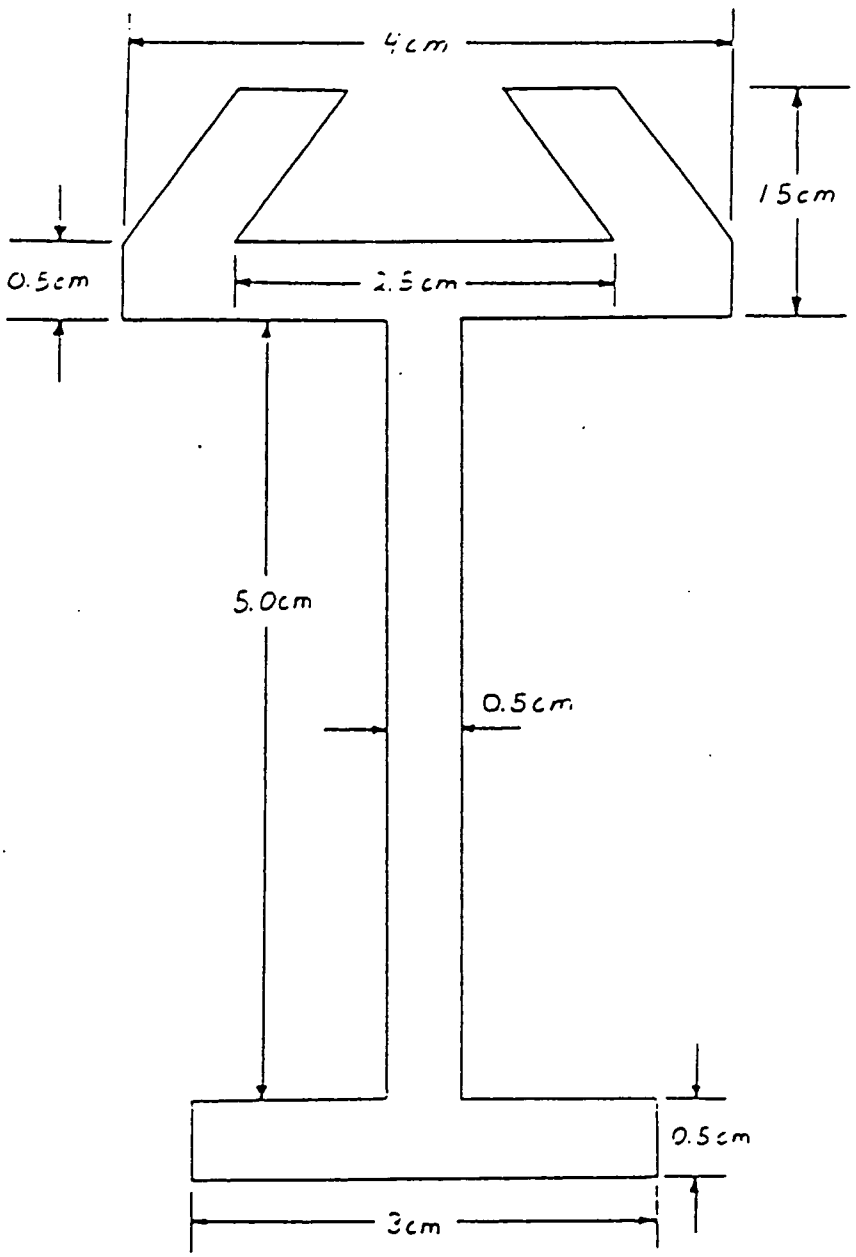

Figure 6: Cross-Sectional View of Launch Rail

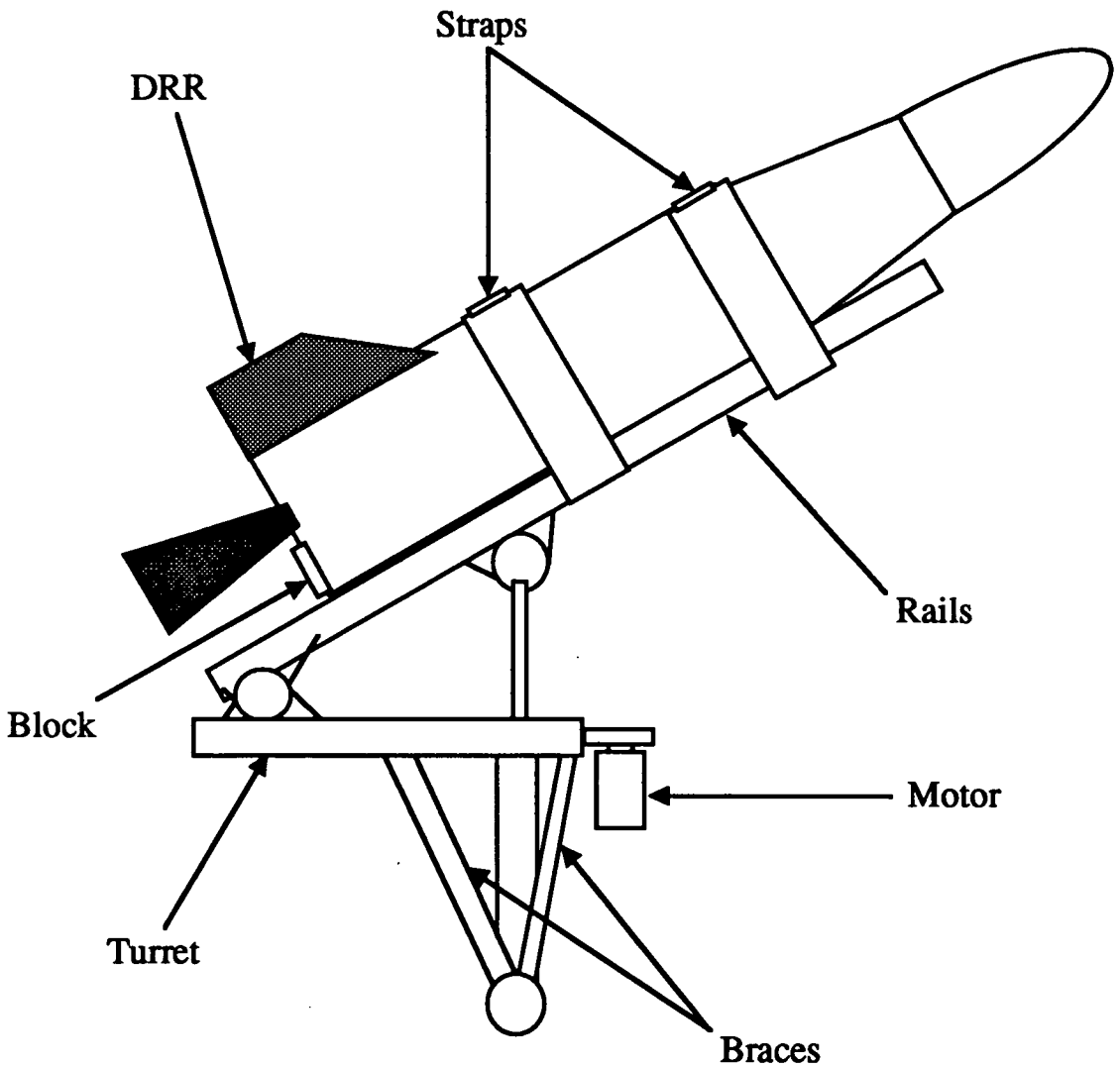

Figure 7: Conceptual Design of DRR Launch System

C-2

The mass of the turret was determined to be approximately 16.7 kg. The mass of the braces connecting the cylinder to the turret was calculated to be approximately 9.4×10^{-3} kg. The total mass of the rail launch system was calculated to be approximately 25 kg. It should also be noted that the masses calculated for this system are rough estimates and were calculated for the sole reason of determining a rough estimate. All calculations and assumptions made concerning the mass of the rail launch system are presented in Appendix G. It should also be noted that the rails will be supported by braces that will be clamped to them from the time of Earth launch until just before the implementation of the lander launch system. This will allow the system to withstand forces up to 10 G's. These braces will also dampen all shocks and vibrations experienced by the rail launch system during Earth to Mars transfer. A conceptual diagram of these braces is shown in Figure 8. The DRR will obviously be strapped to the rail launch system. There will be two straps. One will be located at the top of the DRR fins and the other at the position of the second stage combustion chamber. The straps will be fastened at the top by a pin. Once the pin is removed, springs will force the interlocking components apart thus forcing them to fall away from the DRR. The pins will be removed with the use of the lander robotic arm. A conceptual diagram of the straps and fastening system is shown in Figure 9.

From the mass distribution of the DRR and the rail launch system, the approximate force required by the linear actuator was calculated to be 1731.2 N. This would be the maximum force necessary to lift the launch system in the initial horizontal position. This estimate also takes into account that the acceleration due to gravity on Mars is 3.75 m/s^2. The calculation for the reactions on the cylinder are shown in Appendix F. Several initial cylinder specification estimates have been determined. The length of the cylinder in the retracted position is 0.3 m. This value was estimated using the constraint that the maximum angle of inclination is 30°. Treating the cylinder rod as a column fixed at one end and free at the other, the minimum diameter was determined. This minimum diameter was calculated to be 6.858×10^{-3} m for the aluminum alloy (2014-T6).

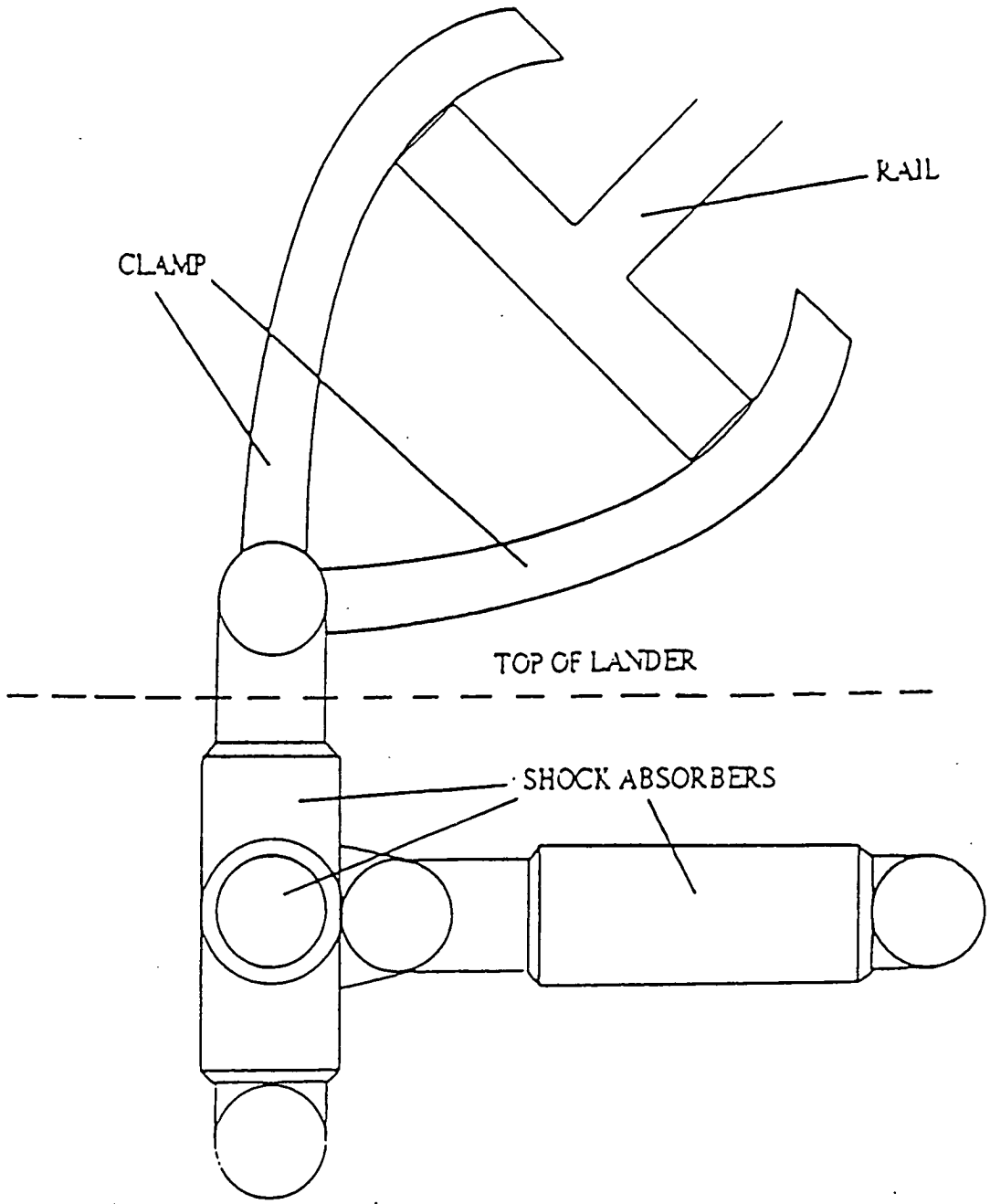

Figure 8: Conceptual Diagram of Rail Support System

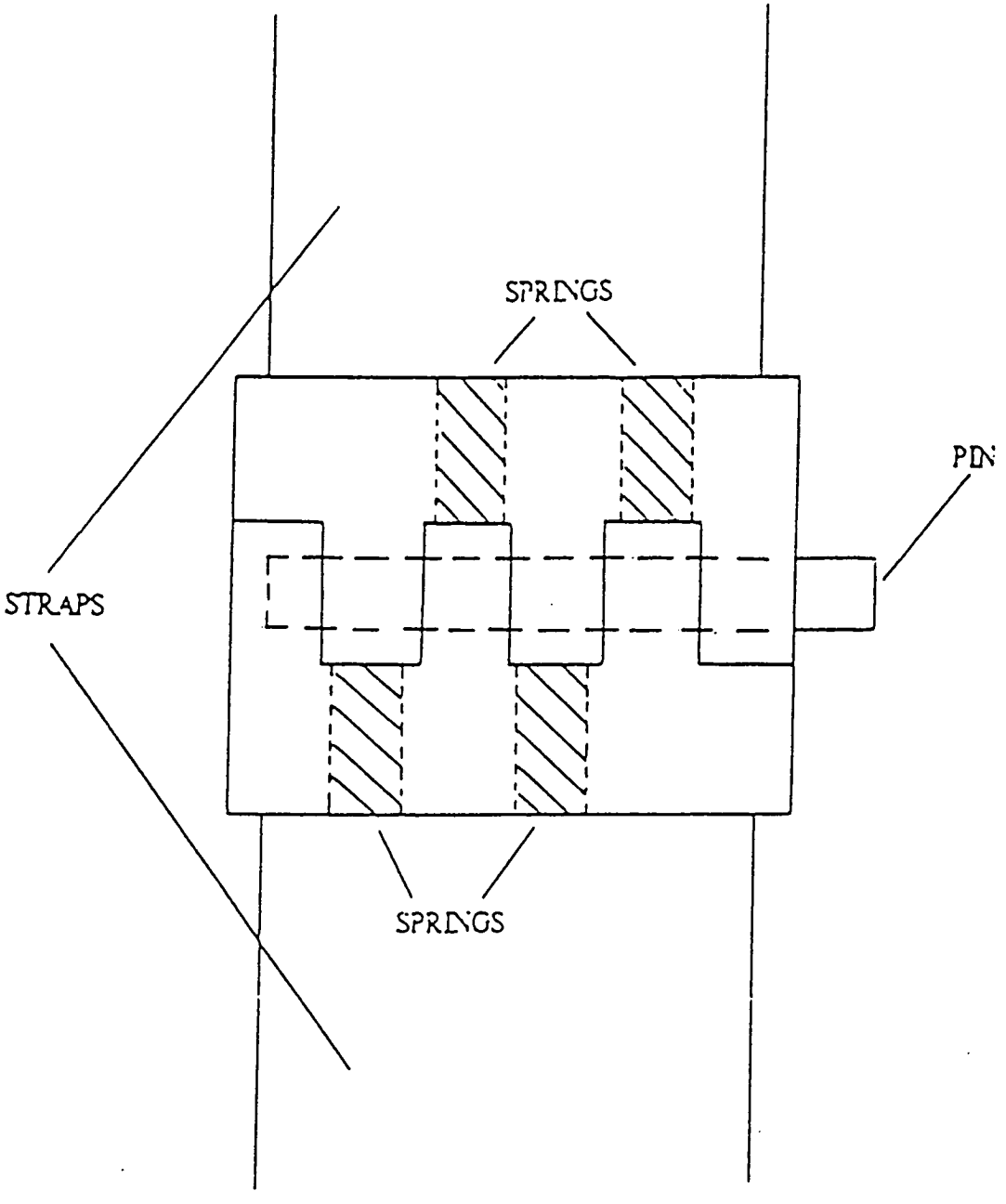

Figure 9: Schematic of Fastening System

Assuming a working rod diameter of 0.0127 m and a piston diameter of 0.025 m, the following cylinder specifications were estimated. The power requirement is approximately 55 watts for a piston velocity of 0.03048 m/s. The fluid flow rate is approximately 0.912 liters per minute and the pressure necessary is 3.55×10^6 N/m^2. The corresponding calculations can be seen in Appendix H. An approximate mass estimate for the cylinder, obtained by tripling the rod mass, is 1 kg.

From the estimated mass of the DRR and the launch system, the torque necessary to rotate the launch system was estimated. Treating the entire system as a rod fixed at one end, the moment of inertia was calculated. Estimating an angular acceleration of 0.1 rad/s^2, the torque was calculated to be 40.3 N·m. This calculation is shown in Appendix H. Once the necessary torque to rotate the launch system was estimated, the specifications for the fluid power motor were approximated. An approximate speed of rotation for the launch system is 1 rev/min. Using a gear ratio of 1:10 for the launch system turret and the motor, the speed of the motor is 10 rev/min and the torque required is approximately 4.03 N m. The corresponding power is 4.23 watts. Since the pressure of the system is 1.5×10^6 N/m^2, the corresponding volumetric displacement for the motor will be 7.137×10^{-3} liters, and the volume flow rate is 7.13×10^{-2} liters/min. All calculations pertaining to the motor are shown in Appendix I. The motor does not need to be designed for repeatability, and assuming the motor is constructed of a material with 1/2 the specific weight of conventional motors, the estimated mass is 2 kg.

The source of power for the fluid power system is the pump. From the estimated cylinder and motor specifications, the pump specifications were estimated. Desiring the speed of the pump to be approximately 114 rev/min, the volumetric displacement will be 8.005×10^{-3} liters, and the volume flow rate will be 0.912 liters/min, at a pressure output of 3.55×10^6 N/m^2. The corresponding torque is 356.2 N·m and the power required would be approximately 54.3 W. The corresponding calculations are shown in Appendix J. The approximate mass of the pump will be similar to the motor, which is 2 kg.

An electric DC motor will be used to drive the pump. Assuming a gear ratio of 1:10 between the pump shaft and electric motor shaft, the speed of the electric motor will be approximately 1140 rev/min and will produce a torque of 356.2 N m. These parameters correspond to a (6 pole) 94 watt (1/8 Hp) DC motor [11]. The corresponding calculations are shown in Appendix K.

Other components in a fluid power system include valves, connectors, and a reservoir. A servo valve is capable of controlling the amount of flow and the flow direction. This type of valve should be adequate for the needs of the system since the pressure necessary for both the hydraulic cylinder and motor remain constant. Its approximate mass is 2 kg. The connectors are simply the hoses that the fluid flows through. The reservoir is the fluid containment device when the system is not in operation. The approximate mass of the reservoir including fluid is 5.5 kg. This mass calculation is shown in Appendix L. The total mass estimate of the fluid power system is 151.5 kg.

Robotic Arm

An all-purpose lander robotic arm (LRA) will be used to collect the contingency sample of regolith. It will also be used to transfer samples from the rover and the core sampler to the DRR. Physical specifications for the LRA were found from Martin Marietta [12]. The LRA will consist of two sections each 1 m in length. This will allow the arm to reach approximately 1.3 m horizontally away from the lander on the surface. This is assuming the base of the lander is located 1 meter above the ground. The shoulder of the LRA has 2 degrees of freedom (DOF) which include pitch and yaw. The base diameter of the LRA is 24 cm. The elbow has 1 DOF which controls pitch. The wrist has 2 DOF which include roll and pitch. There are a total of 5 DOF for the LRA.

The LRA is capable of transferring a container with a mass up to 2.5 kg. The tools required for the LRA are a scoop/sieve, claw, and a grabber. The scoop can acquire about 40 cm^3 of regolith. Once the contingency sample is collected in the scoop, it will be placed in a container. When the regolith container is full, the scoop will be disengaged and the grabber will be engaged. The grabber will be used to pick up small boulders and other objects which may be beyond the function of the claw. The claw will be used to place caps on the containers and then place them on the DRR. The claw will remain attached to the arm for the remainder of the mission. One of the LRA's other functions will be to transfer samples from the rover and core sampler to the DRR. The LRA will also have other tasks to perform. It will be used to position the hoses which will carry aerogel and liquid nitrogen to the sample storage unit in the DRR and will also be used to turn on the valves for these systems. Another use for the LRA is to disconnect the straps which hold the DRR onto the rails of the launch system. A conceptual diagram of the LRA and tools is shown in Figure 10. The mass of the LRA is 26.4 kg and the power required for operation is 100 watts.

The LRA will require the use of a couple of sensory devices. Wrist mounted force/torque sensors will be used as feedback devices when manipulating an object. This will allow an estimate of the weight of the gripped object. The proper quantity of contingency samples will thus be accurately collected.

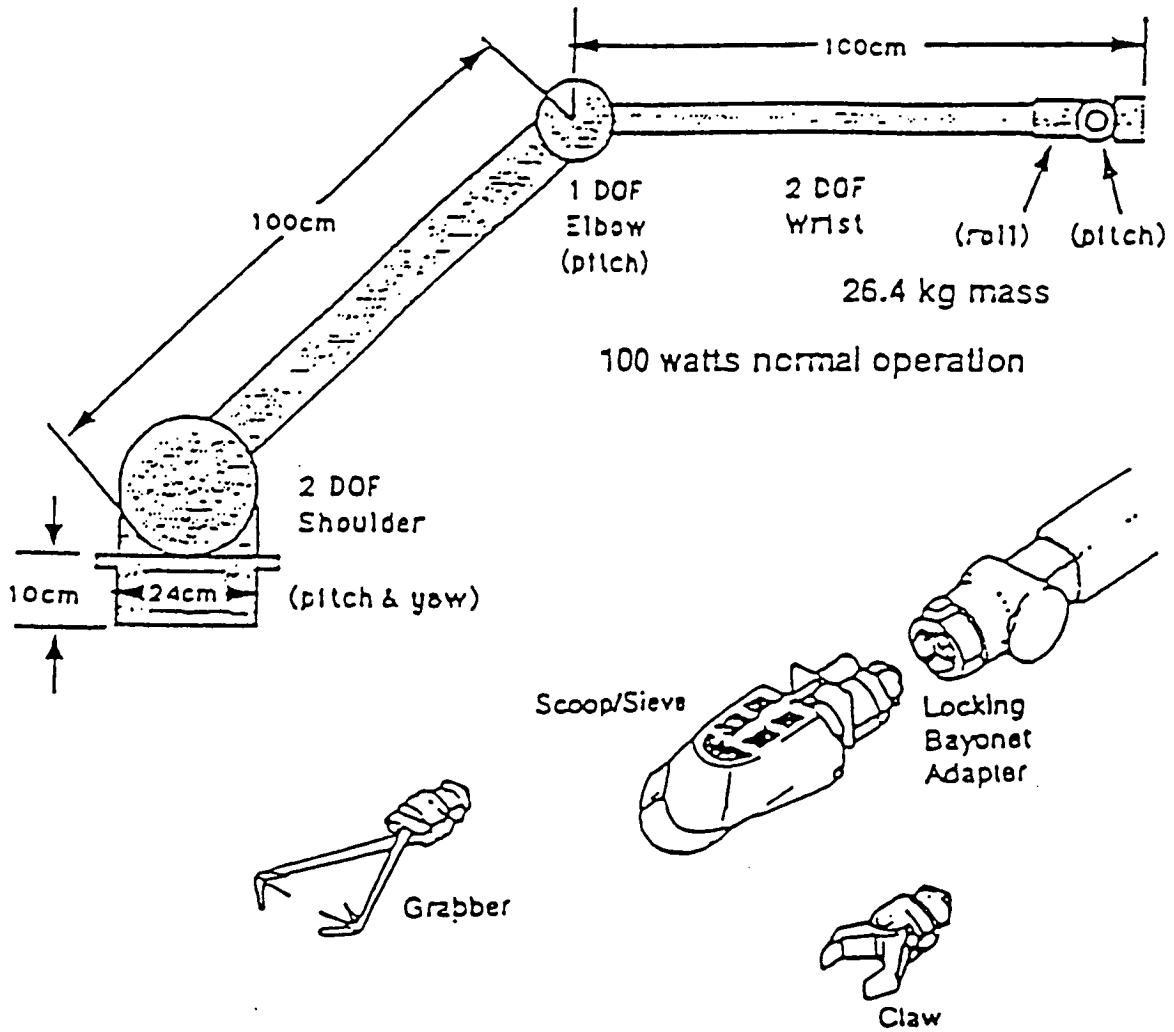

Figure 10: Lander Robotic Arm
(Ref: Martin Marietta, 1990)

An interface with an external vision system will be used to locate the initial position and orientation of an object to be manipulated. This information will guide the LRA to the proper position. Two identical cameras will be positioned atop the lander. This allows for a 3-D vision system which creates perspective and depth. This will allow the exact position of a desired object to be determined. These cameras will be positioned so as to visualize all LRA actions. The design of the cameras must reflect concern for protection from the environment, temperature extremes, and wind blown sand as did the cameras used on Viking 1. The exact design and specifications of the vision system is left to future work.

Lander Sample Acquisition

CORE SAMPLES:

The value of taking core samples has been discussed in many Mars mission reports. Some reports have said that the technology behind a core sampler is too complex to be sent on an unmanned mission. These reports imply that the mass cost in taking such a device would be too great for a system that will not even perform properly [13]. Other reports have stressed the amount of information that can be gained from subterranean samples as taken from a core sampler as opposed to surface samples. Samples taken below the surface provide much more information about the composition of the Martian terrain than surface samples. Geologists have indicated that even a core sample that is disturbed in transit would provide more information than surface samples [14]. Engineers involved with the lunar core sampler development believe that an unmanned core sampler would be able to return a sample [15]. It is for these reasons that it was decided that a core sample would be taken.

It was determined that the core sample will be taken by the lander, since early power estimates indicated that a core sampler's energy needs would be greater than the rover could easily supply. Many other published Mars missions have the core sample being taken by the rover. These missions, however, employ larger rovers than our small scale model and thus would have a larger power supply. These larger rovers would also provide a more stable base from which to take a sample. Thus, the lander was again seen as the better choice in providing a stable base. One disadvantage of taking the core sample from the lander is the contamination of the Martian surface from the heat and exhaust gases of the retrorockets. After taking both the power supply and contamination factors into account, it was decided that the lander would be the more feasible choice for the core sample collection.

In selecting a core sampler type, a total of four were examined: rotary, percussive, rotary-percussive, and thermal. The first three types can be used in either a polar or equatorial sampler, while the thermal is only applicable for an "ice" sample. The rotary

type operates by rotating into the surface to remove the core. It has the advantage of being able to take solid cores or loose, fragmentary cores. Its drawbacks include requiring a coolant system and using a large amount of power for the harder materials that might be encountered. A percussive sampler operates by hammering into the surface and forming a core. Its biggest advantage is that it requires a small power source. It is also able to pull back and cool down if the bit gets too hot. Its largest disadvantage is that, by its deign, it is only able to take solid core samples. A loose sample would slip out each time the drill rose up to hit the surface. A rotary-percussive core sampler combines properties of the aforementioned samplers by being able to work in either mode or a combination of the two. This gives it the advantage of being able to take solid or loose cores while using the mode that requires the least amount of power. It also does not need an active coolant system. The major disadvantages are increased complexity and increased mass over either the rotary or percussive alone. Finally, the thermal sampler uses a current to heat and melt the circumference of the core. This type has very low mass, complexity, and power needs. Unfortunately, it can only drill through ice and would be stopped by any solid rock material.

In evaluating the above types, it was decided that the rotary-percussive type would be the most effective type for both the equatorial and polar lander. The major factor in this decision was the versatility of the model. If the type of material to be encountered was known the core sampler could be designed specifically to meet these needs. This would allow the lowest possible mass and power needs. We do not, however, know what type of material is going to be found and must try to meet all possibilities. The rotary-percussive sampler meets this criterion the best. The thermal sampler was quickly dropped from consideration as it was the least versatile. It would only be effective if we could ensure a polar sample of only ice and maybe some small particulate matter.

Drawings of the prototype rotary-percussive sampler can be found in Figure 11. The actual drilling mechanism can be divided into three parts: the outer core, the inner core, and the bit. The bit is attached to the outer core. The outer core works in either the rotary or percussive mode to produce the core. The bit cuts a ring or "kerf" of material around the core sample. The inner core collects the sample and moves independently of the outer core.

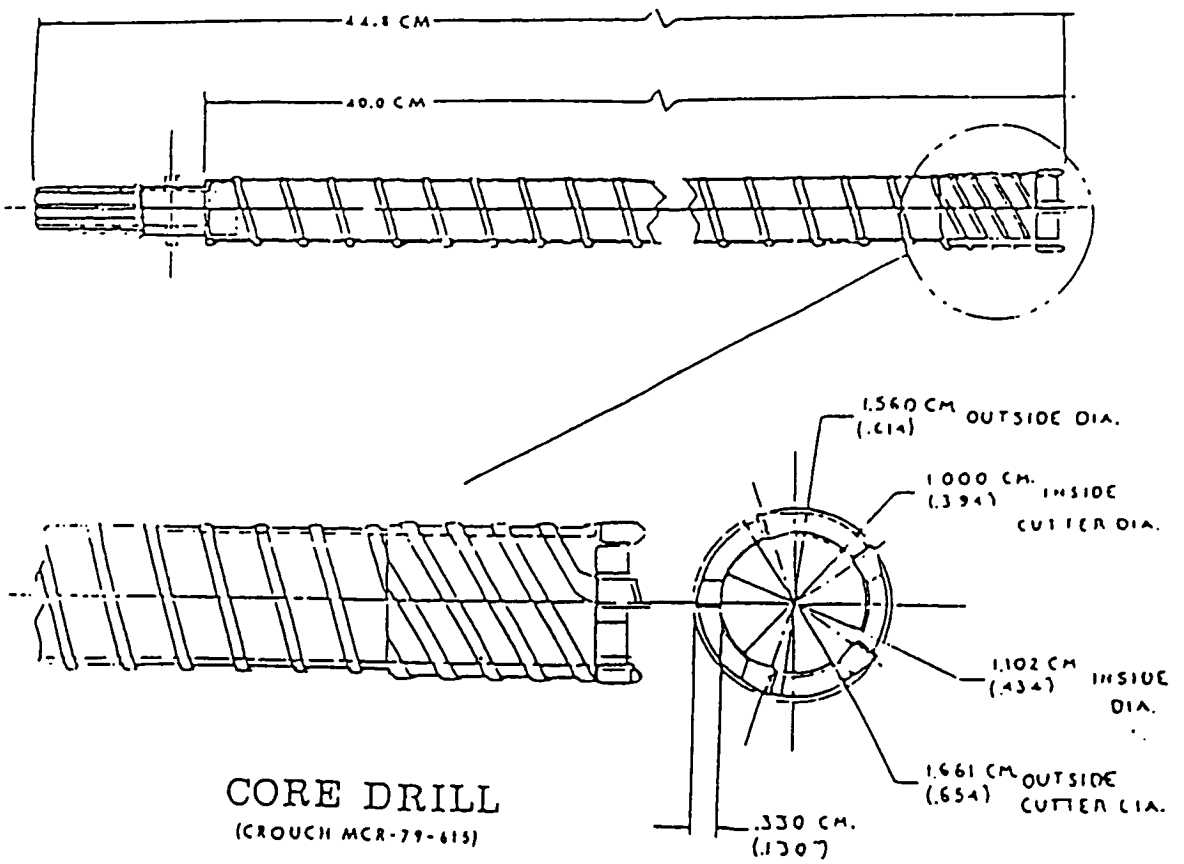

Figure 11: Core Drill Schematic
(Ref: Crouch, 1980)

The drill mechanism is powered by a motor directly above it. The motor and drill mechanism are lowered from the lander to the Martian surface by a support mechanism.

The dimensions of the sampler were dictated by the dimensions of the core to be taken. The core sample will be 40 cm in length and 1cm in diameter. The length of the core should be as long as possible to retrieve the most amount of information about the Martian surface. Limitations were put on this by the dimensions of the DRR. It was determined that a 40 cm sample within its container could be fit into the DRR cargo area. A possibility of increasing the length would have resulted from taking the core in multiple sections. This was decided against because of the amount of complexity that it would add to the sampler. A further consideration was that the chance of sample disturbance increases with multiple sections. The sample diameter was kept small to keep mass low. This also reduces the power needs as the power is proportional to the area of the kerf [15]. A further consideration is that it increases the ability of the sampler to retrieve the core. This is because a large part of the retrieval depends on the frictional forces between the sample and the collection tube. By decreasing the diameter the mass is decreased faster than the surface area of the sample [14].

Many materials were examined in selecting those to be used for the core sampler. The general criteria used in selecting these materials was light weight, high reliability, and minimal contamination. Using a minimum of materials helps to keep the number of contaminants low. Another factor was that the drilling will be taking place at low temperatures. The effect of low temperature needed to be assessed it the design of the components along with the heating associated with the drilling process. Additional factors will be added as each of the major components is considered.

To keep the contamination low it was decided that the same material would be used for both the inner and outer cores. Beyond the general factors, the criteria used was that it should have high shear strength, high elastic modulus, low temperature fracture toughness, low thermal conductivity, and a low ductile-to-brittle transition temperature. The first three criteria relate to the strength of the material under the forces that will be experienced in the drilling process. The last criterion ensures that the material will remain ductile at low temperatures and will not shatter. The low thermal conductivity is important in preventing

thermal contamination to the core sample. Since this is a current technology mission we looked at metals and alloys, ordinary plastics, and polymer matrix composites. A titanium alloy, Ti-6-4, was selected, largely based on past experience. This material was used successfully on the core samplers of the Apollo missions [16]. Titanium is often used for cryogenic applications requiring strength. It also has a very low conductivity. It does have the disadvantages of the possibility of brittle failure and relatively low specific stiffness which means the walls of the cores will have to a little thicker and heavier. Its past success, however, outweighs these drawbacks.

In selecting the bit material, additional criteria were as follows: high hardness for durability in the rotary mode, high impact strength and fracture toughness for the percussive mode, high resistance to thermal shock because of the great variance in temperatures the bit will experience, and a coefficient of thermal expansion that is similar to that of the outer core. The last reason is to ensure that in the heating and cooling process that occurs in drilling the bond between the bit and the core does not loosen from the variance in component sizes. The material selected for our drill bit was an alloy of tungsten carbide with 13% cobalt. The standard bit material for a rotary-percussive drill and the one used on the Apollo drill was tungsten carbide. This is one of the hardest carbides with a strength approaching diamond. It is generally mixed in an alloy of 5 to 15% cobalt to increase ductility and fracture toughness. The Apollo drill used an alloy of 13% cobalt and some chipping was experienced in the percussive mode. This chipping, however, was not enough to prevent cores from being taken and in this mission only one core will be taken [14]. Other materials were considered, but none had the strength of the tungsten carbides. The possibility of putting diamond on the cutting tip of the bit was suggested, but diamond is too brittle to be used in a percussive mode and becomes even more brittle in cold temperatures.

The power needed for drilling was found to be a function of the kerf area and the material being cut. The power requirement of the core sampler when used in the rotary mode is shown in Figure 12.

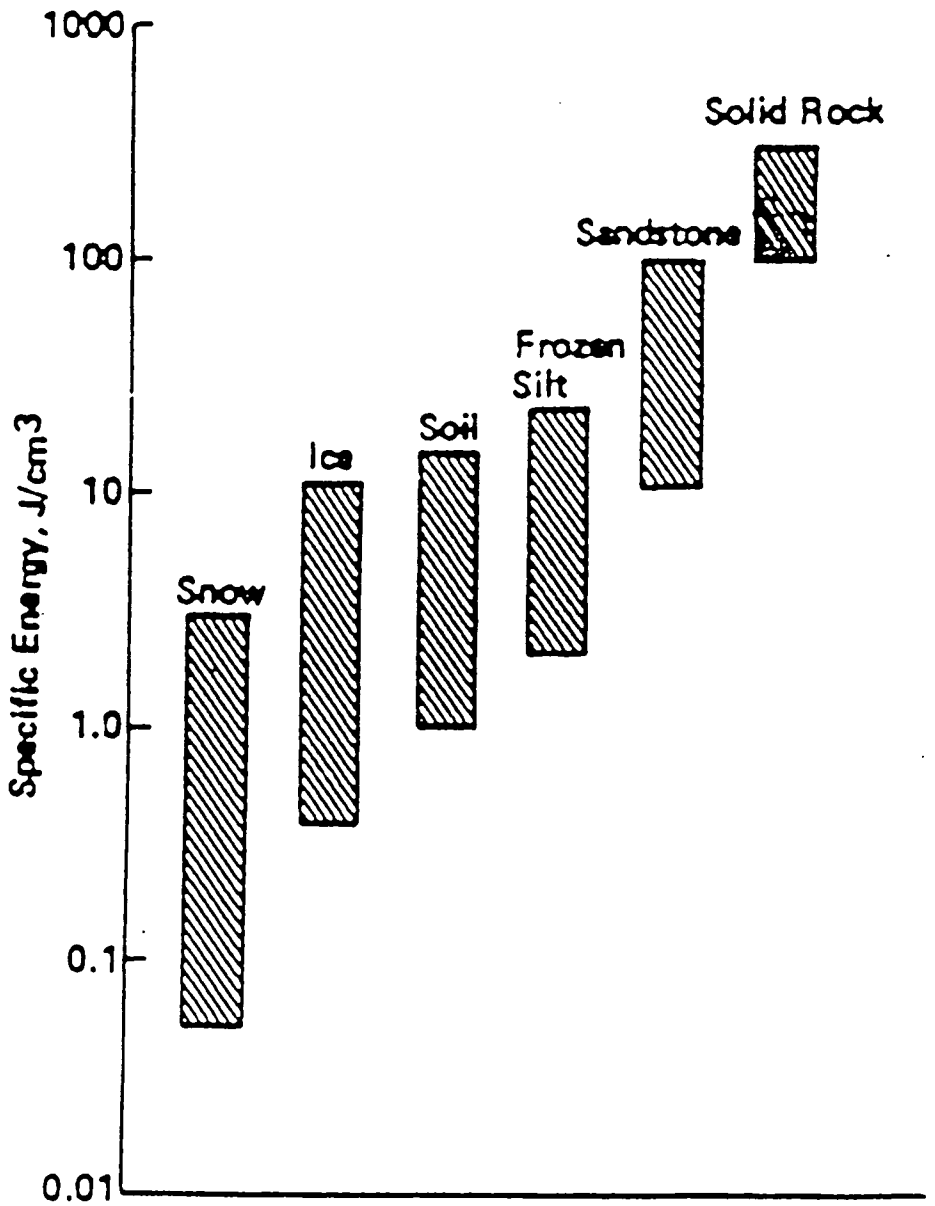

Figure 12: Specific Energy for Rotary Cutting of Various Materials
(Ref: Amundsen, 1987)

The power for use in the percussive mode is a constant value of approximately 170 W. The total power allotted for drilling is 400 W. The actual drilling rate and thus power required will be controlled by an artificial intelligence system designed by Martin Marietta. This system constantly monitors the drilling rate, power draw, and heating of the core bit and core tubes. With this information it determines the optimum drilling rate and proper mix of rotary and percussive modes. The last piece of input is used to monitor heating and determine if the process should be slowed or stopped to allow cooling and maintain the thermal integrity of the sample [14].

The total mass of the core sampler and deployment mechanisms is estimated to be 20 kg. This is based on the mass figures from the Apollo samplers and from scaling done on current prototype sampler masses [17,15]. For sample return, the inner core will have a mass of approximately 36 g. Using average figures of density of rock (3000 kg/m^3) the mass of the equatorial sample was found to be 95 g. An equivalent calculation with the density of ice (1000 kg/m^3) gave a mass of 32 g. Thus the total equatorial and polar core sample return mass was 131 g and 68 g, respectively.

ATMOSPHERIC SAMPLES:

An atmospheric sample contains information that is important in analyzing the surface samples taken. This information is especially important in the case of samples that have been exposed to the atmosphere for an extended period of time. Our mission will take two atmospheric samples. The first, a contingency sample, will have a volume of 160 cm^3 and will be taken as soon as it is determined that any trapped upper atmosphere gases have had a chance to escape and after the lander has cooled to ambient conditions. Because of the latter, it is important that the atmospheric sampler be kept as far as possible from any sources of heat such as the MOD-RTGs. The second sample of 100 cm^3 will be taken sometime after the contingency sample. The second sample will be the one returned to Earth and the contingency sample will only be returned it the rover is unable to complete its mission.

The atmospheric sampler will consist of two hollowed blocks of aluminum and an electronic port system. The interior of each block will be lined with teflon to prevent contamination. The chambers will be kept completely evacuated until the sample is to be taken. In taking the sample a cover plate will be removed from the opening of the appropriate container. The container will remain open for approximately 20 minutes to allow the atmosphere to fill the reservoir and to allow the container to return to ambient conditions after the release of the vacuum. The containers will be sealed with a cover of indium. This element creates an almost impermeable seal and has proven itself effective in the Apollo missions [13].

Lander Descent And Landing

Where a sensible atmosphere is encountered (approximately 250 km altitude), the LFS will orient itself so that the aeroshell faces the direction of travel. The actual lander is upside down so that the retrorockets face upward. At this point, the LFS will be traveling between 15,000 and 16,000 km/hr. The heat generated by the atmospheric drag will erode the aeroshell's silica material. The aeroshell will be shaped to produce some aerodynamic drag.

At approximately 6.0 km the speed of the lander is estimated to be 1600 km/hr. A mortar deployed pilot-chute will pull out the main deceleration parachute. Earlier deployment of this parachute will not be possible because of the lander's high speed. For instance, speeds in excess of 2000 km/hr can destroy the parachute canopy due to large aerodynamic forces. After the deceleration parachute has fully opened, the shock on the system will trigger explosive bolts, and the aeroshell will drop away. The lander will have some initial oscillation when the parachute opens; however, the parachute will dampen it to zero oscillation at time of retrorocket firing.

The parachute will slow the lander's fall to a terminal velocity of approximately 60 m/s. Since the parachute alone will not sufficiently decelerate the lander, four retrorockets will be fired. Calculations indicate that the retrorocket engines will be ignited at approximately 1.6 km altitude to provide a soft landing. The landing gear will be equipped with piston shock absorbers to cushion the landing [5].

LANDER AEROSHELL:

The aeroshell to be used by the lander is based on the aeroshell used in the Viking missions. The lander's aeroshell, however, will have a 4.72 meter outside diameter and a 1.93 meter total height (refer to Figure 13), as compared to the Viking's 3.5 meter by 1.7 meter aeroshell [18]. A direct scaling by surface area of the Viking aeroshell mass to the surface area needed by the lander resulted in a mass estimate of over 300 kg. Since the lander will use modern materials, the mass estimate can be reduced to below 300 kg.

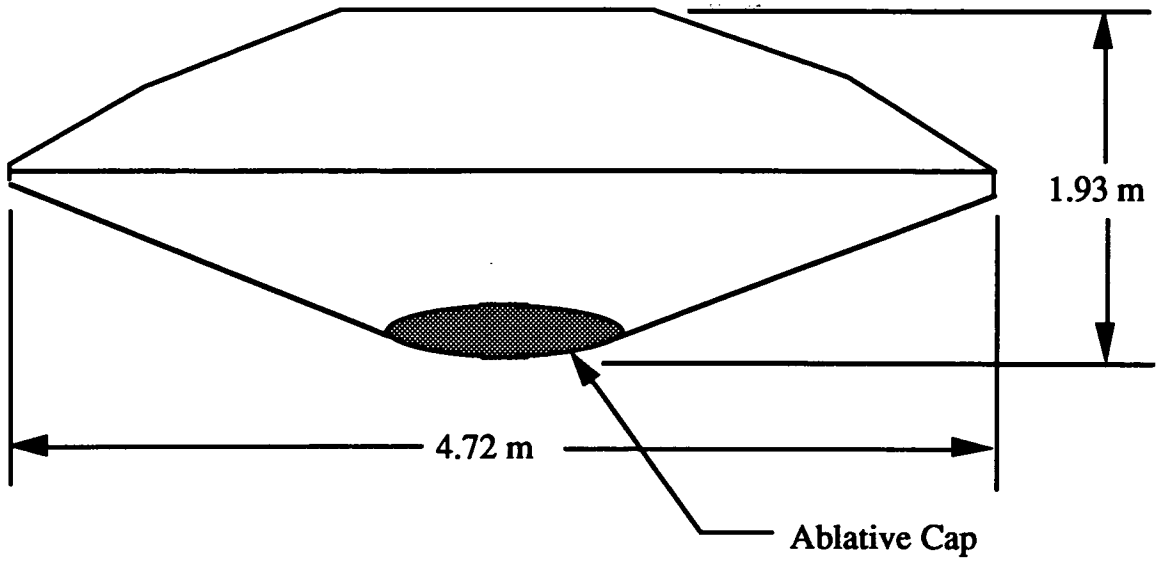

Figure 13 : AEROSHELL CONFIGURATION

The primary material to be used in the lander's aeroshell will be FRCI - 12, a silica based insulation with a density of 252.6 kg/m^3. For one time use, the maximum usable temperature of FRCI - 12 is 1755 °K, but the maximum temperature on the aeroshell can reach 2000 °K. In the region where the temperature will exceed 1755 °K, an ablative material, AVCO H/C 9, will be used. The size and thickness of the AVCO ablative cap must be kept to a minimum, however, due to the high density (513 kg/m^3) of this material. Even using an ablative cap, the total aeroshell density should be less than the aeroshell density in the Viking system, allowing an estimated lander aeroshell mass of 300 kg [18].

The aeroshell will no longer be useful at an altitude of 6.0 km above the landing site and will therefore be discarded. At the time of aeroshell separation from the lander, the lander will have a velocity of approximately 400 m/s. To ensure proper aeroshell jettison, explosive bolts will detach the aeroshell from the lander and small explosives placed within the aeroshell will break the aeroshell and propel the fragments away from the lander. After aeroshell jettison, the lander parachute system will deploy to further decelerate the lander.

PARACHUTE:

Based on the Viking system, the lander's parachute system will be mortar deployed using a pilot-chute to extract a single disk-gap-band main canopy as seen in Figure 14. By scaling the Viking system components to sizes necessary for the lander, it was found that the mortar deployed parachute system will have a mass of 70 kg. The lander's parachute system will contain a 24.4 meter diameter Kevlar main parachute.

Again, using the Viking mission as a model, the deployment of the parachute system will initiate with the mortar firing the pilot-chute into the slip stream at approximately 5275 m above the landing site. At the time the mortar is fired, the lander velocity will be between 430 m/s and 168 m/s [18]. At these velocities, the opening shock on the parachute could be as high as 30 g's. Elastic nylon suspension lines and a shock absorbing bridle assembly will reduce the shock experienced by the lander to under 10 g's.

The parachute system will be discarded at an altitude of 1600 meters above the landing site. At the time of parachute release, the lander have a velocity of 60 m/s. The parachutes will be released by the detonation of explosive bolts at the connection of the bridle assembly to the lander. Rockets will then provide the final deceleration for a soft landing.

The parachute used to decelerate the lander must posses high structural strength to accommodate inflation loads without exceeding weight and volume restrictions. Consequently, a material with a high strength-to-weight ratio which can sustain its strength at high temperatures and high aerodynamic pressure loadings was chosen. The parachute material best suited for decelerating a large mass at high velocity is Kevlar-29 which is produced by E. I. DuPont de Nemours & Company. Kevlar is an aramid fiber that, with the same ultimate strength, has less than one-half the weight and one-third the bulk of nylon materials.

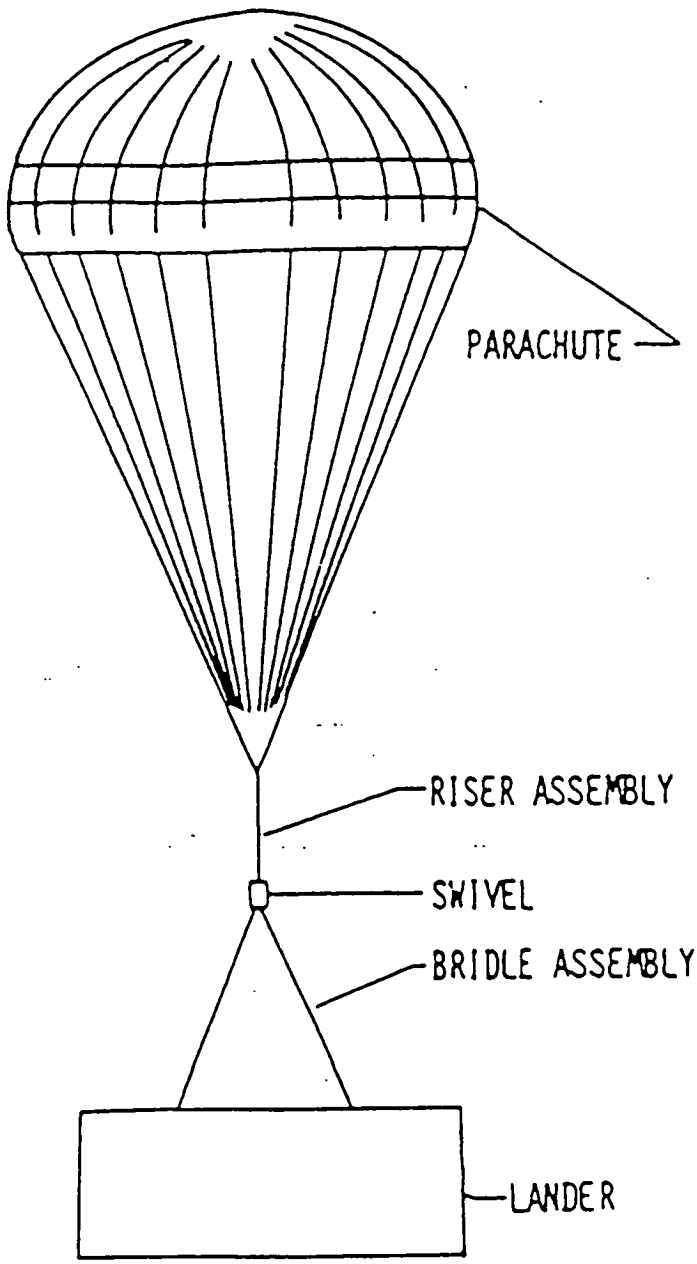

Figure 14: Deployed Parachute System Configuration
(Ref: Lau, 1970)

These characteristics have made Kevlar-29 a very desirable material for use in our deceleration system. The graph in Figure 15 compares tests of parachute strength-to-weight ratios for all-Kevlar, all-nylon, and nylon/Kevlar parachutes as a function of canopy diameter. For canopies of equal diameter, the all-Kevlar parachute consistently achieved the highest strength-to-weight ratio. This is because Kevlar has an ultimate tensile strength of 1.92×10^6 Pa while nylon has one of 5.60×10^5 Pa.

The parachute fibers must be able to physically withstand high temperatures since the temperatures are expected to reach between 230 and 290°C. Studies have shown that Kevlar fibers are more resistant to aerodynamic heating than nylon fibers. Tests also show that nylon parachute components have melted due to stagnation temperatures of 260°C at Mach 3. Kevlar parachute components subject to the same aerodynamic heating experienced no failure. Kevlar is much more resistant to strength degradation at elevated temperatures; it retains half its strength at 290°C, the temperature at which nylon fails completely [19].

Due to the high parachute deployment speed, attention must be given to supersonic characteristics of the parachute. A parachute traveling at supersonic speeds must provide high drag for its weight. The parachute structure must withstand very high canopy pressure loading and aerodynamic heating. Since the parachute will slow the lander down to subsonic speeds, the parachute must operate efficiently for both supersonic and subsonic speeds. For supersonic parachutes, it is necessary to swallow the normal shock wave and contain it in the mouth of the parachute. In order to swallow the shock wave, all of the air mass entering the parachute must pass through the parachute. Therefore, supersonic parachutes are constructed with higher canopy porosity than subsonic parachutes. They are also designed to allow less mass flux to pass out of the canopy at the skirt so that the positive pressure differential at the skirt will cause it to remain fully inflated.

Since high drag efficiency is required at both supersonic and subsonic speeds, conical ribbon parachutes were chosen over special supersonic parachute configurations.

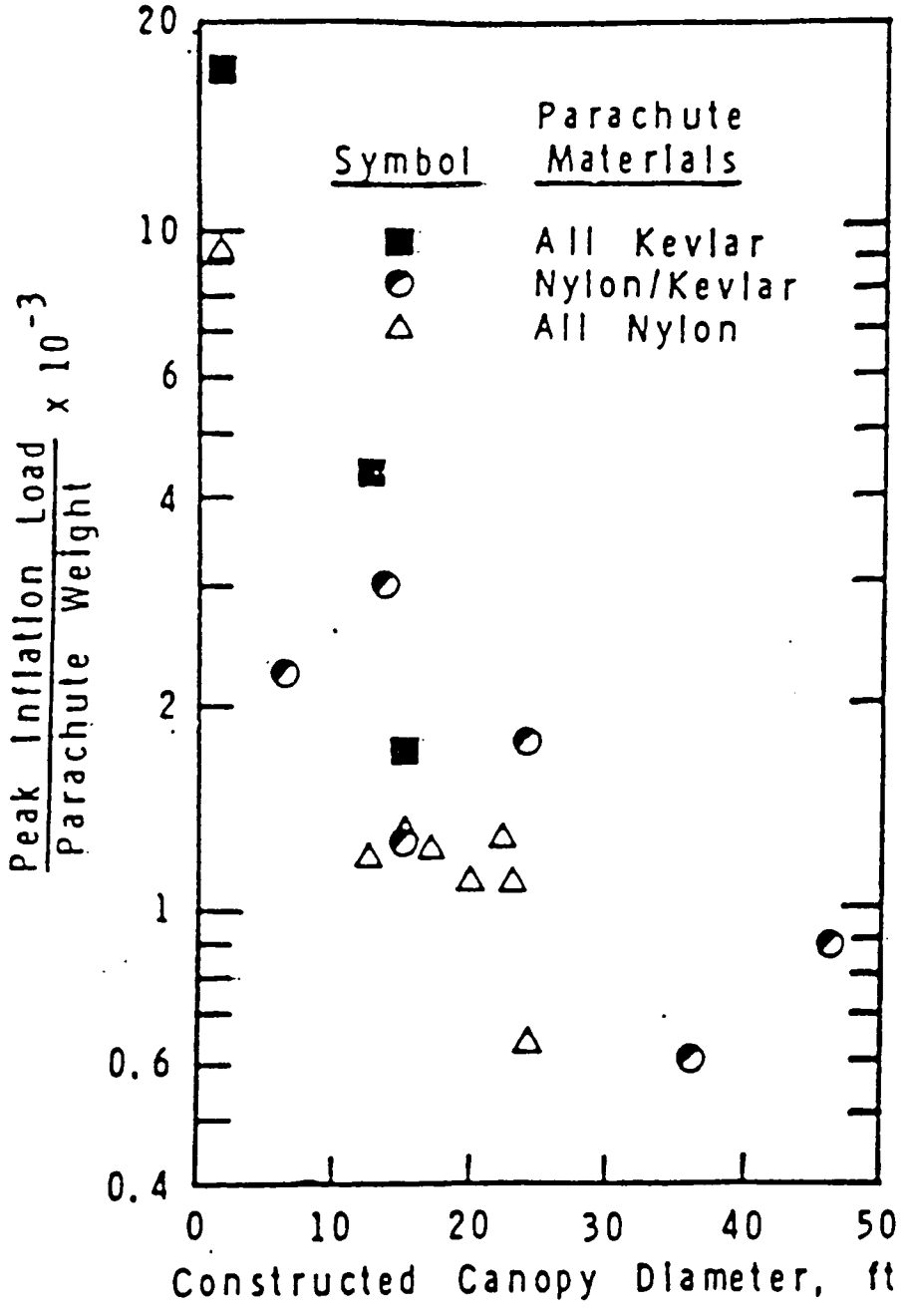

Figure 15: Tested Parachute Strength to Weight
(Ref: Peterson, 1987)

The overall efficiency of a ribbon parachute being used for supersonic and subsonic speeds will be greater than that of a supersonic parachute. This is because the ratio of inlet area (skirt) to outlet area (vent area plus porosity) needed to swallow the shock wave is a function of Mach number. Therefore, supersonic parachutes perform well only over a limited range of Mach numbers. But at lower Mach numbers, performance is reduced because the shock is discharged. Drag efficiency is usually lower than that of the conical ribbon parachute at subsonic speeds because of the higher porosity designed into the canopy [20].

RETROROCKETS:

A nitrogen tetroxide oxidizer (NTO) and hydrazine fuel (MMH) was chosen as the retrorocket's propellant. The propellant was chosen for its storability and for its high Isp value. Storable propellants do not require complicated thermal management systems (i.e., refrigeration systems) which would considerably increase the lander's overall mass.

The tank volumes for the oxidizer and fuel tanks were calculated to be 0.0544 m^3 and 0.0560 m^3, respectively. The spherical storage tanks have inner diameters of approximately 0.47 m. These values were based on a propellant mass of 116.0 kg of which 48.3 kg is MMH and 67.7 kg is NTO. These calculations are based on a mixture ratio of 1.4 (oxidizer/fuel). In order to minimize the overall mass, the propellant tanks will be composed of a carbon composite material.

A program was developed that calculated the burn time, the engine fire altitude, and the mass flow rate of a single engine. Even though the actual lander will have four retrorocket engines, the results of this program are still valid. The results were based on the following assumptions: a propellant I_{sp} value of 300 seconds, an initial lander velocity of 60 m/s downward, a zero landing speed, a lander mass of 1122 kg, a frontal area of 9 square meters, a drag coefficient of 1, and a thrust-to-weight ratio of 1.1. Using these values, the burn time, engine fire altitude, and mass flow rate were calculated to be approximately 73.3 seconds, 1.6 km, and 1.58 kg/s respectively. The program is shown in Appendix M.

The thrust force for each of the four engines was calculated based on center of mass calculations. More detail on the center of mass locations will be provided in the mission integration section. In order to eliminate any moments about the center of mass, each engine will have a different thrust value since the center of mass is not at the geometric center of the lander. A program was used to calculate the thrusts based on three equations: force equation and two moment equations (see Appendix N for program listing). The thrust force for engine four was incremented in steps of ten Newtons and the thrusts for the other three engines were calculated (this method was necessary because there were only three equations for four unknown thrust forces). The most reasonable thrust forces were chosen for the engines. In other words, the thrust force of each engine was chosen so that it would make a meaningful contribution to the overall thrust of the propulsion system. In case of single engine failure, the remaining engines must make up the additional thrust force and stabilize any moments.

After the thrust forces were known, the equivalent exhaust velocities, mass flow rates, and total propellant mass burned during firing were calculated for each engine. The pressure ratio, P_e/P_o, was estimated based on the atmospheric conditions on the surface of Mars. Based on the Galileo spacecraft 400 N MMH/NTO thruster, the chamber pressure was estimated to be 0.7 MPa [21]. The average surface pressure of Mars is approximately 7 millibars (700 Pascals). In order to optimize thrust, one must assume that the exit pressure (P_e) is approximately equal to the atmospheric pressure (P_a). Then the P_e/P_o ratio is 0.001.

In order to optimize the area ratio, one must differentiate the thrust coefficient equation with respect to pressure ratio, P_e/P_o. The thrust coefficient, C_τ, is

$$C_\tau = \sqrt{B\left[1 - x^{\frac{\gamma-1}{\gamma}}\right]} + \left(\frac{P_e}{P_o}\right)\left(\frac{A_e}{A^*}\right) - \left(\frac{P_a}{P_o}\right)\left(\frac{A_e}{A^*}\right) \qquad (2)$$

where

$$B = \frac{2\gamma^2}{\gamma - 1}\left(\frac{2}{\gamma + 1}\right)^{\left(\frac{\gamma+1}{\gamma-1}\right)}, \tag{3}$$

and

$$x = P_e/P_O. \tag{4}$$

Differentiating the thrust coefficient with respect to x gives the optimum area ratio, A_e/A^*.

$$\frac{A_e}{A^*} = \frac{B\left(\frac{\gamma-1}{\gamma}\right)x^{\frac{1}{\gamma}}}{\sqrt{2\left[B\left(1 - x^{\frac{\gamma-1}{\gamma}}\right)\right]}} \tag{5}$$

With γ = 1.26 (for MMH/NTO propellant) and x = 0.001, the optimum area ratio is approximately 60.

For all four engines, the throat area, A*, is

$$A^* = (c^*) \times \frac{m}{P_o} \tag{6}$$

where c* is the characteristic velocity. For the MMH/NTO propellant the characteristic velocity is approximately 1977 m/s [22]. Thus, the throat and exit areas were calculated for each engine nozzle.

The engine chamber area for each engine was found by assuming a chamber gas Mach number of 0.4 [23]. The area ratio, A_C/A^* was obtained by,

$$\frac{A_c}{A^*} = \frac{1}{M_c}\left[\left(\frac{2}{\gamma+1}\right)\left(1 + \frac{\gamma-1}{2}M_c^2\right)\right]^{\frac{(\gamma+1)}{2(\gamma-1)}} \tag{7}$$

where A_C is the chamber area, A* is the throat area, M_C is the gas Mach number in the chamber, and γ = 1.26. This provided an area ratio of approximately 1.61. The program in Appendix N calculated the parameters listed in Table 5.

Table 5 : Engine Parameters

	Engine 1	Engine 2	Engine 3	Engine 4
Engine Mass (kg)	4.0	4.0	7.0	7.0
Thrust (N)	113.8	115.9	1929.2	2490.0
Mass Flow Rate (kg/s)	0.03867	0.03938	0.65551	0.84608
Propellant Used (kg)	2.83601	2.88839	48.07509	62.05116
Equivalent Velocity (m/s)	2943.0	2943.0	2943.0	2943.0
Throat Area (m^2)	0.00011	0.00011	0.00185	0.00239
Throat Diameter (mm)	11.79214	11.90054	48.55109	55.15868
Exit Area (m^2)	0.00655	0.00667	0.11108	0.14337
Exit Diameter (mm)	91.34150	92.18119	376.07511	427.25733
Chamber Area (m^2)	0.00018	0.00018	0.00298	0.00385
Chamber Diameter (mm)	14.96254	15.10009	61.60442	69.98852

A gimbal on each retrorocket engine will be used to change the thrust vector. This will be useful in quick attitude adjustments of the lander during descent. A gimballed engine system has been shown to have negligible losses in specific impulse [24]. Therefore, the presence of this system in the calculated parameters above has been omitted.

LANDING GEAR:

In order for the lander to achieve a safe landing on the Martian surface, several considerations must be addressed. The lander must remain stable through both vertical and horizontal structural vibrations caused from the impact from landing. These vibrations can cause detrimental effects on the lander and its external structure. In addition, several subsystems require motion of their parts such as the robotic arm and the launcher. Other systems generate vibrations indirectly through moving internal components. One example of this is the on-board computer. As a result, structural noise can be produced. The vibrations of the systems can be amplified as they travel through the lander; structure-borne noise is then produced. Also, relatively stationary systems attached to the lander structure can vibrate and add to the structure noise [25]. As a result, an adequate shock system will be required to ensure the stability of the lander.

The lander will utilize a piston shock system similar to that used by aircraft. The piston will consist of two struts - with one fitted into the other. A cushion of air, located in the outer strut's chamber will compress as the inner strut becomes depressed during landing. The strut stroke determines the maximum distance that the inner strut can depress inside the outer member, allowing for enough space for complete compression. This value is determined by the equation:

$$d=\frac{(1.2\times v_o)^2}{2ng} \tag{8}$$

where v_0 is the final velocity of the lander, n-the load factor, and g-the acceleration due to gravity. The load factor for aircraft is set by Federal Aviation Administration (FAA) regulations to be approximately 2.5. This factor will be applied to the lander's piston system. Estimating the lander's final velocity to be 3 m/s, the strut stroke will be 26 cm.

The diameter of the inner strut is determined with the equation:

$$D=\sqrt{\frac{2nmg}{\pi\times P}} \tag{9}$$

where P, the chamber pressure, is estimated to be 2.11 MPa. Assuming that each of the four piston struts will be capable of supporting the full lander mass (m=1050 kg), the inner strut diameter will be approximately 8.81 cm. The area of the surface of the inner strut will be 60.96 cm^2. This is determined from the inner strut diameter and the equation:

$$A_s=\frac{nmg}{P}=\frac{\pi D^2}{4} \tag{10}$$

The force applied on each strut (Fs) will depend on the surface area of the inner strut and the inner chamber pressure:

$$F_s=P\times A_s \tag{11}$$

This force will be approximately 128.8 MN. As the struts depress upon landing, the deceleration force applied on each strut will about 10.3 kN. This assumes that each of the four piston shock struts will carry the full mass of the lander.

One criteria for the piston shock system is that the lander must maintain stability in attitudes up to 10° from the horizontal. Each piston shock will be supported on a foot pad estimated to be 44.1 cm in diameter. A foot pad of this dimension was chosen so that it is five times the size of each inner strut (8.81 cm). This will ensure stability of the lander at any attitude up to 10°. Each foot pad and the strut system will be constructed from aluminum to allow for a strong, lightweight system. Because the lander will achieve a "soft" landing of approximately 3 m/s, heavier and stronger materials such as steel will not be necessary.

When the lander is encapsuled inside the aeroshell during the descent stage, the landing gear will be retracted. The foot pad will be folded towards the outer strut member. The struts will be folded inboard to the lander (refer to Figure 16).

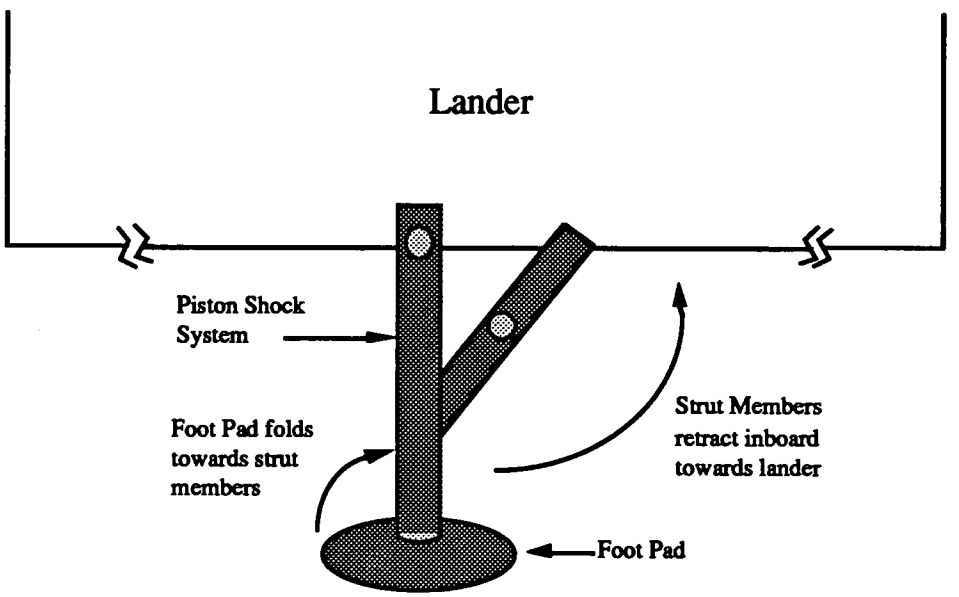

Figure 16: RETRACTION CAPABILITIES OF THE LANDING GEAR

After the aeroshell and parachutes have been ejected and the lander has been decelerated with the thrusters, the landing gear will begin to retract. A layout of the piston shock system is shown in Figure 17.

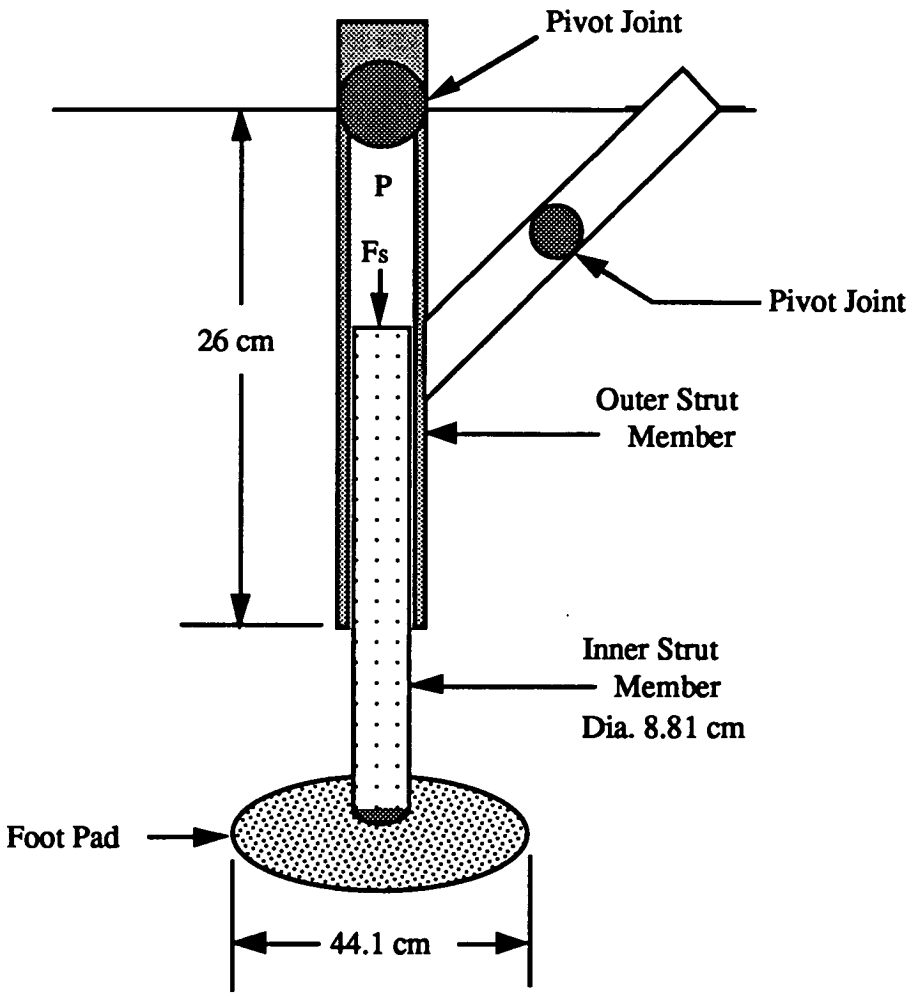

Figure 17: LAYOUT OF LANDING GEAR

MISSION INTEGRATION

The subsystems were placed in the lander according to three criteria: mass, volume, and subsystem constraints. For instance, a constraint for the computer system is that it must not be placed near the RTGs. Using a spreadsheet program, the approximate center of mass was found based on the location of each subsystem. The top view of the lander is shown in Figure 1. The center of mass is located at approximately 30.0 cm and 10.0 cm in the x and z-axes respectively (as measured from the geometric center of the lander). The y-component of the center of mass is located at approximately 3 cm toward the bottom of the lander. The estimated mass and power needs for each subsystem is listed in Table 6.

Table 6 : Subsystem Mass and Power Estimations

Component	Mass (kg)	Power (Watts)
Aeroshell	300.0	---
Camera 1	2.0	5.00
Camera 2	2.0	5.00
Computer	15.0	25.00
Communications	10.0	100.00
Core Sampler	20.0	400.00
DRR	200.0	---
DRR Launcher	41.0	94.00
Engine 1 (w / pump)	4.0	20.00
Engine 2 (w / pump)	4.0	20.00
Engine 3 (w / pump)	7.0	20.00
Engine 4 (w / pump)	7.0	20.00
Fuel (MMH)	48.3	---
Fuel Tank	10.0	---
Oxidizer (NTO)	67.7	---
Oxidizer Tank	10.0	---
Parachute	70.0	---
RTG 1	58.5	247.35
RTG 2	58.5	247.35
Robotic Arm	27.0	100.00
Rover	350.0	N/A
Rover Deployment	30.0	---
Structure	150.0	---
Total Mass	**1492.0**	

A program was developed that calculated the burn time, the engine fire altitude, and mass flow rate of a single engine (see Appendix M). These parameters were calculated by inputting the specific impulse of the propellant, the lander velocity at engine fire, the final velocity at touchdown, the lander frontal area, the drag coefficient, and the thrust-to-weight ratio. Using these parameters, another program (see Appendix N) was used to calculate the thrust values of four retrorocket engines. These thrusts were different because the center of mass was not at the geometric center of the lander. The thrust forces were calculated so that there would not be any moments about the lander's center of mass. Once the thrust forces were calculated, each engine's propellant mass flow rate, throat area, exit area, and combustion chamber area were found.

Since the entire lander system is so complex, the total cost had to be estimated from a generic cost equation:

$$\text{Cost} = 1.72\text{E-}5 * Q^{0.5773} * W^{0.6569} * 58.95^{C} * 1.0291^{Y} * G^{-0.3485} \quad (12)$$

where Q = Number of landers (4; 2 actual landers; 1 for testing, and one for parts)

W = Dry weight (2367 lbm)

C = Culture - measure of mission difficulty (2.4)

Y = Year of initial operation capability (2005)

G = Generation - measure of subsequent variations on a basic design (1.0)

Based on this simple model, the cost of each lander and aeroshell is estimated to be $755 million and $118 million respectively. Thus a total mission cost is estimated to be $1.75 billion [26].

CONCLUSION

The lander design outlined in this report has a total mass of 1492 kg. By using this mass, a total of $873 million per lander was estimated. This cost includes a $118 million aeroshell. The mass and cost estimates of the lander satisfy the restrictions placed on the design.

Further work is needed in some areas. Since the exact dimensions of the lander are known, an aeroshell must be constructed to evaluate aerodynamic properties in order to calculate heat distribution. Once these characteristics are known, a definite thickness and distribution of the two layers can be generated to obtain final mass results. With the exact functions of the lander subsystems known, the amount of data processing required to run all systems can be calculated. A capable computer system can then be integrated. In order to allow for variation in heat transfer throughout the lander, a complex analysis using convection, conduction, and radiation effects must be performed. To properly allow for the g-forces placed on the lander, a finite element algorithm will need to be developed. This will allow for a sound structural design.

By taking into account the criteria imposed on the mission scenario, we believe that the lander design meets the necessary requirements to achieve a successful mission.

APPENDIX A: Solar Cell Comparison

Using the following equation:

$$\phi = (R / R)^2 \phi$$

$R = 149.5E6$ km
$R = 227.8E6$ km
$\phi = 1.35$ kW/m

Solving for ϕ:

$$\phi = 0.5814 \text{ kW/m}$$

Finding the area needed to generate 0.5 kW:

$$P/A = \phi \qquad 0.5 \text{ kW}/A = 0.5814 \text{ kW/m}$$

Solving for A:

$A = 0.8599$ m (*note: this area was calculated assuming 100% efficiency)

Since 100% efficiency can never be achieved, a reference of 15% was used to take into account radiation scattering and other effects.

Therefore:

$$A_{new} = 0.8599 \text{ m} / 0.15 = 5.7327 \text{ m}$$

This area corresponds to a 2.39 m X 2.39 m panel.

In order to obtain a better estimate in terms of mass and dimension, a reference configuration for the Intelsat V was analyzed. General information for the Intelsat V per panel:

dimension	1.6 m X 2.0 m
mass	20.47 kg
power	466.67 W

The power in the reference configuration was based upon a synchronous orbit about the earth, therefore the power and mass estimates had to be corrected for the distance difference to the planet of Mars.

Two panels were used to allow a total surface area of:

$A = 6.4$ m (this value was close to the necessary area calculated for 500 W)

Adjusting the power:

$$\phi = (R / R)^2 \phi \qquad \phi = 145.83 \text{ W/m}$$
$$\phi = 62.81 \text{W/m}$$

Therefore, the power per panel is approximately:

$$P = 201 \text{ W/ panel}$$

Total panel power:

$$P_{tot} = 402 \text{ W}$$

Adjusting the mass: Assuming the use of Aluminum stringers with a honeycomb structure to give better support, since gravity must now be considered, the mass increased to approximately:

$$M = 82.5 \text{ kg}$$

This is an increase of 40 kg. The mass estimate was based upon the different environment for solar cell usage.

The density of Aluminum:

$$\rho = 2700 \text{ kg/m}$$

Therefore assuming volumetric dimensions of:

Length	2.39 m
Width	2.39 m
Thickness	0.01 m

$M = \rho \times V$ $\qquad$ $M = 154.22$ kg

Based on this calculation and the usage of a honeycomb base structure for the lander, we feel the mass estimate of 82.5 kg for the entire system is sufficient.

APPENDIX B: RTG - Size Scaling

The table below shows all pertinent information regarding the prototype MOD-RTG used for this report:

VOLTAGE	30.8 VOLTS
POWER OUTPUT	342.5 WATTS
SPECIFIC POWER	8.4 WATTS/KG
COLD/HOT JUNCTION TEMPERATURE	573 K/1273 K
CONVERTER EFFICIENCY	7.8%
NUMBER OF GPHS MODULES	18
NUMBER OF MULTICOUPLES	144
LENGTH	1.06 M
OVERALL DIAMETER	0.33 M
WEIGHT	41.1 KG
OPERATING LIFE	5 YEARS
STORAGE LIFE	3 YEARS

In order to use the RTG for this mission, approximately 30 kg was allowed for each RTG. Because of the decrease in mass, a scale-down was necessary. Upon speaking to Robert Hartman, it was found that the reduction of modules is about linear down to around 6 modules. Below is a list of the calculations required to scale down a MOD-RTG of about 41.1 kg to 30 kg.

From the table above:

specific power	342.5 W
number of GPHS modules	18

This yields:

19.028 W/module

Also:

RTG mass	41.1 kg
mass/module	2.283 kg/module

By using 30 kg/RTG:

30 kg = (2.283 kg/module)(number of modules)

number of modules = 13

A 30 kg RTG with 13 modules yields a power output of:

(13 modules)(19.028 W/module) = 247.36 W

Total power output then becomes:

$P_{tot} = (247.36)(2)$

$P_{tot} = 494.80$ W

Mass of additional systems related to RTG operation:

Power conditioning	10.3 kg
Energy storage	17.0 kg
Structure	13.0 kg
	40.3 kg

This yields:

40.3/18 = 2.239 kg/module (based on original MOD-RTG)

For 13 modules:

$$M = 29.1056 \text{ kg } (2) = 58.21 \text{ kg}$$

Calculating the exact mass of the RTG using 13 modules, becomes:

(power)/(specific power) = mass
(247.36 W)/(8.4 W/kg) = 29.44 kg

Total mass:

$$M = 2(29.44 \text{ kg}) = 58.89 \text{ kg}$$

Total system mass:

$$M = M + M$$

$$M = 117.0 \text{ kg}$$

APPENDIX C: Radiative Energy (RTG)

Assuming the RTG to be a circular cylinder with the following dimensions:

Length = L = 30.7 inches
Diameter = D = 6.55 inches

For these dimensions, the total outer surface area, neglecting the end caps is:

$$A_{surface} = (\pi)(D)(L) = 631.727 \text{ in}^2$$
$$A_{surface} = 0.408 \text{ m}^2$$

Knowing the surface area from which the radiation is originating, the total radiated heat for a single RTG can be calculated using the Stephan-Boltzmann relation:

$$q = (\varepsilon)(\sigma)(A)(T^4)$$

where ε = emissivity
σ = Stephan-Boltzmann constant
$A = A_{surface}$
T = Outer surface temp. of RTG

For an Aluminum RTG, at 270 ^{o}C:

$$q = (0.90)(5.67\text{E-}8 \text{ W/m}^2\text{K}^4)(0.408 \text{ m}^2)(543 \text{ K})^4$$
$$q = 1810.03 \text{ W}$$

for both RTGs in operation at full power (this most likely will not occur in space):

$$Q = 2 \times q = 3620.06 \text{ W}$$

This is the heat radiated by the RTGs alone, but the radiation from the sun must also be considered. The heat flux at the earth is known to be 1.353 kW/ m^2. However, since the landers will only be in this vicinity for a minimal time, an average flux was used in calculating the radiation incident on the lander.

$$\phi_{av} = 837 \text{ W/m}^2$$

Knowing this value, the following estimate can be made:

$$\phi = 837 \text{ W/ m}^2 = P/A_{incident}$$

where: $A_{incident} = 150 \text{ ft}^2$
$A_{incident} = 13.94 \text{ m}^2$

Therefore, total radiative heat from the sun becomes:

$$P = (837)(13.94)(0.50)$$

*note: the factor of 0.50 comes from the assumption that 50% of the incident radiation will be absorbed.

$$P = 5833.89 \text{ W}$$

Total energy then becomes:

$$E = Q + P = 9453.94 \text{ W}$$

To find the steady state temperature on the lander:

$$E = \varepsilon\sigma AT^4$$

where T is the steady state temperature of the lander. Assuming a emissivity of 0.55, and a total surface area for the lander of 34.6 square meters, the temperature becomes:

$$9453.94 = (0.55)(5.67E\text{-}8)(34.6)(T^4)$$

Solving for T:

$$T = 305 \text{ K}$$

In analyzing this temperature, it is deemed necessary to incorporate some type of shielding around the RTG and possibly around the heat sensitive subsystems. The steady - state temperature will be lower on the surface, due to scattering of the sun's radiation caused by the atmosphere. Also, the winds along the surface of the planet cause convection to occur, reducing the steady - state temperature even further.

Appendix (D): Cylinder Position on Rail Launcher

Constraint: The turret diameter is approximately the same diameter as the DRR to save space.

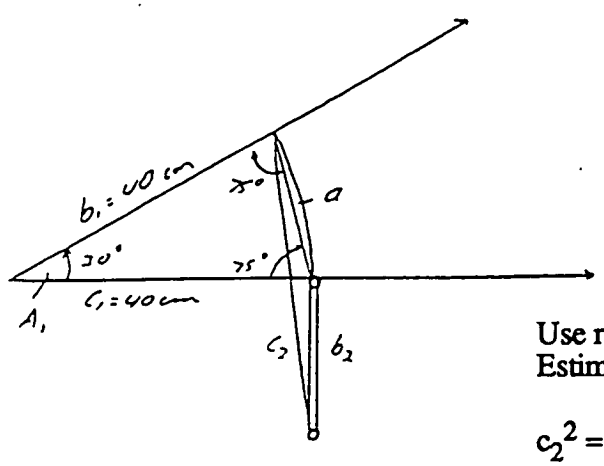

$\theta = A_1 = 30^o$

$\theta = 75^o$

Law of Cosines

$a^2 = b_1^2 + c_1^2 - 2b_1c_1\text{Cos}A_1$

$a = 20.7$ cm

Use rod length = 21 cm
Estimate cylinder length = 30 cm

$c_2^2 = a_2 + b_2^2 - 2ab_2\text{Cos}c_2$

Appendix (E): Rail Specification (Rail Launch System)

Constraints: Y = tip deflection = 1.5 cm
Support from base = 40 cm

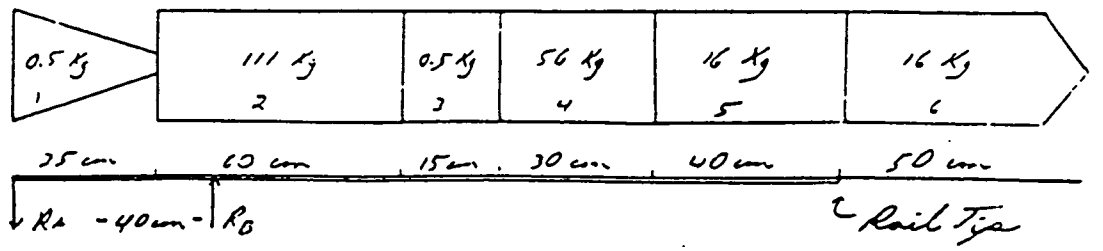

Gravitational Acceleration on Mars = 3.75 m/s^2

W_1 = 2 kg m	= 7.5 N/m
W_2 = 185 kg m	= 693.75 N/m
W_3 = 3.33 kg m	= 12.39 N/m
W_4 = 186.7 kg m	= 700 N/m
W_5 = 32 kg m	= 120 N/m

Ra (1) $\Sigma M_B = 0$ Ra = 1.29 N

Ra (2) $\Sigma M_B = 0$ Ra = 19.5 N Left of B

Ra = 39.02 N Right of B

Ra = 19.52 N

Ra (3) $Ra = \frac{W(a_1^2 - a_2^2)}{2L} = 3.16$ N

Ra (4) $Ra = \frac{W(a_1^2 - a_2^2)}{2L} = 472.5$ N

Ra (5) $Ra = \frac{W(a_1^2 - a_2^2)}{2L} = 187.5$ N

Ra (6) $Ra = \frac{W(a_1^2 - a_2^2)}{2L} = 255$ N

Ra (total) = 936.4 N
Load (total) = 200 kg (3.75 m/s^2) = 750 N

Rb (total) = Ra + Load = 1686.4 N Without Rail Mass

Moment of Inertia

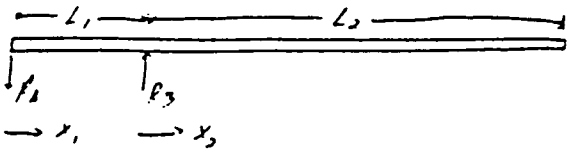

Section 1

Determination of deflection θ at Rb to be used as a boundary condition.

$$M = EI(d^2y / dx^2) = -RaX_1$$

$$EI(dy/dx) = -(1/2)RaX_1^2 + C_1 = EI\theta$$

$$EIy = -(1/6)RaX_1^3 + C_1X + C_2$$

B.C's $X_1 = 0$, $Y_1 = 0$ $\quad EI(0) = 0$, Therefore $C_2 = 0$

$X_1 = L$, $Y_1 = 0$ $\quad EI(0) = 0$, Therefore $0 = -(1/6)RaL_1^3 + C_1L$

$$C_1 = (1/6)RaL^2$$

Thus, $EI\theta = -(1/2)RaX_1^2 + (1/6)RaL_1^2$

$X_1 = L$, Therefore $EI\theta = -(1/3)RaL_12$

Section 2

$$M = EI(d^2y/dx^2) = RbX_2$$

$$EI(dy/dx) = (1/2)RbX_2^2 + C1 = EI\theta$$

B.C. $X_2 = 0$ $\quad EI\theta = -(1/3)RaL_1^2$

$$EI(dy/dx) = (1/2)RbX_2^2 - (1/3)RaL_1^2$$

$$EIy = (1/6)RbX_2^3 - (1/3)RaL_1^2X_2$$

The moment of inertia of two rails must equal the total allowable moment of inertia.

Therefore, $2EIy = (1/6)RbX_2^3 - (1/3)RaL_1^2X_2$

$$I = ((1/6)RbX_2^3 - (1/3)RaL_1^2X_2) / (2Ey)$$

$L_1 = 0.4$ m
$y = 1.0$ cm
$E = 7.308 \times 10^{10}$ N/m^2
$Ra = -936.4$ N
$Rb = 168.4$ N
$X_2 = L_2 = 1.3$ m

Material

Aluminum Aloy (2014-T6)
$E = 7.308 \times 10^{10}$ N/m^2
Specific Weight $= 2.742 \times 10^4$ N/m^3

$I = 3.1127 \times 10^{-7}$

Rail Design and Moment of Inertia

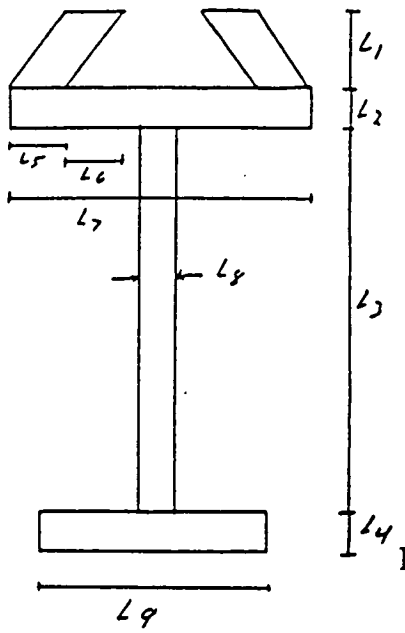

$L_1 = .01$ m
$L_2 = .005$ m
$L_3 = .05$ m
$L_4 = .005$ m
$L_5 = .0075$ m
$L_6 = .0075$ m
$L_7 = .04$ m
$L_8 = .005$ m
$L_9 = .03$ m

Area $= .00075$ m^2

Moment Of Inertia $= 4.0472 \times 10^{-7}$ m^4

Volume of single rail = Length x Area $= 0.001275$ m^3

Weight = Volume x Specific Weight = 35 N

Mass = Weight / Gravitational Acceleration (Earth) = 3.75 kg per rail

Check to see if rail design is acceptable with inclusion of rail mass.

$W_7 = 4.2$ kg/m $= 15$ N/m

Ra(7) = 29.8 N

Ra = 966.2 N
Rb = 1731.2 N

New moment of inertia parameter:

$$I = 3.1969 \times 10^{-7}$$

The new I is less than design I and is therefore acceptable.

Appendix (F): Mass Determination of Rail Launch System.

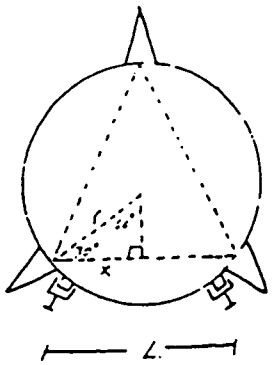

$L = 2X$

$X = .2m \cos 30^{o}$

$L = 0.3464$ m

Quadruple reactions at Ra and Rb to determine the mass of the joints at these positions with a marginal safety factor, since rocket is supported in Earth's gravitational field first.

Ra = 3864.8 N
Rb = 6924.8 N

Shear Stress = P/A $A = \pi R^2$

Hinge (pin) Area = Reaction / Shear Stress

Maximum Shear Stress = 2.2062×10^{8} N/m^2

$A(a) = 1.76 \times 10^{-5}$ m^2

$A(b) = 3.14 \times 10^{-5}$ m

Volume of Pin = L x A

$V(a) = 6.0966 \times 10^{-6}$ m^3
$V(b) = 1.0877 \times 10^{-5}$ m^3

Weight = Volume x Specific Weight (Earth)

$W(a) = 1.6717 \times 10^{-1}$ N
$W(b) = 2.9824 \times 10^{-1}$ N

Mass (pin) = Weight / Gravitational Acceleration (Earth)

$M(a) = 1.536 \times 10^{-2}$ kg
$M(b) = 3.03 \times 10^{-2}$ kg

Assume the mass of each hinge is 3x the mass of the pin.

$M(a) = 4.6 \times 10^{-2}$ kg
$M(b) = 9.12 \times 10^{-2}$ kg

Mass Determination for Turret

Assume reaction at edge of turret is the same as the reaction at B. Use same parameters used for hinge.

Area of turret edge between bearings is 1.57 x 10-5 m^2. Considering a rectangular area, the thickness is the square root of the area.

Thickness = $(1.57 \times 10^{-5}\ m^2) = 3.96 \times 10^{-3}$ m

Outer diameter = 0.5 m
Inner diameter = 0.3 m

Top area = $\pi(Ro^2 - Ri^2) = 0.503\ m^2$

Double thickness of edge for an approximate thickness of the entire turret.

Thickness = 7.92×10^{-3} m

Volume = Area x Thickness = $3.984 \times 10^{-3}\ m^3$

Weight = Volume x Specific Weight = 1.093×10^2 N

Mass = Weight / Gravitational Acceleration (Earth) = 11.14 kg

Assume bearing mass is approximately 1/2 of the turret mass.

Total Mass = 16.7 Kg

Mass of Braces Connecting Cylinder to Turret

Assume total mass of all three braces can be represented by one brace. Double reaction on cylinder for reaction on brace.

Reaction = 3462.4 N

Tensile Stress = P / A

Area = Reaction / Stress

Maximum Tenxile Stess = $4.1366 \times 10^8\ N/m^2$

Area = $8.4 \times 10^{-6}\ m^2$

Approximate (average) brace length = 0.4 m

Volume = 3.36×10^{-6} m^3

Weight = 9.21×10^{-2} N

Mass = 9.4×10^{-3} kg

Additional Masses

Straps x 2 = 0.5 kg
Rail latches x 2 = Negligible

Total Mass of Rail Launch System = 24.5 Kg

Appendix (G): Cylinder Specifications (Rail Launch System)

Reaction on cylinder (Maximum at horizontal position)

$R_b = 1731.2$ N

Round off to 1800 N

Piston Velocity (Desired) = 0.1 ft/sec = 0.03 m/sec

Power = Velocity x force = 0.074 Hp = 54.89 Watts

Determination of Rod Diameter

$Pcr = (\pi^2 EI) / Le^2$

$\sigma cr = (\pi^2 E) / (Le / r)^2$

$Pcr = Pmax = 1800$ N

$\sigma cr = (\pi^2 Er^2) / Le^2 = (1800) / \pi r^2$ Therefore $r^4 = Le^2 (1800) / \pi^3 E$

Constraints: Solid rod
Alluminum Alloy (2014 T6)

$r = 3.4407 \times 10^{-3}$ m

Use diameter = 0.0127 m (Rod)

Piston Area (Desired) = 5.067×10^{-4} m^2

Flow Rate (Q) = Velocity x Piston Area = 1.5201×10^{-5} m^3/s = 0.91 liters/min

Pressure (P) = Force / Area = 3.55×10^6 N/m^2

Power = Piston Velocity x Force = 55 Watts

Appendix (H): Motor Specification (DRR Turret)

Moment of Inertia (I) = $(1/3)ML^3$

Mass (M) = 250 kg
L = 2.2 m

$I = (1/3)ML^2 = 403.33$ kg m^2

Torque (T) = Moment of Inertia x Angular Acceleration (α)

Angular Acceleration (Desired) = 0.1 rad/sec^2

$T = I \alpha = 40.33$ N m

Divide torque by 10 for a gear ratio 1:10 between turret and motor.

T = 40.33 N m /10 = 4.033 N m

Motor

Speed (N) = 10 rev / min

Power (Hp) = TN / 63000 = 0.00567 Hp

Power = 4.23 Watts

Pressure = 3.55×10^6 N/m^2

Volumetric Displacement (Vd) = T(6.28) / P = 0.435 in^3 = 7.137×10^{-3} liters

Flow Rate (Q) = N Vd / 231 = 1.883×10^{-2} gal/min = 7.13×10^{-2} liters/min

Appendix (I): Pump Specification

Flow Rate (max) = 0.912 liters/min

Speed (Desired) = 114 rev/min

Volumetric Displacement = 231 Q / N = 0.49 in^3 = 8.005 x 10^{-3} liters

Pressure = 3.55 x 10^6 N/m^2

Torque = Vd P / 6.28 = 40.21 in lb = 4.51 N m

Power (Hp) = T N / 63000 = 0.0728

Power = 54.28 Watts

Appendix (J): Electric Motor Specifications

Speed = 1140 rev/min

Torque = 40.21 in lb = 4.5 N m

Power = 54.28 Watts

Assume 80 % Efficiency.

Power = 67.85 Watts = 1/10 Hp Motor

Use: [1/8 Hp (6-pole) DC] Motor = 93.25 Watts

Appendix (K): Mass of Fluid Power System

Assume cylinder mass is 3x the mass of the rod.

Rod Area = 5.067×10^{-4} m^2

Volume = 1.0641×10^{-4} m^3

Weight = 2.92 N

Mass = 0.3 kg

Total Mass = 1 kg

Motor & Pump

Mass = approximately 2 kg each

Total Mass = 4 kg

Reservior

The reservoir should have a capacity of three times the volumetric flow rate of the pump.

Reservoir (liters) = 3 x 0.912 liters/min = 2.736 liters

Use water for an approximation of the reservoir mass.

Weight (H_2O) = 9803.2 N/m^3

Volume = 2.3736 liters = 2.736×10^{-3} m^3

Mass = 2.73 kg

Assume structural mass is equivalent to the fluid mass.

Total Mass = 5.5 kg

Servo Valve
Approximately 2 kg

Connectors
Approximately 2 kg

Electric Motor
Approximately 1 kg

Total Mass = 15.5 kg

Appendix (L): Approximate Mass Calculation for RSDS

Rover Mass (max) = 400 kg

Initial loads on system correspond to Earth frame of reference.

Reaction = 3924 N

10 G max force assumed.

Reaction = 39240 N
Reaction per Section = 39240 / 4 = 9810 N

Part C

Length = 1.37 m

Assume entire load is applied at one point.

Reaction = 19620 N

Material

Shear Stress = P / A

Aluminum Alloy (2014-T6)

Area = load / Stress

Maximum Shear Stress = 2.2062×10^8 N/m^2

Area = 8.9×10^{-5} m^2

Volume = 1.22×10^{-4} m^3

Weight = 3.34

Mass = 3.41×10^{-1}

Mass (x2) = 0.682 kg

Part B

Length of B = 1m

Reaction at tip = 9810 N

Moment =2452.5 N m

Max Stress = 4.1366×10^8 N/m^2

Shear Stress = M y / I

M = Moment of Inertia

Assume max deflection (y) = 0.001 m.

Moment of Inertia = 5.9288×10^{-9} m^4

$I = (1/12)bh^3$ Assume b = h for approximation.

$h = (12\ I)^{1/4}$

Area = $h^2 = 2.667 \times 10^{-4}$

Volume = 2.667×10^{-4} m^3

Weight = 7.3 N

Mass = 0.75 kg

Mass (x4) = 3 kg

Part A

Diameter = 0.15 m

Thickness = 0.01 m

Torque = Moment in Part B = 9810 N m

The shear stress in Part A is the same as it is in Part B. Therefore, the mass is equivalent.

Mass (x4) = 3 kg

The design of Part A requires that 1/4 of its volume is filled with fluid. Use water for an approximation of the mass.

Volume = π D t = 0.0047 m^3

1/4 Volume = 1.18×10^{-3}

Weight (H_2O) = 9803.2 N/m^3

Mass = 1.18 kg

Mass (x4) = 4.72

Allow approximately 1/4 kg mass for internal spring.

Mass (x4) = 1 kg

Mass Total = 8.9 kg

Part J (Assume Solid)

Assume max torque equals twice the torque on Parts A or B in Mar's reference frame.

Torque on A or B = 981 N m in Earth's reference frame.

Length of Part J = 1.13 m

Shear Stress = Torque x Radius / Polar Moment of Inertia

Polar Moment of Inertia = $(1/4)\ \pi\ c^4$

Radius = $c = ((4\ T\ ) / (\tau\ \pi))^{1/3}$

T = Torque
τ = Shear Stress

Radius = 1.29×10^{-2}

Area = $\pi\ c^2 = 5.256 \times 10^{-4}$

Volume = 7×10^{-4}

Weight = 1.92×10^{1} N

Mass = 1.95 kg

Remaining Components

The mass of the remaining parts is only an approximation.

Part E (x4) = 4 kg

Part F (x4) = 2 kg

Part G (x4) = 2 kg

Part D (x6) = 2kg

Part I (x4) = 3 kg fron evaluation of Part A

Total Mass Of RSDS = 27.5 kg

```
*********
*                          Group Matulevich                           *
*                        Aerospace Design 401B                        *
*                         Final Design Project                        *
*                                                                     *
*                        Submitted: May 6, 1991                       *
*                                                                     *
*                                                                     *
*   This program is a simple representation of the deceleration of    *
*   a lander.  The puprose of the program is to obtain the reentry    *
*   speeds of the lander at varying altitudes.                        *
*                                                                     *
*                                                                     *
***********************************************************************

*       real vre,phire,bc,h,v,decl,maxdcl,scaleht,grav,rho,pi
        implicit real*8(a-z)

        open(unit = 11, file = 'redat.dat', status = 'unknown')


* initialization of variables

        t = 0.0
        scaleht = 1.0 / 7.315
        delx = 1.0
        vre = 12000.0
        phire1 = -60.00
        pi = acos(-1.0)
        phire = phire1*pi/180.0
        bc = 236.222550045
*       bc = 1135.4981758


* loop which varies altitude

        do 10 h = 150.0,0.0,-delx


* calculates variation of density with altitude

          rho = 1.225 * exp( -scaleht * h )

* calculates reentry velocity with varying density

          v = vre * exp( (1000.0*rho)/(2.0*bc*scaleht*sin(phire)))
          grav = 9.81 * sin(phire)

* amount of deceleration occurring

          decl = ((-0.5*rho*v**2) / bc ) + grav
          decl = decl / 9.81

         if (h.eq.29.0) v1 = v

* takes into account the variation of time with varation in velocity

        if (h .lt. 29) then
            delt = (delx*1000.0) / v1
        else
            delt = (delx*1000.0) / v
        endif

* incrementation of time
```

```
            t = t + delt

            write(11,15)h,v,decl,t
*           print*,h,v,decl,t
10        continue

         close(11)

15      format(5x,f9.3,5x,f12.5,5x,f12.5,5x,f12.6)
        stop
        end
```

```
WATFOR-77 V3.0 Copyright WATCOM Systems Inc. 1984,1988  91 05/05 22:26:14

Options: list,disk,xtype,terminal,extensions,warnings,check,arraycheck

      c*****************************************************************
      c
      c This program uses data from the center of mass calculations for
      c the lander and calculates the thrust force; throat area and
      c diameter; exit area and diameter; chamber area and diameter;
      c propellant flow rate; and total propellant used for each of the
      c four retrorockets.  The specific impulse of the propellant and the
      c total mass of the lander are known to be 300 sec. and 1127 kg.
      c respectively.
      c
      c Variable Directory:
      c
      c isp       : the specific impulse
      c ge        : Earth gravitational acceration at sea level
      c gm        : the Martian surface gravitational acceleration
      c pcham     : the chamber stagnation temperature
      c cstar     : the characteristic velocity of the propellant
      c tb        : the engine burn time
      c pi        : the typical pi constant
      c ueq       : the equivalent exit velocity of the propellant
      c mass      : the total mass of the lander
      c d         : the matrix of constants (from center of mass calculations)
      c x         : the solution matrix (the thrust forces for each engine that
      c             together will cause zero moments about the lander's center
      c             of mass
      c mdot      : the propellant mass flow rate
      c mprop     : the total propellant mass through an engine during burn
      c astar     : the throat area
      c dstar     : the throat diameter
      c ae        : the exit area
      c de        : the exit diameter
      c ac        : the chamber area
      c dc        : the chamber diameter
      c
      c*****************************************************************


     1        dimension d(4,4),x(4),mdot(4),mprop(4),astar(4),ae(4),dstar(4)
*EXT* CC-04 character encountered is not FORTRAN 77 standard
     2        dimension de(4),ac(4),dc(4)
     3        double precision d,x,mdot,mprop,astar,ae,dstar,de,ac,dc,mass,isp
     4        open(unit=12, file = 'thrust.dat',status = 'unknown')

       c Set constants

     5        ge = 9.81
     6        isp = 300.0
     7        pcham = 7e5
     8        cstar = 1977
     9        pi = 3.141592654
    10        tb = 73.34
    11        gm = 3.75
    12        x(4) = 90.0
    13        mass = 1127.0
    14        ueq = isp*ge
```

```
c Increase the thrust on engine 4 in increments of ten Newtons

     15       while (x(4) .le. 2500) do
"EXT" SP-18 WHILE statement is not FORTRAN 77 standard
     16         x(4) = x(4) + 10

     17         d(1,1) = 1.0
     18         d(1,2) = 1.0
     19         d(1,3) = 1.0
     20         d(2,1) = 3.083
     21         d(2,2) = -2.417
     22         d(2,3) = 3.083
     23         d(3,1) = 2.483
     24         d(3,2) = 2.483
     25         d(3,3) = 1.017
     26         d(1,4) = 1.1*mass*gm-x(4)
     27         d(2,4) = 2.417*x(4)
     28         d(3,4) = 1.017*x(4)

c Calls a generic Gaussian elimination routine

     29         call gauss(d,x)

c If the thrust forces for each of the engines are positive, then the
c engine parameters are calculated.

     30         if (x(1) .ge. 0 .and. x(2) .ge. 0 .and. x(3) .ge. 0) then
     31            write(12,6) x(1), x(2), x(3), x(4)
     32            do 10 i = 1, 4
     33               mdot(i) = x(i)/ueq
     34               mprop(i) = x(i)*tb/ueq
     35               astar(i) = cstar*mdot(i)/pcham
     36               ae(i) = 60.0*astar(i)
     37               ac(i) = 1.61*astar(i)
     38               dstar(i) = sqrt(astar(i)/pi)*2000
     39               de(i) = sqrt(ae(i)/pi)*2000
     40               dc(i) = sqrt(ac(i)/pi)*2000
     41               write(12,4) i
     42               write(12,5) mdot(i), mprop(i)
     43               write(12,5) astar(i), dstar(i)
     44               write(12,5) ae(i), de(i)
     45               write(12,5) ac(i), dc(i)
     46               write(12,5)
     47    10       continue
     48         end if
     49         endwhile
     50         close (12)

     51    4    format (1x,i2)
     52    5    format (1x,2(f10.5,3x))
     53    6    format (1x,4(f11.3,3x))
     54         end

c This is a generic Gaussian elimination routine that calculates the
c needed thrust forces so that the lander has zero moments.

     55         subroutine gauss(d,x)
     56         dimension d(4,4),x(4)
```

```
57          double precision d, x

58          n2 = 3 - 1
59          n1 = 3 - 1
60          do 1150 k = 1, n1
61             k1 = k + 1
62             l = k
63             do 1100 i = k1, 3
64                if (abs(d(i,k)) .gt. abs(d(l,k))) l = i
65    1100     continue
66             if (l .eq. k) goto 1120
67             do 1110 j = k, n2
68                dum = d(k,j)
69                d(k,j) = d(l,j)
70                d(l,j) = dum
71    1110     continue
72    1120     do 1140 i = k1, 3
73                piv = d(i,k)/d(k,k)
74                do 1130 j = k1, n2
75                   d(i,j) = d(i,j) - piv * d(k,j)
76    1130        continue
77    1140     continue
78    1150  continue
79          x(3) = d(3,n2)/d(3,3)
80          m = n1
81    1160  m1 = m + 1
82          sum = 0.0
83          do 1170 k = m1, 3
84          sum = sum + (d(m,k)*x(k))
85    1170  continue
86          x(m) = (d(m,n2)-sum)/d(m,m)
87          m = m - 1
88          if (m .ge. 1) goto 1160
89          return
90          end
```

```
Compile time:                     01.49   Execution time:              05.93
Size of object code:               2210   Number of extensions:           2
Size of local data area(s):         869   Number of warnings:             0
Size of global data area:           416   Number of errors:               0
Object/Dynamic bytes free:  365376/46230  Statements Executed:        21958
```

REFERENCES

1. Garner, J.K., Fitzgerald, T.J., and Glasgow, B.B, *A Generalized Method for Optimizing the Mass of Space Power Systems*, Space Nuclear Power Systems, TRW Space and Technology Group, Redondo Beach, CA, 1987, p. 419-427.

2. Agrawal, Brij N., Design of Geosynchronous Spacecraft, Prentice-Hall, Inc., Englewood Cliffs, NJ, 1986.

3. Bents, D.J., *Preliminary Assessment of Rover Power Systems for the Mars Rover Sample Return Mission*, Technical Report, NASA, Lewis Research Center, 1989.

4. Hartman, Robert F., *Current Status of MOD-RTG Program*, 23rd Intersociety Energy Conversion Engineering Conference, Denver, Colorado, July 31-August 5, 1988, p. 153-157.

5. Martin, James S.,Jr., Soffen, Gerald A., Viking 1 Early Results, Scientific and Technical Information Office, NASA, Washington D.C., 1976.

6. Wilhelms, Don, *Venus on a Shoestring*, Air & Space, Smithonian, February / March 1990, pp.83-87.

7. Stokes, Lyle S, *Telecommunications From Lunar Spacecraft*, AIAA Unmanned Spacecraft Meeting, Los Angeles, California, March 1-4, 1965, p.23-34.

8. Roddy, Dennis, Satellite Communications, Prentice Hall, Englewood Cliffs, New Jersey, 1989.

9. *Payload Deployment Method and System*, National Aeronautics and Space Administration Microfiche, Houston, TX, Lyndon B. Johnson Space Center, April 15, 1988.

10. Esposito, A., Fluid Power with Applications, Prentice Hall, 1988.

11. Veinott, C.G., Fractional and Subfraction Horsepower Electric Motors, McGraw-Hill, 1986.

12. *Mars Rover Sample Return-Delivery and Return Study: Final Review*, Martin Marietta, August 14, 1990.

13. Drake, Michael J. *Workshop on Mars Sample Return Science*, N89-18288 thru N89-18372, 1988.

14. Amundsen et al. *Study of Sampling Systems fot Comets and Mars: Final Report*, N89-29292, 1987.

15. Crouch, D. S., *Study of Sample Drilling Techniques for Mars Sample Return Missions*, MCR-79-615, April 1980.

16. Crouch, D. S, *Study of Sample Drilling Techniques for Mars Sample Return Missions*, MCR-78-613, March, 1979.

17. Crouch, D. S., *The Effects of Lunar Probe Data on Lunar Drilling Equipment Design*, AAS 69-679, in Geological Problems in Lunar and Planetary Research, vol. 25, Edited by Jack Greene, Tarzana, CA: AAS, 1971.

18. Lau, Richard A., Hussong, James C., *The Viking Mars Lander Deceleration System*, AIAA Paper No 70-1162, AIAA Deceleration Systems Conference, Dayton Ohio, September 14-16, 1970.

19. Peterson, C.W., *Parachute Materials*, Microfich DE87-014845.

20. Peterson, C.W., *Parachute Materials*, Microfich DE87-014845.

21. Timnat, Y. M., Advanced Chemical Rocket Propulsion, Academic Press, New York, 1987, pp.240-244.

22. Hill, Philip G., Peterson, Carl R., Mechanics and Thermodynamics of Propulsion, Addison-Wesley Publishing Company, Reading, Massachusetts, 1970.

23. Huzel, Dieter K., Design of Liquid Propellant Rocket Engines, 2nd Ed., Rocketdyne Division, North American Rockwell Inc., 1971, p. 8.

24. Sutton, George P., Rocket Propulsion Elements, John Wiley & Sons, Inc., New York, 1986, p. 162.

25. Conway, H.G., Landing Gear Design, Chapman & Hall LTD, London, 1958.

26. Cyr, Kelley, *Cost Estimating Methods for Advanced Space Systems*, SAWE 1856, 1988.

GENERAL REFERENCES

Kourtides, D.A., *Composite Multilayer Insulations for Thermal Protection of Aerospace Vehicles*, Microfich N90-10183.

Brown, W. D., Parachutes, Sir Issac Pittman & Sons, LTD, London, 1951.

Peterson, C. W., *The Aerodynamics of Supersonic Parachutes*, Microfiche DE 87-0148647, 1987.

EXLOG, Coring Operations, International Human Resources Development Corporation, Boston, 1975, pp. 33-49.

Crouch, D. S., *The Effects of Lunar Probe Data on Lunar Drilling Equipment Design*, AAS69-679, Geological Problems in Lunar and Planetary Research, Ed. Jack Green, AAS Publications Office, Tarzana, CA, 1971.

Splettstoesser, John F., Ed.,Ice Core Drilling, University of Nebraska Press, Lincoln, 1976.

Zeilik, Michael, and Gaustad, John, Astronomy: The Cosmic Perspective, John Wiley and Sons, Inc., New York, 1990, p. 358.

Thomson, Ron, et al., *Design of a Sample Acquisition System for the Mars Exobiological Penetrator*, NASA Microfiche, N89-16708, Wisconsin University, May 1988.

Roush, R.G., Powell, T.H., Jr. *Some Systems Considerations for Mars Lander Communications Link Design*, AIAA/AAS Stepping Stones to Mars Meeting, Baltimore, Maryland, March 28-30, 1966, p. 152-159.

Barber, Thomas A., Billy, John M., Bourke, Roger A., *A Systems Comparison of Direct and Relay Link Communications for an Eventual Long Life Mars Surface Experiment*, AIAA/AAS Stepping Stones to Mars Meeting, Baltimore, Maryland, March 28-30, 1966, p. 160-167.

Gamber, R.T., *Subsystem Technology*, Mars Rover Sample Return Delivery and Return Study Final Report, Martin Marietta, October 31, 1990.

Von Braun, Wernher, The Mars Project, The University of Illinois, 1953.

Skrabek, E.A., and McGrew, J.W., *Pioneer 10 and 11 RTG Performance Update*, Space Nuclear Power Systems 1987, Orbit Book Company, Inc., Malabar, Florida, 1987, p. 587-595.

Kourtides, D. A., Pitts, W. C., *Composite Multilayer Insulations for Thermal Protection of Aerospace Vehicles*, NASA Microfiche, N90-10183, December 21,1989.

Beer, F.P., Mechanics of Materials, McGraw-Hill, 1981.

Rocketdyne, *Chemical Propulsion for Lunar / Mars Mission*, Rockwell International, June 19, 1990.

Bennet, Gary L, Lombardo, James J., Rock, B. J., *Power Performance of the General - Purpose Heat Source Radioisotope Thermoelectric Generator*, Space Nuclear Power Systems, Orbit Book Company, Malabar, FL, 1987, p437-449.

Hartman, Robert F., Gorsuch, Paul D., Peterson, Jerry R., *Technology and Hardware Status of Advanced Modular Radioisotope Generator Development*,, Space Nuclear Power Systems, Orbit Book Company, Malabar, FL, 1987, p451-460.

Niggemann, R. E., Lacey, P.,D., *Long- Life, Highly Survivable Rankine Cycle Dynamic Isotope Power Systems* , Space Nuclear Power Systems, Orbit Book Company, Malabar, FL, 1987, p461-467.

Davis, Keith A., Pietsch, Casagrande, Roger D., Brayton, *Dynamic Isotope Power Systems Update*, Space Nuclear Power Systems, Orbit Book Company, Malabar, FL, 1987, p469-482.

Thomson, Ron et al. *Design of a Sample Acquisition System for the Mars Exobiological Penetrator*, N89-16708, May, 1988.

Anderson, Gene, Coring and Core Analysis, Tulsa: Petroleum Publishing Company, 1975.

EXLOG, Coring Operations, Boston: IHRDC Publishers, 1975.

Gamble, Joe D., JSC Pre-Phase A Study Mars Rover Sample Return Mission Aerocapture, Entry, and Landing Element, NASA, May 1, 1989.

Tricamo, S. J., Et Al., Development Implementation and Validation of Control Algorithms for the D., Microfiche No. AD-A222 502, Peritus Inc, Northwood NJ, May 90.

Chapter 3:

MSAV

(Mars Sample Acquisition Vehicle)

Final Report

Submitted By:
The DiPippa Design Group

Chris Avvisato
Frank Capuano
E. Damian DiPippa
Tim Durick
Shahnaz Punjani
Al Soxman
R. Scott Young

Aerospace Engineering 401-B
The Pennsylvania State University
Spring Semester 1991

Abstract

The Mars Sample Return Mission was proposed to gain a better understanding of the Martian environment. This suggested mission scenario consists of using a Centaur G Prime launch vehicle to send sample retrieval equipment to the Martian surface. A lander, rover, and a Direct Return Rocket (DRR) compose the sample retrieval equipment. The lander and rover collect various Martian samples consisting of core, atmospheric samples, regolith, pebbles, rock fragments, and boulder specimens. These samples are placed on the DRR and returned to Earth for scientific study.

The Martian Sample Acquisition Vehicle (MSAV) is one component that is important to the success of this mission. The MSAV is a small, short-range, six-wheeled land rover deployed by a Mars lander. Two individual rovers and landers are used: one in an equatorial region, and the other in a polar region. Each rover uses two robotic arms to obtain Mars regolith, rock fragments, pebbles, and boulder specimens. In addition to these samples, the polar MSAV will also collect an ice sample. The MSAV will package each of the samples and store them in a carbon-carbon basket in preparation for transfer to the DRR. A complete design of the MSAV is presented in this report, discussing mass breakdowns, power requirements, and basic functions of the land rover.

Table of Contents

Acknowledgements

The members of the DiPippa Design Group wish to express their appreciation to the instructors of the spacecraft design class: Dr. Melton, Dr. Thompson, Jay Burton, and Eric Bell. This design group would also like to the thank the other design groups for their cooperation in trading relevant information toward our project.

List of Figures

List of Tables

Nomenclature

Symbol	Description
BCR	Boulder Collection Ring
CBC	Closed Brayton Cycle Dynamic System
DOF	Degrees of Freedom
DRR	Direct Return Rocket
FOV	Field of View
FPSE	Free Piston Stirling Engine
GC	Grabber Claw
GPHS-RTG	General Purpose Heat Source - Radioisotope Thermoelectric Generator
HS	Hoe Scraper
ILC	Integrated Laser Ranger/Camera System
IR	Infrared
JSS	Jaw/Screen Scoop
KBSC	Knowledge-Based Supervisor Controller
MOD-RTG	Modular Radioisotope Thermoelectric Generator
MSAV	Martian Samples Acquisition Vehicle
NHTSA	National Highway Traffic Safety Administration
RF	Radio Frequency
VP	Vibrator Pick

Introduction

Present knowledge of the Martian environment is limited to what is known from a few data sets which include, (i) Earth-based spectroscopy, (ii) Imaging and optical measurements from previous missions to Mars [Mariner, Viking], (iii) Chemical analyses of Martian surface rocks by the Viking landers, and (iv) Analysis of meteorites (SNC Meteorites) that have theoretically originated from Mars [1]. It is for this reason that a Mars Sample Return Mission is needed to learn more about the geology and environment of Mars.

A successful Mars Sample Return mission can be accomplished by returning the following sample set:

Mars Regolith	50 g
Rock Fragment/Chips	1000 g
Pebbles	2085 g
Boulder Specimens	70 g
Core Sample	1256 g
Atmosphere	100 cm^3

A contingency sample will be collected to provide some sort of samples for return to Earth, should there be a failure in the collection of the primary sample set. The contingency sample shall consist of:

Regolith	100 g
Atmosphere	100 cm^3

The mission is expected to be completed between the years 2003 and 2010.

Two MSAVs are landed in two different locations on the Martian surface: one in the equatorial region and the other in a polar region. The equatorial MSAV collects regolith, rock fragments/chips, pebbles, and boulder specimens, while the polar MSAV is responsible for gathering boulder specimens and an ice/regolith sample. Due to the difficulty in separating ice from the regolith, pebbles, and rock fragments/chips, the polar MSAV will collect all of these samples together and place them in a refrigeration unit aboard the Direct Return Rocket.

There are three main systems of this mission: the launch vehicle, the lander, and the rover. Mass and volume restrictions were calculated based on the limited space aboard the lander and the mass capability of the Centaur G Prime launch vehicle. This limits the maximum volume of the MSAV to 167x91x91 cm, and the maximum mass to 350 kg.

Another important requirement for any rover that visits sites on the surface of Mars is autonomous analysis. It should be able to assess the geology of the sites and sample the area effectively with minimum intervention by scientists at Mission Control [1].

Vehicle Design

Vehicle Layout

The Martian Samples Acquisition Vehicle uses three electric motors and added gear drives to enable six-wheel drive, posi-traction mobility (See Figures 1 and 2). It has the advantage of being able to use all six powered traction wheels to surmount obstacles [2]. Particularly important for the polar MSAV, the six-wheeled design allows the

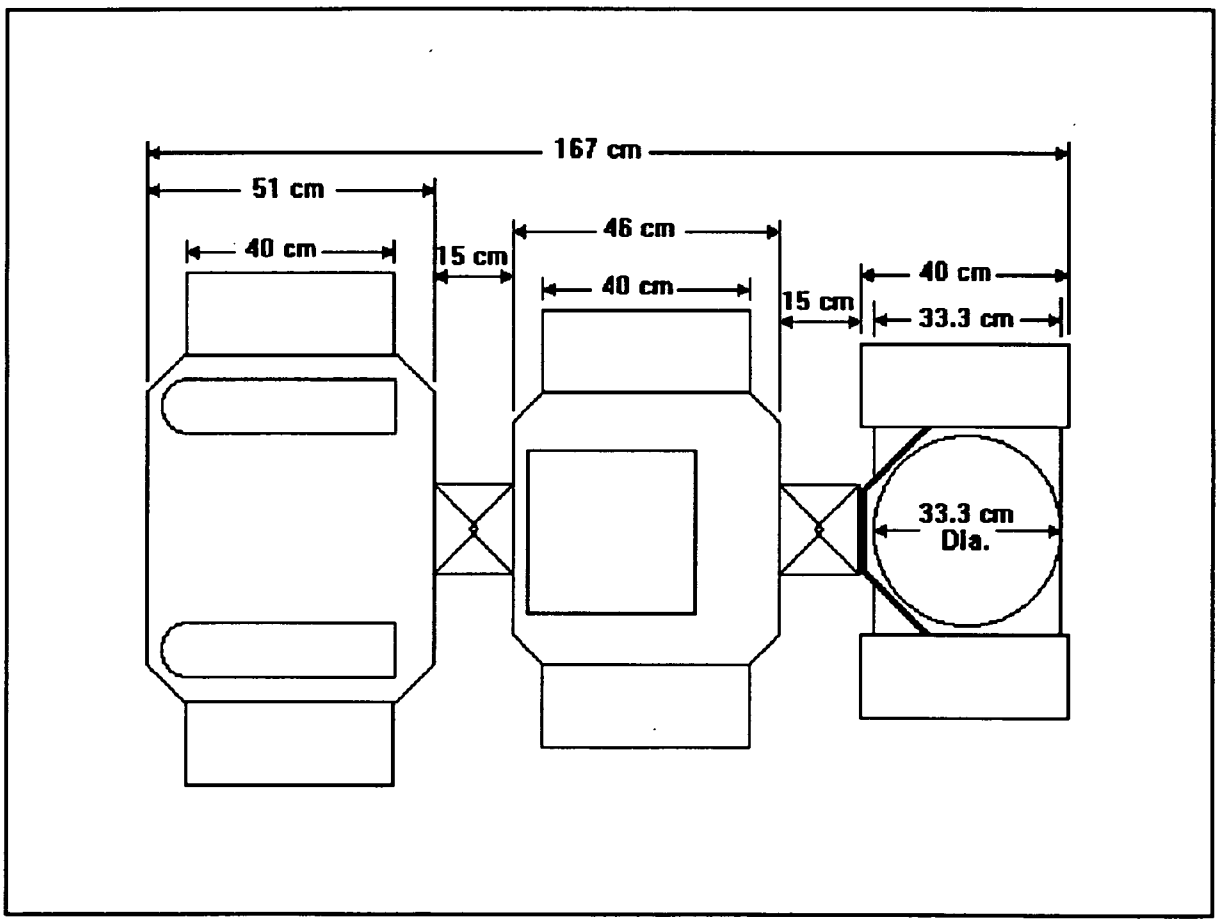

Figure 1. Scale Top View of the MSAV

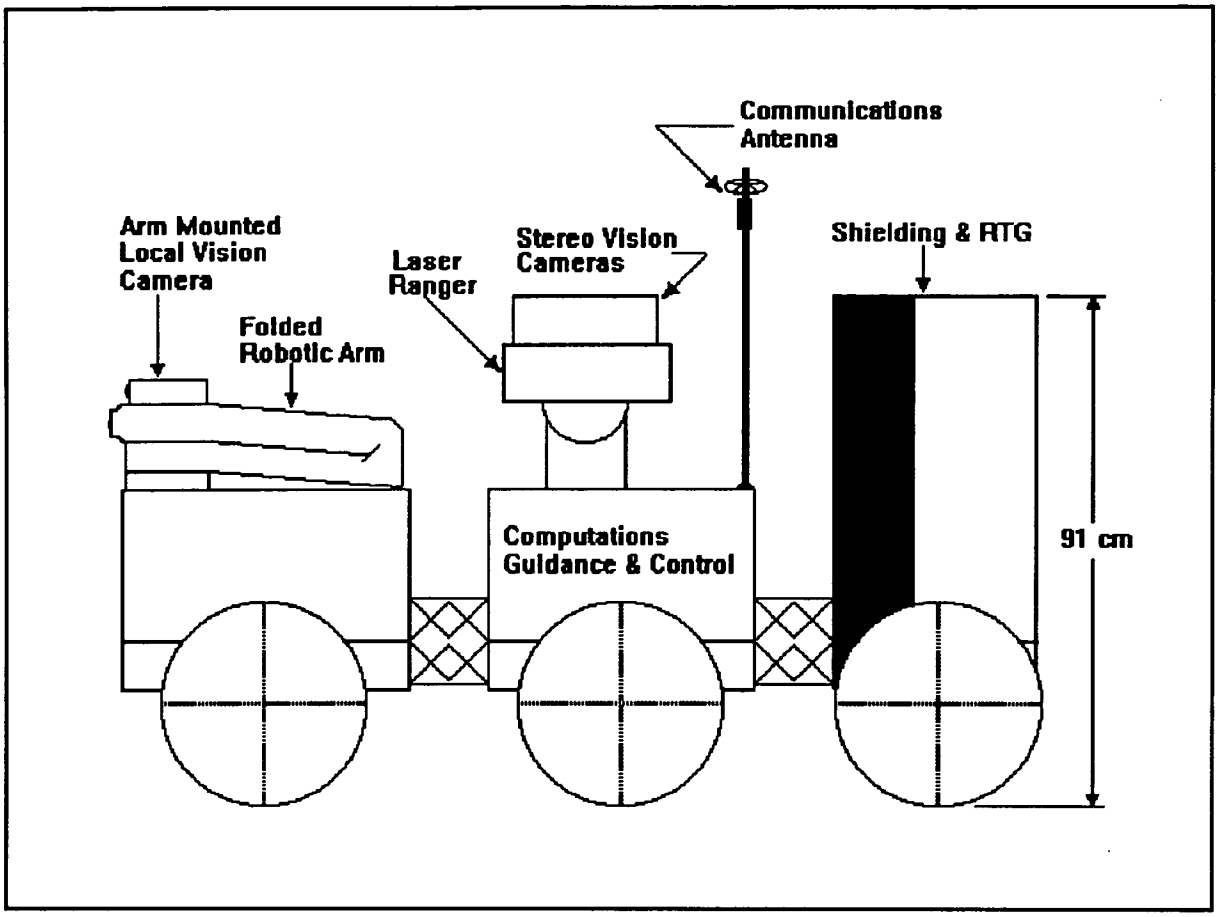

Figure 2. Scaled Side View of the MSAV

vehicle to climb over surfaces which have a low coefficient of friction.

The frame is divided into three units connected by three-degree-of-freedom joints. These joints have enough strength to control any excessive pitch, roll, or yaw in the units, and are capable of moving independently of the others giving the MSAV greater maneuverability.

The first unit contains the sample acquisition systems. Two robotic arms, equipped with local imaging cameras, are attached to the front. A "tool box" containing

different arm attachments is located behind each robotic arm. Once the robotic arms have packaged the samples, the samples are placed in a 18 cm diameter carbon-carbon containment basket located directly behind the robotic arms. Once all of the samples are placed in the basket, the basket is covered with a carbon-carbon lid and aerogel is released into the basket to cushion the samples against strong vibrations and shaking due to motion of the basket. Once all of the samples are securely sealed in the basket, the lander's robotic arm transfers the basket to the Direct Return Rocket.

The center unit of the MSAV contains the imaging, computations, communications, guidance and navigation, and thermal control systems. The systems of this unit are responsible for controlling all of the actions taken by the MSAV.

The rear unit is devoted to the power systems and radiation shielding. Since the RTG supplies the power for the entire rover, minimal design changes made on the RTG resulted in the circular cylinder shape of the rear section. The shielding is directly in front of the RTG with "wings" shielding a portion of the side sections of the RTG. This shielding is important in protecting the electronic equipment located in the center section of the MSAV from harmful radiation being emitted by the RTG.

The length and width of each MSAV unit decreases from front to rear sections. This, along with using chamfers instead of sharp corners allows increased maneuverability for the entire vehicle.

Approximate mass and power breakdowns of the MSAV are shown in Table 1. Mass and power profiles for other rovers ranging from 100 to 600 kilograms were scaled to determine the mass and power profile of some of the systems of the MSAV.

Table 1. MSAV Mass and Power Breakdown

	Mass (kilograms)	Power (Watts)
Communications	2	20
Computations	37	40 - 50
Imaging	25	60
Mobility	5	180
Power systems	79	-
Sample Acquisition	18	28
Structure	49	-
Thermal Control	10	-
Vehicle Control	20	30.2

All of the sub-systems will not be using power at the same time so the total power can exceed the maximum power output by the RTG. The polar MSAV will require added power for the thermal control systems in order to keep electronic systems at a constant temperature in the colder polar environment.

Materials

A Ti-3Al-2.5V titanium alloy will be used for the structure of the MSAV. This alloy is currently being used for the skin over honeycomb structures of aircraft. It is

strong enough to handle the applied loads of the MSAV and is capable of withstanding the extreme temperatures of the Martian environment in both the equatorial and polar regions.

Two other materials -- honeycombed aluminum and composites -- were also considered. Honeycombed aluminum is commonly used for many aerospace applications that require a low-mass structure, but it is highly susceptible to abrasion [3]. For a long-term mission, the violent Martian sandstorms can wear away the aluminum structure which could eventually cause damage to the internal electronic systems of the MSAV.

Composite materials are also considered to be effective for strong, light-weight structures, but many composites will become brittle at the extreme low temperatures of the Martian environment. Also, the cost of producing a strong, lightweight composite capable of withstanding the extreme temperature difference of Mars could prove to be of little benefit.

Tires

The tires on both the equatorial and polar MSAV must be reliable, and they must be maintenance free. Three possible types of tires exist for use with MSAV: air-filled pneumatic tires, Urethane-filled tires, and elastomeric non-pneumatic tires.

Air-filled pneumatic tires are not the most effective tires for the Martian environment. Even the best pneumatic tires are not puncture resistant, and continued

service is required in order to maintain air pressure. A larger volume and mass than allotted would (for the total rover) be necessary for a pneumatic tire to be reliable in the Martian environment.

During the Vietnam conflict, Urethane-filled tires were developed due to the need for a puncture-proof tire system for ground support vehicles [4]. This consists of a 1-to-1 mixture of a patented prepolymer and catalyst which is pumped into a mounted tire. This type of tire has been effectively used in the industrial market for construction and mining vehicles. Since the urethane filling is more dense than air, the overall mass of the tire increases. This added mass is of no consequence when working on Earth, but six Urethane-filled tires would require mass that could be put to better use elsewhere on the MSAV.

The National Highway Traffic Safety Administration (NHTSA) has recently certified the use of elastomeric non-pneumatic tires as spare tires for cars [5]. Cast elastomeric polyurethanes are designed to incorporate two load-carrying members, a web disk, and angled spokes. These spokes connect the inner and outer rings of polyurethane that are bonded to the wheel and tread surfaces (See Figure 3).

The solid structure is capable of carrying high loads in high-speed operations; yet, it has the unusual ability to deform to road surface irregularities and obstacles. Deformations of more than 500% can be sustained with the elastomer returning to its original shape [6]. General Motors and Uniroyal have developed a non-pneumatic tire with 37% less storage volume, and 24% less mass than air-filled pneumatic tires [7].

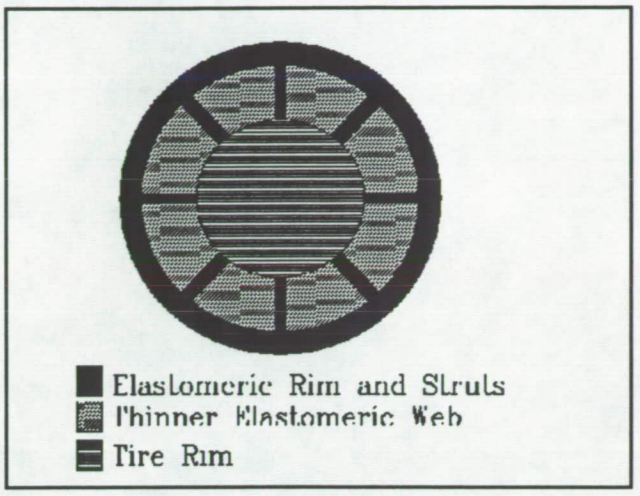

Figure 3. Cross Section of Elastomeric Non-Pneumatic Tire

MSAV uses six elastomeric non-pneumatic tires. Each tire is 15 cm thick with a 40 cm diameter. For the polar MSAV, the tires will have added treads molded to them and a slightly larger surface area for increased traction. Since the tire is solid and contains no encapsulated or pressurized air, it cannot go flat like air-filled pneumatics. It also reduces material usage, yielding a lower mass and requiring less cross-sectional volume to carry similar loads than the other two tires discussed. The elastomeric polyurethane tire is a maintenance-free system in which catastrophic failure is highly unlikely, making it an ideal tire for the Martian environment [6].

Electric Motors

Because of the lack of oxygen on Mars, a conventional combustion engine cannot be used to move the rover. Instead, three electric motors are used. Each motor moves two wheels of the three-unit body. Computer control ensures that the output rpm of the motors is the same so that one part of the vehicle does not "ride up" on the other. Suggested motors for this application are given in Figure 4. Their small size and low mass are advantageous. If the rover encounters an obstacle, an increase of voltage to the motor increases the output torque giving it the necessary force to surmount the obstacle. A bevel gear transmits the power of the motor through the axle to the wheels. Differential gearing allows the outer wheel to turn at a faster rate when the rover is turning. A no-spin locking-type differential commonly used in heavy-duty trucks keeps the wheels from spinning should the rover encounter loose regolith.

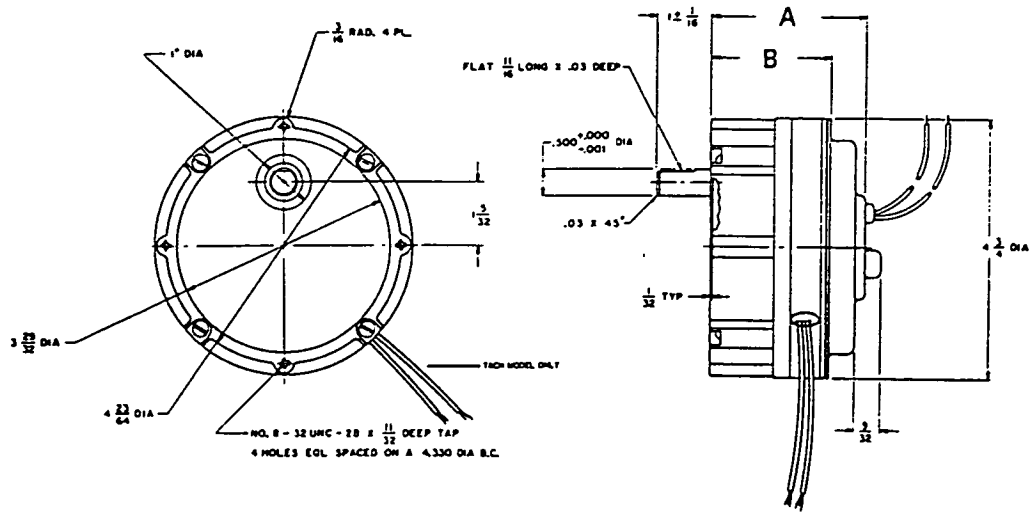

DIMENSIONS	
A	2 - 13/16 ± 1/16
B	2 - 3/16 ± 1/16

U9FGHD dc Gearmotor						
Specifications	**Gear Ratios**					
	15.1:1	25.85:1	48.96:1	79.2:1	99.0:1	148.51:1
Rated Speed (RPM)	200	116	61	38	30	20
Paek Torque (in.-lb)	26	44	84	117	118	119
Rated Torque (in.-lb)	10.7	17.3	32.8	49.7	62.2	80.0
Rated Current (A)	5.2	5.2	5.2	5.2	5.2	4.6
Rated Voltage (V)	12.9	12.9	12.9	12.9	12.9	12.2
Power Out (W)	25	24	24	22	21	19
Radial Load (lbs)	50	50	50	50	50	50
Thrust Load (lbs)	25	25	25	25	25	25
Weight (lbs)	3	3.1	3.1	3.2	3.2	3.2

Figure 4. Specifications of Electric Motors (PMI Motion Technologies)

Sample Acquisition and Packaging

The front section of the MSAV contains all necessary sample gathering devices (See Figure 5). Two 1.15 m robotic arms are attached to the top front portion of the section. Behind each arm is a tool box containing two tools apiece. Each arm primarily uses the tools directly behind it; however, the tools are interchangeable. Located between the arms are two boulder storage rings that either arm can use if necessary. A sample containment basket is located behind the boulder storage rings and its lid is affixed to the front of the section. Once the samples have been packaged, they are placed in the basket. The right arm seals the basket with the lid, and then aerogel is released into it.

Tables 2, 3, and 4 show the parameters for the mechanical arm and the tool attachments.

Table 2. Mechanical Arm Parameters

	Extend/Retract	**Azimuth**	**Elevation**
Maximum Excursion	1.15 m	288°	74°
Operating Force	133 N	10.8 N-m	63.8 N-m
Operating Power	5-13 W	0.4-1.5 W	3-10 W
Control Sensitivity	0.6 cm	0.6°	0.6°

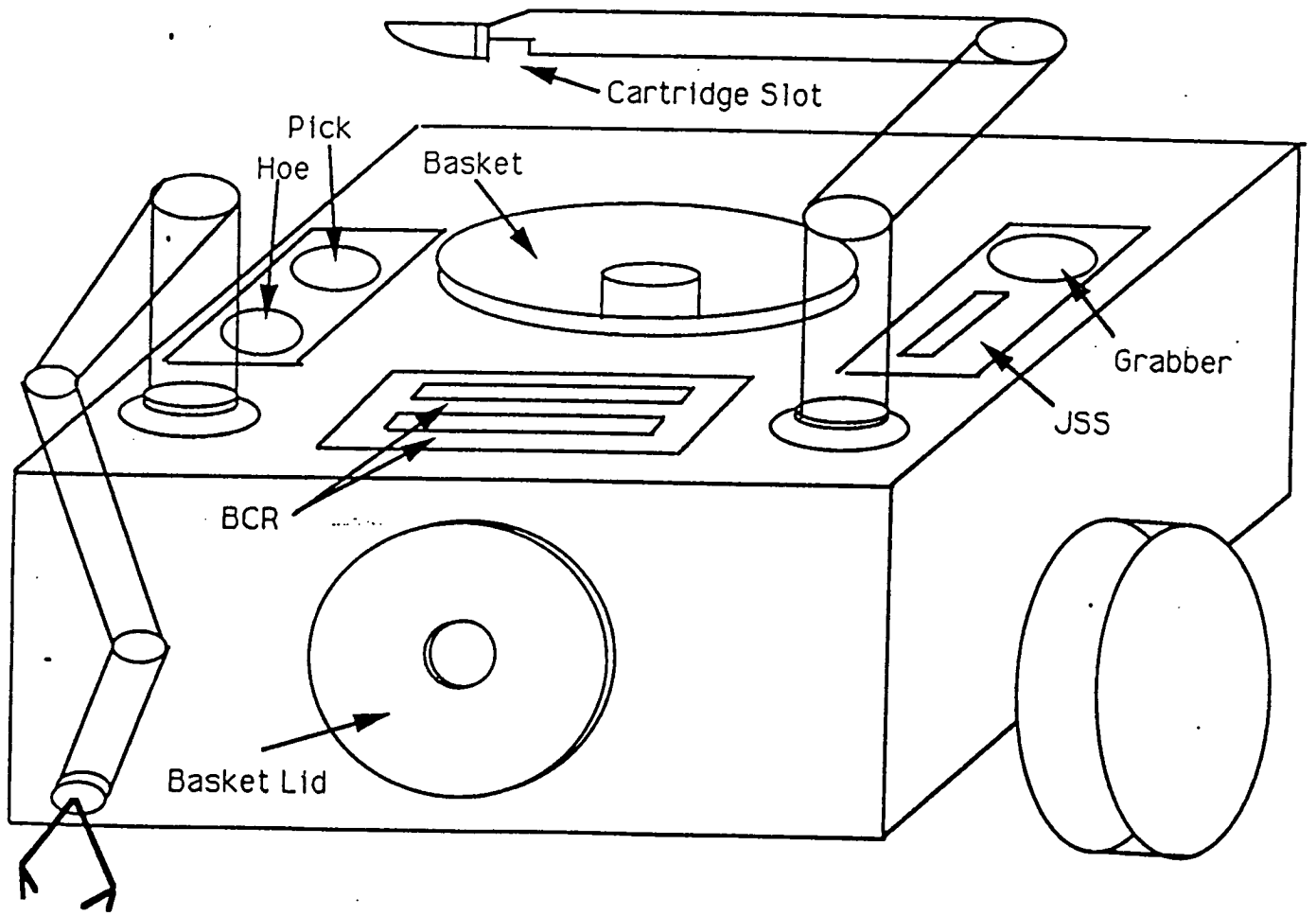

Figure 5. Isometric View of Front Section

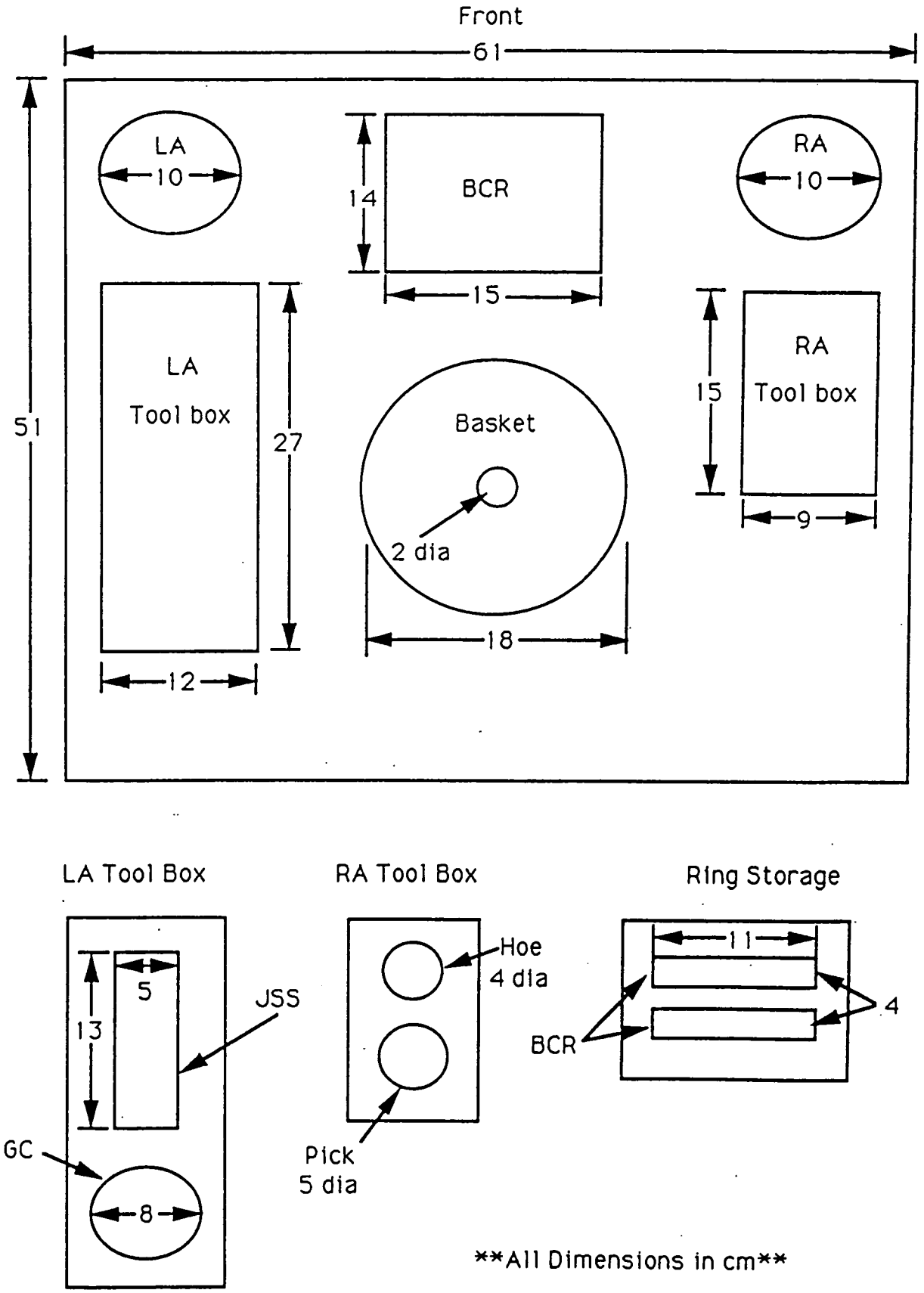

Figure 6. Top View of Front Section

Tool Box

The tool box stores interchangeable sample retrieval devices which consist of:

1) Vibrating Pick (VP) (See Figure 7)
2) Hoe Scraper (HS) (See Figure 8)
3) Grabber/Claw (GC) (See Figure 9)
4) Jaw/Screen Scoop (JSS) (See Figure 10)
5) Six Sample Packaging Cartridges (See Figure 11)
6) Two Boulder Collection Rings (BCR) (See Figure 12)

Table 3. Tool Attachment Parameters

Attachments	Mass (kg)	Power (Watts)
JSS	1.5	3-5
1 BCR	0.75	1
GC	1.25	3-5
VP	0.80	3-5
HS	0.50	2
1 Cartridge	0.10	1
Right Arm	4.50	5-7
Left Arm	5.50	5-7
Basket and Lid	0.25	-

**Parameters are based on Viking Mission Data

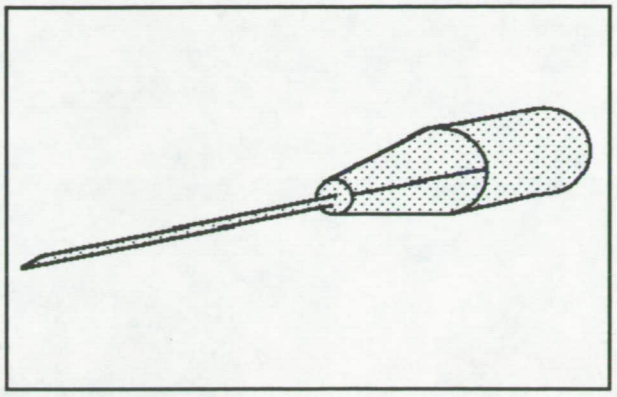

Figure 7. Vibrating Pick Attachment

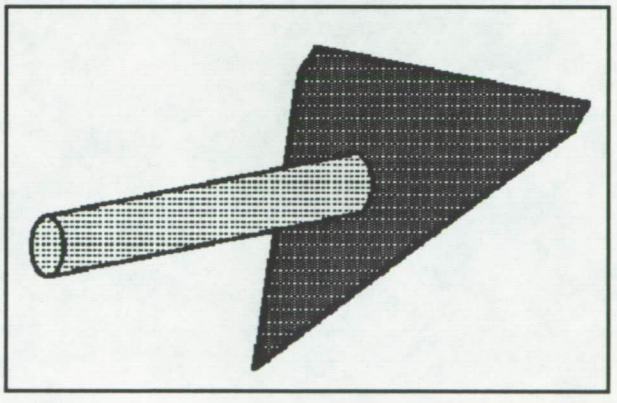

Figure 8. Hoe Scraper Attachment

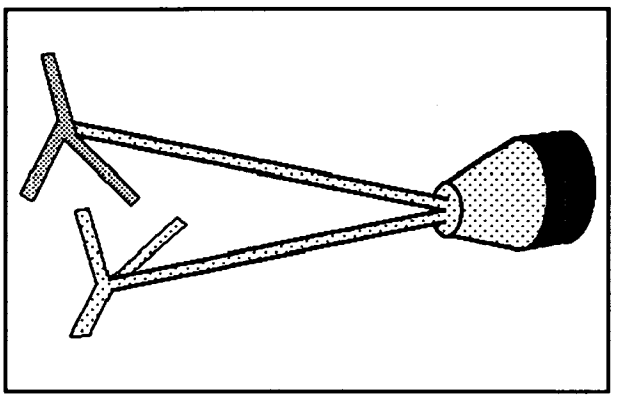

Figure 9. Grabber/Claw Attachment

Table 4. Dimensions of Attachments

Attachment	Dimensions (cm)
BCR	inner diameter: 7 outer diameter: 11
GC	length: 13 diameter: 4
HS	length: 10 sides: 5
Cartridge Bag	25.4 x 7.6 x 7.6
Basket	diameter: 18 depth: 22
JSS	4.5 x 10 x 13

Robotic Arms

The left arm is approximately 10 cm in diameter throughout its length. It collects and packages the regolith, rock fragments/chips, pebbles, and boulder samples. For these tasks, the arm employs the JSS and GC. Six sample packaging cartridges are located inside the arm. Since the cartridges must be able to advance for sample packaging, a joint near the attachment connection is not possible. This results in a maximum of five degrees-of-freedom (DOF) for the left arm.

The right arm has six DOF and a 10 cm diameter that tapers to 5 cm at the tool connection port. This arm uses the VP, HS, and BCR to package the boulder sample. It also aids in gathering specimens for retrieval by the left arm.

Descriptions of Operations

Both arms are used in the collection of each sample. For the regolith sample, the JSS is attached to the left arm, and the HS is attached to the right arm. The right arm uses the HS to make piles of regolith for easy pickup. The JSS scoops up the regolith, tilts up causing the sample to slide toward the arm funneling it into a sample packaging cartridge (See Figure 10C). The rock fragments and pebbles are collected in a similar way. In the event no suitable specimens are found, the right arm uses the VP to flake off rock fragments . It then uses the HS attachment to group together the fragments and

pebbles. The left arm, with the JSS attachment, scoops up the sample. Once the samples have been scooped up, the bottom portion of the scoop swings down on hinges, exposing a screen which sifts out any regolith and keeps only the rock fragments or pebbles (See Figure 10B). After the regolith has been sifted, the JSS is tilted up, and the sample is funnelled into a sample packaging cartridge for storage (see "Sample Packaging Cartridge" section). The procedures of both arms and the JSS will be repeated as many times as necessary to acquire the desired amount of each specimen.

The screen on the JSS is selectively used to acquire the appropriate samples. It obtains regolith-free samples of pebbles and rock fragments. This allows exclusive study of each element of the surface composition. In contrast, pebbles and rock fragments are not sifted out of the regolith sample, so a true representation of the Martian surface can be collected.

Obtaining the boulder sample is more difficult than the previous samples and requires a higher degree of interaction between the two arms. The left arm uses the GC to pick up a boulder sample. The sample size is no larger than seven cm in diameter due to basket dimension restrictions. Equipped with a BCR, the right arm positions itself underneath the sample. The left arm releases the sample into the center of the ring to be packaged by the BCR (see "Boulder Collection Ring" section).

Each sample is placed in the open sample containment basket which is retrieved by the lander. Once a sample is collected, the arm positions itself over the basket. After a sample is packaged, it detaches from the cartridge or ring and falls into the basket. A teflon type plastic completely encloses and protects the sample.

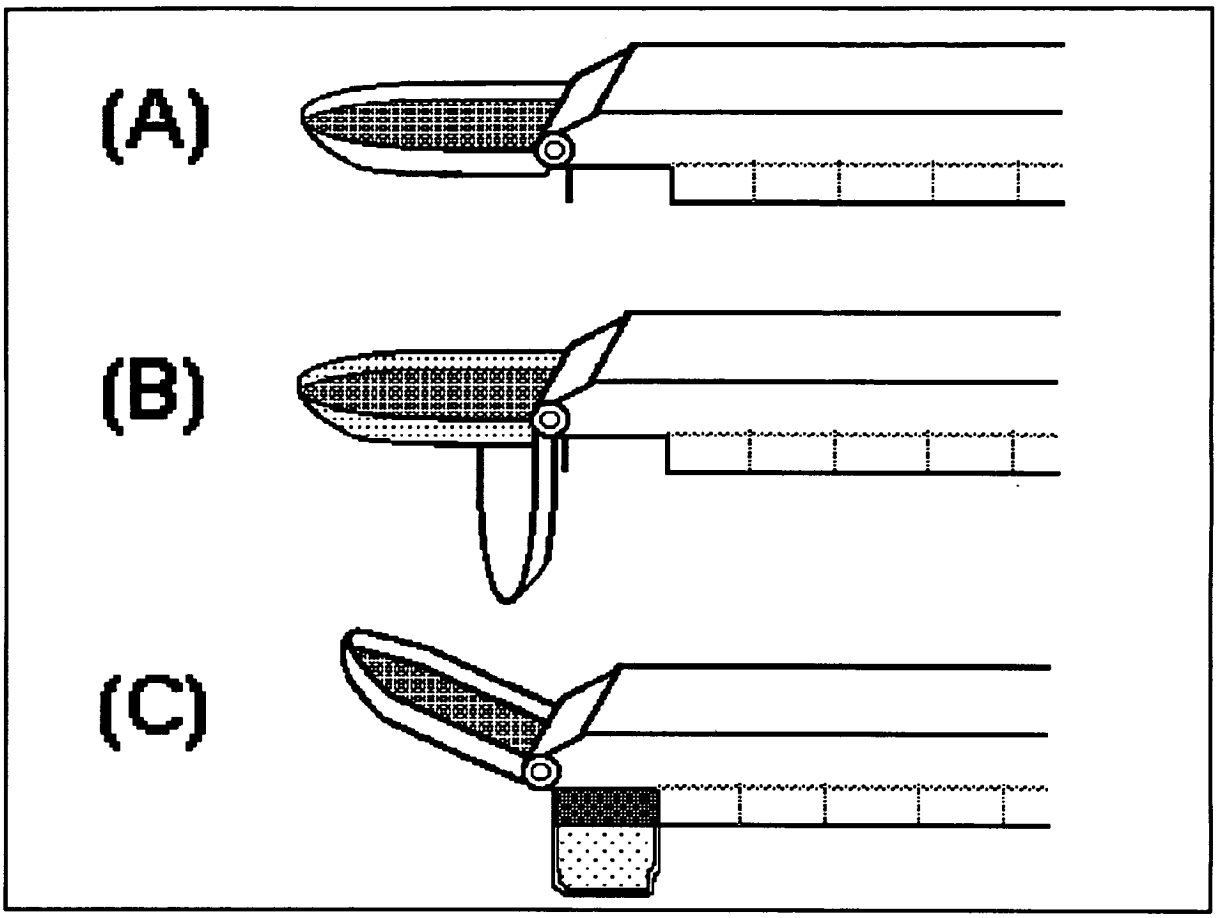

Figure 10. Jaw/Screen Scoop Attachment

After all sample collection and packaging has been completed, the basket is sealed. To seal it, the right arm twists on the lid, and aerogel is released inside in order to cushion the sample. Once the aerogel has filled the remaining volume of the basket, the lander will retrieve the basket for its return trip to Earth.

Sample Packaging Cartridges

There are six sample packaging cartridges stored in the left arm. Each cartridge has a teflon bag capable of holding 1,050 grams of samples (See Figure 11). A thin copper wire runs through the rim of the bag opening. Once a bag is full, a spool device winds the excess copper wire until the bag is closed. The arm then positions the closed bag over the sample containment basket. Then an electric current is passed through the copper wire heat sealing the bag. The heat seal is a result of melting the teflon of the inner surfaces together. By the same token, the current melts the teflon along the outer rim away. This allows the bag to detach from the cartridge and fall into the basket. The empty cartridge is then discarded to allow another to slide into place for further sample packaging. The cartridge is not dropped into the basket with the packaged sample. It is, instead, dropped from the arm and discarded on the Martian surface.

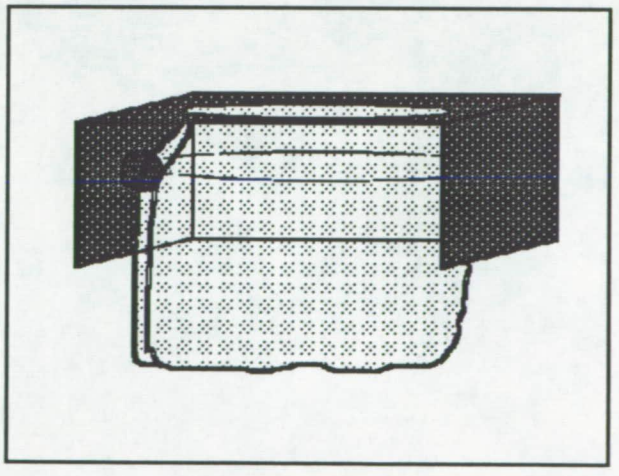

Figure 11. Sample Packaging Cartridge

Other options for the empty cartridges were discussed. Bringing the cartridges back with the samples was thought of as counterproductive. If the packaged sample along with the cartridge were dropped into the basket, it would occupy valuable room and add unwanted mass. The sealed basket and contents cannot be heavier than 6 kg.

A second option was to affix a homing device on each cartridge, and use the discarded cartridge as a marker. A transmitter would have to be placed on each cartridge, in order to later locate the exact spot of sample acquisition. The transmitter would have to be small, light-weight and self-powered. A tiny silicon chip transmitter was developed by Martin Marietta's Oak Ridge National Laboratory. The transmitter chip contains an array of solar cells, a capacitor, control circuitry, and a pair of laser diodes that emit IR radiation at a wavelength of 800 nm. It weighs 35 mg and has a range of 2 km (it was originally designed to be placed on Africanized killer bees to track their migration). This option was abandoned, however, due to the uncertainty that the transmitter's solar cells would be able to collect enough solar energy to power the transmitter. After the cartridge is on the ground, one of many frequent sand storms may bury it entirely, rendering the transmitter chip useless.

After evaluating these options, and finding no way around their shortcomings, they were dismissed. The only option left, beneficial to the mission, was to discard the cartridges on the Martian surface.

Boulder Collection Ring

There are two Boulder Collection Rings (See Figure 12) stored in individual slots between the arms in the front of the rover.

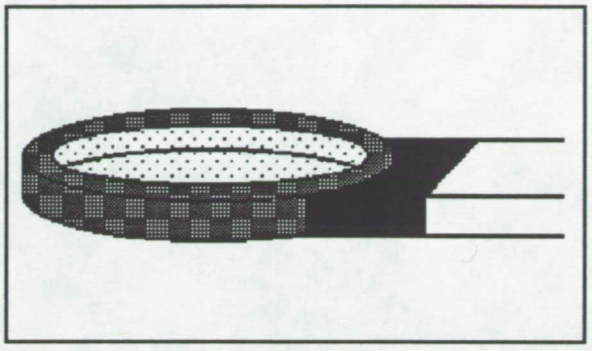

Figure 12. Boulder Collection Ring Attachment

Each ring consists of a thin copper wire, a wire retraction device, and a circular sheet of packaging teflon. The packaging teflon spans the ring opening with the excess rolled up inside the ring. The copper wire is below the packaging sheet, prior to sample packaging, near the bottom edge of the ring. The wire retraction device is located in a section of the ring handle (the ring handle is where the right arm will attach). The wire has two permanent attachment points, one is on the retraction device, while the other is on the ring opposite the ring handle. Once the boulder sample is dropped into the ring, its weight will cause the packaging sheet to unroll. The sheet, having its edge securely clamped within the ring, is allowed to completely unfurl. The wire is then pulled by the retraction device causing the sheet to close. An electric current is passed

through the wire, sealing the package. The arm then positions the storage ring above the sample containment basket. It unclasps the edge of the sheet, releasing the packaged sample. The ring is then returned to its slot for the duration of the mission.

Teflon Packaging

Each sample is packaged in teflon (either in a bag or sheet) before being placed in the basket. Teflon was determined to be the best packaging material to use. It is very ductile and non-reactive. Its non-reactive nature insures no contamination of the samples. Its high ductility allows for the sheets to be partially rolled up inside the BCR, and for the bag to be rolled up inside the cartridges prior to sample acquisition. These two favorable qualities make teflon the choice material for packaging.

Sealing the Basket

The basket and lid are made of a carbon-carbon weave. The basket is doughnut shaped. This material has very low conductivity and is very strong and durable. The low conductivity insures reasonable temperatures inside the basket during the return trip to Earth. Its strength and durability allows for a wall thickness of just 2 mm. In its center is a circular shaft extending the height of the basket. This shaft will house a core sample

which will be inserted through the shaft by the lander after it has retrieved the basket. The core sample is longer than the basket is deep, necessitating circular openings at the top and bottom of the basket as well as through the lid. The shaft also places a restriction on the size of boulder sample that can fit in the basket. The shaft has a 2 cm diameter, and the basket has an 18 cm diameter. This leaves only an 8 cm gap in which samples can be placed. To provide sufficient margin, the sample is limited to a 7 cm diameter.

The lid is screwed onto the front of the rover, with a half twist. Either arm is capable of untwisting the lid from the rover and then, with a half twist, screwing it onto the basket. The attachment ports, at the end of each arm, are able to "grip" the lid in the same way they "grip" each tool attachment. The appropriate connectors for the arm to attach to the lid are outlining the circular hole in the center of the lid.

Once the lid is in place aerogel is released into the basket. Two separate pressure vessels store the two chemicals that form aerogel (tetramethoxysilane and aqueous methanol). Valves connecting these two vessels to a mixing chamber are opened allowing the two to mix together. While in this chamber aerogel is formed using the condensed silica method, which combines the two via hydrolysis and polycondensation. The mixing chamber is connected to the basket, at its base, by a conduit and valve. This final valve opens releasing the aerogel, still in liquid form, into the basket thus filling the remaining volume. Within a few days the aerogel hardens and the basket is ready for transport. The inert aerogel acts as an insulator providing stability and cushioning for the samples during transport.

Polar Samples

The polar samples will be obtained and stored in the same fashion as the equatorial samples. Due to difficulty in obtaining rock and pebble samples only two samples will be collected in the polar region. They are a 70 gram boulder specimen and 2500 grams of regolith. The large regolith sample is necessary because of the ice that laces the surface. Polar ice prevents the sifting of samples which eliminates the need for a screen on the JSS. This also renders the proportions of samples collected indeterminable.

C-3

Imaging System

The imaging system chosen for the Mars Sample Acquisition Vehicle is based on a system developed by Odetics, Inc [8]. This system applies knowledge-based technology to supervise and control both sensor hardware and computation in the imaging system. The end result is what can be called a "smart" camera which would have some decision-making algorithms and would attempt to make the best use of the limited bandwidth for transmission of data.

This imaging system is built around a main unit called the knowledge-based supervisor controller (KBSC). The KBSC is a monitoring and control system which provides sensor control and processing and image control. It is programmed with an internal data base which contains rules, knowledge, data, and researcher's expertise as is relevant to processing the data. The KBSC is used in conjunction with a focal plane processor and image processors.

One of the attractive features of the KBSC is that it combines the use of a laser scanning system with camera imagers. Camera imagers, such as CCD cameras and infra-red cameras, can process images of high resolution but provide poor 3-D contour data. Also, extracting data is extremely computer intensive. On the other hand, laser scanning systems provide range and 3-D contour data, but image detail is poor. The KBSC provides an intelligent fusion of high resolution camera data and laser ranging data to develop an image of high spatial resolution and accurate range to specific objects in the scene.

The function of the integrated laser ranger/camera system (ILC) are shown in Table 5. The range may be provided at a single point or a range image may be generated by scanning the ranger over an area. Several display functions are available such as a contour map and an artificial grid to provide the concept of depth and range to any object in the scene. Camera control functions such as focus and zoom can be performed from the range output. Combining the range with high frequency spatial data can achieve rapid and very reliable camera focus.

Table 5. Integrated Laser Ranger/Camera System Functions

Range to any point in scene
Range image of any area in scene
Display (range image, contour map)
Display depth grid
Display range to any point
Focus Camera
Combine Range and reflectance data

System Overview

An overview of the imaging systems's architecture is illustrated in Figure 13. The areas shown are sensors, focal plane processor, knowledge-based supervisor/controller, image processors, and systems processor. Inputs to the system are supervisory command, channel capacity, and other mission data. The output is edited, classified and coded data, as well as other features and range information.

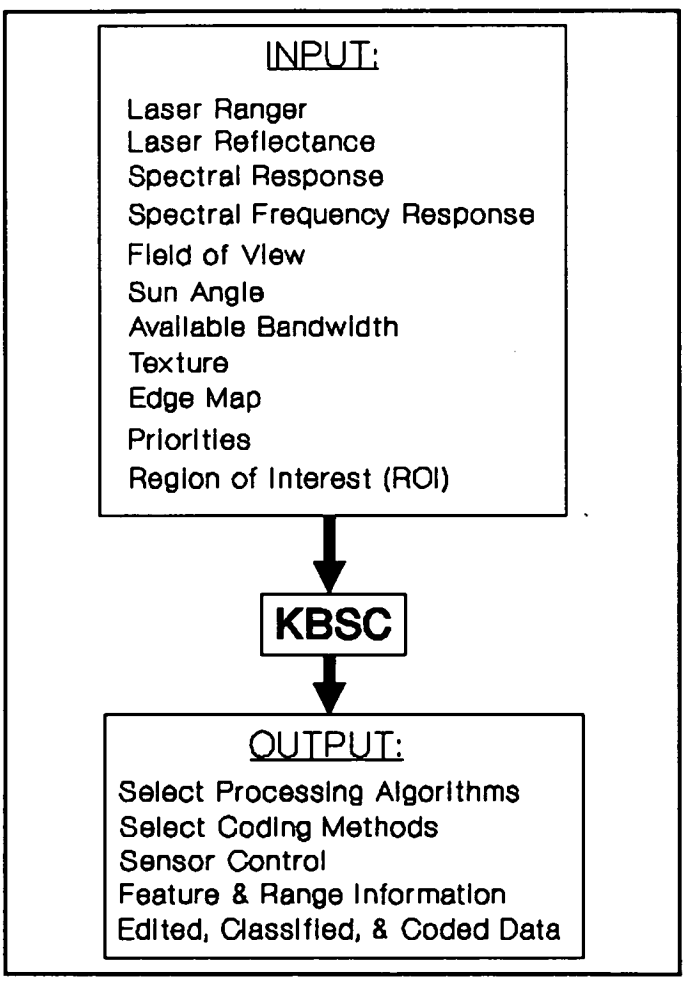

Figure 13. Imaging System Architecture

For this system, data from multiple sensors are collected and sent to the focal plane processor. The imaging sensors used are a color video camera, a infra-red camera, and an imaging spectrometer.

The focal-plane processor uses various numerical techniques along with the KBSC to format the received data to send to the image processor. The KBSC selects which algorithms or techniques are used in order to format the data. The data to be formatted depends on the supervisory command and priorities. For example, if the rover is travelling around searching for samples, the priorities would be imaging for navigation and sample identification.

The image processors edit and code data collected from the imaging sensors and the laser ranger. It is here that the integrated laser ranger/camera system is employed. The image processors use various algorithms to develop and code a high resolution image. Depending on the supervisory command and priorities, the image processors will output coded data and features and range information.

The inputs, output, and control functions of the KBSC system are shown in Figure 14. The inputs to the KBSC can be from image processors such as the spatial frequency, histogram, or other computed characteristics of the image. It may be a supervisory command for a previously identified object or area so as to designate a small region of interest (ROI). Edge information and segmentation may be used to identify specific features in the image. The color, or more generally the spectral response of the image, may be used to identify regions or objects.

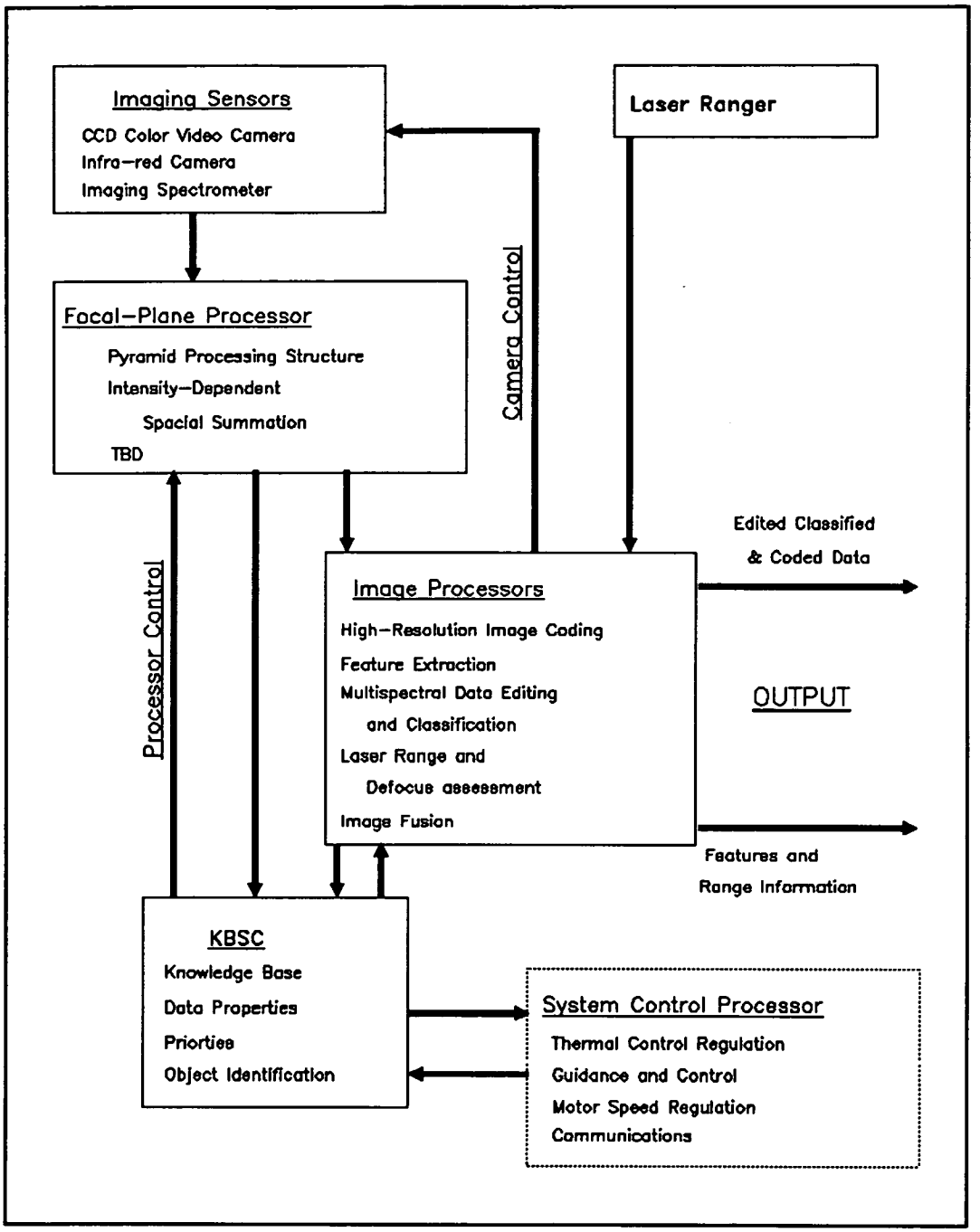

Figure 14. Inputs, Output and Control Functions of the KBSC

From the laser ranger, range and reflectance data may be used with the spatial data to identify features. Laser reflectance values determine the reliability of the range data as well as the reflectance of the target at the laser frequency. The field of view (FOV) may be important when selecting processing algorithms. Sun angle, available bandwidth, and other priorities will be used to select processing algorithms and image coding methods.

Another processor used in accordance with the KBSC is the systems control processor. This processor is represented as a dotted box in Figure 14 since it is not part of the imaging system. This processor is used to regulate and control various systems and devices on the rover. This processor will regulate the temperature of the working fluid for thermal control, modify the output speed of the drive motors, and direct the rover through its chosen path.

Systems Components

Specifications of the laser ranger are listed in Table 6. The KBSC is hosted on a SUN computer and the real-time signal/video processing is on a Datacube pipeline image processor.

The laser scanning system used is a pulse laser ranger. Pulse laser rangers operate on the basis of measuring the time it takes a laser pulse to travel to the object and back to the receiver. The pulse laser ranger was chosen over a continuous wave

laser ranger, which compares the phase shift between the transmitted and received wave, since it requires less computation for range and is generally better for long-range imaging.

Table 6. 501 Laser Ranger Specifications

Range	10 - 500 meters
Accuracy	0.2 meter
Resolution	0.1 meters
Beam Divergence	2.5 meters
Measurement Rate	1 - 2000 firings/second
Mass	3 kilograms
Power	3 Amps @ 12 Volts

The precision pan/tilt platform for the imaging sensors is shown in Figure 15. The laser ranger is mounted on this rotatable head with the CCD and infra-red cameras mounted on top of the laser ranger. The platform is controlled by the SUN computer either to point to a specific object or to scan an area to generate an image.

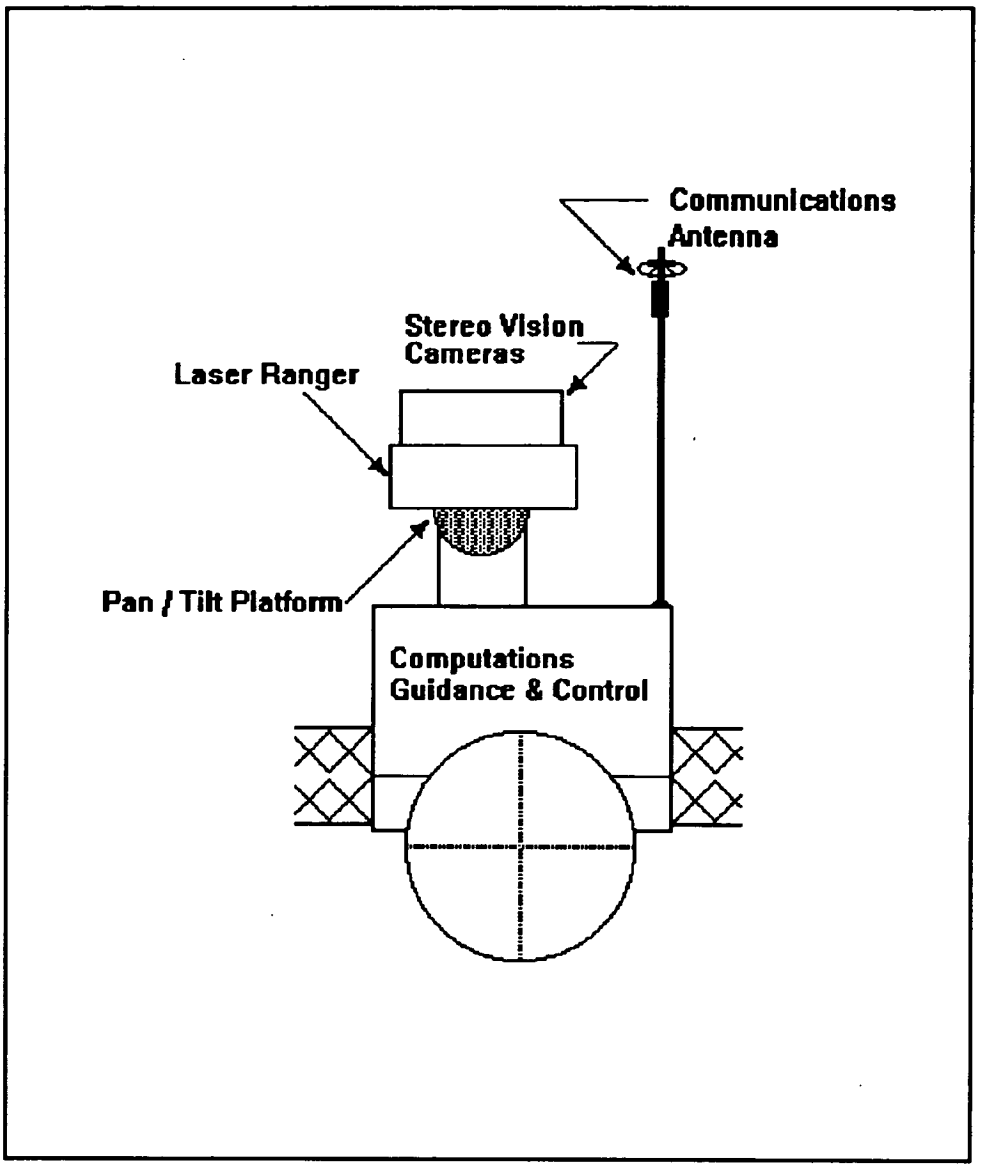

Figure 15. The MSAV Center Section

Guidance and Control

The guidance and control system is similar to that employed by automatic cruise missiles. Satellite maps of the Martian terrain surrounding the proposed landing site are stored in the computer. Infrared sensors and the laser ranger transmit current information about the actual terrain to the main computer which then uses microprocessors to compare the actual data to the maps. The KBSC system can then make course corrections to send the rover to any desired location. Should scientists on Earth wish the MSAV to go to a specified location, data can be transmitted to the lander which will then be relayed to the rover so that the KBSC can make the appropriate course correction.

Communications

A low-frequency radio (RF) link will be used for communication from the lander to the rover. Communication rates will be in the megabit/second range at 100 m, but diminish to 5 kilobytes/second at 5 km. This cost effective method using present day technology is more than suitable for a short-range local rover such as the MSAV.

Power Systems

Once the power requirements for the other onboard systems were set, it was determined that a power output of 200 W would suffice for the MSAV. The alloted mass for the power system was 100 kg, while the allowed volume was 71 x 71 x 71 cm. The system to be used also judged on the following criteria: developmental cost, efficiency, and durability. The five different systems considered were a General Purpose Heat Source Radioisotope Thermoelectric Generator (GPHS-RTG), Modular RTG (MOD-RTG), Closed Brayton Cycle Dynamic System (CBC), Free Piston Stirling Engine (FPSE), and nickel-hydrogen batteries.

This group of systems was quickly reduced to the MOD-RTG and the FPSE. The GPHS-RTG is not as efficient as a MOD-RTG; therefore, a MOD-RTG will give a greater power output for a given size. The CBC is very similar to the FPSE, but the FPSE has fewer moving parts and thus less chance of failure. The performance increases for the Stirling cycle if the size is reduced. Reduction is not so easily accomplished for the CBC. Also, the CBC is very susceptible to elevated background temperatures. Finally, batteries will require solar panels, or some such device, for recharging. This makes the system too bulky and inefficient to be effective.

The MOD-RTG was chosen over the FPSE. The RTG is more durable and has had more development than the FPSE. Furthermore, a cost analysis program was used to determine that the RTG would cost 22% less to develop.

The main difference between the GPHS-RTG and the MOD-RTG is the

modularity. With the MOD-RTG electrical output power can be varied, in increments, to meet user power requirements. This minimizes re-qualification costs for power thermal energy from the heat source to useable electrical energy (See Figure 16).

A report published by General Electric gives physical specifications for a MOD-RTG with a power output of 342 W. It is 1.08 m long, .33 m in diameter, with a mass of 91.1 kg. This data along with a breakdown of module data can be seen in Table 7. This shows that a combination of 11 modules will provide a power output a little over the necessary 200 W. An RTG with 11 modules of approximately 5.08 cm each plus two end closures of approximately 7.62 cm each has a total length of 71.12 cm, a diameter of .33 m, and an output of 209 W. The total mass of 11 modules of approximately 2.28 kg plus the 50 kg converter is just over 75 kg. These rough estimates have been determined to be adequate for the MSAV.

Table 7. MOD-RTG Reference Data

Power Output	342.5 W
Length	1.08 m
Overall Diameter	.33 m
Mass	41.1 kg
Number of GPHS Modules	18
Number of Multicouples	144
Length per Module	~5 cm
Mass per Module	~2.3 kg
Power per Module	~ 19 W
End Closure Length	~ 7.6 cm
General Converter	50 kg

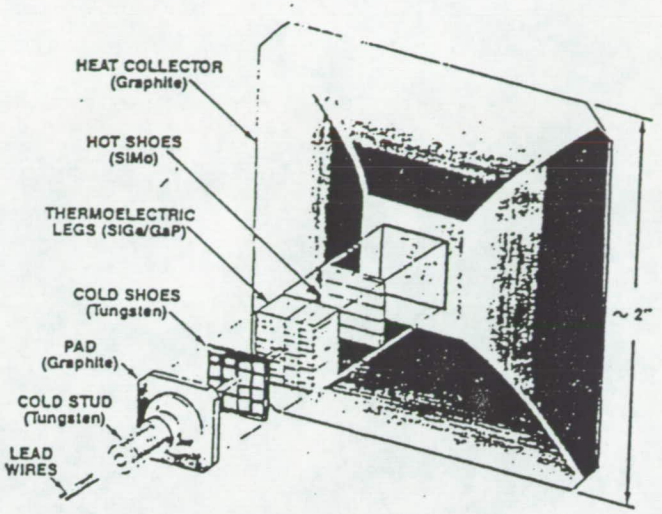

Exploded View of Multi-Couple

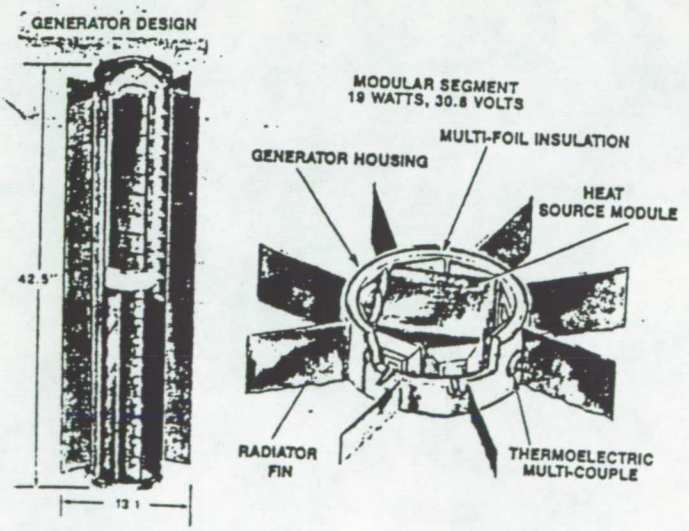

Figure 16. Schematic of Modular RTG

Thermal Control

The temperature extremes on the surface for Mars range from 170 K in winter to 310 K in summer. The electrical equipment has to be kept at about 317 K to function properly. The active thermal control system incorporates heat pipes as the primary means to transfer heat through the various equipment.

Heat Pipe

The heat pipe (See Figure 17) is an effective thermal conductance device able to transport high heat energies between two locations with high efficiency. The heat pipe consists of a container or pipe whose inner surfaces are lined with a capillary wick. Heat from the wick, at the evaporator portion of the pipe, vaporizes the working fluid. The resulting difference in pressure drives the vapor from the evaporator to the condenser where it releases its latent heat of vaporization. The loss of liquid by evaporation results in a liquid-vapor interface in the evaporator entering the wick surface, and developing a capillary pressure. This pressure forces the condensed liquid back to the evaporator for re-evaporation.

Design Considerations

The three basic components of the heat pipe are:

1.) The working fluid
2.) The wick or capillary structure
3.) The container or pipe

In selecting a suitable combination of the above, there were a number of conflicting factors which arose, and the basis for the selections are discussed below.

The Working Fluid

The first consideration was to determine a suitable working fluid. A variety of characteristics had to be examined to determine the most acceptable fluid. The operation vapor temperature ranges for some of the possible selection of fluids are shown in Table 8.

The prime requirements are:

1.) Compatibility with wick and wall materials
2.) Good thermal stability
3.) Vapor pressure not too high or low over the operating temperature range.
4.) High latent heat
5.) High thermal conductivity
6.) Acceptable freezing point

Table 8. Operation Vapor Temperature Ranges

Medium	Melting Point (K)	Boiling Point at Atmospheric Pressure (K)	Useful Range (K)
Helium	1	4	2 to 4
Nitrogen	63	77	70 to 113
Ammonia	195	240	213 to 373
Freon 11	162	297	233 to 393
Pentane	143	301	253 to 393
Freon 113	238	321	263 to 373
Acetone	178	330	273 to 393
Methanol	175	337	283 to 403
Ethanol	161	351	273 to 403

The life of the heat pipe is directly related to the compatibility/incompatibility of the materials. The working fluid had to have good thermal stability over the operating temperature range. The vapor pressure range must be sufficiently great to avoid high vapor velocities which cause large temperature gradients. The pressure must not be too high because of the structural strength of the pipe. In order to transfer large amounts of heat with a minimum fluid flow and maintain a low pressure drop between two points within the heat pipe, the latent heat of vaporization had to be high. Also, the

thermal conductivity of the working fluid had to be high in order to minimize the radial temperature gradient within the heat pipe and to reduce the possibility of fluid boiling at the wick/wall interface.

On the basis of the above criteria, Ammonia, Freon 11 and Acetone are the preliminary choices for the working fluid. Final selection will be based on the choice of pipe material.

The Wick or Capillary Structure

The selection of the wick for the heat pipe depended on many factors, several of which depended on the properties of the working fluid. The prime purpose of the wick was to generate capillary pressure to transport the working fluid from the condenser to the evaporator and be able to distribute the liquid around the evaporator section to the areas where heat will be received by the heat pipe. It also provides the necessary flow passage for the return of the condensed liquid. A composite or arterial wick was chosen over a homogeneous one because it has a higher heat pipe performance. Figure 18 illustrates the arterial wick chosen. This wick system was able to transport the liquid along the pipe with minimum pressure drop.

The Pipe

The function of the pipe is to isolate the working fluid from the outside environment. It had to be leak-proof, maintain the pressure differential across its walls, and enable the transfer of heat to take place into and from the working fluid. Some of the factors in selection of the pipe material were:

1.) Compatibility with working fluid and the external environment
2.) Strength to weight ratio
3.) Thermal conductivity
4.) Ease of fabrication, including weldability, machinability and ductility
5.) Porosity
6.) Wettability

The high strength to weight ratio is important due to rover weight constraints. The material must have a high thermal conductivity to ensure a minimum temperature drop between the heat source, RTG, and the wick. Also, the material had to be non-porous to prevent the diffusion of gas into the heat pipe. The thermal conductivity of some pipe materials considered are given in Table 9.

Stainless steel was suitable for the pipe material and is compatible with the working fluids acetone and ammonia but was not chosen due to its low thermal conductivity and its high weight. Since ammonia was chosen as the working fluid, copper

was not chosen because of it incompatibility with the fluid. Aluminum alloy 6061-T6 was chosen for the tube material because it is compatible with ammonia, light in weight and easy to machine.

Table 9: Choices of Pipe Material

Material	Thermal Conductivity (W/m°C)
Stainless Steel	17.3
Aluminum	205
Brass	113
Copper	394
Glass	0.75
Nickel	88
Mild Steel	45

Variable Control Heat Pipe

The purpose of choosing a variable control heat pipe was to control the operating temperature of the pipe within the design temperature limits of the electronic equipment. Two options of control techniques are listed below.

1. By using thermostatically controlled valves placed at specific locations in the pipe to interrupt fluid to a certain location.
2. By using thermal switches which enable the heat pipe to be switched off and on. This type of variable control was chosen because it had no moving parts and is able to adjust and control the temperature more reliably.

Electric Heaters

If for any reason the heat pipe is unable to perform up to expectations, electric heaters are placed near critical electronic equipment. The heaters are controlled by temperature sensing devices placed in the vicinity of the equipment and a controller which will activate the heaters when necessary.

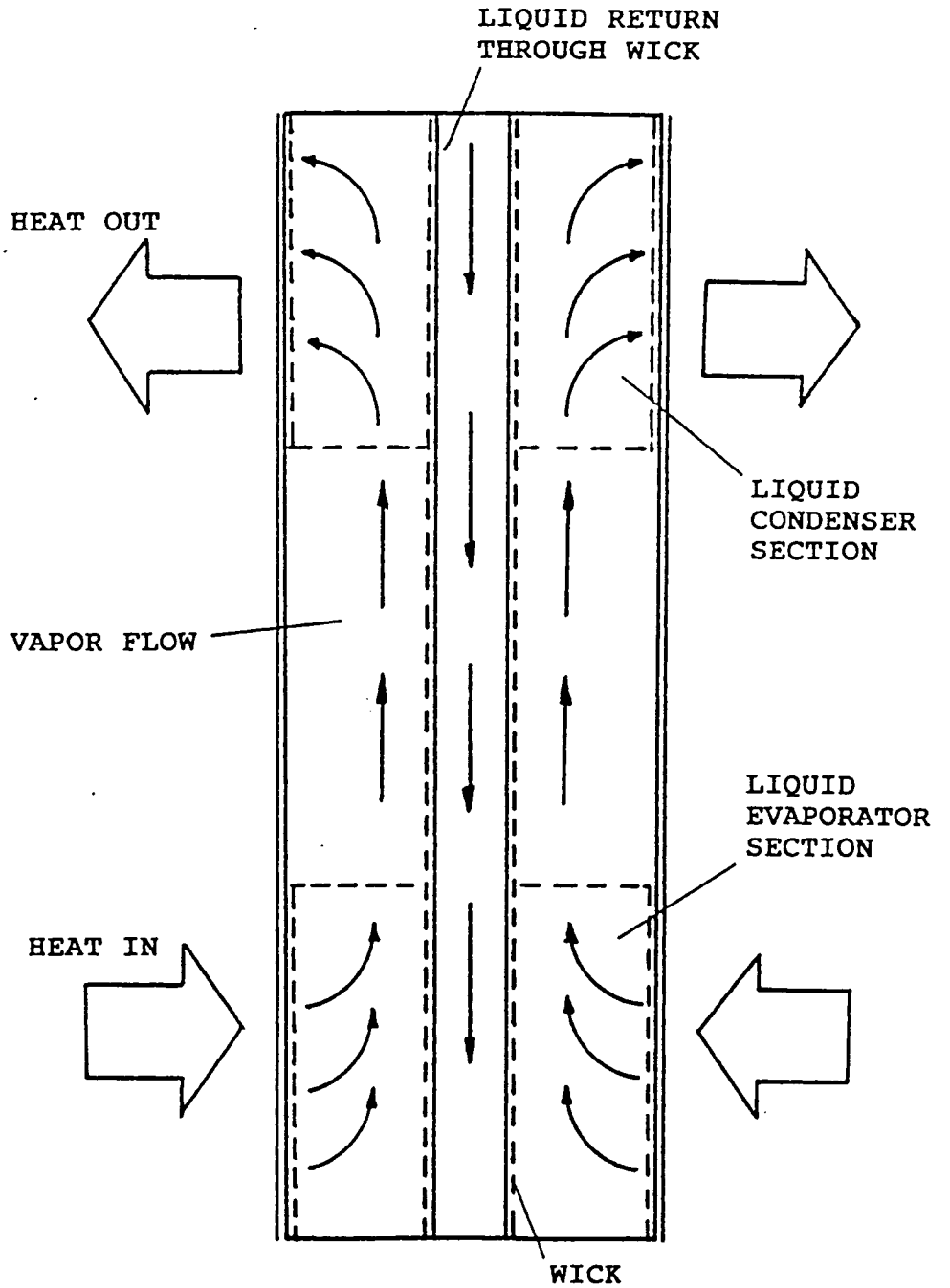

Figure 17. Heat Pipe Schematic

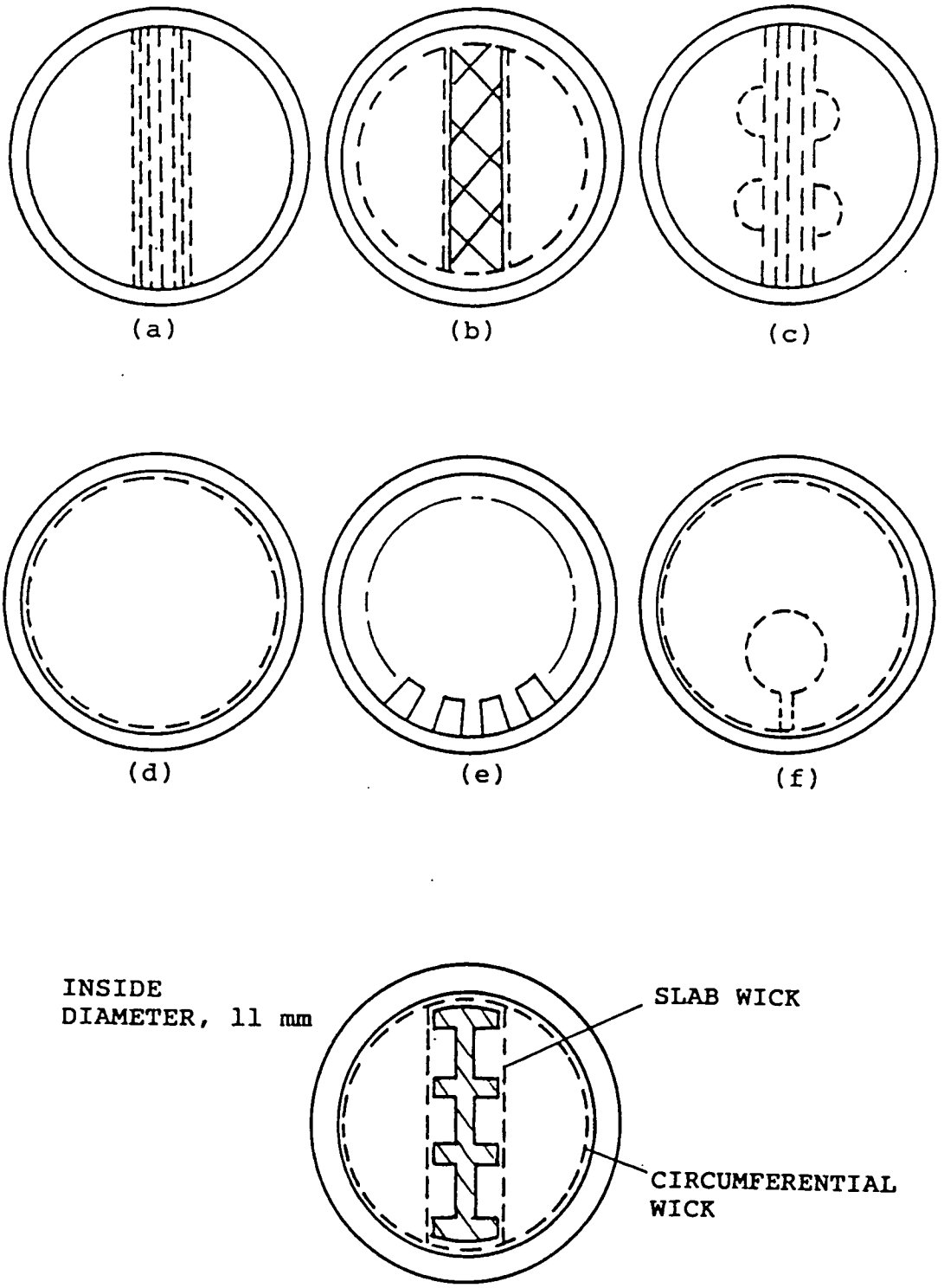

Figure 18. Arterial Wick

Conclusion

The Martian Sample Acquisition Vehicle is a slow-moving short range local rover capable of obtaining the necessary samples for the Mars Sample Return Mission. Many problems are overcome by having a slow-moving rover with a range of one to five kilometers from the landing site. Due to the MSAVs slow speed, roll-over is highly unlikely since the guidance systems will easily be able to steer around any obstacles that may oppose the rover's path. Also, the cost of the MSAV has been estimated to be $708 million using a computerized cost estimate model. For larger long-range rovers, the cost is much greater while performing basically the same mission.

Before actual development of the MSAV, more work will have to be completed on effectively integrating all of the systems through the KBSC control center. Additional research needs to be done on the Martian environment's effect on the Materials chosen for the MSAV, and calculations should be performed to insure that chosen materials are built strong enough to withstand its required loads.

References

[1] Chicarro, A. P., Mission to Mars. Report of the Mars Exploration Study Team, Technical Report, European Space Agency, July 1989.

[2] Pivirotto, and Dias, United States Planetary Rover Status-1989, Technical Report, National Aeronautics and Space Administration, Jet Propulsion Laboratory, California Institute of Technology, May 15, 1989.

[3] Queeny, R., Personal Interview with Dr. Queeny, Professor of Engineering Mechanics, The Pennsylvania State University, January 23, 1991.

[4] Urethane Tire Fill/Lining, Technical Note, Department of the Air Force, April 1990.

[5] "NHTSA Issues Non-Pneumatic Tire Rule Making," Elastomerics, v. 121, p 19, May 1989.

[6] Stokes, L. and Scott Pajtas, "New Non-Pneumatic Polyurethane Tire Based on Innovative Technology," Elastomerics, v. 121, pp 19-23, January 1988.

[7] "Non-Pneumatic Tires," Automotive Engineering, v. 97, p 47, August 1989.

[8] Westrom, G., Knowledge-Based Imaging - Sensor Fusion System, International Workshop on Visual Information Processing for Television and Telerobotics, National Aeronautics and Space Administration, 1989.

General References

Agrawal, Brij N., Design of Geosynchronous Spacecraft, Prentice-Hall, inc., Englewood Cliffs, NJ., 1986.

Bee Nimble, Bee Quick",IEEE Spectrum, pp 18, January 1989.

Bekker, Introduction to Terrain - Vehicle Systems, University of Michigan Press, pp 538-551, pp 679-690, 1969.

Bents, D. J., Preliminary Assessment of Rover Power Systems for the Mars Rover Sample Return Mission, Technical Report, National Aeronautics and Space Administration, Lewis Research Center, 1989.

Boo, J. H., Hartley, J. G., Heat Transfer in Space Systems, Analysis of the Thermal Performance of Heat Pipe Radiators, The American Society of Mechanical Engineers, United Engineering Center, N.Y., 1990.

Boyle, R. V., "Turbines in the Sky, The Power Behind Star Wars?" Mechanical Engineering, pp 38-45, July 1987.

"Carnegie Mellon Develops Six-Legged Robot for NASA's Mars Exploration Mission", Aviation Week & Space Technology, pp 115-117, May 21, 1990.

"Case for Mars," Science and Technology Series, Scientific and Technical Information Branch, Publishing for the American Astronautical Society.

DeMeis, R., "Bridesmaid of Engines Seeks Stardom", Aerospace America, pp 26-28, August 1985.

Dornheim, M.A., "NASA Briefs Contractors on Mars Rover/Sample Return Mission", Aviation Week & SpaceTechnology, pp 22-23, April 6, 1987.

Dunn, P., Reay, D.A., Heat Pipes, Pergamon Press Ltd., 1978.

Hartman, R. F., "Current Status of MOD-RTG Program," Intersociety Energy Conversion Engineering Conference, v. 3, pp 153-157, 1988.

Hrubesh, L. W., "Development of Low Density Silica Aerogel as a Capture Medium for Hyper-Velocity Particles", Lawrence Livermore Lab., Oct. 1, 1989.

Kirby, L., "Real Time Software Controls Mars Robot", Computer Design, pp 60-61, November 1, 1988

LeMay, J. D., Tillostson, Hrubesh, Pekala, "Microstructural Dependence of Aerogel Mechanical Properties", Laurence Livermore National Lab., April 11, 1990.

McCarty, L. H., "A Glutton for Punishment," Design News, pp 103-105, June 8, 1987.

ON MARS: Exploration of the Red Planet (1958-1978), Scientific and Technical Information Branch, National Aeronautics and Space Administration, 1984.

Preliminary Study of Mars Rover/Sample Return Mission, Technical Report, National Aeronautics and Space Administration, January 1987.

Ross, B., "Stirling Machines from Potential to Practicality," Mechanical Engineering, pp 34-42, June 1988.

"Silicon Chip to Track Killer Bees", Design News, pp 24, September 19, 1988.

Strumpf, H. J. and M. G. Coombs, "Solar Receiver for the Space Station Brayton Engine," Journal of Engineering for Gas Turbines and Power, v. 110, pp 295-300, April 1988.

Tilliette, Z. P. and E. Proust and F. Carre, "A Four-Year Investigation of Brayton Cycle Systems for Future French Space Power Applications," Journal of Engineering for Gas Turbines and Power, v. 110, pp 641-646, October 1988.

Tilliette, Z. P., "Advances in Defining a Closed Brayton Conversion System for Future ARIANE 5 Space Nuclear Power Applications," Journal of Engineering for Gas Turbines and Power, v. 109, pp 92-98, January 1987.

Van Ommering, G. and A. Z. Applewhite, Nickel Hydrogen from INTELSAT V to Space Station, Technical Report, GSFL Workshop, pp 387-397, November 1985.

MARS SAMPLE RETURN MISSION
TWO ALTERNATE SCENARIOS

PART II

A HIGH-TECHNOLOGY, HIGH-SCIENCE ALTERNATIVE

MARS SAMPLE RETURN MISSION

MISSION B

RADIO-ISOTOPE TRANSFER VEHICLE

FINAL REPORT

Aerospace Engineering 401B
Detailed Spacecraft Design
The Pennsylvania State University
Spring Semester 1991

GROUP WALTERS

Pat Benson
Steven R. Carbaugh
Jeff Fry
Kevin Gerhart
Wayne Holmberg
Kyle Kelly
Tony Pisano
Jeff Walters

Course Instructors

Robert G. Melton
Roger C. Thompson

ABSTRACT

The Planetary Transfer Vehicle will consist of a radio-isotope engine pod, three fuel tanks, and a sample retrieval bay. Two of the fuel tanks will be expendable and will contain the fuel necessary to get to Mars, where they will be jettisoned. The third tank supports the structure with the engines on one end and the sample retrieval bay on the other. This configuration will allow for maximum protection of electronics, samples, and other sensitive equipment from the radioactive engine core.

The most unique feature of this vehicle is its propulsion system. This system utilizes low-thrust, high-specific impulse (I_{sp}) radio-isotope engines. The engine configuration consists of six small engines (10 kilograms each) surrounding one larger engine (182 kilograms). The large central engine will produce the electrical power for all the ship's needs. The choice of propellants is ammonia (NH_3), for its low density, low cost, and ease of storage. The estimated fuel mass is 12,734 kilograms but this includes a 15% margin of safety. A general program (utilizing low thrusts and spiral transfer orbits) was developed to determine a more accurate propellant mass as a function of the fuel's properties (I_{sp} and density); however, due to time limitations, debugging was never completed.

TABLE OF CONTENTS

LIST OF TABLES

LIST OF FIGURES

LIST OF APPENDICES

INTRODUCTION

The Mars Sample Return Mission is an opportunity for man to explore the possibility of the existence of life-forms on other planets. The project calls for the return of a desired set of surface samples from Mars for study on Earth. These samples will include regolith, atmosphere, pebbles, rock fragments, a core sample, and boulder chips. A contingency sample of 100 grams of regolith and 200 cubic centimeters is collected, while 1000 grams of rock fragments, 2 kilograms of pebbles and a 70 gram core sample comprise the rest of the desired sample set.

This report details the design of a planetary transfer vehicle which will transport the necessary scientific retrieval equipment, as well as a permanent orbiting satellite, to Mars and return the samples to a shuttle-compatible Earth orbit. The only restriction placed on the design is the use of radio-isotope propulsion.

The design philosophy used in this project includes the maximization of the inherent power of the radio-isotope and the integration of subsystems for mass minimization. This philosophy also includes the development of advanced technologies which will further the field of space exploration. With this in mind, the coupling of the propulsion and power subsystems, as well as the coupling of the attitude control propellant and main engine propellant fuels was incorporated into the design.

VEHICLE ELEMENTS

The elements of the Planetary Transfer Vehicle are the Radio-Isotope Engines, the Fuel Tanks, the Sample Retrieval Bay, and the Subsystems. All components of the design have been developed with the a degree of flexibility, in order to facilitate changes in the design. Integration of these components with the other aspects of the mission was the key objective so their ability to be modified was crucial. In addition, the system was designed to keep sensitive equipment as far away as possible from the potentially dangerous radioactive engine core. The structure of this Planetary Transfer Vehicle obtained these goals.

RADIO-ISOTOPE ENGINES

Introduction:

Radio-isotope propulsion offers three attractive characteristics: simplicity, extended power life, and efficient performance. These characteristics can be advantageous in the propulsion application for this mission by reducing propellant requirements (compared with chemical systems), and reducing the flight time of the mission. By integrating the power system with the propulsion system, all power requirements of the spacecraft can also be met. Because of their high performance and inherent design simplicity, radio-isotope thrusters offer high reliability and will out-perform all chemical systems in fuel savings and performance.

Radio-isotope propulsion engines using direct heating consist basically of an isotope-bearing core enclosed in a pressure shell, a nozzle, and a heat rejection mechanism. A propellant such as hydrogen (H_2) or ammonia (NH_3) is heated as it flows through channels in the core and is expanded through the nozzle to produce thrust. This design is similar to solid-core nuclear rockets, but simpler because it involves no critical mass or nucleonic control problems. The power and thrust levels are completely predictable as they decrease as a known function of time depending on the isotope half-life (see Appendix 1).

The performance of a radioisotope engine is limited only by the isotope properties. The continuous release of energy is a problem and must be controlled. Although this release implies heat rejection by radiation to space during no-thrust periods, the system is designed both as a thruster and a radiator which is integrated with an isotope power unit. Due to present aerospace safety requirements, the design will insure complete containment of the radio-isotope material in the event of accidental launch abort or re-entry from orbit.

Engine Characteristics:

Two types of engines will be used for propulsion; solid core and molten core. Six solid core engines, delivering approximately one Newton of thrust each, will be configured around one molten core unit which delivers approximately three Newtons of thrust. The weight of a radio-isotope engine depends strongly on the isotope power density. Low-

power-density isotopes will require considerable isotope investments resulting in large chamber and engine weights. The actual weight also depends somewhat on the design used. Studies of solid core designs indicate that the engine inert weight (all weight except isotope investment) is about 20 to 30 times the isotope investment (Romero, 1965). Thus, lightweight engines are possible if high-power-density isotopes are used.

The operating temperature of radio-isotope engines of the solid-core type (see Figure 1) is dictated mostly by the cladding evaporation rate. The isotope compound can be embedded and clad with a refractory such as tungsten, and if the temperature is kept below 2478 °K (Romero, 1965), several months of continuous thrust are possible without excessive cladding loss. Since no nuclear reaction control is involved, it is possible to design the core for maximum heat transfer in order to avoid excessive temperature spikes that might cause excessive local evaporation. In any case, an outlet propellant temperature of around 2422 °K is a reasonable operating level (Romero, 1965); it yields a specific impulse of around 800 seconds at 101.0 kPa. The thermal efficiency of these engines will be about 70 to 90 percent, depending on the design. The molten core engine makes it possible to obtain much higher propellant temperatures. By using an isotope with a high melting point and heating the working fluid to a temperature of around 4422 °K, a frozen flow specific impulse of approximately 1,200 seconds can be achieved (Romero, 1965).

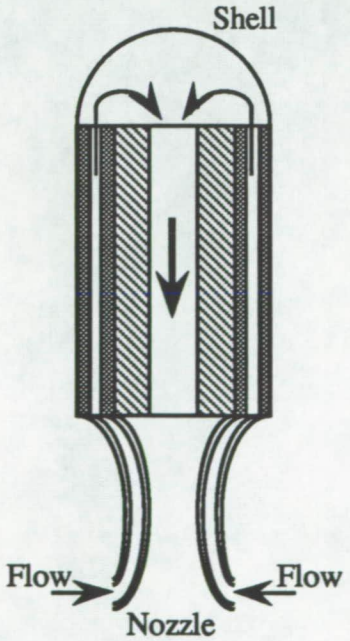

Figure 1: Solid Core Radio-Isotope Engine (Romero, 1965)

Due to the high operating temperatures of the propulsion system, it will be advantageous to supply all power needed for the spacecraft with a thermionic power converter. Thermionic devices convert heat directly into electricity by means of thermionic emission (see Figure 2). A thermionic converter mounted on the surface of the engine core will have 10 to 12 percent efficiency and a specific weight of 1 lb/kW. This is a substantial improvement over the specific weight of solar cells (1,000 lbs/kW) and thermoelectric devices (250 lbs/kW). This system can deliver up to 50 kilowatts of power (Encyclopedia Britannica, 1977).

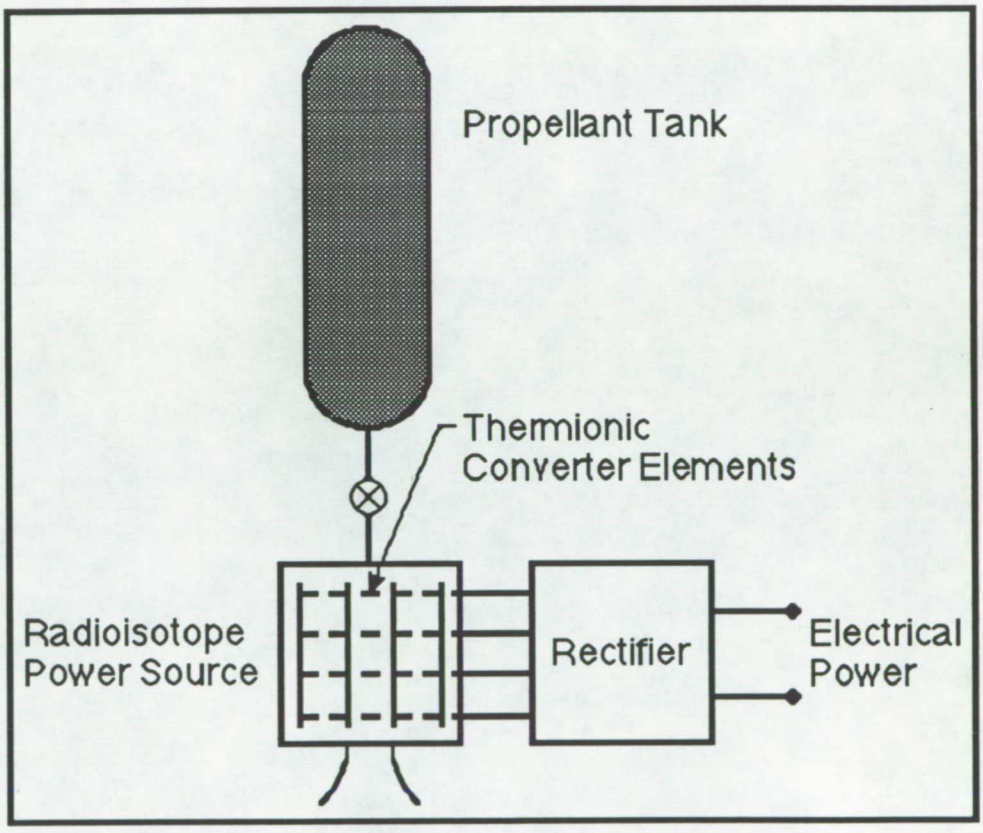

Figure 2: Combined Radio-Isotope Propulsion Engine and Power Cycle (Romero, 1965)

Radio-isotope engines are self-cooled when in the operating condition. During engine off periods, the solid core engines are cooled through a system of radiators and a power unit. A driving fluid for the power cycle, which can be liquid or gas, flows through

the reactor, expands through a turbine, flows through a radiator, and is pumped back to the reactor to complete the cycle. The molten core engine will employ a movable thermal insulator along with the power cycle to control the flow of heat. The thermal insulator can be mechanically removed from the engine, thereby either insulating against the flow of heat or exposing the heat producing section to space for radiation cooling from the outer walls (see Figure 3). An important advantage of this scheme is that it gives engine restart capability which is necessary for the completion of the mission.

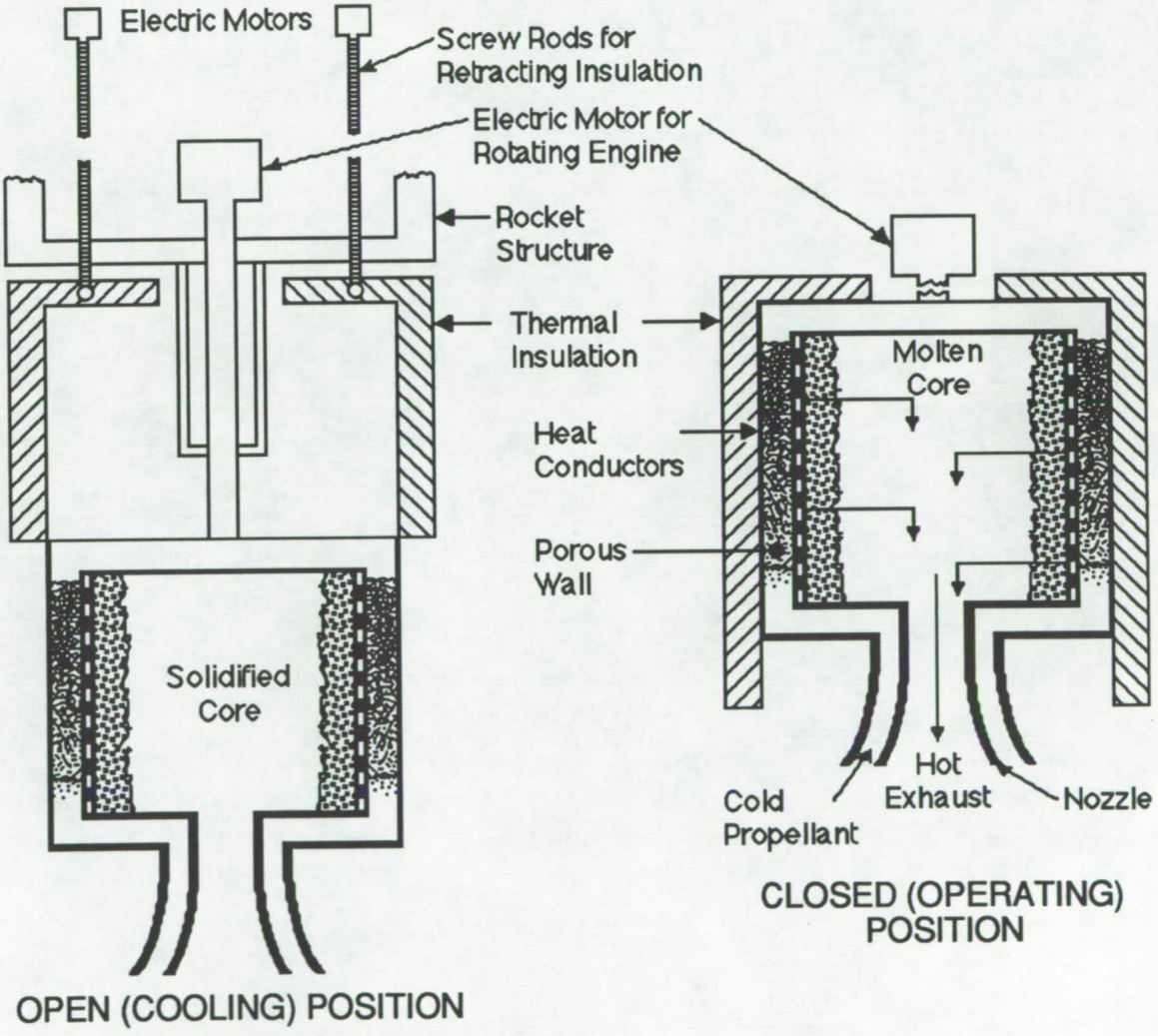

Figure 3: Radio-Isotope Engine Cooled by Movable Thermal Insulators (Romero, 1965)

The heart of a radioisotope engine is the isotope heat source. It must be capable of satisfying the power level, heat flux, temperature, lifetime and duty cycle requirements of the mission. It must also be lightweight and have a configuration which is compatible both with thruster thermal and hydrodynamic characteristics as well as with aerodynamic constraints imposed by aerospace nuclear safety requirements. Additionally, it must have sufficient structural and corrosive integrity to enable it to satisfy rigorous safety qualification testing. One of the important nuclear safety factors is the radiation emitted. The particles emitted may be alpha, beta, or gamma particles or neutrons. Of these, the alpha and beta emitters are preferred because they require less shielding and are easier to handle (see Table 1 for a list of useful isotopes). The isotope chosen for the mission is Curium (Cm-244). Although shielding will be required to protect electronic equipment.from harmful neutron particles, Cm-244 was chosen primarily for its ten-year useful mission life, power density, and low radiation emitted.

The primary components of a heat source are: fuel, liner, strength member, cladding, thermal coatings, and structural heat transfer elements. When selecting the appropriate materials and design for these components, ample consideration must be given to their nuclear, thermal, chemical, metallurgical, and mechanical properties as well as to such matters as fabrication, joining and quality assurance techniques, and to the degree to which the system can be proven through testing with non-nuclear simulated heat sources.

TABLE 1: List of Useful Isotopes (Romero 1963)

Isotope	Decay Production	Half-Life (years)	Melting Point (°C)	Density (kg/m^3)	Specific Thermal Power (w/g)	Useful Mission Life (yrs.)
Pu-238	α	90	. . .	10,000	0.48	10
Cm-244	**α, n**	**18**	**2000**	**11,800**	**2.3**	**10**
Cm-242	α, n	0.44	2000	11,800	120	0.5
Po-210	α	0.38	. . .	9,300	140	0.5
Sr-90	β	28	. . .	5,100	0.20	10
Cs-137	β, γ	27	. . .	3,200	0.07	10
Pm-147	β	2.6	2300	6,600	0.18	2.5
Ce-144	β, γ	0.78	2680	6,400	2.3	1.0
Tm-170	β, γ	0.35	. . .	8,700	1.75	0.5

A composite capsule of the substrate material W-25 Re has been successfully tested and is preferred because of its compatibility with H_2 and NH_3 at all temperatures (Martinez, 1966). The capsule will be fitted with the external tungsten cladding now under development and with the tantalum alloys currently being employed for internal capsule liners. In arc-cast form, it has relatively good creep resistance and ductility and its ability to withstand impact has been experimentally demonstrated to satisfy the impact criteria.

Nozzle efficiency will also play a significant part in engine performance. Nozzle efficiency is defined as the ratio of delivered specific impulse to theoretical specific impulse. Since specific impulse varies approximately as the square root of the absolute temperature, the increase in operating temperature required to offset nozzle losses in maintaining a given performance can be substantial. For example, a 10% loss in nozzle efficiency must be compensated by almost a 20% increase in absolute temperature in order to hold specific impulse constant. Experimental data collected on supersonic nozzle configurations for radio-isotope thrusters showed conclusively that the 20° nozzle produced the highest specific impulse and efficiency was in excess of 99% (Jones & Austin, 1966).

Shielding from radiation hazards for radio-isotope propulsion must be considered during production, launch, and flight. Shielding to protect sensitive instrumentation will be an important factor in the mission and result in extra mass, which affects propulsion system performance. A permissible dosage limit for instruments is approximately 10 million rad total dose. Shadow shielding to protect against solar flares may be used in conjunction with isotope shielding to reduce shielding weight. Final location of the shielding can be specified with the use of the Boeing Company shielding computer code, available for use from Boeing for finalizing the radiation shielding needed.

Conclusions:

Radio-isotope propulsion offers significant advantages and a unique capability as the primary source of thrust for the Mars Sample Return Mission. High specific impulses, increased payload advantage, and high reliability can be realized. Radio-isotope thrusters have been designed and successfully tested and compare favorably with multi-stage

chemical systems. By integrating the radio-isotope unit with the power system, all electrical power for the spacecraft can be supplied. This system should yield a substantial performance dividend for the mission.

FUEL TANKS

The tank configuration will consist of three identical tanks placed side-to-side. The tanks are cylindrical with hemispherical endcaps, and each will have the following properties (see Appendix 2):

Table 2: Tank Specifications

Cylinder Diameter (each tank):	2 m
Height per Tank:	7.9 m
Volume per Tank:	22.577 m^3
Mass per Tank:	2,313 kg (15% propellant mass)
Propellant Mass per Tank:	15,420 kg* of ammonia

(* - includes a 15% margin of safety in total mass of the propellant)

This configuration will withstand higher stresses in the structure than a cylinder with flat ends and thus will decrease the mass needed for construction. The diameter of 2 meters was chosen to accommodate the attachment of the radio-isotope engines (3 meters in diameter) and the sample retrieval bay (1.5 meters in diameter). The height of the tanks results directly from the volume of propellant required (67.731 cubic meters), the number of tanks to be used (3), and the diameter of the tank (2 meters). Since the propellant is ammonia, the tank height is 7.9 meters.

Ammonia (NH_3) is the fuel choice since it is easy to store for prolonged periods of time. For example, ammonia must be kept between 195.2 K and 239.7 K while hydrogen must be kept between 13.8 K and 20.2 K. Obviously, it will be easier (and cheaper in terms of refrigeration) to keep the ammonia inside its temperature range. Ammonia will also be cheaper to use because it only costs $54.33 per cubic meter while hydrogen costs $1,089 per cubic meter (Huzel & Huang, 1971). This amounts to a total savings of approximately $175,949. The multi-tank configuration allows for the jettisoning of empty fuel tanks. This will result in fuel savings since each tank has a mass of 2,313 kilograms.

The engines are connected to the bottom of the center fuel tank and the sample retrieval bay is connected to the top. This configuration allows for maximum separation of the sensitive equipment from the potentially dangerous isotope source. A second advantage to this arrangement is the reduction of in-space assembly. With the engines and the sample retrieval bay already attached to the center tank, the engines can maneuver through space to connect the planetary transfer vehicle to the remaining components (the other two fuel tanks and the lander/communication package).

The sides of the fuel tanks have connection points for attaching the tanks to one another. Since this is accomplished during maneuvers on-orbit, the connection points are designed to simply push together. Once together, fuel and electrical lines remain attached until the peripheral tanks become empty, at which time they are jettisoned.

Also connected to the side of the central tank is the communication dish for the Planetary Transfer Vehicle. Connecting the dish to the central tanks becomes a necessity if it is to avoid the ejectable components of the mission.

SAMPLE RETRIEVAL BAY

The sample retrieval bay is a cylinder with a 1.5 meter diameter and a 2.0 meter height. These dimensions result from the size of the sample return rocket. This rocket has a diameter of 1.22 meters and a height of approximately 1.0 meter. The retrieval bay will be mounted to the top of the central propellant tank and will connect the transfer vehicle to the lander/communications package. This configuration allows for maximum shielding of the transfer vehicle's main computer and communication subsystems which will also occupy the sample retrieval bay. Since the structure of the bay will accommodate the attachment of the lander/communications package to the transfer vehicle, measures have been taken to assure structural integrity under any acceleration caused by thrust loads.

The sample retrieval bay will also house a mechanical retrieval arm to assist in the capture of the samples during rendezvous. During the transfer orbits, the retrieval arm will remain inside the sample storage bay.

SUBSYSTEMS

When examining this spacecraft, there are four primary subsystems to consider: 1) guidance, navigation, and control (GN&C); 2) communications; 3) command and data handling; and 4) power. Each subsystem has its own complications and requirements for the Planetary Transfer Vehicle (PTV). The basic constituents, total mass, and power required for the GN&C, Communications, and Command and Data Handling subsystems are listed in Table 3 and are referred to in each section below.

Guidance, Navigation, and Control:

The GN&C's functions are obviously spacecraft guidance, navigation, and attitude control. Four types of sensors are used for guidance and navigation on the PTV. Each sensor has a specific function for GN&C.

Sun sensors serve as a reference when the PTV must reorient the vehicle from an unwanted attitude. The sun sensors can only define a single axis and therefore will be used along with horizon sensors and magnetometers (when near a planet) to determine attitude data for the three axes.

A star mapper uses star sensors to map out stars in its field of view. The mapper finds a star in the field of view, record's its position, then goes to the next star. The stored data is used to determine the PTV's position in inertial space.

Horizon sensors are infrared sensors which use the IR boundary from the horizons of Earth and Mars as a reference. Since these sensors use a planet to operate, they will only be used near the Earth or Mars.

Magnetometers measure the Earth's magnetic field and data is combined with Sun and horizon data to help establish the spacecraft's attitude. These sensors are used in Earth's orbit when the PTV is assembled before the initiation of the Earth the Mars transfer orbit.

An inertial-measurement unit is used to measure the rotational and translational motions of the PTV. A strap-down unit is implemented for the PTV rather than a gimballed platform. This is done since the gimballed platform is mechanically complex, heavy, and

uses more power than a strap-down unit. A strap-down unit uses high resolution software to resolve the output of the body reference sensors into an inertial reference frame (Wertz and Larson, 1991). A rate gyro is also used, and it supplies readings from each sensor to the onboard computer. Later, these readings can be sent to Earth as required. Using this information, attitude adjustments are then made using arcjets.

Attitude control for the PTV is achieved by twelve ammonia arcjet thrusters, four for each principal axis. Arcjets were chosen over the combination of momentum wheels and thrusters. This choice was made since rough calculations of momentum wheel sizing (comparing to an existing satellite) indicated a momentum wheel would be needed of approximately 8,000 to 10,000 kilograms for a PTV with payload inertia of roughly 3.2 million kg m^2 (Wertz & Larson, 1991). Momentum wheel sizing could be reduced by using a ring mass and increasing the rotational speed but the overall mass of a momentum wheel would still be excessive. A second consideration was the relatively large mass reduction during the life of the mission. At mission start, the mass of the system is approximately 60,045 kilograms. When leaving Mars, the new system mass will be approximately 18,146 kilograms. Obviously, a momentum wheel to control the starting mass would be excessive for controlling the Mars departure mass.

No alternative propellant is needed since the arcjets will use ammonia (the main engine's propellant). The arcjets produce 1.0 Newton of thrust at a power requirement of 7.350 kilowatts each. This is desirable since the molten core radio-isotope engine, at maximum thrust, is predicted to be able to produce up to 25 kilowatts. This is especially an advantage when the PTV conducts its 180° in-plane slew maneuvers which occur midway during the transfer orbit to Mars, twice in Mars orbit, and once for the spiral back to Earth orbit. The maximum power required for the arcjets occurs during the Mars maneuvers where the arcjets require about 15.0 kilowatts of power. The large power margin from the radio-isotope engines will enable all systems on the PTV to remain active during all large power requirement maneuvers. Maximum fuel consumption for the arcjets will also occur at mid-trajectory of the Mars transfer orbit due to the large inertia of the PTV with payload. The fuel expended during this maneuver is predicted to be a total of 0.761 kilograms (see

Appendix 3). This figure is based on acceleration and deceleration firing times totaling 56.02 minutes and a worst case I_{sp} of 450 seconds for the ammonia propellant. From this calculation, a total propellant mass of under 10 kilograms is needed over the entire mission for the arcjets. Since the fuel tanks were designed with extensive margins of safety (see Fuel Tanks section of this report), this mass is not considered a problem.

Communications:

The need for communications with Earth, the Mars lander, the Mars rovers, and the sample return rocket, dictates the use of two communication systems. First, there is a need to receive and transmit signals to Earth ground stations in the Space Ground Link System for carrier tracking, command reception and detection, telemetry modulation and transmission, ranging, and finally subsystems operations. This is done with an S-band communication subsystem. Mass and power requirements for a typical subsystem are shown in Table 3. A suggestion for situations when the PTV is behind Mars is to use the Mars satellite as a relay for Earth communications. This should be considered if this project becomes a reality. As it is now, information concerning the PTV will be stored by Command and Data Handling when communications with Earth are not possible. Once communications with Earth are reestablished, Command and Data Handling will play back all necessary information.

For communicating with the Mars lander, the Mars rovers, and the sample return rocket, the PTV will use a Ka band communication subsystem. Table 3 lists the typical mass and power requirements for a Ku band communication subsystem. Transmission sending and receiving will be accomplished using a 0.9 meter parabolic dish antenna located on the central tank of the PTV. This configuration allows the antenna to be clear of the ejectable portions of the vehicle (the lander/communication package and the peripheral fuel tanks).

Table 3: Mass and Power Requirements for the Planetary Transfer Vehicle's Subsystems

Subsystem	Number	Mass (kg)	Power Required (Watts)
GN&C			
1 Arcjets	12	**	7350.0 (per arcjet)
2 Sun Sensors	6	12.0	18.0
3 Horizon Scanning Sensors & Electronics	2	5.00	10.0
4 Mapper Star Sensors	3	21.0	60.0
5 Magnetometer	1	1.20	< 1.0
6 Inertial Measurement Unit (Strapdown Units and Rate Gyros)	--	--	> 25.0
Communications			
1 S Band	1	28.54	62.5
2 Ka Band*	1	13.3	24.3
C&D Handling			
1 Telemetry	1	2.49	8.75
2 Remote Unit w/mP	1	7.24	27.0
3 RCA STR108	1	3.18	15-17 Playback
4 NASA STD Tape Rec			7-13 Record
			2.3 Standby

*Ka band mass and volume is based on Ku band equipment

Command and Data Handling:

The Command and Data Handling subsystem will receive, decode, process, and distribute spacecraft commands, as well as gather, format, and store data from spacecraft measurements. Mass and power requirements are shown in Table 3. The computer in the Command and Data Handling subsystem will monitor and control the radio-isotope engines, arcjets, and antenna. The computer performs calculations for antenna pointing parameters and does performance limit checks on parameters available for telemetry (Wertz and Larson, 1991).

Power:

Power for the PTV is supplied by the radio-isotope engines (see Radio-Isotope Engines section of this report). A power curve for the mission is shown in Figure 4. This figure breaks the mission up into four phases for the transfer to Mars. Each phase shows the average power needed from the engines. As mentioned earlier, the maximum power needed is 15 kilowatts and will take place at phases 2-3 and 4-5. These power maximums occur during the 180° slew maneuvers during the Mars spiral down trajectory, the Mars rendezvous, and the Earth spiral down maneuvers. Earth spiral down maneuvers are similar to Mars spiral down maneuvers, but are not shown in Figure 4. The maximum power produced by the radio-isotope engines is 25 kilowatts at full thrust which gives the spacecraft a 10 kW power margin at these times.

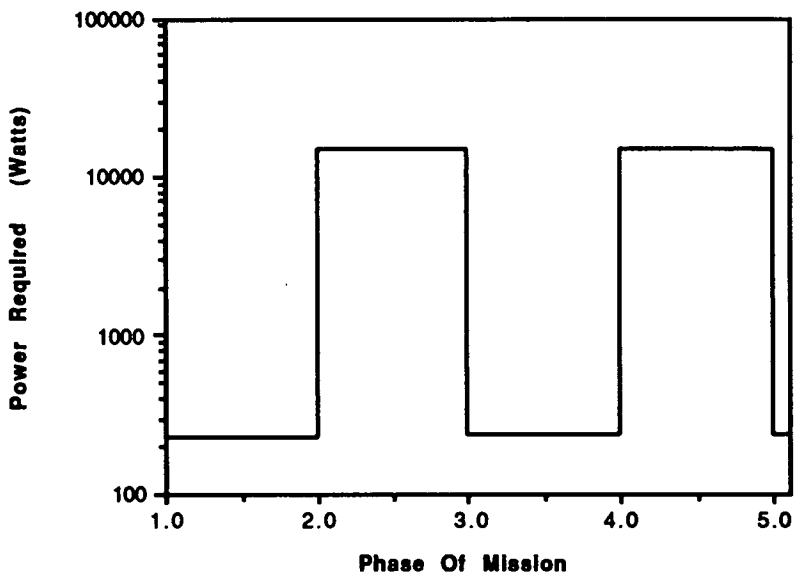

Figure 4: Power Requirements for the Planetary Transfer Vehicle

Phase 1-2: Average power required from Earth until Mars spiral down maneuver

Phase 2-3: Power required for Mars spiral down maneuver

Phase 3-4: Power required for Mars orbit

Phase 4-5: Power required for rendezvous

LAUNCH AND ASSEMBLY

The assembly of the Mars Sample Return Vehicle will be accomplished in four launches of the Titan IV rocket. These launches take into consideration that a Titan IV can carry a payload of approximately 18,000 kilograms in a cargo bay size of 5.2 meters diameter by 17.1 meters length.

The first two launches will carry the two peripheral fuel tanks, the third launch will carry the lander package and the communication satellite, and the fourth launch will carry the third fuel tank, the sample retrieval bay, and the radio-isotope engine pod. This breakdown results from the launch-weight restrictions of the Titan IV rocket, and the desire to separate the delicate scientific equipment (at least to some extent) from the relatively hazardous fuel. Figure 5 shows the relative sizes of the components as they will sit in the Titan IV's cargo bay. The first two Titan IV's will carry approximately 17,733 kilograms each (39,012 pounds at launch), the second will carry approximately 6,483 kilograms (14,263 pounds at launch), and last Titan IV will carry approximately 18,096 kilograms (39,811 pound at launch). The last Titan IV being 96 kilograms over the maximum payload mass allowable should not pose any problems since all fuel estimates are conservative estimates and should decrease in the final analysis.

First and Second Launches:

Titan IV's #1 and #2 will contain the two peripheral fuel tanks. This fuel will be entirely consumed on the voyage to Mars and the peripheral tanks will be jettisoned. Launching the fuel tanks first allows for establishing stable orbits of the hazardous components prior to the launch of the sensitive equipment. This reduces the possibility of having an accident occur in space.

Third Launch:

The third Titan IV launch will carry the lander package and the communications satellite. These parts will be preassembled in the Titan IV's cargo bay to reduce the amount of on-orbit assembly required. Keeping the scientific equipment on a separate launch from

the radio-isotope engines allows for maximum separation of radio-active elements from the rest of the mission's components, thus shielding the sensitive electronics.

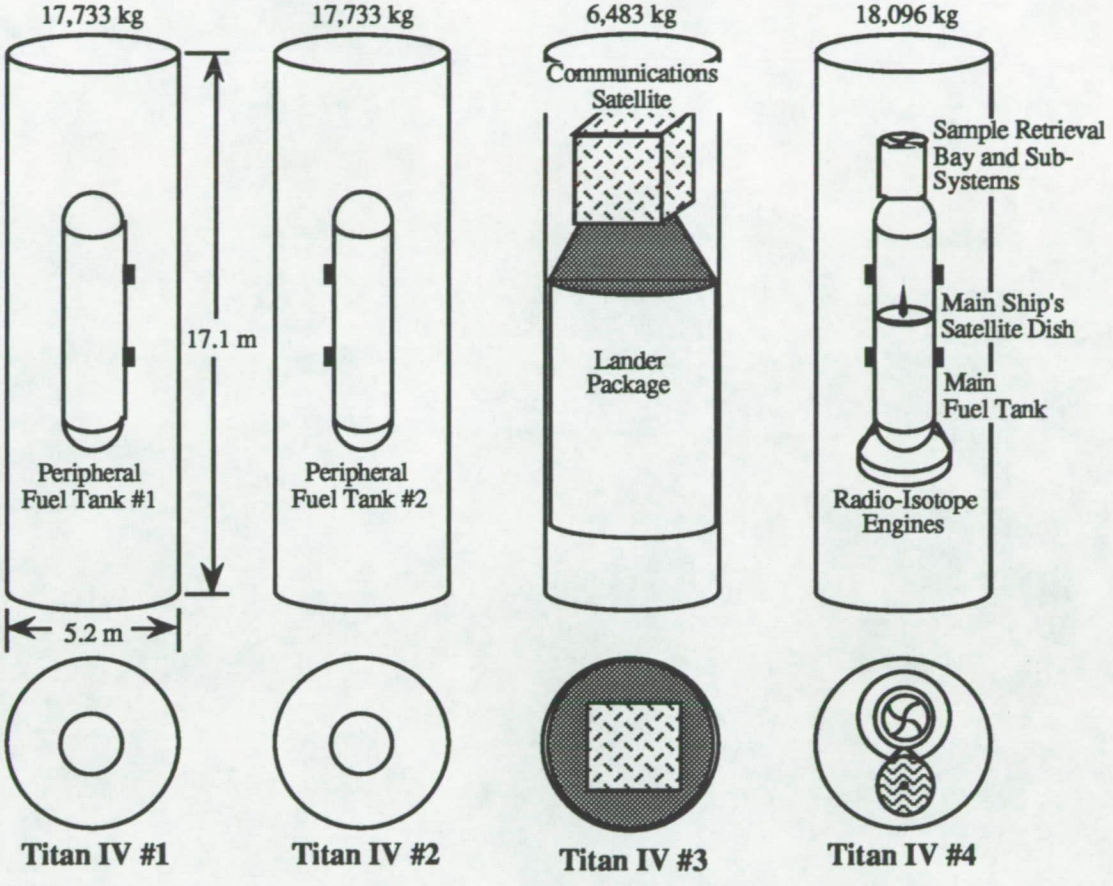

Figure 5: Titan IV Launch Vehicle Configuration

Fourth Launch:

The fourth and final Titan IV will carry the main fuel tank, the radio-isotope engine pod, the sample retrieval bay, and the main ship's communication system. Once the radio-isotope engines are running, this component will rendezvous with the two peripheral fuel tanks and the lander package/communication satellite. Since the last component (with the radio-isotope engines) is the only one with maneuvering capabilities, it was chosen to be the last piece launched so the mission starts as soon as it establishes an orbit around Earth.

Once assembled in space, the entire ship will have the configuration shown in Figure 6. While traveling between the planets, the side of the ship with the satellite dish will always be pointed in the direction of the Earth allowing for constant communications.

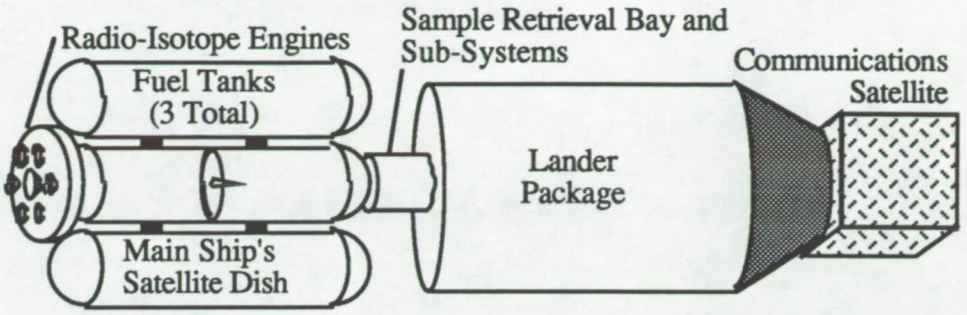

Figure 6: Radio-Isotope Transfer Vehicle - Fully Assembled

TRAJECTORY AND PROPELLANT CONSUMPTION ANALYSIS

Since the radio-isotope transfer vehicle will utilize a constant, low-thrust burn to accomplish the mission, impulse approximations fail to predict the position and velocity of the spacecraft at any given time. Specialized perturbation techniques are better suited to analyze such orbits and several of these techniques were examined.

Three perturbation methods were examined; Cowell's method, Encke's method, and a variation of parameters approach. Of the three, Encke's method was chosen to compute the trajectory and thus the required propellant mass for the mission. Encke's method was chosen over the variation of parameters approach because of its simplicity. Cowell's method was considered; however, the same accuracy can be obtained via Encke's method with much larger time steps, resulting in less computational time. A computer algorithm was developed which will employ Encke's method to determine the affects of perturbation forces on the spacecraft. The program, however, was not completely debugged due to time constraints.

In Encke's method, the difference between the primary accelerations and the perturbing accelerations are integrated. A description of the governing equations and the algorithm appear in Appendix 4.

Some approximations were made with regards to the mission parameters. It was assumed that Mars' orbit lies within the Heliocentric-ecliptic plane and both Mars and Earth are spherical bodies. A patched conic approximation is being used to distinguish the primary accelerations acting on the spacecraft. The gravitational acceleration of the Earth's moon was neglected due to lack of time but a subroutine to include this perturbation would not be difficult to insert into the code. The Martian moons were neglected because of their relatively small sizes.

The perturbing accelerations, those which have magnitudes much lower than the primary acceleration, can be expanded by inserting subroutines into the code. Although plans were to include all perturbations, thrust was the only perturbation taken into account. The direction of the thrust is hard coded into the program and can be changed to include any reasonable orientation by varying two angles.

RENDEZVOUS

The mission profile developed for the Mars Sample Return Mission requires that the collected samples be launched into a Martian orbit. The transfer vehicle, which had previously established a Martian orbit, will rendezvous with the sample rocket. The samples must be retrieved from the rocket and stored on the transfer vehicle before the mission's return to Earth stage can begin.

The rendezvous stage of the mission begins once the samples are collected and placed on the sample rocket. The sample rocket is launched into approximately a 500 km target orbit, which is circular, co-planar and greater than the parking orbit of the transfer vehicle (see Figure 7). The transfer vehicle maneuvers from its current parking orbit into the target orbit approximately 1 kilometer ahead of the samples. The required velocity changes for this maneuver can be calculated using Hill's equations. Hill's equations are as follows:

$$\dot{y}_0 = \frac{[6x_0(nt - \sin nt) - y_0]n \sin nt - 2nx_0(4 - 3\cos nt)(1 - \cos nt)}{(4\sin nt - 3nt)\sin nt + 4(1 - \cos nt)^2} \tag{1}$$

$$\dot{x}_0 = -\frac{nx_0(4 - 3\cos nt) + 2(1 - \cos nt)\dot{y}_0}{\sin nt} \tag{2}$$

where, x_0, y_0 = initial position of the transfer vehicle relative to the sample rocket

n = magnitude of the orbital rate of the target orbit

t = time selected for rendezvous

After arriving in the target orbit, the transfer vehicle rotates 180° and begins the braking maneuver. The braking maneuver is accomplished using the radio-isotope engine, while all required attitude corrections use arcjets. The transfer vehicle maneuvers until the samples are in the retrieval bay. Once in the retrieval bay, the samples are secured by the mechanical retrieval arm located inside the retrieval bay. The location of the bay can be seen in Figure 8.

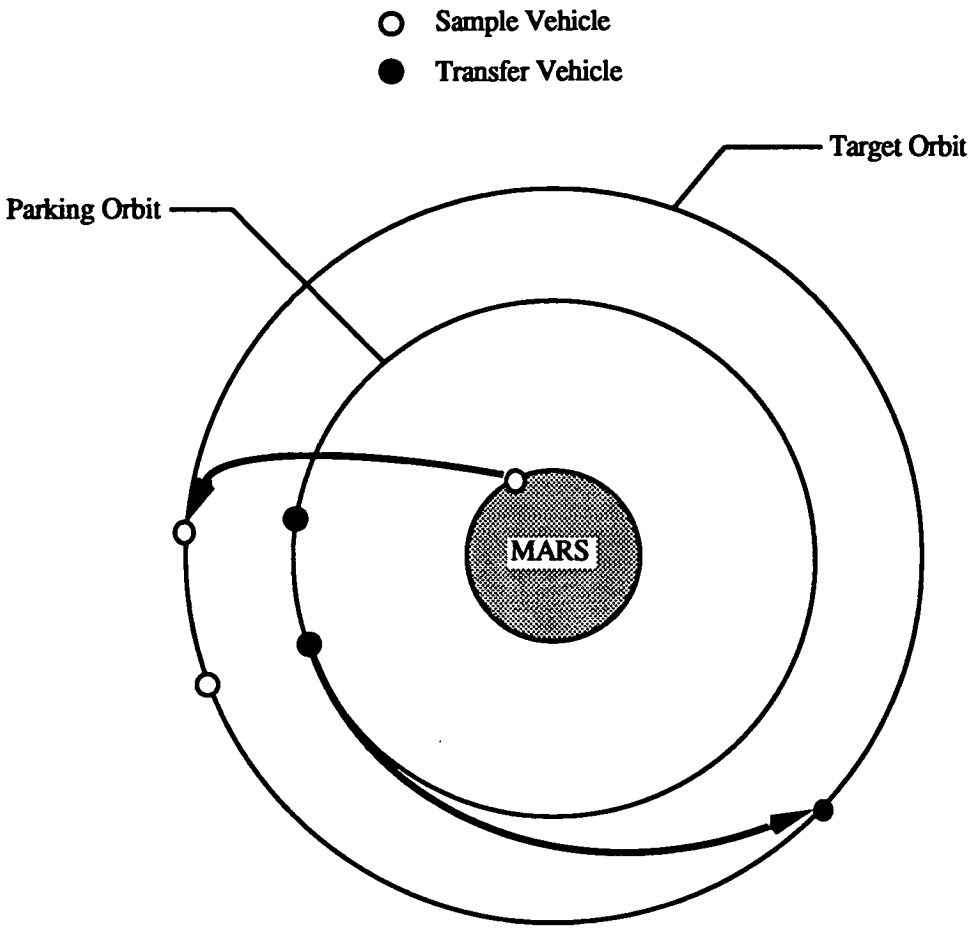

Figure 7: Rendezvous Sequence

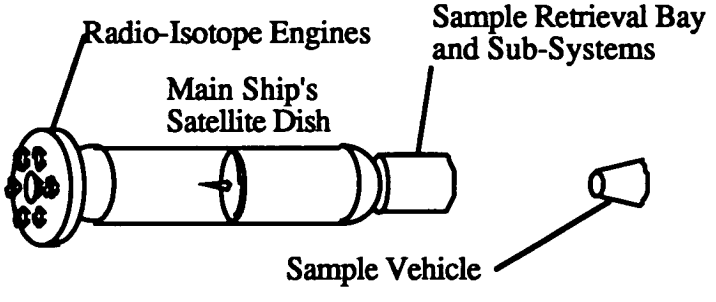

Figure 8: Sample Retrieval

The rendezvous sequence used for this mission was chosen because of the fuel and time saving characteristics. Savings on fuel and time result from utilizing two burns for the maneuver. The first burn changes the transfer vehicle's orbit (parking orbit to target orbit). After establishing the target orbit, the second burn, the braking maneuver, is initiated. Arcjets, which are used for attitude correction, use the same fuel as the radio-isotope propulsion system. Another reason for using this rendezvous scenario is that the sample vehicle does not need an elaborate navigation system or large amounts of fuel, which would be required if the sample vehicle was to initiate the rendezvous with the transfer vehicle.

COST OF THE PLANETARY TRANSFER VEHICLE

The planetary transfer vehicle for the Mars Sample Return Mission has an estimated cost of approximately 1.2 billion dollars. This is based on a launch date in the year 2002, assuming that three such vehicles will be fully equipped. The cost analysis was found using the approach presented in "Cost Estimate Methods for Advanced Space Systems" by Kelley Cyr of the NASA Johnson Space Center (Cyr, 1988). This system bases the system cost on the dry weight, the number of vehicles built and the heritage of the product.

The four launch vehicles, Titan IV - CELL, have an approximate cost of 250 million dollars each, for a Cape Canaveral Launch. These estimates were found using the same cost estimate scheme.

CONCLUSION AND FURTHER INVESTIGATIONS

This design provides a unique proposal for a planetary transfer vehicle for the Mars Sample Return Mission. Advances in propulsion are not only beneficial, but are critical to the advance of space exploration. With this in mind, the radio-isotope transfer vehicle offers aerospace industries and research groups the opportunity to further develop this important area.

Current designs offer the use of conventional propulsion which results in lower mission costs due to heritage. Although the concepts discussed here involve more development costs, the results will have more of an impact on the aerospace industry.

Future Investigations:

The design contains many estimates which must be justified or refined in a final analysis. An in-depth trajectory profile analysis, including all perturbations, should be completed to account for propellant consumption and transfer times. The state-of-the-art arcjets must also be investigated to confirm the use of ammonia as the working fuel and to calculate the power consumption levels. Choices for specific structural materials have not been made and require further investigation. Although the engine is constrained by the current design, more work concerning the cladding is required, in particular, as to which material is best suited for the specific radio-isotope.

REFERENCES

[1] Agrawal, Brij. "Design of Geosynchronous Spacecraft." Prentice-Hall, Inc. Englewood Cliffs, New Jersey, 1986.

[2] Bate, Roger R., Donald D. Mueller, and Jerry E. White. "Fundamentals of Astrodynamics." Dover Publications, Inc. New York, New York, 1971.

[3] Cyr, Kelley. "Cost Estimate Methods for Advanced Space Systems." SAWE Paper No. 1856, Index Cat. #29, NASA Johnson Space Center, 1988.

[4] ELV DATA Base. Eagle Engineering Inc. July 11, 1989.

[5] Huzel, Dieter K. and Huang, David H., "Design of Liquid Propellant Rocket Engines." Rocketdyne Division, North American Rockwell, Inc. NASA Scientific Library, 1971.

[6] Hunter, Maxwell W., II and Howard S. London. Bellconn, Inc. AIAA Unmanned Spacecraft Meeting, Los Angeles, California, March 1-4, 1965.

[7] Interavia Space Directory. Edited by Andrew Wilson, (1989 -1990).

[8] Jones, I.R. and Austin, G.E. "Poodle Isotope Propulsion Technology." Radio-Isotopes for Aerospace. Volume 2. 1966.

[9] Kaplan, Marshall H. "Modern Spacecraft Dynamics & Control." John Wiley & Sons: New York, New York. 1976.

[10] Martinez, John S. "Radio-isotope Propulsion." Chemical, Electrical, and Hybrid Rocket Propulsion. TRW Systems, Chapter 9. 1966.

[11] Pellmann, R. R. "Power Systems for an Unmanned Lunar Roving Vehicle." Bendix Systems Division. Ann Arbor, Michigan. AIAA Unmanned Spacecraft Meeting, Los Angeles, California. March 1-4, 1965.

[12] Peters, Robert L. "Design of Liquid, Solid, and Hybrid Rockets." Hayden Book Company, Inc.: New York, New York. 1965.

[13] Romero, Jacob B. "Radio-Isotope Propulsion." The Boeing Company. Seattle, Washington. Journal of Spacecraft, Volume 1, No.5. May 1964.

[14] Romero, Jacob B. "Potentialities of Radio-Isotope Propulsion for Space Probes." The Boeing Company, Seattle, Washington. AIAA Unmanned Spacecraft Meeting, Los Angeles, California. March 1-4, 1965.

[15] Romero, Jacob B. "Cislunar and Planetary Missions By Thermo-Radio-Isotope Propulsion and Integrated Power." The Boeing Company, Seattle, Washington. XVII International Astronautical Congress, Madrid Spain. October 9-15, 1966.

[16] Sawyer, R. H. "Secondary Propulsion System Capabilities as Compared with Flight Control Requirements." Thiokol Chemical Corporation, Reaction Motors Division. Denville, New Jersey. AIAA Unmanned Spacecraft Meeting, Los Angeles, California. March 1-4, 1965.

[17] Schneiderman, Dan, Glenn Reiff, and J. N. James. "Recent Mariner Spacecraft Missions." Jet Propulsion Laboratory and National Aeronautics and Space Administration. AIAA Unmanned Spacecraft Meeting, Los Angeles, California. March 1-4, 1965.

[18] Strunk, William, Jr., and E. B. White. "The Elements of Style, Third Edition." MacMillan Publishing Co., Inc.: New York, New York. 1979.

[19] "VIKING 1, Early Results." National Aeronautics and Space Administration. Washington, D. C. (1976).

[20] Villers, Philippe. "Application of Solar Sail Attitude Stabilizers to Thermionic Power Generation." Barnes Engineering Company. AIAA Unmanned Spacecraft Meeting, Los Angeles, California. March 1-4, 1965.

[21] Wertz, James R., and Wiley J. Larson. "Space Mission Analysis and Design." Kluwer Academic Publishers: Dordrecht, The Netherlands. 1991.

[22] Wooten, R. W., and E. J. Merz. "Mars - Voyager Systems." General Electric Company, Missile and Space Division, King of Prussia, Pennsylvania. AIAA Unmanned Spacecraft Meeting, Los Angeles, California. March 1-4, 1965.

APPENDIX 1

Isotope Power and Thrust Levels

The power function is:

$$P = P_o e^{-0.693\, t/\tau} \qquad (1)$$

where, P = power

P_o = power at start-up

t = time

τ = isotope half-life

The isotope chosen is Curium (Cm-244), which has a half life of 18 years. Plugging into the equation for predicting power, assuming a mission duration, t, of 2.5 years:

$$P = P_o \times e^{-(0.693 \times 2.5 \text{ years} / 18 \text{ years})}$$

$$= P_o \times e^{-(0.09625)}$$

$$= 0.908\, P_o$$

This means that at the end of the mission, there will be 90.8 percent of the power, and similarly 90.8 percent of the thrust available for use.

APPENDIX 2

Fuel Tank Configuration

	Ammonia	Hydrogen
Density of Liquid State:	683 kg/m^3	71 kg/m^3
Mass of Liquid Required[2]:	46,260 kg	11,715 kg
Mass of Propellant Tanks[3]:	6,939 kg	1,757 kg
Assumed Isp for Propellant[4]:	400 sec	800 sec
Storage Temperature Range:	195.2 °K to 239.7 °K	13.8 °K to 20.2 °K
Price per Cubic Meter[1]:	$54.33	$1,088.66
Number of Tanks[5]:	3	7
Diameter of each Tank[6]:	2 m	2 m
Height of Each Tank[7]:	7.9 m	8.2 m

1 Taken from Huzel & Huang, 1971. Although these values are outdated, using them will provide a margin of safety and/or a basis of comparison.

2 Total fuel needed found by using the rocket equation and two single impulse maneuvers of 3.61 km/sec (Earth to Mars) and 2.1063 km/sec (Mars to Earth). This number includes a 15% margin of safety.

3 This mass (total of all three tanks) is approximated by using 15% of the mass of propellant.

4 The specific impulse used for ammonia is half the value the radio-isotope engines would achieve. This is done to add a margin of safety since these calculations use single impulse maneuvers and not the low thrust techniques. Therefore, the Isp expected from the radio-isotope engines, using ammonia, is 800 seconds.

5 The number of tanks is taken such that the height of each tank remains close to 8 meters for the set diameter of 2 meters. The height of 8 meters results from the height limitations on a Titan IV's cargo bay (see notes 6 and 7).

6 The diameter is chosen to accommodate the attachment of the radio-isotope engines (3 meters in diameter) and the sample retrieval bay (1.5 meters in diameter).

7 Height is found from the equation for the volume of a cylinder and the volume of a sphere, combined and solved for the height of the cylinder plus diameter of the sphere,h (see Figure 9).

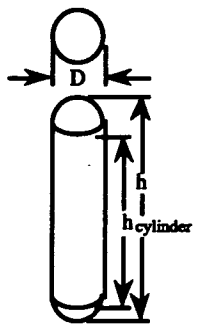

Figure 9: Cylindrical - Spherical Tank Dimensions

From basic Geometry:

$$V_{sphere} = \frac{4}{3}\pi R^3 \qquad \text{(SE 1)}$$

$$V_{cylinder} = \frac{1}{6}\pi h_{cyl} R^2 \qquad \text{(SE 2)}$$

$$h_{cylinder} = h - D \qquad \text{(SE 3)}$$

and the volume of one tank will be:

$$\begin{aligned} V_{per\ tank} &= V_{sphere} + V_{cylinder} \qquad \text{(SE 4)} \\ &= \frac{4}{3}\pi R^3 + \frac{1}{6}\pi h_{cylinder} R^2 \\ &= \frac{4}{3}\pi\left(\frac{D}{2}\right)^2 + \frac{1}{6}\pi(h-D)\left(\frac{D}{2}\right)^2 \\ &= \frac{1}{6}\pi D^3 + \frac{h}{4}\pi D^2 - \frac{1}{4}\pi D^3 = \frac{V}{n} \end{aligned}$$

Where V is the total volume of 'n' tanks, so rearranging gives:

$$\frac{h}{4}\pi D^2 = \frac{V}{n} + \frac{1}{12}\pi D^3$$

and finally the expression of the Height of the Cylindrical - Spherical Tanks:

$$h = \frac{4V}{\pi D^2 n} + \frac{D}{3} \qquad \text{(SE 5)}$$

where, h = height of each tank
V = total volume of propellant
n = number of tanks
D = diameter of the tanks.

APPENDIX 3

Arcjet Fuel and Power Calculations

Symbol List:

F = Force

I = Inertia

L = Total Lever Arm

N = Newton

P = Power

g = Gravity of Earth

m = Meters

t = Time

t_{fire} = Firing Time of Arcjets

I_{sp} = Specific Impulse

η = Efficiency of Arcjet

θ = Angle of Rotation

$d\theta/dt$ = Angular Velocity

$d\theta^2/d^2t$ = Angular Acceleration

sec = Seconds

Problem:

A 180° x-axis rotation is needed

Assumptions:

Rotation takes one day	(86,400 sec)
Accelerating 5% of time	(4,320 sec)
Decelerating 5% of time	(4,320 sec)

Inertia* = 3,000,000 kg m^2

Calculations:

$d\theta/dt = 180° / 86{,}400 \text{ sec} = 2.0833 \text{ E-}3° / \text{sec}$

$d\theta^2/d^2t = d\theta/dt \times 1/t = 2.0833 \text{ E-}3° / \text{sec} / 4{,}320 \text{ sec}$

$= 4.822 \text{ E-}7° / \text{sec}^2$

Force required for rotation time:

$F = I \times (d\theta^2/d^2t) / L$

$= 3{,}000{,}000 \text{ kg m}^2 \times 4.822 \text{ E-}7° / \text{sec}^2 / 8.5 \text{ m}$

$= 0.17019 \text{ N}$

A total force of 0.17019 N is required for a one day 180° rotation. But there will be two arcjets firing at one Newton with total lever arm of 8.5 meters**.

$1 \text{ N} / 0.17019 \text{ N} = 5.875$

Therefore, the firing time of the arcjets is 735.22 sec. and the total firing time for the total maneuver is 1,470.44 seconds or 24.51 minutes.

The mass of propellant required for one arcjet, given a worst case specific impulse of 450 seconds, is given by:

$Mp = F t / (I_{sp} g)$

$Mp = 1.0 \text{ N} \times 1{,}470.44 \text{ sec} / (450 \text{ sec} \times 9.81 \text{ m/sec}^2)$

$= 0.333 \text{ kg}$

The power required for one arcjet is:

$$P = F \times I_{sp} \times g / (2 \times \eta)$$

The efficiency of an arcjet is approximately 0.3

$$P = 1.0\ N \times 450\ sec. \times 9.81\ m/sec^2 / (2.0 \times 0.3)$$

$$= 7.35\ kilowatts$$

* An initial estimate of inertia was calculated to be 3,000,000 for the PTV and payload with a center of mass positioned on the PTV.

** A length of 8.5 meters is the maximum lever arm attainable with the configuration of the Planetary Transfer Vehicle.

APPENDIX 4

Spiral Orbit Trajectory Program Development

The governing equations in Encke's method are outlined below.

$$\ddot{\vec{r}} + \frac{\mu}{r^3}\vec{r} = \vec{a}_p$$

$$\ddot{\vec{\rho}} + \frac{\mu}{\rho^3}\vec{\rho} = 0$$

where $\vec{r}$ = radius vector of actual, perturbed orbit

$\vec{\rho}$ = radius vector of reference orbit

$\vec{a}_p$ = all perturbing accelerations acting on the spacecraft

$\delta\vec{r} = \vec{r} - \vec{\rho}$

$\ddot{\delta\vec{r}} = \ddot{\vec{r}} - \ddot{\vec{\rho}}$

This leads to the difference equation to be integrated;

$$\ddot{\delta\vec{r}} = \vec{a}_p + \frac{\mu}{\rho^3}\left[(1 - \frac{\rho^3}{r^3})\vec{r} - \delta\vec{r}\right]$$

This is further reduced to eliminate $(1 - \rho^3/r^3)$, which results in a small number. The final form is given below.

$$\ddot{\delta\vec{r}} = \vec{a}_p + \frac{\mu}{\rho^3}\left\{\left[1 - (1 - 2q)^{-3/2}\right]\vec{r} - \delta\vec{r}\right\}$$

$$q = -\frac{\rho_x\delta x + \rho_y\delta y + \rho_z\delta z}{\rho^2} + (O)^2$$

Initially, the reference orbit coincides with the actual perturbed orbit and the forces acting on the spacecraft are calculated. The difference between the the actual orbit and the

reference orbit at some later time (t +Δt) is then calculated using a fourth-order Runge Kutta technique. From this difference, the actual position and velocity vector of the spacecraft is calculated. If the difference between the actual orbit and reference orbit exceeds a specified value (ϕ), rectification occurs and the reference orbit once again coincides with the actual orbit. Beyond a certain radius relative to Earth, the spacecraft will enter the sphere of influence of the Sun, at which time the gravitational attraction of the Sun becomes the primary acceleration acting on the spacecraft. As the spacecraft reaches this critical radius, checks will be made to ensure that the spacecraft does not miss Mars all together. Checks are also included to ensure that the magnitudes of the perturbing accelerations do not exceed the magnitude of the primary acceleration. Once the spacecraft reaches its final position, the elapsed time along with the propellant mass flow rate can be used to determine the required propellant. The program listing along with all subroutines can be found in Appendix 5.

APPENDIX 5

Spiral Orbit Trajectory Program

(NOTE: This program was not completely debugged due to time constraints.)

MAIN PROGRAM:

```
      parameter (n=3, m=3, k=1, k1=1, k2=2, k3=3, phi=0.01, ndim=3, nvar=2)
      implicit double precision (a-h, p-z)
      implicit integer (i-o)
      dimension drx(ndim), dry(ndim), drz(ndim), rmat(n, m), rmatr(n, m),
     #ap(m,k), acc(m, k), rhop(m, k), rho(m, k), vrp(m, k), vr(m, k), at(m),
     #drdot(ndim), temp(ndim), g1(ndim), g2(ndim), g3(ndim), g4(ndim)
      external de
c
      pi = 3.141592654
      ri = 0.75 * sqrt(3.) * 6378.145
      rj = 0.75 * 6378.145
      rk = 0.0
      vi = (-0.5 / sqrt(2.)) * 7.90536828
      vj = 0.5 * sqrt(1.5) * 7.90536828
      vk = (1 / sqrt(2.)) * 7.90536828
      u = 3.986E+5
      drx(1) = 0.0
      dry(1) = 0.0
      drz(1) = 0.0
      drx(2) = 0.0
      dry(2) = 0.0
      drz(2) = 0.0
      zmagr = dsqrt(ri**2 + rj**2 + rk**2)
      zmagv = dsqrt(vi**2 + vj**2 + vk**2)
      print*,zmagr
      print*,zmagv
      call orbel(zmagr, ri, rj, rk, zmagv, vi, vj, vk, zn, rh, e, zi, comega,
     #zomega, energy, theta,u,angl,tau,pi,a)
      q = 0.0
c.....          Reference orbit angles, I.C.'s
      anglr = angl
      comegr = comega
      zomegr = zomega
      zir = zi
      thetar = theta
      zmrho = zmagr
      taur = tau
      ar = a
      er = e
c....           Mass, Thrust, Thrust angles
      zmo = 74616.75
      t =  9.0
      beta = 0.0
      alpha = 0.0
```

```
c....
      time = 0.0
      h = 1800
      kmax = 5
c.....
      call rmatx(rmatr, comegr, zomegr, zir, anglr)
      call rmatx(rmat, comega, zomega, zi, angl)
c....
      do 10 i = 1, kmax
        t = 9 * exp(-0.693 * time / 568036800.)
        t = t/1000.0
        zmdot = (t * 1000.) / (800 * 9.81)
        zm = zmo - zmdot * time
        call thrust(t, zm, at, theta, beta, alpha)
        ap(1,1) = at(1)
        ap(2,1) = at(2)
        ap(3,1) = at(3)
c....
        call xfer(rmat, ap, acc, n, m, k)
c....
        call rk4(drx, drdot, de, time, h, ndim, nvar, temp, g1, g2, g3, g4, ier,
     #   acc, k1, u, q, zmrho, ri)
        call rk4(dry, drdot, de, time, h, ndim, nvar, temp, g1, g2, g3, g4, ier,
     #   acc, k2, u, q, zmrho, rj)
        call rk4(drz, drdot, de, time, h, ndim, nvar, temp, g1, g2, g3, g4, ier,
     #   acc, k3, u, q, zmrho, rk)
        time = time + h
        zmdr = dsqrt(drx(1)**2 + dry(1)**2 + drz(1)**2)
c....
        call ref(time, ar, er, rhop, thetar, u, energy, pi, taur, vrp, zmrho)
        call xfer(rmatr, rhop, rho, n, m, k)
        call xfer(rmatr, vrp, vr, n, m, k)
c....
        ri = drx(1) + rho(1,1)
        rj = dry(1) + rho(2,1)
        rk = drz(1) + rho(3,1)
        zmagr = dsqrt(ri**2 + rj**2 + rk**2)
        vi = drx(2) + vr(1,1)
        vj = dry(2) + vr(2,1)
        vk = drz(2) + vr(3,1)
        zmagv = dsqrt(vi**2 + vj**2 + vk**2)
        print*,zmagr
        print*,zmagv
c....
        call orbel(zmagr, ri, rj, rk, zmagv, vi, vj, vk, zn, h, e, zi, comega,
     #zomega, energy, theta, u, angl, tau, pi, a)
        call rmatx(rmat, comega, zomega, zi, angl)
c.....
        q = (-1.0)*(rho(1,1)*drx(1) + rho(2,1)*dry(1) + rho(3,1)*drz(1)
     #    + rho(3,1)*drz(1))/zmrho**2
c....
        ratio = zmdr/zmrho
```

```
        if (ratio .gt. phi) then
            comegr = comega
            zomegr = zomega
            zir = zi
            zmrho = zmagr
            thetar = theta
            ar = a
            er = e
            taur = tau
            call rmatx(rmatr, comegr, zomegr, zir, anglr)
        endif
c....
      print*,time, zmagr, zmagv
 10   continue
      end
```

SUBROUTINE ORBEL:

```
c-------------------------------------------------------
c.... Subroutine orbel computes the orbital elements for a
c.... given position and velocity vector.
c.... NOTE: r & v must be represented in I,J,K coord.
c-------------------------------------------------------
      subroutine orbel(r, ri, rj, rk, v, vi, vj, vk, n, h, e, i, comega, omega,
     *ener, theta, u, angl, tau, pi, a)
      double precision r, ri, rj, rk, v, vi, vj, vk, h, hi, hj, hk, n, ni, nj,
     *e, ei, ej, ek, i, comega, omega, theta, ener, s, u, nedot, rvdot,
     *erdot, njdot, ekdot, pi, angl, nk, tau, a
c.....
      hi = rj*vk - vj*rk
      hj = (-1.0)*(ri*vk - vi*rk)
      hk = ri*vj - vi*rj
      h = dsqrt(hi**2 + hj**2 + hk**2)
c.....
      ni = (-1.0)*hj
      nj = hi
      nk = 0.0
      n = dsqrt(ni**2 + nj**2)
c.....
      s = v**2 - (u/r)
      rvdot = ri*vi + rj*vj + rk*vk
      ei = (1/u)*(s*ri - rvdot*vi)
      ej = (1/u)*(s*rj - rvdot*vj)
      ek = (1/u)*(s*rk - rvdot*vk)
      e = dsqrt(ei**2 + ej**2 + ek**2)
c.....
      i = dacos(hk/h)
c.....
```

```
      if (i .eq. 0.0) then
        angl = datan2(ej,ei)*(180.0/pi)
      else
        angl = 0.0
      endif
c.....
      if (abs(i) .gt. 0.0 .and. abs(n).gt.0.0) then
       comega = dacos(ni/n)
       njdot = nj
       if (comega .gt. pi) then
         if (njdot .gt. 0.0) then
           comega = comega - pi
         endif
       endif
c......
       nedot = ni*ei + nj*ej + nk*ek
       omega = dacos(nedot/(n*e))
       ekdot = ek
       if (omega .gt. pi) then
        if (ekdot .gt. 0.0) then
         omega = omega - pi
        endif
       endif
      endif
c.....
      ener = v**2/2 - u/r
      a = (-1.0)*u/(2*ener)
      tau = 2*pi*dsqrt(a**3/u)
c.....
      erdot = ei*ri + ej*rj + ek*rk
      theta = dacos(erdot/(e*r))
      if (theta .gt. pi) then
       if (rvdot .gt. 0.0) then
         theta = theta - pi
       endif
      endif
      if (i .le. 0.00001) then
        comega = 0.0
        omega = 0.0
      endif
      i = i*(180.0/pi)
      comega = comega*(180.0/pi)
      omega = omega*(180.0/pi)
      theta = theta*(180.0/pi)
      return
      end
```

SUBROUTINE RMATX:

```
c-------------------------------------------------
c.... Subroutine rmatx sets up the directional cosine matrix
c.... necessary to transform, P,Q,W coordinates into I,J,K
c.... coordinates.
c.... NOTE: variable 'angle' is used only if Comega and Omega are
c.... undefined, (ie. Comega = Omega = 0)
c-------------------------------------------------
      subroutine rmatx(rmat, comega, omega, i, angl)
      double precision rmat(3, 3), comega, omega, i, angl, wangl
c.....
      wangl = (-1.0)*angl
c.....
      If (i .eq. 0.0) then
        rmat(1,1) = dcos(wangl)
        rmat(1,2) = dsin(wangl)
        rmat(1,3) = 0.0
        rmat(2,1) = (-1.0)*dsin(wangl)
        rmat(2,2) = dcos(wangl)
        rmat(2,3) = 0.0
        rmat(3,1) = 0.0
        rmat(3,2) = 0.0
        rmat(3,3) = 1.0
      Else
        rmat(1,1) = dcos(comega)*dcos(omega) - dsin(comega)*
     *dsin(omega)*dcos(i)
        rmat(1,2) = (-1.0)*dcos(comega)*dsin(omega) - dsin(comega)*
     *dcos(omega)*dcos(i)
        rmat(1,3) = dsin(comega)*dsin(i)
        rmat(2,1) = dsin(comega)*dcos(omega) + dcos(comega)*
     *dsin(omega)*dcos(i)
        rmat(2,2) = (-1.0)*dsin(comega)*dsin(omega) + dcos(comega)*
     *dcos(omega)*dcos(i)
        rmat(2,3) = (-1.0)*dcos(comega)*dsin(i)
        rmat(3,1) = dsin(omega)*dsin(i)
        rmat(3,2) = dcos(omega)*dsin(i)
        rmat(3,3) = dcos(i)
      Endif
      Return
      End
```

SUBROUTINE THRUST:

```
c-------------------------------------------------
c.... Subroutine thrust computes the acceleration of the S/C
c.... due to the thrust component
c.... NOTE: The components of acceleration are in P,Q,W coord.
c-------------------------------------------------
```

```
      subroutine thrust(t, m, at, theta, beta, alpha)
      double precision t, m, at(3), theta, beta, alpha, gamma
c.....
      gamma = theta - beta
      at(1) = (-1.0)*(t/m)*dsin(gamma)
      at(2) = (t/m)*dcos(gamma)
      at(3) = (t/m)*dsin(alpha)
      return
      end
```

SUBROUTINE XFER:

```
c-------------------------------------------------------
c.... Subroutine xfer multiplies the two matrices rmat and perf in
c.... in the following way.
c.... {resul} = {rmat}{perf},   where
c.... {rmat} = any matrix with dimensions (n x m)
c.... {perf} = any matrix with dimensions (m x k)
c.... {resul} = resulting matrix with dimensions (n x k)
c-------------------------------------------------------
      subroutine xfer(rmat, perf, resul, n, m, k)
      integer i, j, k, m, n, p
      double precision rmat(n, m), perf(m, k), resul(n, k)
      do 40 p = 1,k
       do 50 i = 1,n
          resul(i,p) = 0.0
        do 55 j = 1,m
           resul(i,p) = resul(i,p) + rmat(i,j)*perf(j,p)
55      continue
50     continue
40    continue
      return
      end
```

SUBROUTINE RK4:

```
C     ************************************************************************
C     * Integrates a set of first-order differential equations               *
C     *   using a Runge-Kutta fourth-order method.                          *
C     *                                                                     *
C     * Author: R. G. Melton                                                *
C     * Revised: 2/18/88                                                    *
C     ************************************************************************
C
```

```
      SUBROUTINE RK4(X, XDOT, de, TIME, H, NDIM, NVAR, TEMP, G1, G2, G3,
     #G4, IER, acc, loc, u, q, zmrho, r)
C
      IMPLICIT DOUBLE PRECISION (a-h, p-z)
      IMPLICIT INTEGER (i-o)
      DIMENSION X(NDIM), XDOT(NDIM), TEMP(NDIM)
      DIMENSION G1(NDIM), G2(NDIM), G3(NDIM), G4(NDIM), acc(3,1)
      EXTERNAL de
      IF (NVAR .GT. NDIM) THEN
        IER = 1
        RETURN
      ELSE
        IER = 0
      END IF
      CALL de(X,XDOT,TIME,NDIM,NVAR,acc,loc,u,q,zmrho,r)
      DO 100 I = 1,NVAR
        G1(I) = H * XDOT(I)
  100 CONTINUE
      DO 200 I = 1,NVAR
        TEMP(I) = X(I) + G1(I)/2.
  200 CONTINUE
      CALL de(TEMP,XDOT,TIME+H/2.,NDIM,NVAR,acc,loc,u,q,zmrho,r)
      DO 250 I = 1,NVAR
        G2(I) = H * XDOT(I)
  250 CONTINUE
      DO 300 I = 1,NVAR
        TEMP(I) = X(I) + G2(I)/2.
  300 CONTINUE
      CALL de(TEMP,XDOT,TIME+H/2.,NDIM,NVAR,acc,loc,u,q,zmrho,r)
      DO 350 I = 1,NVAR
        G3(I) = H * XDOT(I)
  350 CONTINUE
      DO 400 I = 1,NVAR
        TEMP(I) = X(I) + G3(I)
  400 CONTINUE
      CALL de(TEMP,XDOT,TIME+H,NDIM,NVAR,acc,loc,u,q,zmrho,r)
      DO 450 I = 1,NVAR
        G4(I) = H * XDOT(I)
  450 CONTINUE
      DO 500 I = 1,NVAR
        X(I) = X(I) + 1/6. * (G1(I) + 2. * (G2(I) + G3(I)) + G4(I))
  500 CONTINUE
      RETURN
      END
```

SUBROUTINE DE:

```
      subroutine de(dr, drdot, time, ndim, nvar, acc, loc, u, q, zmrho, r)
```

```
c-----------------------------------------
c  subroutine that has the differential equation that is solved
c  with Runge Kutta Method
c-----------------------------------------
      implicit double precision (a-h, o-z)
      dimension dr(ndim), drdot(ndim), P(0:1000), acc(3,1)
      external binom
c
      call binom(p, q, iw)
      drdot(1) = dr(2)
      drdot(2) = acc(loc,1) + (u/zmrho**3) * (p(iw)*r - dr(1))
c
      return
      end
```

SUBROUTINE BINOM:

```
      subroutine binom(p, q, iw)
c-----------------------------------------------------
c  Subroutine binomial computes the quantity 1 - (1-2q)^-(3/2).
c  The answer is stored in the last element in the column
c  matrix P(#).
c-----------------------------------------------------
      implicit double precision (a-h, p-z)
      dimension p(0:1000)
c
      k = 1
      is = 0
      p(0) = 3 * q
      phi = 1.0E-20
c
      do 5 i = 3,500,2
       is = is + 1
       k = k + 1
       mF = 1
c
        do 10 j = 1,k
         mF = mF * j
 10      continue
c
       num = 1
c
        do 15 l = 1,i,2
         num = num * (l + 2)
 15      continue
c
       p(i-1) = ((-1.0)**is) * (num * q**k) / mF + p(i-3)
       iw = i-1
```

```
      diff = abs(p(i-1) - p(i-3))
      if (diff .le. phi) then
        p(iw) = (-1)*p(iw)
        go to 20
      end if
 5   continue
 20  return
     end
```

SUBROUTINE REF:

```
c-------------------------------------------------------------
c   Subroutine ref computes r & v of a perfect
c   Keplerian orbit for a given Tp (time since periapsis)
c-------------------------------------------------------------
      subroutine ref(dtime, a, e, rho, theta, u, energy, pi, tau, vr, mmrho)
      double precision  dtime, ecan(5000), p, a, theta, e, ce, mrho,
     *u, diff, pi, rho(3, 1), vr(3, 1), energy, rvdot,
     *thetc, tau, ratio, mmrho
c....
      ecan(1) = 0.0
      do 30 j = 1,5000
        ecan(j + 1) = e*dsin(ecan(j)) + dsqrt(u/a**3)*dtime
        ce = ecan(j +1)
        diff = dabs(ecan(j + 1) - ecan(j))
        if (diff .lt. .000000001) then
          go to 300
        endif
30    continue
c.....
300   mrho = a - a*e*dcos(ce)
      thetc = (a*dcos(ce) - a*e)/mrho
      theta = dacos(thetc)*(180.0/pi)
      ratio = dtime/tau - int(dtime/tau)
      if (ratio .gt. 0.5) then
        theta = (180.0 - theta) + 180.0
      endif
      p = a*(1.0 - e**2)
      rho(1,1) = mrho*dcos(theta*pi/180.0)
      rho(2,1) = mrho*dsin(theta*pi/180.0)
      rho(3,1) = 0.0
      mmrho = dsqrt(rho(1,1)**2 + rho(2,1)**2 + rho(3,1)**2)
      vr(1,1) = dsqrt(u/p)*(-1.0)*dsin(theta*pi/180.0)
      vr(2,1) = dsqrt(u/p)*(e + dcos(theta*pi/180.0))
      vr(3,1) = 0.0
      rvdot = rho(1,1)*vr(1,1) + rho(2,1)*vr(2,1) + rho(3,1)*vr(3,1)
      energy = (-1.0)*u/(2*a)
      end
```

Chapter 5:

Communications and Tracking Satellite for the Mars Sample Return Mission

Group Martincic Final Report
Aerospace 401B
Spring Semester 1991

Group Members:

Harry Anderson
Ron Brubaker
Paul Fedor
John Martincic
Joe Pampanin
Pamela Presutti
Glenn Webb

ABSTRACT

The Mars Sample Return Mission's (MSRM) communications system is a 250 kg three-axis stabilized satellite with a five year design lifetime in a nearly circular Mars orbit whose period is one half the sidereal period of Mars. The satellite will establish this orbit by detaching from the transfer vehicle at the correct altitude during the descending spiral approach to Mars and make little, if any, corrections to this acquired orbit.

The satellite has a design EOL power requirement of 250 watts: 100 watts will be allocated for communications, 75 watts for momentum wheels for attitude control, and the remaining 75 watts for housekeeping functions. The power will be provided by two solar arrays each 1.9 m by 1.9 m. These solar arrays will be of the flexible rollup type which have a BOL energy density of 20 W/m^2 at Mars.

Communications will be carried out on the K_a band both to Earth and to all rovers and the lander/ base on Mars. The transmission rate will be 64 KBPS for all transmissions at a bandwidth of 38.4 kHz. The communications process consists of receiving messages, storing them in the onboard computer, and retransmitting them. The onboard computer has a storage capacity of 50 MB which translates to 13.02 min of continuous transmission at 64 KBPS.

TABLE OF CONTENTS

LIST OF FIGURES

LIST OF TABLES

LIST OF APPENDICES

INTRODUCTION

One of the necessary components of any successful scientific space exploration mission is a communications system. Without this, all of the valuable information obtained during the mission would be useless. Also, any other mission component which requires monitoring or control from outside sources would be lost.

The Mars Sample Return Mission (MSRM) is one such scientific mission. The architecture of this mission includes a stationary lander/base, a limited range land rover, two long-range Aereon type rovers, and two small sample return rockets. All of these components require a communications system in order to ensure an overall mission success. In addition, some of the mission components will also require tracking so that the communications satellite will actually be a communications/ tracking satellite.

There are several mission requirements that have had a direct impact on the final design and configuration of the MSRM communications/tracking satellite. One is that the two Aereon rovers must be able to send both data and video images to Earth stations and receive all commands for movement from Earth. Secondly, the two Aereon rovers must be tracked by the satellite as their journey progresses.Thirdly, the land rover must be able to access the data that will be available from the Mars Orbiter in order to navigate and be able to send video images to Earth stations. Lastly, as the mission comes to a close, the Aereon rovers must be given the proper information regarding their position so that they can launch the sample return rockets in the direction of the main lander/base.

The communications/ tracking satellite described in this report and depicted in Fig 1 is believed to be the best means of achieving these goals.

ORBIT PARAMETERS

The orbital parameters set for the communications/tracking satellite are a nearly circular orbit at an altitude of 9292 km with a period that is one-half the sidereal period of Mars. This orbit will be established simply by detaching from the transfer vehicle assembly at the proper time during the spiral in approach to Mars. The attainment of the required orbit is possible since at most points along the spiral approach path, the altitude and velocity of the transfer vehicle assembly define a nearly circular orbit. It was not necessary to completely circularize the orbit because none of the ground stations required very stringent transmission times and the transmission times will change throughout the mission as the Aereon rovers circumnavigate the globe.

Coupled with the rotation of Mars, this orbit will provide the satellite with a chance to communicate with the lander/ base and the three rovers at least once each Martian day. Maximum transmission times available for the lander/base and the land rover are both about 9.5 hours per Martian day. For the Aereon rovers, maximum transmission times will vary between 5 and 9.5 hours per Martian day depending upon their latitude. As the Aereons near the poles, the lower transmission times will only be available.

In this orbit, the satellite will be able to see most of the surface of Mars (Fig 2). This is mainly attributable to the satellite's altitude. With a 24 degree inclination, relative to the equator of Mars, about half of the polar regions will be accessible. The 24 degree inclination will be provided by Mars's natural tilt and the fact that the satellite will have been inserted into its orbit while in the ecliptic.

This orbit was chosen to be the best solution to meet the overall demands set by the lander/base, land rover, and Aereon rovers. These requirements were the number of transmissions per Martian day, length of the transmission window, and length of each transmission.

Other orbits were studied, but none could meet the mission requirements as well as the one described above. For example, a Molniya type orbit could provide close to 23 continuous hours of transmission time per Martian day for the lander/base and land rover,

but, as the Aereon rovers would eventually circumnavigate the globe, their transmission times would be cut to about 1 hour per Martian day. This would be completely undesirable, making such an orbit infeasible. A Mars-synchronous orbit would present similar problems; i.e., a Mars-synchronous orbit would make over half of the planet's surface inaccessible to the Aereon rovers because the Aereon rovers must be tracked by the satellite.

COMMUNICATION SYSTEM

Overview:

The communications system of the communication tracking satellite (CTS) is required to provide communication between Earth, the limited range Mars rover, the Mars Orbiter, the Mars base, the orbiting transfer vehicle, and the two Aereon rovers. In providing a link between these systems, the CTS will need to handle various forms of information including data and video images from the rovers, movement commands from Earth, and navigational assistance from the Mars Orbiter.

The Aereon rovers will be transmitting both data and still video signals describing their current operating status and the surrounding conditions. They will rely on the CTS to provide a link to Earth for the relaying of movement commands and general instructions. The minimization of total mass is a requirement for these vehicles, so the signal from the CTS must be strong enough so that the Aereon communications system meets stringent mass and volume requirements.

The limited range land rover is semiautonomous; therefore, communication will only be required for the relaying of navigational mapping data from the Mars Orbiter imaging satellite to the rover. This data will be downloaded by the CTS to the rover and will consist of a series of detailed maps of the surface immediately surrounding the rover for use in navigation.

Contact with the Mars base will be required for tracking purposes. Range-rate data for the CTS, which will enable the satellite to determine its exact orbit and position, will be determined by the base and relayed to the satellite. This link is also provided as an emergency backup communications system for the Mars base in case a breakdown occurs in its link with the orbiting transfer vehicle.

A link with the transfer vehicle is provided as a backup precaution. In the event that either orbiter loses contact with Earth, it can route its information through the link existing with the other orbiter. Also, if communication is interrupted between the transfer vehicle and the Mars base, the CTS will be able to complete that link.

The CTS will provide communication by receiving data from the transmitting end of the link, storing that data onboard the satellite, then transmitting the stored data to the receiving end of the link after all the data has been uploaded to the CTS. This will enable the CTS to conserve power by never sending and receiving data at the same time. Mass can also be conserved because this system allows for the use of only one set of uplink/downlink frequencies without the problem of interference effects, enabling the satellite to carry less signal generating equipment than would be necessary if more frequencies needed to be produced.

Frequency Band Selection:

The K_a band, with an uplink frequency of 30 GHz and a downlink frequency of 20 GHz will be employed by the satellite for all communications. It was decided that the link to Earth must be at a frequency that was not oversaturated by existing communications so that the weak signal received from the CTS could be detected without a great deal of interference. For this reason, the C band and the X band were eliminated as possibilities for the CTS. Since the CTS was designed to handle still video signals and needed to transmit those images in a limited amount of time, a frequency that could provide a high transmission rate was necessary. The 2.4 kilobits per second (KBPS) provided by the available bandwidth of the S and L bands was determined to be insufficient for this mission, so a higher frequency band was deemed neceassary. Current technology can provide reliable communications equipment for frequencies up to about 100 GHz, but expensive high technology equipment is necessary for equipment designed to transmit at higher frequencies than the K band. Therefore, the best possible frequency selection for this mission is the K band, which encompasses the range of 10.9 GHz - 36.0 GHz. Due to expanding use of the lower end of this band, the higher end, specifically the Ka band, was chosen for this mission.

Power and Signal Generation:

The communications system of the satellite was allocated 100 watts of power and will use traveling wave tube amplifiers (TWTA's) for the generation of the output signal. It

was determined that for the given size of the solar array, 100 watts would be the maximum amount of power that could be devoted to communications. Using TWTA's, a 30 W generated output signal will be obtained, using a value of 30 % for the overall efficiency of the communications system. TWTA's were chosen over solid state power amplifiers (SSPA's) due to their proven reliability over the past 25 years, their high efficiency, and their ability to deliver a higher power output signal than current SSPA's [4].

Antennas:

The CTS will utilize two 1.2 m diameter Cassegrain reflecting antennas for communications purposes--one for communication with vehicles on the surface of Mars and one for all other communications links. The use of two antennas with one directed at each member of a communication link eliminates the problem of having to acquire a different target for every burst of data, and provides for a backup in the event of the failure of one antenna. 1.2 meters was determined to be a sufficient diameter for the antennas due to their signal boosting characteristics (see section on surface vehicle communications requirements), and not so large as to cause problems due to unnecessarily raising the total mass of the spacecraft and causing structural problems associated with the stowing of the antennas during the transfer to Mars.

Data Transfer:

A data transfer rate of 64 KBPS was chosen for the CTS due to a request for a short time transfer of the still video images taken by the Aereon rovers. The images will be of composed of a 500 X 1000 pixel grid with a 4 bit per pixel coded shading scheme. 16 such images will be sent at a time. The limited range land rover requires upwards of 100 daily transmissions of pictures from the Mars Orbiter with a 512 X 512 pixel grid and a 4 bit per pixel coded shading scheme. A 64 KBPS data rate can accomplish the transmission of the set of Aereon images in 125 seconds, and the land rover images in 16 seconds. A higher data rate would require a higher signal power from the CTS which would not be feasible for the time it would save. A storage capacity of 50 MB was chosen for the CTS to enable a 13.02 minute continuous communication upload time.

Signal Modulation:

The signals received and transmitted by the CTS will be modulated using the quaternary-phase phase-shift-keyed system (QSPK) and will utilize a bandwidth of 38,400 Hz. QSPK modulation is the most common form of modulation currently being used for digital communications and is well suited to the type of data flowing through the CTS. The required bandwidth for the filtered signal was determined from the following equation [1]:

$$B = 1.2/T \text{ Hz} \qquad (1)$$

where:

B = required bandwidth

T = symbol rate of source signal

Since two signals are combined to form a QPSK signal, a 1/T of 32,000 Hz is used for a data rate of 64 KBPS, and the required bandwidth of 38,400 Hz was determined.

Specifications:

Table 1: Communications System Specifications

System Mass:	120 Kg
Output Signal Power:	30 W
Power Input:	100 W
Signal Generation:	TWTA
Frequency:	30/20 GHz
Bandwidth:	38400 Hz
Modulation:	QPSK
Transmission Rate:	64 KBPS
Storage Capacity:	50 MB

Requirements for Receivers on Mars:

Listed in Table 2 is a summary of the gains and losses affecting the communications link signal. The gains for the Aereon rovers were based on the utilization of a 0.15 m parabolic antenna for communications purposes. The limited range land rover will use a 0.25 m parabolic antenna for reception.

The path loss was determined based on the maximum distance possible for communications, 12223 km, which is based on a 15° angle of the antenna with the surface. The equation used to calculate this loss was[5]:

$$P_L = (4\pi r/\lambda)^2 \qquad (3)$$

where:

P_L = path loss
r = distance traversed by the signal
λ = wavelength of the signal

Table 2: Signal Gains and Losses (Mars Surface)

Signal Power:		17.77	dB
CTS Antenna Gain:	Uplink	50.0	dB
	Downlink	46.46	dB
Path Loss:	Uplink	143.7	dB
	Downlink	140.2	dB
Aereon Gain:	Uplink	31.9	dB
	Downlink	28.4	dB
Rover Gain:	Uplink	36.3	dB
	Downlink	32.8	dB
Signal to Noise Ratio:		18.5	dB

The antenna gains were determined using the following equation [8]:

$$G = 4\pi A\eta/\lambda^2 \qquad (2)$$

with:

G = Antenna gain

A = Antenna Area

η= Efficiency (assumed to be 0.70 [1])

λ = Wavelength of signal

Using these figures, the downlink signal received by the Aereons will be of strength -50.57 dB when entering the receiver. This translates to a signal power of 8.77 X 10^{-6} W, which should be easy to amplify. As a comparison, the signal received by a private home satellite television receiver is 4 pW [4].

Earth Station Requirements:

Using the same method as in the above section, the gains and losses the signal experiences during transmission to Earth are listed in Table 3. The gain for the Earth station was determined assuming communication facilities will be provided by NASA's Deep Space Network (DSN) on 120 m diameter dishes.

Table 3: Signal Gains and Losses (Earth)

Signal Power:		14.77	dB
CTS Antenna Gain :	Uplink	50.0	dB
	Downlink	46.46	dB
Path Loss:	Uplink	293.6	dB
	Downlink	290.1	dB
DSN Gain:	Uplink	90.3	dB
	Downlink	86.8	dB

TRACKING

There are several main tracking requirements for the communications and tracking satellite (CTS). First, it must be able to locate the rovers on the Martian surface so the phased-array antenna can be aimed to establish a communications link. Accuracy to within 10° is required for this task; however, the location of the Aereons must be determined more precisely in order to record exactly where, on the surface, the samples are obtained. This accuracy is not required for the limited range rover, however, which can determine its precise location on its own.

The communications and tracking satellite will use the communications radar, antennas and power sources to track its subjects. The stationary Mars lander will aid the satellite in providing the necessary range and rate information. The base will relay its position to the satellite, providing a reference by which to locate other vehicles. The Aereons will send out a beacon which the satellite can locate and lock on to at every pass and receive and transmit information. The satellite will implement the range and range rate system [6], patented by NASA, Lyndon B. Johnson Space Center, in 1988, to determine the locations of the Aereons.

The rover will be capable of determining its location, and will be capable of finding the satellite to relay information and position. It can also provide another reference to the satellite, it will have detailed maps of the surface, and can communicate through the satellite to Earth to determine its general location.

POWER

The communications and tracking satellite (CTS) will need sufficient power to communicate with the Earth ground station, two Aereon rovers, the limited range land rover, and the Mars base. Additional power is needed for attitude control, active thermal control, telemetry, and several motors onboard the spacecraft including the antenna pointing motors and the suntracking motors for the solar arrays. Appendix 3 gives a breakdown of exactly how much power each system on the satellite requires.

Flexible roll-up solar arrays will be used to supply the 250 watts needed to power the CTS. The solar blankets are stored on a cylindrical drum and are deployed using a boom system which pulls the blanket from the drum while a damping force on the drum keeps the solar panel array taut.

A simple algorithm [1] was used to determine the size and mass of a possible solar array configuration (see Appendix 1). All major assumptions for this size and mass estimation are given in Table 4. Using these assumptions, the solar panel arrays were estimated to be 1.9 m x 1.9 m. Changes were made to the algorithm, which was devised for a satellite in Earth orbit, based on expected conditions in the Mars orbit. The solar array temperatures were cut in half as a reasonable approximation. Results showed that the subsystem will have a mass of approximately 15 kg total.

A dual bus system will be used to regulate battery depth of discharge, increase reliability, and protect against failures. Since 1000 charge-discharge cycles will be needed, the system will use NiCd batteries. At a 55 % depth of discharge, the NiCd batteries must be kept between 32° F and 115° F in order to maintain the minimum 1000 cycle life (Fig 3). Small thermal radiators and heaters will be used to control temperature. Finally, a shunt dissipative regulator (Fig 4) is used as a power transistor.

Table 4: Major assumptions for determining solar array dimensions

Mission life: 5 years
Bus voltage: 42V during sunlight and minimum 28V during eclipse
Load: 250 Watts (see Appendix 3 for Load Calculation)
Array: Suntracking flat panels
Radiation degradation factors
    current 8.6 %
    voltage 4.2 %
Solar intensity facors
    summer solstice 0.7498
    autumnal equinox 0.9867
NiCd batteries with maximum DOD of 55 %
Minimum discharge voltage = 1.1V
Two independent bus systems
Three-axis stabilized satellite

Solar cells @ 25° C
Size: 2 X 4 cm Thickness: 0.025 cm

Coverglass: Cesium-doped microsheet of 0.015 cm thickness

I_{mp} = 0.2966 A I_{sc} = 0.315 A
V_{mp}= 0.45 V V_{sc}= 0.548 V

Solar array temperature:
    Summer Solstice: 19° C
    Autumnal Equinox: 25° C

Temperature coefficient at EOL:

α_I = 0.24 mA/°C

α_V = -2.2 mV/°C

PROPULSION

The propulsion system of the CTS will need only to make minor orbital corrections and minor attitude adjustments to back up the momentum wheel system. No propulsive burn will be necessary to achieve the orbit since the spacecraft is placed into orbit by the transfer vehicle.

A computer program was developed to determine the propellant mass required for the five-year lifetime of the CTS based on equations given in Agrawal [1]. The program is attached as Appendix 2, and the results based on propulsion being used for only inclination stationkeeping and longitudinal stationkeeping show that 20 kg of fuel will be sufficient for a reaction control system which has a mass of 5 kg.

The propellant used will be nitrogen tetroxide/monomethylhydrazine, which is a hypergolic bipropellant. This was chosen due to its advantages in I_{sp} over mono-propellants, and the elimination of an ignition system usually necessary for a bipropellant system.

STRUCTURES

The structure of the satellite must support a variety of loads and provide sufficient volume and mounting area to accommodate all the subsystems in the spacecraft. Some of the loads to be considered are operating thrusts, centrifugal stresses, radiation pressure, and micrometeorite impacts. The limits of these structures is dependent on mass limitations. The design of this structure must meet all requirements while optimizing the stiffness/strength to weight ratio.

Two ways of meeting the requirements is through selection of materials and type of design. Considering material selection and cost some ideal materials would be aluminum, magnesium, stainless steel, Invar, Titanium, graphite-reinforced phenolic, fiberglass epoxy, and beryllium [7]. Since the CTS is three-axis stabilized, a central thrust tube is surrounded by equipment panels to form a box structure with the solar cells mounted on deployable rollout panels. Included in the design are support struts which are used to improve stiffness/strength. In addition to the primary structure, secondary structures are used for mounting of items such as antenna reflectors and feed assemblies. Due to the mass limitations imposed on the CTS, corrugated aluminum will be used for the thrust tube and brackets and an aluminum honeycomb core faced with carbon fiber sheets for the panels.

THERMAL CONTROL

The CTS will rely entirely upon passive thermal control devices for both heat dissipation and heat retention. Only for critical components of the CTS which require heating, will active thermal control devices be used.

The two primary sources of heat that must be dissipated by the passive control devices are solar radiation and internally generated heat from the instrumentation. The solar radiation will be dealt with primarily by coating the outer surface of the CTS, minus the north and south sides, with low alpha white paint so that the CTS does not absorb much of the radiation in the first place in much the same manner as IntelSat VII [2,3]. The internally generated heat will be dealt with in two ways. First, the north and south sides of the CTS will be covered with mirrored surfaces made of Teflon, Kapton, and Mylar to allow most of the internal heat to pass through them. Secondly, small heat pipes will be used to aid in the dissipation of the heat generated by the TWTA's, the largest producer of waste heat in the CTS. Heat retention, wherever necessary in the CTS, will be provided by insulation in varying amounts depending upon the sensitivity of each of the CTS's components to extremes in temperature.

Heating, which is provided by active control devices, will only be done for those components of the CTS that are very vulnerable to low temperatures. The active control devices used for this purpose will be small heat sensitive resistive heaters which will utilize power from the electrical system.

ATTITUDE CONTROL SYSTEM

Stabilization:

The CTS will be stabilized in three axes during the operational mission phase, with one of the communications antennas always directed towards Mars and the solar array panels rotating twice per day to remain facing the sun. The attitude control subsystem stabilizes the flight system and adjusts the spacecraft orientation to maintain proper pointing of the Mars-directed antenna. This subsystem employs zero-bias momentum derived from three separate reaction wheels provided for all three axes to achieve three-axis stabilization in the operation orbit. This zero-bias is a very precise system because the axes are independently controlled and adjusted in orbit.

Attitude Control Subsystem:

The attitude control subsystem consists of pointing and attitude sensors, sensor electronics, an attitude control and digital processor, and mechanical drives. The pointing sensors are a star sensor and sun sensor. The star sensor will precisely measure the pointing angle with respect to a known reference. For the CTS, the primary pitch and roll attitude sensor is an autotrack feed system utilizing the Mars antenna. Yaw attitude is determined using the star sensor. Because the accuracy of the star sensor is in the arc-second range, the star sensor will be used for attitude determination along with the sun sensor. The satellite will employ fixed-head star trackers to search their field of view and acquire stars. The fixed-head star trackers were chosen above gimbaled star trackers because of their light weight and generally smaller size. The image detecting device used by the fixed-head star tracker is a charge coupled device (CCD). Also, the fixed-head tracker requires no mechanical action which would reduce their long term reliability. The sun sensors will aid in positioning the solar arrays and protecting the star trackers.

The star tracker for this mission will use a version of the P8600 CCD supplied by English Electric Valve Co. (EEV) [9]. This is a 385x288 pixel frame-transfer device and was selected primarily because of its potential low noise performance and because the type

used (P8604) is packaged with an integral Peltier cooler, which enables more computing power for nonuniformity correction. Listed in table 5 are the measured performance parameters of the high accuracy star trackers using this CCD. These attitude measurement and control system (AMCS) star trackers, which are mission-critical items, are a special concern for long-term reliability. The AMCS trackers' absolute accuracy is improved by simultaneously tracking a fiducial star, an artificial light source generated within the telescope that gives information on the misalignment between the telescope and the star tracker boresight. An AMCS star tracker optical subassembly can be viewed in Figure 5.

The sensor electronics system will process the sensors' output signals to produce a properly calibrated message. The autotrack error signals are referenced to the command carrier uplinked from the main reference and received by the Mars antenna beam fixed on the main reference.

The attitude control and digital processor accepts the error message from the sensor electronics system and determines corrective action based on preprogrammed instructions that can be modified by the command carrier. This is then uplinked from the main reference and received by the Mars antenna beam fixed on the main reference.

The mechanical drives include three momentum wheels and an easily applied sensitive gyroscope which is used to control the attitude of the spacecraft. The sensed errors in roll, pitch, and yaw are corrected by applying torques about the appropriate flight system axes. The Attitude Control subsystem design provides 0.05-degree stationkeeping accuracy along with 0.025-degree pointing accuracy for the CTS communications antennas.

Table 5: Star Tracker Performance [9]

Application	attitude control
Field of view	5.9 x 4.4
Lens focal length	82 mm
Sensitivity, GO stars, Mv	6.5 to 0
Total signal for minimum star brightness(electrons)	1.7 x 10E4
Noise equivalent angle(NEA) (1 , one axis,faintest stars)	
pointing	0.5 arcsec
scanning	< 5 arcsec
Systematic errors	
pointing	2 arcsec
scanning	< 5 arcsec
Update period	1 s
Star acquisition time	4 s
Magnitude accuracy	+0.25 Mv
Mass	
camera unit + baffle	8 kg
electronics unit	5 kg
Power	16.4 W

Hardware:

The three separate momentum wheels are used for stabilizing against disturbance torques, absorbing cyclic torques, and transferring momentum to the satellite body for the execution of slewing maneuvers. The capacity of the reaction wheels will be approximately 0.41 kg m^2/s. The same momentum can be achieved with a small, high-speed flywheel or with a large low-speed one, but the smaller wheel is favored because of its size and weight. The high-speed smaller wheel has the disadvantage of greater wear on its bearings, but the five year design lifetime of the CTS is far less than other satellites employing the same size wheels. Typical values of momentum wheel parameters are given in Table 6.

Table 6: Typical Values of Momentum Wheel Parameters [9]

Manufacturer	Mass (Kg)	Moment of Inertia (KgxM2)	Speed Range (RPM)	Angular Momentum (KgxM2/s)
APL	3.18	0.0115	2000	2.41 @ 2000 RPM
BENDIX	8.84	0.0880	1450	11.52 @ 1250 RPM
	2.36	0.0034	1400	0.45 @ 1250 RPM
	5.13	0.0297	900	2.79 @ 900 RPM
ITHACO	3.72	0.0060	600-2000	1.49 @ 2000 RPM
	6.71	0.0272	1000-2000	5.69 @ 2000 RPM
RCA	18.66	3.4604	95-392	128.03 @ 353 RPM
	18.66	14.43	120-160	128.03 @ 353 RPM
SPERRY	13.38	0.1913	2000	40.07 @ 2000 RPM

The three momentum wheels used for this mission are similar to those used in the Skylab attitude control system. The momentum wheels have mass of approximately 1.34 KG each and require an operating power for each wheel in the range of 24.9 - 49.8 W.

To complement the momentum wheels, bipropellant gas jets will be used to produce thrust to provide the spacecraft with a backup system for spacecraft stability and orientation and also to maintain proper pointing of the communications antennas. The resultant torques and forces will be used to adjust the spacecraft's orbit, and to control the attitude of the spacecraft and speed of the reaction wheels.

CONCLUSION

The communications and tracking satellite (CTS) designed herein for the Mars Sample and Return Mission (MSRM) will provide tracking information for the Aereon rovers and will fulfill nearly all of the communications needs for the mission. After the mission is completed, the satellite will remain in orbit until too many of the main systems fail or the solar panels cease to provide enough power for the vital systems of the satellite. After the samples are returned to Earth, the Aereons will continue to explore the planet, and the data collected will be relayed to Earth via the CTS.

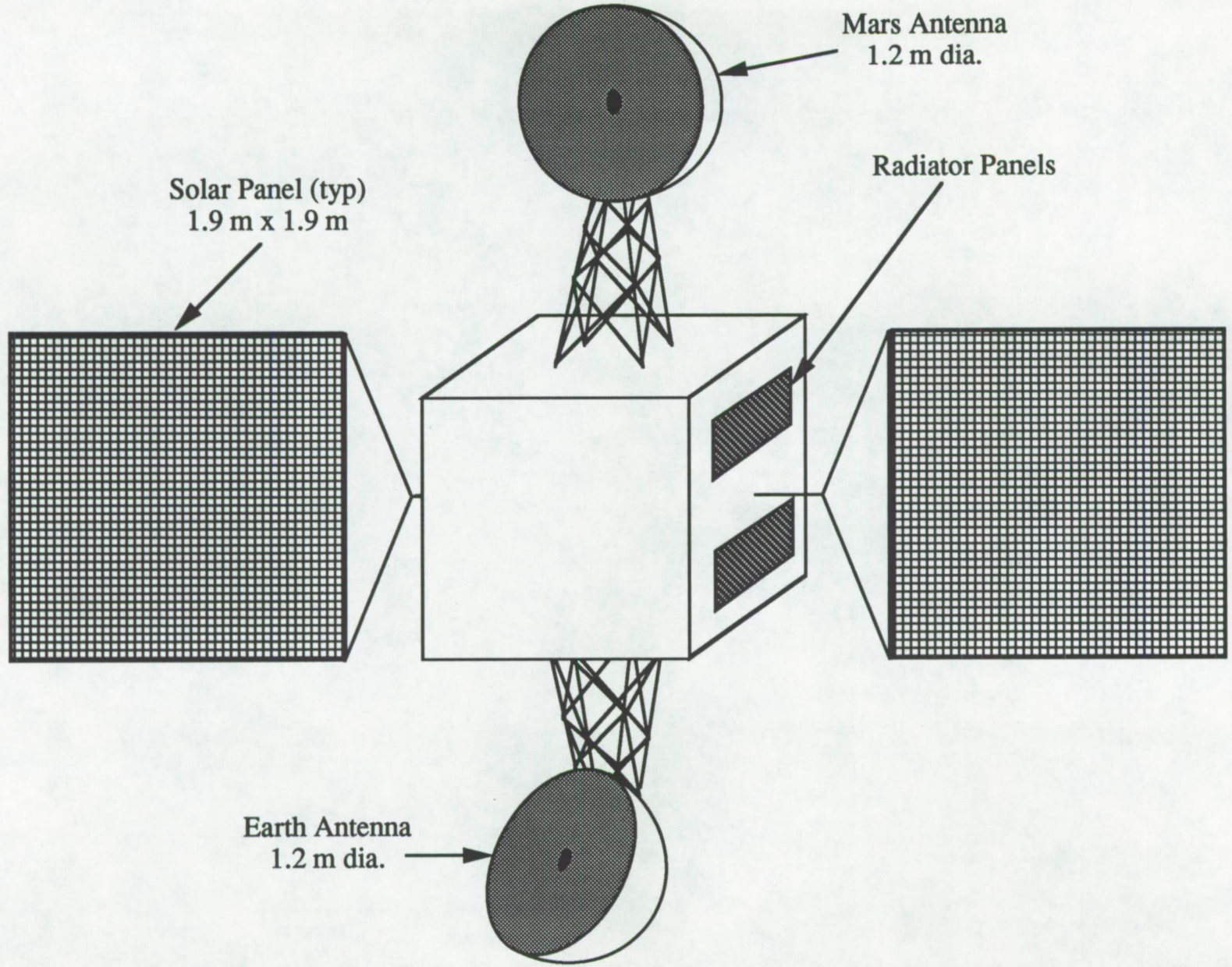

Figure 1: Deployed Satellite Configuration

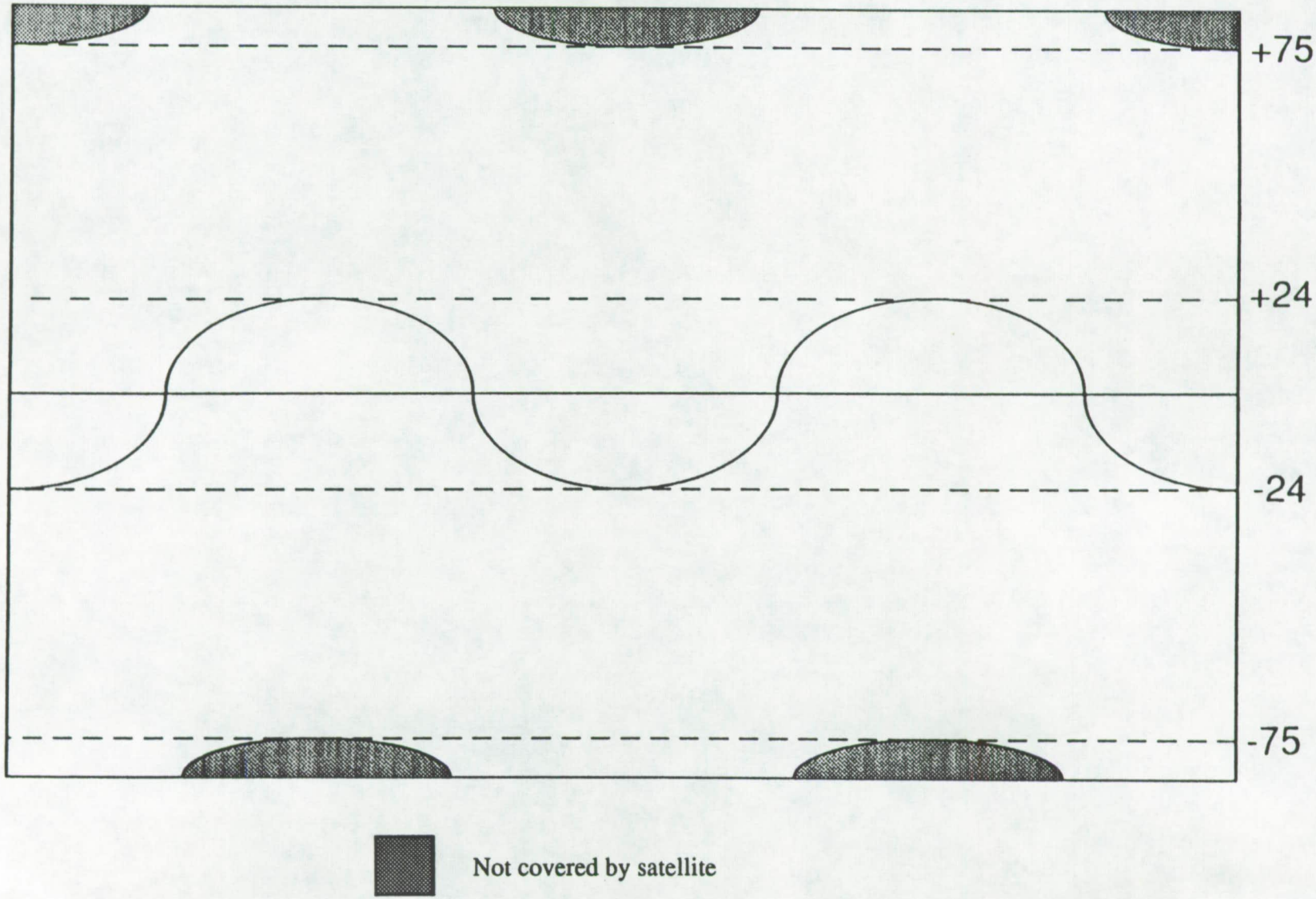

Figure 2: Communications Satellite Path and Coverage Area

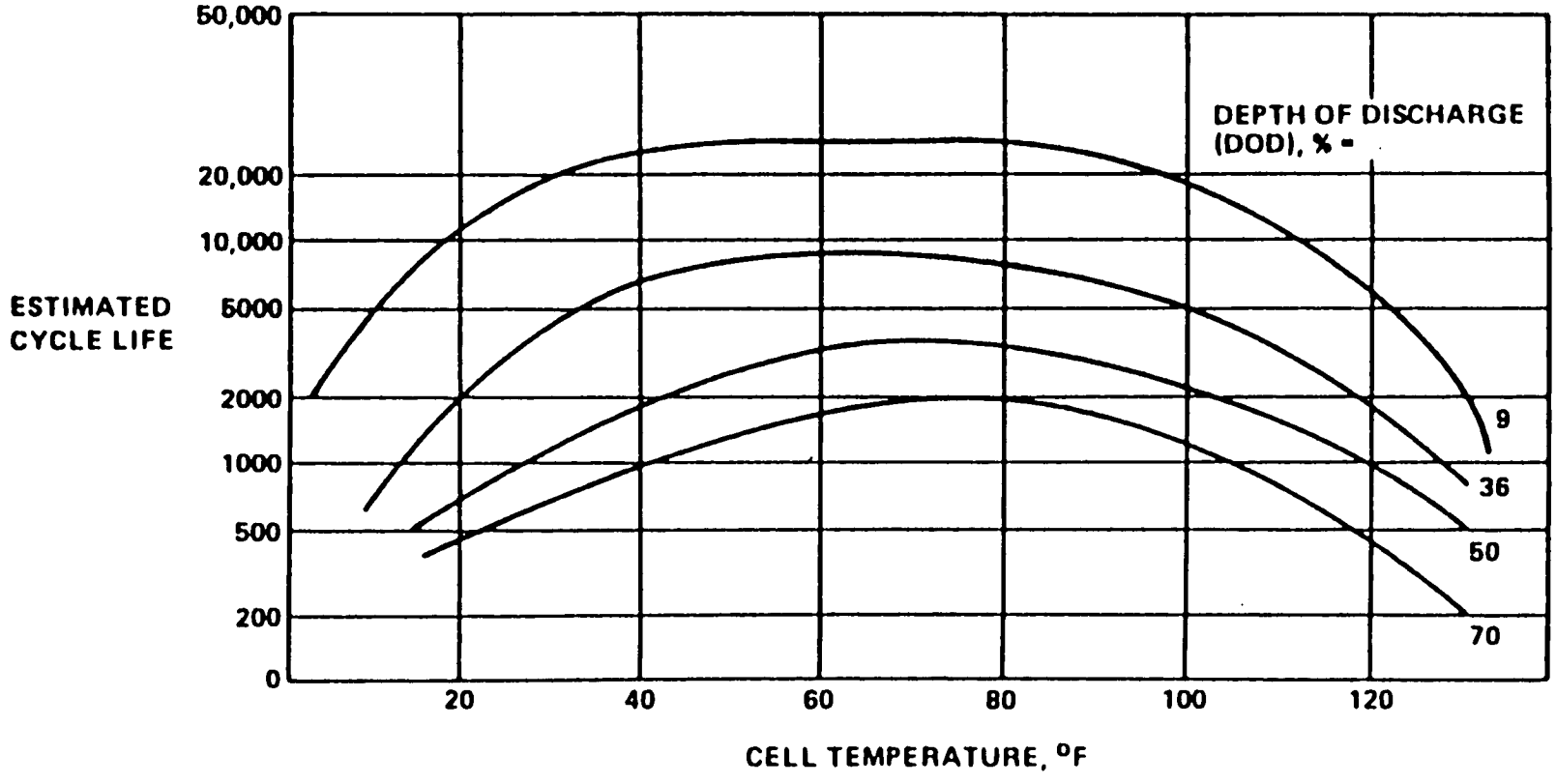

Figure 3: Nickel-Cadmium Battery Cycle Life [1]

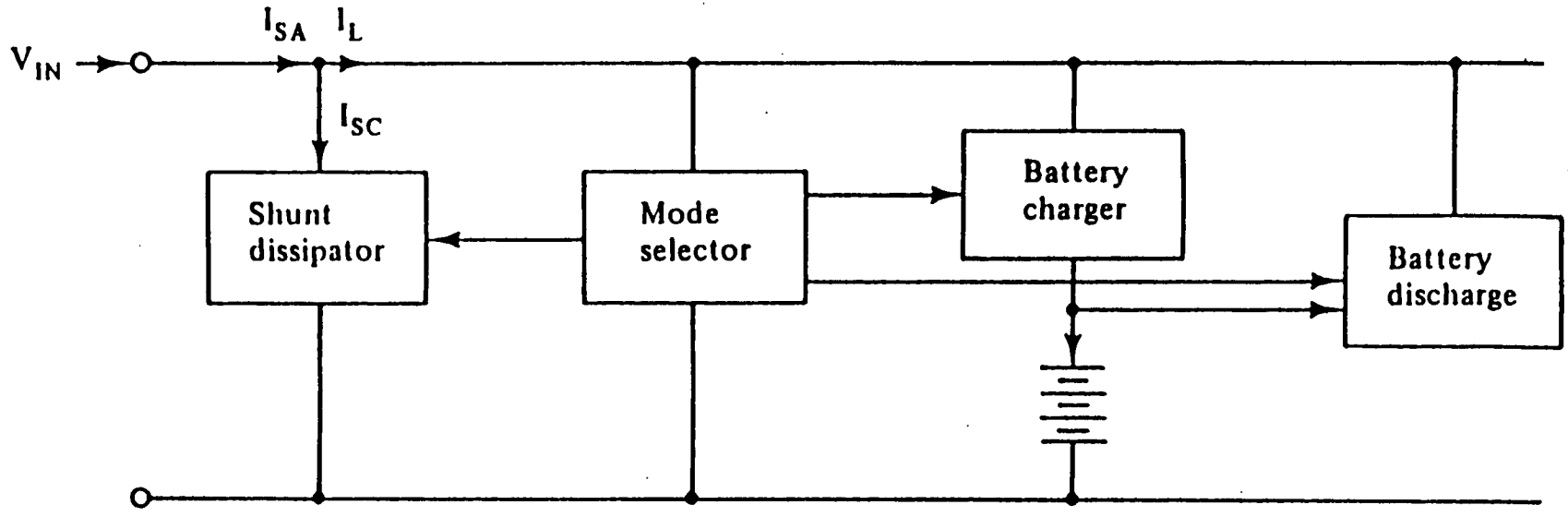

Figure 4: Shunt Regulator [1]

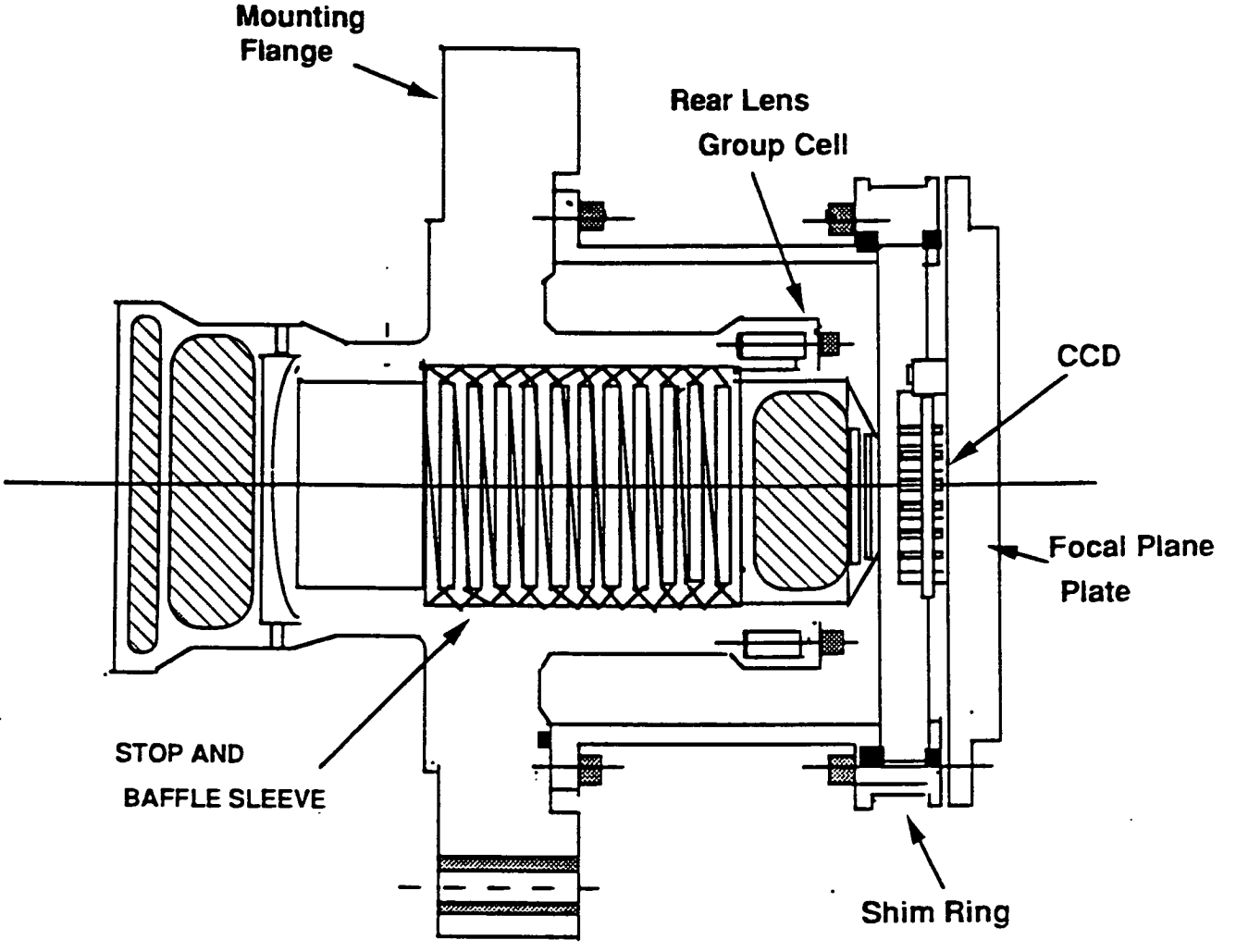

Figure 5: Section Through AMCS Star Tracker Optical Subassembly [Wertz, 1978]

REFERENCES

1. Brij N. Agrawal, Design of Geosynchronous Spacecraft, Prentice-Hall, Englewood Cliffs, NJ, 1986.

2. Collection of Technical Papers, *11th AIAA International Communication Satellite Systems Conference and Exhibit,* AIAA, 1988.

3. Collection of Technical Papers, *13th AIAA International Communication Satellite Systems Conference and Exhibit,* AIAA, 1990.

4. Robert L. Douglas, Satellite Communication Technology, Prentice-Hall, Englewood Cliffs, NJ, 1986.

5. Gerard Maral, Satellite Communications Systems, Wiley, New York, 1986.

6. Mars Rover Sample Return Mission Navigation System Studies, Charles Stark Draper Laboratory, Inc., Cambridge, MA, 1988.

7. Wilbur L. Pritchard and Joseph A Scilli, Satellite Communications Systems Engineering, Prentice-Hall, Englewood Cliffs, NJ, 1986.

8. Satellite Communications Systems, B. G. Evans, London, 1987.

9. James R. Wertz, Spacecraft Attitude Determination and Control, 1978.

APPENDIX 1: EXAMPLE USING POWER ALGORITHM

Batteries:

$V_{DB} = (N-1)V_D - V_D$
$28 = (N-1)(1.1) - 1.1 \Rightarrow N = 27.45 \Rightarrow 28$
$V_{DB} = 27 \times 1.1 - 1.1 = 28.6V$

$C = (Pt)/V_{DD}DOD) = [(125W)(1.2\ hr)/(28.6V)(0.55)] = 9.54\ Ah$
$C/15 = 0.636$
$C/45 = 0.212$

$V_{BC} = (1.5 \times 27) + (3 \times 0.8) = 42.9\ V$
$V_{CA} = V_B - V_{BUS} + V_{CD} = 42.9 - 41.5 + 1.75 = 3.15\ V$

Equinox:

$P_{charge} = (current)(voltage) = (0.636)(42.9) = 27.3$

$t_{recharge} = (P_{discharge})(t_{discharge})/(P_{charge})^n$

Summer Solstice:

$P_{charge} = (0.212)(42.9) = 9.09\ W$

Solar Array Design

Design Load at Equinox:
$(1.1)(50 + 32.6) = 90.9\ W \Rightarrow 45.45\ W$ per bus

Design Load at Summer Solstice:
$(1.1)(50 + 9.09\ W) = 65.0\ W \Rightarrow 32.5\ W$ per bus

$I = [I_{mp} + \alpha_I(T - 25)]K_A{}^iK_D{}^iK_S = [0.2966 + 0.24E\text{-}3\ (39\text{-}25)](0.96)(0.8853)(0.7498)$
$I = 0.191\ A$

I_T = Power/Bus Voltage = 32.5/42 = 0.774 A

Number of cells in parallel for each wing (N_P):
$N_P = I_T/I = 0.6786/0.1911 = 3.55$

Solar Cell Voltage
$V = [V_{mp} - DV + \alpha_V(T - 25)]K_E{}^V = [0.45 - 0.005 + (-0.0022)(39-25)](0.974)$
$V = 0.4034\ V$

Number of cells in series for each wing (N_S):

N_S = (Bus Voltage + Bus Voltage Drop)/Cell Voltage = (42 +1.8)/0.4034

N_S = 109 cells

Solar cell current and voltage at EOL Autumnal Equinox:

I = [0.2966 + 0.24E-3(49-25)](0.96)(0.8853)(0.9867)

I = 0.2535 A

V = [0.45 - 0.005 - 0.0022(49-25)](0.974)

V = 0.3820 V

Current per bus:

I_T = (0.2353)(3.55) = 0.90 A

V_{BUS} = (109)(0.3820) - 1.8 = 39.84 V <= 40 V

Total power output:

P_{OUT} = 2(0.90)(40) = 72 W

Design load at Equinox:

PEQ = 60.99 W => Power Margin = 11 W

Charge Array:

N_S = 3.15/0.4034 = 7.8 => 8

N_P = 0.127/0.2535 = 0.5 => 1

Solar Panel Design:

Number of cells in parallel and in series can be determined from desired current and voltage. For this example, twenty cells in parallel and ninety-six cells in series are needed to generate the required current and voltage, respectively. This results in a panel size of 7.22 m^2.

APPENDIX 2:
PROGRAM TO DETERMINE REQUIRED PROPELLANT

```
      program propellant
+  ************************************************************
* programmed by:  Ron Brubaker
* programmed for:  Aerospace 4013
************************************************************
      real mp(50), v(15), isp, g, mi, il(5), lt(11), n(11), mpac(50)
      integer i, j, k, l, p
*** input data tables ***
      il(1) = 0.1
      il(2) = 0.5
      il(3) = 1.0
      il(4) = 2.0
      il(5) = 3.0
      lt(6) = 0.1
      lt(7) = 0.2
      lt(8) = 0.5
      lt(9) = 1.0
      lt(10) = 2.0
      lt(11) = 3.0
      n(1) = 21.0
      n(2) = 4.0
      n(3) = 2.0
      n(4) = 1.0
      n(5) = 1.0
      n(6) = 59.0
      n(7) = 42.0
      n(8) = 26.0
      n(9) = 19.0
      n(10) = 13.0
      n(11) = 11.0
      v(1) = 10.7
      v(2) = 53.65
      v(3) = 107.30
      v(4) = 214.56
      v(5) = 321.76
      v(6) = 0.15
      v(7) = 0.21
      v(8) = 0.33
      v(9) = 0.46
      v(10) = 0.66
      v(11) = 0.80
*** input constants ***
      mi = 250.0
      g = 9.81
*** begin loop for finding mp with station keeping mode ***
      isp = 285.0
      do 20 i = 1, 11
         z = -((v(i)*n(i))/(isp*g))
         mp(i) = mi*(1-exp(z))
20    continue
*** begin loop for finding mp with attitude control mode ***
      isp = 175.0
      do 40 j = 1, 11
         z = -((v(j)*n(j))/(isp*g))
         mpac(j) = mi*(1-exp(z))
40    continue
```

```
*** begin print routine ***
      print*, 'Mp values for Inclination Station Keeping'
      print*, ' Incl limit        Mp'
      do 60 k = 1, 5
         print501, il(k), mp(k)
60    continue
      print*, 'Mp values for Longitudinal Station Keeping'
      print*, ' Long Tol          Mp'
      do 80 l = 6, 11
         print501, lt(l), mp(l)
80    continue
      print*, 'Mp values for Inclination Attitude Control'
      print*, ' Incl limit        Mp'
      do 100 m = 1, 5
         print501, il(m), mpac(m)
100   continue
      print*, 'Mp values for Longitudinal Attitude Control'
      print*, ' Long Tol          Mp'
      do 120 p = 6, 11
         print501, lt(p), mpac(p)
120   continue
501   format(1x, f7.1, 5x, f10.2)
      end

Ready; T=0.01/0.05 11:35:11
fvcg rocket fortran
** VS Fortran Level 2.4 invoked to compile source file ROCKET.FORTRAN.
VS FORTRAN VERSION 2 ENTERED.   11:35:20

**PROPELLANT** END OF COMPILATION 1 ******

VS FORTRAN VERSION 2 EXITED.    11:35:22

** ROCKET FORTRAN * compiled with no warnings or errors.
Loader invoked and working...
DMSLIOZ40I Execution begins...
Mp values for Inclination Station Keeping
 Incl limit        Mp
      0.1          19.31
      0.5          18.47
      1.0          18.47
      2.0          18.47
      3.0          27.18
Mp values for Longitudinal Station Keeping
 Long Tol          Mp
      0.1           0.79
      0.2           0.79
      0.5           0.77
      1.0           0.78
      2.0           0.77
      3.0           0.79
Mp values for Inclination Attitude Control
 Incl limit        Mp
      0.1          30.67
      0.5          29.38
      1.0          29.38
      2.0          29.37
      3.0          42.73
Mp values for Longitudinal Attitude Control
```

```
Long Tol          Mp
    0.1          1.29
    0.2          1.28
    0.5          1.25
    1.0          1.27
    2.0          1.25
    3.0          1.28
Ready; T=0.23/0.35 11:35:24
spool console close stop
```

APPENDIX 3: POWER BREAKDOWN

Subsystem	Power (W)
Communications	100
Star Tracker	15
Momentum Wheels	75
Thermal Control	20
Motors	20
Battery Charging	20
TOTAL POWER	250

Chapter 6:

Mars Sample Return Mission

Aerospace 401B Detailed Spacecraft Design

Lander Base and Mars Ascent Vehicle

Final Written Report

Group Members:

Steven Douglas
Tim Herald
John Karol
Judine Perreault
Tony Valasek
Mike Vascsinec

ABSTRACT

Upon establishing a stable 500 km (310.7 mi) parking orbit above the Martian surface, the transfer vehicle and lander separate. Once the biconic aeroshell is free of the transfer vehicle, it begins its descent through the Martian atmosphere. At six km in altitude, a combination of parachutes and retrorockets is used to insure a safe landing. Upon stabilization on the surface, the lander collects the contingency samples and then deploys the rovers for sample collection. As samples are returned, the lander's articulated arm collects sample canisters and loads them onto the Mars Ascent Vehicle (MAV). Upon completion of the collection phase, the MAV is launched from the lander and establishes a 500 km (310.7 mi) orbit through the application of a two stage burn. The transfer vehicle intercepts the ascent vehicle and the samples are transferred. Once the samples are transferred, they continue on to Earth via the transfer vehicle.

TABLE OF CONTENTS

LIST OF FIGURES

LIST OF TABLES

INTRODUCTION

Mars Sample Return Mission B utilizes an RTG powered transfer vehicle, an orbiter, a lander, a surface rover, and two Aereons. The lander, which houses the rover and Aereons during transfer, was designed to meet requirements during Martian descent, surface, and ascent operations. Descent required designing a suitable aeroshell and retrorockets to place the lander and its payload safely on Mars. Surface operations required designing the following subsystems: communications, thermal control, robotic arm, and power. Ascent will be performed by a two-stage Mars Ascent Vehicle (MAV).

As with all aerospace design concepts, cost effectiveness, weight considerations, and feasibility were major factors of concern. The lander design was based on guidelines and restrictions imposed by the integration team and the other groups involved with Mission B. The major restrictions imposed by the launch vehicle were mass budgets and ferrying limitations. Subsystems, such as communications, power, and the ascent vehicle placed further dimensional guidelines, as well as redundancy requirements, on the lander design; however, successful integration has resulted in a feasible lander design.

1.0 ATMOSPHERIC DESCENT

1.1 The Aeroshell

The factors to be considered in aeroshell design include aerothermodynamic heating (convective and radiative), trim angle of attack, and packaging to satisfy center of mass (CM) requirements. Three design approaches were investigated. They included a blunt body (L/D=0.24), symmetric biconic (L/D=0.7), and a symmetric bent biconic (L/D=1.5), as shown in Figure 1. The parameters established in rating the designs of these aeroshells involved how well each satisfied the above mentioned design factors.

Originally developed by personnel at the Johnson Space Center (JSC), a symmetric biconic aeroshell is a possible method of achieving moderate L/D's, and relatively low ballistic coefficients (BC) and wing loading values. This design can also fly at an angle of attack significantly higher than that required to achieve maximum L/D. The relationship between a given biconic with an L/D=0.5-0.7 and the BC is insensitive to the aeroshell configuration. This does not hold true for any other range of L/D. Minimum heating rate and acceleration were also found to correspond to an L/D=0.6. These results showed that as the CM moves aft, the BC decreases, the angle of attack increases, the L/D decreases, and the vehicle stability increases. The total volume of the aeroshell is 141.70 m^3 and may also be designed to have a 23.2 m^2 radiator on the lee side to reject radioisotope thermoelectric generator (RTG) heat. The design of the biconic takes into account all aft flow as well. The volume of the shell may be scaled down or up so it should be noted that this number may be altered as needed for the design of the lander. The mass estimate is between 700-800 kg. The resulting L/D of 0.6 is adequate to handle the approach navigation corridor [1].

The aerodynamic navigation corridor (ANC) is defined as the set of all deorbit trajectories that result in the proper orbital conditions at the atmospheric interface. Due to design limitations, this corridor must be adapted to satisfy vehicle entry requirements. The flyable entry corridor is then defined as the ANC reduced by vehicle design limitations [2].

The flyable corridor is primarily constrained by the five-g acceleration limit imposed by NASA for sample preservation. The corridor is defined by L/D=0.6 for V=4.46 km/s (upper limit) and L/D=1.1 for V=3.41 km/s (lower limit). Larger corridors can be achieved through higher accelerations, but this could compromise the stability of the vehicle. Corridor width may be specified by the range in flight path angle at the atmospheric interface. Through the use of data collected from the Viking missions, the interface was found to occur at an altitude of 140 km. The width of the flyable corridor must also be large enough to compensate for the uncertainties associated with the flight. Flight uncertainties may result from erroneous atmospheric modeling, unpredicted aerodynamics, and mid-course correction errors. These mission uncertainties are assumed to impose a +/- 0.5° corridor width requirement. This assumption dictates a flyable corridor width of 1.0° to ensure a successful deorbit to atmosphere maneuver [3].

An L/D=0.22-0.24 (Blunt Body) requires a 2.0° corridor at five g's and therefore does not meet the mandatory requirement of a 1.0° flyable entry corridor. The blunt body also has a deployability requirement to its disadvantage, and it also requires significant development in terms of material technology. The symmetric bent biconic (L/D=1.5) experiences severe heating, dynamic pressures and g-loading during descent which deems it impractical for the mission. The symmetric biconic configuration (L/D=0.6) has proven to have the least risk while meeting all of the mission's performance requirements. Its L/D is also sufficient enough that autonomous navigation in the encounter phase is unnecessary [2]. Unlike the blunt body, this design does not require extensive new technological developments but its performance has yet to be investigated. Since the mission can not make use of a blunt body or bent biconic, the only feasible decision is to utilize the biconic design.

It has been decided that the symmetric biconic is 5.0 m in diameter and 11.91 m in length. The diameter is limited by the maximum allowable payload faring of the Titan IV and it was determined from the lander design considerations that a length of 11.91 m would be appropriate for payload storage. The biconic has a constant L/D and is flown at an angle of attack of 40°.

1.1.1 Configuration Summary

Two biconic aeroshell configurations have been investigated for the mission. The two shapes are similar except that one has a larger nose radius (approximately 1.159 vs. 0.305 m) and a smaller front cone angle (15.7° vs. 23.55°) [5]. The designs are illustrated in Figure 2. The increased nose radius reduces the maximum L/D, increases the angle of attack, and reduces the BC at the maximum L/D. It should be noted that even if both configurations are flown at a 40° angle of attack or an L/D = 0.6, the only noticeable difference in aerodynamic performance is a 2-3% forward shift in the location of the CG in the larger nose radius design. This interesting result shows that if an L/D as low as 0.6-0.7 is used, the nose shape can be modified for packaging or local thermal concerns without significant changes in the aerodynamic performance of the aeroshell [5].

Inherent to the design is a parameter comparable to wing loading on an airplane and is known as the lift coefficient (LC). This parameter is a measure of the maneuverability of the vehicle and is determined by dividing the BC by L/D. It is perhaps more significant than either L/D or the BC in assessing the ability of the aeroshell design to accommodate the required flight corridor size with the minimum heating rate [5]. A low LC allows the vehicle to pull out to level flight at a higher altitude if necessary. It should also be noted that the minimum value of LC occurs at a value of L/D=0.6.

Additional design investigations proved that, with a total corridor height equivalent to a 2° total variation in entry flight path angle, an L/D=0.6 is adequate. The requirement for entry-to-landing is even less demanding on L/D, but a low BC contributes to desirable conditions at parachute deployment, including lower dynamic pressures and velocities.

The use of this biconic configuration and the reduction of its BC by flying at a higher angle of attack than required for maximum L/D, has several advantages. These include increased stability due to a larger negative pitching moment, easier packaging due to an aft displacement of the CM, a larger reduction in the BC which reduces aeroheating and yields lower dynamic pressures at parachute deployment, and less sensitivity to nose bluntness [5].

1.1.2 Effect of Mach Number on Aerodynamic Performance

Investigation into Mach number effects leads to the conclusion that L/D, angle of attack (a), and drag coefficient (C_d) vary with Mach number, as can be seen in Figure 3. These values are representative of a CG position located at approximately 56.5% of the body length [5]. It should also be noted that the lift coefficient remained nearly constant, varying from 1.0 to 1.1 over the total Mach number range. From Figure 3, it can be seen that both the angle of attack and drag coefficient decrease and L/D increases as Mach number decreases.

1.1.3 Pressure Distribution

Pressure contours for the two aeroshell configurations are illustrated in Figure 4. These contours were generated at a Mach number of 26 and an angle of attack of 40°. From this figure, it can be seen that the pressure concentration is located at the nose cone and on the lower atmospheric contact surface. Structural and thermal designs take these pressure concerns into account. Structural strength will be greater at these points to ensure that the design is not compromised. Thermal protection is greater in these regions to ensure that the aluminum structure does not exceed 177°C.

1.1.4 Thermal Protection System (TPS)

The primary objective of thermal analysis is to estimate the maximum temperatures and total weight of the TPS for the aeroshell. The aeroshell's aluminum structural skin requires a thickness of .254 cm and must not exceed a temperature of 177°C. In order to decide what materials to use for thermal protection, an analysis of the crucial heating points must be done.

The analysis can be broken down into six axial divisions along the aeroshell with each division broken into six circumferential segments (see Figure 5) [5]. Heating to panels located in section B can be taken to be the average of the windward and side panels. Heating to section D (leeward side) can be considered to be 1/3 that of section B [5]. At first consideration, most of the windward temperatures could exceed the 1500°C limit generally associated with the Fiber-Fiber Rigid Composite Insulation (FRCI) tiles that are

used on the Space Shuttle; however, additional research revealed that these portions of the vehicle may remain below 1500°C and the FRCI tiles may be used on the aeroshell. Some portions of the vehicle (i.e. D-the leeward section) remain below 1090°C and may be covered with Felt Reusable Surface Insulation (FRSI) as used on the lower heating regions on the Shuttle Orbiter [5].

The additional research into the "hot spots" on the aeroshell involved studying the boundary layer created upon atmospheric entry. It was discovered that if laminar flow exists over the entire vehicle, these "hot spots" could be insulated with FRCI tiles. Preliminary calculations by the Martin Marietta Aerospace Group indicate that if flight criterion developed from Space Shuttle flight data can be applied to the biconic configuration, then laminar flow would occur over the entire body for the duration of its use. The shuttle criterion is defined as the momentum thickness Reynolds number divided by the local Mach number and is equal to 290. This criterion applies to the forward portion of the orbiter. This section of the orbiter is similar in cross-section to the biconic configuration with the larger nose cone. The shuttle flight data was collected in the presence of these TPS tiles and was flown at an initial reentry angle of attack of 40°. Since the TPS tiles and the 40° angle of attack are both factors in the design of the Mars aeroshell, the correlation of data is a good approximation. This collection of data leads to a projected TPS weight of between 224kg and 292 kg. Figure 6 illustrates a cross-section of the proposed TPS. It consists of the thin aluminum structure covered by Q-Felt, ZrO_2 Felt and an advanced Carbon-Carbon tile. It should be noted that a low TPS weight is required if laminar flow is to exist over the vehicle [2].

1.2 Descent

1.2.1 Orbital Mechanics

Once the transfer vehicle establishes a 500 km orbit above Mars, procedures for the descent phase will commence. Considering the path from orbit to atmospheric interface as a Hohmann transfer, orbital mechanics theory was used to determine the point of

atmospheric penetration. This flyable corridor can be determined based on the time of departure from Earth and the projected time of established Martian orbit. All the deorbit calculations are independent of departure time.

Hohmann transfer calculations include calculating the true anomaly (n), speed (v), flight path angle (f) and the radial distance (r) of the vehicle in orbit. It was determined that the vehicle will be traveling at 3.331 km/s and a radial distance of 3880 km. Atmospheric interface occurs at a radial distance of 3520 km at which point flight mechanics dominate the problem.

1.2.2 Flight Mechanics

Flight mechanics calculations are initiated at the atmospheric interface. Since the velocity at this point was initially unknown, a numerical solution of the descent trajectory was required. Before the solution could be implemented, the initial conditions of the trajectory had to be determined. Since the vehicle must be slowed to Mach 2 at 6 km before the parachutes and aeroshell can be deployed, the speed at this point could be determined.

From previous Viking mission temperature data, the temperature at 6 km was found to be 211 K[4]. This altitude also corresponds to a ratio of specific heats (g) of 1.33896. The molecular weight of carbon dioxide, Mars' primary atmospheric compound, is 44.0098. Assuming that CO_2 is a perfect gas,

$$V = M\,a \quad (1)$$

where,

$$a = [g\,R/M\,T]^{1/2} \quad (2)$$

The speed at the 6 km altitude was found to be .4623 km/s. In order to solve for the interface speed, the equations of motion of the aeroshell at any altitude between entry and jettison must be derived. Two second-order equations were found, which can be decomposed into four first-order equations. Using the Runge-Kutta numerical method of integration, and the initial conditions established by the orbital mechanics calculations, the velocity at the interface can be determined. A driver routine was created to establish the initial conditions for the Runge-Kutta subroutine but the numerical solution remains to be

completed. The equations for true anomaly, speed, and flight path angle are:

$$n = -\cos^{-1}\left[\frac{2r_a r_p - r(r_a + r_p)}{r(r_a - r_p)} \right] \quad (3)$$

$$v = \text{sqrt}\left[2\,m\,\{ 1/r - 1/(ra + rp) \} \right] \quad (4)$$

$$f = \cos^{-1}\left[\text{sqrt}\left[r_a r_p / \{ r(r_a + r_p) - r2 \} \right] \right] \quad (5)$$

1.2.3 Navigation Systems

Navigation measurements can be taken immediately after the deorbit burn, through atmospheric entry, and down to the release of the parachutes. The general navigation scheme onboard the descent/entry lander is to collect navigation measurements from the sensors when permitted by attitude orientation. This method allows the sensors to collect data through opportunity viewing without expending additional fuel for special maneuvers. Opportunity viewing can be described as collecting data when the vehicle's attitude orientation permits unobstructed viewing. The navigation sensors include gyros and accelerometers for inertial stability only, ground beacon ranging or Doppler sensors, and radar altimeters. It should be noted that all the sensors in this mission are generic representations of current hardware and additional research could improve each sensor's efficiency.

1.2.3.1 Gyros and Accelerometers

Inertial navigation uses gyros and accelerometers. This segment of navigation is vital during the deorbit burn since all other methods of navigation are inoperable during this time. Gyros are used to maintain knowledge of inertial and relative attitude and have errors due to misalignments and drift rates about all three axes [5]. Accelerometers are used to maintain knowledge of inertial position and velocity and have errors due to scale factor and bias.

1.2.3.2 Ground Beacon Ranging and Doppler Sensors

These sensors require that a previous mission place a beacon near the desired landing point. This beacon could be placed during the Mars Observer Mission or this option could be implemented after the first successful Mars Sample Return Mission. If the beacon is in place, it must have a transponder. This places a requirement on the lander and the beacon that they must both have transmitters and receivers. This 2-way ranging and/or Doppler Shift can be very accurate with the beacon location being the biggest error. To simplify the design, the beacon could have a transmitter only, enabling the lander to need only a receiver. The 1-way ranging measurement has an error an order of magnitude larger than 2-way ranging because of clock/timing uncertainties between the beacon and lander [2].

1.2.3.3 Radar Altimeters

Radar altimeters simply bounce a signal from the lander to the ground and back and measure range and Doppler shifts. The Viking lander had a 4-beam radar configuration to measure directional Doppler and a wide beam radar to measure range [5]. For terminal descent, the altimeter is critical in providing relevant surface information. The largest source of error is terrain height uncertainties.

1.2.4 Parachutes

Deceleration in a rarefied atmosphere such as Mars introduces the problem that speed of a vehicle can only be reduced to 200-250 m/sec or so before collision with the surface, because of the low density of the atmosphere near the surface. This does not allow enough time to release a standard canvas parachute. A parachute must then be designed so that it can be released at a much higher speed, approximately Mach 2, which is reached at an altitude of 6 km. This in turn creates other obstacles that have to be avoided [6]. For one, a high strength material which can withstand high loads is necessary in the design of the parachute. This is due to restrictions imposed on the design by the parachute's deployment. One solution to this problem is to reduce the loads on the parachute by releasing several different parachutes. A second method is by staging one

parachute. The second method is used in this mission due to the savings in material, thus reducing the total mass. The characteristics of parachutes at subsonic and supersonic speeds is shown in Figure 7.

Another problem involves the supersonic deployment of the parachutes. A vacuum can form behind the lander, introducing the possibility that a parachute might be sucked into it. Therefore, the deployment will be controlled by a forced charge. This system is initiated by using a shaped charge to cut the aft section of the parachute, on which the charge is mounted. This system is lighter, less complicated, and less expensive, compared to a fuel-consuming engine release system [6].

Another factor is that the supersonic parachute must be stable, must withstand high canopy pressure loading, ribbon flutter, and aerodynamic heating associated with both subsonic and supersonic flow. A conical ribbon parachute will be used due to its superior performance in both types of flow and at high dynamic pressures, associated with parachute deployment [6].

The conical ribbon parachute best satisfies characteristics for this mission. Figures 8 and 9 show the comparison between conical ribbon parachutes and hemisflow parachutes. It can be seen in these figures that the conical parachute has a higher drag coefficient at lower Mach numbers and provides a constant drag coefficient at high Mach numbers, while the hemisflo parachute has a decreasing drag coefficient with increasing Mach numbers. Also, a higher drag will be needed at low Mach numbers since the velocity is higher at lower altitudes on Mars, rather than what has been experimented with on Earth [6]. Figure 10 shows the configuration of the 21 ribbon, 20 degree conical ribbon parachute.

The parachute suspension lines will consist of 6000 lb, one-inch wide Kevlar webbing. The radials are continuations of the suspension lines with 2400 lb Kevlar tape backing, which provides stabilization [6].

1.2.5 Retrorockets

At an altitude of 6 km, where the aeroshell is jettisoned, the lander will be traveling at a speed of Mach 2. At this point, a command from an accelerometer signifies the

initiation of the parachute deployment sequence. The full deployment will occur when sonic velocity is reached. At an altitude of 1.5 km, the parachutes will be jettisoned by a forced release. An altimeter will initiate the command to ignite the liquid hydrazine retrorocket system. There are three retrorockets situated in such a manner that roll and pitch maneuvers can be conducted. The mass of each of these retrorockets is 150 kg, consuming 210 kg of liquid hydrazine fuel. These retrorockets will reduce the vehicle's speed to approximately 2 to 4 m/sec, which is acceptable for a safe landing [7].

2.0 THE LANDER BASE

2.1 Communications

The communications subsystem for the lander is an interface for both the orbiter and the return vehicle, transmitting and receiving various information about the mission. Also, the lander will transmit a homing beacon to all of the rovers on the surface. In normal operations, the communications subsystem will transmit and receive signals at various frequencies unique to the lander.

The communications within the lander will consist of two main subsystems: the communications subsystems, and the command and data handling subsystem. After collecting data from the entire lander, the command and data handling subsystem (C&DH) will decode, process, and distribute lander commands. It also gathers, formats, stores, and transmits telemetry data from spacecraft measurements. After formatting the data, the C&DH will send the telemetry data to the communication subsystem in real time, or store the data for transmission, depending on the data rates (see Figure 11).

If the data cannot be sent in real time, it will be stored in a flight recorder. For storage of the lander's data, the Lockheed 4200 series tape recorder will be used. This recorder has a total data storage of up to 80 million bits, with record data rates of 512 kbps. Power requirements for the recorder are: 2-4 W for record, 4 W for playback, and .2 W for standby. The total mass of the recorder is 2.95 kg.

Three data rates are required for the lander subsystem: one for commands, one for health and status reports, and one for mission objectives such as video imaging. Commands require data rates of 1000 bps, while health and status telemetry will transmit at 2500 bps. Video imaging will require the largest data rate at approximately 100 kbps.

The C&DH will consist of a central processing unit, remote units, and a computer. The central processing unit receives demodulated information and routes it to either the remotes or the computer. It also receives, formats, and routes telemetry to the transmitter part of the transponder. The remote units can receive and process commands and requests for data. The entire C&DH has a mass of 15 kg and a power requirement of 45 W.

After the C&DH formats the data, the information is sent to the communications subsystem. The specific function of the communications subsystem includes two-way communication with the return vehicle and the orbiter. The communications subsystem is one of the most important subsystems of the lander, since it directly interfaces with every system of the lander, with the exception of the propulsion system. The communication subsystem receives information and commands from Earth via the communication satellite or transfer vehicle, while simultaneously transmitting video imaging, periodic health and status, and general information such as location and tracking of sample projectiles.

Because of the importance of the communications subsystem, redundancy is designed into the system with the addition of a second transponder (see Figure 12). The purpose of the transponder is to transmit telemetry, and to receive and detect commands. Both transponders will transmit and receive signal paths in parallel, to assure accurate communications. The total mass of the communications subsystem is 13.3 kg, with each transponder weighing 4.45 kg. Power requirement for the receiver and transmitter is 4.3 watts and 20.0 watts respectively, thus resulting in a 24.3 watt power requirement for the communications subsystem [8].

The frequency range used in the two-way communication with the orbiter and the return vehicle is within the Ka-band, which includes frequencies in the 20-30 GHz range. The advantage of these high frequencies is that the size of the dish antennas is greatly reduced. For Ka-band frequencies, a 0.9 m dish will be required for transmitting and receiving of signals.

The one-way radio beacon is an additional communications subsystem used to provide the Aereons and land rovers with a navigational marker. This subsystem will consist of a 7 inch antenna and a transmitter with a mass of 3 kg. Total power requirement of this subsystem is 3 W.

In summary, the total communications subsystem will have a mass of approximately 35 kg, with a total power requirement of 75 watts. The subsystem will transmit at a telemetry rate of 15 kbps, storing the accumulated data for later transmission. In addition, the subsystem will require approximately 0.015 cubic meters, excluding the 0.9 m antenna dish.

2.2 Thermal Control

The thermal control system (TCS) must maintain the lander and its components within certain temperature limits. These limits are summarized in Table 1.

Table 1: Typical Spacecraft Temperature Limits

Spacecraft Electronics	0-40 °C
Batteries	5-20 °C
Structure	-45-60 °C

The TCS will sustain the lander in the space environment, where heat will be generated by the engines, and the various RTG's located on the rover, Aereons, and the lander itself. Furthermore, heat will be generated during the Martian descent from both the frictional effects of the atmosphere and the retrorockets. On the Martian surface, heat sources will include the RTG, communications equipment, batteries, and solar radiation. The contribution from solar radiation was determined to be minimal.

The main obstacle for the TCS, in both environments, is the lander's 290 W RTG. Generating at 7.25% efficiency, it will create 4000 W of thermal energy, with temperatures of 1275 K and 575 K at its hot and cold shoes, respectively [9]. Two thermal control devices, heat pipes and pumped refrigeration loops, were considered to cool the RTG in both the space and Martian environments.

2.2.1 Heat Pipes

A heat pipe is a self-contained device which uses a two-phase fluid flow to provide high thermal conductivities. A heat pipe (shown in Figure 11) consists of two sections: the evaporator and the condenser. At the evaporator section, heat is added which vaporizes the working fluid. The vapor then flows to the condenser, where the condensing gas releases heat. The liquid then returns to the evaporator portion and the cycle is repeated.

The heat pipe requires no outside pumping device. As the fluid is condensed a pressure drop occurs, and as it vaporizes, the fluid experiences a pressure rise. This resulting pressure gradient pumps the working fluid [9].

The axial heat flux of a typical 1.27 cm diameter heat pipe is 5080 W cm, which means the pipe can transfer 508 W over 10 cm. Another attractive feature of heat pipes is that by choosing a suitable working fluid, the heat pipe will be stable in a radioactive environment.. This is important since the RTG uses radioactive materials to generate power. Nevertheless, the heat pipe does have one limitation -- it must be aligned horizontally in a gravitational field. If not aligned properly, the pipe's performance will be severely hampered [8].

2.2.2 Mechanically Pumped Loop

The other thermal control device considered was a continuously circulating refrigeration loop. In this device, thermal energy would be transferred, using a pump, from the heat source to either the radiator or a heat sink. The working fluid in the loop can either be a liquid metal or a gas. The liquid metals have greater thermal conductivities, greater operating temperatures, and because of their higher molecular weight, less pumping requirements than a gas working fluid. However, in addition to corrosion and oxidation problems, liquid metals have poor characteristics in a radioactive environment. In comparison, a Helium-Xenon gas mixture is very stable in radiation, because both gases are inert. Furthermore, a Helium-Xenon mixture combines the high thermal conductivity of a low molecular weight gas (He), with the pumping efficiency obtained with a higher molecular weight gas (Xe).

2.2.3 Design

The thermal control during all portions of the mission will depend mainly on dissipating the heat from the RTG. This 290 W RTG, operating at about 7.25% efficiency, will generate approximately 4000 W of heat [10]. During space flight and surface operations, eight to ten heat pipes will transfer this heat to a radiator assembly.

The heat pipes were chosen as the main thermal control device because they require no power input and are more reliable than a pump. Since the heat pipe has no moving mechanical parts, it is less likely to break down. Conversely, the refrigeration cycle uses a pump, which would be difficult to run continuously over several years.

Since the heat pipes will not function during launch, ascent, and descent operations due to the orientation of the lander, a refrigeration loop will be necessary. Because the radiator will be covered by the aeroshell on the launch pad, a pump will be connected to an external sink for heat dissipation. During ascent and descent, in addition to the radiator being covered, the heat pipes will not be horizontal. Therefore, the pump will be employed to transfer the RTG's heat to a heat sink. This heat sink will consist of a solid-liquid phase change material (PCM). During ascent and descent, heat will be transferred to the sink melting the PCM. Once in the radiator is deployed, the PCM is allowed to cool and it returns to solid form. The refrigeration loop can also be used as a backup to the heat pipes in case of unexpected problems [8].

Further thermal control will be provided by small electrical heaters and insulation layers. The electrical heaters were compared with radioisotope heater units (RHU's), each of which provides one watt from the natural decay of 2.7 g of PuO_2. These RHU's, which were used on Galileo, are lightweight, reduce electrical power requirements, and decrease electromagnetic interference; however, the mass savings would be offset by extra shielding requirements, and the lander's 290 W RTG would have plenty of excess capability. Therefore, electrical heaters, coupled to temperature sensors, will warm the isolated portions of the craft [11].

Insulation layers will also be needed around the RTG and along the external walls. Insulation around the RTG will contain its heat, protecting surrounding instruments and minimizing heat transfer to the payload. Also, insulation around the external wall will protect the lander from the sometimes cold Martian environment.

2.3 Articulated Arm Subsystem

The robotic arm serves two main purposes: to collect the contingency and core samples from the surface and to transport the samples from the Martian land rover to the ascent vehicle. Figure 14 shows the arm and its degrees of freedom. The mass of the arm is estimated to be 100 kilograms, and approximately 200 watts is needed for power. The arm segments have a circular cross section with a vertical support, both having a thickness of 2 millimeters. Motors in the shoulder, elbow and wrist joints are supplied with power

from the power subsystem, by wires which run through the arm.

The arm consists of two main segments, each 3 m in length and 20 cm in diameter. A third segment, one meter long, can be extended from the outer arm section to give the arm a total length of 7 meters. The arm has six degrees of freedom: two from the wrist and the shoulder, one in the elbow, and one for the extension of the wrist from the outer arm section. The rest position of the arm corresponds to the angles in Figure 14, all having a value of zero. There are three attachments for the wrist: a core drill, a scooper, and a claw. The attachments are stored on the lander where the arm is folded up as shown in Figure 15. During the mission, the arm will be able to use whichever attachment is needed, without the other two attachments interfering. A camera located in the wrist provides vision for an accurate location of the land rover when it returns with the Martian samples. Once the land rover returns, the camera takes several pictures of the rover from different locations. The images are sent back to Earth for computer analysis. Then by triangulation, the exact location of the sample canister, with respect to the arm, is known and the angles defined in Figure 14 will be known .

Once the lander has settled on the Martian surface, the arm will begin to collect the contingency samples. Supports that keep the arm in place for the journey to Mars are removed and the arm unfolds from the lander. The arm then connects the core drill to the wrist. The arm moves so that the angles in Figure 14 result in alpha 1 = 121.2°, alpha 2 = 0°, beta 1 = 90°. Now the third segment of the arm can be extended so that the core drill runs directly into the surface. Once the drilling is complete, the arm transports the sample to a contingency container, located near the attachment compartment.

The arm then goes to the attachment compartment, returns the core drill, and connects the scooper to the wrist. The scoop will have a capacity of 600 cm^3. The arm will shovel up the regolith and place it, with the core sample, into the contingency container. Now the arm can return the scooper to the attachment compartment and return to the arm's storage position, waiting the land rover return. If for some reason the land rover cannot return with its samples, the arm will take the container with the contingency samples and place it in the ascent vehicle.

When the land rover returns, it must approach within 1.5 meters of the lander for the arm to reach the sample container. The arm will then attach the claw to the wrist and extend it to the rover. With the aid of the camera within its wrist, the arm can locate the canisters by the triangulation method previously described. The canisters are then removed and loaded onto the MAV. Once all 55 containers have been transported to the MAV, the robotic arm's duties are complete.

2.4 Power Subsystem

The electrical power system consists of the power source, the power distribution subsystem, and the power regulation and control subsystem. The power source generates power by converting heat to electrical energy. The power distribution subsystem consists of the cabling, fault protection, and switching gear to turn power on and off, depending on the lander's power load. The power regulation subsystem converts the bus voltage into various AC or DC voltages for distribution to the electrical instruments [8].

The lander's power source will be a Radioisotope Thermoelectric Generator (RTG). An RTG is a device that converts heat from naturally decaying radioactive isotopes directly into electricity. The lander will use a General Purpose Heat Source RTG (GPHS-RTG), containing 10.7 kg of PuO_2, to generate 290 W (BOM) and 250 W (EOM). This RTG, shown in Figure 16, was used on the Galileo Mission and incorporates a modular design, which allows the power output to be reduced at times of low demand.

This modular design uses eighteen modules, each of which is autonomous and equipped with its own safety provisions. Each module consists of a graphite block that encases two graphite cylinders. Each cylinder contains two pellets of PuO2 encased in iridium. This construction provides, in addition to support, protection during ground operations, re-entry impact, and post-impact environmental contamination [10].

The module stack is constrained by locking members and packaged in an axial compression system to minimize any individual lateral motion of the modules. The thermoelectric converter also provides axial support to the module stack. It consists of 576 SiGe unicouples, each with hot and cold side temperatures of 1275 K and 575 K, respectively [10].

The RTG also has a gas management device and a pressure release valve. The management assembly maintains the internal environment of the RTG, while the pressure relief valve serves as a vent for the inert gas contained within the RTG. This gas allows partial power operations on the launch pad and protects various refractory materials during storage and ground operations.

The RTG was chosen as the power source because of its reliability and experience in space applications. It has been previously proven in more than twenty spacecraft missions, which include Pioneer, Viking, Voyager, and all but the first manned Apollo landings. A design having a smaller version of the GPHS-RTG, coupled with several batteries, was also considered because of the RTG's excess power generation. The robotic arm needs 250 watts for a relatively short period of time, and the next highest requirement was 75 W for the communications system. Therefore the RTG will be generating a substantial amount of excess power. The proposal was to use a 75 W RTG to power the communications and other subsystems, and supply enough batteries to power the robotic arm, when it was needed. This would ease the thermal control system and radiation shielding requirement.

Both Nickel-Hydrogen (NiH_2) and Lithium Thionyl Chloride ($Li/SOCl_2$) batteries were considered. Although the NiH_2 batteries had suitable charge and discharge characteristics, their relatively moderate energy density (25-40 Whr/kg) would have added considerable mass [12]. The $Li/SOCl_2$ cells had a high energy density(130-350 Whr/kg), but a short lifetime and unsuitable charge and discharge characteristics [13].

The power distribution subsystem consists of cabling, fault protection, and a switching gear. It should be designed with minimum power loss, survivability, cost, reliability, and power quality taken into account. These are each further dependent on the requirements of other subsystems, which are as yet unknown.

The power control and regulation subsystem converts the bus voltage into various AC or DC voltages for distribution to electrical components. Typical spacecraft subsystems may require low to high DC or single or triple phase AC, all of which need to be converted from the RTG's 28 V DC bus. By utilizing DC voltage in as many instruments as possible, the number of converters can be reduced, keeping mass of the power system at a minimum.

The power control and regulation subsystem is, like the distribution system, dependent on demands of thermal control, entry-attitude control, communication, and the other subsystems. These requirements will need expert, detailed research to determine optimum operating conditions.

2.5 Lander Design

The design of the lander is a product of constraints placed on it by the subsystems housed within it and by the other vehicles it transports. These are the rovers, the Mars Ascent Vehicle (MAV), communications, thermal control, the articulated arm, and power subsystems. Constraints were also placed on the design by Earth launch vehicle ferrying dimensions and Martian atmospheric descent requirements.

Within the lander, storage space must be allocated for the transportation and deployment of two Aereons and one land rover. The two Aereons must each be stored flat and in single file, with each requiring storage dimensions of 1.7 x 1.12 x 3.2 m. The lander must also house compressed hydrogen gas in a spherical pressure vessel, 1m in diameter, with a hose connected to each Aereon. The hoses must each be 27.5 m in length, due to deployment restrictions (see the report on Aereon design). The land rover must also be stored flat, requiring a 2.1 x 1.6 x 4.0 m storage space. The lander must have a ramp that has an inclination of no more than 30 degrees from horizontal, due to deployment requirements. This is satisfied by a ramp formed by a side panel of the lander that is hinged at the bottom and opens by rotating outward and down (see Figure 17).

The lander must be designed with the capability of launching the Mars Ascent Vehicle (MAV), which it carries. This is satisfied by allowing space for a cylinder 2 m in diameter and 2 m in length to be mounted on top of the lander. To aid in the sample recovery, the top 0.5 m of the MAV cylinder will be opened by the robotic arm, for the on-loading of sample canisters. After a successful sample retrieval, the MAV will launch from on top the lander, virtually destroying the existing lander base.

To dimension the lander accurately, launch and transfer vehicle restrictions must be considered. These restrict the descent aeroshell to 5 m in diameter, thus constraining the lander to fit within a cylinder 5 m in diameter (see Figure 18). The positioning of the

thermal and power subsystems must also be considered. Each must be placed according to their own specification, contributing their own loading upon the lander.

Taking all constraints into account, a lander design can be formulated (see Figure 18). Subsystem and total vehicle mass are shown in Table 2.

The material from which the lander's structure is made will be primarily Aluminum, due to the low drag and heating characteristics it will experience during the descent.

Table 2: Mass Breakdown

Component	Mass (kg)
Communications	35
Thermal	55
Power	45
Retrorockets	450
Robotic Arm	100
Rovers	2000
MAV	1087
Aeroshell	800
Structural Mass*	1000
Total	**5572**

* estimated from total lander dry mass [8]

2.6 Cost Analysis

Using the cost model developed for advanced space systems, by Kelley Cyr at Johnson Space Center, cost estimates for the lander, the MAV, and the lander's aeroshell can be made, and are presented in Table 3.

Table 3: Cost Estimate

Component	Cost (million $)
Lander	1943.18
MAV	611.19
Aeroshell	381.26
Total	**2935.6**

3.0 MARTIAN ASCENT

3.1 Mars Ascent Vehicle

The Mars Ascent Vehicle (MAV) is designed to transport the sample set from the surface of Mars to the orbiting transfer vehicle. The design of the MAV is shown in Figure 19. It is 2 meters in height and 1.46 meters in diameter. There are two rocket stages. The first is a solid rocket stage used to get the MAV to an altitude of 500 km, and the second stage is a small liquid propellant system to insert the rocket into its final desired orbit. The solid rocket casing is made of titanium alloy. This material was chosen for its high stress level and its relatively low weight [14]. A foam insulation will serve two purposes, it will help keep both the solid and liquid propellants warm on the cold surface of Mars, and will also protect the outer casing from the high temperature of the solid rocket engine.

The MAV will initially be propelled by PU/AP/AL, a solid grain propellant. The advantage of a solid propellant system over a liquid system is that it is much simpler and more conducive to the atmosphere of Mars. A large chemical engine would require a cooling system, two or more bulky fuel tanks, and numerous pipes, pumps, and valves. Keeping the liquid fuels stable at their proper storage temperatures on Mars would also require an additional heating/cooling system. The solid propellant system is lighter and much less complex than the chemical system in that there are no pumps or valves needed.

The type of propellant chosen, PU/AP/AL, was picked over other solid fuels for its high Isp, low density, and slow burning rate (see Table 4).

Loading the samples onto the MAV was also a design consideration. Because of the canister size and configuration, the nose cone of the rocket was designed to be flipped over by the robotic arm, revealing the sample collection compartment. The MAV, with the nose cone flipped over, will receive the samples from the rovers via the robotic arm of the lander. The sample canisters will be loaded in a pattern resembling a honeycomb. There will be nineteen clusters of seven hexagon canisters. The land rover can only hold a few canisters at a time, so the MAV will store empty canisters and trade them for full ones from the rover.

Table 4: Characteristics of PU/AP/AL Propellant *

Fuel	Aluminum Powder (AL)
Oxidizer	Ammonium Perchlorate (AP)
Binder	Polyurethane Polyether (PU)
Isp Range	260 - 265 seconds
Flame Temperature	2982 - 3315 °C (5400-6000 °F)
Density	0.0174 kg/cm^3 (0.064 lb/in^3)
Burning Rate	0.685 cm/sec (0.27 in/sec)

*Taken from [14]

When the MAV is full of samples, the robotic arm of the lander will reattach the nose cone of the rocket by flipping it back over, and the liftoff process will begin. An electronic igniter will light the solid grain and the rocket will begin its two-stage burn to rendezvous with the orbiting vehicle. The first stage is a near-vertical climb with a gravity turn, reaching a flight path angle of 45° at burnout. This occurs 73 seconds into the flight, at an altitude of 52.1 km. At this point, explosive bolts will release the lower portion of the rocket that includes the spent solid propellant system. The rocket will then be in an elliptical orbit with apogee at the final, desired altitude of 500 km [15]. At this altitude, the MAV will perform another burn, with its small Hydrazine/H_2O_2 liquid chemical propellant system, to increase its speed and establish it in its final orbit (see the appendix for calculations involving the MAV). At this time, a small S-band homing device will lead the transfer vehicle to it.

A liquid chemical propellant was needed for the second stage, because the thrust must be throttled in flight. Many short bursts of thrust will effectively maneuver the MAV into the final orbit. The characteristics of Hydrazine/H_2O_2 are shown in Table 5. The Hydrazine fuel and H_2O_2 oxidizer were chosen over fuels and oxidizer combinations mainly for their good storability characteristics. They can be stored in tanks over long periods and at many temperatures, without decomposition or change of state [14]. Its capability of withstanding a wide variety of temperatures requires only a small amount of insulation to keep the chemicals warm on the surface of Mars.

Table 5: Characteristics of Hydrazine/H_2O_2 (90%) *

Oxidizer	H_2O_2
Fuel	Hydrazine
Oxidizer-Fuel Mix Ratio (by weight)	1.5
Flame Temperature	2298.89°C (4170°F)
Ratio of Specific Heats	1.25
Bulk Density (80°F)	1.2 gm/cm^3 (0.043 lbm/in^3)
Specific Impulse	245 seconds

*Taken from [14]

CONCLUSION

The goal of this report was to provide a broad perspective of the lander base and the subsystems housed within it. Although, attention was made to make all presented information as detailed as possible, further advanced design work is needed in numerous areas. For one, the knowledge of an exact Mars entry window would aid in attaining an accurate velocity profile for entry. Also, the biconic aeroshell, used in this mission, has never been experimentally tested, but has been analytically shown feasible. Another area, needing work, is the lander design. Advanced structures work will be needed for the precise placement of the subsystems, and there mounting harnesses, to obtain an optimum center of mass location.

Another advantage of the mission is its lower cost repeatability. Due to the rover components remaining on the surface, a return lander unit would not require a payload bay for the rovers.

After a total assessment of this mission segment profile, we believe that a high level of confidence can be maintained, about the Lander Base and MAV. Though, more work can be done, a very good start has already been accomplished.

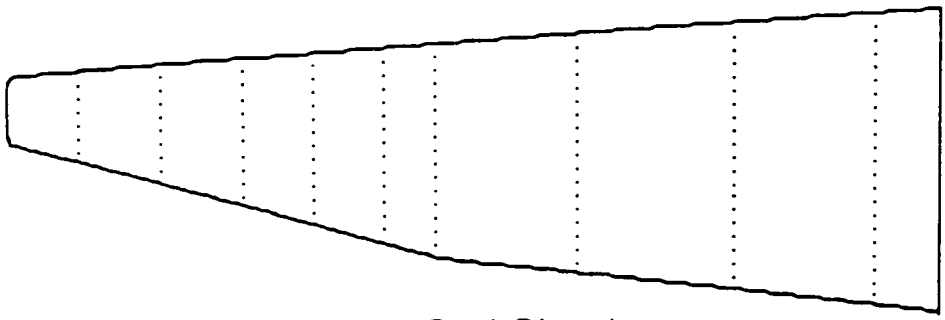

Bent Biconic
alpha = 16°, L/D = 1.5
"Mars Rover Sample Return (MRSR) Program-Aerocapture, Entry, and Landing (AEL) Conceptual Study", Martin Marietta, page 4-10

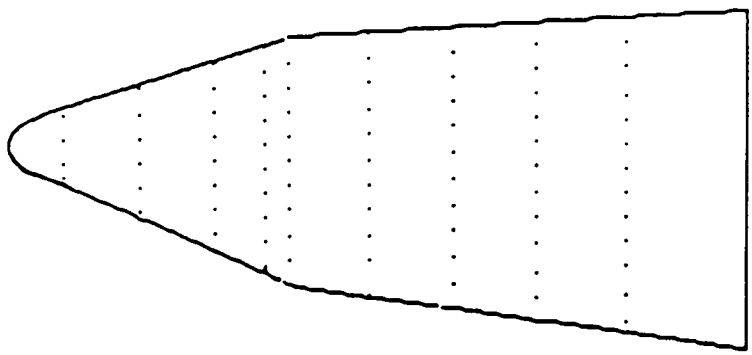

Biconic
alpha = 40°, L/D =0.6
"Mars Rover Sample Return (MRSR) Program-Aerocapture, Entry, and Landing (AEL) Conceptual Study", Martin Marietta, page 4-10

Blunt Body
alpha = -21°, L/D =0.3
alpha = -34°, L/D =0.5

"Aerodynamics Requirements of a Manned Mars Aerobraking Transfer Vehicle", NASA Langley Research Center, page 5

Figure 1: Aeroshell Configurations

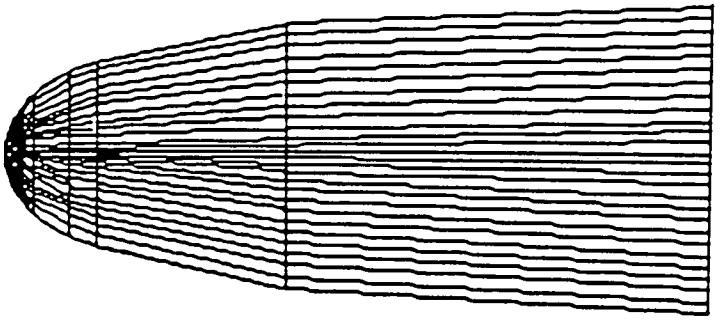

N_r = 1.159m
N_a = 15.7°
alpha = 40°
L = 11.91m
L/D = 0.6

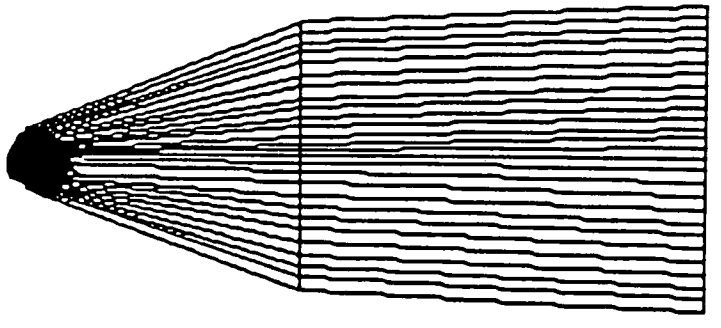

N_r = 0.305m
N_a = 23.55°
alpha = 40°
L = 11.91m
L/D =0.6

Figure 2: Biconic Configurations
[Martin Marietta, 1988]

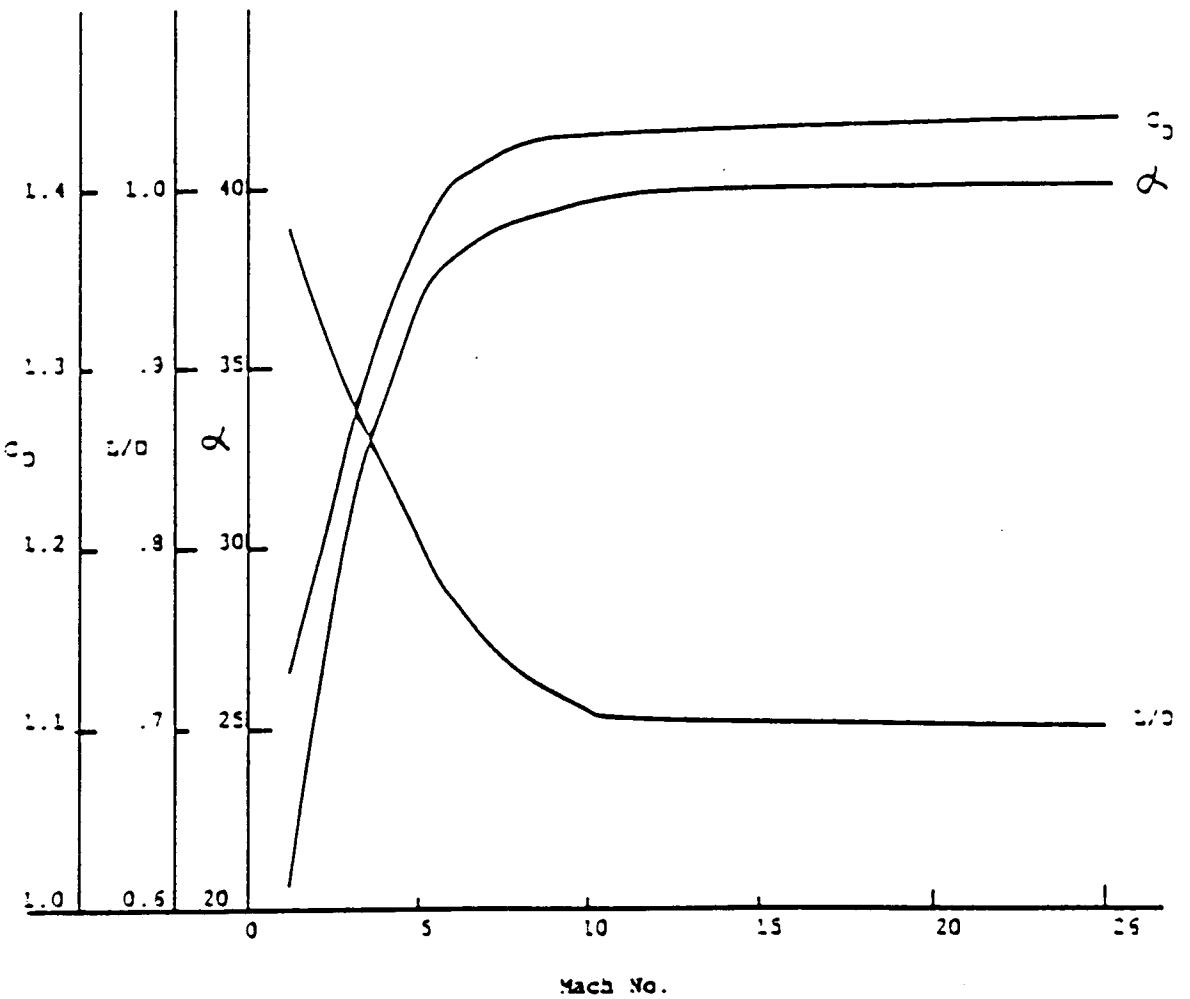

Figure 3: Biconic Characteristics ($X_{cg}/1 = 0.565$)

[Martin Marietta, 1988]

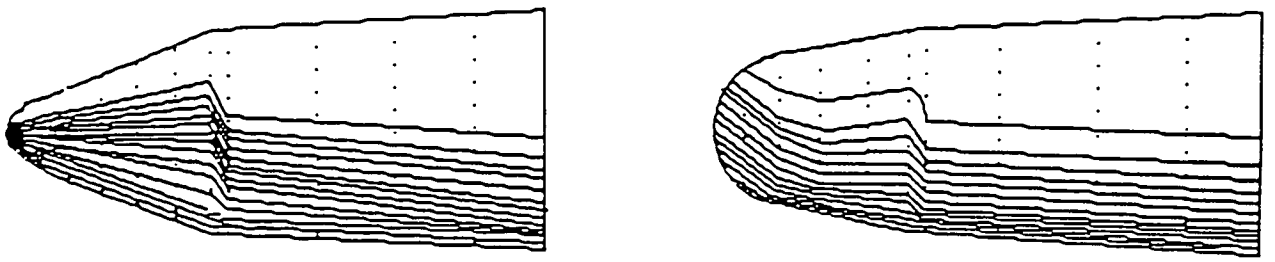

Figure 4: Pressure Distributions for Two Biconic Configurations
[Martin Marietta, 1988]

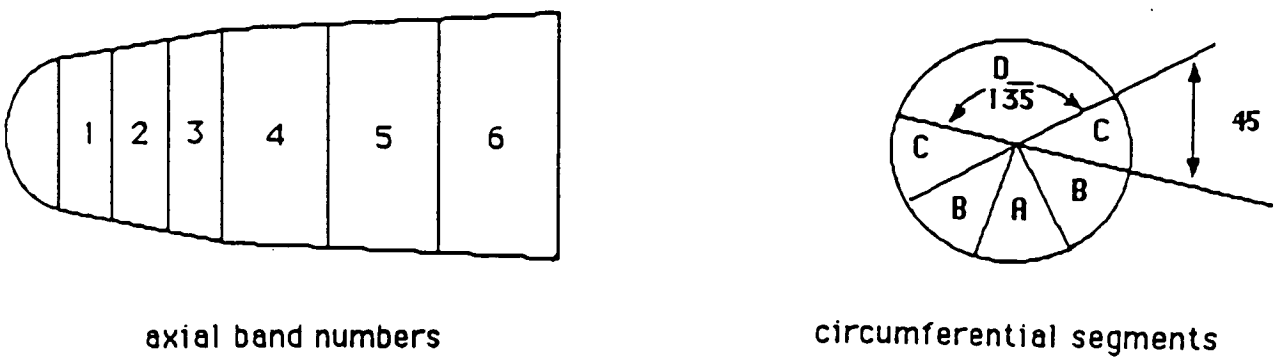

Figure 5: Thermal Protection System Panel Locations
[Martin Marietta, 1988]

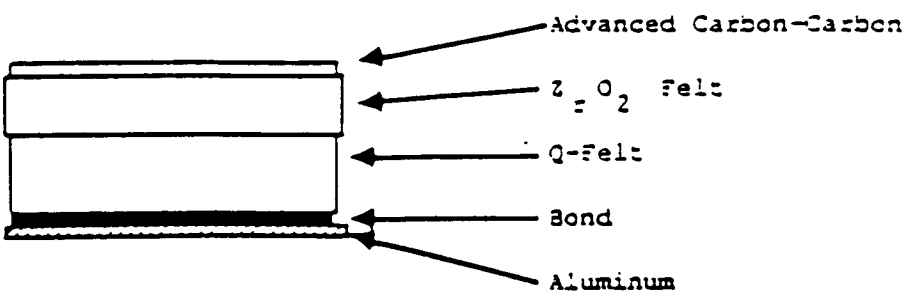

Figure 6: Thermal Protection Tile Concept
[Martin Marietta, 1988]

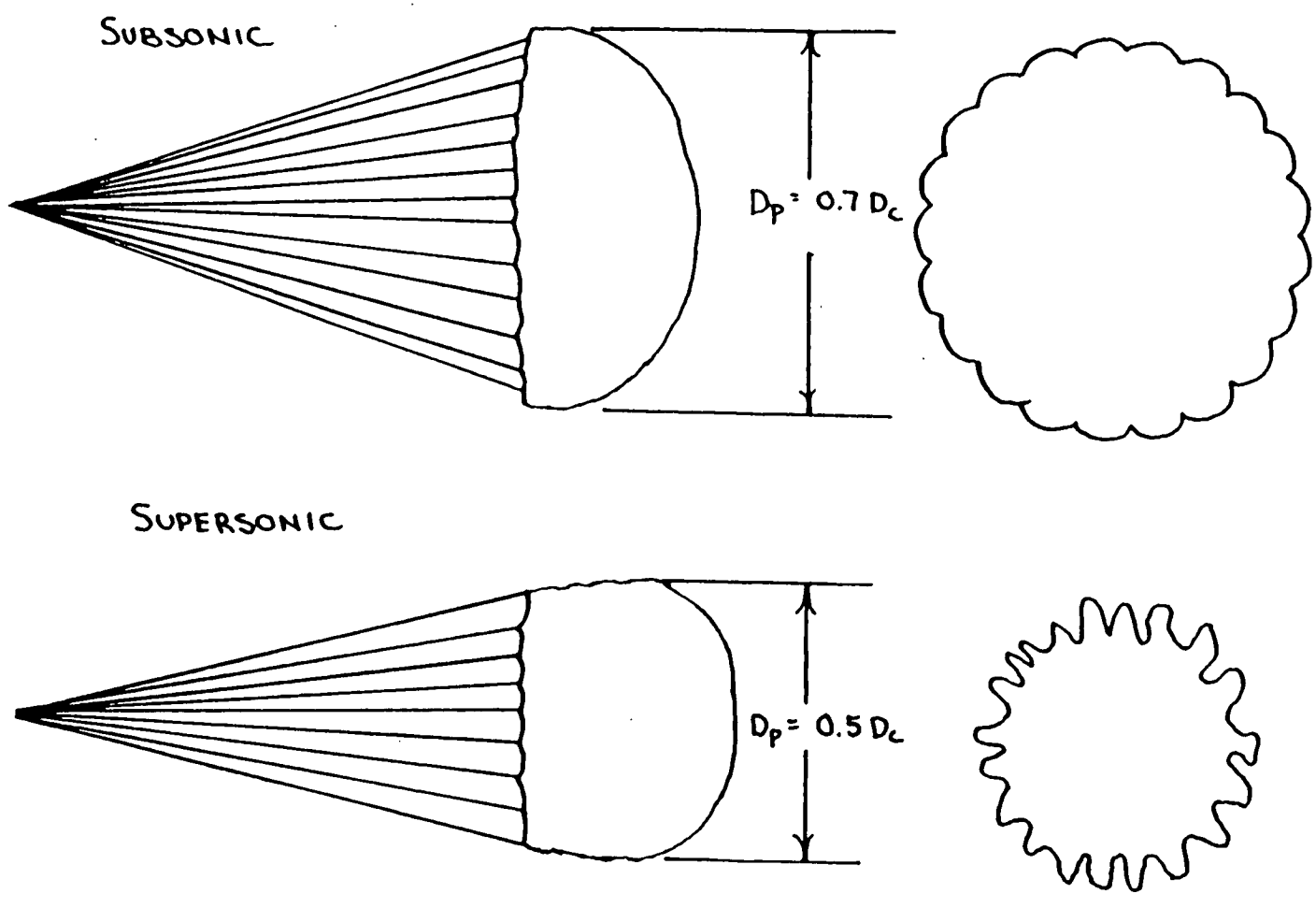

Figure 7: Shape of Conical Ribbon Parachutes at Subsonic and Supersonic Speeds
[Peterson, 1987]

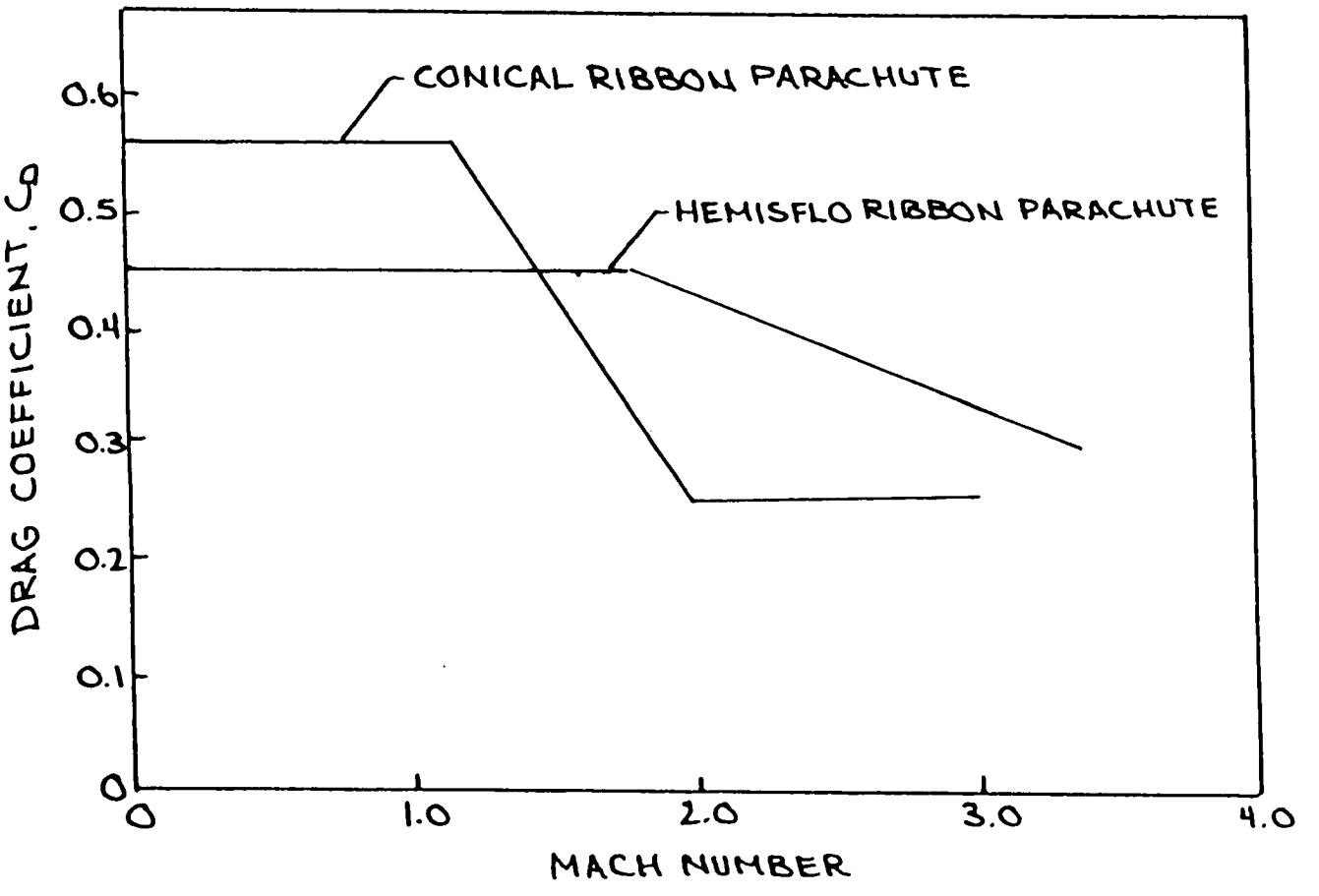

Figure 8: Comparison of Drag Coefficient vs. Mach Number for Conical Ribbon and Hemisflo Parachutes
[Peterson, 1987]

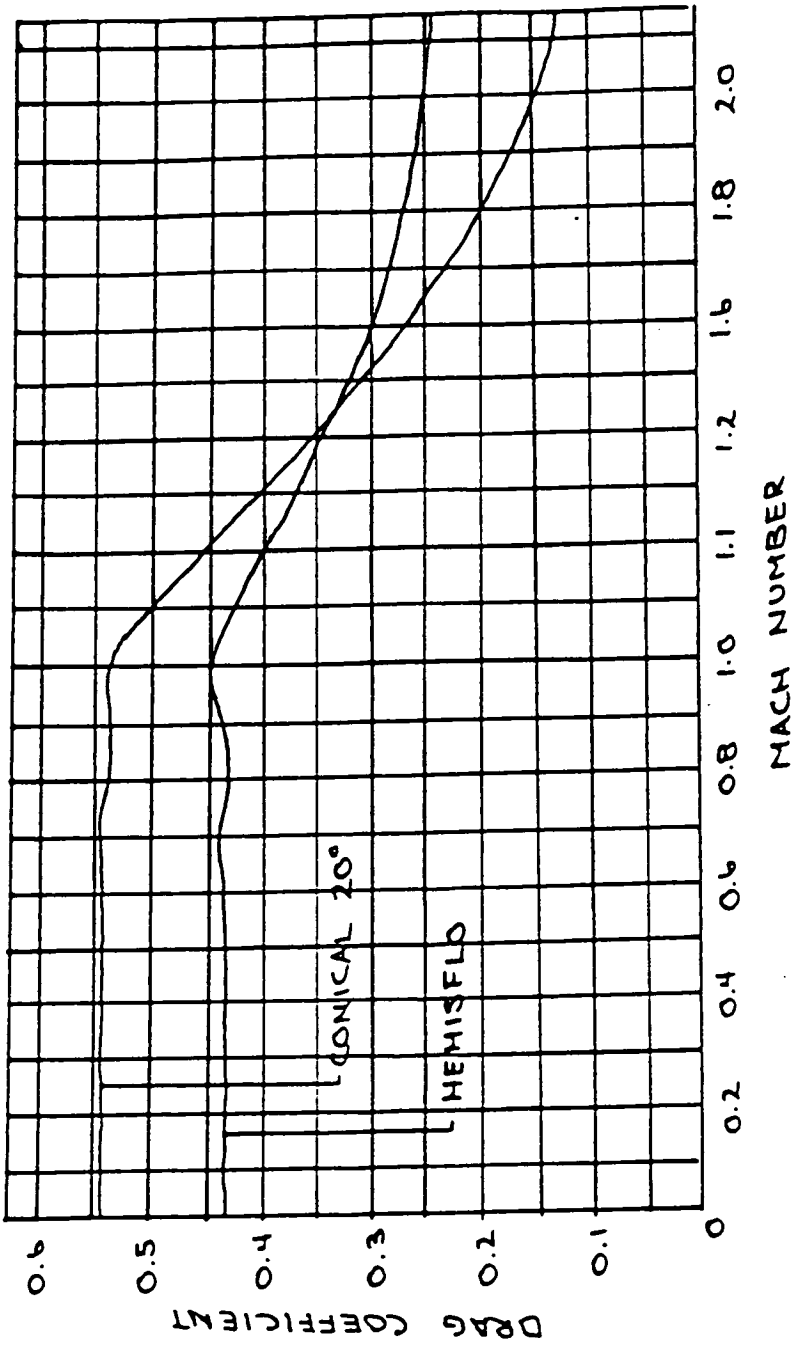

Figure 9: Drag Coefficients for Ribbon Parachute Configurations
[Peterson, 1987]

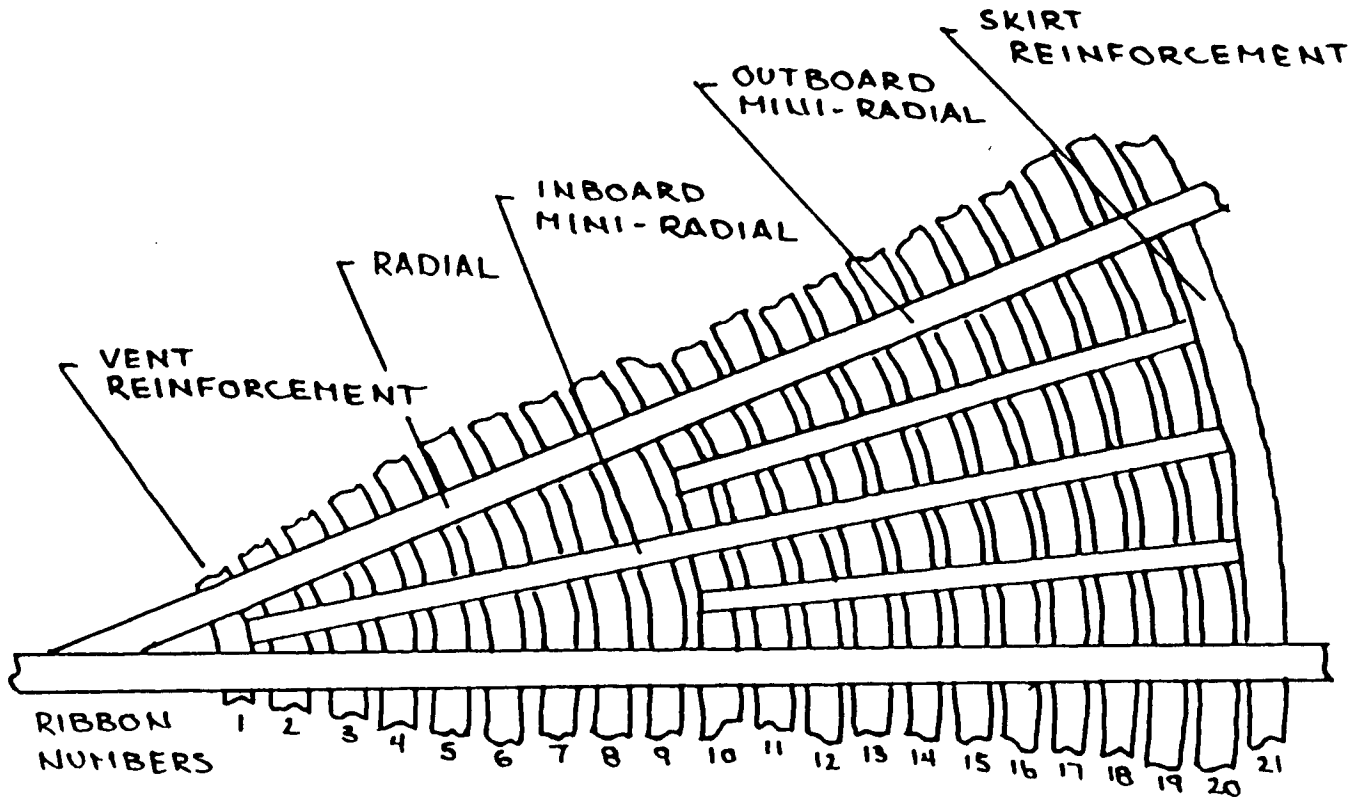

Figure 10: Twenty-one Ribbon, 20° Conical Parachute Designed for Mach 2 Deployment
[Peterson, 1987]

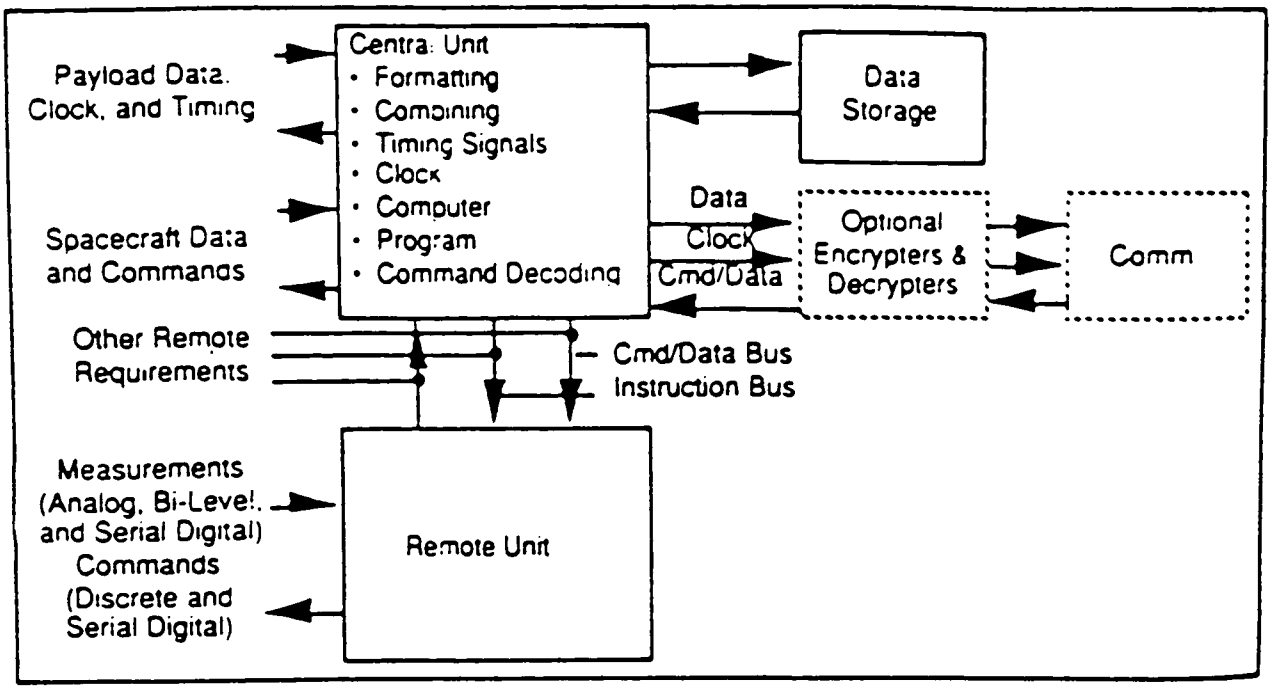

Figure 11: Block Diagram for a Command and Data Handling Subsystem

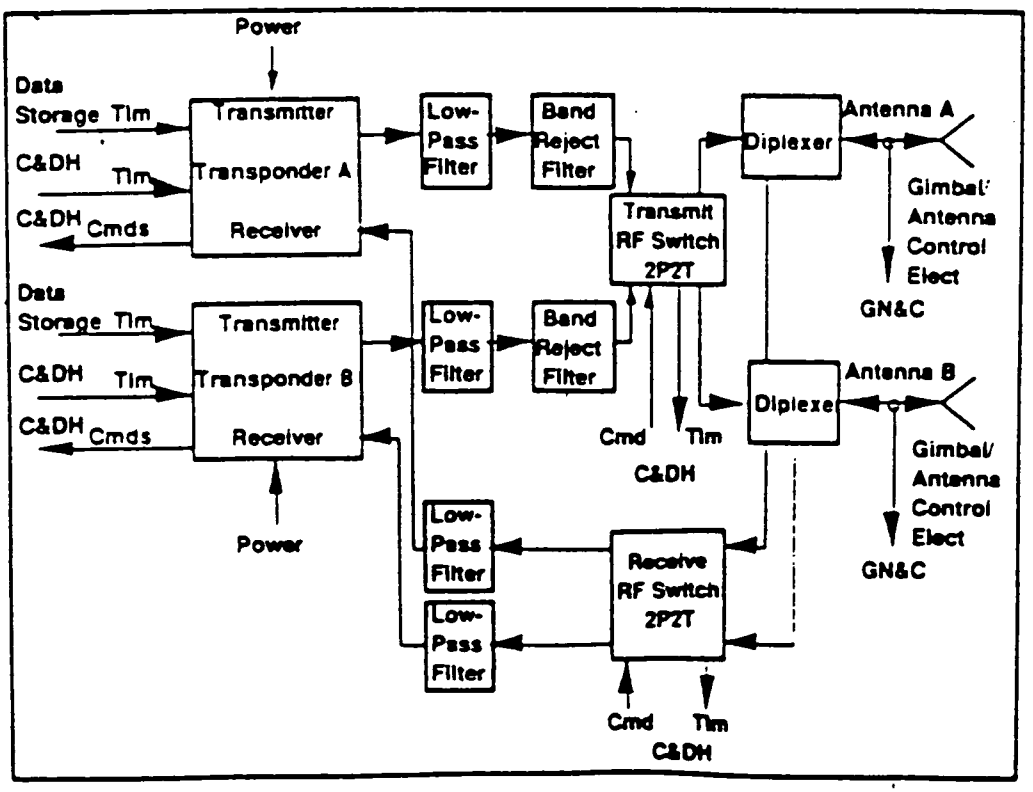

Figure 12: Block Diagram of a Generic Communications Subsystem

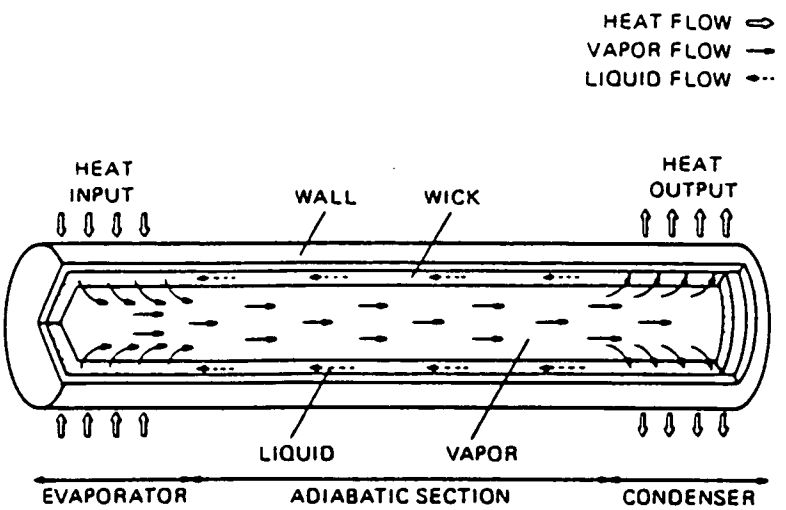

Figure 13: Heat Pipe Operating Principle
[Los Alamos National Laboratory]

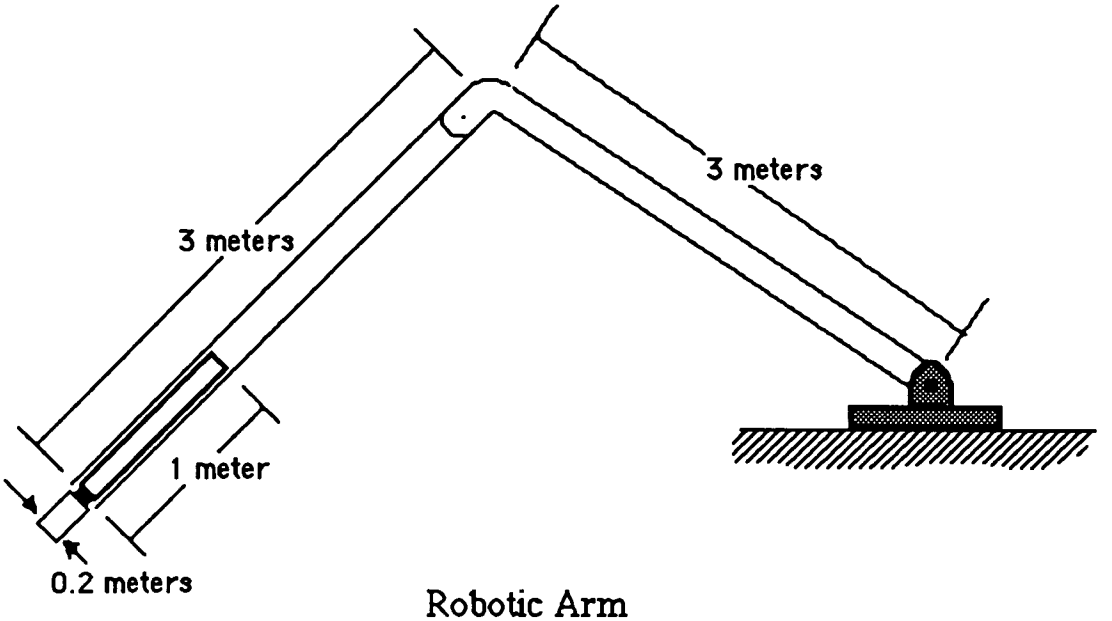

Robotic Arm

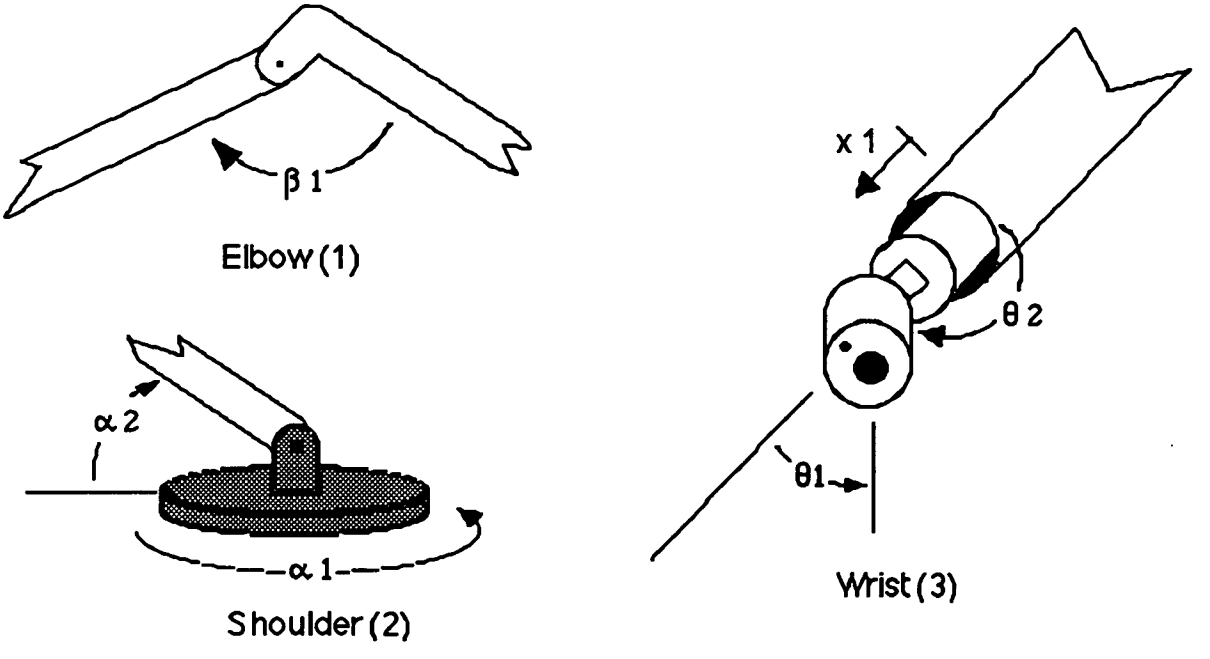

Degrees of Freedom

Figure 14: Robotic Arm and Degrees of Freedom

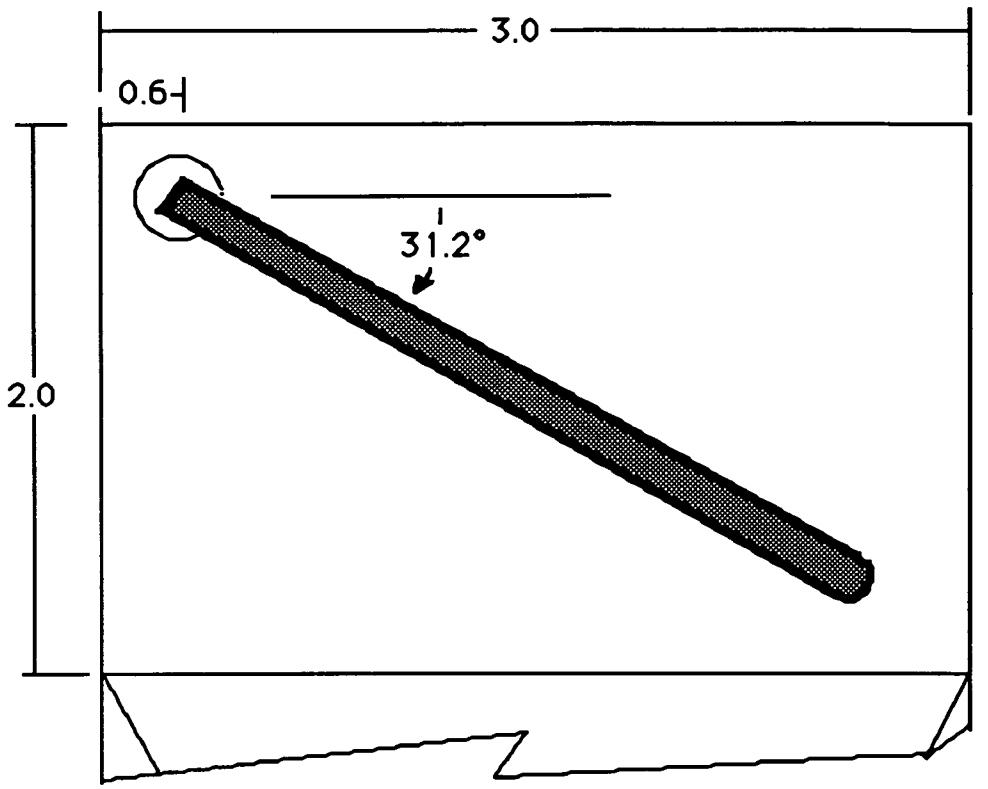

Top View

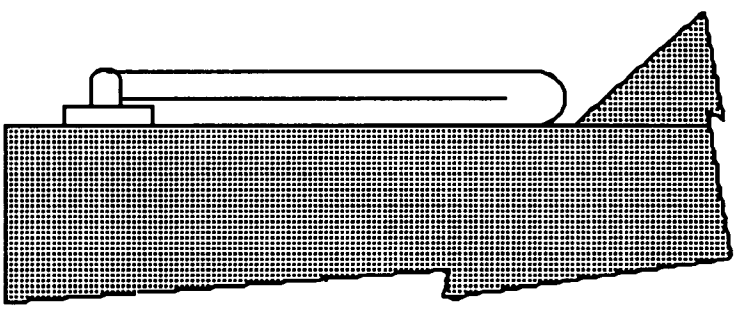

Side View

Figure 15: Rest Position of Robotic Arm
(All units in meters)

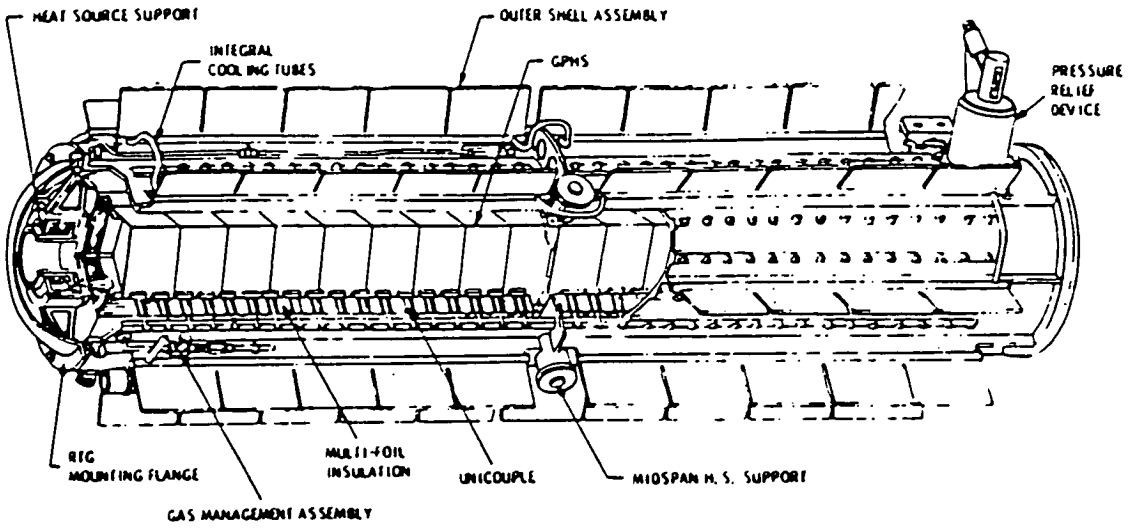

Figure 16: General Purpose Heat Source RTG
[U.S. Department of Energy and General Electric Co.]

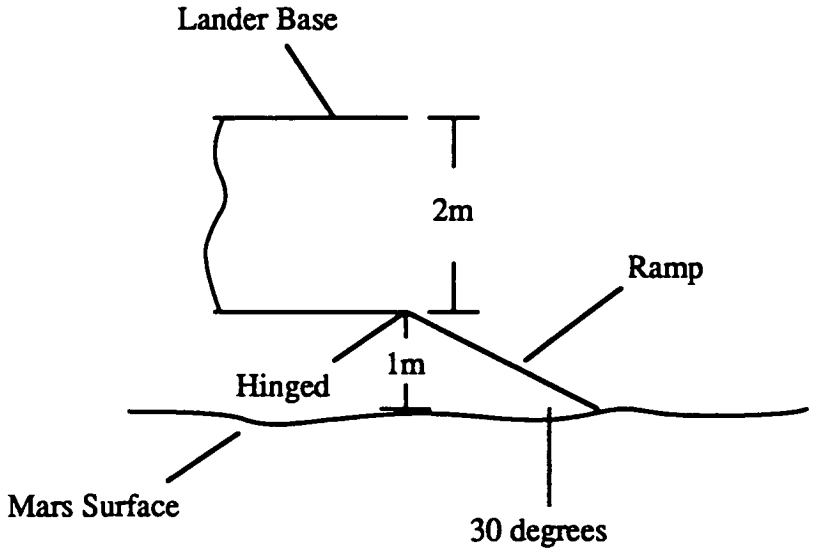

Figure : 17 Ramp Design

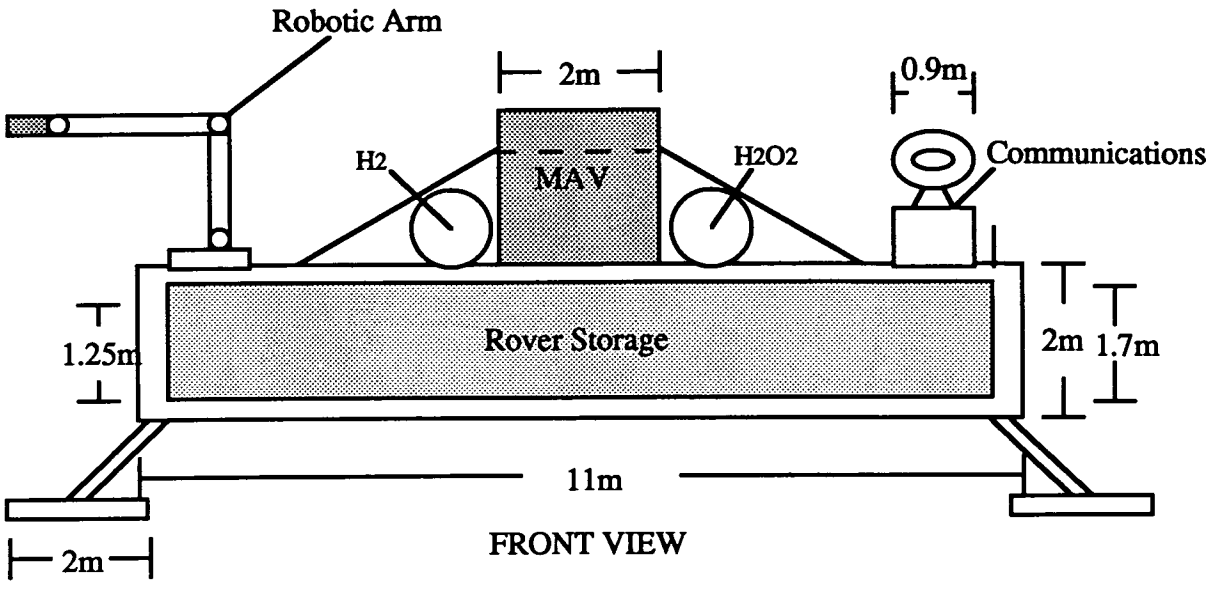

FRONT VIEW

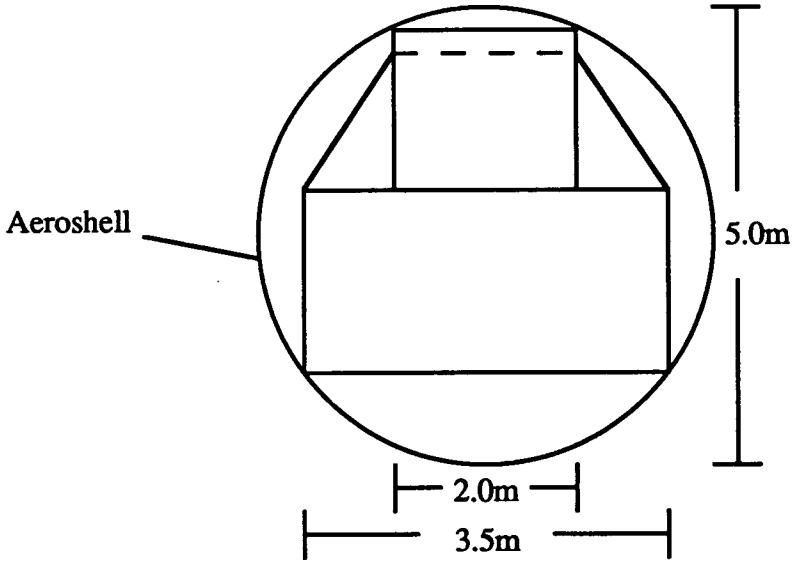

SIDE VIEW

Figure: 18 Lander Design (Front and Side)

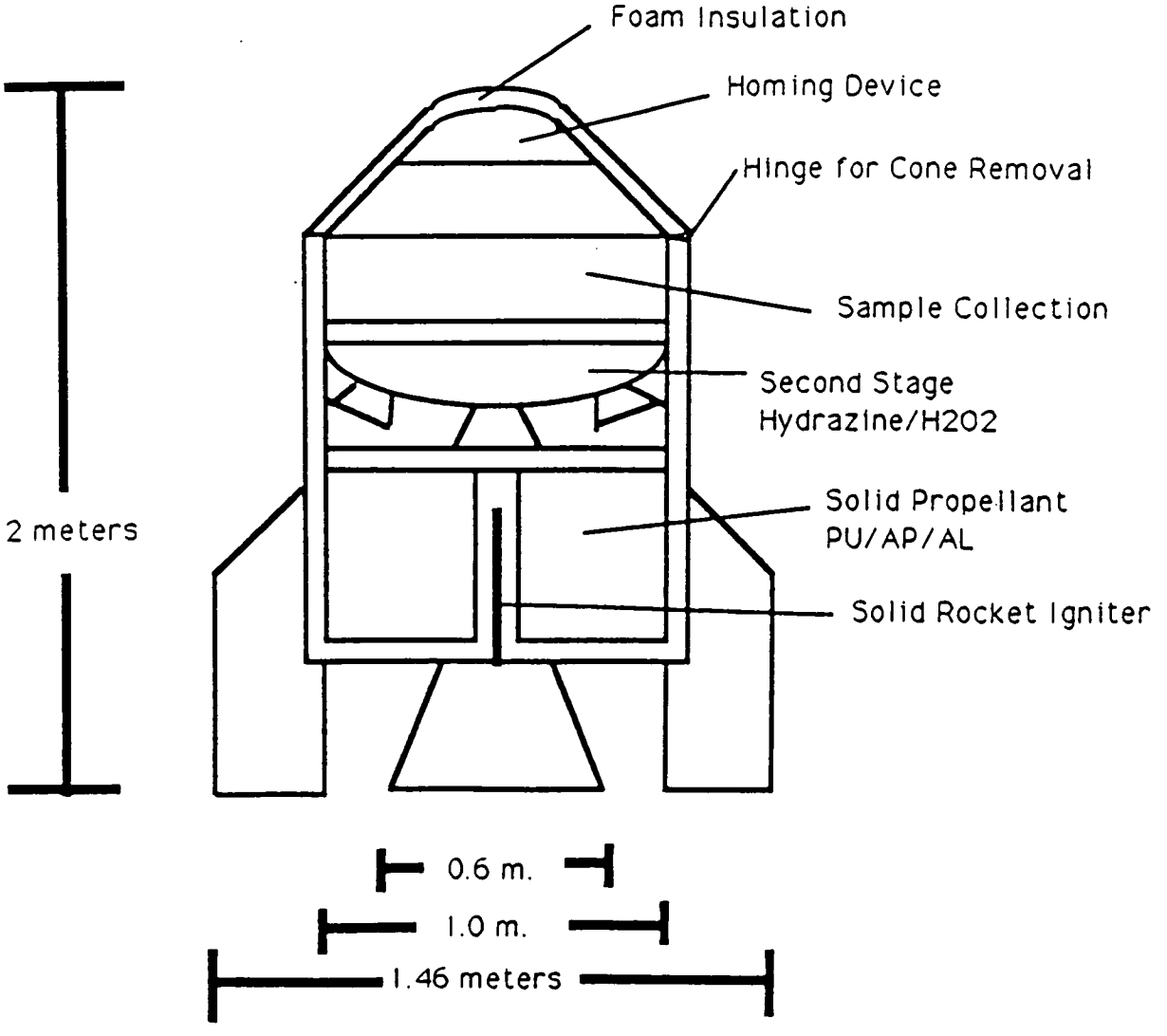

Figure 19: Mars Ascent Vehicle

REFERENCES

[1] Gamber, R.T., and Rogers, J.A. "Aerocapture, Entry, and Landing Systems for the Mars Rover Sample Return Mission." AIAA 27th Aerospace Sciences Meeting, V.9, AIAA 89-0422. Martin Marietta Astronautics Group.

[2] Freeman, D.C., Powell R.W., and Braun, R.D. "Manned Mars Aerobrake Vehicle Design Issues." IAF 90-197. NASA Langley Research Center.

[3] Braun R.D., and Powell R.W. "Aerodynamics Requirements of a Manned Mars Aerobraking Transfer Vehicle." NASA Langley Research Center.

[4] NASA Technical Memorandum 100470, "Environment of Mars." October 1988. Figure2-2 and Figure 2-3.

[5] "Mars Rover Sample Return (MRSR) Program-Aerocapture, Entry, and Landing (AEL) Conceptual Study -- Final Report." September 1988. Martin Marietta Astronautics Group.

[6] Peterson, Carl W. Aerodynamics of Supersonic Parachutes. Sandia National Laboratories, 1987.

[7] Popov. Descent Vehichles. NASA, June 1985.

[8] Wertz, James R., and Wiley, Larson R. Space Mission Analysis and Design. Kluwer Academic Publisher, 1991.

[9] Agrawal, Brij N. Design of Geo-Synchronous Spacecraft. Prentice-Hall, 1986.

[10] Angelo, Joseph A., Jr. and Buden, David. Space Nuclear Power. Orbit Book Company. 1985.

[11] Draft Environmental Impact Statement of Galileo Mission (Tier 2) Office of Space Science and Applications, Solar System Exploration Division. Washington, DC. December 1988. N9022148.

[12] Bush, Donald. Evaluation of Terrestrial Nickel-Hydrogen Cells and Batteries. DE88-01470 Sandia National Labs. Albequerque. May, 1988.

[13] Zolla, A. E. and Tura, D. D. 250 AH/90 A Active Lithium-Thionyl Chloride Cell for Centaur-G Applications. Atlus Corporation, San Jose,CA. 1989 Goddard Space Flight Center Battery Workshop. November 18-19, 1986.

[14] Hill and Peterson, Mechanics and Thermodynamics of Propulsion. Reading, Massachusetts: Addison-Wesley, 1970.

[15] Bate, Mueller, and White. Fundamentals of Astrodynamics. New York: Dover Publications, 1971.

APPENDIX: MAV CALCULATIONS

Propellant PU/AP/AL

I_{sp} = 260 sec. on Earth = 666.5 sec. on Mars

U_{eq} = 2550 m/s

propellant density = 17419.188 N/m^3

volume = 0.393 m^3

weight = 6845.74 N

Mass = 697.83 kg.

radius of grain is 0.5 m.

rate of burn is 0.00685 m/s

t_b = 72.96 sec.

mass flow rate = 9.56 kg/sec.

Thrust = mass flow rate x Ueq = 24,225 kg-m/sec2

U_{exit} = 1740 m/s

M(propellant) = M_p = 697.83 kg.

M(payload) = M_l = 200.00 kg.

M(structure) = M_s = 389.91 kg.

Note: Structure mass includes Titanium alloy casing (300 kg.), second stage propulsion system (34.5 kg), insulation (40 kg.), and homing device (10 kg.).

M(total) = Mo = 1287.73 kg.

M(burnout) = Mb = 1287.73 - 697.83-182 (structure) -30 (insulation) = 377.9 kg.

R = Mo/Mb = 3.407

Maximum altitude = Ue2(lnR)/(2gm) - Ue tb(R/(R-1) x ln(R) -1) = 501.2 km.

Burnout altitude = -UetblnR/(R-1) + Uetb - 0.5gmtb2 = 52.1 km.

Chapter 7:

Mars Land-Based Rover

Final Report

Aerospace 401B - Detailed Spacecraft Design
The Pennsylvania State University

Spring Semester 1991

Submitted by Group Scheeser:

Philip Angelo
Daniel Berardo
Mark Elphinstone
Donald Ermel
Thomas Manning
David Morgan
Michael Scheeser

ABSTRACT

Upon landing on the Martian surface, the Mars land rover will be deployed by rolling down the ramp provided by the lander. The rover will then travel within a 25 km radius of the lander to carry out its primary mission of collecting 57 kg of samples from the surface. Its secondary mission is to recover samples from the Aereons if they fail to return to the lander. A fast and efficient navigation system controlling a six-wheeled, three-body, articulated cab-linkage rover with roll-over recovery capability was determined to be the most suitable for achieving the goals of this mission. Power requirements will be met with a modular radioisotope thermoelectric generator using an alkali metal thermoelectric converter to convert the heat from the generator to electricity. Thermal control of the rover will be accomplished by active systems (oxygen filled heat pipes) and passive elements (white paint, thermal louvers, and exposure to the atmosphere for convection and radiation of the heat) that are commonly used in industry. The rover will use a robotic 5 Degree-Of-Freedom (DOF) acquisition and 7-DOF manipulation arm, in conjunction with three different drills, to collect the samples. Sample analysis and validation will be accomplished by an optical microscope, an alpha proton X-ray spectrometer, a differential scanning calorimeter, a neutron spectrometer, and an electromagnetic sounder contained within the rover. All samples will be placed, sealed, and dated in hexagonal shaped canisters that will be used universally in all sample acquisition components of the mission. After all samples have been acquired, the canisters will be brought to the lander for placement in the payload bay of the ascent vehicle where they will be launched for return to Earth. The rover will continue on an extended mission of analyzing the Martian terrain, sending detailed maps of the surface to Earth.

TABLE OF CONTENTS

NOMENCLATURE

AMTEC	alkali metal thermal converter
APXS	alpha particle x-ray spectrometer
BASE	beta-alumina solid electrolyte
DOF	degree-of-freedom
DSC	differential scanning calorimeter
EGA	environmental gas analyzer
EMS	electromagnetic sounder
FWPF	fine weave pierced fabric
GIS	graphite impact shells
GPHS	general purpose heat source
INS	inertial navigation system
IPRP	independently programmable rotary & percussive
ISCA	interim sample canister assembly
MAV	Mars ascent vehicle
MLR	Mars land rover
MSRM	Mars sample return mission
NS	neutron spectrometer
OM	optical microscope
RTG	radioisotope thermoelectric generator
SARS	sample acquisition robotic system
SES	sample experiment suite

LIST OF FIGURES

LIST OF TABLES

1.0 INTRODUCTION

Mission Profile B of the Mars Sample Return Mission (MSRM) requires the use of a Mars Transfer Vehicle, a deployable Mars lander/base, two Aereons, a land rover, and a Mars Ascent Vehicle to accomplish the mission. An integral part of the MSRM is a large land-based planetary exploration vehicle, the Mars Land Rover (MLR), which is used to collect the majority of the samples for the mission. This report will focus on the overall design characteristics of the MLR.

In addition to mechanical design concepts, other factors such as feasibility, weight restrictions, size limitations, and cost were considered during the development of the MLR. The six primary subsystems considered in this report are navigation, mobility, sample acquisition and retrieval, power systems, communications, and thermal control. Navigation and mobility requirements for the MLR dictate that a semi-autonomous control system implementing high resolution navigation equipment be integrated with a highly flexible multi-cab rover. The MLR must contain a sample acquisition, analysis, and preservation system capable of retrieving core samples, large amounts of rock specimens, and various soil samples while minimizing the total rover payload requirements. The MLR will be in operation for an extended period of time and will require an effective thermal control and power system, as well as a communication system that will enable it to remain in contact with all components of the mission. Specific mission requirements state that the MLR have a maximum range of 200 km, and remain under a mass of 1000 kg. The concepts and requirements for the MLR have been researched and developed for this final report.

2.0 NAVIGATION

2.1 Navigation Criteria and Concept

A fast and efficient navigation system is needed to ensure overall mission success. In an interplanetary mission, the navigation system for a remote sample collection vehicle must maximize the vehicle's computational speed, while minimizing Earth communication time. Semi-autonomy thus becomes a necessity, since it reduces the amount of communication time needed as well as periods of vehicle inactivity.

The chosen concept uses a semi-autonomous design which ranges from full autonomy for simple tasks to complete dependence on Earth for highly complex vehicle activities. The three major tasks that the vehicle must achieve in autonomous navigation are normal maneuvering functions, collection and processing of terrain data, and Earth communications. Other functions are also performed autonomously, but under direct supervision by mission control. These include maneuvering in close quarters, roll-over recovery, and extraction from vehicle entrapment. The more specific operations are fully explained in the chapter dealing with vehicle mobility. The basic design of the MLR is illustrated in Figure 1.

2.2 Basic Navigation Technique

To minimize the number of sensing, control, and computational components required on the MLR, the navigation system utilizes function redundancy, a method of comparing data from multiple information gathering sources to increase the reliability of the information, for path finding and position estimation. In this application of the concept, a comparison is made between local terrain data received by both the Mars Orbiter and the onboard image processors of the MLR. The first step in path determination is the downloading of 1-meter resolution stereo images from the Mars Orbiter to Earth. From this data, a rover path is determined (with a length of approximately 10 kilometers) by

mission control. This information is then transmitted to the vehicle. These images are compared to high resolution depth maps (precision of approximately 1 cm) created by scanning laser range finders and stereo vision cameras located on the vehicle. The depth maps are created through the stereo process of matching and triangulation. The MLR analyzes the matched maps, then plans a local path (of approximately 10 meters) that avoids observed obstacles. On board, the vehicle simulates the maneuvers required along the planned path to create its own collection of sensor expectations that are used during path execution. The MLR then follows the path while monitoring its sensors for conflicting conditions. Once the short path is completed, the vehicle acquires a new set of local terrain images and processes this information to determine its next 10 meter path. This semi-autonomous operation of the MLR is illustrated in Figure 2 [Wilcox, et al, 1987].

The computations needed to process images may require roughly 60 seconds. If these are needed every 10 meters and it takes the MLR approximately 30 seconds to traverse 10 meters, the resulting average rate of travel is 10 meters every 90 seconds, which is approximately 10 km/day. If a 10 km path is designated from Earth each time, only one communication per day will be required unless an emergency, such as vehicle roll-over, dictates additional attention from mission control.

2.3 Terrain Data Processing and Navigation Systems

The combination of craters, pits, rocks, crevasses, and slopes on the martian surface presents many opportunities for vehicle entrapment and/or rollover. There are several types of computations that need to be performed by the rover during its surface movements. These include the processing of a surface or topographical map, the matching of this map to the global data base, analyzing the traversability of the area, planning the local path, and monitoring the execution of that path.

Negotiation of local terrain is determined through a combination of stereo vision and structured light vision (a method of depth characterization accomplished by controlling

and recording lighting on objects), while the stability characteristics are identified by testing the surface with the front section of the MLR and the onboard manipulators. The manipulator arms can be used to test the soil stability in front of the vehicle and around its forward periphery. The use of electromagnetic propagation characteristics provides a means of assessing the strength of homogeneous soils prior to vehicle commitment. When the front section of the MLR encounters unstable or non-negotiable terrain, the vehicle simply stops and determines a new course of action. Even if the front body collapses through the surface and is no longer supported, the main body has enough mass to support it and keep the entire rover from falling forward into the unstable soil. Terrain sensing is an important advantage of the Attached Scout (described below), and some of the primary sensor and control systems are shown in Figures 3 and 4 [McTamaney and Douglas, 1988]. Sensors include:

- external contact and proximity sensors on all bodies
- structured light vision sensors
- inertial navigation system (INS)
- manipulator force and position sensors
- camera on the hand
- articulation force and steering position sensors
- camera platform position and orientation sensors
- active and passive onboard beacons
- onboard range finder and optical beacon navigation sensors
- onboard star tracker
- tilt sensors

Some of the control elements of the MLR include:

- sensor platform position and orientation control
- steering geometry modeling
- attached scout force control for hazard detection
- attached scout coordination for hazard crossing
- catastrophe protection and compromise recovery
- manipulator assisted hazard detection
- nonholonomic steering geometry

3.0 MOBILITY

3.1 Mobility Criteria

The criteria for the mobility of this vehicle are very specific. It must be able to negotiate rocks and steps up to 1 meter in height, and traverse crevasses of up to 1.5 meters in width. Climbing requirements make it necessary for the vehicle to maneuver on slopes of ± 30 degrees. Terrain on the martian surface calls for high traction mobility that allows the vehicle to operate efficiently in loose sand conditions. The MLR will act as a failsafe in case of minor system failures that might occur on the Aereons or the Mars Ascent Vehicle (MAV). In case of damage to the Aereons, the MLR is designed to locate the mini-rocket and retrieve the Aereon's samples from this rocket. This may require that the MLR cover a total radial distance of 200 km. Because of the equipment carried onboard and the precision of the manipulators, the MLR can also be used to repair minor damage to the MAV through direct control from Earth. The MLR mobility concept was developed from an existing rover design referred to as the Attached Scout (see Figure 5), where the Attached Scout is the front section of the MLR. Dynamic constraints for the rover are governed by the equations shown in Appendix 1.

3.2 Mobility Concept

The concept chosen to meet the mobility criteria is a six-wheel, three-body rover that utilizes an articulated cab linkage. All axles are powered and vehicle control information is obtained primarily from force transducers at each wheel location. Six 1 meter diameter, 1/2 meter wide wheels are independently powered to provide maximum drive train capacity. They are conical in shape, and rely on interior drives and high connecting axles for rotation. These internal drives consist of the drive motor, clutch, and transmission components. This system requires 8 drive motors to function, but it can still maneuver normally with a minimum of 6 motors. The MLR can sustain a maximum speed

of 13 cm/sec (11 km/day), but usually cruises at a speed of 10 cm/sec (9 km/day). Deeply grooved wheel segments (grousers) give the vehicle its high traction capabilities [McTamaney and Douglas, 1988]. The grouser is able to dig into softer soil and grip projections and points on rock surfaces. The first two wheels serve as the front cab's maneuvering system, and are independently suspended by articulated torsion bars, sustaining a maximum pivot rotation of 30 degrees. The other two sets of wheels function in the same manner for the remaining two cabs. Steering is achieved by driving outer and inner wheels at different speeds on their independently driven axles. Both the front and rear axles are steerable using a wagon-wheel type mounting. The MLR has a turning radius of approximately 2.6 meters.

The front and rear connectors for the three cabs are 3-DOF powered joints. This enables them to provide additional steering in cases of drive motor incapability, as well as the raising or lowering of a particular vehicle segment. Roll axes allow raising either the right or left side wheel on either the front or rear axle as required by the terrain. Axle raising can be accomplished with a pitch motor, while individual wheels can be raised by using the powered roll. Pivot, pitch, and roll of the joints is allowed during normal vehicle operation and movement so as to conform to the terrain and keep all wheels in contact with the surface.

3.3 Application of Mobility Concept

Not all hazards can be avoided and many unavoidable hazards cannot be negotiated. Providing the vehicle with the capability to extract itself from entrapment is a design option that must, therefore, be considered. Air bags, jacks, winches, grappling hooks and other auxiliary devices can be used to free the MLR from pits, burial, and entanglements.

The general movement of the vehicle across the martian surface is something that must also be given consideration in the application of the vehicle's mobility systems. As this vehicle utilizes a multi-functional drive system, several options are usually available to

complete a particular maneuver. In the case of obstacles, the axles can crawl up or be power lifted by their powered pitch axes over the obstacle (see Figure 6). In most cases, a combination of both will be used, where power lifting takes over when crawling slows to an inefficient level. Descending steps are negotiated in much the same manner. Powered axle-pitch changes are not usually necessary for descent.

Crevasse traversal can be accomplished by two means. In the first approach, the roll and pitch axes are locked, and the front joint is extended as the crevasse is crossed on an oblique angle (see Figure 7a). In the second approach (see Figure 7b), the middle axle is moved forward to stabilize the rear vehicle section, and the front axle is raised by its powered joint. The vehicle is then maneuvered such that the middle axle is within close proximity of the crevasse edge, and the front section can be lowered safely across the crevasse. It is then safe for the MLR to cross the obstacle.

The wheels are equipped with force transducers that continuously monitor the loading conditions on their respective wheel. In this way, rocks, pits, craters, and slopes can be actively sensed and negotiated. An inclinometer, which is a device that measures the position of the rover relative to the local vertical, is employed to measure an approaching slope, while wheel slip sensors test the coefficient of friction between the wheel and the surface. In this way, the vehicle can stop itself before attempting to descend a slope that it cannot successfully climb when returning. Simple pressure detectors extended from the vehicle are used to provide warnings of unanticipated obstacles or departures from course.

A situation may arise where adverse terrain conditions cause vehicle roll-over. The vehicle utilizes a self-righting system that employs its powered joints to recover from any such scenario. Total roll-over is avoided by the use of fitted roll bars found at opposite ends of the vehicle. These bars limit maximum roll-over to 90 degrees from the surface normal. The roll-over recovery technique is as follows: first, the middle section is rotated to a horizontal position. The forward axle joint is then angled upward to raise the front section off of the ground, while subsequently lowering the middle section to the ground.

Once this is complete, the fore-body is rotated to a horizontal position. Now the middle axle is shifted to the rear, causing the rear body to come off the ground. Then, the rear body is rotated to a horizontal position, thus completing the rollover recovery maneuver. This sequence is illustrated in Figure 8.

4.0 SAMPLE ACQUISITION, ANALYSIS & PRESERVATION

4.1 Introduction

The success of the Mars Sample Return Mission is directly dependent on the ability of the land rover to effectively determine sites which contain valuable surface samples. For a fully capable semi-autonomous rover, it is assumed that geologists will pick sampling sites and transmit a single command for sample acquisition. Once a desired sampling site has been determined, the rover must have the ability to plan and execute the necessary movements to place the rover's sampling mechanism within range of the sampling site. This will require imaging and ranging instrumentation to provide precise sample location and a multi-DOF robotic system to acquire the samples. Because there are many different materials to be sampled on Mars, flexibility in sampling methods is an important criterion. Once the samples have been collected, the rover must contain an equipment suite which determines the samples elemental, chemical, and physical properties without producing cross-contamination. Once this is completed, the rover will process the results through its computers and determine which samples to keep. The samples which meet the mission requirements must be placed in containers and properly stored within the rover until the rover returns to the MAV.

4.2 Sample Acquisition

The Mars land Rover will be working in conjunction with two Aereon rovers to meet the sample requirements specified by NASA. Because of the Aereon's limited payload capabilities, the MLR will be responsible for collecting the majority of the rock and regolith/conglomerate samples. The MLR sample acquisition goals were determined on the basis that the primary function of the rover was to provide a detailed analysis of a localized Martian environment which placed emphasis on larger rock samples and core samples. The sampling goals are shown in Table 1.

Because of the MLR's enhanced stability and control system, it will perform all sample acquisitions of rock fragments/chips, pebbles, and boulder specimens. To perform these functions the MLR will be equipped with three primary sample acquisition subsystems: a 5-DOF robotic acquisition arm, a 7-DOF robotic manipulation arm, and core drill. The MLR is designed to perform its sample experiments within a 25 km radius of the MAV, and is capable of traversing a distance of 10 km a day under optimal conditions. A 25 km radius corresponds to a surface area of roughly 1963.5 km^2, which provides a large enough sampling area to ensure an adequate diversity in samples.

4.2.1 The Sample Acquisition Robotic System

The Sample Acquisition Robotic System (SARS) will consist of a 7-DOF manipulation arm and a 5-DOF acquisition arm, as shown in Figure 9. Each arm will contain appropriate position, velocity, force, vibration, and thermal sensors. For redundancy, each arm will have the capability to perform many of the actions of the other, but each will be optimized for its own range of functions.

The 7-DOF manipulator arm is a high-resolution arm capable of delicate motion and precision. This arm will perform the majority of operations requiring high levels of accuracy. Its operations will include transferring samples to containers and exchanging tools on the acquisition arm when necessary. The manipulator arm is capable of accessing the complete sampling tool kit. The manipulator arm has two axes of motion (rotations) at the point where the arm attaches to the rover, one axis at the elbow, one axis between the elbow and wrist, and three axes of motion at the wrist where the tools are attached.

The acquisition arm will be used mainly for operations requiring strength. Its design is very rugged and will require less positioning accuracy. The acquisition arm contains the core drill. The acquisition arm also has at its disposal the complete kit of sampling tools. The arm has sufficient mobility and electrical connections to access each tool. The acquisition arm has two rotational axes of motion at the point where the arm

attaches to the rover, one degree of freedom at the elbow and only rotation at the wrist where the tools are attached. Because of the vibrational loads applied by the core drill and shock loads associated with the impact of chipping, the acquisition arm will contain an advanced and extremely efficient sensor-based reflex mechanism to quickly retract or adjust tools and avoid system level damage.

The complete kit of sampling tools is illustrated in Figure 10. The tools are designed with two identical bayonet lock connections, one at 180 degrees from the tool head and the other at 90 degrees to the first connection. This enables the tool to be exchanged between the acquisition arm and the manipulator arm. The 90 degree connection is primarily designed for the manipulator arm with its three degrees of freedom at the wrist.

The SARS is capable of recalibrating its instruments and sensors prior to any sampling. This includes the calibration of the control systems for each arm and the detection of possible tool slippage.

4.2.2 Contingency Sample

The primary contingency sample will be collected by the lander using a robotic system equipped on the lander. This contingency sample will include regolith and atmospheric samples. Another level of contingency planning is to send the MLR on an initial regolith retrieval expedition that will involve little risk and be performed within the range of the lander sensing equipment. This expedition would be devoted to the collection of as many different regolith samples as possible from minimum risk areas near the lander. A special sample canister would then brought back to the lander and placed in the ascent vehicle ready for launch. This process could periodically be repeated, replacing the initial contingency sample if more interesting samples were found during the mission life of the MLR. A total of 2 kg of regolith is the goal for this contingency sample. The contingency sample canister would be a small cylinder using a metal seal ring with a protective cover that is removed before final sealing.

4.2.3 Regolith Sampling

The scientific requirements for the sampling of regolith on Mars include surface material, deeper and partially frozen regolith, unconsolidated fines, and wind blown or settled dust [Clark and Amundsen, 1987]. The collection of regolith will be accomplished using both the acquisition and manipulator arms. The SARS provides a flexible and reliable means of sample acquisition that prevents cross-contamination. A list of regolith sampling techniques is given in Table 2.

The Martian soil is of great interest, especially in areas where the Martian environment has eroded the surface to provide access to the layered deposits and fluvial deposits which contain materials carried by a distant and extinct water source. A complete sample set of the regolith will include the wind-blown surface layer, eolian or settled particles, and deeper undisturbed soil. These different types of regolith samples will be collected using two different techniques for each specimen to ensure redundancy and avoid cross-contamination.

The topmost layer of fine soil is of scientific importance because it can represent eolian materials transported from remote areas of Mars [Clark and Amundsen, 1987]. This layer will be sampled using two different techniques. The first technique is straight-forward and uses the manipulator arm equipped with the scoop to obtain fine grains on the surface to be tested. Once collected, the samples are taken from the surface and deposited in the Sample Experiment Suite (SES), where they are analyzed for their quality and importance. Any samples deemed worthy of return will then be placed into canisters and stored within the thermally controlled sample storage area The second method requires the acquisition arm to expose a surface area of sticky tape to be gently lowered to the Martian surface. The soil and dust adhering to the tape will then be collected by the manipulator arm and stored in a sample canister. Numerous tape samples can be collected in this manner.

Another sample of interest are the eolian grains produced by the Martian winds. Two methods will be employed to perform this type of sampling. The first method incorporates the same adhesive tape used in the sampling of the topmost layer; however, the tape will be deployed for long-term use on the sides of the MLR. When the MLR returns to the lander at the end of the mission life, these samples will be collected by the manipulator arm and placed in a sample canister. Another method of sampling to collect a vast number of impinging particles is the Mars wind sock. This device consists of half cylinders of fabric to collect the particles and wind vanes to keep the rotatable assembly pointed into the wind. The fabric cylinders are stretched on a lightweight structure of wires that can easily collapse for storage. This assembly will be deployed at the beginning of the mission relatively close to the lander. At the end of the mission the bag will be removed from the wire frame, and rolled up for insertion in a return canister.

The deeper and undisturbed soil of the Martian surface will be collected using two very different methods. The first method is simple and provides large amounts of deep regolith. The technique involves the clearing or trenching of the surface soil by the acquisition arm and the tools at its disposal. Next, the manipulator arm will obtain large segments of the newly exposed soil using the scoop/sieve. These samples will then be taken to the SES where they will be sifted by the sieve to remove any larger rock particles. Any samples deemed worthy of return with then be placed into canisters and stored within the sample storage area. The second method involves the collection of deeper soil samples by using a mini-core drill attached to the sample acquisition arm of the SARS. This device will be discussed in more detail in section 4.2.5.

4.2.4 Rock Sampling

Rocks to be sampled have been broken down into three different classifications. The first group are pebbles. These include all natural rock formations existing on the surface and in the soil that are small enough to fit into the sample canisters without any

manipulation. The next group are rock fragment or chips. A rock fragment/chip is a section of rock that must be manually removed or chipped from the surface of a larger rock specimen. The last group, boulder specimens, includes all naturally formed boulders and any exposed bedrock slabs of substantial size and consistency.

The simplest way to obtain a diverse sample of pebbles is to scoop up quantities of regolith and sieve out the pebbles and lithic fragments. This process can be aided by the use of the rake, broom and hoe/scraper tools in the sample kit, and these functions will be performed by the acquisition arm. To ensure a wide variety of pebble specimens, the sieve utilizes 10 different sized screens that can be changed by the manipulator arm. A total sample mass of 13 kg will be collected for this classification.

A total of 10 kg will be sampled from the weathered rinds of larger rocks. Samples of larger rocks can be produced by picking, chipping or crushing to obtain representative fragments. These methods will be used to obtain 6 kg of larger rock fragments and 4 kg of crushed rock specimens. Loose rocks must be held stationary by one of the rock-holding mechanisms available to each of the rover arms. These tools use two hinged levers, each with three stiff, splayed fingers, to capture a rock from opposite sides [Clark and Amundsen, 1987]. These tools are very flexible in terms of the size of rock it can hold. Once the specimen is stationary, the free arm is capable of using the positionable chipper or the rock pick to obtain samples. These methods will be employed to obtain the fragment specimens. A tool available to the acquisition arm, simply referred to as a rock crusher, will be utilized to obtain crushed rock specimens. A stationary rock crusher mounted to the SES is also available for larger specimens. Once collected, all specimens must be validated by SES analysis before they are placed in sample canisters.

There are several methods for obtaining fragments from stabilized rock. The first method is to subject the rock to steady vibrations to weaken sections of the larger rock; a vibrating pick is used to accomplish this goal. A maneuverable pick is recommended because it allows the selection of a desired spot on a boulder for chipping. The weakened

sections may sufficiently chip or crumble for sample collection or may require the aid of a spring-loaded chipper to break off small chips and flakes from the impact point. Another approach is to attach a large sledgehammer to the rover, which can be used to break chips from boulders and bedrock. A combination of the acquisition arm at the top of the handle of the sledgehammer and the manipulator arm at the bottom of the handle of the sledgehammer would be sufficient for operating the sledgehammer. The head of the hammer would be left hollow during transport and filled will Martian soil just after landing. The sledgehammer would also be useful in obtaining seismic data. Recorders placed a small distance from the rover could measure seismic waves produced by the sledgehammer striking either bedrock or an impact plate on the soil surface [Clark and Amundsen, 1987]. This information would be useful in determining bedrock layers and depth. The most difficult method of obtaining boulder specimens is to use core drilling. These cores would be around 5 mm in diameter and taken by a drill separate from the regolith drill (See Section 4.2.5). All boulder specimens would be subject to SES analysis for validation before being stored in the sample canisters. A total of 13 kg from a diverse set of boulder specimens will be collected during the mission life of the rover.

4.2.5 Drilling Techniques

4.2.5.1 Regolith Drilling

In order to obtain sample levels of the Martian regolith soil, a conventional core drill could not be used since it could not retain the noncohesive material of the soil during withdrawal. Because of this, a sand drill will be used. The sand drill was chosen since it could obtain regolith samples without loosing the sample during withdrawal and could also take the samples in levels. This is a solid-bit drill with an internal movable structure of pistons (see Figure 11). As the drill is progressing to a set depth, the pistons are closed.

When the desired depth is attained, the pistons are open, revealing cups inside the drill for retaining soil. The drill then rotates until the cups are filled, at which time the pistons close and the drill is withdrawn from the soil. The sand drill is used as an attachment to the 5-DOF arm.

4.2.5.2 Rock Drilling

One method of obtaining a large rock or boulder specimen is coring. Coring a large rock was chosen since it would obtain a more representative sample of the entire depth of a weathered or stratified rock. The mini-core drill used for this procedure is 1 cm in diameter and 20 cm in length and made of a titanium alloy with a tungsten carbide cutter. These materials were also used in the Apollo drill and chosen for their very low thermal conductivity and hardness properties. As with the sand drill, the mini-coring drill is an attachment to the 5-DOF arm.

When a core sample is drilled, the base of the core may not break off from the rest of the rock. To overcome this problem, a second hole must be drilled at an angle to the core and intersect it near its base. This will break the core sample at the point of intersection and allow the specimen to be withdrawn. A diagram of this procedure can be found in Figure 12. Although the thermal effects have not been tested for a drill of such a small diameter, they have not been found to harm the sample during previous drilling procedures. This is further explained in the next section.

4.2.5.3 Core Drilling

A 2 m core sample of the Martian soil was desired for the mission. The drill used to obtain this sample is a rotary-percussive drill, chosen so that minimum disturbance of the core sample is achieved. The core drill is mounted through the mid-section of the MLR for stability during drilling.

The core drill is a double-barrel design chosen so that the outer tube can retain the shape of the hole without it collapsing while core sample sections are taken. The outer tube is composed of two 1.75 x 125 cm sections that lock together during the drilling procedure. The inner tube is a 1.5 x 25 cm section that locks at the bottom of the outer tube. Both the inner tube and outer tube are made of titanium alloy. The outer tube has a cutter made of tungsten carbide which is used for the drilling and the inner tube is used to obtain the core sample. During drilling, the inner tube remains stationary, so that the core sample is not disturbed by wall friction.

After a 20 cm core sample is taken, the 5-DOF arm removes the inner tube by attachments and stores the sample in a single hexagon canister as discussed in section 4.4. During withdrawal of the inner tube, the core sample is not likely to be lost since there is a large ratio of support area to core mass. For this reason, no core catcher was necessary on the drill. Once the tube is stored, another tube is placed into the drill and locked into position for drilling. This procedure continues until the 2 m depth is obtained.

Tests have been performed to determine the effect that heating due to the drilling procedure would have on a similar core sample [Clark and Amundsen, 1987]. The results showed that the core surface heated by 358 K, and the inner portion heated to a temperature approximately 20 K above the ambient. From this information, it is unlikely that heating will destroy any information resident in the rock. Since the drilling is performed in sections, there is more time for cooling of the drill which further lowers the heating effects.

To minimize the core sample disturbance, the drilling procedure is overseen by an independently programmable rotary and percussive (IPRP) microprocessor. This is done since different drilling methods are best for different soil properties. The microprocessor responds to the type of material being drilled, monitors the effectiveness of the cutting, and speeds or slows the drill accordingly. Also, all information about the parameters of the drilling is stored during operation.

4.3 Analysis and Validation

There exist numerous methods of sample determination. Some studies on sampling recommend an autonomous rover capable of performing highly detailed sample analysis, while other studies suggest larger sample payloads using less sophisticated analysis and validation equipment. Extremely sophisticated analysis and validation instruments require longer operation times, during which the MLR is stationary. Since advantages and disadvantages exist to each method, the MLR utilizes a moderately sophisticated Sample Experiment Suite (SES) which contains a 100 kg thermally insulated sample storage bay. The SES consists of a complex series of instrumentation designed to identify and analyze any given sample. Once a sample is collected it must pass through all of the instruments of the SES before validation can be obtained. The SES consists of an optical microscope (OM), an alpha proton X-Ray spectrometer (APXS), a differential scanning calorimeter (DSC), an environmental gas analyzer (EGA), a neutron spectrometer (NS), and an electromagnetic sounder (EMS).

The purpose of the OM is for the validation of rock fragments, pebbles, and boulders. The OM is located on the MLR's 7-DOF manipulation arm with an auxiliary light source for illumination. The OM is used to characterize individual materials at the scale of individual mineral grains with stereo view. The OM is equipped with a 1 cm field of view and 0.005 cm resolution with 10^6 bits per image for stereoscopic viewing. Once the sample has been identified by the OM, the 7-DOF manipulation arm collects the sample and places it in the interim sample canister assembly (ISCA) for analysis by the SES.

The APXS is one tool of the SES designed to perform the elemental analysis of collected samples. The APXS can determine elemental composition up to 0.1 atom percent with a required counting time of at least 4 hours. The APXS uses a Curium source (Cm-242) and can detect elements with atomic numbers up to titanium-81. For elements heavier than titanium, an additional auxiliary source is required. The x-ray detector is a Ge detector with active cooling required below the Mars daylight ambient condition which will be

accomplished by the instrumentation thermal control system (described in Section 6.1). For operation at night, cooling may not be required.

The DSC and the EGA are the main instruments used in the SES unit to detect and identify volatiles and mineral phases. The DSC determines the chemical properties of a sample such as phase changes and evolved gases. This is done by varying the sample temperature with time and measuring the heat input relative to a standard sample. The evolved gases are transported to the EGA where they are identified. The DSC is destructive, so only a portion of the sample to be analyzed is prepared and used for the test.

The EGA receives the head gases produced by the DSC and analyzes them to determine volatiles and compounds. The compounds in the Mars atmosphere are expected to have a molar mass of 100 grams or less. The baseline requirement for the EGA is to detect masses up to 200 grams.

The NS is an important device needed to detect the presence of water and organics on Mars. The NS is located under the MLR and is shielded from the RTG's. The NS relies on the detection of thermal neutrons to determine the presence of water and organics. Thermal neutrons are produced when hydrogen is present in a material. Hydrogen has a very high cross-section and is able to capture thermal neutrons. The detection of excessive thermal neutrons will be an indication of water in the Martian soil. The neutron sources for the NS are the RTG's on the MLR.

The Electromagnetic Sounder (EMS) is another device which was considered for the MLR. The EMS is located under the MLR and is used to determine the vertical subsurface structure of the ground.

4.4 Containment and Preservation

The sample storage system is a very important part of this mission. To simplify the design, a universal sample canister system for all parts of the mission (Aereons, land rover, and ascent vehicle) will be used. All samples must be stored to keep them in the condition

in which they were collected. The storage device must be able to withstand a 5 g acceleration (the ascent from Mars to the return vehicle) and keep the sample intact and reduce contamination from solar radiation. The sample storage canisters should maximize the amount of sample volume and mass for different types of samples and be able to be easily handled by the rovers and lander while isolating the samples from each other.

A cylindrical and hexagonal shape of the canisters was considered, because many of the samples taken will be tubular and both shapes will hold tubular samples well. To determine if the shapes can withstand the 5g's, both shapes were examined with two different finite element codes using an arbitrary material. The codes employed were the IDEAS code, a commercially available code, and Wonderfem, a code developed by the Penn State University Engineering Mechanics department. The deflections in the hexagon shape were less than the cylinder by 10% and the stresses were larger in the hexagon than the cylinder by 20%.

The hexagon shape allows for a more volume efficient method for storing the samples because of the minimum space allowed between canisters. Since all samples will have to be restricted to a certain size, both shapes would have the same sample mass characteristics. Additionally, flat surfaces are more easily handled by the robotic arms of the rover, Aereon, and lander, making the hexagon shape more appealing for all aspects of recovery. Both shapes can easily isolate samples from each other. With all of the requirements examined, the hexagon shape proved to be the best choice for a sample canister.

Seven hexagon canisters will be attached together to form a tray for storage of samples, with a total of 13 of these trays on the mission, and all of them will be handled by the MLR. This tray must be smaller than 20 cm in diameter and 21 cm in height, as required by the mini-rockets in the Aereons (see Figure 13 for actual dimensions). For large samples, i.e. boulders fragments, there will be 6 seven-hexagon canister systems with the inner canister walls removed as shown in Figure 14. Storage of the core samples

will be accomplished by putting the samples in 10 single hexagon canisters, 21 cm in length (see Figure 15). Since the core sample will be sensitive to the Martian atmosphere, a small copper lid will be placed on top of the canister for immediate sealing from any contamination. Twenty-six more single hexagon canisters will be available and the Aereons will use six of these, while the MLR will use the remaining twenty.

The material that was chosen was A357.0 Alloy. This Al-Si-Mg alloy was chosen because of its excellent casting characteristics; it is heat treatable, provides the highest strengths available in commercial castings, has good toughness, and has excellent corrosion resistance. After running the finite element codes with this material, the stresses were found to be within 40% of the yield strengths in any direction.

The canisters will be placed in a thermally buffered, hermetically sealed payload bay Sample Can, as shown in Figure 16, with sensitive samples placed in the center of the configuration. The thermal buffer material will act as an insulation from unforeseen temperature gradients encountered in Earth re-entry. The buffer must be leak proof to prevent loss and contamination of the buffer material. The buffer will be silica ceramic foam. It will be placed in the payload bay Sample Can and be pre-formed in a shape to accept the canisters in the configuration of Figure 15. This foam has a high temperature limit (1650°C), low density (0.32 g/cm^3) and a high compression strength (52 kg/cm^3), which would allow for a fairly light and strong support structure. This type of buffer also acts as a radioactity shield, which can decrease the chances of sample contamination.

The seal will be made of a soft metal, so that when contact is made, the sealing of the two surfaces will be easy. Picking a good material for the seal is just as important as getting the samples, for contaminated samples are worthless. The material chosen must not be one to be expected on the Martian surface, because when the sealing takes place, sealant particles may chip off into the samples and destroy their integrity. Using the rarest material might be a good choice, but a more common material is better one. A more common material, such as copper, will not affect any geologic readings of samples because it is not a

trace element and it is expected to find a large percentage of copper on the Martian surface as found by the Viking mission. Once all the sample canisters are placed in the payload bay can, the can's lid will be opened to a 150° angle, at which point the copper seals will expose themselves for use. The lid will then be closed and locked into place with simple side clamps. The samples are then ready for ascent and the return trip to Earth.

5.0 POWER SYSTEM

5.1 General Description

A modular Radioisotope Thermal Generator (RTG) will be used to generate the power for the MLR. The RTG consists of two stacks of eight General Purpose Heat Sources (GPHS) arranged in a space saving design as shown in Figure 17. One stack of GPHS modules will have 24 alkali metal thermoelectric conversion (AMTEC) modules and the other will have 32 AMTEC modules. Three AMTEC modules surround each GPHS module in one stack and four AMTEC modules surround each GPHS module in the other stack. The total of 56 AMTEC modules, each producing 10.6 watts at 19 volts, will provide the required average power of 500 watts. Batteries supplement the RTG during peak power usage and will recharge when the rover is using less than 563 watts. The total power source has dimensions of 60 x 45 x 40 cm. The power system also includes ceramic supports to hold the GPHS modules in place and thermal insulation to keep the system components at their respective temperatures.

The GPHS modules provide the thermal energy and the AMTEC modules provide conversion from thermal to electrical power. The AMTEC modules protrude 10 cm from the GPHS module and will act as heat radiators. The current leads from the modules carry the electricity produced from the power source to the rover. The AMTEC modules will be wired in parallel, in case of a failure. Therefore, the failure of one module will not result in a decrease in power system voltage.

The power system is designed to limit volume and mass which are conflicting goals. The design decreases the volume but slightly increases the mass. Also, since the AMTEC modules are a small fraction of the total mass in the small radioisotope-based power system, efficiency is the overriding factor. Therefore, increasing the current collector and lead mass will increase the system efficiency by reducing the resistant losses inherent in a collection device. The increased efficiency of AMTEC allows for a

subsequent reduction of the most massive components of the system for the same electrical output.

The GPHS heat source and the storage system are both readily available and accessible. The AMTEC modules are still in the developmental stages at the Jet Propulsion Laboratory in Pasadena, CA.

5.2 Heat Source

The heat source for the power system is made up of 16 general purpose heat source (GPHS) modules. Each module has over all dimensions of 9.71 x 9.31 x 5.3 cm. and a mass of 1.45 kg. Each module gives a total thermal power of 250 watts. The modules are placed one on top of the other, in two stacks of eight modules. Each stack is placed in the center of the converter elements and held in place by ceramic supports.

The fuel that is used in the GPHS is PuO_2. The plutonium isotope has a half-life of 87.8 years which will result in a 3.4% reduction in thermal power after 40,000 hours. This means that there would be a 5%, or 15 watt, loss in electrical power in this time. Since our mission is shorter than this time, the loss in electrical power will not be a concern.

A sectioned view of the heat source module is shown in Figure 18. Each module contains four fuel pellets of PuO_2. Each fuel pellet is enclosed within a vented, iridium alloy capsule. This capsule provides containment of the isotope. Two cylindrical graphite impact shells (GIS) surround the capsules and are designed to withstand, if necessary, impact associated with launch and mission aborts. Each GIS contains two fuel capsules. The GIS is made of fine weave pierced fabric (FWPF) which is a three dimensional carbon-carbon composite. All of these parts are contained in a shell which is also made of FWPF.

5.3 Thermoelectric Conversion

Alkali metal thermoelectric converters (AMTEC) are used as a direct energy conversion device. AMTEC is a very favorable system because it has no moving parts and a fairly high efficiency. Since it is a static system, maintenance is simple. The efficiency of the system is 14.1% as shown in Table 5. There are a total of 56 AMTEC modules, each produces 10.6 Watts of power. The voltage in each module is 0.68V. Each module is connected in parallel with one other module. Therefore, there are 28 sets of modules which are then connected in series. This set up provides 563 Watts at 19.1 Volts. If a module fails the power will drop by 10.6 Watts but the voltage will remain the same.

The AMTEC is a thermally regenerative electrochemical device for the direct conversion of heat to electrical energy. The device accepts a heat input at 1100 to 1300 K and produces a direct electrical current with predicted efficiencies between 15 and 30%. The system uses saturated Sodium as its working fluid. The Sodium moves around a closed thermodynamic cycle between two heat reservoirs. A beta"- alumina solid electrolyte (BASE) physically separates the high temperature reservoir from the low temperature heat sink, as shown in Figure 19. The vapor pressure of Sodium in the hot zone is about one atmosphere and in the cold zone about 10^{-5} atmosphere [Bankston and Williams, 1988]. The pressure difference causes a voltage to develop across the BASE. The Sodium atoms cannot pass through the BASE so they separate into Sodium ions and electrons. The BASE is an excellent conductor of Sodium ions and an extremely poor conductor of electrons; therefore, the Sodium ions pass through it. An external path is provided for the electrons to leave the liquid phase Sodium, travel through a load, and return to the lower potential region through an electrode where they recombine with the Sodium ions at the interface between the BASE and the electrode.

The AMTEC module is shown in Figure 20. The figure does not include the refill inlet for Sodium. The high pressure and high temperature region exists from the evaporator to the closed end of the BASE. This region consists of a Sodium-filled lining

on the evaporator tube and BASE, and enclosing a Sodium vapor space. Thermal energy input into the evaporator causes the Sodium in the inner wick to evaporate and flow to the BASE region where it condenses [Sievers and Banston, 1988]. Approximately eighty percent of the condensed Sodium returns to the evaporator through the inner wick and does not do any work. The rest of the pressurized Sodium ionizes. The Sodium ions pass through the BASE and the electrons are conducted along the Sodium filled wick to the outer surface of the module evaporator and through the electromagnetic (EM) pump where the current leads are placed. The current is returned to the grid which surrounds the BASE. The grid distributes the electrons to the electrode where they recombine with the Sodium ions that passed through the BASE. The neutral Sodium vapor atoms then pass through the porous heat shield and condense on the wick of the low temperature condenser wall. Liquid Sodium in the low temperature and low pressure condenser region is sent back to the high pressure evaporator region through a small DC electromagnetic pump and the Sodium return line.

Three key components that make the AMTEC an efficient device are the electromagnetic pump, a BASE to metal seal, and the electrodes. The electromagnetic pump must maintain the pressure difference between the high and low pressure reservoirs and it must return Sodium to the high pressure side at about 1 cm^3/hr-amp of AMTEC current. The EM pump has recently been developed at JPL. Currently, the pump is a 15 cm piece of 0.125 in outer diameter by 0.006 in. wall thickness type 304 stainless steel tube with a pump section 1.3 cm long flattened to a gap of 0.002-0.003 in. An electromagnet with a gap of 0.02-0.03 inches delivered a magnetic flux density $1x10^{-4}$ I/g Wb/m^2 where I is the total magnet current in amps and g is in meters. Iron pole pieces were electrically isolated from the pump section by 0.001-0.003 in. sheets of mica. The magnet coil and pump were electrically in series [Underwood and Sievers, 1989]. The electric current leaving the module will power the EM pump. The pump will extract only a small percent of the cell power.

There have been problems developing a BASE to metal seal because the BASE tubes operate at temperatures between 1075 and 1275K. One method that has had some success at joining materials of this type at these temperatures is active metal brazing. This process is based on the high chemical activity of one or more of the constituents of the braze filler material that results in compound formation with both the refractory metal structure and the ceramic during the brazing cycle [Underwood and Sievers, 1989]. Effective seals were made by active metal brazing of BASE to Nb or Ta using alloys of TiCuNi, TiNi and TiNiCr. The Ta/TiCuNi/BASE and Nb/TiCuNi/BASE systems were used without failure or observed degradation in a AMTEC recirculating cell test.

The numbers provided in Table 5 are based on a thin Molybdenum electrode with a power density of 0.65 W/cm^2. Molybdenum electrodes are the most well understood of the electrodes and their performance is now highly repeatable. Very thin Molybdenum films, 0.5 micron thick, with overlying current collection grids have exhibited significant increases in stable power densities. Experiments and modeling show that the Molybdenum electrodes are capable of up to 0.7 W/cm^2. Most recently the best 0.5 micron Mo electrodes have given stable power densities of about 0.45 W/cm^2 for 200 hours at about 1160 K [Williams and Nukamura, 1990]. AMTEC is still under development, but should be available in the next few years. Platinum/Tungsten electrodes have produced even higher power densities, but will not be used because less is known about their transport mechanisms; therefore, no predictions of performance are available.

Although AMTEC is currently the most efficient static conversion system it possesses many energy losses. As mentioned earlier, resistance losses are reduced by increasing the mass of the current collector and lead. Conduction losses occur from the evaporator to the radiator shell along the lower insulated segment of the shell. This loss is minimized by making this section wall thin and long. The EM pump magnet also provides a heat loss path, since the permanent magnet must be maintained below its Curie temperature by allowing it to radiate to space. This loss can be controlled by providing

small gaps in the magnet pole pieces in which radiation is the only active mechanism of heat transfer, without significantly reducing the magnetic flux. Radiation heat loss from the heat source and evaporators can be controlled by insulation [Sievers and Bankston, 1988].

5.4 Storage

Power storage in batteries is necessary to provide excess power at peak power operating times. Also, if several blocks of the RTG fail, the batteries could be used to supplement the remaining power plant. The mission progress could be slowed to provide battery recharging whenever necessary. The power output by the RTG is 563 W, and whenever more power is required, the batteries will supply it. Two lithium-titanium-sulfide batteries will be used because they can store the energy needed and withstand the extreme temperature drop during the Martian nights.

6.0 COMMUNICATIONS

6.1 High Frequency Communications

The communications system will enable the MLR to stay in contact with all mission elements, except the Mars Transfer Vehicle. The primary communication will be through the Mars communications satellite that is established as part of this mission. Links will only be made once a day for a maximum of 5 hours per day. The link will be made on the Ka band with a 30 GHz uplink and 20 GHz downlink. The information will be sent at a rate of 64 Kbytes per second.

To enable the communications to operate at the previously stated conditions, a parabolic antenna with a minimum power output of 30 W is required. The size of the MLR's antenna will be a 0.23 m diameter, with a powered, 360° rotating base. The antenna will have a dome over the parabolic dish that will act as a one way mirror, and only be used for high frequency transmission.

The most important communication of the entire mission for the MLR is the receipt of the 1 m resolution picture of the landing site from the Mars Orbiter. So, the optical imaging reception capabilities are quite high on the MLR.

6.2 Low Frequency Communications

The MLR is required to retrieve a mini-rocket if an Aereon is not able to return to the lander to load its samples on the MAV. The retrieval is accomplished through an S-band, low frequency homing beacon. A low-frequency antenna, essentially a small wire like a car radio antenna, will be used to receive the pulses sent by the mini-rocket. The MLR will follow the signal until the mini-rocket is located and get the samples for delivery to the MAV.

The exact procedure that will be performed for the retrieval of the mini-rocket is as follows. The Aereon will communicate to the lander and MLR that the launch of the mini-

rocket is necessary and that the lander should prepare for its delivery; the MLR will finish the sample collections that it was currently performing and prepare for the incoming signal. Upon receiving the signal, the optimum path will be computed and traversed until the Aereon samples have been recovered. The optimum path to the MAV will then be computed and traversed for the delivery of all samples collected by the MLR and Aereon to the MAV.

7.0 THERMAL CONTROL

7.1 Requirements

Since the mission of the rover will extend over a number of years (including the extended mission), a passive thermal control system is not enough to control temperatures for all rover systems. Known requirements are:

- withstand the range of Martian temperatures throughout the mission (180 - 310 K)
- keep all instrumentation at an equilibrium temperature between 300 and 350 K
- keep electrical motor temperatures below 325 K
- increase temperatures in an emergency (Dust storms can create enormous amounts of unwanted convection)
- keep the communications antenna from distorting and bending due to solar radiation and cosmic rays
- keep the external temperature of the rover as low as possible during transit to Mars.

7.2 Passive Elements

In order for the rover to adapt to the large temperature ranges on Mars, an overall thermal control system is needed. Several passive and one active technique will be used to insure that proper temperatures are kept throughout the mission. One simple passive technique that will be used is to paint the outer surface of the rover with white paint containing a nonspherical pigment. A nonspherical pigment creates a radiation pattern that will increase that amount of reflection on a surface over a spherical pigment [Shafey and Kumitomo, 1980].

The second technique will use thermal louvers on the outer structural skin to allow heat radiation and convection to occur from the inside of the structure to the atmosphere. Hwangbo and Kelly suggest the quickest response comes from using a bimetallic actuator,

each metal with a very different coefficient of thermal expansion than the other (thus creating a larger deflection between the two metals when there is a temperature change). The actuators in this system are, in practice, like the closed-loop feedback thermostats found in most homes today (i.e. they are just two different metals bonded together in a coil to create a deflection when there is a temperature change). Finally, the RTG's will be exposed to the Martian atmosphere using convection and radiation to carry off some of the excess heat.

Initial estimates and difficulties with active controls directed the analysis of the thermal control of the antenna towards a more passive system for hindering solar radiation and cosmic ray thermal affects. A number of existing passive controls were studied and a combination of existing systems was decided upon. The resultant system is able to keep heat distortion on the antenna to a minimum.

7.3 Active Systems

The rover's temperature will need to be controlled during transit to Mars, since it is located directly above the fuel tanks in the Mars Lander. The RTG's will have a skin temperature of 600 K and are the only components producing any heat during transit. The internal instrumentation must also be kept warm during transit because of the extreme temperatures in space.

To keep the external temperature of the rover at a minimum during transit, a simple heat pipe/liquid bath configuration is used. Oxygen was chosen as the working fluid for this system through a comparison of several papers dealing with fluids in heat pipes [Wright, 1980; Schlitt et al,1974; and Harwell and Ollendorf, 1980]. The RTG's will be kept in a bath of liquid oxygen that will be contained by a cylindrical pressure vessel at the start of the mission. As the oxygen begins to boil off, it will go through a set of heat pipes that are threaded throughout the MLR. This, in turn, will keep the instrumentation and

motor warm during transit. The condensed gas will then go back to the liquid bath via the wicks in the pipes.

When the MLR is deployed on the surface, the liquid will be pumped into the heat pipes and sealed. The pressure vessel will be removed for radiation and convection to take over the thermal control of the RTG's.

During night operations, the active controls will, depending on the conditions, be operating at low power levels. The controls will then be checked for any problems and self-correcting adjustments will be made at this time.

8.0 SYSTEMS INTEGRATION

After all constraints, requirements, and needs of each of the sub-systems were met, the final details of their integration were accomplished. The navigation computers and sensors are housed throughout the entire structure. The SARS and SES are located on the front cab of the MLR, while the RTG's are located in the aft section. The canisters and the core drill are located in the middle section. Table 6 gives a mass breakdown of all the major subsystems on the MLR. The mass of the Sample Can is seperate, since it is stored in the MAV for the entire mission.

After an estimate of the time required for building, testing, and duplication of the MLR, an estimated cost of $1.1 billion was determined for the successful development of the MLR. This estimate was calculated from an equation given in Appendix 3.

9.0 RECOMMENDATIONS AND CONCLUSIONS

Although the cost estimate for this mission subsystem appears quite high, the overall versatility of the MLR more than proves its worth. The MLR can provide up to four major fuctions in this mission. These include sample acquisition and preservation, Mars surface mapping, Aereon rescue, and basic MLR and lander repair. The subsystems of the MLR are designed for high versatility and reliability so that task encounters can be solved as quickly and efficiently as possible without compromising the the mission requirements or the integrity of the MLR.

More exact analysis is needed in all of the MLR subsystems before the testing phase can be reached. Specifically, advancement in the central computing system must be made before full integration of the MLR's subsytems can be accomplished.

Once these goals have been achieved, and the MLR proves itself in testing, this system should be an effective element in this Mars sample return mission.

Table 1 Mass Breakdown of Samples Collected

Sample	Mass (kg)
Mars Regolith	6
Pebbles	13
Rock Fragments/Chips	10
Boulder Specimens	13
Core Sample	13
Contingency Sample	
Mars Regolith	2
Total	57

Table 2 Regolith Sampling Techniques

Tool	Technique
Mini-coring Drill	Sample small cores of regolith, including frozen sections
Trencher	Digging device to expose and collect deeper soil in a trench
Scoop	Take samples of surface soil
Contact Sampler	Maze trapping of topmost soil grains
Wind Sock	Strains windblown particles from atmosphere (long term)

Table 3 Comparison of Canister Shapes*

Requirement	Cylinder	Hexagon
Stress accommodation	good	fair
Deflection accommodation	fair	good
Samples intact	good	good
Reflection characteristics	fair	excellent
Volume efficiency	fair	excellent
Mass Efficiency	good	good
Handling by robotic arms	fair	good
Isolation of samples	good	good

*all comparisons are with respect to each other

Table 4 Operating Characteristics of Radioisotopes Powered AMTEC System Concept

Total thermal power (W)	2864
GPHS surface temp (K)	1261
BASE temp (K)	1200
Condenser temp (K)	606
BASE thickness (mm)	0.8
Electrode emissivity	0.7
Condenser emissivity	0.05
Heat shield emissivity	0.2
Module voltage	0.68
BASE current density (A/cm^2)	0.65
Number of modules	56
Diameter of BASE (cm)	0.8
Length of BASE tubes (cm)	9.0
Net electrical power (W)	563
System efficiency (%)	14.1
Total mass of system (kg)	42.9
System specific power (W/kg)	13.1

Table 5 Mass Breakdown of AMTEC Power Source

Component	Mass (kg)
GPHS	23.2
Multi-foil insulation	3.2
Aluminum support structure	3.9
Ceramic module supports	2.9
Module evaporators	2.0
BASE tubes	0.4
Inner and outer current collectors	1.1
Leads	0.8
Condenser shell	2.5
EM pumps	2.9
TOTAL	42.9

Table 6 Mass Breakdown of Mars Land Rover

Subsystem	Mass (kg)
SARS (loaded with samples)	250
(dry at launch)	50
Mobility	250
(includes drive train, tires, motor, etc.)	
Power Source	43
Thermal Control	75
Structure	332
Total	950 (loaded)
	750 (dry)
Sample Can (with canisters)	150

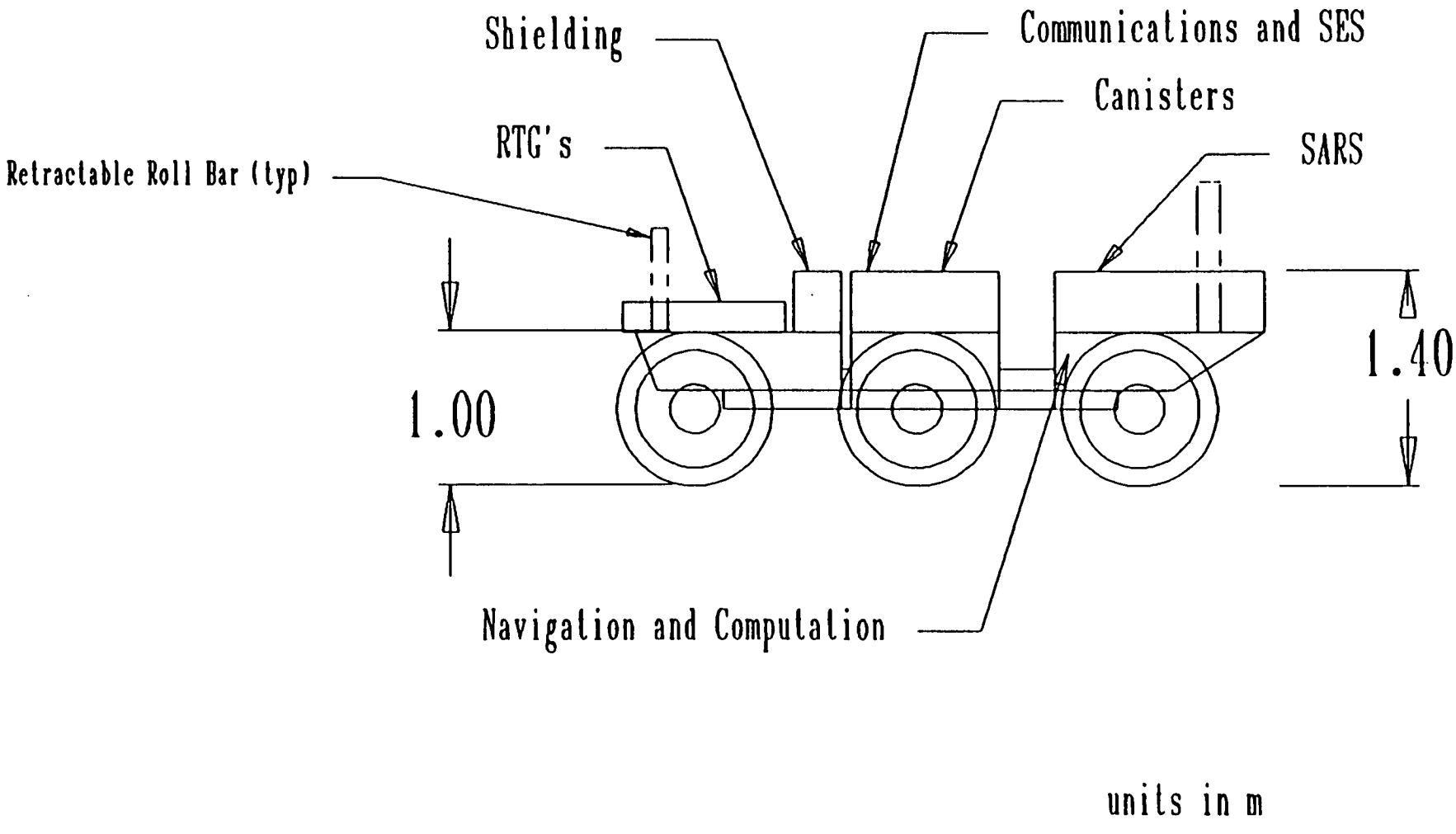

Figure 1: Basic Design of the Mars Land Rover (MLR)

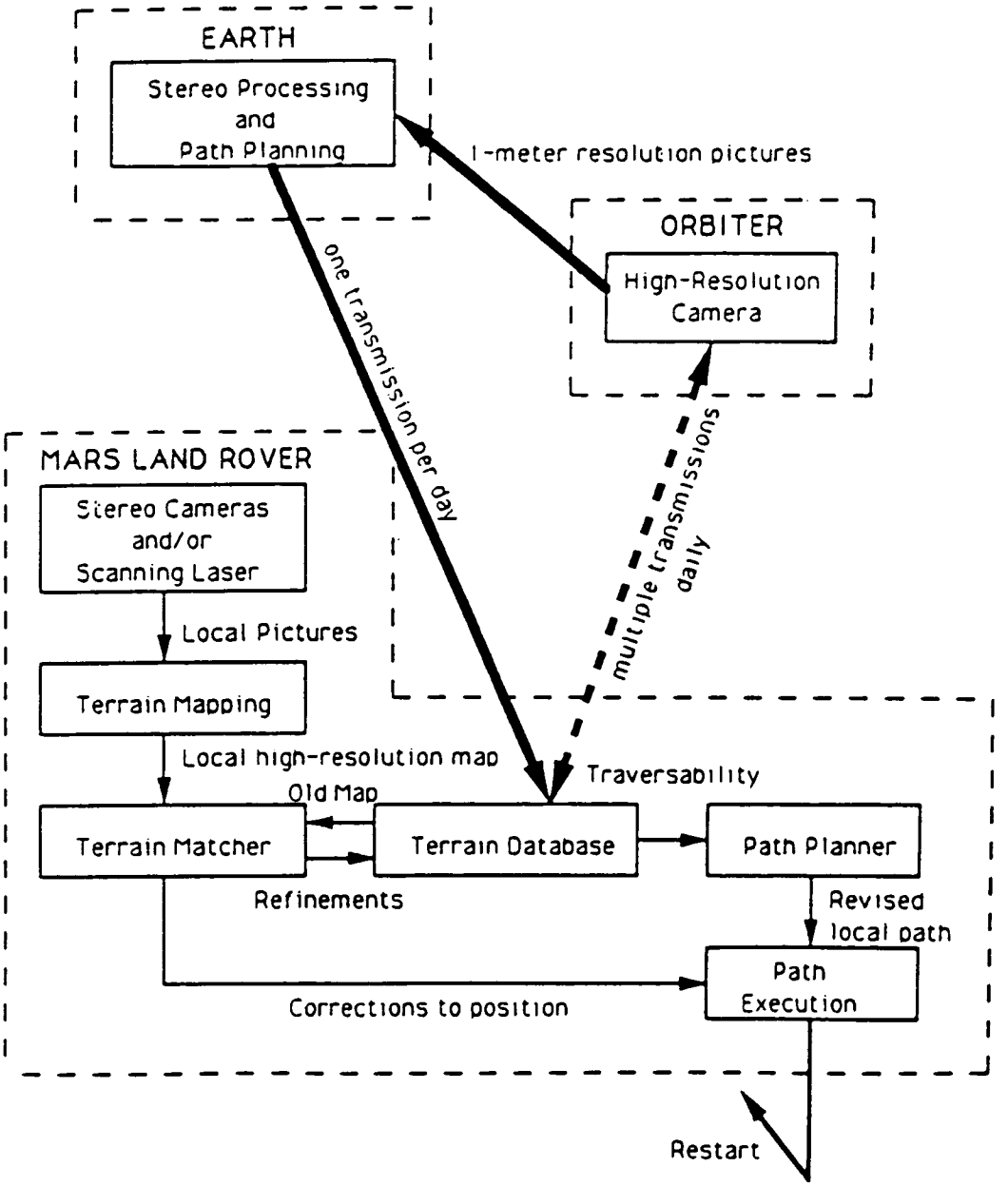

Figure 2: Navigation Algorithm
(B. Wilcox, et al, 1987)

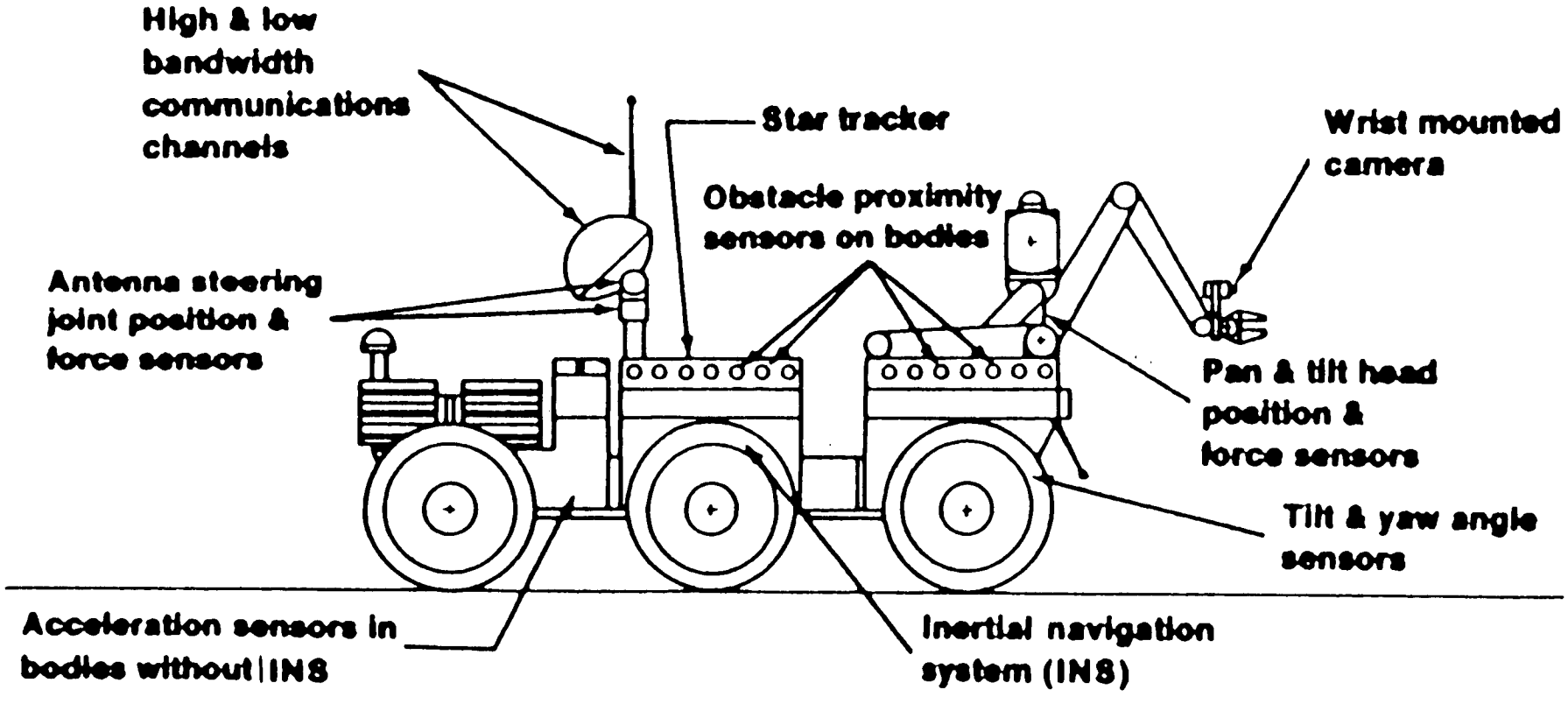

Figure 3: Navigation Systems - Side View
(McTamaney and Douglas, 1988)

Figure 4: Navigation Systems - Top View
(McTamaney and Douglas, 1988)

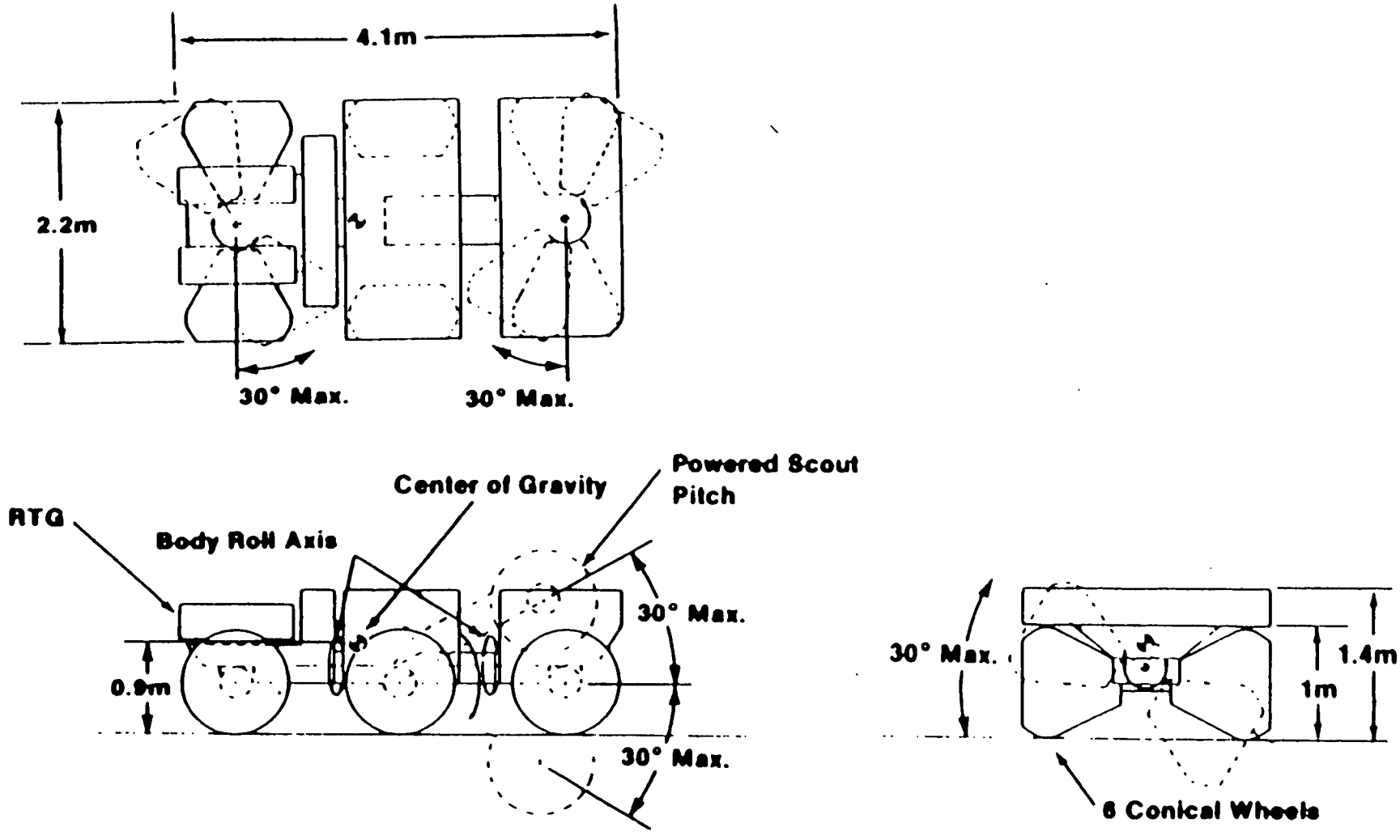

Figure 5: Mobility Concept
(McTamaney and Douglas, 1988)

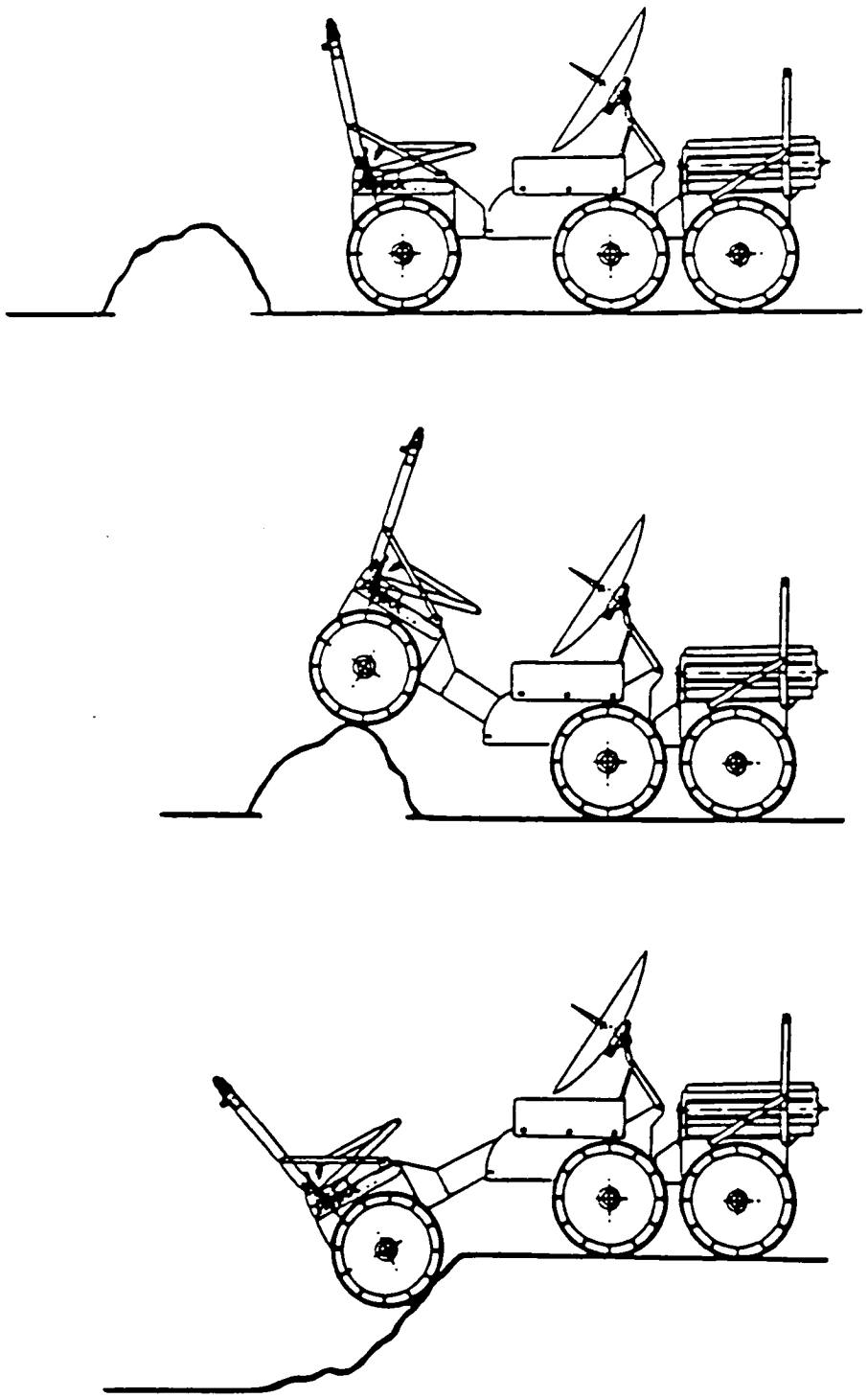

Figure 6: Step Ascension and Descension
(McTamaney, 1989)

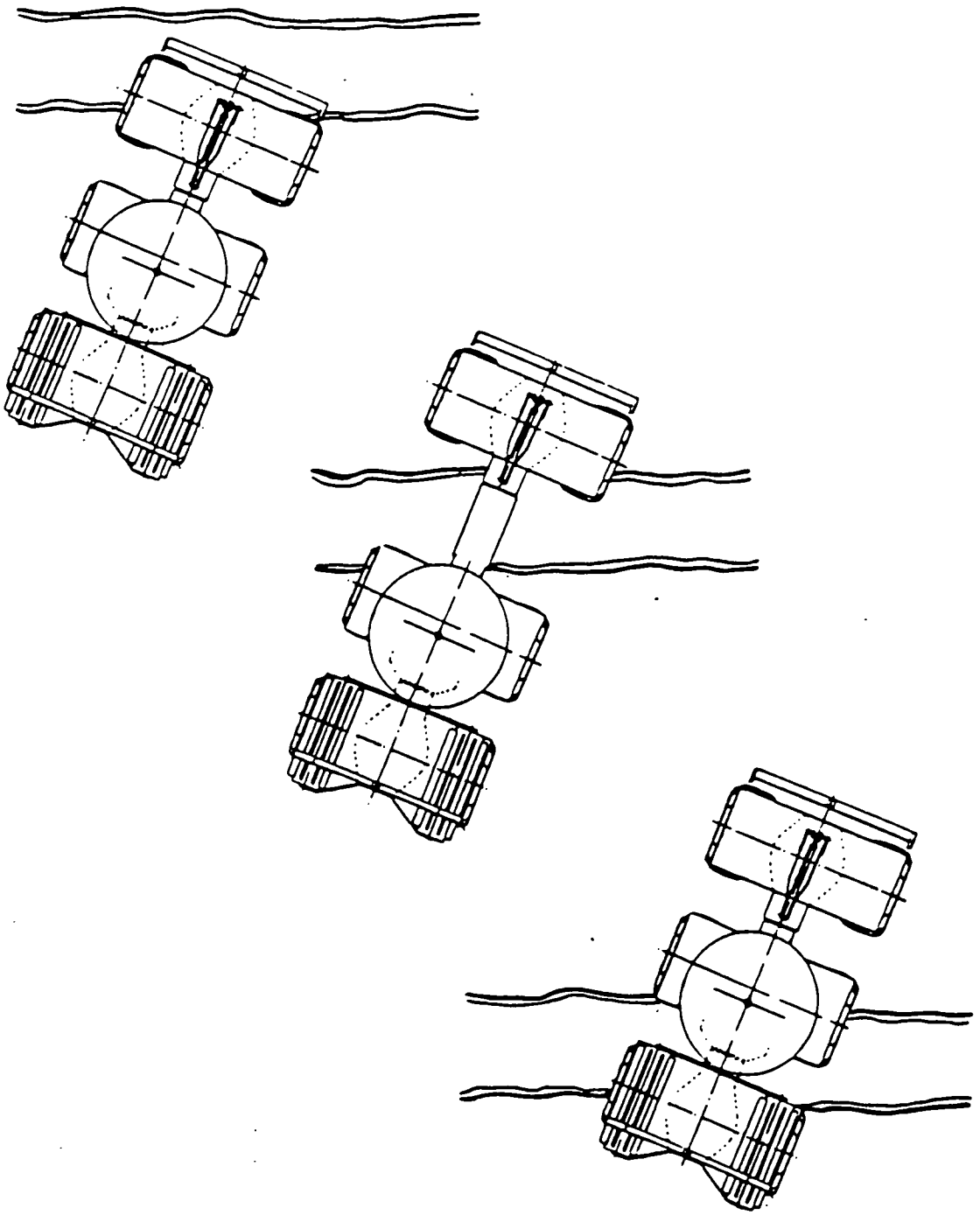

Figure 7a: Crevasse Traversal
(McTamaney, 1989)

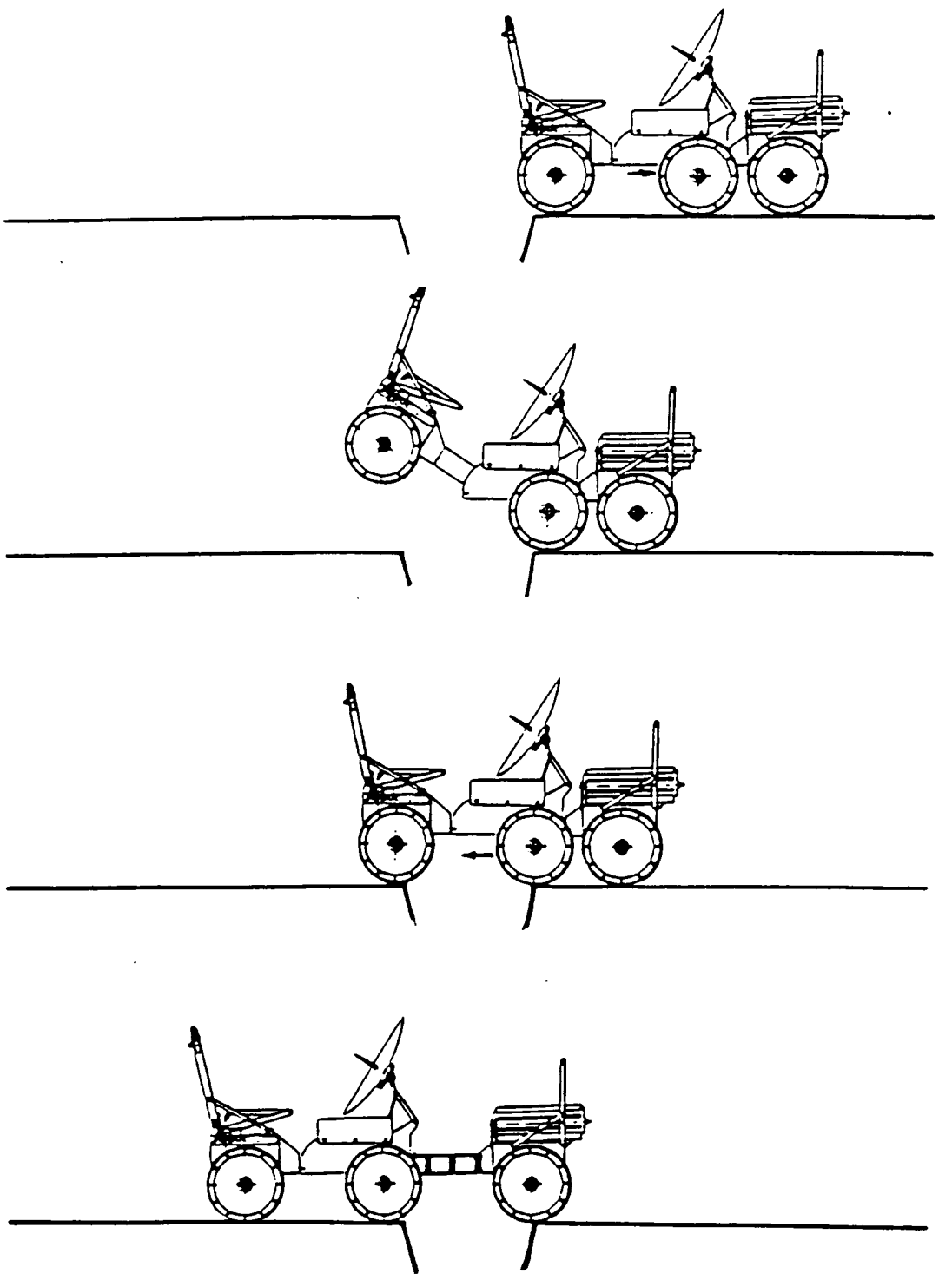

Figure 7b: Crevasse Traversal
(McTamaney, 1989)

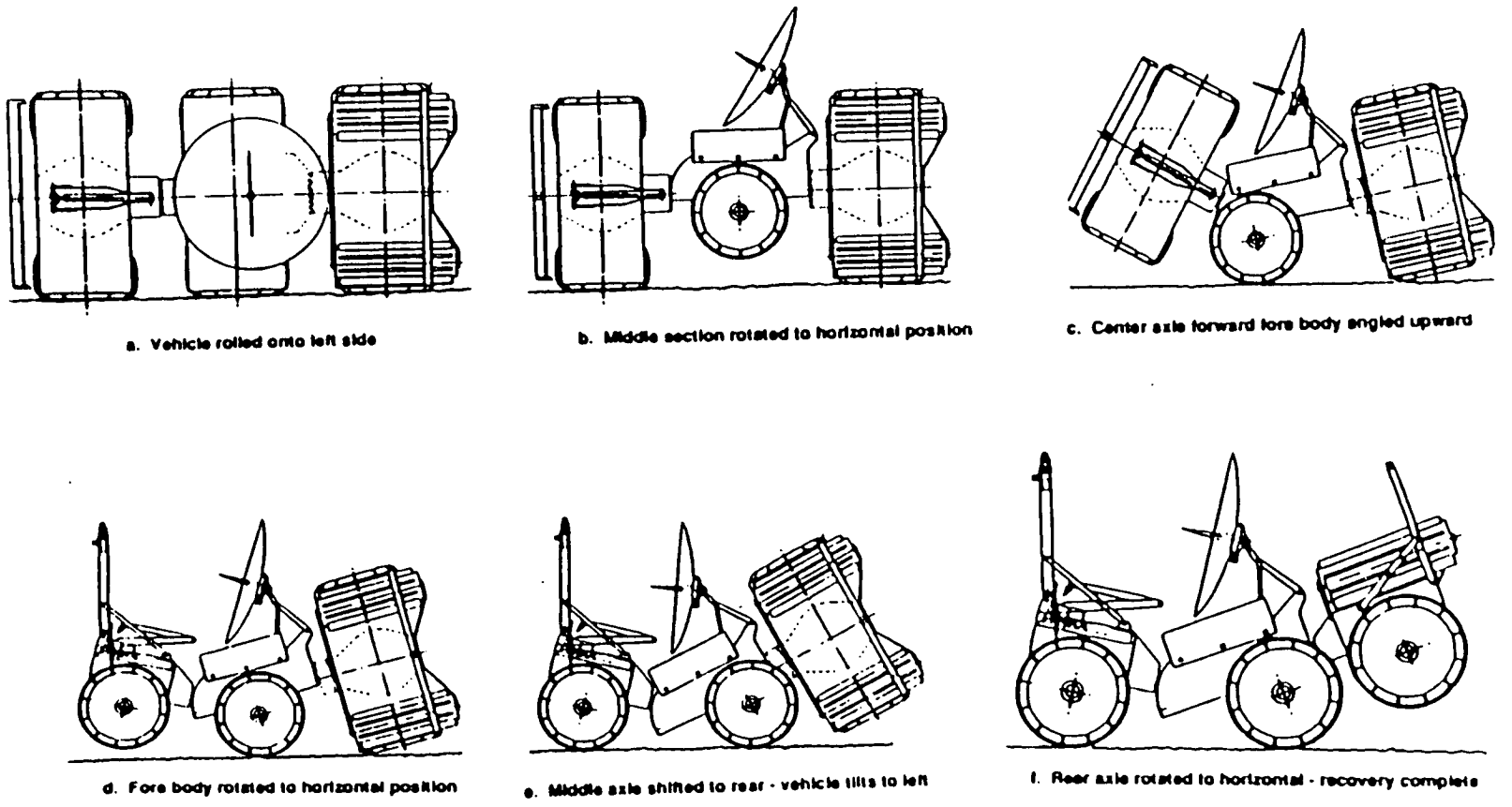

Figure 8: Roll-Over Recovery
(McTamaney, 1989)

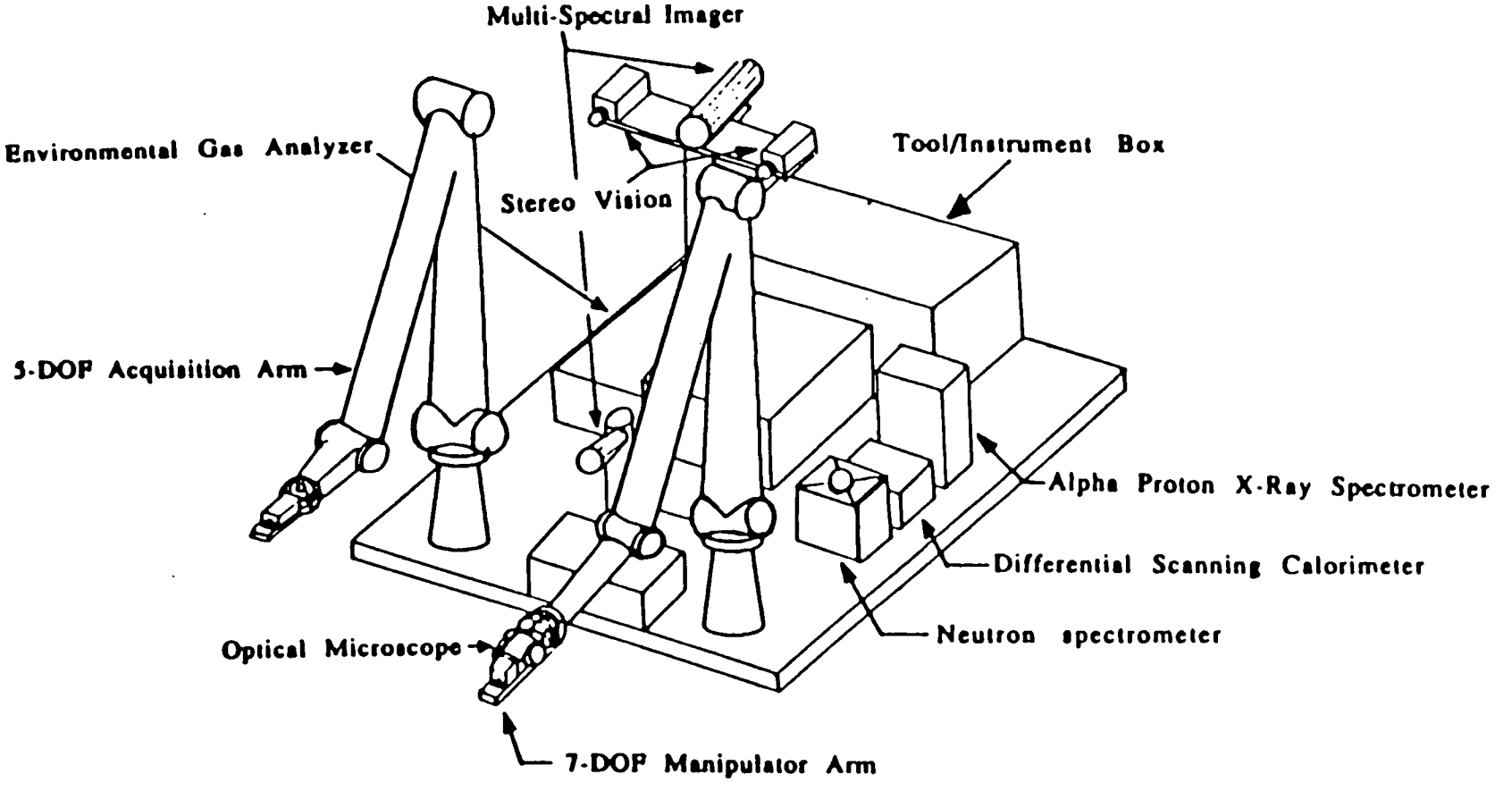

Figure 9: Sample Acquisition Robotic System (SARS)

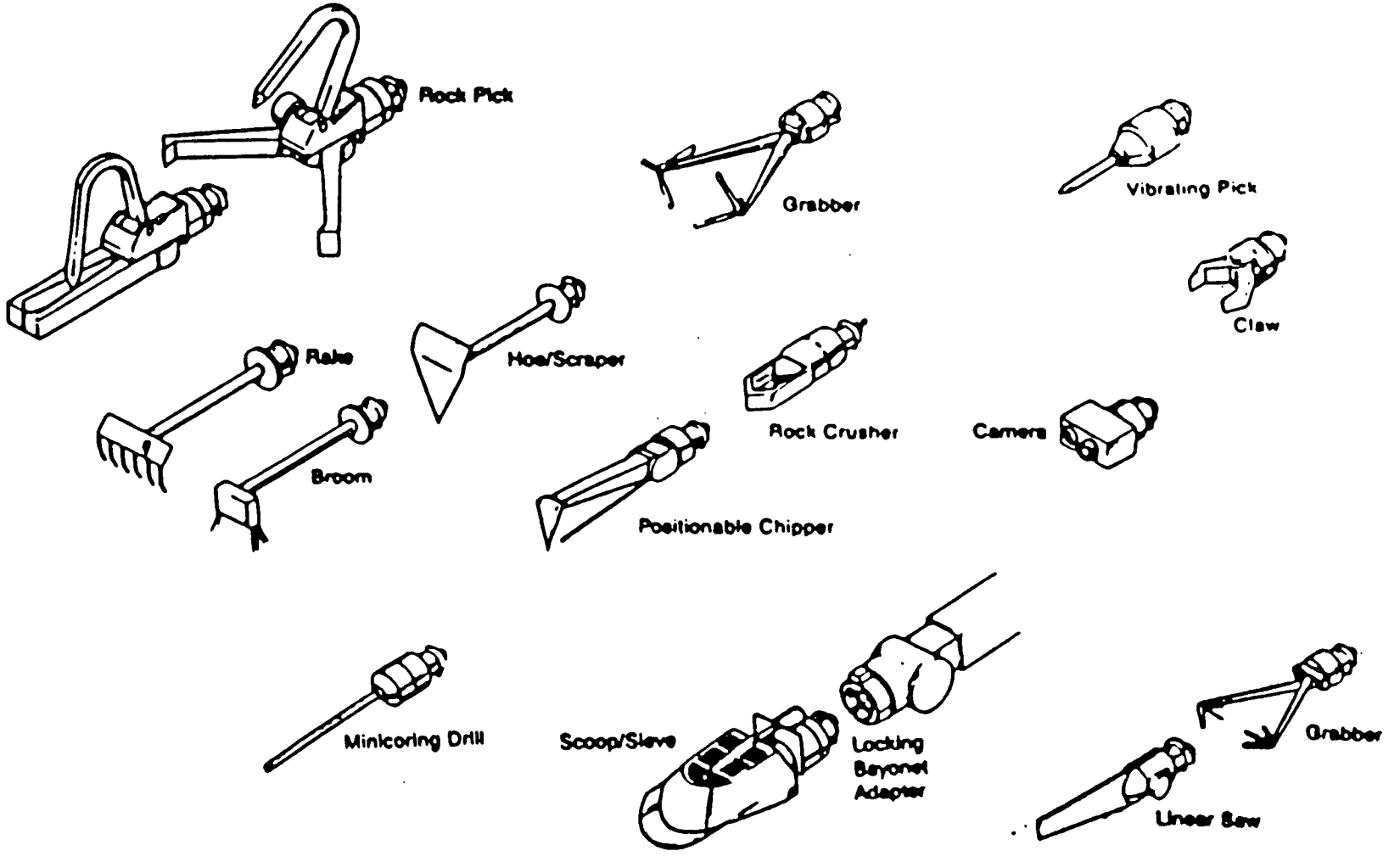

Figure 10: Instrument/Tool Kit
(Clark and Amundsen, 1987)

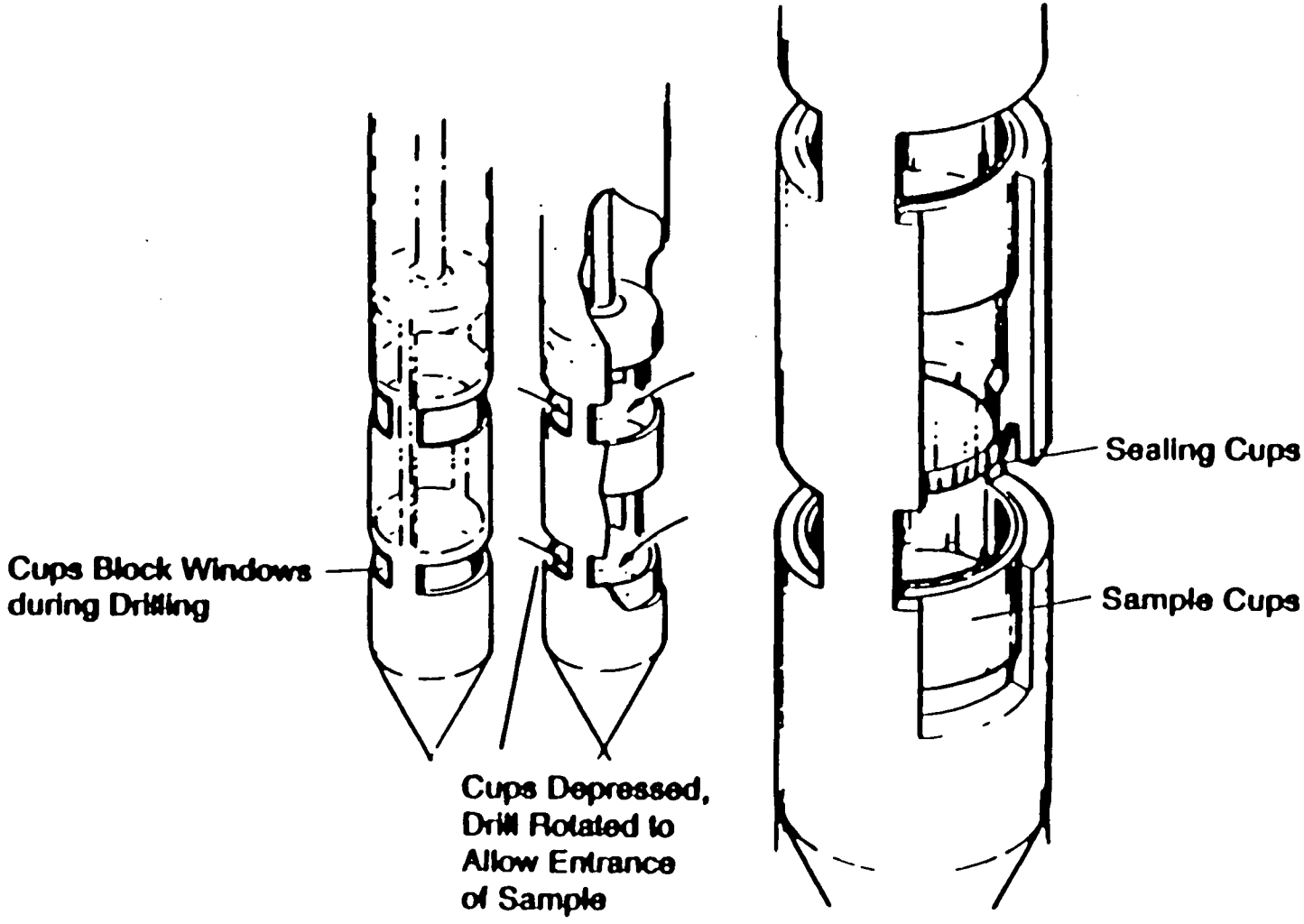

Figure 11: Sand Drill
(Clark and Amundsen, 1987)

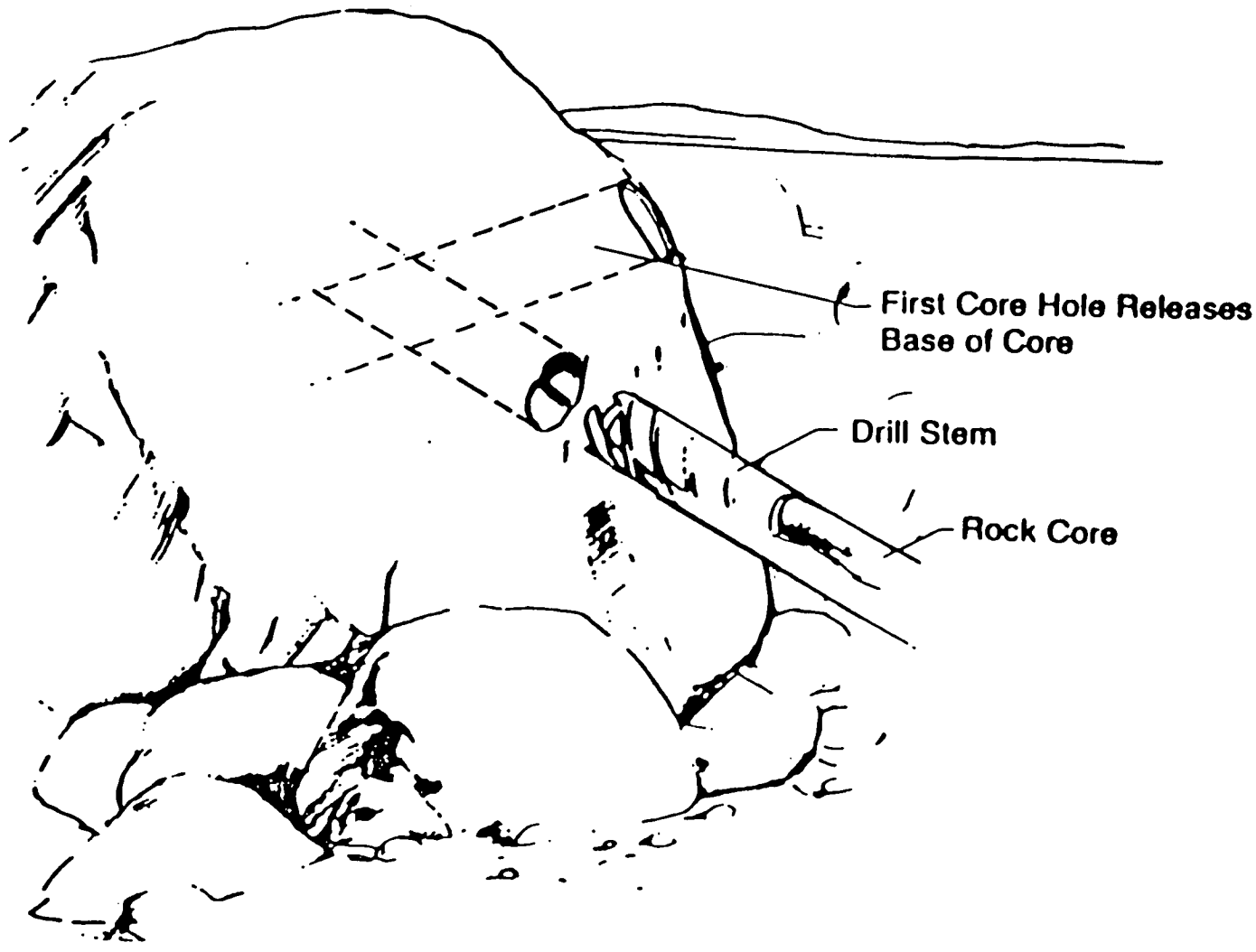

Figure 12: Rock Drilling Procedure
(Clark and Amundsen, 1987)

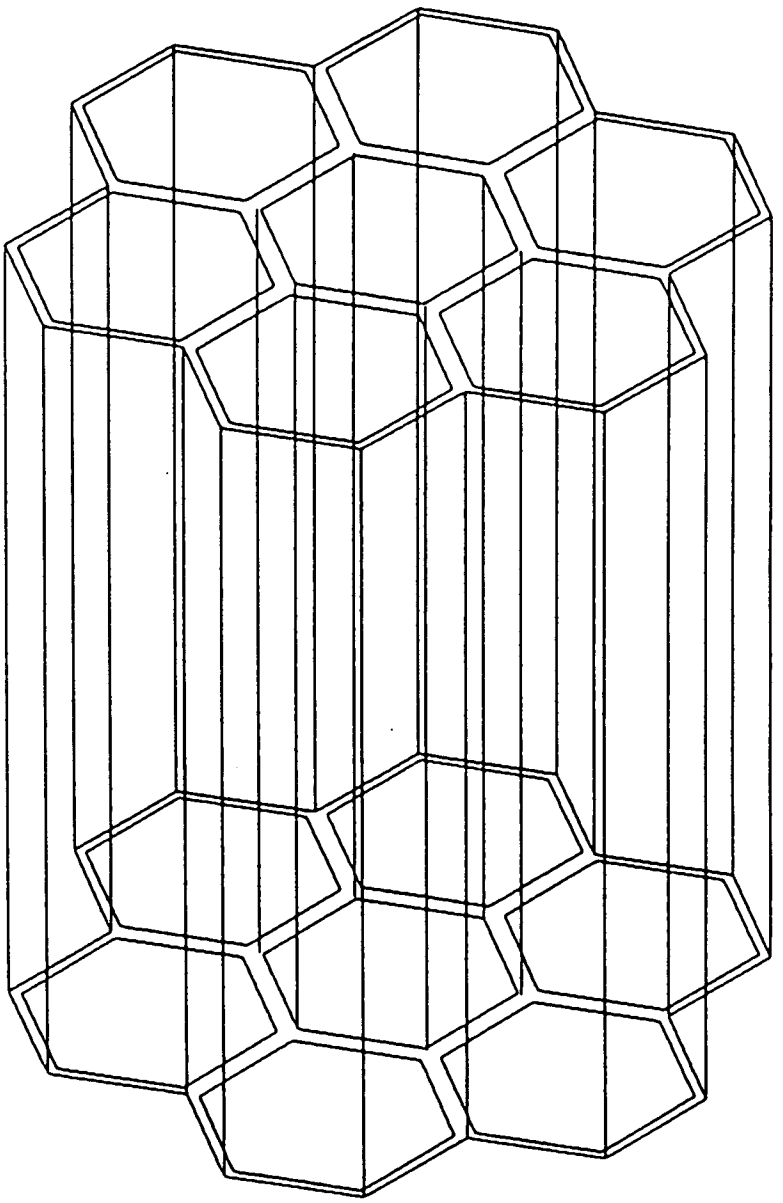

Figure 13a: Seven Hexagon Canister System

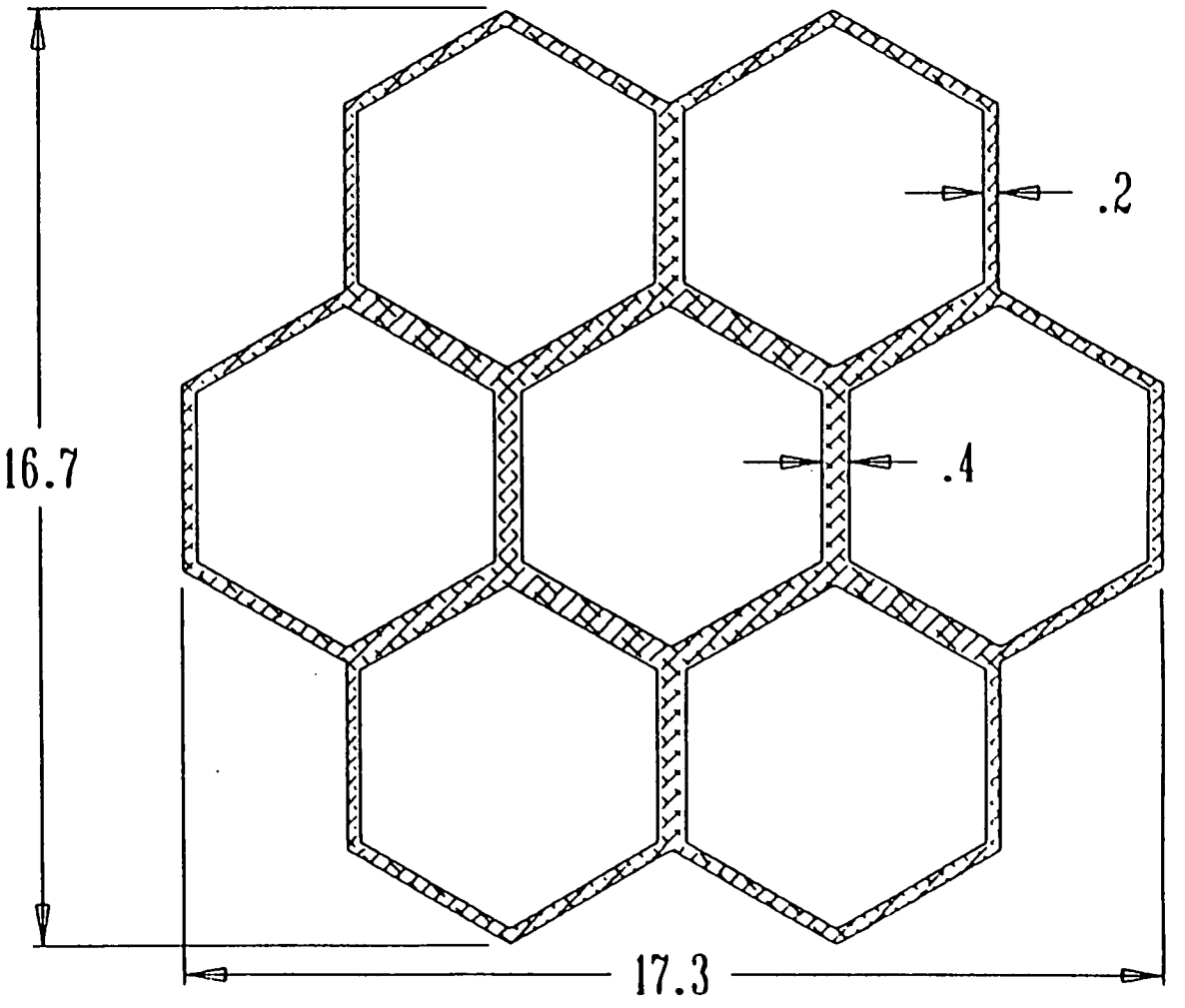

Figure 13b: Seven Hexagon Canister System - Top View

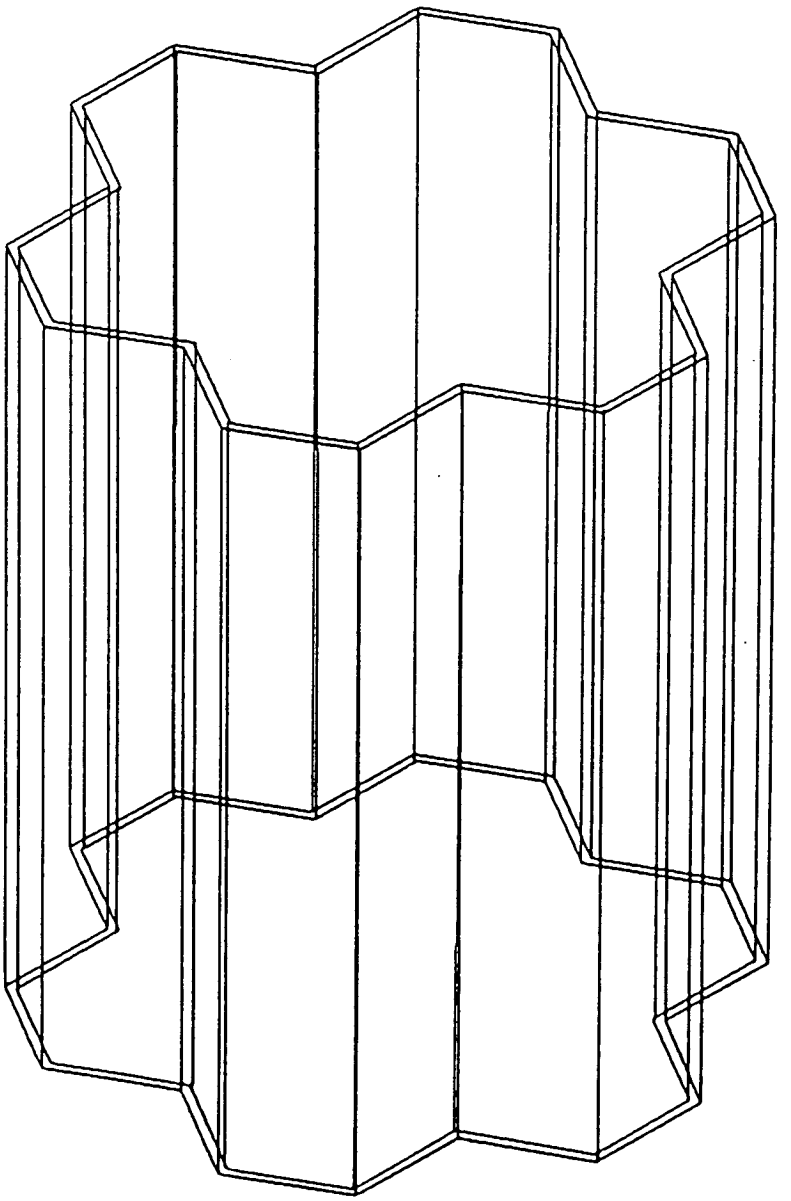

Figure 14: Large Hexagon Canister

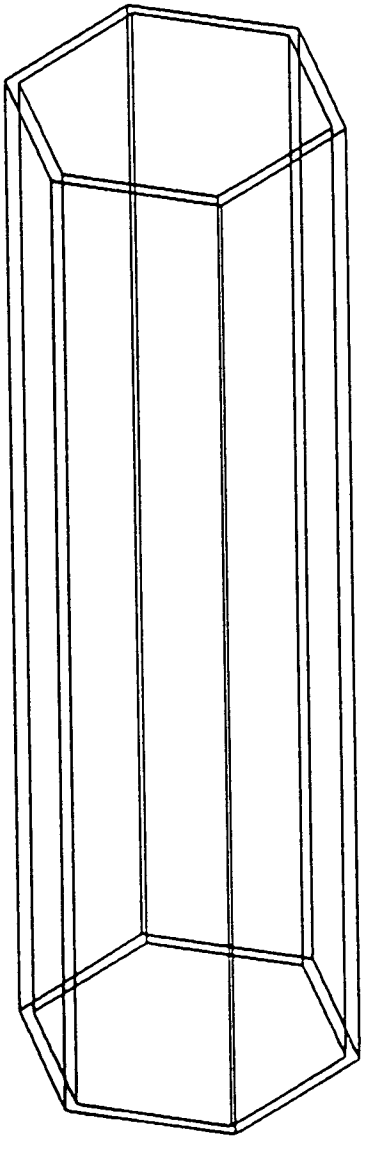

Figure 15: Single Hexagon Canister

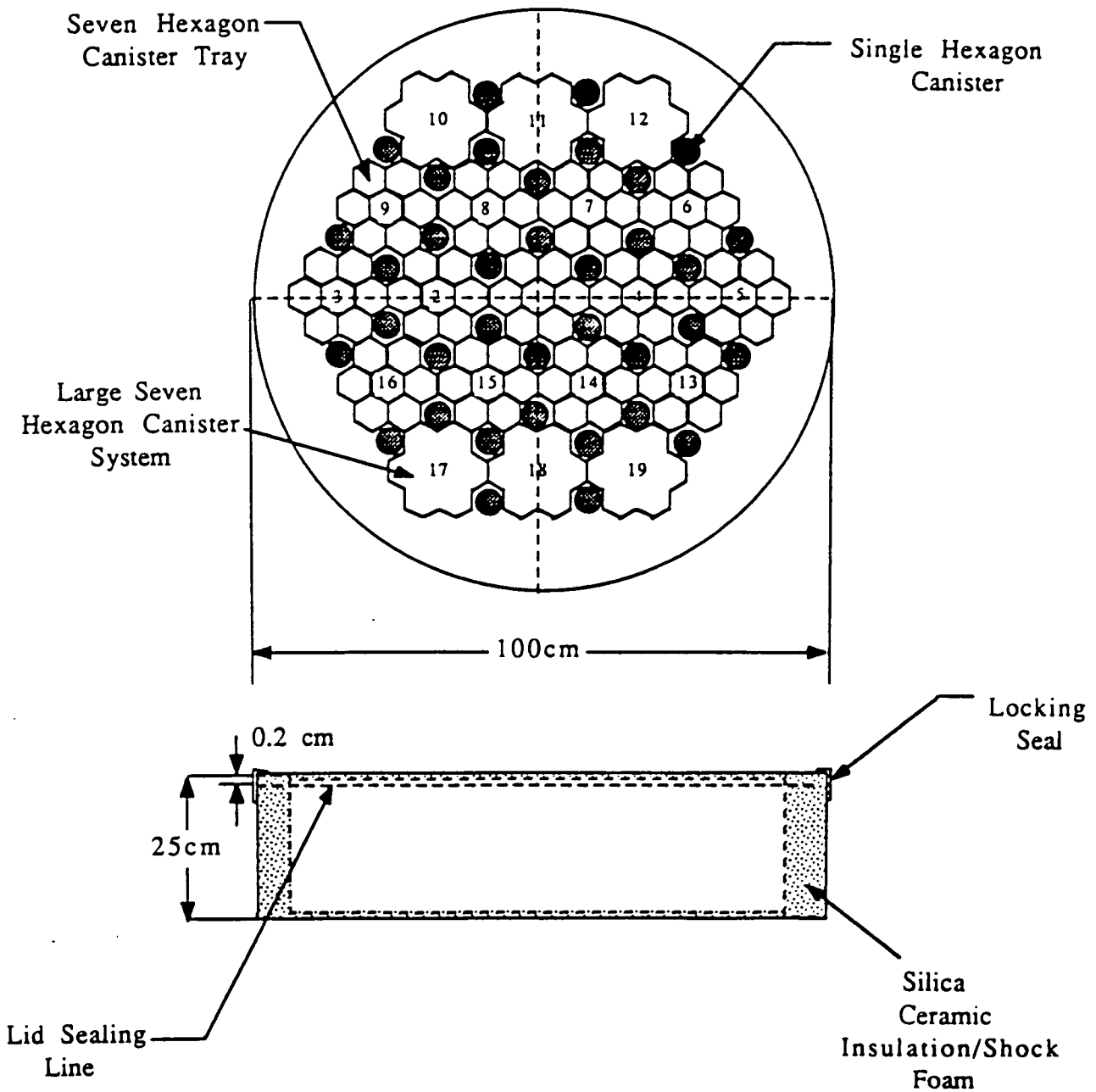

Figure 16: Sample Can

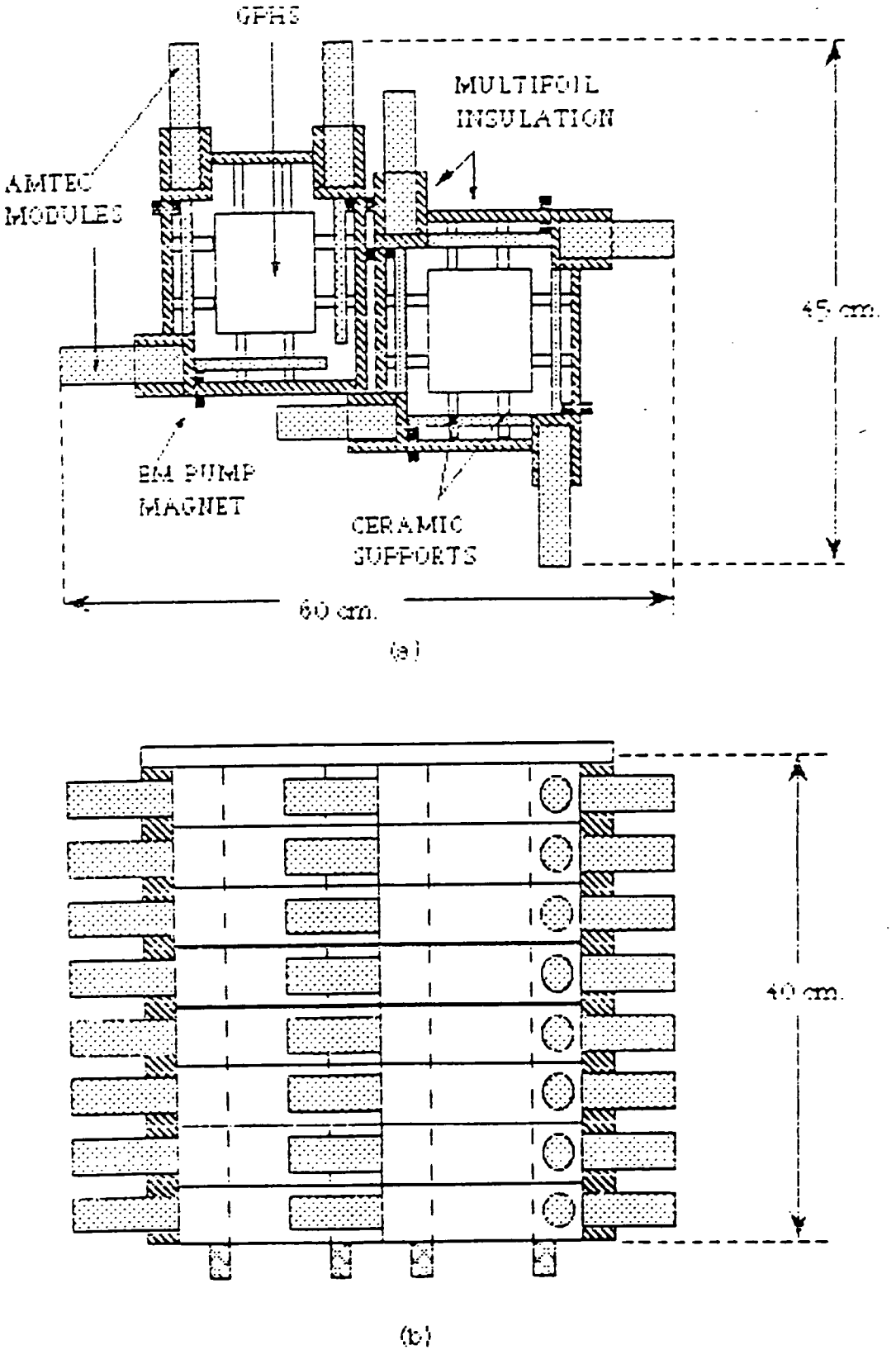

Figure 17: RTG Design - (a) Top View, (b) Side View

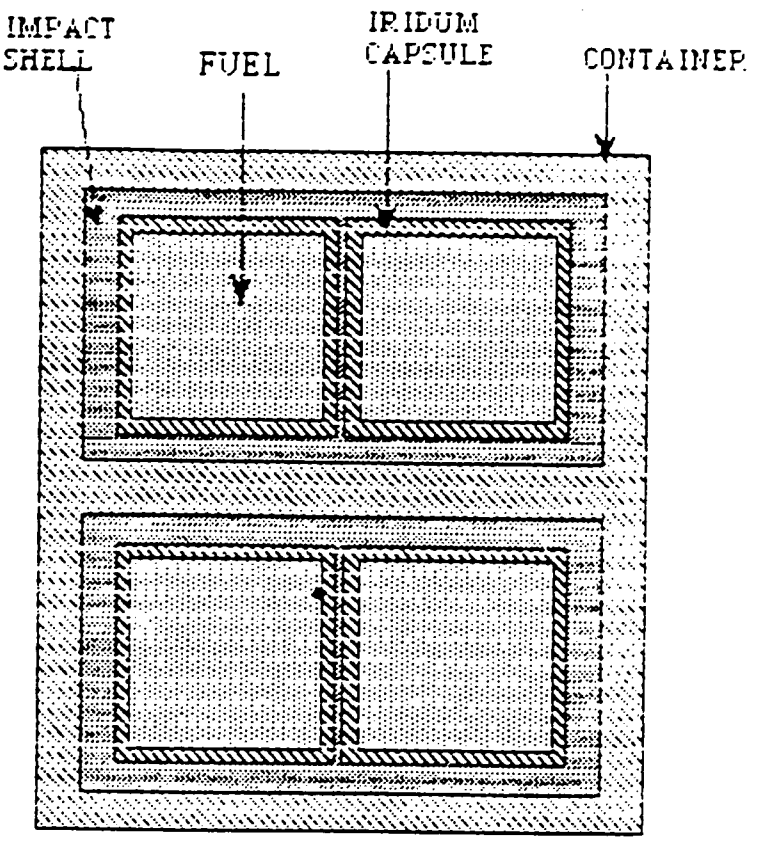

Figure 18: General Purpose Heat Source
(Schock, 1981)

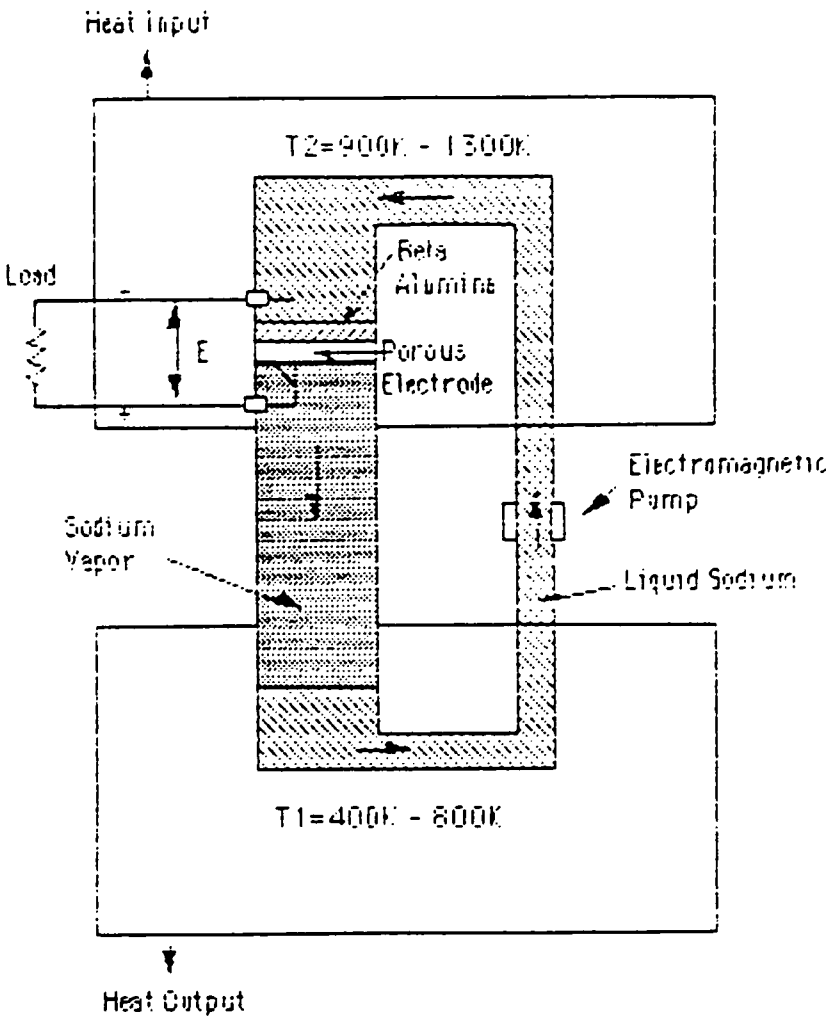

Figure 19: AMTEC Cycle
(Bankston and Williams, 1988)

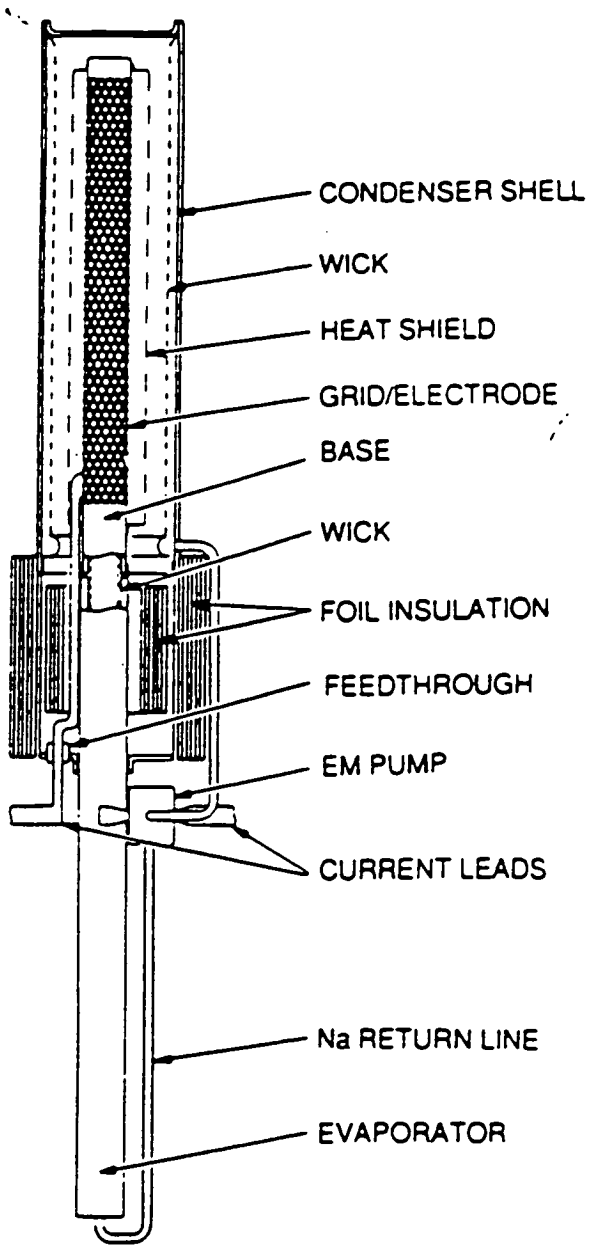

Figure 20: AMTEC Module Configuration
(Sievers Bankston, 1988)

REFERENCES

Acker, W. L., Basic Procedures for Soil Sampling and Core Drilling, Acker Drill Co. Inc., Pennsylvania, 1974.

Agrawal, Brij N., Design of Geosynchronous Spacecraft, Prentice-Hall Inc., Englewood Cliffs, New Jersey, 1986, Chapter 5.

AIAA, "Aerospace Design Engineers Guide," American Institute of Aeronautics and Astronautics, New York, New York, 1987.

Allen, David H. and Walter E. Haisler, Introduction to Aerospace Structural Analysis, John Wiley & Sons, New York, New York, 1985.

Bankston, C.P., et al,"Recent advances in Alkali Metal Thermoelectric Converter (AMTEC) electrode performance and modeling", Space Structures, Power, and Power Conditioning, Proceeding of SPIE Vol. 871, 1988, pp 64-67.

Bents, David J., (NASA Lewis Research Center), "Preliminary Assessment of Rover Power Systems for the Mars Rover Sample Return Mission", 1989.

Brennan, P.J., M.J. Suelau, R. McIntosh, "Low-Temperature Phase-Change Material Package," AIAA paper 77-762, presented at the 12th Thermophysics Conference, Albuquerque, New Mexico, June 27-29, 1977.

Brown, Theodore L. and H. Eugene Lemay Jr., Chemistry, The Central Science, Prentice-Hall Inc, Englewood Cliffs, New Jersey, copyright 1985.

Chielewski, A.B.,"Improved Techniques for Predicting Spacecraft Power", Energy-New Frontiers, Vol. 1, 1987, pp 392-395.

Clark, B. C. and R. J. Amondsen, "Study of Sampling Systems for Comets and Mars," NASA paper N89-29292, final report prepared by Martin Marietta, March 1987.

Clark, S.C. and G.E. Allen, "Thermo-Mechanical Design and Analysis System for the Hughes 76-in. Parabolic Antenna Reflector," AIAA paper 82-0864, presented at the 3rd AIAA/ASME Joint Thermophysics, Fluids, Plasma & Heat Transfer Conference, St. Louis, Mo., June 7-11, 1982.

Cockfield, R.D., Hartman, R.F and Kelly, C.E, "RTG Power sources for the International Solar Polar Mission," 1980 Intersociety Energy Conversion, Vol. 2.

Foldes, P. and M.W. Dienemann, "Large Multibeam Antennas for Space," Jouranl of Spacecraft and Rockets, Vol. 17, July-Aug. 1980, pp. 363-371.

Glaser, Peter E., Igor A. Black, Richard S. Lindstrom, Frank E. Ruccia, and Alfred E. Wechsler, "Thermal Insulation Systems," NASA SP-5027, 1967.

Gumenskii, B.M. and Komarov, N. S., Soil Drilling by Vibration, Consultants Bureau, New York, 1961.

Harwell, W. and S. Ollendorf, "The Heat Pipe Thermal Canister," AIAA paper 80-1461, presented at the AIAA 15th Thermophysics Conference, Snowmass, Co., July 14-16, 1980.

Harwell, W., R. Haslett, and S. Ollendorf, "Instrument Canister Thermal Control," AIAA paper 77-761, presented at the 12th Thermophysics Conference, Albuquerque, New Mexico, June 27-29, 1977.

Hwangbo, Han and W.H. Kelly, "Transient Response of Thermal Louvers with Bimetallic Actuators," AIAA paper 80-1539, presented at the AIAA 15th Thermophysics Conference, Snowmass, Co., July 14-16, 1980.

Kelley, C., "Cost Estimating Methods for Advanced Space Systems," SAWE Paper No. 1856, 1988.

Lehtinen, A.M., "Controllability Analysis for Passively and Actively Controlled Heat Pipes," AIAA paper 77-776, presented at the 12th Thermophysics Conference, Albuquerque, New Mexico, June 27-29, 1977.

McTamaney, L. S. and Douglas, B. D., "Mars Rover Concept Development," SPIE Paper 1007-13, Presented at Mobile Robots III Conference, Cambridge, Massachusetts, November 10-11, 1988.

MIL HDBK-5D, Metallic Materials and Elements for Aerospace Vehicle Structures.

MIL HDBK-251, Reliability/Design Thermal Applications.

Padgett, David L. and Leroy S. Fletcher, "The Thermal Contact Conductance of Dissimilar Metals," AIAA paper 82-0885, presented at the 3rd AIAA/ASME Joint Thermophysics, Fluids, Plasma & Heat Transfer Conference, St. Louis, Mo., June 7-11, 1982.

Schlitt, K.R., P.J. Brennan and J.P. Kirkpatrick,"Parametric Performance of Extruded Axial Grooved Heat Pipes from 100^{o} to 300^{o}K", AIAA paper 74-724, presented at the AIAA/ASME Thermophysics and Heat Transfer Conference, Boston, Mass., July 15-17 1974.

Schiller, Zvi and J. C. Chen, "Optimal Motion of Autonomous Vehicles in Three Dimensional Terrains," Proceedings of the 1990 IEEE International Conference on Robotics and Automation, May 13-18, 1990, Cincinnatti, Ohio.

Schneider, P. J., "Correlation of Low-Density Thermal-Protection Materials in Mild Heating Environments," AIAA paper 74-77, presented at the 12th Aerospace Sciences Meeting, Washington D.C., Jan 30-Feb 1,1974.

Schock, A., "Modular Isotopic Thermoelectric Generator", 1981 Intersociety Energy Conversion, Vol. 1.

Shafey, Hamdy M. and Takeshi Kunitomo, "Radiative Properties of a Painted Layer Containing Nonspherical Pigment," AIAA paper 80-1521, presented at the AIAA 15th Thermophysics Conference, Snowmass, Co., July 14-16, 1980.

Shirbacheh, M.,"Small Reactor Power Systems for Space Application", Energy-New Frontiers , Vol. 1, 1987, pp 396-400.

Sievers, R.K., Bankston, C.P., "Radioisotope Powered Alkali Metal Thermoelectric Converter Design for Space Systems", Proceedings of the 23rd Intersociety Energy Conversion Engineering Conference, Vol. 3, 1988, pp 159-167.

Steele, W. H. and H. B. McKee, "A Precise Satellite Thermal Control System Using Cascaded Heat Pipes," AIAA paper 77-777, presented at the 12th Thermophysics Conference, Albuquerque, New Mexico, June 27-29, 1977.

Underwood, M.L., Sievers, R.K., "AMTEC Recirculating Test Cell Component Testing and Operation", Proceedings of the 24th Intersociety Energy Conversion Engineering Conference, Vol. 6, 1989, pp 2833-2839.

Van Wylen, Gorden J. and Richard E. Sonntag, Fundamentals of Classical Thermodynamics, John Wiley & Sons, New York, New York, copyright 1985.

Williams, R.M., Jeffries-Nakamura, B., "Lifetime Studies of High Power Rhodium/Tungsten and Molybdenum Electrodes for Application to AMTEC", Proceedings of the 25th Intersociety Energy Conversion Engineering Conference, Vol. 2, 1990, pp 413-419.

Wright, J.P., "Development of a 5 W 70 K Passive Radiator," AIAA paper 80-1512, presented at the AIAA 15th Thermophysics Conference, Snowmass, Co., July 14-16, 1988.

Appendix 1: Mobility Constraints

Dynamic constraints are an important consideration for this rover system, since terrain conditions are unknown and rover operations are not necessarily performed by human operators. The constraints to which the rover must conform can be represented by a series of equations that the rover's sensing and computing systems can follow [Schiller and Chen, 1990].

To set up the constraints, the following set of vectors are needed:

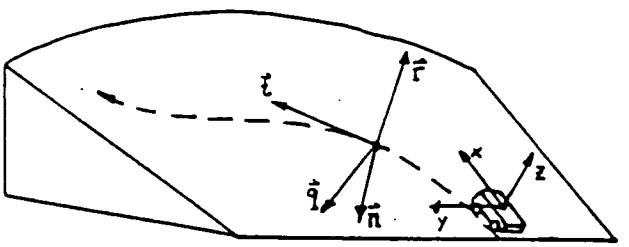

n - radius of curvature

q - rover's y-axis rotation

r - path normal

t - path tangent

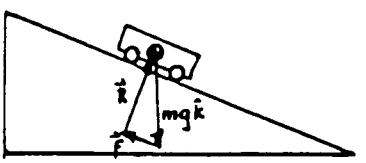

R - reaction force

F - friction force

mg k - gravitational force

Figure A1: Vehicle Reference Frame and Force Diagram

Now paramaterizing by a distance "S" at point "P":

$$\vec{t}=\frac{dP}{dS} \qquad \vec{n}=\frac{\kappa d^2P}{dS^2} \qquad \kappa=\frac{1}{|\vec{n}|_P} \tag{1}$$

yields the following equation of motion:

$$f_t\vec{t}+f_q\vec{q}+R\vec{r}-mg\hat{k}=mk\vec{n}\dot{S}^2+m\vec{q}\ddot{S} \tag{2}$$

and friction and normal forces:

$$f_t = mgk_t + m\ddot{S} \tag{3}$$

$$f_q = mgk_q + mkn_q\dot{S}^2 \tag{4}$$

$$R = mgk_t + mkn_t\dot{S}^2 \tag{5}$$

where:

$$\vec{F} = f_t\hat{t} + f_q\vec{q} \tag{6}$$

Now the dynamic constraints can be set up.

Engine Torque: The torque applied by the engine on the wheel translates to a friction force f_t applied between the wheel and the ground. Positive torque is applied in the direction of motion, while negative torque is applied in the opposite direction. These represent the maximum equivalent engine force and the maximum braking force respectively.

$$F_{min} \le f_t \le F_{max} \tag{7}$$

Substituting equations (3)-(5) into (7) yields:

$$\frac{F_{min}}{m} - gk_t \le \ddot{S} \le \frac{F_{max}}{m} - gk_t \tag{8}$$

These limits can be assumed constant and independent of rover speed.

Sliding: This constraint is a function of the friction force between the wheels and the surface being traversed. The following equation can be used to represent the maximum friction force relative to the normal reaction force and the coefficient of friction, respectively:

$$F^2 = f_t^2 + f_q^2 \le \mu^2 R^2 \tag{9}$$

If this equation is violated, the vehicle will slide.
Substituting equations (4)-(6) into equations (9) yields the following quadratic inequality:

$$\ddot{S}^2 + 2gk_t\ddot{S} + \kappa\left(n_q^2 - \mu^2 n_r^2\right)\dot{S}^4 + 2g\kappa\left(k_q n_q - \mu^2 k_r n_r\right)\dot{S}^2 + g^2\left(k_q^2 + k_t^2 - \mu^2 k_r^2\right) \le 0 \tag{10}$$

Now the sliding constraint becomes a function of velocity, acceleration, and path geometry. The feasible acceleration or deceleration of the rover is obtained by solving for the acceleration:

$$\ddot{S}_{dec} \leq \ddot{S} \leq \ddot{S}_{acc} \tag{11}$$

where:

$$S_{dec} = gk_t - \sqrt{a\dot{S}^4 + 2b\dot{S}^2 + c} \tag{12}$$

$$S_{acc} = gk_t + \sqrt{a\dot{S}^4 + 2b\dot{S}^2 + c} \tag{13}$$

and

$$\begin{aligned} a &= \kappa^2\left(\mu^2 n_r^2 - n_q^2\right) \\ b &= g\kappa\left(\mu^2 k_r n_r^2 - k_q n_q\right) \\ c &= g^2\left(\mu^2 k_r - k_q^2\right) \end{aligned} \tag{14}$$

There is also a limit on the acceleration from the velocity, because the value under the square root must always be non-negative, which is represented by equation (14).

$$\Delta = a\dot{S}^4 + 2b\dot{S}^2 + c \geq 0 \tag{15}$$

Contact: This constraint becomes a necessity at higher vehicle velocities because if the vehicle loses contact with the ground due to terrain irregularities, tip-over can occur. Using equation (5) a limit for the vehicle's range of velocity is found to be:

$$\dot{S}^2 \leq \frac{-gk_r}{\kappa n_r} \tag{16}$$

Note that k_r is always positive to avoid any inverted slope condition.

Tip-Over: Again velocity becomes a limit depending on the aspect ratio (height to width) of the vehicle. The reaction and friction forces in this constraint are combined for all wheels into two equivalent forces to simplify the governing equations. The force equation is written as follows:

$$f_q^2 \leq \left(R\frac{b}{h}\right)^2 \tag{17}$$

Substituting equations (5) and (8) into (17) yields the final velocity limiting equation:

$$\kappa^2\left(n_q^2-\beta^2 n_r^2\right)\dot{S}^4+2g\kappa\left(k_q n_q-\beta^2 k_r n_r\right)\dot{S}^2+g^2\left(k_q^2+\beta^2 k_r^2\right)\leq 0 \tag{18}$$

where $\beta = (b/h)$.

Appendix 2: Calculation of Canister Properties

The body of the text gives the results for picking the general shape of the canisters for the samples. Since the hexagon canister was chosen, all the property calculations were done using the hexagon shape. The thickness of each hexagon, the height of the canister, the thickness of the top and bottom caps, and the mass of each canister were assumed all unknown and therefore varied in all calculations to allow for any constraints given by the intergration team of the mission. The properties of interest for the canisters were the cross sectional area left in the sample can for insulation and shock absorbing materials, the volume available in each type of hexagon configuration for samples, the mass of each type of canister, and the total mass of all canisters.

The attached computer program was developed prior to any known constraints in mass and size, but after the decision to go with a hexagon shape canister. The outer diameter of the canister was assumed to be the diameter of a hexagon inscribed in a circle of diameter ro. The inner wall was assumed to be a hexagon inscribed in a circle of diameter ro - th, where th is the thickness of the walls of the canister.

The volume in each type of canister was computed by simply summing the total cross sectional area for each type and multiplying that value with the height. Once the total planar cross sectional area for all of the canisters was computed, the cross sectional area in the sample can was lessened by the amount used by the canisters. The remaining area was then used to compute the volume used by the insulation and shock absorbing material by multiplying by the height of the sample can.

Having already computed the total volume used by each type of canister, the mass of each type of canister was calculated by multiplying the density of the used material by its known volume. Initially, a guess of the size of the hexagon was made and the mass for different types of material was computed. From this, a material that had more than just lightweight properties inherent to it made it more appealing for a choice of material.

After a period of looking at various materials, the physical constraints were known and used to help in the analysis. The hexagonal configurations that were chosen are shown in Figures 13a through 15. The physical parameters that were input to the computations are:

Diameter of outer circle of inscription = 3.33 cm

Height of the inner walls of the canister = 18 cm

Diameter of sample can = 100 cm

Thickness of the hexagonal walls = 0.2 cm

Thickness of the top and bottom caps = 1.5 cm

Density of the material = .0026839 kg/(cm^2) {A357.0 Alloy}

See attached data for the results of the program when run with these values.

```
      PROGRAM CAN
      real ia,innvol,lstvol,lsmss,lwalls
C*********************************************************************
C*********************************************************************
C*                                                                   *
C*       This program was written by Thomas E. Manning II            *
C*     on 30 mar 91                                                  *
C*                                                                   *
C*     latest update: 26 apr 91                                      *
c*                                                                   *
C*********************************************************************
C*   this program calculates the available cross sectional area left *
C*   in the sample can for use by the silica foam, the volume        *
C*   available in each type of canister for the samples, the         *
C*   mass of each canister, and the total mass of all canisters.     *
C*********************************************************************

* set constants

* dnsty = the density of the material for the canisters (kg/cm**3)
* cd    = sample can diameter (cm)
* h     = height of the canister without the top and bottom (cm)
* capt  = height of the top cap of the canister (cm)
* capb  = height of the bottom cap of the canister  (cm)
* pi    = the constant pi
* th    = the thickness of the canister walls (cm)
* ro    = diameter of a cricle in which the outer most hexagon is
*         inscribed
      dnsty= 0.0026839
      cd=100.
      pi=acos(-1.)
      h=18.0
      capb=1.5
      capt=1.5
      ht=capb +capt + h
      th=0.2
      ro=3.33
**********************************************************************
*     areas of inner and outer hexagons
**********************************************************************
```

```
* compute outside area of one hexagon tubes
    oA = 6*ro**2*(cos(pi/6)*sin(pi/6))
* compute inside area of one hexagon tubes
    iA  = 6*(ro*cos(pi/6)-th)*(ro*sin(pi/6)-tan(pi/6)*th)
* compute total area of total 7 section hexagon combination
    oAA = 7*oA
*****************************************************************
*              canister area in sample can
*****************************************************************
* cross sectional area of sample can
    carea = (PI* ((cd/2)**2.) )
* remaining cross sectional area of sample can
    canara = carea - (19*oAA) - 36*oa
*****************************************************************
*     volume available in canisters
*****************************************************************
* only 13 trays will have inner walls

* sample volume in single hexagon
     spvlsi = ia * h
* sample volume in seven hexagon system
     spvlse = spvlsi * 7
* volume of inner walls cut out for the large seven hexagon system
* volume of walls (20 sides, 3.33 cm long h cm high, and .2 cm thick)
     innvol = 24 * ro * th * h
* sample volume in large seven hexagon system is inner walls plus
* sample volume in seven hexagon system
     spvlls = spvlse + innvol
* total volume available for samples
     tsmpvl = 13*spvlse + 36*spvlsi + 6*spvlls
*****************************************************************
*     mass of containers
*****************************************************************
* volume of canister wall material (h cm high, not including the base
* and cap), in one tray
*********************************************************
*          seven hexagon system
*********************************************************
* volume of canister walls for group of 7 hexagons
    svol = (oa-ia)*7*h
```

```
* volume of base (capb cm high)
     basvol = capb*oaa
* volume of cap (capt cm high)
     topvol = capt*oaa
* volume of one tray
     tryvol = basvol + topvol + svol
* mass of one tray
     trymss=dnsty*tryvol
*********************************************************
*     single hexagon
*********************************************************
* volume of walls for single hexagon tube
     swlvol = h*(oa-ia)
* volume of base of single hexagon tube
     sbsvol = capb*oa
* volume of cap of single hexagon tube
     stpvol = capt*oa
* single hexagon total volume of material
[redacted]
     sinvol = swlvol + sbsvol + stpvol
* mass of single hexagon tube
     sinmss = sinvol * dnsty
*************************************************************
*     large seven system
*************************************************************
* volume of walls (18 sides, 3.33 cm long 17 cm high, and th cm
thick)
     lwalls = 18 * ro * th * h
* volume of base and top is the same as seven hexagon system
* total volume of large seven hexagon system
     lstvol = lwalls + topvol + basvol
* mass of the large seven hexagon system
     lsmss = dnsty * lstvol
*********************************************************
*   total mass
*********************************************************
     totmss = 6*lsmss + 26*sinmss + 13*trymss
*********************************************************
*    output results
*********************************************************
```

```
      open(unit=9,file='canister data',status='old')
      write(9,*)
      write(9,*)
      write(9,*)'the cross sectional area '
      write(9,3)'available in the sample can  is',canara,' cm**2'
      write(9,*)
      write(9,*)
      write(9,*)'the volume available for samples in:'
      write(9,*)
      write(9,3)'a single hexagon canister is',spvlsi,' cm**3'
      write(9,3)'all of the single hexagon canisters is',36*spvlsi,' cm*
     +*3'
      write(9,*)
      write(9,3)'A seven hexagon canister system is',spvlse,' cm**3'
      write(9,3)'all of the seven hexagon canisters is',13*spvlse,' cm**
     +3'
      write(9,*)
      write(9,3)'a large seven hexagon system is',spvlls,' cm**3'
      write(9,3)'all of the large seven hexagon systems is',6*spvlls,' c
     +m**3'
      write(9,*)
      write(9,3)'all canisters is',tsmpvl,' cm**3'
      write(9,*)
      write(9,*)
      write(9,*)'the mass of:'
      write(9,*)
      write(9,3)'a single hexagon system is',sinmss,' kg'
      write(9,*)
      write(9,3)'a seven hexagon system is',trymss,' kg'
      write(9,*)
      write(9,3)'a large seven hexagon system is',lsmss,' kg'
      write(9,*)
      write(9,3)'all canisters is',totmss,' kg'
      write(9,*)
      write(9,*)
      write(9,3)'the height of the canisters is',ht,' cm'
      close(9)
    3  format(a41,f15.4,a7)
      STOP
      END
```

Canister data from Can Fortran

the cross sectional area available in the sample can is	2985.1233	cm^2

the volume available for samples in:

a single hexagon canister is	449.1416	cm^3
all of the single hexagon canisters is	16169.0977	cm^3
A seven hexagon canister system is	3143.9912	cm^3
all of the seven hexagon canisters is	40871.8828	cm^3
a large seven hexagon system is	3431.7031	cm^3
all of the large seven hexagon systems is	20590.2188	cm^3
all canisters is	77631.1875	cm^3

the mass of:

a single hexagon system is	0.4183	kg
a seven hexagon system is	2.9283	kg
a large seven hexagon system is	2.2029	kg
all canisters is	62.1612	kg
the height of the canisters is	21.0000	cm

Appendix 3: Cost Estimate Calculation

This appendix shows how the the cost estimate of the MLR was calculated using the NASA/Johnson Space Center Advanced Space Systems Cost Model.

W = Weight = 750 kg
Q = Quantity = 3
Y = Year = 2005 - 1900 = 105
G = Generation = 1
C = Culture Factor = 2.4

$$\text{Cost} = 0.0000172Q^{0.5773} - W^{0.6569} - 58.95^{-C} - 1.0291^{Y}(G)$$

Cost = 1.0936 Billion Dollars (U.S.)

Chapter 8:

The Mars Aereon Sample Collector

Final Report
Aerospace 401B - Detailed Spacecraft Design
Spring Semester 1991

The Norin Group

Alexander Barnes

Darrin Brendel

David Criswell

Thomas Cuff

Lee Greenwood

Todd Martin

Scott Norin

Stephanie Sroczyk

ABSTRACT

A detailed design of the Martian Aereon Sample Collector for use on a Mars Sample Return Mission is presented. The main objective of the overall mission is to return mineralogical and atmospheric samples from the planet Mars to Earth by the year 2010. The specific objectives of the Aereon Sampler are to acquire samples from diverse locations across the planet as well as survey geographic features of the Martian terrain. Connected by the orientation wires, the balloon and rover comprise the two individual components of the Aereon Sampler. The all-wheel-drive rover serves as the command center of the entire vehicle. Two Aereon Samplers are delivered to the Martian surface by means of a surface lander, where they are deployed, inflated and launched. By utilizing the unique characteristic geometry of the Aereon, the vehicle is capable of generating its own propulsion via buoyancy and mass center shifting. This enables the vehicle to control its direction in tandem with the direction of the Martian jet stream which varies with altitude. Both Aereon Samplers are intended to start near the equator, from which one will sample the northern hemisphere and the other will sample an equatorial region. Samples are collected using a multi-tool manipulator arm and are transferred to the Sample Delivery Rocket, both systems being located onboard the rover. Samples are returned to the initial landing sight utilizing the Sample Delivery Rocket where they are delivered to a scouting rover via parachute. The focus of this investigation is the description of the final detailed design of the entire vehicle. Discussion of the Aereon Sampler design is divided into three sections: the Mission Scenario, Vehicle Configuration and Flight Performance, and the Vehicle Subsystems.

ACKNOWLEDGEMENTS

Group Norin would like to thank the instructors of our Aerospace Spacecraft Design Class, Dr. R. Thompson and Dr. R. Melton, and teaching assistants Eric Bell and Jay Burton. We would also like to thank the following faculty for their assistance: Dr. C. Camci, Dr. A Stiehl, Dr. M. Maughmer and Dr. I. Harrison. Special thanks to our families and friends, for their patience while our time was occupied by this and other projects.

TABLE OF CONTENTS

LIST OF TABLES

LIST OF FIGURES

NOMENCLATURE

ACS	Autonomous Control System
BIPS	Brayton Isotope Power System
DIPS	Dynamic Isotope Power System
FPSE	Free Piston Stirling Engine
GPHS-RTG	General Purpose Heat Source RTG
MAV	Mars Ascent Vehicle
MCS	Mars Communication Satellite
MOD-RTG	Modular RTG
RTG	Radio-isotope Thermoelectric Generator
SDR	Sample Delivery Rocket
SSC	Sample Storage Container

CHAPTER I
INTRODUCTION

Presented is a detailed design of a lighter-than-air balloon to gather samples of the Martian environment. This vehicle differs from other balloons planned for Mars in that it uses the Aereon principal for propulsion. The Aereon principal was developed by Dr. Solomon Andrews of New Jersey in 1862. Certain orientations of the Aereon's ellipsoid balloon generate thrust as the vehicle rises and falls. Hereafter, the lighter-than-air balloon is referred to as either the Aereon or Aereon rover.

The Aereon is part of a complete scenario for a Mars Sample Return Mission, and must rely on other mission components to deliver Martian samples to Earth. These include a Mars Communications Satellite (MCS) and a land rover, in addition to the Mars descent and ascent vehicles. The use of these components place constraints on the design of the Aereon, which are mentioned in this report.

Two identical Aereons are used to collect samples from a wide range of the planet's surface. One Aereon explores the northern hemisphere, and the other explores the equatorial region. Both make use of the Martian jet stream and winds, which run predominantly from west to east. The objective of each Aereon is to circumnavigate the planet, and in so doing, deliver samples from a wide range of the planet to the land rover to be taken to the Mars Ascent Vehicle (MAV). Upon completion of the acquisition of samples, the MAV will deliver them to Earth via an Interplanetary Transfer Vehicle. In addition to collecting samples, another objective of the Aereon is to geographical and environmental information for landing sites of future manned missions.

The body of this paper is divided into three main sections: mission scenarios, Aereon balloon and flight performance, and vehicle subsystems. The mission scenarios section discusses the Aereons' missions, and how they will be completed. The Aereon balloon and flight performance section deals with the shape and size of the balloon, and its

controllability in flight. The Aereon subsystems section describes some of the main components of the Aereon. Future questions that need to be addressed are mentioned in the recommendations and conclusions.

CHAPTER II
MISSION SCENARIO

2.1. Introduction

Within the mission scenario section contains two sub-sections: 1) Mission Procedure, and 2) Candidate Landing Sites and Trajectories. The Mission Procedures section describes the deployment and inflation of the Aereon Balloon, the sample collection process as well as the deployment and launch of the Sample Delivery Rocket. The Candidate Landing Site section lists possible landing sites and the flight paths necessary for the intended mission objectives.

2.2. Mission Procedures

2.2.1. Aereon Deployment and Balloon Inflation Procedure

The Aereon deployment and balloon inflation are illustrated in Figure 2.1. The mission begins with the deployment of the Aereon rovers. The two Aereons are stored in tandem inside the descent vehicle and are deployed one at a time. The main balloons are stored underneath the rovers when in the descent vehicle. The first step is to deploy an unloading ramp from the descent vehicle to the ground. As the rover goes down the ramp to the surface, the balloons are unpacked from beneath the rover.

The small drogue balloon is used to lift the main balloon off of the Martian surface so that it is not damaged during inflation..The drogue balloon is the first balloon to be inflated using hydrogen from the storage tanks inside the descent vehicle. When the drogue balloon is in the air, the main balloon is suspended above the surface in preparation for inflation.

Once the balloon is fully unpacked, a hose from the decent vehicle hydrogen storage tank fills the reserve hydrogen tank inside the rover. This tank is used to replenish hydrogen in the main balloon during the mission. The reserve tank used to replenish lost

hydrogen is connected to the main balloon by another hose. Once the reserve tank has been filled, a bypass valve inflates the main balloon. The balloon is inflated to the point where it reaches its lift off volume. The lift off volume is the point where the balloon has slightly less lift than is needed to raise the rover. Once the balloon is filled, the hose from the descent vehicle is disconnected from the rover. At liftoff, the rover is approximately 100 meters away from the descent vehicle, which ensures that the balloon does not collide with the descent vehicle while being carried by the wind. This distance roughly corresponds to the overall length of the balloon.

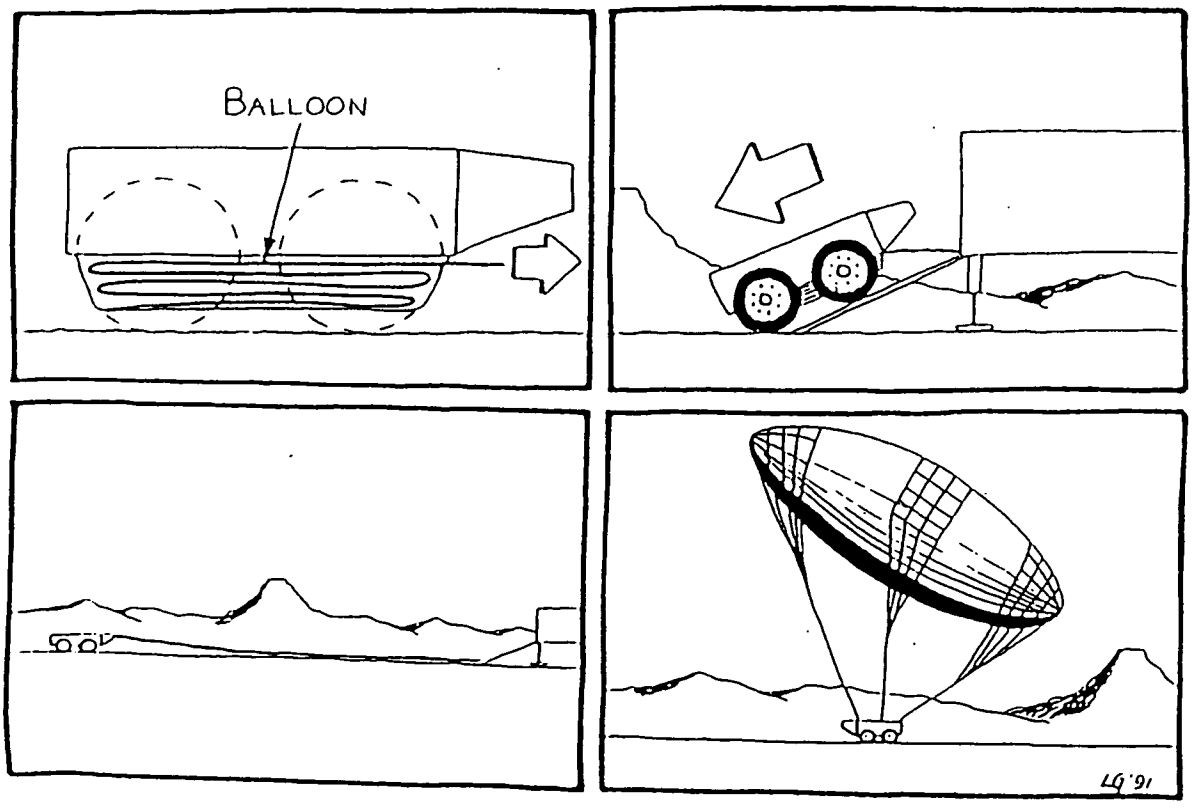

Figure 2.1. Vehicle Deployment and Balloon Inflation Process.

2.2.2. Sample Collection Procedure

Each Aereon circumnavigates the planet, collecting samples from a wide variety of sites. The landing sequence is as follows: as the vehicle approaches a target site, the on-board compressor pumps low-density H_2 out of the balloon and into the high-density storage tank until a slow rate of descent is reached, as determined by the onboard radar altimeter (a much smaller version of the instrument used by the Magellan spacecraft to map the surface of Venus). After touchdown on the surface, the compressor continues to deflate the balloon until buoyancy is reduced to the point where horizontal friction between the surface and the wheels is equal to some factor of safety times the drag force of wind gusts on the balloon. If this condition is reached quickly enough, there will be no dragging of the vehicle along the surface.

The arm's stereoscopic camera now digitizes several images of the immediate surroundings and transmits them to Earth as soon as the communications window opens. Teleoperators, under the advice of a team of geologists and planetary scientists, then transmit the vehicle's next move. If an interesting specimen is seen which is beyond the reach of the robot arm, the operator will instruct the vehicle to switch on its electric drive train and drive closer. This procedure could be as simple as using a mouse to point a cursor on the operator's video monitor to the destination point. A redundant verification system will be in place to prevent transmission of erroneous commands. Similarly, the operator could use the mouse to instruct the robot arm to scoop up a particular patch of soil or saw a slice off of the face of a selected boulder.

Computers on board the vehicle would be responsible for simpler matters such as steering around obstacles. Use of this semi-autonomous control system, as opposed to a fully autonomous system where the robot arm grabs rocks at random, would vastly increase the scientific returns of the mission. It would be difficult to program a computer to discriminate between common rocks and samples of greater geological interest.

If the mission takes place during the 2004-2005 time frame, when the distance from Mars to Earth is approximately 56×10^6 km, the round-trip radio signal time will be only 6.2 minutes. Even at longer distances, there will be plenty of time for many communications exchanges at each sample collection site.

The collected samples are stored in the Sample Storage Container (SSC). The SSC consists of a series of interlocking trays with hexagonal compartments. The hub of each tray has a connector much like those of the robot arm's tools (see Section 4.9). This allows the robot arm to attach directly to the trays and process them. This connector is also used to attach a lid to each tray, and the lid also has a connector so that the arm can lift it, and the filled tray, and put them into the Mars Ascent Vehicle (MAV).

Before sample collection begins, all trays are stored in a single column. Next to the trays is an empty column where trays will be moved when full. When the first empty tray is full, the robot arm picks it up and places it at the bottom of the empty column. The arm then picks up the lid of the next empty tray and places it on the first full tray. This procedure is repeated until all the trays are full. During transportation, when no samples are being collected, both columns of trays are covered with a sliding door to prevent samples and trays from falling out.

After the operators have thoroughly investigated a given site, they issue the command to take off and give the latitude and longitude of the next site. Takeoff is effected by opening the valve on the ballast balloon until sufficient lift is achieved. The Aereon flies from site to site, following a predetermined route which is flexible enough to take advantage of the changing wind conditions as measured from orbit (see Section 4.6).

2.2.3. Sample Delivery Rocket Launch Procedure

Each Aereon is equipped with a single Sample Delivery Rocket (SDR) used to transfer the collected samples to the MAV. The SDR is launched after an amount of samples equal to the SDR's payload capacity has been collected, or in the event of an

Aereon malfunction, whichever comes first. The launch procedure is as follows: the SDR assembly is rotated 90° so that the SDR is vertically oriented as seen in Figure 2.2. The support legs on each corner of the SDR assembly are deployed and the entire assembly is lowered to the surface. Next, the SDR assembly is detached from the rover. The rover then moves a safe distance away from the SDR to protect the balloon from damage during launch. Once the balloon is at a safe distance, a radio command is sent to the SDR, which then launches towards the MAV. When the SDR lands in the vicinity of the MAV, the land-based rover uses its robot arm to put the samples into the MAV for return to Mars orbit and eventually to Earth for analysis. Once the SDR has been launched, the Aereon will further explore the Martian terrain to gather geographical and environmental information for future manned missions to Mars.

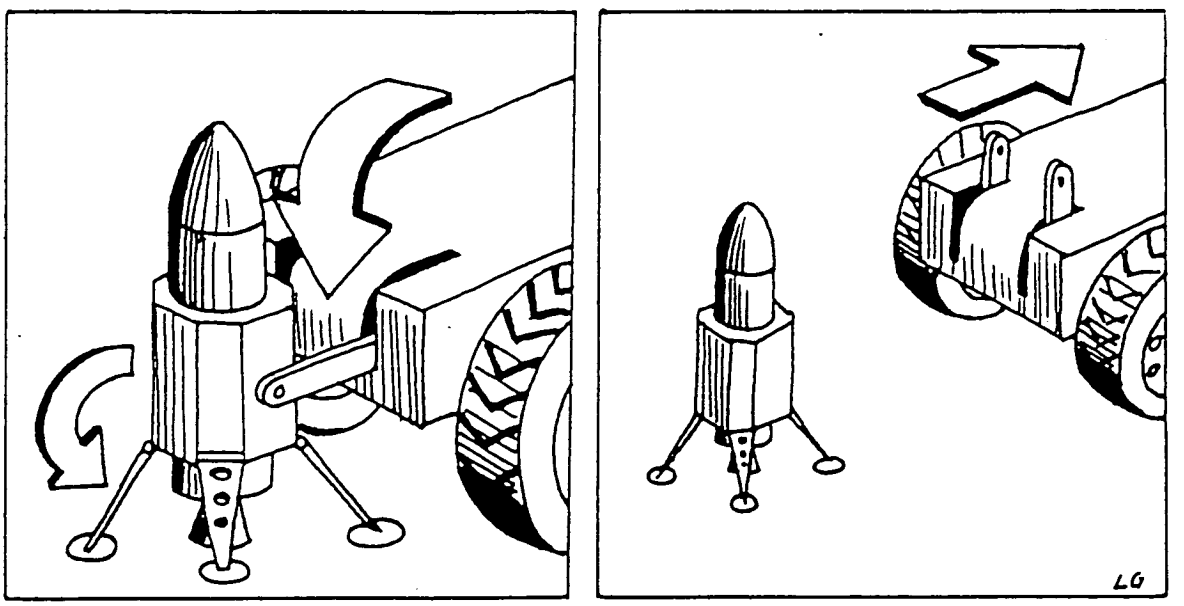

Figure 2.2. Deployment Procedure of the Sample Delivery Rocket

2.3. Candidate Landing Sites and Trajectories

One possible route of exploration to be taken by an Aereon vehicle is described in this section. It should be emphasized that this route is only one possible outcome. While the wind currents on Mars do follow general patterns, there are also day-to-day variations in those patterns which would make an inflexible flight plan impossible to meet. An actual flight plan would be designed by expert scientists to maximize the scientific returns of the mission, and would include many alternate sites and contingency sub-plans to allow for changing wind conditions. In the following flight plan, site numbers are as shown in Figure 2.3.

Site	Latitude/ Longitude	Description
		Main Landing Site
M	5.5° S / 74.5°	Candor Mensa. A large side canyon associated with Valles Marineris. The wheeled rover will encounter extensive areas of flat terrain on the floor of the valley and a wide variety of materials to sample. Valles Marineris is a fault which exposes layered canyon walls which were once 7 km below the surface and contain material ranging from ancient to young. Barchan dunes, representative of dunes elsewhere on Mars, lie on valley floor as well as possible dry lake beds and waterlain sediments. Robbins (1989) proposes sampling iron ore to scan for "bacterial mineral precipitates." "...the scientific rewards [of landing a spacecraft on the floor of Valles Marineris] would be so great that such a landing should be considered..." (Lucchitta, 1988).
		Aereon I - Northern Hemisphere
1	18.95° N / 53.5°	Maja Valles. Sedimentary deltas exist at the mouth of three dry riverbeds. Streamlined islands, sinuous ridges, and possible scoured bedrock are also present for sampling and observation. Crust surrounding dry lake bed is of the oldest rock unit on Mars.
2	22.52° N / 47.97°	Chryse Planitia / Viking 1. This is perhaps the site which will yield the most practical information. At the time of the sample return mission, the Viking landers will have been exposed to the Martian environment for at least 27 years. By sawing off and returning small samples of Viking which have been in contact with air and soil, we will be able to measure the resistance to weathering and corrosion of various man-made materials. This information will advance the ultimate goal of building durable structures for a manned Mars base. The immediate area around Viking 1 was well-documented visually; new images of the area would determine the any changes (erosion, shifting of dunes, etc.). It may be possible for the Aereon to send a radio command to Viking 1 to turn its antennae back towards Earth and resume transmissions. The Viking aeroshell impacted about 1 km north of here and formed a small crater. Sampling ejecta from this crater would allow

		acquisition of material previously at a depth of 2 m without a long core drill. Determining the absolute age of a sample of the plains here is ideal for calibration of the crater-count surface dating curve (Craddock, 1989).
3	40.9° N / 10°	Northern Cydonia / Pyramid City. This is a site of great popular interest. An unusual rock formation, 1 km wide, is shaped like a human face. Nearby lies a set of pyramid-shaped objects. Close observation and possibly sampling could resolve the outspoken controversy of these geographic features.
4	30° N / 327°	Arabia. Obtain the composition of these ridged plains, possibly volcanic.
5	45° N / 251°	Utopia. An area of extensive water and mud flows; possible ground ice.
6	48° N / 226°	Utopia Planitia / Viking 2. If the visit to Viking I was highly successful, mission directors may decide to stop here as well.
7	33° N / 212°	Northern Elysium. Sampling the flank of volcano Hecates Tholus may determine whether Martian volcanism was "explosive in nature." Aereon could determine whether controversial channels here were carved by water or debris flow.
8	27° N / 185°	Elysium. Sample plains flows from Elysium Mons.
9	2° S / 159°	Medusae Fossae. Pole may have been located here in the past; the easily erodible sediments here my be freeze-dried remnants of polar layered terrain.
10	4.7° S / 147.5°	Mangala Valles East. Interfaces between young basaltic flows and underlying ancient cratered terrain.
11	11° N / 137°	Olympus Mons South Scarp. Search for fissure vents (possible origin of local lava flows); sample wind streaks of contrasting albedo.
12	12.5° N / 125.5°	Tharsis-Olympus Pass. Sample young lava flows and aureole deposits of Olympus Mons.

Return to Main Landing Site.

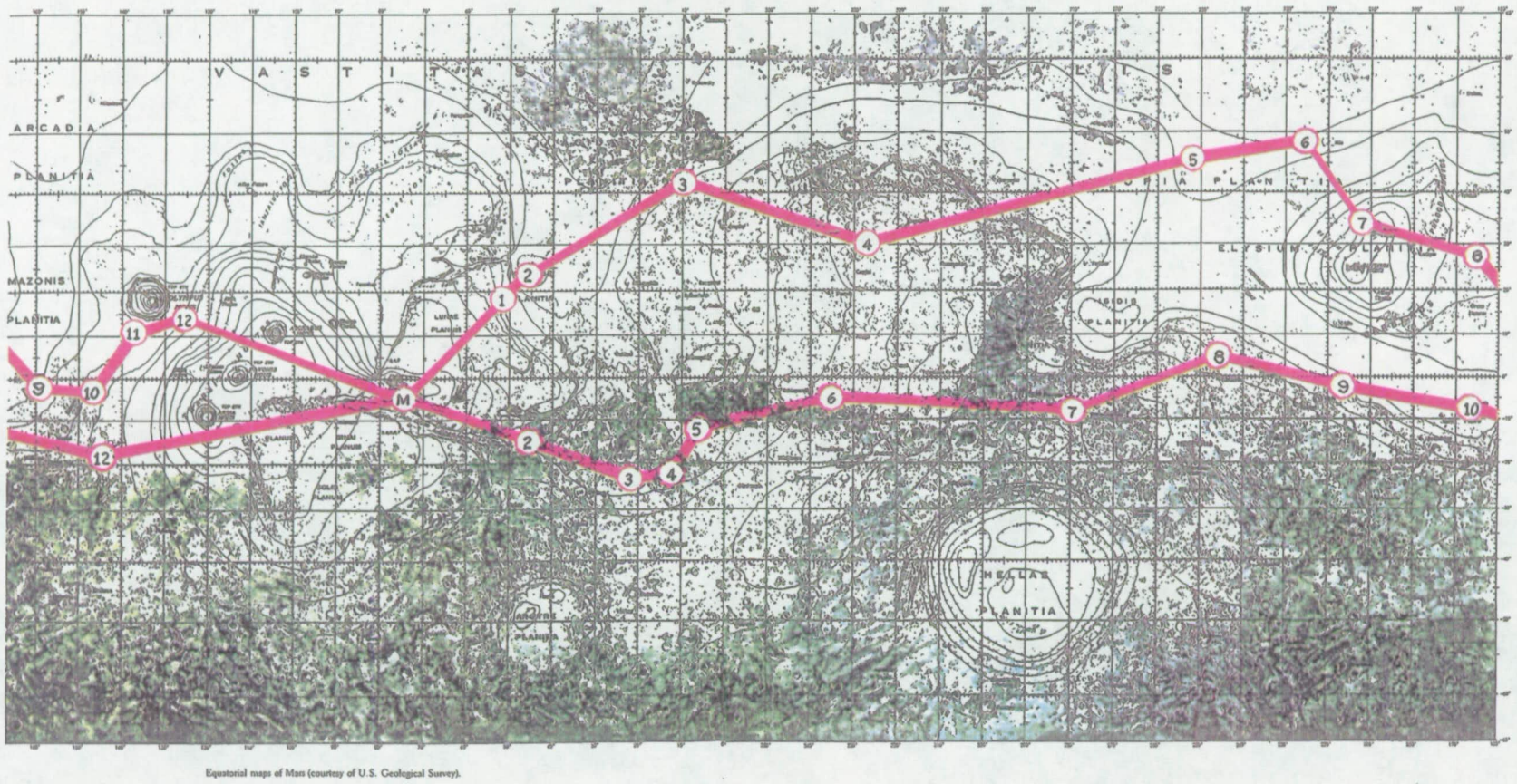

Figure 2.3. Candidate Landing Sites for the Aereon Sampler [Carr, 1981]

CHAPTER III
AEREON BALLOON AND FLIGHT PERFORMANCE

3.1. Balloon Material

Two materials for the balloon skin were studied: Mylar and Polyethylene. Their properties are summarized in Table 3.1. In addition to having a greater specific strength, Mylar also has a minimum operating temperature of 83 K [USU 1987, p. 10], which is less than the coldest temperatures expected to be encountered at Mars. For these reasons, Mylar is chosen as the balloon material.

Table 3.1. Comparison of Balloon Skin Materials

Material	Mylar [source: USU 1987, p. 10]	Polyethylene [source: Harrison 1991]
Yield Stress, σ_y, at room temperature (MPa)	97	13.8
Volume Density, ρ (kg/m^3)	988	930
Specific Strength (σ_y/ρ)	9.82E4	1.48E4

Permeability of a membrane varies exponentially with temperature. The permeability constant of hydrogen gas through Mylar film was found experimentally to be 0.025 at 0 °C and 0.120 at 50 °C (units, cm^2 / s / cmHg) [Tuwiner, 1962]. Using these two data points with the relationship

$$P=P_0 \times \exp(-E_p/RT)$$

where E_p is the activation energy of permeation, R is the universal gas constant, and T is absolute temperature, the two unknowns E_p and P_0 were found to be E_p = 23.03 kJ/mol and $P_0 = 4.74 \times 10^{-14}$. The relationship of permeability and temperature is graphed in Figure 3.1. Note that at typical Martian temperatures (≈ -40 °C), P is only 8% of its room

temperature value. Assuming this value for T, a 100 day mission, balloon skin thickness of 2.048×10^{-5} m, and a surface area of 8027 m^2, 0.0729 kg of hydrogen will diffuse out of the balloon. This amount is negligible compared to the the total mass of hydrogen on board (23 kg).

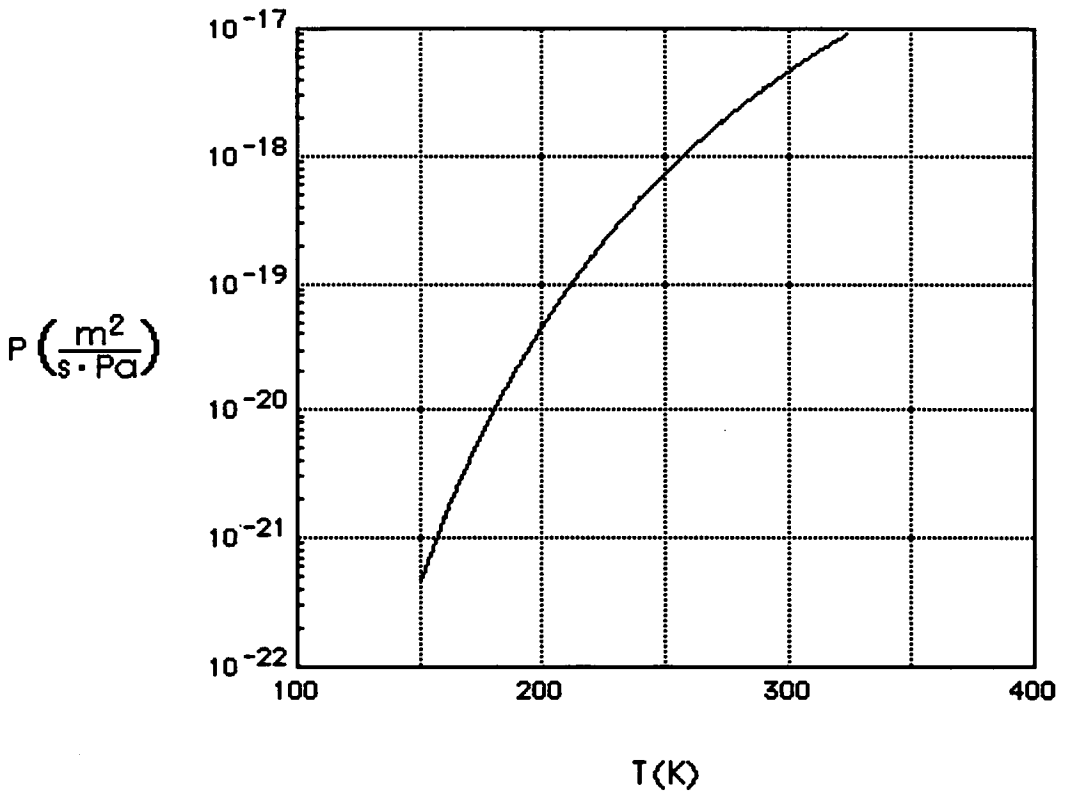

Figure 3.1. Permeability of Hydrogen through Mylar as a Function of Temperature.

3.2. Balloon Shape and Size

The Aereon is basically an airfoil rotated 90°. While an airfoil generates lift as a propulsive device drives it forward through the air, the Aereon generates thrust as positive or negative buoyancy causes it to rise or fall. The shape of the balloon is determined from an engineering trade-off between two opposing goals: high thrust/drag ratio and low weight. The balloon is so large that the mass of the skin of the balloon is a major component of the total vehicle mass. The balloon volume is strictly a function of vehicle mass and maximum desired altitude. To enclose this volume in a weight-efficient manner, the chosen balloon shape must have a low surface-area/volume ratio.

Aerodynamically speaking, the ideal shape of the body would be a nearly flat plate. This would provide maximum thrust for a given rate of climb. Unfortunately, this body has a surface-area to volume ratio which approaches infinity. The best surface-area to volume ratio is afforded by a sphere, but because of its symmetry, the sphere produces zero forward thrust as it changes altitude. The ellipsoid shape was chosen as a practical compromise which produces a vehicle of reasonable size and adequate performance. Another shape which might be chosen is a fattened triangular shape described as a "deltoid pumpkinseed." This shape, which has a higher thrust to drag ratio but a somewhat lower surface-area to volume ratio, was used in Aereon research vehicles flown in New Jersey in the 1960's. Minimizing surface area is not as important for flight in Earth's atmosphere because the greater density of Earth's air yields a much smaller balloon volume. A comparison of these bodies is shown is Figure 3.2.

An ellipsoid fineness ratio, defined as the major axis length divided by the minor axis length, of two minimizes the drag coefficient of the balloon [McCormick]. This corresponds to an eccentricity of approximately 0.866. Now that the shape has been defined, the actual dimensions of the balloon can be determined.

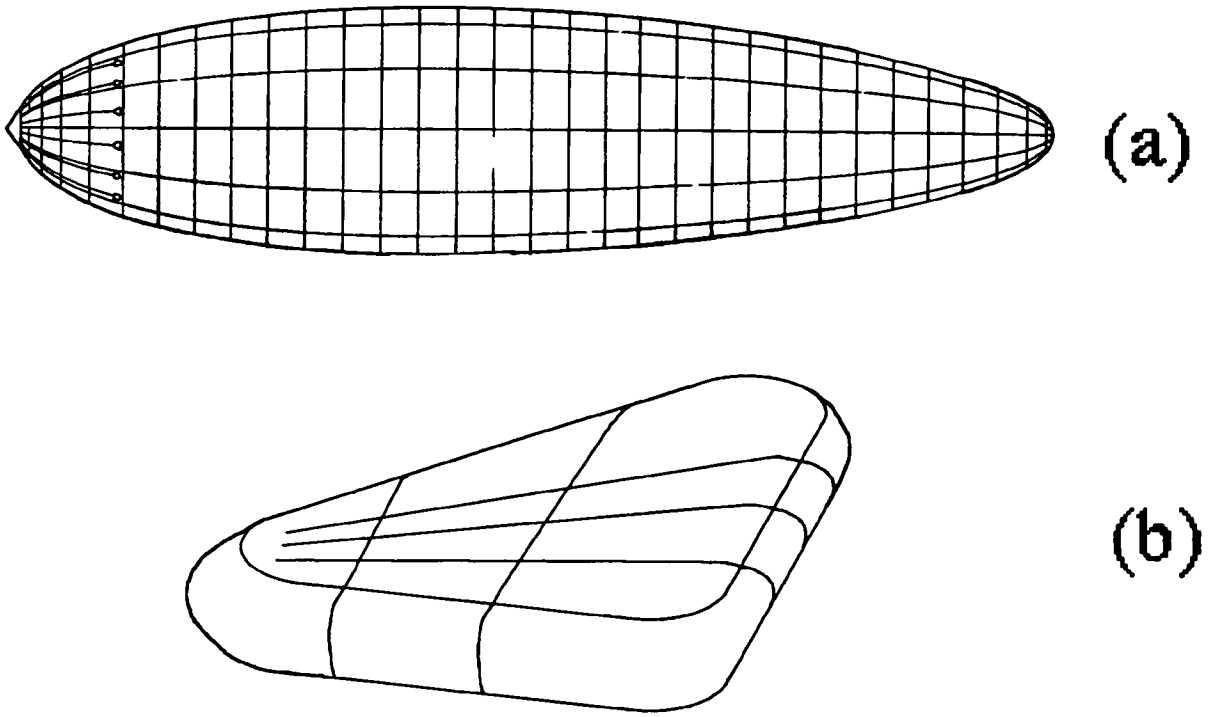

Figure 3.2. The ellipsoidal (a) and "deltoid pumpkinseed" (b) Aereon shapes.

In addition to its mass, the balloon's size is driven by the desired altitude range of the Aereon. In the worst case flight conditions, the Aereon must be able to attain an altitude of 6 km. This altitude allows the Aereon to fly over most of the Martian terrain, with some room for maneuvers which generate Aereon thrust. On the other hand, during the best case flight conditions, the Aereon must be able to stay on the ground without decreasing its volume to less than 75% of its maximum volume. As explained in Section 3.5.1, the balloon's volume decreases when it descends due to the ballast balloon being inflated. The related contracting and expanding of the balloon stresses its skin, and thus large volume changes should be minimized.

The worst flight conditions, when the Aereon attains its lowest maximum altitude, correspond to the lowest ambient pressure and highest ambient temperature. The best flight conditions are simply the opposite of the worst flight conditions. The ambient Martian

pressure and temperature, like Earth's, vary daily, seasonally, and by latitude. The surface pressure and surface temperature range from 650 Pa to 900 Pa and 150 K to 300 K respectively. Applying these conditions to the two cases described in the previous paragraph, a minimum and maximum balloon volume are calculated. Because the two cases conflict with each other, the minimum volume is greater than the maximum volume. As a compromise, the average of the two volumes is chosen, giving the balloon a maximum volume of 46,150 m^3 and a constant 23.04 kg of hydrogen. The maximum altitudes that can be attained with this balloon are shown in Figure 3.3.

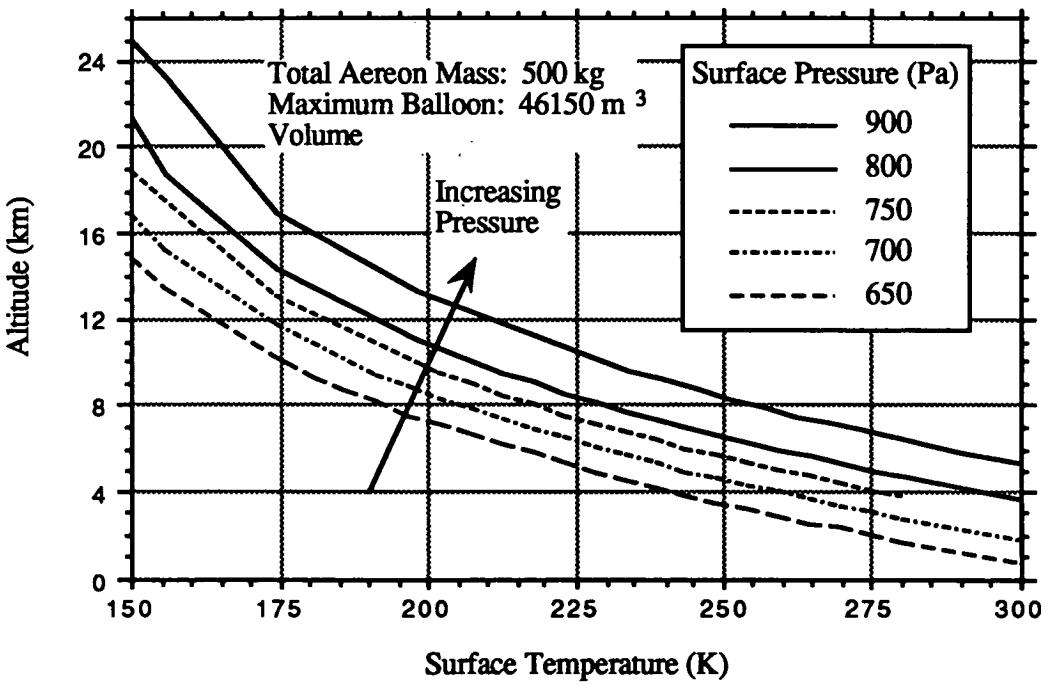

Figure 3.3. Maximum Altitude Attainable by the Aereon

The mass of the balloon depends on the thickness of its skin. The thickness, in turn, is dependent on the maximum stress that the balloon can withstand before yielding. The stress in the balloon skin is approximated by the equation for hoop stress, which is considered to be conservative since it is twice the longitudinal stress. The internal pressure

of the balloon only needs to be great enough to support the weight of its skin. A maximum pressure of 1.05 times the ambient pressure is assumed. Later calculations will show that this pressure is also conservative. In addition, a factor of safety of 2.5 is used to account for the Mylar becoming brittle. The yield stress for Mylar shown in Table 3.1 is at room temperature, or approximately 300 K. The temperature that the balloon is exposed to at Mars may be as low as 150 K. Decreasing the temperature decreases the yield strain and increases the modulus of elasticity. The relationship between yield stress, strain and modulus of elasticity is given by

$$\sigma_y = E\,\varepsilon_y$$

where E and ε_y are the modulus of elasticity and yield strain respectively. It is not known whether the change in modulus of elasticity offsets the reduction in yield strain; thus, the factor of safety is used to account for this. The safety factor of 2.5 is the maximum allowable without the resulting balloon skin mass becoming too large. The balloon skin thickness, then, is calculated to be 20.48 μm. Although this thickness is small, it is greater than three times the smallest thickness achievable using current technology [Harrison 1991]. The resulting skin mass is 135.58 kg. In addition, the balloon skin has an area density of 20.23 g/m^2. Using this area density, the balloon must have an internal gage pressure of 0.08 Pa, which is less than the assumed pressure of 5% of the ambient, in order to support the balloon's weight. The balloon characteristics are summarized in Table 3.2.

Table 3.2. Main Balloon Characteristics

Volume	46,150 m^3
Fineness Ratio (eccentricity)	2.0 (0.866)
Maximum Length	70.64 m
Maximum Diameter	35.32 m
Skin Thickness	20.48 μm
Mass	135.58 kg
Mass of Hydrogen	23.04 kg

The final balloon calculation concerns the size of the spherical ballast balloon. A large ballast balloon increases the amount of ballast the Aereon can take on without pressurizing the ballast balloon and decreasing the volume of the main balloon. The affect of changing the ballast balloon's size is shown in Figure 3.4. The ballast balloon is completely filled at the point where the slope of the curve changes. Below this point, the volume of the main balloon decreases. At the smaller ballast balloon sizes, the main balloon's volume must be less than 75% of its maximum value in order to land. In addition, the pressure ratio in the ballast balloon at the surface is 1.074, 1.061 and 1.053 for the 8, 10, and 12 thousand m^3 cases respectively.

A ballast balloon larger than what is shown in Figure 3.4 may be desirable, but the ballast balloon's size is limited by the mass of its skin. Taking these factors into consideration, a ballast balloon volume of 12,000 m^3 is chosen. For simplicity, the ballast balloon has the same material and thickness as the main balloon. The characteristics of the ballast balloon are summarized in Table 3.3.

Table 3.3. Ballast Balloon Characteristics

Volume	12,000 m^3
Diameter	28.40 m
Skin Thickness	20.48 μm
Mass	51.3 kg

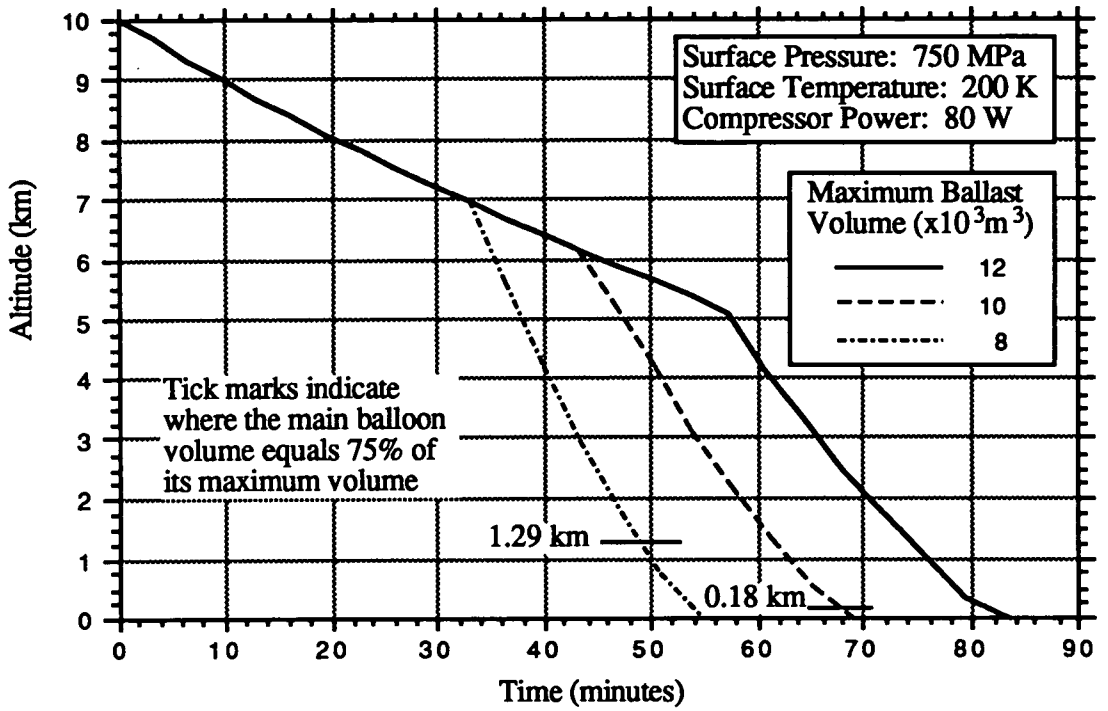

Figure 3.4. Affect of Different Ballast Balloon Volumes on the Aereon's Descent

3.4. Atmospheric & Environmental Conditions

In order to design the Aereon Sampler for maximum maneuverability, it is crucial to know what atmospheric and topographical conditions the Aereon may encounter. Ambient temperature and pressure affect the overall performance of the Aereon's buoyancy and dynamic behavior.

Data collected from the Viking missions show the Martian ambient surface temperature ranges from 150 K to 300 K, and the surface pressure ranges from 5.9 to 15.0 millibars. The ambient pressure varied in seasonal patterns (Figure 3.5). Lowest pressure occurs between the northern summer and northern fall, while highest pressure occurs in the northern winter [Carr 1981]. Surface temperature variations have been modeled as a function of latitude, longitude and season (Figure 3.6). Temperature models have also been produced for dust storm / dust free seasons as a function of altitude and latitude (Figure 3.7). Temperature variations would be experienced by the Aereon Sampler over the course of a day could vary by as much as 110 degrees Kelvin over a seven hour period (Figure 3.8). These models show the variable range of temperatures that the Aereon would experience traveling across the planet.

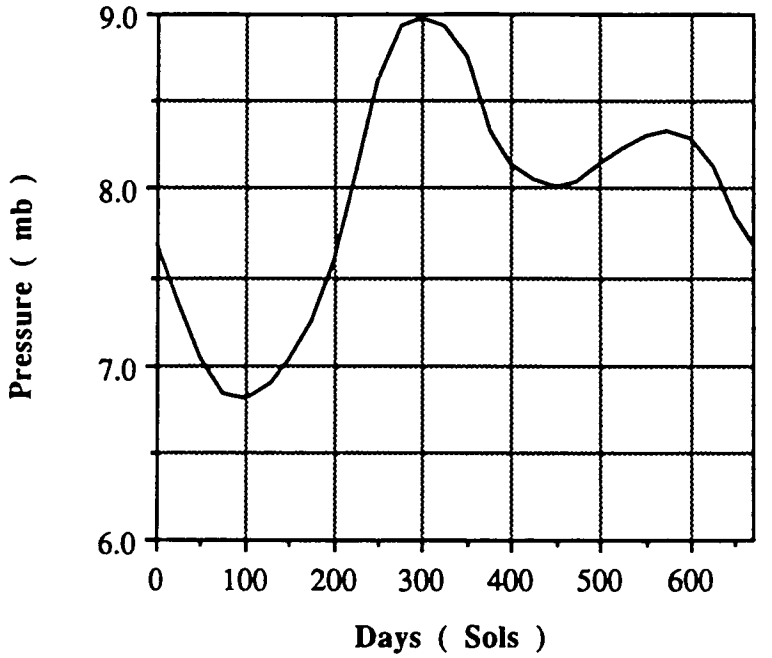

Figure 3.5. Seasonal Pressure Variation Measured from Viking One[Carr 1981].

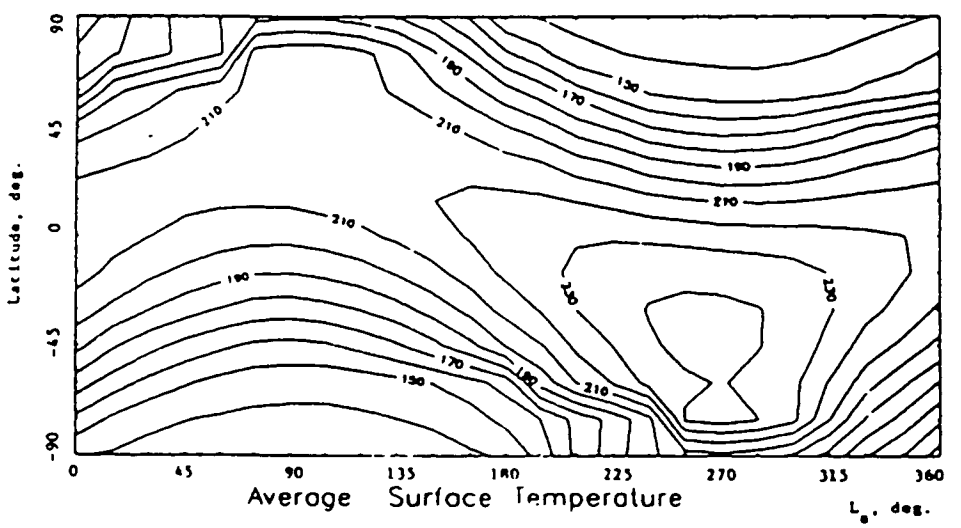

Figure 3.6. Average Surface Temperature Variations Across Longitude and Latitude [Justus 1989].

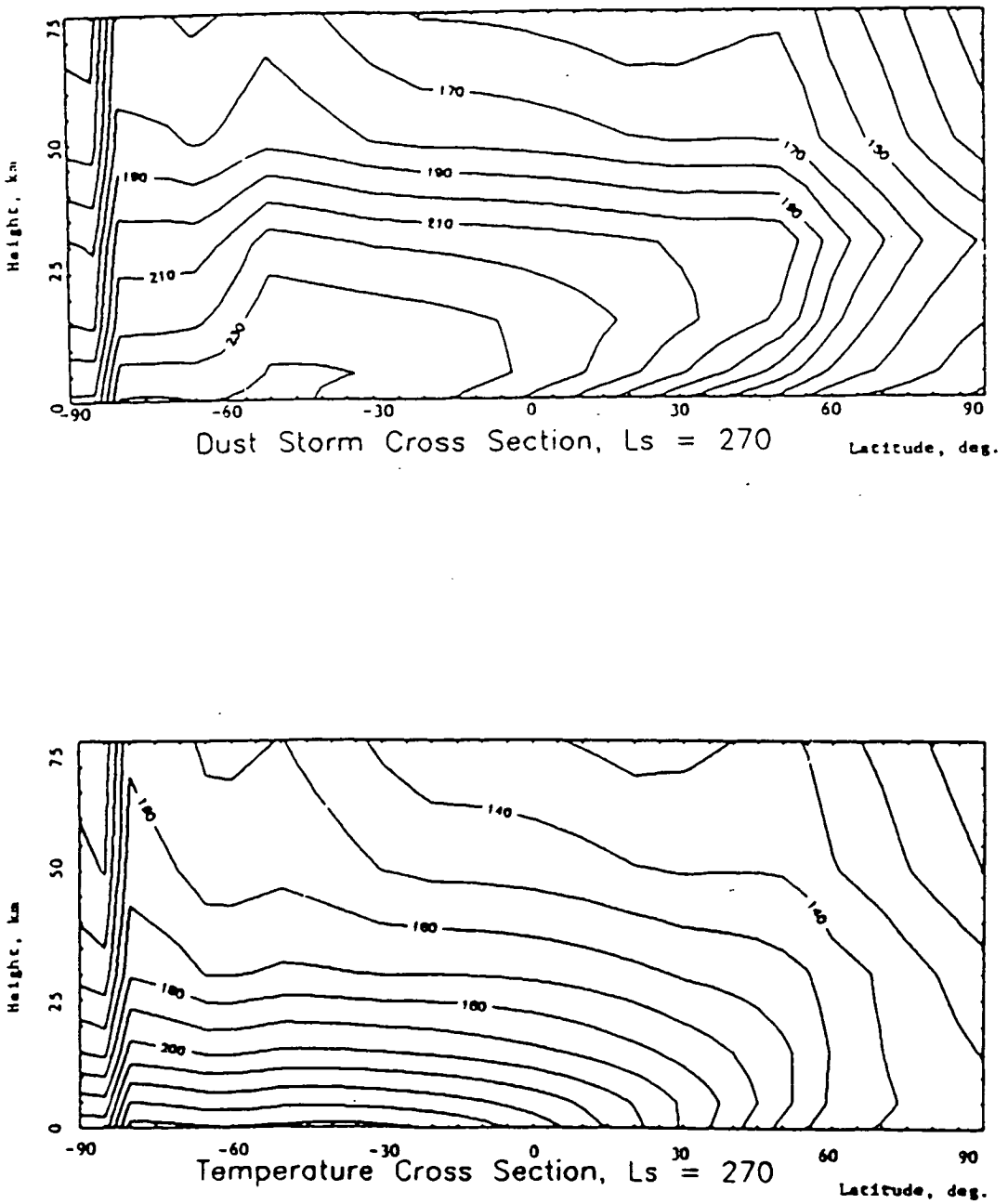

Figure 3.7. Variation of Temperature with Altitude and Latitude For Dust Storm & Dust-Free Seasons [Justus 1989].

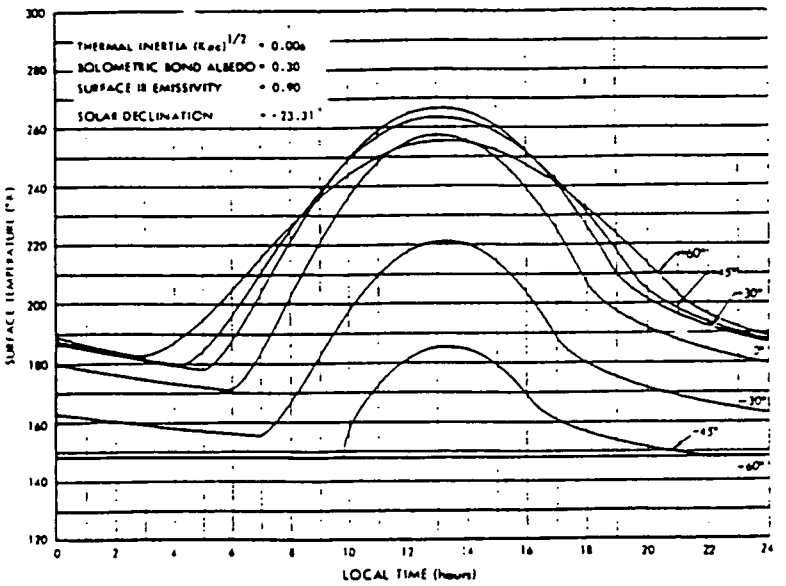

Figure 3.8. Variation of the Surface Temperature Over the Martian Day [Carr 1981].

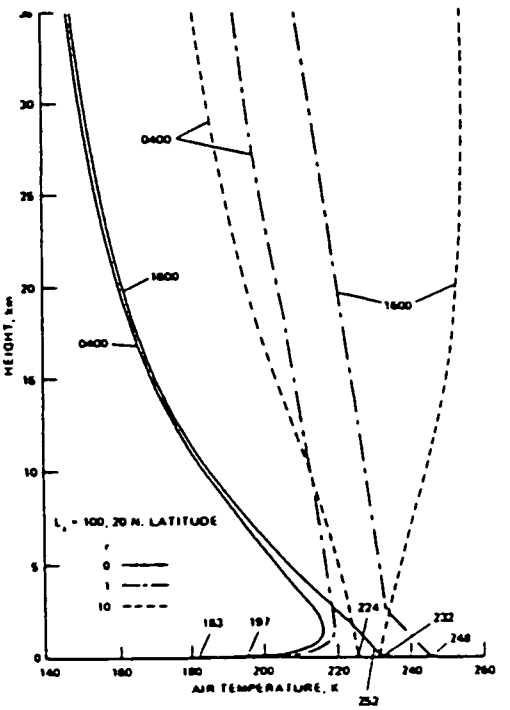

Figure 3.9. Variation of Ambient Temperature Versus Altitude [Carr 1981].

Elevations on the surface are known from the topographical maps that were produced from Mariner mission photographs. The planet Mars has a large variation in its surface elevation, which is shown by the large offset of the planet's gravitational potential (Figure 3.9). The average mean pressure at the zero level elevation is 6.1 millibars. The elevation of Mars surface ranges from -3 km to 26 km atop Olympus Mons [Batson 1979]. It may be impossible for the Aereon to reach the higher elevations, due to the low density of the Martian atmosphere. In order to reach the higher altitudes, the volume of lifting gas required by the Aereon would be enormous and impractical.

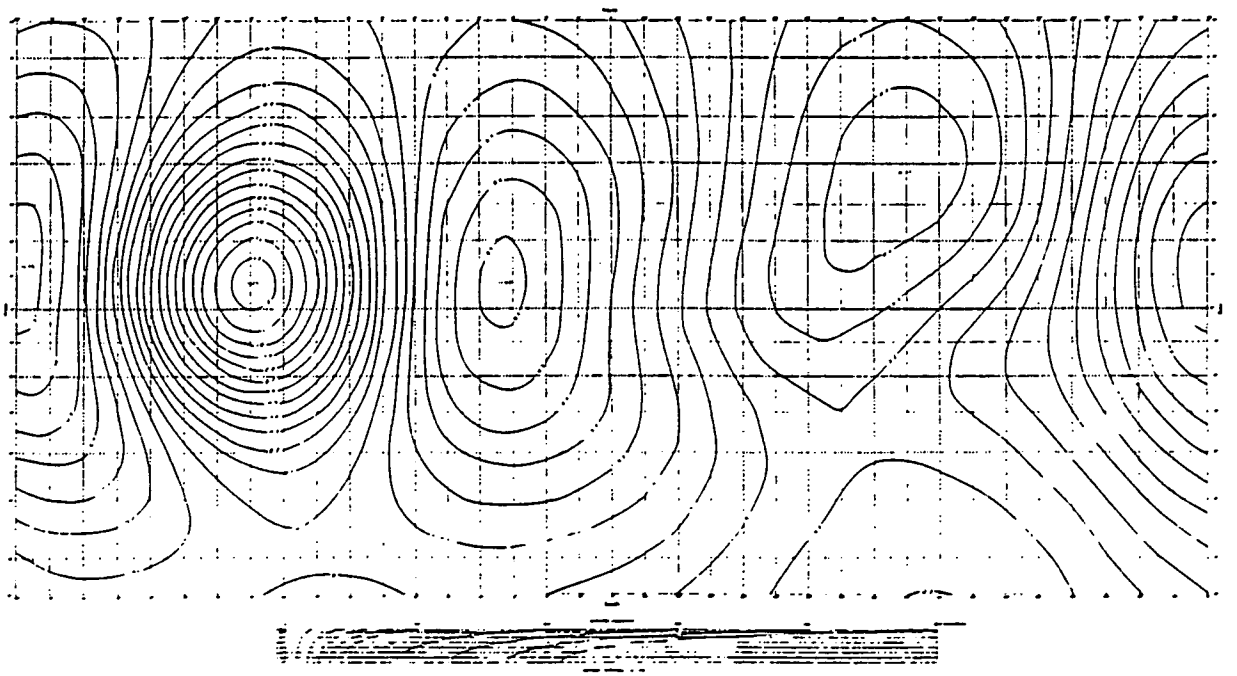

Figure 3.10. Gravitational Potential Offset of Mars [Batson 1979]

The Martian winds pose the most dominant threat to the Aereons. Winds in the upper atmosphere (40 km above the Martian datum elevation) can reach up to 140 meters per second (313 mph), but the Aereon is not expected to fly so high (Figure 3.11). Of some concern, however, are the reports of Martian dust devils existing near the planet's

surface. After the two year survey of the Viking orbiters, ninety-seven dust devils were observed. These dust devils occurred at regions of 20° latitude, north and south of the subsolar point. Dust devils were sighted only on afternoons in the summer season. Their elevation is approximated at just under 7 kilometers and are under 250 meters wide [NASA 1988].

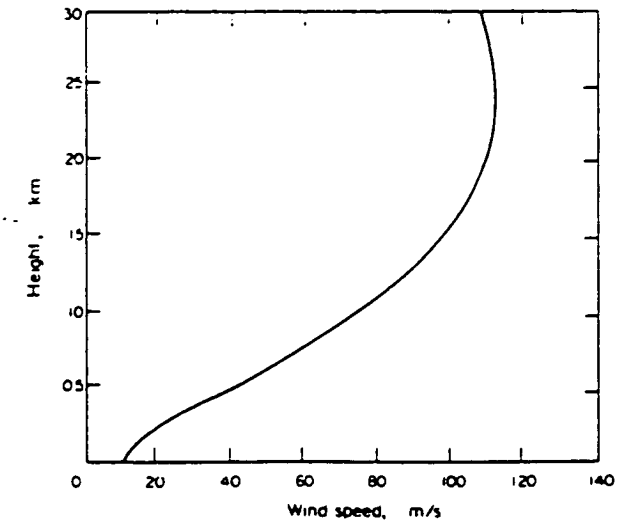

Figure 3.11. Wind Velocity Profile With Respect to Altitude [Kondratyev 1982].

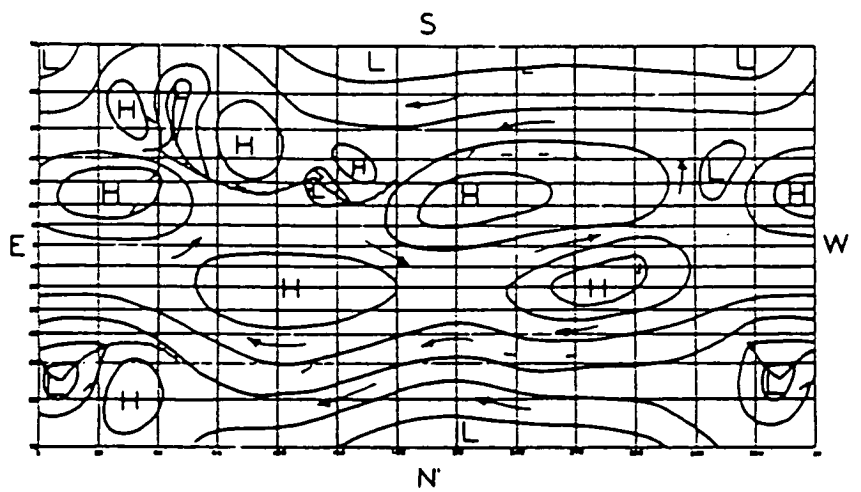

Figure 3.12. Sample Wind Directions of the Martian Atmosphere [Kondratyev 1982].

3.5. Aereon Flight Performance

3.5.1. Balloon Ascent and Descent

The process used by the Aereon to descend and ascend is similar to that used by submarines to submerge and surface. A submarine has tanks which it fills with sea water in order to descend below the ocean's surface. When the submarine wants to surface, it forces the water from its tanks. Instead of water, the Aereon uses Martian air. The Aereon's "tank" is a balloon contained within the main, hydrogen balloon. This inner balloon is referred to as the ballast balloon. At the Aereon's maximum altitude, which varies due to seasonal and diurnal variations of temperature and pressure, the ballast balloon is empty. In order to descend, a compressor fills the ballast balloon with air, which increases the total mass of the Aereon. Since the main balloon cannot expand, the Aereon descends until the mass of air displaced by the balloon once again equals the total mass of the Aereon. In order to ascend, the process is reversed. The air is pumped out of the ballast balloon by the same compressor that filled the ballast balloon.

The method of the Aereon descent is illustrated in Figure 3.13. Initially, the volume of the main balloon remains constant. The expansion caused by filling the ballast balloon is offset by the decrease in volume of the hydrogen. The hydrogen's volume decreases as the Aereon descends due to an increase in the ambient pressure, which in turn increases the density. This can be seen in Figure 3.14. Since the mass of hydrogen in the balloon is constant, the volume decreases.

When the ballast balloon reaches its maximum volume, the main balloon begins to shrink. Shrinking the main balloon decreases its buoyancy force. The combined effects of increasing the Aereon's mass and decreasing the balloon's buoyancy force cause the Aereon to descend faster, compared to when the balloon volume is constant. The same holds true for when the Aereon is rising.

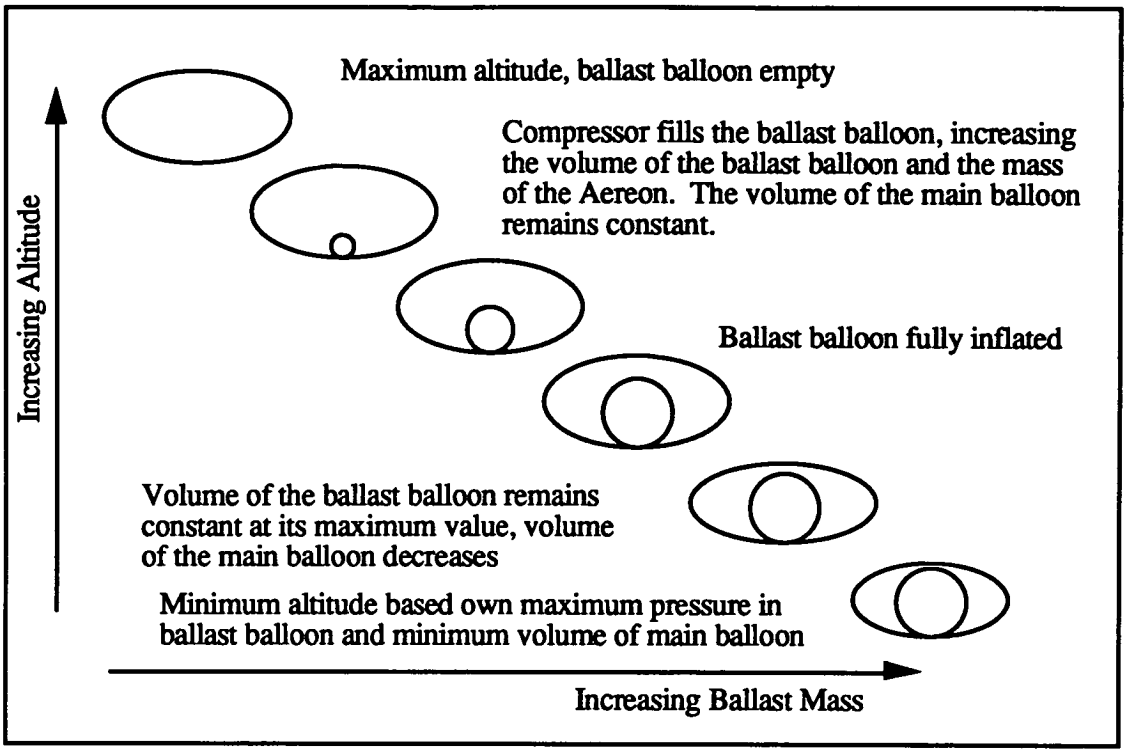

Figure 3.13. Aereon Descent Using a Ballast Balloon

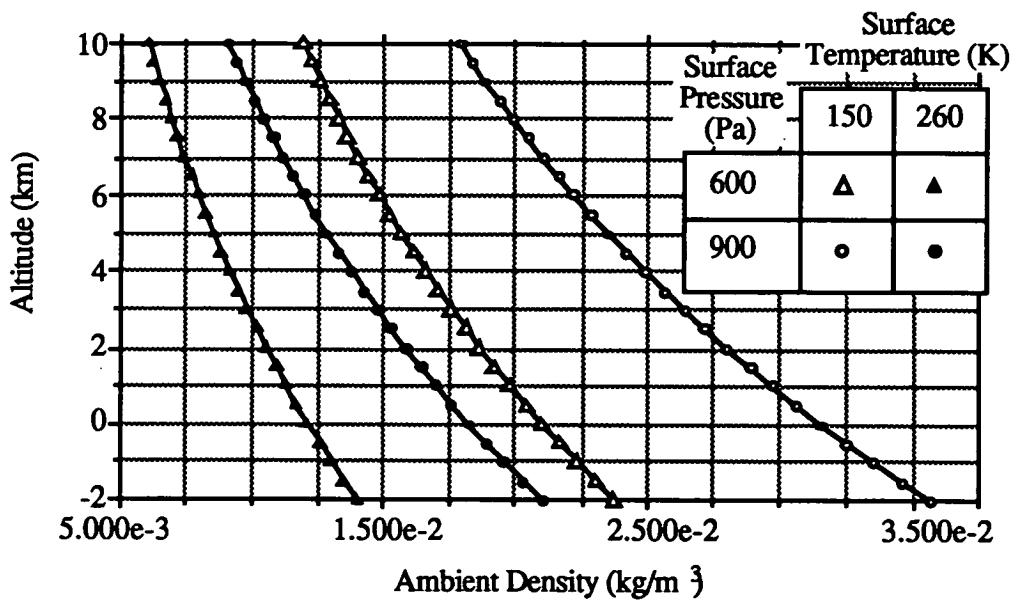

Figure 3.14. Density as a Function of Altitude, Pressure and Temperature

3.5.2. Aereon Thrust and Maneuverability

The Aereon concept is accredited to Dr. Solomon Andrews, who proposed the idea in 1862 and went on to build and successfully fly an Aereon in 1864 to speeds of 25 mph. His success demonstrates that his theory is valid. This theory describes the controlled propulsion of a balloon without the use of engines. A spherical balloon, when ascending or descending, does so vertically in the absence of wind, similar to a cork in water. An oblong balloon behaves similar to a board in the water, which moves laterally in addition to vertically if tilted at an angle. Constant foreword motion can be achieved by alternately pointing the nose upward until the maximum altitude is reached, and then pointing the nose downward. This is illustrated in Figure 3.15.

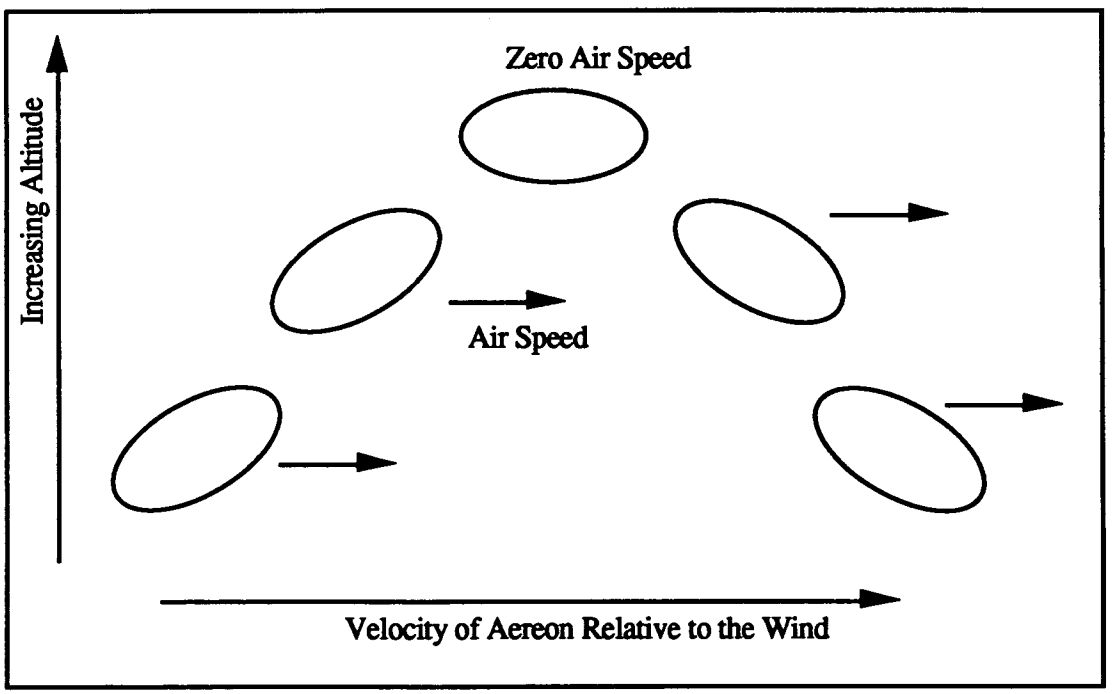

Figure 3.15. Generation of Aereon Thrust

The actual air speed attainable by the Aereon depends on the rate of climb or descent, and the Aereon balloon's angle of attack. Wind tunnel tests showed that an angle of attack of 30° maximizes the Aereon thrust. From trigonometry, at an angle of attack of 30°, the Aereon thrust is twice the rate of climb or descent. The rate of descent is calculated from the mass flow achievable by the compressor at a given power input. This rate varies with altitude, pressure and temperature, as shown in Figure 3.16. By taking the slope of the curves in Figure 3.16, the Aereon can descend at a maximum rate between 1.5 and 4 m/s, giving the Aereon an air speed of between 3 and 8 m/s. This air speed compares favorably to the Martian wind speeds, which range from 5 to 24 m/s, allowing the Aereon to travel in almost any direction desired. The Aereon can control its direction, or relative ground speed, while in flight as shown in Figure 3.17. The ground speed is simply the vector addition of the wind speed and the Aereon's air speed. In addition to being able to control the air speed, the Aereon can also choose its wind speed, to a limited extent, by choosing the altitude at which it flies. The wind speeds at Mars, like those at Earth, vary with altitude.

If the Aereon is not oriented in the proper direction with respect to the wind, it must be turned about its yaw axis. Turning the Aereon about its yaw axis may prove to be difficult. One method proposed is to attach a sail between the balloon and gondola. This system, however, is complicated due to the instruments located on top of the gondola, and also may not be very effective. A simpler system is illustrated in Figure 3.18. It consists of sticking a parachute out to the side of the gondola, similar to placing a paddle into the water from a moving boat. The drag force caused by the parachute creates a torque which tends to turn the Aereon. Preliminary analysis, however, shows that this system also may not be very effective as the time to turn 90° is on the order of hours.

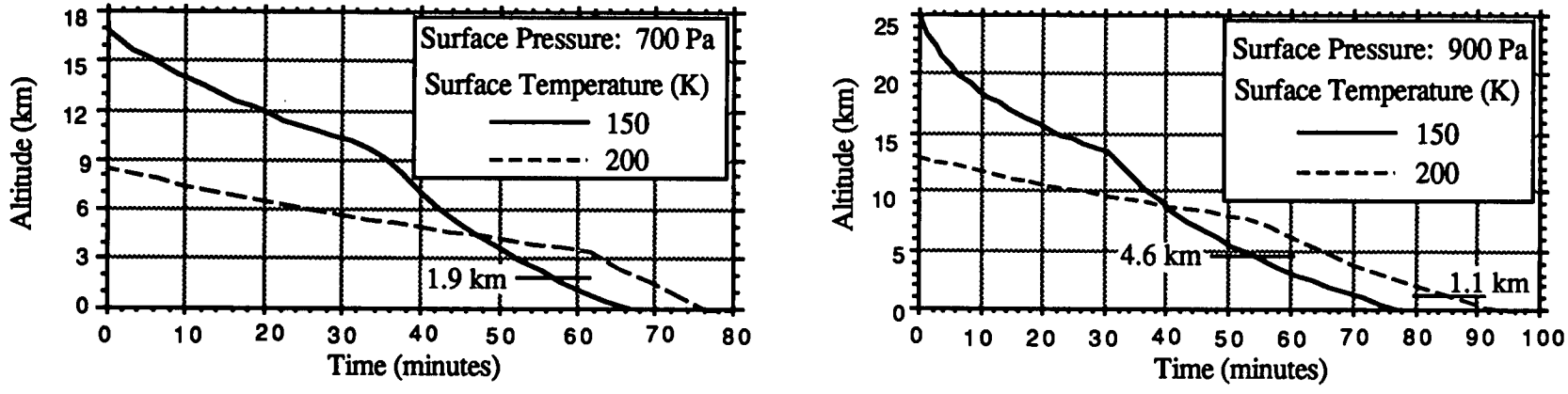

(a). Constant Pressure Descent Rates at Different Temperatures

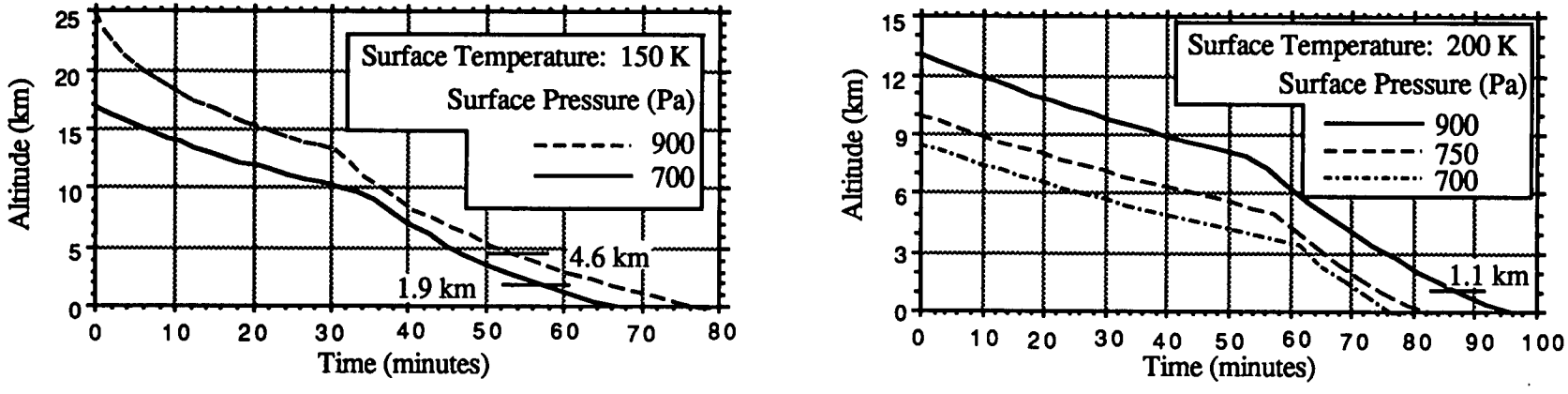

(b). Constant Temperature Descent Rates at Different Pressures

Figure 3.16 Aereon Descent Profiles at Different Pressure and Temperature Conditions

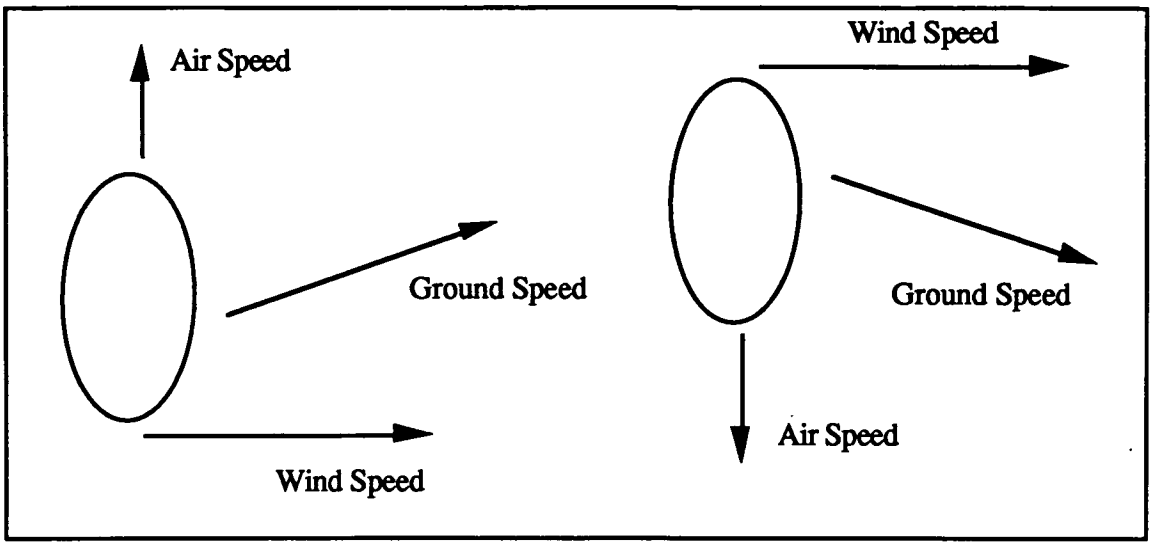

Figure 3.17. Aereon Ground Speed versus Air Speed

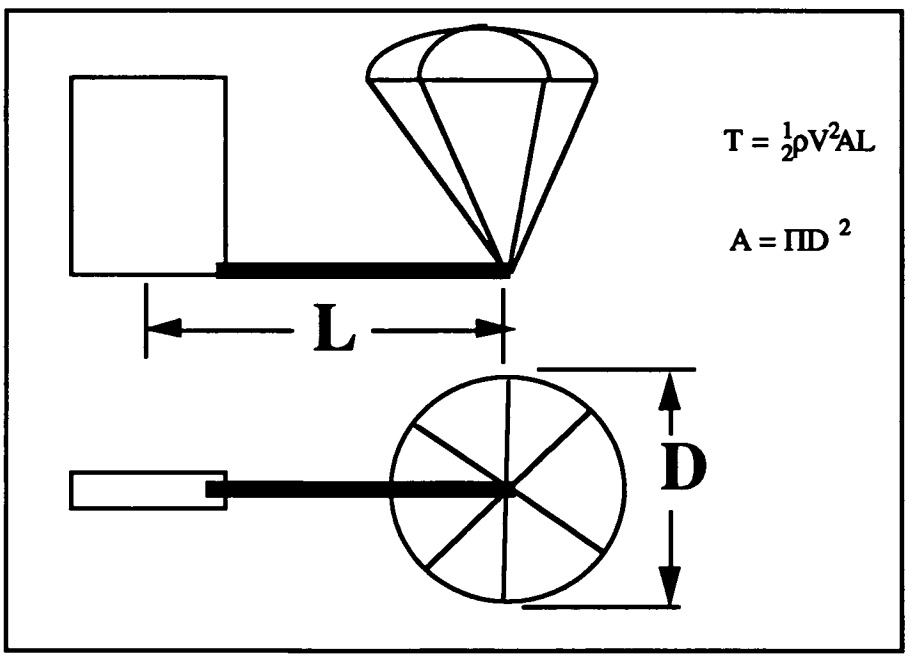

Figure 3.18. Aereon Turning System

CHAPTER IV
VEHICLE SUBSYSTEMS

4.1. Chassis Structure

The structural design of the rover that has been developed is shown in Figure 4.1. In designing the structure, the location and masses of the subsystems are considered. Using basic structural design analysis, elements are connected at nodes where loads are applied. The frame consists of 1 inch square I-beams with a thickness of 0.25 inches. These I-beams are 6060-T6 aluminum, reinforced with composite end caps. One proposed composite to use is Kevlar. Kevlar is an ideal choice because of its high strength and light weight. Out of the plethora of possible materials, these are considered most advantageous in satisfying mass and support strength constraints. The total mass of the aluminum - composite structure is 65.363 kg. This structure serves as a support for the exterior skin of the rover which is made of a light-weight composite material which resists degradation to radiation in the Martian environment. Kevlar is a proposed composite for the skin of the rover. The structure is arranged in accordance with the positioning of the systems inside the rover, and is designed to protect the interior components from damage due to loads present upon landing. Additional finite element analysis needs to be performed to determine a complete stress analysis of the structure.

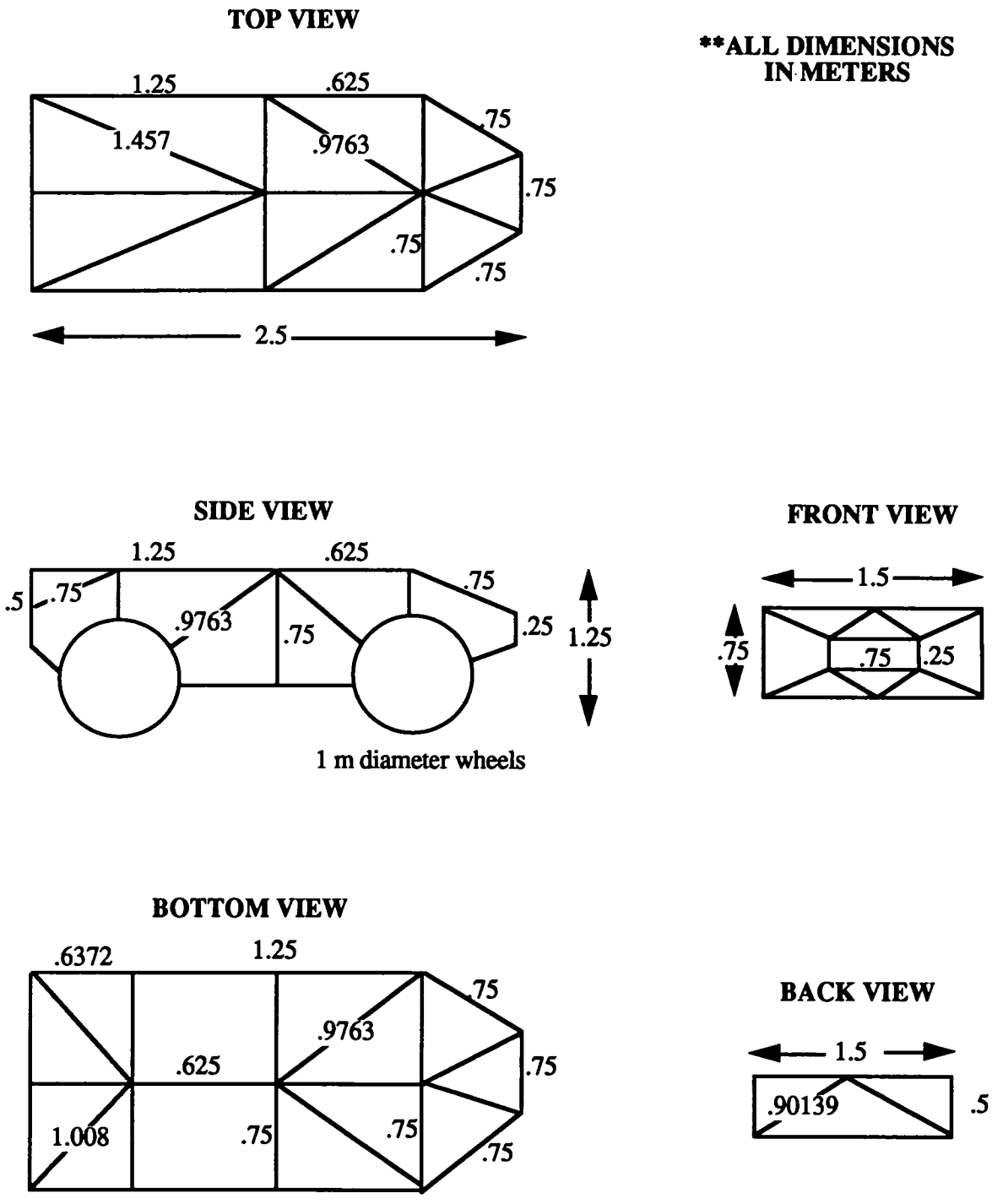

Figure 4.1. Rover Chassis Structure.

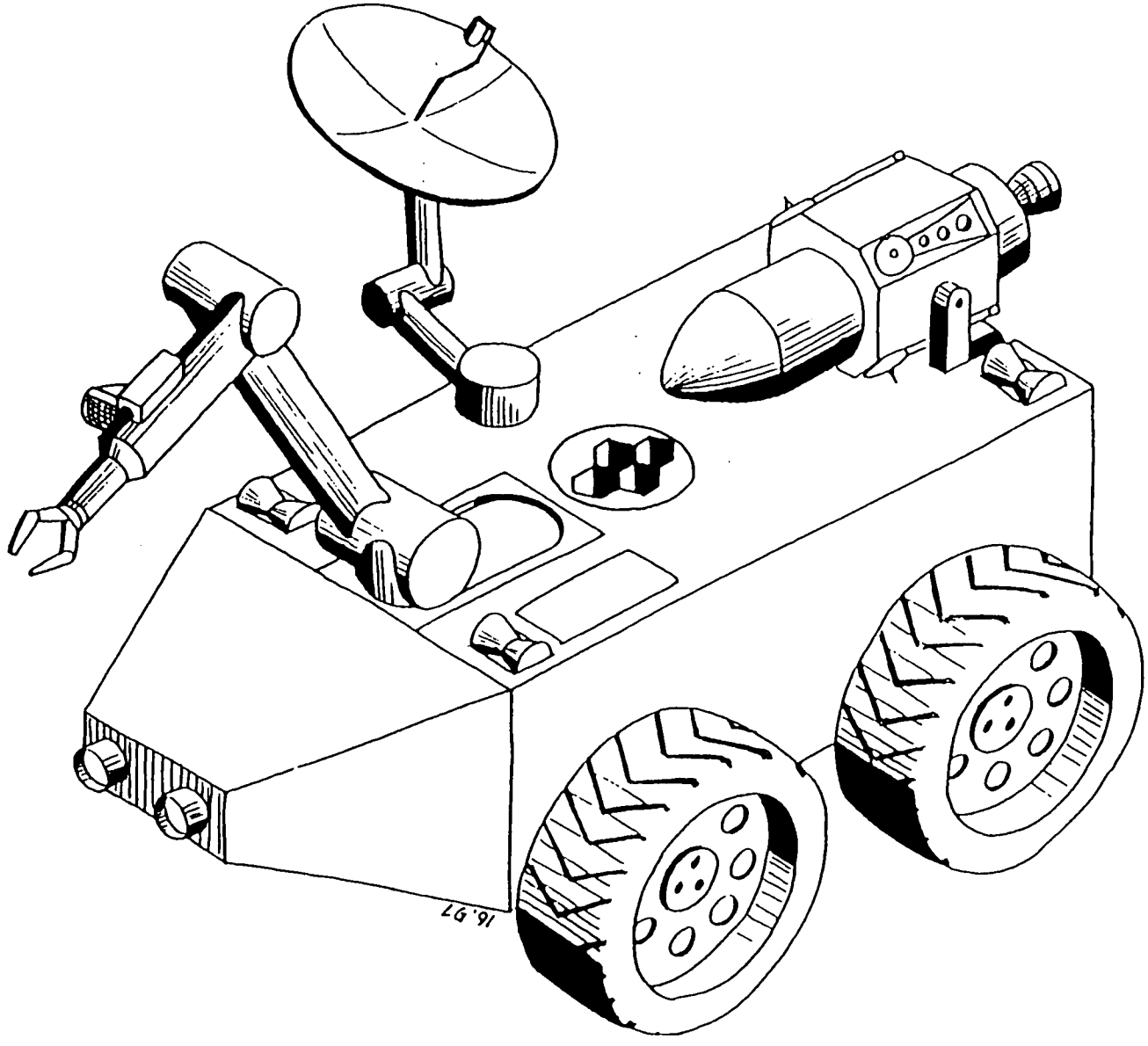

Figure 4.2. Rover Exterior Sub-Systems

4.2. Harnessing Cable System

The drive motor for the surface locomotion system also drives the pulley system for balloon attitude control. The forward and rearward cables are wound to a common spool. Each cable is wound opposite to the other. This allows one cable to unwind as the other is wound. The shaft for the pulley system is located above the drive motor (Figure 4.5). To provide torque to the pulley system a shaft with threaded ends is utilized. In order to control the direction of spool rotation, the torque direction of the motor is varied. The lifting action of the balloon pulls the cable which is being unwound. To change the attitude of the balloon the drive motor operates with less than maximum power input.

4.3. Electric Power System

A MOD-RTG (Modular-Radioisotope Thermoelectric Generator) is used to generate the electricity required to run the Aereon's systems and instruments. It is the latest RTG space power source currently being developed by NASA. It builds on the extensive history of RTG based space power sources used by previous NASA missions, the most recent being the GPHS-RTG (General Purpose Heat Source) used by the Galileo and Ulysses spacecraft (Bennett, et al. 1987).

The MOD-RTG has a specific power output design goal of greater than 7.7 W/kg with a minimum 5 year operating life. It is expected to be ready for production of flight units in the early 1990's (Hartman, et al. 1987).

The main goal of the MOD-RTG design is modularity, i.e. the ability of the MOD-RTG to be scaled to any desired power level. Thus, building a MOD-RTG to fit the power level required by the Aereons should not be a problem. A power output of 120 W is deemed necessary to operate the various systems and instruments on the Aereon, shown in Table 4.1. Martian air is forced over radiators to cool the RTG. Using the data for the GPHS-RTG, the RTG will experience a thermal loss of 0.8 % W / year.

Table 4.1. Power Requirements

	(W)
Wheels	80
Compressor	80
Scientific Instruments	45
Communications	65
Balloon Tethers Winch	80
RTG Cooling Fans	7

The MOD-RTG mass breakdown and operating characteristics are shown in Tables 4.2 and 4.3 respectively.

Table 4.2. Power System Mass (USU 1987)

	(kg)
RTG	15
GPHS	1.0
Supports	0.8
Power Distribution Unit	5.0
Total	21.8

Table 4.3. MOD-RTG Characteristics

Power Output (BOM)	120 W
Converter Efficiency (Berts 1988)	7.5 %
Radiator Temperature	570 K
Length and Diameter (Hartman, et al. 1985)	0.44 m x 0.33 m
Optimum Load Voltage (Hartman, et al. 1985)	28.6 V
Open Circuit Voltage (Hartman, et al. 1985)	52.0 V

4.4. Compressor System

A reciprocating, single stage, double-acting compressor feeds Martian atmosphere to and from the ballast balloon. Comparison of different compressors shows that, with power and size constraints, this is the best compressor to achieve the desired goal. Both rotary and centrifugal compressors are too large for the Aereon mass constraints. A rotary compressor requires more power than a reciprocating compressor. The ability to use the reciprocating compressor to pump the air from the ballast balloon allows for increased altitude control during descent. The volume displaced per stroke is 0.0283 cubic meters. The bore diameter is 0.2540 meters and the stroke is 0.5588 meters [Brown 1986] (Figure 4.3).

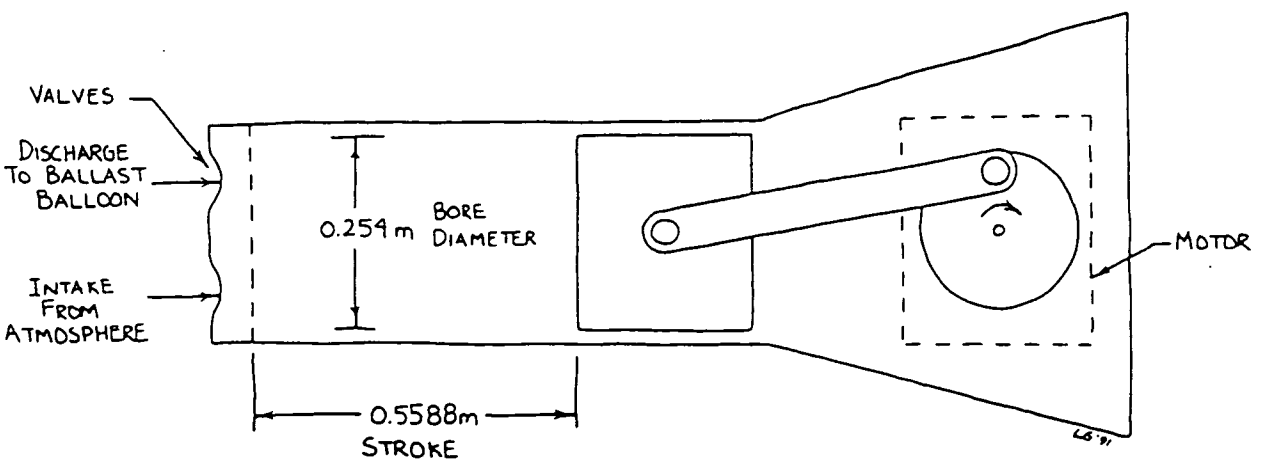

Figure 4.3. Compressor Dimensions

The mass flow rate of the martian air into the ballast balloon is controlled by varying the volume flow rate of the compressor. Changing the input power varies the compressor speed and, in turn the volume flow rate (Figure 4.4). A constant mass flow rate is attained by varying the volume flow rate via input power with a varying density. A maximum of 1000 rpm is attainable by the reciprocating compressor [Brown 1986]. This corresponds to a volume flow rate of 0.47 cubic meters per second, which is more than necessary to control the altitude of the Aereon.

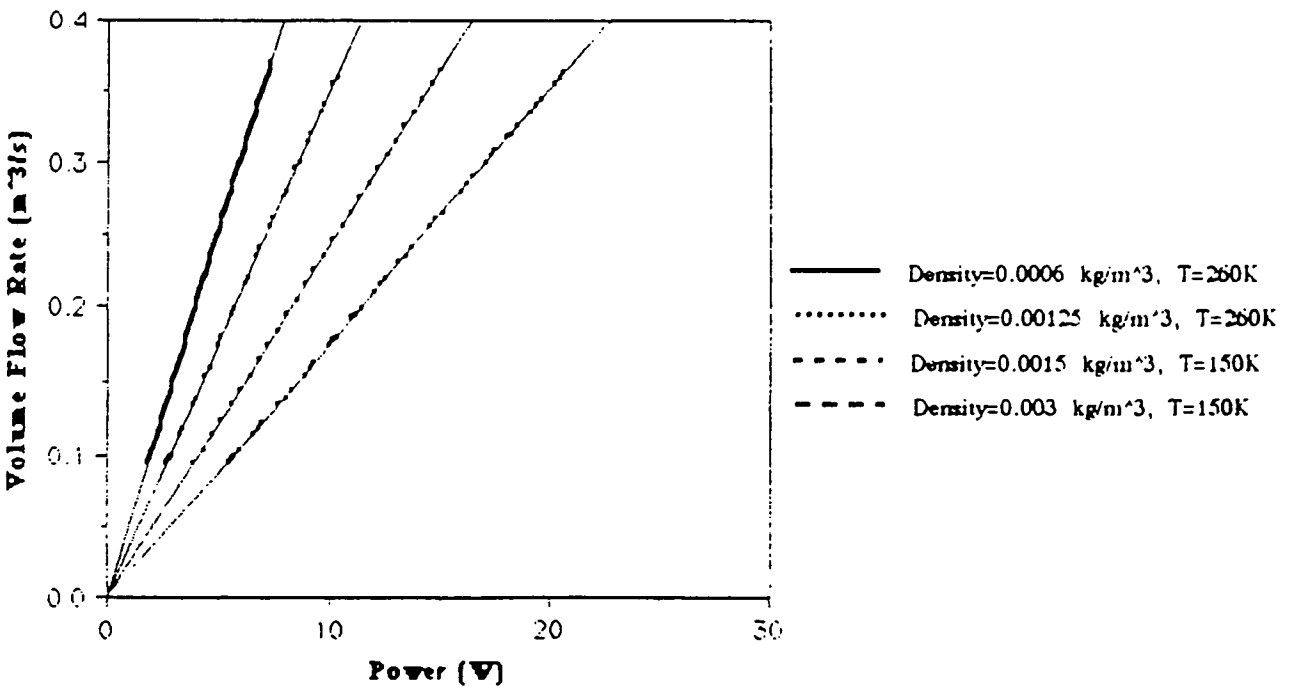

Figure 4.4. Volume Flow Rate vs. Power

4.5. Hydrogen Storage Tanks

The hydrogen which is used in the Aereons is stored initially in a tank on the lander. In addition to this tank, there is also a tank on each of the Aereon rovers. These tanks are designed to replenish any hydrogen which may be lost by dissociation through the balloon skin. Spherical tanks are used since they provide the most volume for the least amount of surface area, which is beneficial for the mass constraint. Hydrogen can either be stored as a liquid at a very low temperature or as a gas at a very high pressure. A cryogenic, or low temperature system, requires a refrigeration unit which can be very massive. A high pressure system requires a tank with much thicker walls than that of a cryogenic system, which also adds to the total mass. A high pressure system was chosen because it was found to be lighter and less complex than a cryogenic system. To save additional mass, the storage tanks are constructed of a very light-weight composite material. Leakage of hydrogen from the tanks is prevented by using a metal-foil liner on the inside of the tanks.

The use of composite tanks with load sharing metallic liners was tested and proven in various space systems. Typically, composite tanks are designed for applications with low life cycles. Since these tanks are only filled and emptied once, composite tanks perform well. To keep costs at a minimum, 6061-T6 aluminum is chosen as the liner material because of its low cost, ease of manufacturing, and low density. Aluminum demonstrates excellent fatigue resistance in other pressurized tank applications. The liner of the tank consists of two aluminum hemispheres 5.08×10^{-4} meters thick that are welded at the equatorial region and overwrapped with carbon-epoxy composite. A four ply quasi-isentropic carbon fiber laminate with a failure stress of 910 MPa is used. The approximate density of this material is 1378 kg/m^3. The size of the spherical tank is determined by knowing the mass of hydrogen in the balloon. A computer code was written in which the tank diameter and thickness are varied and the corresponding tank volume, pressure, and

mass are calculated. The development of this code and the results can be found in Appendix A.

An important design consideration is the separation of the liner from the inside of the composite shell. When the temperature drops, the metal foil contracts while the composite material shrinks very little. The solution to this problem is to apply a liner containing fibers of Spectra 1000 between the aluminum liner and the composite shell. Spectra 1000 is a high-strength, high-modulus material that expands with decreases in temperature. Therefore, as the temperature decreases, the Spectra 1000 liner expands and pulls the aluminum liner back against the composite tank. Both liners are relatively thin in comparison to the thickness of the composite material and do not add significant mass or decrease total volume.

From the results of the computer code found in Appendix A, a lander tank of 1.5 meters in diameter and 0.0225 meters thick is chosen. For this tank, the mass is calculated to be 235 kg with a storage pressure of 0.546×10^8 Pa. Since the tanks on the rovers hold approximately 10% of the balloon volume, tanks 0.5 meters in diameter and 0.0205 meters thick are chosen. These tanks have a mass of 25 kg each and the storage pressure is 0.149×10^9 Pa.

4.6. Surface Locomotion System

The surface locomotion system propels the Aereon when it is on the ground (Figure 4.5). A slow walking speed of 1 m/s on a level surface was set as the design goal. In addition, a 20 percent grade was assumed to be the maximum slope that the Aereon would climb. The mass of the Aereon used was 500 kg. Four one meter diameter, non-pneumatic, polyurethane wheels provide the traction with the ground. The coefficient of rolling friction is assumed to be 0.012 [Moore 1975].

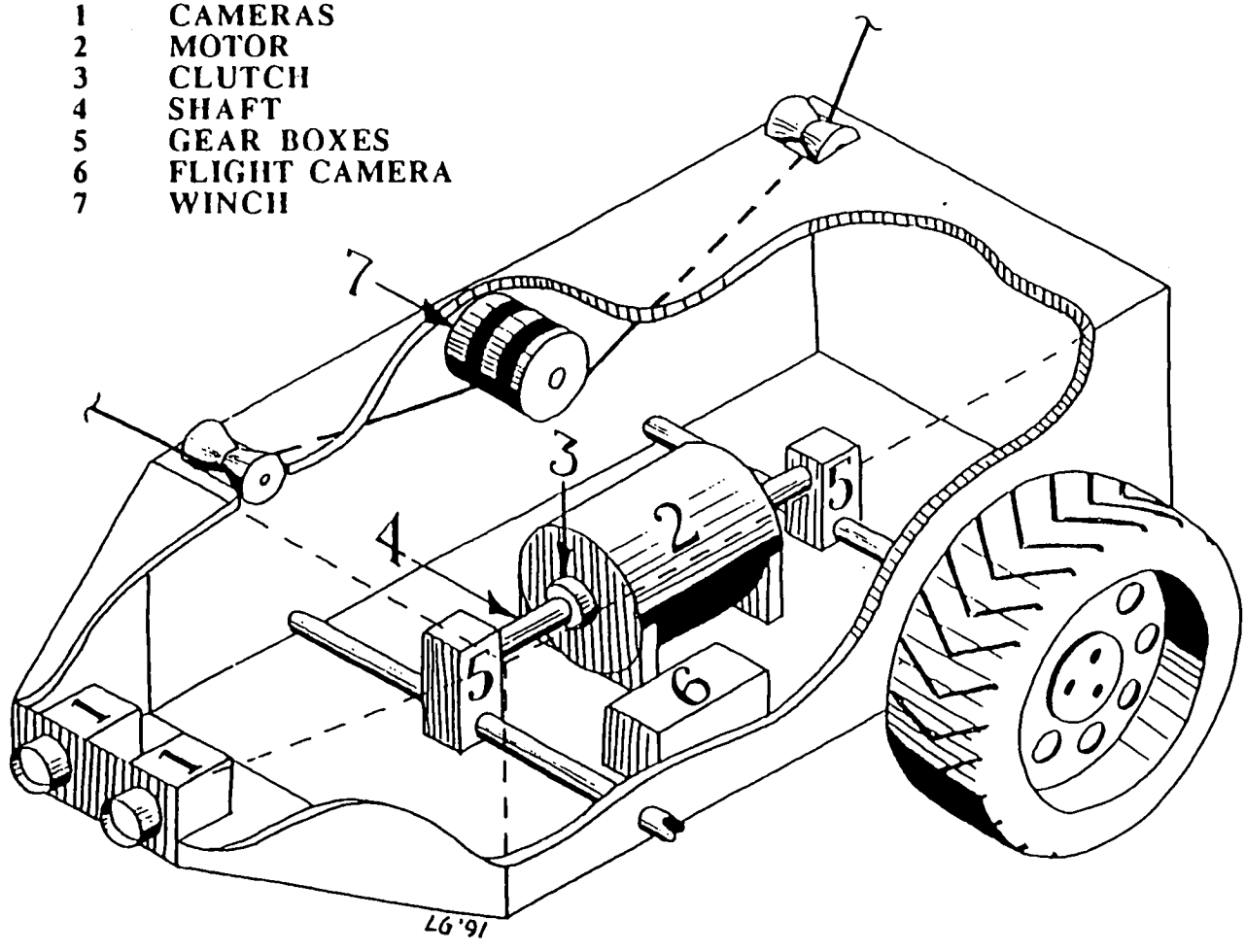

Figure 4.5. Rover Locomotion System

A four wheel drive transmission, running off of a common drive shaft, provides torque to the wheels. Each pair of wheels is attached to a rigid shaft. Both viscous and inertia effects are considered through the shaft. A gear ratio of 1:2 for each transaxle is employed, with 90% efficiency in the gear train assumed.

Over level ground with no obstacles, the required torque on each wheel is 2.79 Nm. At the design goal of 1 m/s, this gives a required power input of 3.10 Watts. This is well within the power system's range. At the maximum grade of 20 percent, the torque per wheel is 48.29 Nm. This yields 53.66 Watts required to move at 1 m/s. The system is allowed a maximum of 80 Watts.

The range of the Aereon ground movement is limited to the lifetime of the power source, the characteristics of the driver motor, and the surrounding Martian terrain where it lands. The effects of the Martian atmosphere may shorten the lifetime of the motor through deterioration of the lubricants. This deterioration is not envisioned to be a problem during the Aereon's mission life.

4.7. Landing Survival System

To collect samples, the Aereon must descend and land on the Martian surface. It is possible that the Aereon may make a hard landing which could damage the internal components of the rover. In addition to a hard landing, internal components such as the motor and power systems vibrate while operating, which can transmit noise and stress to surrounding instruments and structures, resulting in fatigue and reduced reliability of the system.

To control vibrations from inner systems, the motor and power systems are equipped with L-mounts to help damp out vibrations. These mounts have a low ratio of horizontal-to-vertical stiffness and horizontal self-centering damping. These characteristics hold vibration in rocking modes to low magnitudes.

To help prevent the possibilities of landing and vibration damage, the Aereon is equipped with a piston-shock absorbing system. The Aereon landing environment is modeled after that of an aircraft. Sources of vibration, shock, and noise are similar to those of an aircraft which include air turbulence, compressor noise, structural resonances, and most important, landing impact. Being modeled after an aircraft landing system, the piston-shocks have a load factor of 2.5 which is in accordance with FAA regulations. The piston consists of two struts which fit inside each other with compressed air inside. A typical strut pressure of 3000 psi is assumed. An impact velocity of 2 m/s is approximated for landing on the Martian surface. With an impact velocity of 2 m/s and a maximum Aereon mass of 500 kg, a strut stroke of 11.75 cm results. This strut stroke corresponds to how much the shock depresses upon impact. The diameter of the shock is calculated to be 6.074 cm with a corresponding length of 18 cm. There are four piston shocks on the rover, one at the support of each of the four wheels. The four shocks correspond to a total mass of 7.255 kg. Piston shocks are chosen because of the similarity of the Aereon landing system to an aircraft landing system and because of their presumed similar performance.

4.8. Autonomous Control System

In order for the mission to be carried out with safety, there is a need for an Autonomous Control System (ACS). A multi-input / multi-output control system acts as the central nerve center for vehicle operations. Commands from Earth as to the flight of the vehicle take too long for assured safe operations to be performed. The ACS required for the mission is relatively complex compared to the types of control systems used in current spacecraft. Decision making processes based on surrounding geographic information and desired tasks is evaluated at a high rates of speed in coordination with driving the real time performance of the vehicle.

Operations that the ACS drives such as the directional maneuvers and thrust production depend upon the temperature, pressure, wind speed and direction. The orbiting communications satellite determines wind speed and direction variations in the altitude. Information about the varying wind layers is transmitted to the Aereon Sampler, from which the ACS determines which altitude is optimal for reaching its destination. Constant communication with the orbiting satellite is not planned, so an update of the wind layers is received on every possible flyby. Determining the position on the planet seems impossible since compass readings do not exist in the weak magnetic field. Updates as to the current position are received from the communications satellite. Information as to the possibility of a global dust storm is received from the orbiter. In addition to the planetary information, changes in the mission plan are transmitted to the Aereon Sampler.

Through the use of the onboard instruments, information on the surrounding geographic terrain is found with the stereoscopic cameras. A computer representation of the surrounding area is generated. With this model, the ACS evaluates what maneuvers to perform to evade obstacles in the flight path, and what maneuvers are needed to land at a collection site.

The ACS requires adequate intelligence to perform the tasks for deployment of the Aereon Sampler from the lander. Collection of the samples require the ACS to drive the robot manipulator arm, and to store samples in the sample collection containers. Operations include loading the Sample Delivery Rocket and deploying it for launch (Figure 4.6).

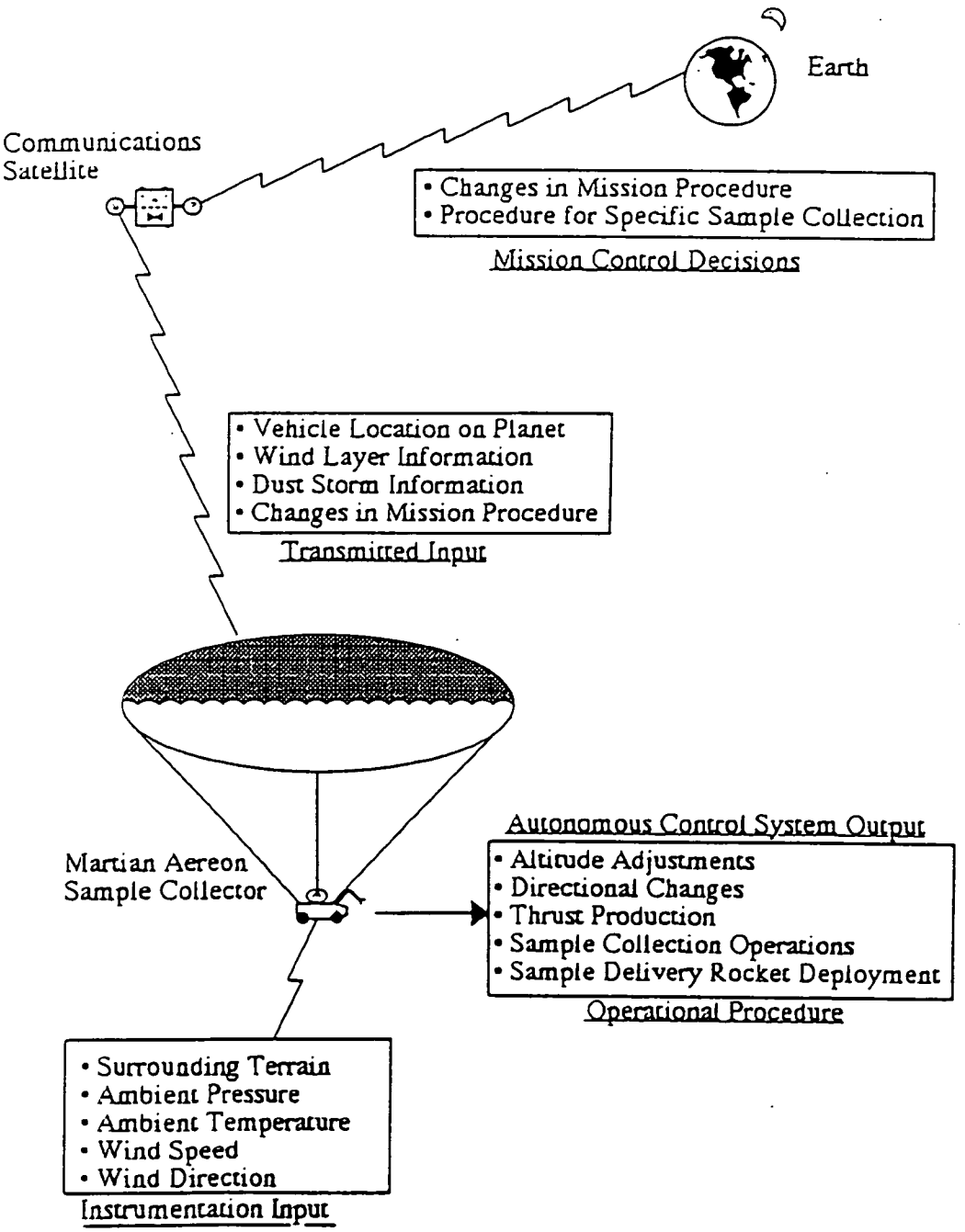

Figure 4.6. Autonomous Control System Operations Schematic.

4.9. Robot Manipulator Arm and Tools

The choice of which robotic arm to use on the rover was made on the basis of mass, size, material, and power constraints. The robotic arm shown in Figure 4.7 is used to collect samples from various landing sites on the planet. It is located 1.875 meters from the front of the rover.

The arm uses two different interlocking tools to collect the samples. Both tools are shown in Figure 4.8. The first tool is a grabber that is used to pick up samples from the surface of the planet. The grabber is chosen for its extended reach as compared to a claw.

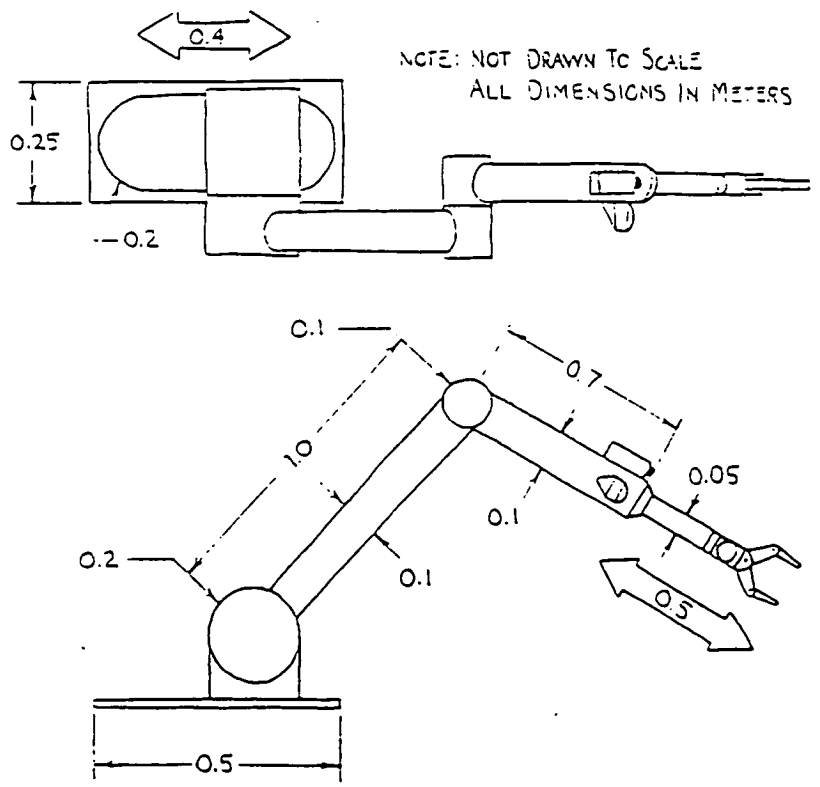

Figure 4.7. Robotic Arm

The second tool is a scoop / sieve combination. The robot arm does not make use of a rock pick or any cutting devices such as a linear saw. Samples which are already lying loose on the surface are simply picked up by the arm and stored in the sample storage containers. The reach of the arm can be extended 0.17 meters beyond the original arm length if it becomes necessary to collect a sample at a considerable distance from the rover. The arm reach is made extendable through the use of a retractable extension placed on the end of the arm closest to the surface.

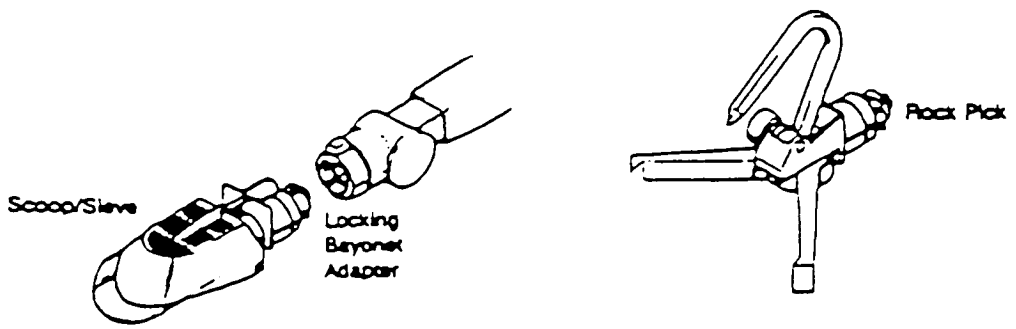

Figure 4.8. Robotic Arm Tools. [Reiber 1988]

The maneuverable arm is powered through the use of an RTG. The total power required to operate the arm with the RTG is 27 watts. The base-sweep of the arm, moves in a horizontal direction, and is powered with an electric motor placed within the base of the arm. Vertical arm movement is made possible through the use of autonomous control computers on-board the rover. The arm may be directly controlled by mission operators on Earth at those times when communication is established between the communication satellite and the rover. A camera is placed near the far end of the arm to observe which sample the arm is collecting. In addition to camera observations, a pre-programmed sample limitation device is located in the collection end of the arm. Due to material constraints, the arm is only capable of picking samples of up to 1.24 kg off the Martian surface.

The arm is made of a heavy aluminum alloy which is wrapped with Kevlar composite fibers for reinforcement. This material choice is made because the mass of the arm is limited to a maximum of 19.5 Kilograms. This mass is extremely low compared to the rest of the Aereon rover.

The two previously mentioned tools, which are used by the robotic arm, are stored in a small storage compartment located next to the arm. Each tool is attached to the end of the arm at different times.

Due to the dust storms that may be encountered while the Aereon is traversing the Martian surface, the robotic arm is stored in a compressed position on the surface of the rover. This compressed storage precaution saves the arm from being ripped off or damaged during atmospheric travel. Aereon vehicle drag is also reduced if the arm is not directly in the free stream flow field.

4.10. Scientific Instruments

While the major function of the Aereon is to collect samples, various scientific data is also collected on the Martian surface. This data is collected with the help of various instruments (Figure 4.9). These instruments are listed and described below.

4.10.1 Atmospheric Composition and Structure

The purpose of the atmospheric analysis that will be performed is to identify the composition of the Martian atmosphere and to determine constituent abundance. The composition of the atmosphere is studied by sampling the Martian air at intervals, and analyzing these samples with a mass spectrometer. The position at which each sample is taken is referenced by the use of a radar altimeter. By using these two instruments in conjunction, atmospheric data can be correlated with planetary location. A cross section of the lower atmosphere can be studied during the aerial mission of the Aereon [USU, 1987].

KEY

1 H2 TANK
2 COMPUTER
3 TOOLS
4 SAMPLES
5 ATOMIC MASS SPECTROMETER
6 METERORLOGICAL DEVICES
7 COMPRESSOR
8 RTG
9 RADAR ALTIMETER

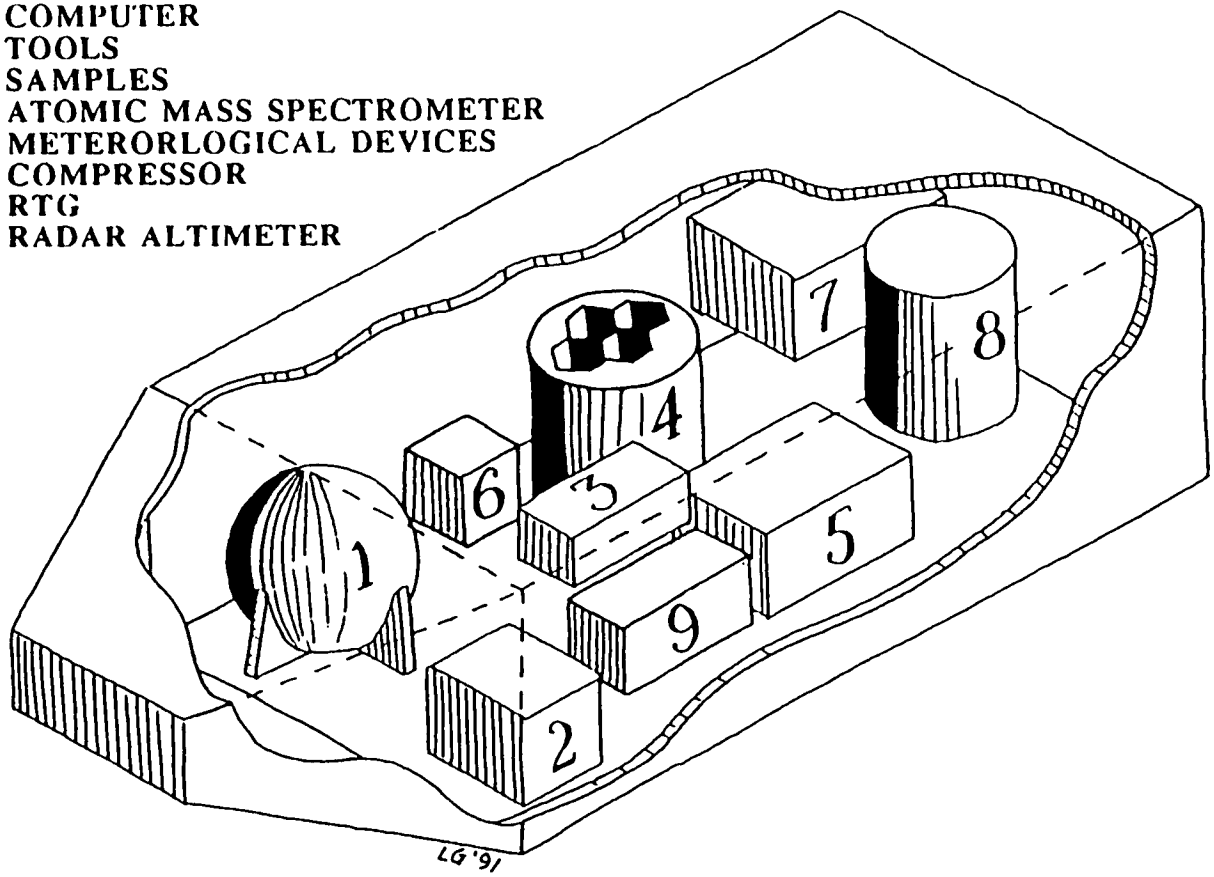

Figure 4.9. Rover Internal Components

4.10.2 Aerial Photography

The aerial photography mission uses lightweight stereoscopic cameras, allowing a 3-D image to be produced. Each camera has a mass of 2 kg. Two cameras are located in the front of the rover for forward view. Two are located on the bottom of the rover for aerial photography. These cameras are used in conjunction with the radar altimeter to map the surface of the planet. One camera is chosen to be located on the robot arm which allows sample collection to be monitored. The location of cameras is chosen so as to function both during flight and when grounded. Depending on the rovers ability to relay data to the communications satellite, imaging may be processed continuously, or may be stored in on-board computers for later transmission.

4.10.3 Meteorology Devices

Various transducers are arranged with the computer system to characterize the environment during the Aereon's flight and descent. These transducers consist of temperature, pressure, density, wind speed, and direction, and solar flux sensors. These transducers measure their respective quantities, with data relayed through the Aereon's on-board computer.

4.10.4 Instrument Arrangement Consideration

There are several constraints imposed by the position of various instruments and they are as follows, (USU, 1987).

1. Temperature sensors are shaded so as to keep them in thermal balance with the atmosphere.
2. The radar altimeter is placed on the bottom of the rover, where it is always facing the ground.
3. Air intakes are provided for the mass spectrometer and pressure sensors.

4. The RTG and other instruments are arranged such that the landing dynamics are stable.
5. The RTG must be insulated to prevent contamination to the computers, meteorological transducers and the mass spectrometer.

The total mass of the instrument package is 18.8 kg and the power requirement is 25 W. From a long list of possible instruments for the Aereon to use some were eliminated because of the weight constraint. The four main instruments, mass spectrometer, radar altimeter, meteorological transducers, and cameras, are chosen because of their need and versatility. Only some planetary measurements need to be taken, resulting in the most vital instruments accompanying the Aereon on its mission. These instruments can perform desired functions, and because of the lowered number of instruments, the mass is lowered.

4.11. Sample Delivery Rocket

The Sample Delivery Rocket (SDR) is proposed as a contingent system to deliver the samples from the Aereon to the vicinity of the lander base and land rover if the Aereon is unable to do so. Three cases are envisioned where the SDR must be utilized: (1) The balloon becomes disabled, (2) the Aereon land unit becomes stuck such that it cannot be pulled out by the balloon, and (3) the Aereon is blown off course and is unable to reach the range of the land rover (200 km). To prevent total loss, the SDR would be launched if the land rover's range is within that of the SDR.

The SDR is designed to be a single-stage rocket carried by the Aereons as shown in Figure 4.10. The requirements and parameters that affected the design are the need for simplicity, autonomy, and low mass. Because of these specifications, the amount of samples to be collected by each Aereon is limited to 7 kg or 1340 cm^3. The structure must be lightweight but durable. For this reason a carbon-epoxy composite material is used for the structure. The solid propellant is wound with the material to minimize the structural mass.

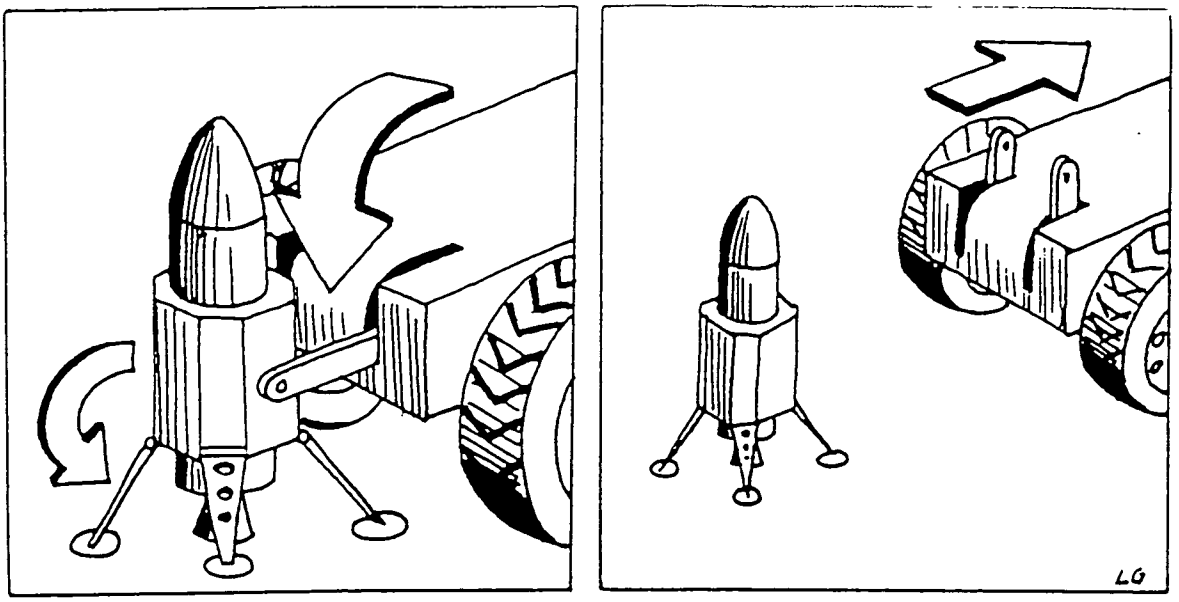

Figure 4.10. Deployment of the Sample Delivery Rocket.

A maximum range of the rocket is set at 200 km. Since the land rover has a range of 200 km, the samples can be delivered from approximately 400 km from the lander base. By setting the range, the burnout velocity can be calculated using ballistic trajectory relations [Bate, Mueller, and White 1971]. Choosing a propellant mass (which is the major contributor) and structural ratio allows the calculation of the payload mass. Approximate dimensions of the rocket can then be determined.

The nose section of the SDR contains the parachute, guidance and control systems, and the homing beacon. The middle section contains the samples. The samples are housed in storage containers compatible with those of the land rover (see Section 4.12). The lower section is a solid propellant chamber. The propellant is wound with carbon composite fiber to reduce the structural mass. A star bore of the solid propellant prevents structural heating until the final seconds of the burn. This type of pattern allows a thrust profile that is near maximum a few seconds into the burn when trajectory adjustments are made.

4.12. Sample Storage Containers

The sample containment units used by the Aereons must be compatible with those used by the land rover; the compartments are hexagonal. Three single hexagonal compartments are used by each Aereon. They are designed with the same requirements as those of the land rover: (1) Structural integrity to withstand the 5 g acceleration of the Mars

Ascent Vehicle, (2) minimum solar radiation contamination, (3) maximization of storage space utilization, (4) sample isolation , and (5) keeping the samples intact.

The SDR and Aereon each have a set of three of the hexagonal compartments for sample storage. Smaller separate containers that fit inside the compartments contain the samples. They are stacked inside the compartments such that the bottom of one container is the lid to the other. If copper is used on the rim and base of the canisters, the robotic arm can create a seal by tapping the top container. Another method for sealing the compartments is using two different substances on the rim and base of the containers that form a bond when placed together. This latter method provides difficulty in storage of the containers because they would have to be isolated from each other to prevent accidental sealing. By using the copper, the containers may be stacked in storage without sealing.

CHAPTER FIVE
RECOMMENDATIONS AND CONCLUSIONS

5.1 Overall Mass Breakdown of the Aereon

The total mass breakdown of the Aereon is shown in Table 5.1. A mass budget of 500 kilograms was allotted to each Aereon. Much work was done to keep within the mass restriction of 500 kg. The Aereon balloon is optimized for size which required some components originally designed to be removed to make room for the SDR. The basic chassis structure was designed without the use of finite element analysis. Further analysis of the structure is needed to determine structural stability. All mass values are estimates from density-volume calculations, catalog specifications and engineering judgement. The total mass of the Aereon is 452 kilograms.

Table 5.1 Final Mass Breakdown of the Aereon

Subsystem	Report Findings (kg)
Balloon Skins	187
H_2 and Reserve H_2 Tank	39
Instruments, RTG, and Supporting Systems	47
SDR	11
Rover Structure, Wheels and Motor	133
Communications Equipment Computers and Data Storage	35

5.2 Cost Analysis of the Aereon

The total cost of each Aereon in millions of dollars was determined from the following equation [Cyr 1988]:

$$\$ = 1.72\ E\text{-}5 * Q^{0.5773} * W^{0.6569} * 58.95^{C} * 1.0291^{Y} * G^{-0.3485}$$

G (generation) = 1

Q (quantity of prototypes) = 4

W (weight) = 500 kg

C (Culture Factor) = 2.4

Y (year of start up) = 2002

From this model, the total cost of each Aereon is determined to be $ 633 million.

REFERENCES

Agrawal, Brij N., Design of Geosynchronous Spacecraft, Prentice Hall Inc., 1986.

Alerich, Walter N., Electric Motor Control, Delmar Publishers, Inc., Albany, New York, 1965.

Barry, Application Selection Guide, Barry Wright Corp., 1977.

Bate, R.R., Mueller, D.D., and White, J.E., Fundamentals of Astrodynamics, Dover Publications, Inc., New York, New York, 1971.

Batson, R.M., Bridges, P.M., and Inge, J.L., Atlas of Mars - The 1:5,000,000 Series, National Aeronautics and Space Administration, U.S. Government Printing Office, Washington, D.C., 1979.

Berts, David J., Preliminary Assessment of Rover Power Systems for the Mars Sample Return Mission, NASA LeRC, 1989.

Burgeson, John, E., "Reinforcing Linear for Composite Cryogenic Tanks," NASA Tech Briefs, June 1990.

Burgess, Charles P., Airship Design, Ronald Press Company, New York, 1927.

Camci, C. Dr., 'Aerospace Engineering 430 - Rocket Propulsion Class Notes', Department of Aerospace Engineering Pennsylvania State University, Spring, 1991.

Carr, Michael H., The Surface of Mars, Yale University Press, 1981.

Chamberlain, Joseph W., Theory of Planetary Atmospheres, Academic Press, Inc., 1978.

Charles C. Libby, Motor Selection and Application, McGraw Hill Book Company Inc. New York, 1960.

Coiffet, Philippe, Robot Technology Modeling and Control, Prentice-Hall Inc., 1983.

Craig, John J., Adaptive Control of Mechanical Manipulators, Addison-Westley Publishing Company, 1955.

Cyr, Kelley, 'Cost Estimate Methods For Advanced Space Systems', NASA Johnson Space Center, 1988, SAWE Paper No. 1856.

DeLaurier, J.D. and Hui, K.C.K., 'Airship Survivability in Atmospheric Turbulence', AIAA Lighter-Than-Air Technology Conference, 1981, AIAA Paper 81-1323.

DeLaurier, J.D., 'Refinements and Experimental Comparisons of Stability Analysis for Aerodynamically-Shaped Tethered Balloons', AIAA Lighter-Than-Air Systems Technology Conference, 1975, AIAA Paper No. 75-943.

Heinsheimer T.F., Friend, R.C., and Siegel, Neil G., 'Concepts for Autonomous Flight Control for a Balloon on Mars', NASA Paper N89-15600.

Hill, and Peterson, Mechanics and Thermodynamics of Propulsion, McGraw Hill, 1965.

Holland, John M., Basic Robotic Concepts, Howard W. Sams and Co., Inc., 1983.

Hookway, R.O. and Pretty J.R., 'HASPA Flight Control Concepts', AIAA Lighter Than Air Technology Conference, 1975, AIAA Paper No 75-942.

Jackson, J.P. and Dichtl, R.J., The Science and the Art of Hot Air Ballooning, Garland Publishing, Inc., New York, 1977.

Kaplan, Marshall H., Modern Spacecraft Dynamics and Control, John Wiley & Sons, 1976, pp. 72-108, 308-29.

Kondratyev, K.Y. and Hunt, G.E., Weather and Climate on Planets, Pergamon Press Ltd., 1982.

Larson, George, Blimp!, Van Nostrand Reinhold Co., 1981, pp. 19-20.

Leovy, Dr. Conway, "The Meteorology of Mars", The NASA Mars Conference - Proceeding of the NASA Mars Conference, American Astronautical Society, Vol. 71, 1988.

McCormick, Barnes W., Aerodynamics, Aeronautics, and Flight Mechanics, John Wiley & Sons Inc., 1979.

Moore, D.F., The Friction of Pneumatic Tyres, Elsevier Scientific Publishing Co. New York, 1975.

NASA, Survey of Gas-Correlation Spectroradiometry: The principal application is remote sensing of atmospheres, 1990.

R.L. McItyre, Electric Motor Control Fundamentals 2nd Ed., McGraw Hill Book Company Inc., New York, 1960.

Reiber, Duke B., "The NASA Mars Conference", Proceedings of the NASA Mars Conference, American Astronautical Society, Vol. 71, 1988, pp. 303-472.

Taylor, Janes D., 'The Variable Geometry Airship: A Challenge in Lighter-Than-Air Systems Design.', AIAA 8th Lighter-Than-Air Systems Technology Conference, 1989.

Tiller, Dale, B., " Design and Development of a Carbon Overwrapped, Aluminum Lined Spherical Pressurant Tank," AIAA 1990.

TRW Mars Rover Sample Return Delivery and Return Study Interim Report, June 1990, pp. 5.18-5.28.

Tuwiner, Sidney B., Diffusion and Membrane Technology, Weinhold Publishing Corp., New York, 1962.

USU (Utah State University), Mars Lander/Rover Vehicle Development: An Advanced Space Design Project for USRA and NASA, 1987.

Weisel, William E., Spacecraft Dynamics, McGraw Hill Book Co., 1989, pp. 188-91.

APPENDIX A
CALCULATION OF THE HYDROGEN STORAGE TANK SPECIFICATIONS

The hydrogen tanks used on the lander and rovers are constructed of a four ply quasi-isotropic carbon composite. The maximum stress at failure is assumed to be 910 MPa and the material density is approximately 1378 kg/m^3. The tank liner is 6061-T6 aluminum with a thickness of 5.08 x 10^{-4} meters and a density of 2.71 x 10^3 kg/m^3. The pressure in the tank is assumed to follow the relation:

$$P = \frac{4\sigma t}{d}$$

Since the stress is known, values of diameter (d) and thickness (t) are assumed and the tank pressure is calculated. For a given value of d and t, the tank volume and mass are calculated using:

$$V = \frac{4}{3}\pi\left(\frac{d}{2}\right)^3$$

$$V_{amb} = \frac{4}{3}\pi\left[\left(\frac{d}{2} + t_{amb}\right)^3 - \left(\frac{d}{2}\right)^3\right]$$

$$V_{liner} = \frac{4}{3}\pi\left[\left(\frac{d}{2} + t_{liner}\right)^3 - \left(\frac{d}{2}\right)^3\right]$$

$$mass = \rho_{amb} V_{amb} + \rho_{liner} V_{liner}$$

To find the volume that the hydrogen occupies when released from the balloon, the following equation is used.

$$V_{atm} = \frac{P_{tank}\, V_{tank}\, T_{amb}}{T_{tank}\, P_{amb}}$$

The hydrogen is assumed to be stored at a temperature of 400° K. Ambient conditions are assumed to be:

$$T_{amb} = 130.13° \text{ K}$$

$$P_{amb} = 277.18921 \text{ Pa}$$

The following computer code computes these values by varying the values of the diameter and thickness.

```
0       C*************************************************************
        C*    Program to find the pressure, volume, mass for a spherical     *
        C*            composite tank of varying diameter and thickness.      *
        C*    written by Lee Greenwood                                       *
        C*    Aerospace 401B Spring 1991                                     *
        C*************************************************************
      1       real d,t,temp,v,vcomp,mass,denh2,stress,pi,cdens
*EXT* CC-04 character encountered is not FORTRAN 77 standard
      2       real pa,ta
        C*************************************************************
        C*    d       = tank diameter                                        *
        C*    t       = tank thickness                                       *
        C*    temp    = tank storage temperature                             *
        C*    vcomp   = volume of composite material required                *
        C*    mass    = total mass of the empty tank                         *
        C*    denh2   = density of hydrogen                                  *
        C*    stress  = stress in the composite at rupture                   *
        C*    cdens   = density of the composite                             *
        C*    pa      = ambient pressure                                     *
        C*    ta      = ambient temperature                                  *
        C*    vatm    = volume occupied when release into the balloon        *
        C*    v       = volume inside the tank                               *
        C*    p       = pressure inside the tank                             *
        C*    tliner  = thickness of the aluminum liner                      *
        C*    linden  = liner density                                        *
        C*************************************************************

        C*************************************************************
        C*    Initialize constants                                           *
        C*************************************************************
      3       r      = 4157.2
      4       temp   = 400.0
      5       ta     = 130.13
      6       pa     = 277.18921
      7       stress = 910e6
      8       cdens  = 1378.0
      9       pi     = acos(-1.0)
     10       d      = 0.50
     11       t      = 0.001
     12       tliner = 5.08e-4
     13       linden = 2.71e3
     14       do 10 i = 1,4
     15          PRINT 70,'DIA(m)','THICK(m)','PRESS(Pa)'
             +   ,'VOL(m**3)','MASS(kg)','ATM VOL(m**3)'
     16    70    format ('1',5(a9,4x),a13/1x,78('='))
     17          v = (4.0/3.0) * pi * (d/2.0)**3
     18       do 20 j = 1,50
     19          p      = (4.0*stress*t) / d
     20          vcomp  = (4.0/3.0)*pi*(((d/2.0) + t)**3 - (d/2.0)**3)
     21          vliner = (4.0/3.0)*pi*(((d/2.0) + tliner)**3 - (d/2.0)**3)
     22          mass   = cdens * vcomp + linden * vliner
     23          denh2  = p / (r*temp)
     24          vatm   = (p*v*ta) / (temp*pa)
```

```
      25        print 50,d,t,p,v,mass,vatm
      26    50  format (1x,2(f9.4,3x),g9.4,3x,3(f10.3,3x))
1     27        t = t + 0.0005
      28     20 continue
      29        d = d + 0.5
      30        t = 0.001
      31     10 continue
      32        end
```

1 DIA(m)	THICK(m)	PRESS(Pa)	VOL(m**3)	MASS(kg)	ATM VOL(m**3)
0.5000	0.0010	.7280E+07	0.065	2.170	559.218
0.5000	0.0015	.1092E+08	0.065	2.716	838.826
0.5000	0.0020	.1456E+08	0.065	3.265	1118.435
0.5000	0.0025	.1820E+08	0.065	3.816	1398.043
0.5000	0.0030	.2184E+08	0.065	4.369	1677.653
0.5000	0.0035	.2548E+08	0.065	4.925	1957.261
0.5000	0.0040	.2912E+08	0.065	5.482	2236.868
0.5000	0.0045	.3276E+08	0.065	6.042	2516.474
0.5000	0.0050	.3640E+08	0.065	6.604	2796.081
0.5000	0.0055	.4004E+08	0.065	7.168	3075.688
0.5000	0.0060	.4368E+08	0.065	7.734	3355.295
0.5000	0.0065	.4732E+08	0.065	8.303	3634.902
0.5000	0.0070	.5096E+08	0.065	8.873	3914.509
0.5000	0.0075	.5460E+08	0.065	9.446	4194.117
0.5000	0.0080	.5824E+08	0.065	10.021	4473.723
0.5000	0.0085	.6188E+08	0.065	10.599	4753.332
0.5000	0.0090	.6552E+08	0.065	11.179	5032.938
0.5000	0.0095	.6916E+08	0.065	11.761	5312.543
0.5000	0.0100	.7280E+08	0.065	12.345	5592.152
0.5000	0.0105	.7644E+08	0.065	12.931	5871.758
0.5000	0.0110	.8008E+08	0.065	13.520	6151.371
0.5000	0.0115	.8372E+08	0.065	14.111	6430.977
0.5000	0.0120	.8736E+08	0.065	14.704	6710.582
0.5000	0.0125	.9100E+08	0.065	15.299	6990.191
0.5000	0.0130	.9464E+08	0.065	15.897	7269.797
0.5000	0.0135	.9828E+08	0.065	16.497	7549.406
0.5000	0.0140	.1019E+09	0.065	17.099	7829.012
0.5000	0.0145	.1056E+09	0.065	17.704	8108.617
0.5000	0.0150	.1092E+09	0.065	18.311	8388.230
0.5000	0.0155	.1128E+09	0.065	18.920	8667.832
0.5000	0.0160	.1165E+09	0.065	19.531	8947.441
0.5000	0.0165	.1201E+09	0.065	20.145	9227.051
0.5000	0.0170	.1238E+09	0.065	20.761	9506.652
0.5000	0.0175	.1274E+09	0.065	21.380	9786.262
0.5000	0.0180	.1310E+09	0.065	22.000	10065.871
0.5000	0.0185	.1347E+09	0.065	22.623	10345.480
0.5000	0.0190	.1383E+09	0.065	23.249	10625.086
0.5000	0.0195	.1420E+09	0.065	23.877	10904.691
0.5000	0.0200	.1456E+09	0.065	24.506	11184.301
0.5000	0.0205	.1492E+09	0.065	25.139	11463.906
0.5000	0.0210	.1529E+09	0.065	25.773	11743.516
0.5000	0.0215	.1565E+09	0.065	26.411	12023.121
0.5000	0.0220	.1602E+09	0.065	27.050	12302.730
0.5000	0.0225	.1638E+09	0.065	27.692	12582.340

0.5000	0.0230	.1674E+09	0.065	28.336	12861.941
0.5000	0.0235	.1711E+09	0.065	28.982	13141.551
0.5000	0.0240	.1747E+09	0.065	29.631	13421.160
0.5000	0.0245	.1784E+09	0.065	30.282	13700.766
0.5000	0.0250	.1820E+09	0.065	30.936	13980.375
0.5000	0.0255	.1856E+09	0.065	31.592	14259.980

1 DIA(m)	THICK(m)	PRESS(Pa)	VOL(m**3)	MASS(kg)	ATM VOL(m**3)
1.0000	0.0010	.3640E+07	0.524	8.666	2236.871
1.0000	0.0015	.5460E+07	0.524	10.841	3355.307
1.0000	0.0020	.7280E+07	0.524	13.021	4473.738
1.0000	0.0025	.9100E+07	0.524	15.205	5592.176
1.0000	0.0030	.1092E+08	0.524	17.393	6710.613
1.0000	0.0035	.1274E+08	0.524	19.586	7829.051
1.0000	0.0040	.1456E+08	0.524	21.783	8947.477
1.0000	0.0045	.1638E+08	0.524	23.985	10065.906
1.0000	0.0050	.1820E+08	0.524	26.190	11184.336
1.0000	0.0055	.2002E+08	0.524	28.401	12302.762
1.0000	0.0060	.2184E+08	0.524	30.615	13421.199
1.0000	0.0065	.2366E+08	0.524	32.835	14539.625
1.0000	0.0070	.2548E+08	0.524	35.058	15658.051
1.0000	0.0075	.2730E+08	0.524	37.286	16776.484
1.0000	0.0080	.2912E+08	0.524	39.518	17894.914
1.0000	0.0085	.3094E+08	0.524	41.754	19013.348
1.0000	0.0090	.3276E+08	0.524	43.995	20131.770
1.0000	0.0095	.3458E+08	0.524	46.241	21250.184
1.0000	0.0100	.3640E+08	0.524	48.490	22368.633
1.0000	0.0105	.3822E+08	0.524	50.745	23487.063
1.0000	0.0110	.4004E+08	0.524	53.003	24605.492
1.0000	0.0115	.4186E+08	0.524	55.266	25723.918
1.0000	0.0120	.4368E+08	0.524	57.534	26842.332
1.0000	0.0125	.4550E+08	0.524	59.806	27960.781
1.0000	0.0130	.4732E+08	0.524	62.082	29079.211
1.0000	0.0135	.4914E+08	0.524	64.363	30197.641
1.0000	0.0140	.5096E+08	0.524	66.648	31316.070
1.0000	0.0145	.5278E+08	0.524	68.938	32434.480
1.0000	0.0150	.5460E+08	0.524	71.232	33552.930
1.0000	0.0155	.5642E+08	0.524	73.531	34671.359
1.0000	0.0160	.5824E+08	0.524	75.834	35789.789
1.0000	0.0165	.6006E+08	0.524	78.141	36908.219
1.0000	0.0170	.6188E+08	0.524	80.453	38026.648
1.0000	0.0175	.6370E+08	0.524	82.770	39145.051
1.0000	0.0180	.6552E+08	0.524	85.091	40263.480
1.0000	0.0185	.6734E+08	0.524	87.416	41381.906
1.0000	0.0190	.6916E+08	0.524	89.746	42500.336
1.0000	0.0195	.7098E+08	0.524	92.080	43618.762
1.0000	0.0200	.7280E+08	0.524	94.419	44737.227
1.0000	0.0205	.7462E+08	0.524	96.763	45855.656
1.0000	0.0210	.7644E+08	0.524	99.110	46974.047
1.0000	0.0215	.7826E+08	0.524	101.463	48092.512
1.0000	0.0220	.8008E+08	0.524	103.820	49210.941
1.0000	0.0225	.8190E+08	0.524	106.181	50329.367
1.0000	0.0230	.8372E+08	0.524	108.548	51447.797
1.0000	0.0235	.8554E+08	0.524	110.918	52566.223
1.0000	0.0240	.8736E+08	0.524	113.293	53684.652

1.0000	0.0245	.8918E+08	0.524	115.672	54803.078
1.0000	0.0250	.9100E+08	0.524	118.057	55921.508
1.0000	0.0255	.9282E+08	0.524	120.445	57039.934

1 DIA(m)	THICK(m)	PRESS(Pa)	VOL(m**3)	MASS(kg)	ATM VOL(m**3)
1.5000	0.0010	.2427E+07	1.767	19.489	5032.953
1.5000	0.0015	.3640E+07	1.767	24.376	7549.434
1.5000	0.0020	.4853E+07	1.767	29.269	10065.918
1.5000	0.0025	.6067E+07	1.767	34.169	12582.398
1.5000	0.0030	.7280E+07	1.767	39.074	15098.879
1.5000	0.0035	.8493E+07	1.767	43.987	17615.359
1.5000	0.0040	.9707E+07	1.767	48.906	20131.809
1.5000	0.0045	.1092E+08	1.767	53.832	22648.281
1.5000	0.0050	.1213E+08	1.767	58.763	25164.734
1.5000	0.0055	.1335E+08	1.767	63.703	27681.207
1.5000	0.0060	.1456E+08	1.767	68.648	30197.680
1.5000	0.0065	.1577E+08	1.767	73.599	32714.133
1.5000	0.0070	.1699E+08	1.767	78.558	35230.582
1.5000	0.0075	.1820E+08	1.767	83.522	37747.055
1.5000	0.0080	.1941E+08	1.767	88.494	40263.516
1.5000	0.0085	.2063E+08	1.767	93.472	42779.988
1.5000	0.0090	.2184E+08	1.767	98.456	45296.461
1.5000	0.0095	.2305E+08	1.767	103.447	47812.895
1.5000	0.0100	.2427E+08	1.767	108.445	50329.367
1.5000	0.0105	.2548E+08	1.767	113.450	52845.840
1.5000	0.0110	.2669E+08	1.767	118.460	55362.313
1.5000	0.0115	.2791E+08	1.767	123.478	57878.785
1.5000	0.0120	.2912E+08	1.767	128.501	60395.219
1.5000	0.0125	.3033E+08	1.767	133.532	62911.727
1.5000	0.0130	.3155E+08	1.767	138.569	65428.164
1.5000	0.0135	.3276E+08	1.767	143.613	67944.625
1.5000	0.0140	.3397E+08	1.767	148.664	70461.063
1.5000	0.0145	.3519E+08	1.767	153.721	72977.563
1.5000	0.0150	.3640E+08	1.767	158.785	75494.000
1.5000	0.0155	.3761E+08	1.767	163.855	78010.500
1.5000	0.0160	.3883E+08	1.767	168.932	80526.938
1.5000	0.0165	.4004E+08	1.767	174.015	83043.375
1.5000	0.0170	.4125E+08	1.767	179.105	85559.875
1.5000	0.0175	.4247E+08	1.767	184.203	88076.375
1.5000	0.0180	.4368E+08	1.767	189.306	90592.813
1.5000	0.0185	.4489E+08	1.767	194.416	93109.313
1.5000	0.0190	.4611E+08	1.767	199.533	95625.750
1.5000	0.0195	.4732E+08	1.767	204.656	98142.188
1.5000	0.0200	.4853E+08	1.767	209.786	100658.688
1.5000	0.0205	.4975E+08	1.767	214.923	103175.125
1.5000	0.0210	.5096E+08	1.767	220.066	105691.625
1.5000	0.0215	.5217E+08	1.767	225.216	108208.063
1.5000	0.0220	.5339E+08	1.767	230.374	110724.563
1.5000	0.0225	.5460E+08	1.767	235.537	113241.063
1.5000	0.0230	.5581E+08	1.767	240.707	115757.500
1.5000	0.0235	.5703E+08	1.767	245.884	118274.000
1.5000	0.0240	.5824E+08	1.767	251.067	120790.438
1.5000	0.0245	.5945E+08	1.767	256.257	123306.875
1.5000	0.0250	.6067E+08	1.767	261.454	125823.375
1.5000	0.0255	.6188E+08	1.767	266.658	128339.813

1 DIA(m)	THICK(m)	PRESS(Pa)	VOL(m**3)	MASS(kg)	ATM VOL(m**3)
2.0000	0.0010	.1820E+07	4.189	34.601	8947.484
2.0000	0.0015	.2730E+07	4.189	43.277	13421.227
2.0000	0.0020	.3640E+07	4.189	51.974	17894.969
2.0000	0.0025	.4550E+07	4.189	60.666	22368.707
2.0000	0.0030	.5460E+07	4.189	69.369	26842.445
2.0000	0.0035	.6370E+07	4.189	78.094	31316.199
2.0000	0.0040	.7280E+07	4.189	86.814	35789.902
2.0000	0.0045	.8190E+07	4.189	95.539	40263.590
2.0000	0.0050	.9100E+07	4.189	104.275	44737.340
2.0000	0.0055	.1001E+08	4.189	113.038	49211.012
2.0000	0.0060	.1092E+08	4.189	121.791	53684.801
2.0000	0.0065	.1183E+08	4.189	130.555	58158.473
2.0000	0.0070	.1274E+08	4.189	139.340	62632.188
2.0000	0.0075	.1365E+08	4.189	148.120	67105.875
2.0000	0.0080	.1456E+08	4.189	156.906	71579.625
2.0000	0.0085	.1547E+08	4.189	165.702	76053.375
2.0000	0.0090	.1638E+08	4.189	174.527	80527.063
2.0000	0.0095	.1729E+08	4.189	183.340	85000.750
2.0000	0.0100	.1820E+08	4.189	192.164	89474.500
2.0000	0.0105	.1911E+08	4.189	201.015	93948.188
2.0000	0.0110	.2002E+08	4.189	209.856	98421.938
2.0000	0.0115	.2093E+08	4.189	218.702	102895.625
2.0000	0.0120	.2184E+08	4.189	227.559	107369.313
2.0000	0.0125	.2275E+08	4.189	236.444	111843.063
2.0000	0.0130	.2366E+08	4.189	245.318	116316.813
2.0000	0.0135	.2457E+08	4.189	254.202	120790.563
2.0000	0.0140	.2548E+08	4.189	263.114	125264.188
2.0000	0.0145	.2639E+08	4.189	272.016	129737.938
2.0000	0.0150	.2730E+08	4.189	280.928	134211.688
2.0000	0.0155	.2821E+08	4.189	289.845	138685.375
2.0000	0.0160	.2912E+08	4.189	298.791	143159.125
2.0000	0.0165	.3003E+08	4.189	307.730	147632.813
2.0000	0.0170	.3094E+08	4.189	316.676	152106.500
2.0000	0.0175	.3185E+08	4.189	325.643	156580.250
2.0000	0.0180	.3276E+08	4.189	334.610	161054.000
2.0000	0.0185	.3367E+08	4.189	343.583	165527.750
2.0000	0.0190	.3458E+08	4.189	352.561	170001.438
2.0000	0.0195	.3549E+08	4.189	361.567	174475.125
2.0000	0.0200	.3640E+08	4.189	370.567	178948.875
2.0000	0.0205	.3731E+08	4.189	379.573	183422.563
2.0000	0.0210	.3822E+08	4.189	388.590	187896.313
2.0000	0.0215	.3913E+08	4.189	397.634	192370.063
2.0000	0.0220	.4004E+08	4.189	406.667	196843.688
2.0000	0.0225	.4095E+08	4.189	415.711	201317.438
2.0000	0.0230	.4186E+08	4.189	424.778	205791.188
2.0000	0.0235	.4277E+08	4.189	433.839	210264.875
2.0000	0.0240	.4368E+08	4.189	442.910	214738.625
2.0000	0.0245	.4459E+08	4.189	451.988	219212.313
2.0000	0.0250	.4550E+08	4.189	461.093	223686.063
2.0000	0.0255	.4641E+08	4.189	470.187	228159.750

APPENDIX B

DRAG DETERMINATION FOR THE AEREON BALLOON

The Aereon configuration is shown in Figure 1.1. Total Aereon drag is determined through the use of the following equations:

- Calculation of transition point: $x = \nu Rx / U_x$

  Assume: $R_x = 3 \times 10^5$

  $x = (7.325 \times 10^{-4}) (3 \times 10^5) / 5$ m/sec.

  $x = 43.95$ m

- Calculation of Reynolds number based on Aereon length: $R_l = \rho U l / \mu$

  $R_l = (2 \times 10^{-2}$ kg/m^3) (5 m/sec.) (70.64 m) / 1.465 x 10-5 N-sec./m^2

  $R_l = 4.82 \times 10^5$

- Calculation of turbulent skin friction coefficient: $C_f = 0.455 (\log_{10} R_l)^{-2.58}$

  $C_f = 0.455 (\log_{10} 4.82 \times 10^5)^{-2.58}$

  $C_f = 5.14 \times 10^{-0.03}$

- Dynamic pressure calculation: $q = 1 / 2pU^2$

  $q = 1/2 (2 \times 10^{-2})$ (5 m/sec.)^2

  q = 2.5 x 10-1 N/m^2

- Total skin friction drag if all flow were turbulent: $D = qS_wC_f$

  $D = (2.5 \times 10^{-1}) (6074.69$ m$^2) (5.14 \times 10^{-0.03})$

  $D = 7.81$ N

- Laminar skin friction calculation: $C_f = 1.328\ R_l^{-1/2}$

  $C_f = 1.328\ (4.82 \times 10^5)^{-1/2}$

  $C_f = 1.9128 \times 10^{-0.03}$

- Drag for laminar flow portion: $D = qC_f S_w$

  $D = (2.5 \times 10^{-1}\ N/m^2)\ (1.9128 \times 10^{-0.03})\ (6074.69\ m^2)$

  $D = 2.95\ N$

- Skin friction drag if flow were turbulent over leading edge: $C_f = 0.455\ (\log_{10} R_x)^{-2.58}$

  $C_f = 0.455\ (\log_{10} 3 \times 10^5)^{-2.58}$

  $C_f = 5.657 \times 10^{-3}$

- Drag for turbulent boundary layer: $D = qC_fS_w$

  $D = (2.5 \times 10^{-1}\ N/m^2)\ (5.657 \times 10^{-3})\ (6074.69\ m^2)$

  $D = 8.59\ N$

- Final Drag on entire Aereon: D = Total Skin Friction - (Turbulent B.L. -Laminar Drag)

  $D = 7.81\ N - (8.59 - 2.95)$

  $D = 2.17\ N$

  Total Drag Coefficient: 1.3958×10^{-3}